Bioreporters for mode of action-informed antibiotic screening and their transcriptional regulation in *Bacillus subtilis*.

Dissertation

der Mathematisch-Naturwissenschaftlichen Fakultät

der Eberhard Karls Universität Tübingen

zur Erlangung des Grades eines

Doktors der Naturwissenschaften

(Dr. rer. nat.)

vorgelegt von

Katharina Wilma Wex

aus Mosbach (Baden)

Tübingen

2021

Gedruckt mit Genehmigung der Mathematisch-Naturwissenschaftlichen Fakultät der Eberhard Karls Universität Tübingen.

Tag der mündlichen Qualifikation:	21.12.2021
Dekan:	Prof. Dr. Thilo Stehle
1. Berichterstatterin:	Prof. Dr. Heike Brötz-Oesterhelt
2. Berichterstatter:	Prof. Dr. Wolfgang Wohlleben
3. Berichterstatter:	Prof. Dr. Fabian Commichau

TABLE OF CONTENTS

ABBREVIATIONS

µg	microgram
µm	micrometer
µM	micromolar
µL	microliter
σ (σ^A, σ^B, etc.)	sigma factor (Sig) (A, B, etc.)
ADEP	acyldepsipeptide
Ala	alanine
ATP	adenosine triphosphate
asRNA	antisense RNA
A-site	acceptor/aminoacyl site (ribosome)
BMM	Belitzky minimal medium
(M)bp	(Mega) base pair(s)
Ca^{2+}	calcium
cAMP	cyclic adenosine monophosphate
CHL	chloramphenicol
CCCP	carbonyl cyanide m-chlorophenyl hydrazone
CFU	colony forming units
CIP	ciprofloxacin
Da	dalton
DACA	DNA affinity capturing assay
DACT	actinomycin D
DAP	daptomycin
DCM	dichloromethane
DMSO	dimethyl sulfoxide
DNA	desoxyribonucleic acid
DOX	doxycycline
dTMP	deoxythymidine monophosphate
FID	fidaxomicin
ECF	extracytoplasmic function
e.g.	*exempli gratia*
ERY	erythromycin
etc.	*et cetera*
EtOAc	ethyl acetate
EtOH	ethanol
i.e.	*id est*
IPM	imipenem
h	hour
HPLC-MS	high performance liquid chromatography
HTH	helix-turn-helix
LB	lysogeny broth
mg	milligram
$MgCl_2$	magnesium chloride
MeOH	methanol
min	minute
MIC	minimal inhibitory concentration
MOA	mode(s) of action
mRNA	messenger RNA
MS	mass spectrometry
NaCl	natrium chloride
OD_{600}	optical density at λ=600 nm
PCR	polymerase chain reaction
PG	peptidoglycan
P-site	peptidyl site (ribosome)
RAE	rifampin-associated element
RNA	ribonucleic acid
RNAP	RNA polymerase
RIF	rifampin
RLU	relative luminescence units
SPT	spectinomycin
sRNA	small RNA
tRNA	transfer RNA
TMP	trimethoprim
UDP-MurNAc-pp	uridine diphosphate-N-acetylmuramyl-pentapeptide
UTP	uridine triphosphate
UTR	untranslated region
UV-Vis	ultraviolet-visible
VAN	vancomycin
v/v	volume per volume
WT	wildtype
w/v	weight per volume
X-Gal	5-bromo-4-chloro-3-indolyl-ß-D-galactopyranoside
ZOI	zone of inhibition

ZUSAMMENFASSUNG

Der Großteil der heutzutage angewandten Antibiotika gehört zur Gruppe der Naturstoffe oder wurde durch Modifizierung einzelner funktioneller Gruppen von ihnen abgeleitet. Auf der Suche nach neuen Antibiotika konzentrieren sich viele aktuelle Forschungsprojekte erneut auf Naturstoffproduzenten, da Naturstoffe komplexe physiochemische Eigenschaften bezüglich einer guten bakteriellen Aufnahme, intrazellulären Verfügbarkeit und Bindung an die Zielstruktur in sich vereinen und durch rationales Design nur sehr schwer nachzuahmen sind. Es besteht die gerechtfertigte Hoffnung, dass die Untersuchung neuer Produzentenstämme aus weniger erforschten Nischen potenziell neue antimikrobiell wirksame Substanzen hervorbringt. Außerdem konnte durch Genomsequenzierung festgestellt werden, dass viele Produzentenstämme das Potential besitzen zusätzliche Sekundärmetabolite zu synthetisieren, welche in sogenannten kryptischen oder stillen Genclustern codiert sind. Die Aktivierung dieser Gencluster, z.B. durch die Anzucht der Produzentenstämme unter neuen Wachstums- oder Stressbedingungen, die genetische Manipulation der Genregulation oder die heterologe Genexpression, ist ebenso Bestandteil aktueller Forschung. Um diese Auswahl an potenziellen Naturstoffproduzenten effektiv zu beproben, benötigt man, neben verbesserten Aufreinigungs- und Dereplikationsmethoden, vor allem schnelle, robuste und selektive Screeningmethoden, welche einen hohen Informationsgehalt generieren.

In dieser Arbeit wurde ein Agar-basierter Bioreporteransatz entwickelt und validiert, der ein kombiniertes Bioaktivitäts- und Wirkmechanismus (MOA)-informiertes Screening ermöglicht. Die verwendeten ß-Galaktosidase-basierten *Bacillus subtilis* Bioreporter-konstrukte zeigten eine selektive Induktion bei antimikrobieller Interferenz mit einem der Hauptstoffwechselwege: DNA-Synthese (P_{yorB}-*lacZ*), RNA-Synthese (P_{rpt}-*lacZ* und P_{helD}-*lacZ*), Proteinbiosynthese (P_{bmrC}-*lacZ*, selektiv für Translationsarrest) und Integrität der Zellhülle (P_{ypuA}-*lacZ* und P_{liaI}-*lacZ*). Die Induktionsspezifität der Bioreporterstämme im Agar-basierten Testverfahren wurde unter Verwendung von ~90 Referenzantibiotika mit bekanntem MOA bestätigt. Da P_{rpt} als Bioreporter bisher unbeschrieben war, musste seine Induktionsspezifität und -sensitivität in Bezug auf RNA-Stress sowohl im Agar-basierten Ansatz sowie in einem flüssigen, Luciferase-basierten System eingehend profiliert werden. Nach der Validierung der Bioreporterstämme, ermöglichte der Agar-basierte Test die Charakterisierung unbekannter, antimikrobieller Wirkstoffe, wie z.B. die Untersuchung von Microcionamid A und C. Generell wies die Bioreporter-basierte MOA-Profilierung den Hauptstoffwechselweg auf, welcher durch die antibiotische Aktivität spezifisch gehemmt

wurde, und ermöglichte die Auswahl geeigneter Folgestudien zur Aufklärung der molekularen Zielstruktur.

Weiterhin wurde der Agar-basierte Bioreporteransatz auf seine Anwendbarkeit im direkten Screening von Antibiotika-Produzentenstämmen untersucht. Es konnte nachgewiesen werden, dass produzierte antimikrobielle Wirkstoffe durch die direkte Untersuchung von Agarproben oder Kulturüberständen der kultivierten Produzentenstämme sensitiv detektiert und bezüglich ihres MOA profiliert werden können, ohne dass eine initiale Wirkstoffaufreinigung erforderlich war. Dies war besonders interessant, da Antibiotika-Produzentenstämme oft das genetische Potenzial besitzen, verschiedene antimikrobielle Sekundärmetabolite zu synthetisieren, welche mit Hilfe der zusätzlichen MOA-Information der Bioreporterstämme schnell unterschieden werden können. Das Testverfahren bietet zudem den Vorteil, den gesamten Aufreinigungsprozess eines Wirkstoffes zu überwachen, da unbearbeitete Produzentenstämme, Extrakte, fraktionierte Proben oder Reinsubstanzen auf das Vorhandensein der zuvor detektierten Aktivität inklusive Bioreportersignal getestet werden können. Es konnte weiterhin gezeigt werden, dass der Agar-basierte Bioreporteransatz in der Lage ist, Polypharmakologie oder synergistische Effekte von antimikrobiellen Substanzen sensitiv nachzuweisen.

Die selektive Hochregulierung der ausgewählten *B. subtilis* Bioreportergene durch antibiotische Interferenz mit einem der oben genannten Hauptstoffwechselwege war in einer früheren Transkriptom-Studie entdeckt worden. Die Funktion und Regulation der identifizierten *B. subtilis*-Gene sind jedoch nur teilweise charakterisiert. Ein besseres Verständnis der initiierten Stressantworten, welche die selektive Induktion der Gene regulieren, ermöglicht eine verfeinerte MOA-Charakterisierung der induzierenden Antibiotika und erlaubt potenziell neue Einblicke in zelluläre Anpassungs- oder Resistenzmechanismen. Daher wurde in dieser Arbeit die Regulation der Bioreportergene *rpt*, *helD* und *yorB* untersucht, welche nach Behandlung mit RNA-, respektive DNA-Synthese-hemmenden Antibiotika selektiv hochreguliert werden. Bezüglich der Genregulation von *rpt* und *helD* ließen die Induktionsprofile von P_{rpt} und P_{helD} nach Antibiotikabehandlung, welche zusätzlich in einem quantitativen, Luciferase-basierten Reportersystem gemessen wurden, auf einen ähnlichen Regulationsmechanismus schließen. Weitere Ergebnisse wie Promotor-Deletionsstudien und DNA-Affinitäts-Capturing-Assays, deuteten darauf hin, dass die SigA-regulierten Gene *rpt* und *helD* zu einer *cis*-kodierten Antisense-RNA-regulierten Stressantwort gehören, welche möglichweise selektiv durch das zelluläre Erkennen blockierter RNA-Polymerase-Komplexe induziert wird. Zudem konnte nachgewiesen werden, dass das SPß-Prophagenprotein YorB

LexA-reguliert und somit Teil der SOS-Antwort in *B. subtilis* ist. Schließlich wurde die bisher nicht charakterisierte Funktion von Rpt (früher PpS/YppS) aus *B. subtilis* aufgeklärt. Es konnte gezeigt werden, dass Rpt eine selektive Resistenz gegen Rifamycine verleiht, indem es diese spezifisch phosphoryliert und damit inaktiviert.

SUMMARY

Most of todays applied antibiotics belong to the group of natural products or have been derived from them, by modifying individual functional groups. In the search for new antibiotics, current research is again concentrating on natural product discovery, since those compounds combine complex physiochemical properties with regard to good bacterial uptake, intracellular retainment, and target engagement, which cannot simply be mimicked by rational design. There is justified hope that the investigation of new producer strains from less explored niches could reveal new natural products. Genome sequencing has also shown that many producer strains possess the potential to synthesize additional secondary metabolites, which are encoded in so-called cryptic or silent gene clusters. The activation of those gene clusters, e.g., by cultivation of the producer strains under different growth or stress conditions, genetic manipulation of gene regulation, or heterologous expression, is also part of current research. In order to effectively screen all those potential natural product producers, improved purification and dereplication methods are required and, above all, fast, robust, and selective screening procedures, which generate high content information.

In this thesis, an agar-based bioreporter approach was developed and validated, which allows for combined bioactivity and mode of action-informed screening. The employed ß-galactosidase-based *Bacillus subtilis* bioreporter constructs showed selective induction upon antimicrobial interference with one of the main metabolic pathways: DNA synthesis (P_{yorB}-*lacZ*), RNA synthesis (P_{rpt}-*lacZ* and P_{helD}-*lacZ*), protein biosynthesis (P_{bmrC}-*lacZ*, selective for translation arrest) and integrity of the cell envelope (P_{ypuA}-*lacZ* and P_{lial}-*lacZ*). Induction specificity of the bioreporter panel in the agar-based setup was confirmed using a large set of ~90 reference antibiotics with known MOA. Of note, P_{rpt} had not previously been described as bioreporter and was therefore extensively profiled for its induction specificity and sensitivity upon RNA stress in the agar-based assay as well as in a liquid, luciferase-based system. After validation of the bioreporter panel, the agar-based approach allowed the characterization of unknown antimicrobial agents, like the investigated compounds microcionamide A and C. Generally, the bioreporter-based MOA profiling indicated the metabolic pathway(s) of antibiotic interference and allowed for the selection of adequate MOA follow-up studies to elucidate the exact molecular target.

Furthermore, the agar-based bioreporter approach was evaluated for its applicability in direct screening of antibiotic producer strains. It could be proven that produced antimicrobials can be sensitively detected and MOA-profiled by direct probing of agar plugs or culture supernatants of the cultivated producer strains, with no need for initial compound

purification. This finding was especially interesting as antibiotic producer strains often possess the genetic potential to synthesize different antimicrobial secondary metabolites, which can rapidly be distinguished using the additional MOA information of the bioreporter panel. The assay also bears the advantage to monitor the entire purification process of a bioactive substance, allowing to test unprocessed producer strains, extracts, fractionated samples, or pure substances for the presence of the previously detected activity and bioreporter signal of interest. It could further be shown, that the agar-based bioreporter approach is able to sensitively detect polypharmacology or synergistic effects of antimicrobial substances.

The specific upregulation of the selected *B. subtilis* bioreporter genes upon antibiotic interference with one of the upper mentioned main metabolic pathways was discovered in a previous transcriptome study. However, the function and regulation of the identified *B. subtilis* genes are only partially characterized. A better understanding of the initiated stress responses that regulate selective gene induction would enable a refined MOA characterization of the inducing antibiotics, and potentially allow new insights into cellular adaptation or resistance mechanisms. Hence, regulation of the bioreporter genes *rpt*, *helD*, and *yorB*, which are selectively upregulated upon exposure to antibiotics that inhibit RNA or DNA synthesis, respectively, was investigated in this work. For gene regulation of *rpt* and *helD*, the induction profiles of P_{rpt} and P_{helD} upon antibiotic treatment in a quantitative, luciferase-based reporter system, already pointed at a similar regulation mechanism. Further results like promoter deletion studies or DNA affinity capturing assays indicated, that the SigA-regulated genes *rpt* and *helD* both belong to a *cis*-encoded antisense RNA-regulated stress response, which is proposed to be selectively induced by the cellular sensing of stalled RNA polymerase complexes. The SPß-prophage protein YorB was proven to be LexA-regulated and thus part of the SOS response in *B. subtilis*. Finally, the function of *B. subtilis* Rpt (formerly PpS/YppS), which had not been previously characterized, was elucidated. It could be shown that Rpt confers selective resistance to rifamycins by phosphorylation inactivation.

LIST OF ALL PUBLICATIONS

Accepted publications

Publication 1

Wex, K. W., Saur, J. S., Handel, F., Ortlieb, N., Mokeev, V., Kulik, A., Niedermeyer, T. H. J., Mast, Y., Grond, S., Berscheid, A.*, Brötz-Oesterhelt, H.* (2021). Bioreporters for direct mode of action-informed screening of antibiotic producer strains. Cell Chemical Biology. DOI: 10.1016/j.chembiol.2021.02.022

Publication 2

Mokhlesi, A., Stuhldreier, F., **Wex, K. W.**, Berscheid, A., Hartmann, R., Rehberg, N., Sureechatchaiyan, P., Chaidir, C., Kassack, M. U., Kalscheuer, R., Brötz-Oesterhelt, H., Wesselborg, S., Stork, B., Daletos, G., Proksch, P. (2017). Cyclic cystine-bridged peptides from the marine sponge *Clathria basilana* induce apoptosis in tumor cells and depolarize the bacterial cytoplasmic membrane. Journal of Natural Products 80, 2941-2952.

Manuscript in preparation

Manuscript 1

Wex, K. W., Franz-Wachtel, M., Kulik, A., Macek, B., Brötz-Oesterhelt, H., Berscheid, A. Expression of the *Bacillus subtilis* genes *rpt* (formerly *pps*/*yppS*) and *helD* is specifically induced by RNA polymerase stalling and regulated by a *cis*-encoded antisense RNA.

* Shared senior authorship

DECLARATION OF PERSONAL CONTRIBUTION

Publication 1

The study concept was designed by me, Anne Berscheid and Heike Brötz-Oesterhelt. The bioreporter construction, validation and all related bioreporter experiments were conducted by me. Cultivation experiments of known producer strains were done by me. Cultivation of all uncharacterized producer strains of the Tübingen strain collection as well as the selective follow-up of some actinomycetes strains, including compound purification and deconvolution experiments, were conducted by Julian S. Saur, Franziska Handel, Nico Ortlieb, Vladislav Mokeev, and Andreas Kulik. All authors discussed and analyzed data. The paper was written by me, Anne Berscheid and Heike Brötz-Oesterhelt and edited by all authors. All containing figures were prepared by me. I took part in the revision process, by performing requested experiments and revising the manuscript under supervision of Anne Berscheid and Heike Brötz-Oesterhelt.

Publication 2

I was involved in the mode of action profiling studies and tested the substances microcionamide A and C against the *Bacillus subtilis* bioreporter panel. All bioreporter strains used in this study were generated and validated by me. I drafted the results of the agar-based bioreporter approach for the manuscript, prepared Figure 5 and wrote the corresponding methods section under the guidance of Anne Berscheid and Heike Brötz-Oesterhelt.

Manuscript 1

The study concept was devised by me and Anne Berscheid. All mutants used in this manuscript have been constructed by me, while the *B. subtilis* knockout and knockdown libraries were acquired from Addgene and initially provided by Carol Gross. Experimental design and data analysis was performed be me and Anne Berscheid, while I conducted all experiments myself, with the exception of the following. The detection of phosphorylated rifampin via HPLC-MS analysis was done by Andreas Kulik. Liquid chromatography-nanospray tandem mass spectrometry (NanoLC-MS/MS) analysis and data processing of the DNA affinity capturing assay (DACA) samples was performed by Mirita Franz-Wachtel. Data was discussed by me, Anne Berscheid and Heike Brötz-Oesterhelt. The manuscript was written by me under the supervision of Anne Berscheid. Furthermore, I prepared all figures that are contained in the manuscript.

1. INTRODUCTION

1.1. Current importance of antibiotic research

Antibiotic discovery was initiated with the finding of anti-*Treponema pallidum* (pathogen causing syphilis) bioactivity of the synthetically prepared salvarsan in 1909, followed by the incidental discovery of the first natural product penicillin in 1928. In the subsequent, so-called golden era of antibiotic discovery (~1940-1960), the scientific community uncovered a large variety of bioactive compounds, that still build the bases of the majority of today's antibiotic treatment options (Figure 1). Already at that time the parallel emergence of antibiotic resistance was described (Welsch, 1952; Eagle, 1954; Clatworthy et al., 2007).

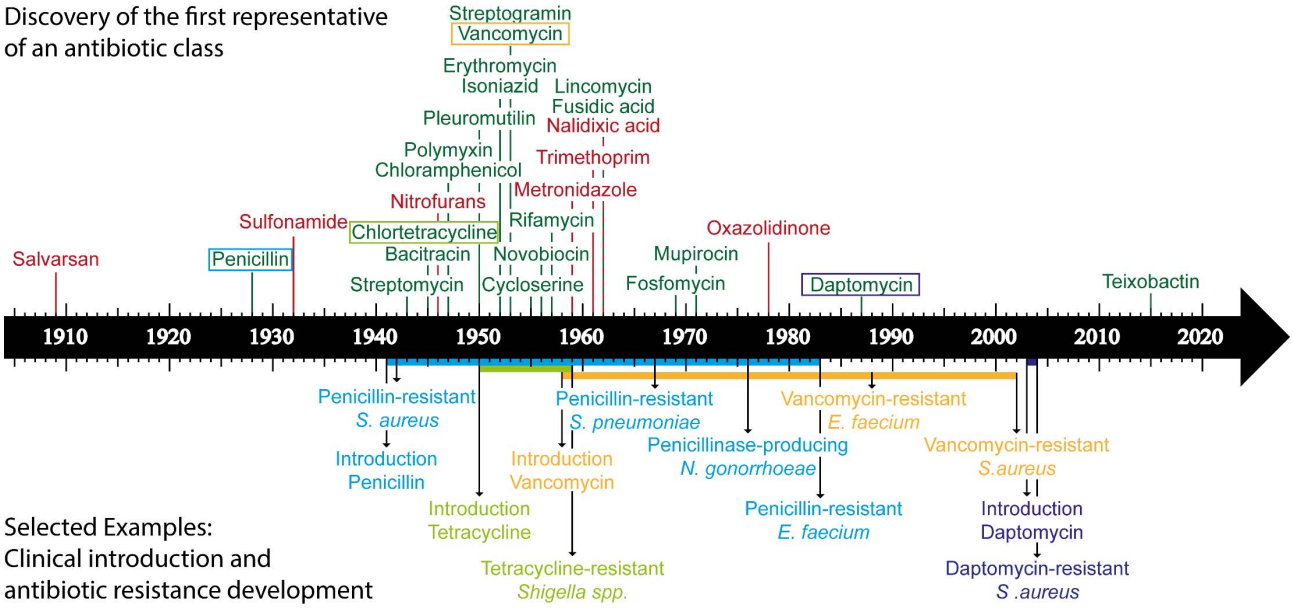

Figure 1. Timeline of antibiotic discovery and resistance development. The upper part depicts the year of discovery for the first identified representatives of each antibiotic class (Silver, 2011; Ling et al., 2015). Natural products are highlighted in green, while synthetically derived compounds are marked in red. Colored boxes indicate antibiotics that were further investigated in this graph for parallel resistance development (lower part). The lower section shows the resistance development against some exemplarily chosen antibiotics after clinical introduction. Resistant pathogens depicted are *Staphylococcus aureus* (*S. aureus*), *Shigella* spp., *Streptococcus pneumoniae* (*S. pneumoniae*), *Neisseria gonorrhoeae* (*N. gonorrhoeae*), and *Enterococcus faecium* (*E. faecium*) (Centers for Disease Control and Prevention, 2013; Centers for Disease Control and Prevention, 2020).

What did not appear as a great threat back then as antibiotic resources seemed to be infinite, has become a major problem in recent years, with dried-out pipelines in antibiotic discovery and rising numbers of (multi-) resistant pathogenic bacteria (O´Neill, 2014; Frieri et al., 2017; Aslam et al., 2018). Multiple factors have been adding to this shortage: the imprudent use of antibiotics in agriculture (e.g., for artificial animal fattening or factory farming) (Landers et al., 2012; Manyi-Loh et al., 2018; Yang et al., 2019), the enhanced medical application of broad-spectrum antibiotics (often misused or used for preventive measures) (Schroeck et

al., 2015), the general difficulty to find new antibiotic scaffolds in a more exploited environment, the shrinking efforts in antibiotic research made by pharmaceutical companies due to its non-profitable and tedious developmental process, the more rapid spread of antibiotic resistance in a globalized world (MacPherson et al., 2009) and finally, the environmental accumulation of all produced and applied antibiotics (e.g., in the waste water of antibiotic production facilities or municipal sewage) (Kraemer et al., 2019; Davies and Davies, 2010). Although public awareness of the growing threat of antibiotic resistance is rising, there is need for further education, as for example awareness studies revealed misbeliefs concerning the appropriate application of antibiotics or the antibiotic resistance development, i.e., the majority of people asked thought, that humans and not bacteria become antibiotic resistant (World Health Organization, 2015). In 2014, an expert committee predicted that by 2050 antimicrobial infections will constitute the most frequent cause of death (O´Neill, 2014). Although it is difficult to predict the extent of such prognoses, we are indeed facing a post-antibiotic future, if the antibiotic resistance problem is not promptly tackled from multiple sides. On the one hand our generation has to learn to responsively handle the remaining precious drugs, e.g., by restricting the medical application or following a more sustainable antibiotic-free agriculture, while, on the other hand, we have to invest in the discovery and development of new antimicrobial agents, which can only be achieved by an extended and stably financed antibiotic research.

1.2. Antibiotic discovery and development

In recent years, only few antibiotics could successfully pass through all clinical trials, with the majority of approved antibiotic agents comprising derivatives of known antibiotic classes (Hutchings et al., 2019). To counteract antibiotic resistance development, there is the urgent need to find new antimicrobial scaffolds, that either show new binding modes on characterized targets or interfere with new targets, thereby avoiding cross-resistance (Bush et al., 2011; Walsh and Wencewicz, 2014). Furthermore, resistance breaking agents are of interest, which specifically combat resistance in combinational treatment with currently applied therapeutics (Bush and Pucci, 2011; Melander and Melander, 2017; Laws et al., 2019) or compounds that tackle non-essential virulence pathways (i.e., biofilm formation) (Rasko and Sperandio, 2010; Martínez et al., 2019). Research groups are also working on antimicrobial, immunomodulatory agents, that support the inherent host immune response for more effective elimination of invading pathogens (Liu et al., 2006; Ting et al., 2020).

To date, antibiotic research mostly followed two main strategies: the target-based screening for and rational optimization of (semi-)synthetic molecules versus the activity-based

screening of naturally or (semi-) synthetically derived samples (Brötz-Oesterhelt and Sass, 2010; Singh et al., 2011). For the former, huge efforts had been invested into developing low-molecular molecules that displayed optimized binding to the purified bacterial target site of interest *in vitro*. Unfortunately, when tested *in vivo* they often only showed weak antimicrobial activity, as the predicted targets were not essential in the nutrient-rich host environment, prone to mutation or could easily be bypassed by acquiring requisite reaction products from the surrounding (Brötz-Oesterhelt and Sass, 2010). Furthermore, their physiochemical properties often allowed for improved target-binding, but did not meet the demands necessary for bacterial cell entry or escaping efflux mechanisms (Brötz-Oesterhelt and Sass, 2010; Tommasi et al., 2015). The results indicate the difficulties of computationally predicting suitable bacterial target structures or the impact of molecular modifications of antimicrobials on every step necessary for effective target engagement in bacterial whole cell systems. In contrast, natural products have evolved complex physiochemical properties to combine efficient target-binding, optimized bacterial cell entry, good cytoplasmic retainment, and resistance-slowing polypharmacology, which make them a promising source for potentially new antimicrobial scaffolds (Brötz-Oesterhelt and Sass, 2010; Bérdy, 2012; Wright, 2017). This superiority is also displayed by the vast majority of all applied antibiotics having derived from natural products (Newman and Cragg, 2016; Wright, 2017). Nonetheless, the major bottleneck in natural product discovery is the frequent rediscovery of previously isolated compounds (Tulp and Bohlin, 2005; Genilloud, 2017). To overcome this problem, current research tries to follow new paths, e.g., by investigating newly discovered or underexplored antibiotic producer species, which colonize more specialized environmental niches (Wohlleben et al., 2016; Zipperer et al., 2016; Nithya et al., 2018). Furthermore, genomic approaches revealed that producer strains indeed often possess large numbers of antibiotic gene clusters and therefore the potential to produce new antimicrobial secondary metabolites, i.e., indicated by metagenomic data from non-cultivable microorganisms or the existence of silent gene clusters (Wohlleben et al., 2016). To free those capacities, different strategies are developed in order to indirectly (e.g., by growth under stress conditions or in cocultivation) (Seyedsayamdost, 2014; Yoon and Nodwell, 2014; Netzker et al., 2015) or directly modulate the producer strains gene expression (Mao et al., 2018; Culp et al., 2019; Wang et al., 2019) or to heterologously express the gene cluster of interest (Nah et al., 2017).

In parallel, further development of improved extraction methods, facilitated deconvolution strategies and appropriate high-throughput screening technologies to efficiently purify, unravel and prioritize potentially interesting bioactive molecules are required (Carrano and

Marinelli, 2015; Ventura et al., 2017). As indicated above, especially bioactivity-based whole cell screenings are of interest, as they reflect the antibiotic's potency to overcome the cumulative bacterial obstacles (e.g., membrane barriers, inactivating enzymes, or efflux systems). Selection and prioritization can be accomplished by application of pathogen-specific counter-screenings (Murray et al., 2019) or eukaryotic toxicity assays, but also by an early mode of action (MOA) classification (Fischer et al., 2004; Urban et al., 2007; Nonejuie et al., 2016; Wolf and Mascher, 2016; Wex et al., 2021).

1.3. Antibiotic modes of action

Antibiotics are agents that inhibit bacterial growth and reproduction (bacteriostatic) or lead to bacterial cell lysis (bactericidal). Antibiotic action can be broad-spectrum by interference with target structures or biosynthetic pathways, which are of common importance and accessible in all bacteria (Pham et al., 2019) or narrow-spectrum, thereby tackling only a subset of bacteria, which possess species-specific target structures, target essentiality or target accessibility (Melander et al., 2018; Alm and Lahiri, 2020). In that regard, antibiotic accessibility (and therefore also antibiotic activity) is often impeded in Gram-negative bacteria, due to their additional outer membrane permeability barrier (Hancock, 1997). To date, most applied antibiotics interfere with enzymes or the cellular structure of one of the four major biosynthetic pathways of bacteria, thereby inhibiting DNA synthesis, RNA synthesis, protein biosynthesis or unbalancing cell envelope integrity (Figure 2) (Bassetti et al., 2013; Wetzel et al., 2021), while each pathway contains multiple antibiotic target options, with the following sections exemplarily characterizing some of those pathway-specific antibiotic MOA.

1.3.1. Interference with DNA synthesis

DNA synthesis can be impaired by hampering the function of replication enzymes, by interference with the nucleotide precursor supply, or by intercalation into DNA. The synthetic group of quinolones inhibits both essential bacterial type-II topoisomerases, DNA gyrase, and DNA topoisomerase IV, with some of those derivatives showing preference for one of those enzymes (Fournier et al., 2000). DNA gyrase is also targeted by other antibiotics like aminocoumarins, simocyclinones, cyclothialidines, or zoliflodacin, which is currently in phase-III clinical trials (Basarab et al., 2015a; Khan et al., 2018). Limitation of the nucleotide precursor supply is, e.g., implemented by the MOA of trimethoprim and sulfonamides, which interfere with different steps of the folate biosynthesis (Wormser et al., 1982). Furthermore, the antibiotic 5'-fluorouracil limits the intracellular deoxythymidine monophosphate (dTMP)

levels by inhibition of the thymidylate synthase (Cohen et al., 1958; Longley et al., 2003; Oe et al., 2020). Of note, 5'-fluorouracil was shown to possess a dual MOA and can additionally be metabolized and incorporated into mRNA, thereby impairing protein synthesis (Cohen et al., 1958; Singh et al., 2015). Impairment of DNA structure is a MOA that in most cases goes hand in hand with a high eukaryotic cytotoxicity, as the DNA target is conserved in eukaryotes. Therefore, those antibiotics are primarily applied in anticancer therapy rather than antimicrobial chemotherapy (Godzieba and Ciesielski, 2020). There are intercalating agents like doxorubicin, alkylating agents like mitomycin C, or minor-groove binders like netropsin (Bhaduri et al., 2018). DNA-binding compounds most likely affect both, DNA and RNA synthesis, but can show (species-specific) preferred primary inhibition of a single of those two pathways (Harvey et al., 1976; Opperman et al., 2016).

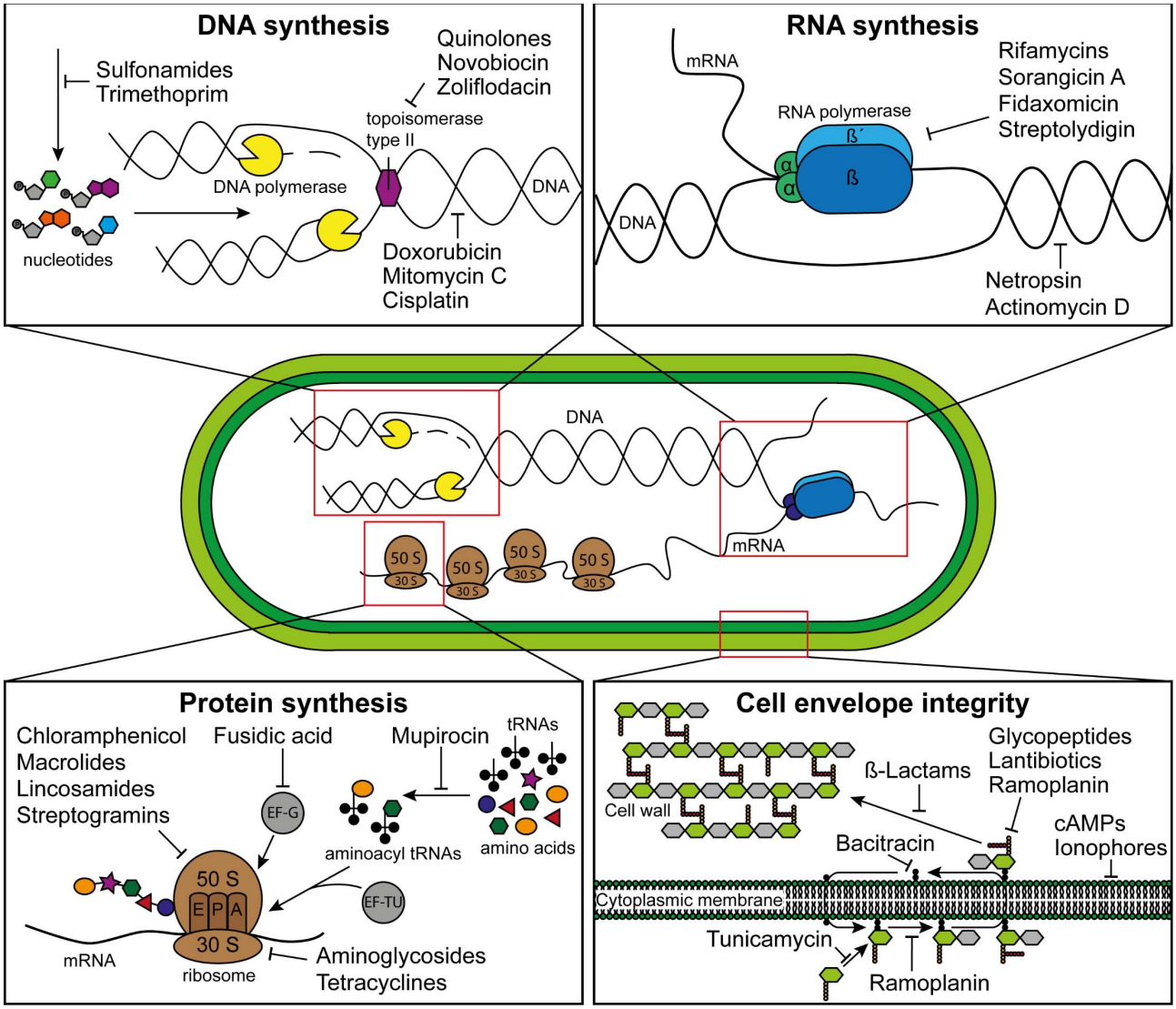

Figure 2. Schematic overview of antibiotic interference with the bacterial main metabolic pathways. Depicted are different antibiotic target structures or enzymes in one of the respective pathways: DNA synthesis, RNA synthesis, Protein biosynthesis, or maintenance of cell envelope integrity. The schematic overview of antibiotics interfering with cell envelope integrity was partly adapted from Schneider and Sahl, 2010.

1.3.2. Interference with RNA synthesis

The main target of RNA synthesis impairment is the DNA-dependent RNA polymerase (RNAP), which usually consists of the subunits $\alpha_2\beta\beta'\omega$ (core RNAP) and a promoter-binding sigma factor. Rifamycins inhibit the progression of the RNAP by sterically blocking its exit tunnel and thereby the release of the nascent messenger RNA (mRNA) (Floss and Yu, 2005). They can therefore only inhibit RNA synthesis initiation for mRNA chains between 3-7 nucleotides, which did not yet leave the exit tunnel, while they cannot affect RNA synthesis progression at later time points (Campbell et al., 2001; Floss and Yu, 2005). The antibiotics streptovaricin and sorangicin A possess a similar transcription inhibition mechanism and bind to the same RNAP binding pocket. Resistance mutations against rifamycins in the ß-subunit of the RNAP similarly affect streptovaricin activity, while sorangicin A only shows partial cross-resistance (Wehrli and Staehelin, 1971; Campbell et al., 2005). Transcription initiation is further inhibited by fidaxomicin or α-pyrone antibiotics, like myxopyronin or corallopyronin, which interfere with different steps in open complex formation (Tupin et al., 2010; Artsimovitch et al., 2012). Elongation of RNA synthesis is impaired by streptolydigin, tirandamycin, or pseudouridimicin. While streptolydigin freezes the nucleotide addition cycle and other catalytic RNAP reactions (Temiakov et al., 2005), the nucleoside analog pseudouridimicin competes with uridine triphosphate (UTP) for RNAP binding, thereby hampering native UTP addition to growing mRNA chains (Maffioli et al., 2017). Thiolutin and holomycin are also discussed to inhibit RNA synthesis. However, current studies indicate that the inhibitory action is rather an indirect effect based to their ability to act as chelating agents for zinc ions, which active RNAP is dependent of (Chan et al., 2017). Transcription is also affected by DNA-binding agents (see chapter 1.3.1.). A prominent example is the intercalator actinomycin D, which was shown to preferably inhibit RNA synthesis, while impairment of DNA synthesis could only be observed at highly elevated antibiotic concentrations (Hollstein, 1974).

1.3.3. Interference with protein synthesis

Impairment of protein biosynthesis is very diverse and can be achieved by direct interference with the ribosome, amino acid supply or nascent polypeptide chains. Bioactive agents like chloramphenicol, macrolides, ketolides, lincosamides, or streptogramins, all interact with the 50S ribosomal subunit. Chloramphenicol blocks ribosomal progression by binding to the acceptor (A)-site and inhibiting the peptidyl transferase reaction (Wilson, 2009). Similarly, streptogramins of the A-type yield this blockage by interference with the ribosomal peptidyl (P)-site (Vannuffel and Cocito, 1996). Macrolides, ketolides, lincosamides, and

streptogramins of the B-type are described to block the ribosomal exit tunnel, which hinders mRNA translocation and destabilizes nascent peptide chains (Tenson et al., 2003). Current research implicates that the macrolide-dependent translation arrest is selective for nascent peptide chains of specific proteins and might be part of a peptide-based translation control (Vázquez-Laslop and Mankin, 2018). Of note, although rather known for introducing translation arrest, some 50S inhibitors like chloramphenicol, erythromycin, and lincomycin were also discussed to cause selective stop codon readthrough but no miscoding, thereby bypassing translation termination by incorporation of an amino acid (Thompson et al., 2004). Tetracyclines or aminoglycosides target the 30S subunit of the ribosome. While tetracyclines prevent the attachment of aminoacyl-transfer RNAs (tRNA) to the ribosomal A-site (Chopra et al., 1992), aminoglycosides interfere with protein synthesis by alteration of the A-site conformation, thereby leading to the unspecific incorporation of aminoacyl-tRNAs (Krause et al., 2016). The resulting mistranslated peptides are in most cases non-functional and are thought to introduce cell membrane damage (Davis et al., 1986). Further targets of antibiotic translation inhibition are aminoacyl-tRNA synthetases, which catalyze the loading of amino acids to their cognate tRNAs. Mupirocin (pseudomonic acid) blocks the function of the isoleucyl-tRNA synthetase by competitive binding with isoleucine, thereby depleting the isoleucine-charged tRNA levels (Khoshnood et al., 2019). Thiostrepton and fusidic acid both interfere with GTP-dependent translocation of the ribosome along the mRNA by inhibition of the elongation factor (EF)-G (Walter et al., 2011; Borg et al., 2015). Elfamycins were shown to inhibit the function of another bacterial translational GTPase, the EF-thermo unstable (TU), which is responsible for the aminoacyl-tRNA loading to the ribosomal A-site (Prezioso et al., 2017). A different kind of protein synthesis impairment is introduced by puromycin, which leads to premature termination of translation and the intracellular accumulation of short peptide chains. Puromycin resembles a tyrosyl-tRNA structure but can be incorporated for every amino acid into the growing peptide chain, precluding further extension (Aviner, 2020).

1.3.4. Impairment of the cell envelope integrity

The cell envelope is targeted by antibiotic interference with cell wall biosynthesis or the permeabilization of the cytoplasmic and/or outer membrane. While the cell wall shapes the bacterial cell and provides the essential rigidity, its biosynthesis is a highly dynamic process that allows for stable growth and cell division, thereby recycling peptidoglycan (PG) components (Johnson et al., 2013). Amino acid analogs like D-cycloserine or fosfomycin target the cytoplasmic production of the PG building block, uridine diphosphate-N-

acetylmuramyl pentapeptide (UDP-MurNAc-pp) by interference with the alanine (Ala) racemase and the D-Ala-D-Ala ligase or the inhibition of the UDP-N-acetylglucosamine 1-carboxyvinyltransferase MurA, respectively (Neuhaus and Lynch, 1964; Lambert and Neuhaus, 1972; Silver, 2017). Membrane-associated steps of cell wall biosynthesis are inhibited by uridyl peptide antibiotics like tunicamycin, which hamper MraY function and thereby the formation of lipid-I, or by ramoplanin, which was proposed to interfere with lipid-II formation via inhibition of MurG and FemXAB aside from its primary MOA by preventing lipid-II from being transglycosylated (compare below) (Brandish et al., 1996; Schneider and Sahl, 2010). In the periplasm glycopeptides, like vancomycin, teicoplanin, or balhimycin, can bind to the D-Ala-D-Ala terminus of the flipped lipid-II pentapeptide and sterically block transglycosylation and transpeptidation (Reynolds, 1989; Schäberle et al., 2011; Zeng et al., 2016), while lantibiotics or ramoplanin tackle the carbohydrate pyrophosphate moiety of lipid-II, either blocking incorporation into the PG layer (mersacidin-like lantibiotics or ramoplanin) or triggering the formation of a defined membrane pore (nisin-like lantibiotics) (Brötz et al., 1998; Cudic et al., 2002; Schneider and Sahl, 2010). Bacitracin blocks the bactoprenol-mediated precursor recycling by extracellular, zinc-dependent complex formation with undecaprenyl pyrophosphate, which upon complexation is unable be dephosphorylated and flipped back into the cytosolic compartment (Schneider and Sahl, 2010; Economou et al., 2013). The most important and also diverse class of antibiotics is comprised by ß-lactam antibiotics. Penicillins, cephalosporins, carbapenems, or monobactams irreversibly bind and inactivate the D-D-transpeptidase and D-D-carboxypeptidase activity of penicillin-binding proteins, by mimicking their substrate, the D-Ala-D-Ala terminus of the PG disaccharide pentapeptide monomer (Schneider and Sahl, 2010).

While the cell wall is the stabilizing component, membranes form selective barriers, which allow for controlled uptake and efflux of different molecules. Some compounds show interaction with specific bacterial lipid components, like the clinically important antibiotic daptomycin. Although the MOA is still not fully elucidated, it could be shown that upon complexation with calcium (Ca^{2+}), daptomycin specifically binds to the anionic phospholipid phosphatidylglycerol and is able to form tripartite complexes with undecaprenyl-coupled cell envelope precursors, thereby impairing cell wall biosynthesis and leading to massive membrane rearrangements (Müller et al., 2016; Grein et al., 2020). Ca^{2+}-daptomycin binding to phosphatidylglycerol was further discussed to lead to the formation of a pore-like complex, that causes dissipation of the cellular membrane potential (Grein et al., 2020; Straus and Hancock, 2006). Ionophores can modulate the membranes' ion permeability by acting as

ion carriers or by building ion channels. They often possess antimicrobial activity provoking a disturbed intra- and extracellular ion equilibrium, an altered electrochemical gradient, and/or a lower proton motive force, which hampers ATP production (Gale et al., 1981; Kevin II et al., 2009). Membrane-targeting cationic antimicrobial peptides (cAMP) use the negative charge on the outer leaflet of the bacterial membrane, containing negatively charged phospholipids (e.g., phosphatidylglycerol or cardiolipin), lipoteichoic acids (cytoplasmic membrane of Gram-positive bacteria) or lipopolysaccharides (outer membrane of Gram-negative bacteria), to establish strong electrostatic membrane interactions and accumulate at its surface. Currently, different models of cAMP membrane impairment are discussed, including pore formation, unfavorable effects on the membrane integrity, and detergent-like membrane destabilization (Kumar et al., 2018), while the MOA might be dependent on the steric and physiochemical properties of each agent. Compounds that specifically permeabilize the outer membrane are of special interest for combinational therapy as they might allow target engagement of effective antimicrobial substances, which normally cannot overcome the outer membrane barrier (Field et al., 2016; Choi and Lee, 2019; Li et al., 2021). Polymyxins (polymyxin B or colistin) were described to disrupt the outer and to some extent the inner membrane, thereby mainly targeting Gram-negative bacteria. However, their killing mechanism is not merely outer membrane-related and remains to be resolved (Trimble et al., 2016).

1.3.5. Further modes of action

Another way of tackling the bacterial metabolism is to unbalance the level of newly synthesized proteins as shown by acyldepsipeptides (ADEPs) (Brötz-Oesterhelt et al., 2005). ADEPs act by a dual MOA on the Clp protease: they compete with binding of the ATPase-component to the ClpP proteolytic core, thereby impairing its native function in proteolysis and additionally deregulate its function by initiating an unspecific degradation of nascent polypeptides, less structured proteins (Kirstein et al., 2009), and the essential cell division protein FtsZ (Silber et al., 2020; Sass et al., 2011). Antibiotics like cerulenin or triclosan affect bacterial cell viability by impairing *de novo* fatty acid synthesis. In *Escherichia coli* cerulenin hampers the function of the enzymes FabH and FabB, while triclosan inhibits FabI (Heath et al., 1999; Heath and Rock, 2004). Of note, cerulenin was also shown to inhibit eukaryotic sterol and fatty acid synthesis (Funabashi et al., 1989; Nomura et al., 1972).

In principle, every bacterial cell structure or metabolism could be targeted by an interfering molecule, but microbial growth inhibition or cell lysis depend on the targets indispensable

function in the bacterial cell combined with the lack of a timely cellular adaptation process. Indispensability of a target is discussed to enhance the evolutionary selection pressure for bacterial adaption and the development and spread of resistance, i.e., by target mutation, enzymatic inactivation, or efflux mechanisms (Rasko and Sperandio, 2010). With the rise of antibiotic resistance, there is a constant need for new antimicrobial agents. Therefore current research is following two leads: on the one hand, screening for antimicrobials that tackle essential pathways either by showing new binding properties on well described targets (Basarab et al., 2015b), interference with new targets in well described metabolic pathways (van Eijk et al., 2017), or by hindrance of new biosynthetic pathways (Mak et al., 2012; Sass and Brötz-Oesterhelt, 2013; McVey et al., 2020). On the other hand, identification of resistance breaking compounds or anti-virulence agents, which counteract bacterial biofilm formation, toxin production or interfere with bacterial quorum sensing and therefore reduce bacterial pathogenicity (Rasko and Sperandio, 2010; Martínez et al., 2019). As most virulence factors are non-essential for bacterial survival they are proposed to be less prone to rapid antibiotic resistance development (Rasko and Sperandio, 2010). Furthermore, those anti-virulence compounds could also be used in combinational treatment with applied antibiotics (Rezzoagli et al., 2020). The applicability of antibacterial agents in human therapy is very often limited by the agents' selectivity in counteracting bacterial survival, while leaving eukaryotic cells (mostly) unaffected. Hence, antibiotic target structures and MOA that are specific for bacteria, constitute the preferred basis for new drug candidates. However, preceding human application all promising agents have to undergo detailed investigation to fully exclude toxic side effects, e.g., by alternative (eukaryotic) targets or secondary effects. Especially in the search for new, resistance breaking antibiotics it is difficult to maintain the high standards of currently applied antibiotics (Rolain and Baquero, 2016). Of note, antibacterial agents that show high cytotoxicity are often further investigated and developed for their application in anticancer chemotherapy (compare DNA-binding agents in chapter 1.3.1.) (Phillips et al., 2000; Yun et al., 2019).

1.4. *Bacillus subtilis* and its transcriptional gene regulation mechanisms

B. subtilis is a rod-shaped, Gram-positive bacterium, that is classified into the phylum of Firmicutes (Piggot, 2009). The non-pathogenic strain is commonly found in soil, where it is able to survive under facultative anaerobic conditions (Nakano and Zuber, 1998). Its low GC content genome contains approximately 4.2 Mbp, which include ~4100 coding regions (Kunst et al., 1997). *B. subtilis* is capable of quorum sensing (Kalamara et al., 2018), biofilm formation (Arnaouteli et al., 2021), cannibalism (González-Pastor, 2011), or natural

competence development, the latter allowing rapid adaptation by internalization of exogenous DNA (Piggot, 2009; Brito et al., 2018). Furthermore, in order to survive under extreme stress conditions, it is able to form heat resistant, dormant endospores (Errington, 2003). In recent years, in addition to research on the elucidation of the mentioned survival strategies or the general lifestyle of *B. subtilis*, a rich selection of genomic (Kunst et al., 1997; Zhang et al., 2016), transcriptomic (Hutter et al., 2004; Freiberg et al., 2006; Nicolas et al., 2012), and proteomic (Bandow et al., 2003; Ravikumar et al., 2018) data sets became available, making *B. subtilis* the best studied Gram-positive model organism. The extensive characterization of *B. subtilis* allows a more detailed picture of the different bacterial gene regulation mechanisms.

Generally, gene regulation is one of the most important cellular processes as bacterial survival is dependent on a tightly regulated, but yet quickly adaptable gene expression, which limits needless consumption of energy and other resources and sustains the fitness by allowing rapid adaptation to changing environments or different growth conditions.

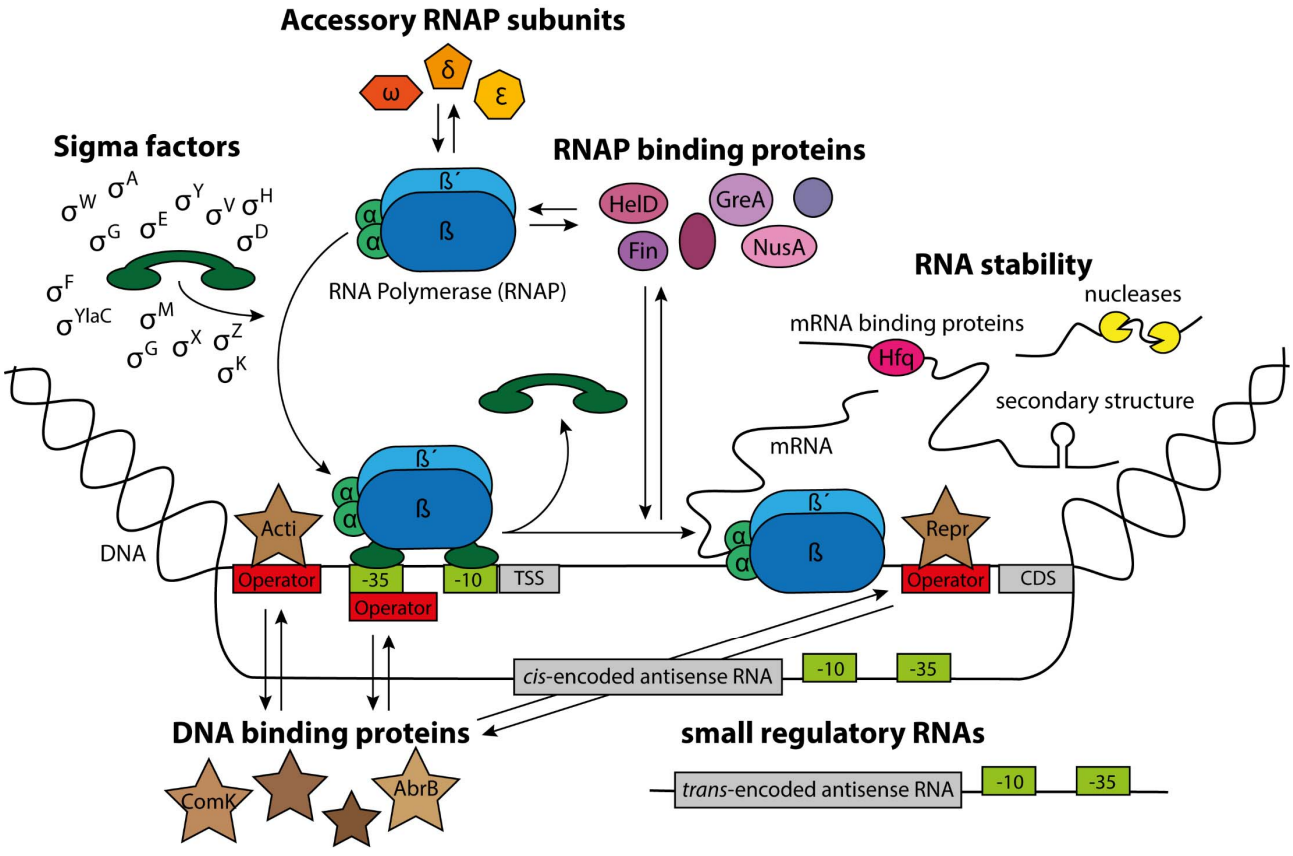

Figure 3. Schematic overview of the main transcriptional and post-transcriptional regulation processes in *B. subtilis*. The upper DNA strand depicts an exemplary promoter region, that precedes the coding region (CDS) of a transcribed gene. After formation of the RNAP holoenzyme (sigma factor bound to the core RNAP), the sigma factor enables selective binding of the transcription complex to the respective sigma factor binding site indicated by its characteristic -10 and -35 binding region. After successful transcription initiation, the sigma factor dissociates from the complex and transcription starts at the transcriptional start site (TSS). DNA-binding proteins shown in the graph are activators (Acti) and repressors (Repr). The regulatory mechanisms depicted are further described in detail in the following sections.

This chapter will mainly focus on transcriptional regulation including some post-transcriptional regulatory mechanisms (Figure 3), which represent, aside from translational regulation or proteolytic mechanisms, only one dimension of the overall regulation of *B. subtilis* metabolism.

1.4.1. *B. subtilis* sigma factors

RNA synthesis is initiated upon sigma (σ) factor binding to the core RNAP, while the σ factor recruits the RNAP to the respective promoter region, allows for promoter melting and initiates strand separation (Huang et al., 1997; Du Toit, 2014). The best-investigated Gram-positive model bacterium *B. subtilis* possesses the essential primary σ factor SigA (σ^A), which regulates the transcription of housekeeping genes, and additionally at least 17 alternative σ factors, which determine promoter selectivity (Helmann and Moran, 2001; Ayala et al., 2020). Alternative σ factors compete with SigA for RNAP binding and promote a selective transcription of their respective growth phase-dependent or stress-responsive regulons. This alternative transcription is regulated via the modulation of the intracellular concentration of different σ factors, their activity and also availability, i.e., titrated by anti-σ factors, anti-anti-σ factors, or other transcriptional regulators (Ayala et al., 2020). The general stress σ factor SigB is the most prominent representative of the alternative σ factors. It is stimulated upon a variety of stress (e.g., heat, salt, or ethanol stress) and starvation stimuli (e.g., phosphate or glucose limitation) and regulates the expression of approximately 150 genes, some of which are involved in cellular stress adaptations or virulence (Hecker et al., 2007). SigD was shown to regulate genes involved in flagellar assembly, motility, chemotaxis, and the expression of the major vegetative autolysins, thereby determining heterogenic subpopulations of sessile and motile *B. subtilis* cells, which might be advantageous to colonize both, the current location, while motile cells are able to expand into potentially favorable niches (Helmann and Moran, 2001; Mukherjee and Kearns, 2014). *B. subtilis* endospore formation represents the last resort in physiological adaptation to environmental and nutritional stress. SigH can contribute to the initiation of endospore formation, as it was shown to control the expression of several genes encoding for sporulation proteins, i.e., the phosphorelay response regulator Spo0A, which is the key regulator of sporulation, Spo0F, KinA, as well as the transcription of the *spoIIA* operon, containing the forespore-specific early σ factor SigF, its anti-σ factor SpoIIAB, and its anti-anti-σ factor SpoIIAA (Britton et al., 2002; de Hoon et al., 2010). Besides influencing sporulation initiation, SigH was further described to play a role in natural competence and controls various physiological processes during transition to stationary phase (Britton et al.,

2002). After sporulation initiation, the process of endospore formation is spatially and temporally regulated by various σ and transcription factors, but nevertheless they are highly interlinked (de Hoon et al., 2010). In the forespore, early gene expression is driven by SigF, followed by SigG-regulated finalization of the forespore formation. In the mother cell, the transcription of early sporulation genes is controlled by SigE, before the SigG-regulated SigK-dependent expression of 150 late mother cell-specific genes kicks in (de Hoon et al., 2010; Higgins and Dworkin, 2012). *B. subtilis* also possesses seven extracytoplasmic function (ECF) σ factors, which are in most cases co-transcribed in an operon together with their specific anti-σ factor. Upon the respective cell envelope stress signal, the membrane-localized anti-σ factor is inactivated, which allows the initiation of the ECF σ factors' transcriptional stress response (Helmann, 2016). While SigY, SigZ, and YlaC are still poorly characterized, SigM, SigW, SigX, and SigV were shown to be activated in response to cell envelope stress and control cell surface-related functions (Helmann and Moran, 2001; Gaballa et al., 2017). Although partly overlapping in their promoter recognition sites, induction by SigM, SigW, SigX, and SigV could be assigned to different regulatory stress responses. SigM induction was detected upon impairment of cell wall biosynthesis, heat shock, osmotic, acid or superoxide stress and correlated with adaptive expression of resistance proteins, detoxification enzymes, and genes important for cell division and maintenance of PG integrity (Eiamphungporn and Helmann, 2008). The ECF σ factor SigW responds to alkaline stress, membrane active detergents, and different cell envelope targeting antibiotics like vancomycin or nisin. SigW was shown to be involved in the adaptive expression of different detoxification enzymes and resistance mechanisms that e.g., alter the membrane composition or contribute to lantibiotic resistance or fosfomycin inactivation (Helmann, 2016). Stimulatory stress signals affecting SigX-dependent regulation partially overlap with the ones described for SigM and SigW. SigX initiates the expression of genes known to introduce membrane modifications that decreases the negative net charge of the outer leaflet of the bacterial membrane, thereby potentially protecting the cell from cAMP inhibitory action (Helmann and Moran, 2001). Furthermore, SigX seems to play a role in biofilm architecture, septum formation and cell wall biosynthesis (Souza et al., 2014). SigV is specifically induced upon lysozyme treatment, while it is located and expressed in the same operon with OatA, a PG O-acetyltransferase which is interestingly connected with lysozyme resistance (Souza et al., 2014; Helmann, 2016).

1.4.2. Accessory RNAP subunits and RNAP-binding proteins

Accessory RNAP subunits or RNAP-binding proteins can also modify the transcription process by alteration of RNAP activity, selectivity, or DNA-binding capacity. While the α (RpoA), β (RpoB), and β' (RpoC) RNAP subunits are essential, the δ (RpoE), ε (RpoY), and ω (RpoZ) subunits are dispensable (at least under laboratory conditions) and therefore considered accessory subunits (Weiss and Shaw, 2015). RpoY and RpoZ are poorly characterized in Gram-positive bacteria. The RpoZ subunit was shown to co-purify with the essential RNAP subunits (α, β, β′) in a 2:1:1:1 ratio ($\alpha_2\beta\beta'\omega$) during exponential and stationary growth in *B. subtilis*, whereas RNAP subunit stoichiometry was not altered during sporulation, or following stress conditions (Nicolas et al., 2012; Weiss and Shaw, 2015). Recent studies in *S. aureus* revealed that RpoZ might possess a chaperone-like function, which supports folding and subsequent association of the RpoC subunit with the residual RNAP subunits. Interestingly, a deletion of RpoZ is connected with RNAP complex instability and the increased binding of alternative σ factors, indicating a stress adaptation mechanism (Weiss et al., 2016). The RpoE subunit modifies transcription in several ways. It initiates preferred transcription of strong promoters by destabilizing DNA-RNAP interactions during open promoter complex formation and was shown to be important for bacterial general fitness, adaptation to environmental stress conditions, and virulence development (Weiss and Shaw, 2015). Furthermore, it overall enhances transcriptional activity as well as RNAP recycling, two processes which are further boosted by its synergistic action with the RNAP-binding protein HelD (Wiedermannová et al., 2014; Pei et al., 2020).

The elongation factors NusA associates with the progressing RNAP complex after dissociation of the σ factor and was shown to be involved in RNAP pausing and intrinsic transcription termination (Yakhnin and Babitzke, 2002; Mondal et al., 2016). The elongation factors NusB and NusG are also capable of RNAP binding (Doherty et al., 2006). While in *B. subtilis* their exact functions remain elusive, they both seem to play a role in transcription termination, with NusG also affecting RNAP pausing and translocation (Yakhnin and Babitzke, 2002; Doherty et al., 2006). A further example for the modification potential of RNAP-binding proteins is the enzyme Fin, which was described to modulate transcription by competing with SigF for the same RpoC-binding site, thereby inhibiting SigF regulation and initiating the transition to a SigG-mediated late forespore regulation (Wang Erickson et al., 2017).

1.4.3. DNA-binding transcription factors

Another way of regulating gene expression is facilitated by DNA-binding transcription factors (TFs), which can influence RNAP promoter-binding as well as RNA synthesis progression. DNA-binding is most commonly associated with a TFs helix-turn-helix (HTH) motif, which allows them to specifically bind a respective DNA operator motif (Brennan and Matthews, 1989). After association with the respective operator site, activators stimulate transcription by supporting RNAP recruitment to suboptimal promoter sequences or by structural remodeling of the promoter site. In contrast, repressors negatively modulate gene expression by steric hindrance of RNAP-binding and -progression, alterations of the local DNA structure and its accessibility, or counteraction of the positive regulation by another TF (Bervoets and Charlier, 2019). In *B. subtilis*, TF-dependent regulation is mostly implemented by repressors, which are described to constitute the majority of DNA-binding TFs in this organism. Furthermore, many, often global, regulatory TFs can act as both, repressor and activator (Moreno-Campuzano et al., 2006). Known examples in *B. subtilis* are the ambiactive TF ComK, the key regulator of competence development (Susanna et al., 2006) or the transition state regulator AbrB, which coordinates adaptive, post-exponential gene expression (Hoch, 2017). The majority of two-component systems also utilizes this way of gene regulation to adapt to changing environmental conditions. While the membrane-bound histidine kinases are capable of sensing extracellular stimuli and mediate the activation of intracellular response regulators, the response regulators often constitute TFs, which are able to initiate cellular adjustments by modulating an adaptive gene expression (Fabret et al., 1999). Of note, many promoter regions also possess several repressors and/or activator binding sites that allow for the integration of various modulatory signals and a more interlinked and fine-tuned transcriptional response. The activity or DNA binding capacity of TFs is either regulated by their intracellular abundance, influenced by binding of small effector molecules to allosteric sites of some TFs, or by chemical modification (e.g., phosphorylation) (Bervoets and Charlier, 2019).

1.4.4. Regulatory small RNAs and RNA stability

Gene regulation complexity is yet further multiplied by a group of regulatory small RNAs (sRNA), the so-called antisense RNAs (asRNA). Their RNA-RNA regulation can be classified into *cis* or *trans* acting, meaning that asRNAs are encoded complementary to their target RNA in the same loci or are located and produced at a different position in the chromosome, respectively. While *cis*-encoded asRNAs display perfect complementary sequence homology, *trans*-acting asRNAs only possess limited complementarity with their

targeted mRNA and therefore often depend on RNA-binding chaperones like Hfq (Oliva et al., 2015). Upon target-binding, asRNAs can alter mRNA stability, promote degradation, modify regulator accessibility, or regulate translation of the respective mRNA (Oliva et al., 2015; Ul Haq et al., 2020). *Cis*-encoded regulatory elements are further discussed to directly interfere with transcription of the complementary target RNA, e.g., by steric hindrance of the complementary occurring RNAP initiation and progression, which is a process that happens most likely in accordance with the respective asRNA regulation (Bordoy and Chatterjee, 2015).

Having outlined different mechanisms of direct modulation of the transcription process, an additional regulatory level of gene expression is represented by the intracellular stability of the respective transcription products. The mRNA half-lives in *B. subtilis* vary from approximately 1 min to more than 15 min, which largely influences the intracellular levels of mRNA available for subsequent translation (Hambraeus et al., 2003). Generally, mRNA stability is influenced by its secondary structure, the RNA degradosome, including different endo- and exonucleases, RNA-binding proteins, potential 5' or 3' untranslated regions (UTRs), sRNA interactions, or ribosome binding (Bechhofer and Dubnau, 1987; Dambach et al., 2013; Vargas-Blanco and Shell, 2020). It was shown for some bacteria, including *B. subtilis*, that upon various stress conditions the half-live of their transcriptome is altered, allowing a rapid, adaptive, and selective translation of genes important for cellular adaptation and survival (Vargas-Blanco and Shell, 2020).

1.5. Aims of this thesis

Natural product discovery was and remains the most promising source in the search for new antibiotics. One goal of this thesis was the development and validation of a rapid, robust, and selective antimicrobial screening tool on the basis of different *B. subtilis* bioreporter strains, that combines the activity-based agar diffusion approach, commonly used in antibacterial screening, with reliant MOA information. For this, promoter regions of different bioreporter genes, which had previously been shown to be selectively upregulated only upon treatment with antibiotics interfering with the same metabolic pathway (Mascher et al., 2004; Freiberg et al., 2006; Urban et al., 2007), were fused to a detectable reporter gene. Upon antibiotic exposure, the bioreporters should specifically and sensitively signal interference with the main metabolic pathways: DNA synthesis, RNA synthesis, protein biosynthesis and the maintenance of cell envelope integrity. After validation of the bioreporter assay using a large set of pure reference antibiotics with known MOA to ensure their MOA profiling capacity in this setup, the assay was meant to be utilized as an entry test

for MOA classification of uncharacterized antimicrobial substances, thereby allowing the selection of adequate follow-up studies to elucidate the exact molecular target structure. In this regard, a further aim was to utilize the bioreporter suite to acquire MOA information about the newly discovered antibacterial secondary metabolites microcionamide A and C, produced by the fungus *Clathria basilana*.

As most MOA profiling tools are dependent on more or less purified antimicrobial agents, the objective was to adapt the agar-based bioreporter approach for direct screening of antibiotic producer strains, with no need for any upfront extraction or purification procedure. This was to be followed by the investigation of a large set (~500) of partly uncharacterized actinomycetes strains of the Tübingen strain collection, with the aim to verify the MOA classification potential of the bioreporter approach in direct screening and to potentially identify new antimicrobial compounds.

Specific upregulation of the *B. subtilis* genes upon antibiotic treatment had been discovered in previously published transcriptome studies (Hutter et al., 2004; Freiberg et al., 2006). Although the genes were shown to be selectively induced upon antibiotic interference with a specific metabolic pathway, to date their function and regulation remains only partly characterized. Therefore, the further goal of this thesis was to elucidate the transcriptional regulation of the bioreporter genes *yorB*, *rpt,* and *helD* involved in signaling DNA and RNA stress, respectively, with particular focus on the new bioreporter gene *rpt*. The in-depth characterization of their gene regulation aimed for an improved understanding of the cellular adaptions initiated by *B. subtilis* in response to RNA and DNA stress signals and *vice versa*, to better profile the MOA of antibiotics, causing *B. subtilis* to initiate a stress response that leads to the selective induction of those bioreporter genes. This investigation was especially interesting, as my bioreporter results indicated that the promoters P_{rpt} and P_{helD} are induced similarly in response to different RNA synthesis inhibiting antibiotics, pointing at a potentially similar way of regulating *rpt* and *helD* gene expression in *B. subtilis*. To date, Rpt (formerly PpS/YppS) has not been characterized in *B. subtilis*. Therefore, an additional objective of this thesis was the elucidation of its function, in order to understand the potential benefit for the *B. subtilis* cell to strongly upregulate *rpt* expression in response to RNA stress.

2. SUMMARY OF RESULTS

2.1. The agar-based bioreporter approach

2.1.1. Validation of sensitivity and induction specificity

B. subtilis was chosen as model organism, due to the rich selection of different data sets characterizing its transcriptomic, proteomic, or phenotypical stress response upon exposure to different antibiotics (Bandow et al., 2003; Freiberg et al., 2006; Nonejuie et al., 2016). Furthermore, the Gram-positive organism is highly susceptible to most antibiotics, allowing a bioreporter-based MOA profiling for the majority of antimicrobial agents, while the antibiotic MOA information is often directly transferable to pathogenic species. For bioreporter construction, the promoters of the *B. subtilis* genes *yorB*, *ypuA*, *liaI (yvqI)*, *bmrC* (*yheI*), and *helD* (*yvgS*), which had previously been described to be specifically upregulated upon antibiotic stress (Hutter et al., 2004; Freiberg et al., 2006; Urban et al., 2007; Mascher et al., 2004; Wenzel et al., 2014), were individually fused during this thesis project to the ß-galactosidase gene *lacZ* and genomically integrated into the *amyE* locus of the sporulation deficient strain *B. subtilis* 1S34 (Piggot, 1973). After the construction of the five different *B. subtilis* bioreporter strains, indicative of DNA stress (P_{yorB}-*lacZ*), RNA stress (P_{helD}-*lacZ*), translation arrest (P_{bmrC}-*lacZ*) or impairment of cell envelope integrity (P_{ypuA}-*lacZ* and P_{liaI}-*lacZ*) and the subsequent optimizations of the agar-based bioreporter approach in regard to maximal induction sensitivity, each bioreporter was validated for MOA specificity using a subset of 90 pure reference antibiotics with well characterized MOA. Of note, bioreporter-based MOA profiling results were obtained rapidly, after overnight incubation. It could be proven that in the agar-based bioreporter approach P_{yorB}-*lacZ*, P_{bmrC}-*lacZ*, P_{ypuA}-*lacZ,* and P_{liaI}-*lacZ* sensitively and specifically detect antibiotics interfering with their respective biosynthetic pathway (Figure 1 and Table S1, Publication 1). P_{helD}-*lacZ* showed specific, but only weak induction signals upon treatment with RNA synthesis inhibitors in the agar-based bioreporter approach (Figure S1, Publication 1), which did not meet our goal of robust and sensitive MOA detection in this screening setup. After re-analyzing previous microarray data (Freiberg et al., 2006) we identified the *B. subtilis* gene *rpt* (formerly *ppS*/*yppS*; the new annotation is based on our elucidation of its function as rifampin phosphotransferase in chapter 2.2.2), which showed massive upregulation after treatment with the RNAP inhibitors corallopyronin and rifampin. And indeed, the alternative RNA stress bioreporter P_{rpt}-*lacZ* displayed strong and selective induction solely by RNA stress inducing compounds in the agar-based bioreporter setup (Figure S1 and Table S1, Publication 1). For example, P_{rpt}-*lacZ* showed selective induction of all RNAP inhibiting compounds,

including rifamycins, streptovaricin, corallopyronin A, fidaxomicin, sorangicin A, or streptolydigin, and intercalating agents that are described to inhibit RNA synthesis (e.g., actinomycin D and echinomycin). For signaling cell envelope stress, two different bioreporters were employed to better characterize antimicrobial MOA interfering with this pathway. P_{ypuA}-*lacZ* responded more broadly to the disturbance of cell wall biosynthesis or cell membrane integrity, while induction of P_{lial}-*lacZ* seemed to signal stress upon interference with membrane-associated steps of the undecaprenyl precursors (e.g., lipid-II) cycling, necessary for cell wall biosynthesis. P_{yorB}-*lacZ* inducing compounds like quinolones, doxorubicin, mitomycin C, or phleomycin all showed an additional weak signal for P_{ypuA}-*lacZ*, which was not detected in a luciferase-based liquid system (Urban et al., 2007) and might hint at the sensitive detection of secondary effects in the agar-based setup due to bioreporter overnight incubation (Table S1, Publication 1). None of the five reporter strains were induced upon treatment with ionophores (e.g., nigericin), fatty acid synthesis inhibitors (e.g., triclosan), protein synthesis inhibitors that act by miscoding (e.g., kanamycin), by impairment of aminoacyl-tRNA synthesis (e.g., mupirocin), or by antimicrobial agents causing protein stress (e.g., diamide) (Table S1, Publication 1).

Generally, the agar-based bioreporter assay is bioactivity-dependent, as the induction signal forms at the borders of the zone of inhibition (ZOI), where the antibiotic concentration is appropriate to cause a cellular stress response that leads to selective induction of the bioreporter genes. All bioreporters sensitively responded to interference with their respective pathways even upon treatment with low antibiotic concentrations, with the bioreporters P_{yorB}-*lacZ* and P_{rpt}-*lacZ* sensing subinhibitory antibiotic concentrations (induction was visible without detection of ZOI) of ciprofloxacin (0.01-0.025 µg) or fidaxomicin (0.01-0.05 µg), respectively (Figure S2, Publication 1).

2.1.2. MOA profiling of microcionamide A and C

Having evaluated the specificity and sensitivity of the agar-based bioreporter approach, the tool was applicable for MOA profiling of uncharacterized compounds. Our collaboration partners in Düsseldorf provided us with the pure substances microcionamide A and C, that showed strong cytotoxic activity against different tumor cell lines (A-2780, Ramos, Jurkat J16, Nomo-1, HL-60) ranging from 2.6-28 µM for microcionamide A and 0.45-1.9 µM for microcionamide C (Table 5, Publication 2). While both compounds were shown to induce apoptotic cell death in human lymphoma and leukemia cell lines (Figure 3, Publication 2), only microcionamide C appeared to interfere with autophagic processes under starvation conditions in embryonic fibroblasts (Figure 4, Publication 2). The compounds showed no

activity up to 100 µM against *Mycobacterium tuberculosis* as well as Gram-negative pathogens, like *Enterobacter aerogenes*, *Klebsiella pneumoniae*, *Acinetobacter baumannii, Pseudomonas aeruginosa*, and *E. coli*. The minimal inhibitory concentration (MIC) for *S. aureus* and *E. faecium* were determined to correspond to 6.3 µM (microcionamide A and C) and 12.5 µM (microcionamide A and C), respectively (MIC experiments were conducted by Jan Straetener and Dr. Anne Berscheid with the exception of *M. tuberculosis*, which was tested by our collaboration partners in Düsseldorf) (Table S10-2, Publication 2). The agar-based bioreporter approach was applied as an entry test to elucidate the overall metabolic pathway of interference. Bioreporter-based MOA profiling revealed a selective induction of P_{ypuA}-*lacZ* and P_{lial}-*lacZ* for both compounds, hinting at membrane-associated disturbance of the undecaprenyl precursors cycling (Figure 5, Publication 2). Based on those results adequate follow-up studies were selected to further confirm the proposed MOA. Jan Straetener and Dr. Anne Berscheid conducted a membrane potential assay in *S. aureus* NCTC8325 that strongly indicated dissipation of the membrane potential already at low antibiotic concentrations below the MIC (0.2 µM for microcionamide A, 0.8 µM for microcionamide C) (Figure 6, Publication 2).

2.1.3. Direct screening of antibiotic producer strains

A further aim of this thesis was to establish the agar-based bioreporter approach in direct screening of antibiotic producer strains to gain additional, reliant MOA information on the produced antimicrobials, with no need for initial and laborious compound purification. The setup was validated using six well-characterized actinomycetes producer strains, that were known to produce the natural products rifamycin B (*Amycolatopsis mediterranei* NBRC 14843), porfiromycin (a mitomycin C derivate) (*Streptomyces ardus* NBRC 13490), novobiocin (*Streptomyces niveus* NBRC 12917), erythromycin (*Saccharopolyspora erythraea* NBRC 13426), chloramphenicol (*Streptomyces venezuelae* NBRC 13096), or ADEP (*Streptomyces hawaiiensis* NRRL 15010). Each producer strain was individually cultivated for several days on solid media for optimal antibiotic production. After cultivation, agar plugs of each producer strain were sampled, embedded in the bioreporter-strain containing agar and incubated overnight. After incubation, all bioreporter strains showed the expected induction pattern, with the bioreporter signal matching the MOA of the produced antibiotic (Figure 2, Publication 1).

In a subsequent screening approach of uncharacterized producer strains, approximately 500 actinomycetes strains of the Tübingen strain collection were evaluated in the direct agar-based bioreporter approach. Producer strains were cultivated on at least two different

solid media and initially tested for *B. subtilis* 1S34 activity, with 240 of them lacking activity. Of note, 280 of the 500 actinomycetes strains were additionally tested against *E. coli* ATCC25922 to evaluate their Gram-negative bioactivity and to check for Gram-negative-only activities, which would hint at an outer membrane target that is not covered by our Gram-positive *B. subtilis* bioreporter strains. Of the 280 samples, 38 showed bioactivity against both, *B. subtilis* 1S34 and *E. coli* ATCC25922, while no bioactivity could be detected that was selectively present only for *E. coli* ATCC25922 (Data S1, Publication 1). The remaining 270 *B. subtilis*-bioactive actinomycetes were analyzed in the agar-based bioreporter approach against the full bioreporter panel. For 94 actinomycetes samples we could detect at least one reliable bioreporter signal. Of note, after incubation, some actinomycetes agar plugs showed blue coloration themselves. If this coloration was visible for all five bioreporters, we classified the signal as unspecific, and attributed it to the actinomycetes' potential to produce an inherent ß-galactosidase. For some agar plugs such unspecificity could be excluded, yet they yielded an induction of more than one bioreporter, either hinting at the production of multiple antimicrobial compounds, or implicating a dual MOA of a single antimicrobial agent. In order to validate the obtained MOA information and to check for potentially new antimicrobial activities, an extended subset of the bioreporter inducing actinomycetes as well as few non-inducing activities were further investigated to identify the produced bioactive compounds. Extraction of one Petri dish of the grown producer strain (the same that was initially used for the agar-based bioreporter screening) was in most cases more than sufficient for compound deconvolution via agar extraction, high-performance liquid chromatography-mass spectrometry (HPLC-MS) analysis, and/or HPLC-tandem MS (HPLC-MS-MS) analysis (purification and dereplication experiments were conducted by our collaboration partners mentioned in Publication 1). Notably, bioreporter application also allowed to monitor the whole purification procedure, by testing culture supernatants, extracts, fractionations, or pure substances for the initially observed induction pattern (Figure 3, Publication 1). In total, 28 compounds were dereplicated, that validated the reliability of the agar-based bioreporter approach but were not new to the scientific community (Table 1, Table S3, and Data S2, Publication 1). However, some of the antimicrobial agents, like telomycin, had not previously been described to be produced by the Tübingen strain collection. Generally, the bioreporter signals concurred with the described MOA of the 28 dereplicated antimicrobial agents in all cases. For instance, investigation of the strain Tü2108 yielded a selective induction of the translation arrest bioreporter (P_{bmrC}-*lacZ*), while dereplication uncovered the substance berninamycin. In the literature, berninamycin is described to bind to the ribosomal 50S subunit and inhibit protein

synthesis progression by hindering the incorporation of amino acids (Reusser, 1969), which perfectly suits the bioreporter profiling results. For strain Tü2641, impairment of cell envelope integrity (P_{ypuA}-*lacZ*) combined with the further indication of the inhibition of cell membrane-associated steps of undecaprenyl precursors cycling (P_{liaI}-*lacZ*) were signaled by the bioreporter panel. The following purification and dereplication procedure revealed the production of the cyclic depsipeptide antibiotic telomycin. Although the exact MOA of telomycin is not fully understood, it was shown to exhibit bactericidal activity upon binding to the membrane phospholipid cardiolipin (Johnston et al., 2016). The DNA stress bioreporter (P_{yorB}-*lacZ*) was shown to be induced by the cultivated producer strain Tü2471, which turned out to produce the DNA-binding agent chrysomycin A, that was shown to inhibit DNA synthesis (Wei et al., 1982). Substances dereplicated from non-inducing samples possessed MOA that were known not to be covered by the applied bioreporter panel (e.g., ionophores like monactin (TüG102), omomycin (TüG343), or boromycin (GöK12/9)) (Table S1, Publication 1), with some of them producing substances with up to date poorly characterized MOA. Strain Tü2401 produced two different substances, albomycin δ_1 and C-1027 under liquid or solid cultivation conditions, respectively. The additional information of the differential bioreporter signal for both unpurified samples (agar plug or culture supernatant) allowed an early discrimination of the diverse production pattern (Figure 4, Publication 1). Negative controls, like solvents, commonly purified bioactive metabolites from actinomycetes, or media components, were also tested for antimicrobial activity and bioreporter induction, but were shown not to interfere with the agar-based bioreporter setup (Table S2, Publication 1).

2.1.4. Further applications in polypharmacology and synergism

For the producer strain GöK16/4 a triple induction of P_{yorB}-*lacZ*, P_{rpt}-*lacZ*, *and* P_{bmrC}-*lacZ* was detected. What was initially hinting at the production of multiple antimicrobials could be traced back to the single compound chartreusin (Table S3 and Data S2, Publication 1). Testing the pure substance against the different bioreporters confirmed the induction pattern seen for the producer strain and indicated interference with multiple bacterial targets by the single compound chartreusin (Figure 5A, Publication 1). Detection of polypharmacology was further validated by the investigation of the recently published antimicrobial substance SCH-79797, which was described to possess a dual MOA interfering with folate metabolism and bacterial membrane integrity (Martin et al., 2020). The agar-based bioreporter approach reliably confirmed this dual MOA profile, with SCH-79797 inducing both cell envelope stress

bioreporters (P_{ypuA}-*lacZ* and P_{liaI}-*lacZ*) in combination with the DNA stress bioreporter (P_{yorB}-*lacZ*) (Figure 5B, Publication 1).

The bioreporter tool was also investigated for its application in detecting synergistic antibiotic effects. For this, we spotted trimethoprim next to a subinhibitory concentration of sulfamethoxazole on a P_{yorB}-*lacZ* containing agar plate. When gradually diminishing the spotting distance, an additional induction zone could be identified, that confirmed the synergistic effect of both substances to interfere with DNA synthesis (Figure 5C, Publication 1).

2.2. In-depth characterization of the *B. subtilis* genes *rpt* and *helD*

2.2.1. Induction of P_{rpt}, P_{helD} and P_{yorB} bioreporter constructs in response to RNA and DNA stress

RNA and DNA synthesis are two independent processes that are essential for bacterial growth, yet they both utilize the same DNA template and therefore need to be tightly coupled to guarantee unaffected performance of both metabolic pathways. Hence, we further analyzed the *B. subtilis* stress response upon treatment with antibiotics that target transcription and/or replication, focusing on the bioreporters P_{rpt}-*lacZ* and P_{helD}-*lacZ* signaling RNA stress and P_{yorB}-*lacZ* for the detection of DNA stress. In contrast to P_{helD}-*lacZ,* the P_{rpt}-*lacZ* construct was shown to additionally detect DNA-binding agents that interfere with RNA synthesis (Figure S1, Publication 1). Interestingly, P_{rpt}-*lacZ* covered intercalators like echinomycin or the minor groove binder netropsin, which did not induce stress sensed by our DNA stress reporter P_{yorB}-*lacZ.* Vice versa*,* intercalators like doxorubicin or the alkylating agent mitomycin C selectively signaled interference with DNA synthesis by the sole induction of the DNA stress bioreporter P_{yorB}-*lacZ*. Only few DNA-binding antibiotics, like chartreusin or gilvocarcin V, showed an induction of both, the RNA and DNA stress bioreporter (Figure 1 and Table S2, Manuscript 1).

In the agar-based setup, the induction strength of P_{helD}-*lacZ* was generally weaker in comparison to P_{rpt}-*lacZ* upon treatment with the different RNAP inhibitors (Figure S1, Publication 1 and Figure 1, Manuscript 1). We therefore hypothesized, that the induction upon treatment with DNA-binding agents seen for P_{rpt}-*lacZ* might be missed for P_{helD}-*lacZ* due to the generally lower induction signal, and that P_{rpt}-*lacZ* and P_{helD}-*lacZ* might actually be induced by a similar set of antibiotics via the same stress response. In order to most sensitively quantify the induction strength of both RNA synthesis bioreporters, the *Photorhabdus luminescens* luciferase-based bioreporters P_{rpt}-*luxABCDE* and P_{helD}-*luxABCDE* were constructed. For better comparison, both bioreporters were

investigated in Belitzky minimal medium (BMM) in order to monitor their expression under similar growth conditions. After 210 min, P_{rpt}-*luxABCDE and* P_{helD}-*luxABCDE* were selectively induced by RNA synthesis inhibitors (Figure 2 and Table S3, Manuscript 1), with comparable induction patterns for all antibiotics tested. RNA synthesis inhibitors again yielded higher induction fold changes for P_{rpt}-*luxABCDE* in comparison to the fold changes observed for P_{helD}-*luxABCDE* (Figure 2 and Table S3, Manuscript 1), thereby supporting our hypothesis that DNA-binding agents interfering with RNA synthesis might be missed in the agar-based setup due to the generally weaker induction strength of P_{helD}-*lacZ.* Nevertheless, the evaluation in a luciferase-based system sensitively detected that P_{rpt}-*luxABCDE* and P_{helD}-*luxABCDE* are strongly induced by the same RNAP-binding agents, but are also responsive to the same DNA-binding agents, thereby supporting the idea of a similar gene regulation mechanism.

2.2.2. Function of Rpt and HelD in response to RNA stress

Both bioreporter genes, *rpt* and *helD*, are selectively upregulated only upon treatment with RNA synthesis inhibitors. Hence, their role in conferring resistance to those strongly inducing substances was investigated. MICs of different antibiotics were determined for the different knockout mutants *B. subtilis* 168 Δ*rpt* and *B. subtilis* 168 Δ*helD.* For comparison, we used *B. subtilis* 168 Δ*amyE* as a reference strain to determine wildtype (WT) MIC levels. Of note, the *amyE* gene encodes for a non-essential α-amylase, that is frequently used as an integration target site in *B. subtilis* (Shimotsu and Henner, 1986; Härtl et al., 2001). As *amyE* inactivation did not have negative impact on growth in other (Juhas and Ajioka, 2016) and our experiments, we chose this deletion mutant as an unrelated control, as it had undergone the similar knockout procedure in comparison to the other knockout strains of interest. *B. subtilis* 168 Δ*rpt* showed a 16-32-fold, 4-8-fold, and 4-fold lower MIC for rifamycin SV, rifampin, and rifabutin, respectively, while all other tested RNA synthesis inhibitors matched WT MIC (Table 1, Manuscript 1). Prior to this work, the function of Rpt had not been determined in *B. subtilis*. Based on sequence homologies, *rpt* was either annotated as a phosphoenolpyruvate synthase, an enzyme important in gluconeogenesis (McCormick and Jakeman, 2015), or a rifampin phosphotransferase enzyme, which selectively inactivates rifamycins (Spanogiannopoulos et al., 2014). The results of the antibiotic susceptibility testing supported the idea of Rpt being a selective rifamycins inactivating phosphotransferase enzyme. To verify the effect of *rpt* deletion, the knockout mutant *B. subtilis* 168 Δ*rpt* was complemented using an integrative, isopropyl-β-D-thiogalactopyranoside (IPTG)-inducible S707-*rpt* construct (*B. subtilis* 168 Δ*rpt aprE*::P_{Spac}-

S707-*rpt*). Of note, S707 was described to be the 5' untranslated region (UTR) of the *rpt* gene (Nicolas et al., 2012). Upon IPTG induction, the rifampin MIC returned to WT level (Table S1, Manuscript 1).

Heterologous overexpression of *B. subtilis rpt* in *E. coli* XL1 blue (*E. coli* XL1 blue pBS2E-P_{Spac}-S707-*rpt*), which is naturally devoid of a Rpt enzyme homolog, led to high-level rifampin resistance (128-fold MIC increase) (Table S1, Manuscript 1). To confirm that *B. subtilis* Rpt is able to inactivate rifampin by phosphorylation, IPTG-induced cultures of *E. coli* XL1 blue pBS2E-P_{Spac} (Vector control, which is devoid of S707-*rpt*) and *E. coli* XL1 blue pBS2E-P_{Spac}-S707-*rpt* were grown for 24 h in the presence of 100 µg/mL rifampin. Culture supernatants were subsequently investigated via HPLC-MS analysis (all HPLC-MS experiments have been conducted by Andreas Kulik). While the mass of unmodified rifampin (*m/z* 821.3) was present in all samples, the mass of phosphorylated rifampin (*m/z* 901.3) was only detectable upon overexpression of *B. subtilis rpt,* proving the function of *B. subtilis* Rpt as rifampin phosphotransferase enzyme (Figure S1, Manuscript 1). On the basis of this function elucidation, we proposed the name *rpt* for *B. subtilis ppS*/*yppS* and Rpt for the corresponding protein. Of note, the name *rph* - in the style of the first discovered rifampin phosphotransferase found in actinomycetes called *rph* (Spanogiannopoulos et al., 2014) - was already taken in the *B. subtilis* gene annotation and thus no longer available.

HelD was previously described to bind to the RNAP and enhance transcriptional activity as well as the recovery of stalled RNAP (Wiedermannová et al., 2014; Newing et al., 2020; Pei et al., 2020). A deletion of *helD* did not influence the MIC values for most antibiotics tested, but the mutant showed a more sensitive phenotype upon treatment with the closely related antibiotics corallopyronin A (16-fold) and myxopyronin A (> 32-fold) (Table 1, Manuscript 1). A similar trend could be observed for *B. subtilis* 168 Δ*rpoE* (Table 1, Manuscript 1), which was also chosen for MIC determination on the basis of its described function to act cooperatively with HelD on transcriptional (re-)cycling (Wiedermannová et al., 2014; Pei et al., 2020).

2.2.3. Upregulation of *rpt* and *helD* in response to RNAP stalling

As indicated by the investigation of P_{rpt}-*lacZ* and P_{helD}-*lacZ* (Table S2, Manuscript 1), but also P_{rpt}-*luxABCDE* and P_{helD}-*luxABCDE* (Figure 2 and Table S3, Manuscript 1), both bioreporters respond to a panel of differently acting RNA synthesis inhibitors. Deduced from the MOA of those structurally diverse compounds, the mechanism of RNAP stalling was suspected to represent the common stress signal leading to selective *rpt* and *helD*

upregulation. To investigate this hypothesis, the background expression (luminescence signal of untreated cells grown in BMM after 210 min) of P_{rpt}-*luxABCDE* was monitored in different knockout mutants (Δ*helD*, Δ*rpoE*, Δ*mfd, and* Δ*uvrB)*, that are described to affect transcription in *B. subtilis*. For this, the plasmid pBS3Clux-P_{rpt}-*luxABCDE* was transferred into the respective naturally competent *B. subtilis* 168 deletion mutants, where the reporter construct P_{rpt}-*luxABCDE* was genomically integrated into the *sacA* locus. As reference strain we used the isogenic *B. subtilis 168* Δ*amyE. B. subtilis 168* Δ*perR* was chosen as negative control*,* which is devoid of the transcriptional repressor of peroxide stress (Giedroc, 2009) and should not have direct effects on *rpt* expression. Interestingly, *B. subtilis 168* Δ*helD* and *B. subtilis 168* Δ*rpoE* showed significantly enhanced P_{rpt}-*luxABCDE* background expression in comparison to *B. subtilis 168* Δ*amyE*, while all other knockout strains displayed values close to the reference background luminescence of *B. subtilis 168* Δ*amyE* (Figure 3, Manuscript 1).

2.2.4. Regulation of gene expression of *rpt* and *helD*

Transcriptional regulation was first investigated using different promoter deletion or promoter modification constructs. For *rpt* and *helD*, we could delete the upstream promoter region up to the previously proposed SigA-dependent promoter sites (constructs P_{rpt_123bp}-*lacZ* and P_{helD_120bp}-*lacZ*) (Nicolas et al., 2012), with no changes in the respective expression pattern (Figure 4, Manuscript 1). Upon deletion of the -35 region of the SigA binding sites, both constructs (P_{rpt_108bp}-*lacZ* and P_{helD_113bp}-*lacZ*) could not (or only very weakly) be induced upon RNA synthesis stress by e.g., rifampin or fidaxomicin anymore, which confirmed their dependency to be expressed by this housekeeping σ factor (Figure 4, Manuscript 1). Interestingly, both promoters natively possess a 102 bp (*helD*) or 110 bp (*rpt*) long 5'UTR (Figure S3B, Manuscript 1). An alignment of the promoter fragments P_{rpt_123bp} and P_{helD_120bp}, which both retained induction specificity, revealed a highly conserved 13 bp nucleotide motif at the downstream end of both promoter regions (Figure S4, Manuscript 1). In order to investigate the regulatory impact conferred by this region we deleted the last 14 bp (P_{rpt}) and the last 15 bp (P_{helD}) of their downstream promoter regions, including the conserved 13 nucleotides. The larger deletion of P_{helD} is due to one additional nucleotide that is present only in the P_{helD} 13 bp consensus sequence (compare Figure S4, Manuscript 1). Upon deletion of this motif, both constructs, $P_{rpt\_Del14bpDS}$-*lacZ* and $P_{helD\_Del15bpDS}$-*lacZ*, showed enhanced background expression and loss of induction specificity, indicating that this region is essential for the selective upregulation of *rpt* and *helD* due to transcriptional stress (Figure 4, Manuscript 1). To verify that this effect was not

solely due to the shortening of the respective 5'UTR, a *rpt* promoter construct was generated, that was randomly modified in 6 out of 13 of the conserved nucleotides, thereby keeping the length of the 5'UTR unchanged. Nevertheless, a modification of this region ($P_{rpt\_Modi14bpDS}$-*lacZ*) also led to a deregulated *rpt* expression (Figure 4A, Manuscript 1). The generation of a construct only containing the SigA binding site of P_{rpt} fused to the *lacZ* reporter ($P_{rpt\_onlySigA}$-*lacZ*) revealed that the observed deregulated *rpt* expression by deletion or modification of the conserved 13 bp nucleotide motif basically resembles a constitutive SigA-dependent expression, hinting at a repressive mechanism that controls induction specificity at the downstream end of the promoter (Figure 4A, Manuscript 1). Deregulation was also confirmed in a quantitative system. $P_{rpt\_Del14bpDS}$-*luxABCDE* showed significantly higher background luminescence signals in comparison to the unmodified P_{rpt}-*luxABCDE*, with an approximately 68-fold higher background expression after 210 min of growth (Figure 5A and Figure 5C, Manuscript 1). Furthermore, it was not inducible after antibiotic treatment for none of the compounds tested (Figure 5B, Manuscript 1). A comparison of the relative luminescence units (RLU) in relation to OD_{600} demonstrated that upon induction of P_{rpt}-*luxABCDE* by RNA synthesis inhibitors the values approximated to the (untreated) background levels measured for $P_{rpt\_Del14bpDS}$-*luxABCDE* (Figure 5C, Manuscript 1).

Aiming to identify a TF that regulates *rpt* expression, we tried to detect DNA-binding proteins that specifically bind to the conserved 13 bp, which had been found to confer induction specificity. The DNA affinity capturing assay (DACA) is a sensitive method to identify such proteins. Here, DNA-bound proteins are co-purified with the biotin-tagged DNA fragment of interest and analyzed via semi-quantitative mass spectrometry (the latter has been performed by our collaboration partner Mirita Franz-Wachtel). Four different DNA fragments were investigated for their protein binding capabilities: three versions of the *rpt* promoter fragment and, as an independent control, one *yorB* promoter fragment (fragment 4, 200 bp of length), that should identify unspecific DNA-binding proteins. For the *rpt* promoter fragments, the largest one comprised 200 bp containing the conserved 13 bp (fragment 1), while the other two were shortened by 30 (fragment 2) or 126 nucleotides (fragment 3) at the downstream end, thereby deleting the 13 bp consensus motif and further parts of the 5'UTR, respectively (Table S4, Manuscript 1). After incubation with *B. subtilis* cytoplasm, the DNA-bound proteins were purified and identified via NanoLC-MS/MS analysis. Interesting candidates were followed up by expressing P_{rpt} bioreporter constructs in the respective *B. subtilis* deletion mutant of the detected protein, assuming that the missing regulatory protein leads to the observed deregulation of *rpt* expression. The method was verified for *yorB* regulation, which had previously been proposed to be LexA-dependent (Au et al., 2005)

and showed specific induction of SOS response inducing antibiotics (Table S1, Publication 1) (Urban et al., 2007). And indeed, in the DACA experiment, LexA could be detected in highly elevated label-free quantification (LFQ) levels for fragment 4 (Table S6, Manuscript 1), while subsequent expression of P_{yorB}-*lacZ* in *B. subtilis* 168 Δ*lexA* displayed enhanced background expression and deregulated induction specificity (Figure S6, Manuscript 1) as it had been seen for P_{rpt} upon deletion or modification of the 13 conserved nucleotides (Figure 4, Manuscript 1). However, fragment 4 also showed enhanced binding of other transcriptional regulators like Xre or GamR (YbgA) (Table S6, Manuscript 1). Nevertheless, expression of P_{yorB}-*lacZ* in *B. subtilis* 168 Δ*gamR* did not influence the bioreporter's background expression or induction specificity (Figure S6, Manuscript 1), indicating that *yorB* induction upon DNA stress is selectively regulated by LexA. Although, we could confidently confirm the method by proving the LexA-dependent regulation of *yorB* expression and also identified several promising candidates by DACA, which showed preferred binding to the *rpt* promoter fragments, we were unable to find a DNA-binding protein that conferred induction specificity to *rpt* in follow-up experiments be the validated procedure. While some of the 45 tested candidates had minor modulatory effects on the background expression of P_{rpt}-*lacZ*, none led to the loss of induction specificity (Table S5 and Table S7, Manuscript 1).

Further analysis of the P_{rpt} and P_{helD} revealed two SigA bindings sites on the complementary strand. Interestingly, for both of them, the -35 region of the SigA binding site is located in the region of the conserved 13 nucleotides (Figure 6A, Manuscript 1) (Nicolas et al., 2012). The opposite strand of the *rpt* promoter was described to encode a small RNA (sRNA) called ncr1015 (120 bp) or S708 (628 bp), dependent on the study (Irnov et al., 2010; Nicolas et al., 2012). For the *helD* promoter region, no complementary sRNA has been annotated, but transcript levels on the complementary strand seemed to be upregulated under some growth conditions (Nicolas et al., 2012; Zhu and Stülke, 2017). We therefore hypothesized, that *rpt* and *helD* are both regulated by a complementarily expressed asRNA (*cis*-encoded asRNA) mechanism. To test this, the -10 region of the SigA binding site of the complementary sRNA ncr1015/S708 was modified, while leaving the conserved 13 nucleotides that were previously shown to confer induction specificity unchanged (Figure 6B, Manuscript 1). This manipulation also led to *rpt* deregulation and loss of induction specificity (Figure 6C, Manuscript 1), pointing at a role of the complementary expression of the *cis*-encoded sRNA in *rpt* repression.

2.2.5. Conservation of *rpt* regulation in other Bacillales

Homologs of *B. subtilis* Rpt could confidently be detected in different Actinomycetales, Myxococcales, Clostridiales, and Bacillales, while they were only considered homologous if they possessed a protein identity > 0.5 (Kanehisa and Goto, 2000) and a conservation of the reported rifamycin-binding sites (Stogios et al., 2016). A previous study of Spanogiannopoulos and colleagues showed that some actinomycetes utilize a rifampin-associated regulatory element (RAE) in order to control *rph* (encodes for a Rpt homolog in actinomycetes) expression (Spanogiannopoulos et al., 2014). Upon investigation of the promoter regions of the different *rpt* homolog containing bacteria, the RAE was detectable in many Actinomycetales, while minor variations of the regulatory element were even present in some Myxococcales (Figure 7, Manuscript 1). However, the promoter regions of all other examined bacterial orders were devoid of the RAE motif (Figure 7, Manuscript 1). As my regulatory studies had shown that the specific upregulation of *rpt* and *helD* gene expression was dependent on the conserved 13 nucleotides (compare chapter 2.2.4.), all promoter regions were investigated for this motif. Interestingly, the 13 bp consensus motif located in the *B. subtilis* P_{rpt} region was identified for a subgroup of different *rpt* homolog containing Bacillales (e.g., *Bacillus licheniformis* ATCC14580 (NC_006270.3), *Paenibacillus lautus* (NZ_CP032412.1), *Bacillus amyloliquefaciens* MT45 (NC_014551.1), and *Brevibacillus formosus* (NZ_CP018145.1)) (Figure 7 and Figure S7, Manuscript 1). In those strains the *rpt* homologs were located at different positions in the chromosome and flanked by a variety of different genes. Nevertheless, an alignment of the different potential promoter regions revealed a conservation of approximately 200 bp containing all regions that we hypothesize to play a regulatory role in *rpt* expression in *B. subtilis* 168: the SigA binding site of P_{rpt}, the ribosomal binding site in P_{rpt}, and the SigA binding site of the complementary sRNA ncr1015/S708 (Figure S8, Manuscript 1). In comparison, *rpt* promoter regions of other Bacillales, that were devoid of the 13 bp consensus sequence (Figure 7, Manuscript 1), including the *Bacillus cereus* group, did not display any sequence similarity to the conserved promoter region of ~200bp.

3. DISCUSSION

3.1. The agar-based bioreporter approach

3.1.1. Sensitivity and specificity of the bioreporter strain induction

The model organism *B. subtilis* was selected as strain background for the agar-based bioreporter approach, with the advantages lying in its good characterization concerning e.g., transcriptomic or proteomic data sets (Bandow et al., 2003; Fischer et al., 2004; Freiberg et al., 2006) and its high susceptibility to most antibiotics, which allows MOA profiling for the majority of antimicrobials. Although the target-area of antibiotic interference can most often be transferred to other bacteria, some of those antibiotics would not be able to approach their targets in Gram-negatives due to the additional outer membrane barrier that restricts compound permeation. Furthermore, antimicrobials that selectively target specific structures or enzymes of the outer membrane (Hart et al., 2019) would of course not be covered in our Gram-positive bioreporter approach, but could easily be detected in a Gram-negative activity-based counter-screening (compare *E. coli* ATCC25922 screening in chapter 2.1.3.). The agar-based bioreporter screening of pure compounds with known MOA confirmed a reliable detection of antibiotic interference with the main biosynthetic pathways: DNA synthesis (P_{yorB}-*lacZ*), RNA synthesis (P_{rpt}-*lacZ*), translation arrest (P_{bmrC}-*lacZ*), and impairment of cell envelope integrity (P_{ypuA}-*lacZ* and P_{liaI}-*lacZ*). Bioreporter induction occurred after overnight incubation at the borders of the ZOI, where the antibiotic concentration was not high enough to kill the bacterial cell, but sufficient to cause an adaptive cellular stress response. The size of the ZOI was not only dependent on the antibiotic's activity but also on its agar diffusion potential. Testing different dilutions of one antibiotic revealed the high sensitivity of the bioreporters even at low antibiotic concentrations. For P_{yorB}-*lacZ* and P_{rpt}-*lacZ* induction was even detectable upon treatment with subinhibitory concentrations of ciprofloxacin or fidaxomicin, respectively.

Generally, the antibiotic induction profiles of P_{yorB}-*lacZ,* P_{bmrC}-*lacZ,* and P_{ypuA}-*lacZ* were comparable to the results obtained by Urban and colleagues in a luciferase-based liquid system (Urban et al., 2007), while we extended the panel of tested reference antibiotics. Only after treatment with quinolones, mitomycin C, or phleomycin a divergent weak induction signal of P_{ypuA}-*lacZ* could be detected*,* additionally to the expected P_{yorB}-*lacZ* signal*.* We hypothesize that this induction is due to the readout after overnight incubation in the agar-based setup in comparison to the readout after 3 h in the luciferase-based liquid system, the former potentially revealing long-term secondary antibiotic effects. One explanation for the P_{ypuA}-*lacZ* induction by this group of antimicrobials could be their

ability to induce oxidative stress, which might impair the function of proteins relevant for maintenance of cell envelope integrity (Dwyer et al., 2007; Dapa et al., 2017; Hong et al., 2019). Generally, P_{ypuA}-*lacZ* was upregulated by all antibiotics that disrupt cell envelope integrity, with the exception of ionophore antibiotics. Previous studies postulated that *ypuA* is expressed from a SigM-dependent promoter (Jervis et al., 2007). However, ECF σ factor binding sites are often described to possess a specificity for one σ factor but sometimes also allow the recognition of other ECF σ factors (Helmann, 2016). Interestingly, *ypuA* expression was also shown to be modulated by SigV (Zellmeier et al., 2005), which supports the finding that P_{ypuA} is broadly induced by diverse cell envelope interfering agents. In comparison to P_{ypuA}-*lacZ,* P_{lial}-*lacZ* induction could only be observed for glycopeptides, lantibiotics, daptomycin, telomycin, ramoplanin, bacitracin, or lysolipin I, while the large group of ß-lactams did not yield an induction signal. *LialI*, which encodes for a small membrane protein, is located in the hexacistronic operon *lialIH-liaGFSR*, which is autoregulated by the three-component system LiaFSR (Jordan et al., 2006; Radeck et al., 2017). Based on the MOA of inducing antibiotics, Mascher and colleagues proposed *lial* induction to be responsive to perturbations of the lipid-II cycle (Mascher et al., 2004). However, *lial* induction was also shown to be triggered by unspecific stressors, such as alkaline shock or exposure to detergents (Radeck et al., 2017). Not surprisingly, most of the P_{lial}-*lacZ* inducing antibiotics tested in this thesis are described to interfere with different steps of bactoprenol-mediated precursor cycling (Schneider and Sahl, 2010). Bacitracin, for example, is known for its zinc-dependent binding to the extracellular undecaprenyl pyrophosphate, which upon complex formation cannot be dephosphorylated and recycled into the cytosolic compartment (Schneider and Sahl, 2010; Economou et al., 2013). The MOA of daptomycin, telomycin, and lysolipin are until now not fully elucidated. Nevertheless, it was postulated that Ca^{2+}-daptomycin activity and its insertion into the membrane is dependent on the level of the anionic phospholipid phosphatidylglycerol in the membrane (Miller et al., 2016; Müller et al., 2016; Taylor and Palmer, 2016; Grein et al., 2020), while the MOA of telomycin seems to be dependent on the bacterial phospholipid cardiolipin (Epand et al., 2016; Johnston et al., 2016). Those results suggest that *lial* might also be induced upon interference with phospholipid components of the cytoplasmic membrane. However, Ca^{2+}-daptomycin was recently shown to form tripartite complexes with undecaprenyl-coupled cell envelope precursors upon phosphatidylglycerol-binding (Grein et al., 2020), thereby impairing undecaprenyl precursor cycling. It therefore remains elusive, if *lial* induction could generally be caused by an impairment of membrane integrity upon phospholipid-binding or if substances like telomycin, which show selective binding to

cardiolipin might also possess currently unknown mechanisms to affect undecaprenyl precursor cycling. Of note, the dissipation of membrane integrity by ionophores, which act as ion carriers or initiate the formation of ion channels thereby modulation the membranes' ion permeability, does not lead to an induction of *lial*.

The upregulation of P_{bmrC}-*lacZ* was observed for antibiotics inducing translation arrest by various MOA. For example, chloramphenicol or erythromycin directly bind to the 50S ribosomal subunit and inhibit the peptidyl transferase reaction, or the translocation of the polypeptide chain by blockage of the ribosomal exit tunnel, respectively (Tenson et al., 2003; Wilson, 2009). Tetracyclines bind to the 30S ribosomal subunit and stall the ribosome by inhibiting the aminoacyl-tRNA from binding to the ribosomal A-site (Chopra et al., 1992). Inhibitors of EF-G, like fusidic acid of thiostrepton, prevent the ribosomal progression by blocking the GTP-dependent translocation of the ribosome (Borg et al., 2015). The *bmrC* gene encodes for a subunit of the multidrug ABC transporter BmrCD (Torres et al., 2009). However it remains puzzling, why *bmrC* expression is induced by such a structurally diverse group of translation stalling agents, although a *bmrCD* deletion mutant did not display increased sensitivity to any of the tested compounds inducing its induction (Torres et al., 2009). Due to the structural diversity of inducing substances one can hypothesize that *bmrC* is induced by a specific stress response signal upon translation arrest, rather than a direct drug sensing mechanism. Protein synthesis inhibitors that led to miscoded proteins (e.g., aminoglycosides), blocked aminoacyl-tRNA synthesis (e.g., mupirocin), or acted by abortive translation (e.g., puromycin) induce different kinds of stress and did not yield a P_{bmrC}-*lacZ* signal. An exception is represented by the aminocyclitol antibiotics spectinomycin and hygromycin B, which are often described as untypical aminoglycosides. Both are associated with ribosomal stalling rather than miscoding (Borovinskaya et al., 2007; Borovinskaya et al., 2008) and accordingly induced P_{bmrC}-*lacZ*. Puromycin and classical miscoding agents, like kanamycin or streptomycin, increase the intracellular levels of non-functional, aberrant peptides or proteins, which bacterial cells try to counteract by the initiation of the so-called heat-shock response (Bandow et al., 2003; Shaw et al., 2003; Freiberg et al., 2006; Kindrachuk et al., 2011). This stress response typically leads to the upregulation of chaperones (e.g., DnaK or GroEL/S) and proteases (e.g., ClpCP), trying to restore cellular protein homeostasis (Hecker et al., 1996; Elsholz et al., 2017). Exposure to mupirocin was shown to evoke the stringent response in *B. subtilis* (Bandow et al., 2003), as mupirocin depletes the isoleucine-charged tRNA levels by its competitive binding with isoleucine to the isoleucyl t-RNA synthetase (Khoshnood et al., 2019), thereby mimicking amino acid starvation conditions.

DNA stress was detected upon treatment with inhibitors of the bacterial type-II DNA topoisomerases (e.g., quinolones or novobiocin), the nucleotide precursor supply (e.g., trimethoprim or 5'-fluorouracil), or by some intercalators or alkylating agents (e.g., daunomycin or mitomycin C, respectively). As expression of *yorB* was shown to be LexA-dependent (see chapter 2.2.4), it can be concluded that all P_{yorB} inducing compounds lead to an initiation of the SOS response in *B. subtilis*. *YorB* encodes for a protein of unknown function and was shown to be located in a SPß-prophage derived chromosomal region (Kunst et al., 1997). Based on its origin and its strong and selective LexA-regulated induction, it is tempting to hypothesize that the temperate bacteriophage uses *yorB* expression by the bacterial SOS response to sensitively sense and react to the host´s struggle for survival, e.g., by influencing the decision of the bacteriophages to leave the host by initiation of a lytic cycle. Interestingly, this mechanism was described for the GIL01 bacteriophage. After infection of *Bacillus thuringiensis*, the GIL01 bacteriophage exploits the transcriptional repressor LexA of its host for maintenance of the lysogenic state. However, upon DNA damage LexA-dependent repression is abolished, which induces the expression of genes involved in virion maturation and host lysis and thereby entrance into the lytic cycle of GIL01 bacteriophage (Fornelos et al., 2018).

The bioreporter P_{helD}-*lacZ* showed selective but weak induction only of RNAP-binding agents in the agar-based bioreporter assay. We therefore re-analyzed previously conducted microarray data (Freiberg et al., 2006) and established the P_{rpt}-*lacZ* bioreporter as an alternative, which displayed strong and selective induction of direct RNAP inhibiting substances (e.g., rifampin or fidaxomicin), but also weaker signals for DNA-binding agents that block RNA synthesis (e.g., actinomycin D, echinomycin or netropsin). Interestingly, DNA-binding agents, that did not show an induction signal for P_{yorB}-*lacZ*, could be successfully detected with P_{rpt}-*lacZ*, while only few antibiotics, like chartreusin or gilvocarcin V, were able to induce both, P_{rpt}-*lacZ* and P_{yorB}-*lacZ* (see chapter 2.2.1.). Generally, DNA-binding agents most likely act as roadblocks hindering both metabolic pathways, replication and transcription, as both metabolic processes are dependent on the same DNA template. Nevertheless, it could be shown for some antibiotics like actinomycin D or mitomycin C, that they primarily interfere with transcription or replication, respectively (Harvey et al., 1976). The bioreporters seem to sensitively detect those preferences by selectively inducing P_{rpt}-*lacZ* (actinomycin D) or P_{yorB}-*lacZ* (mitomycin C). The MOA of DNA-binding agents are often not well described in bacteria due to their eukaryotic toxicity and primary application in anticancer chemotherapy. Studies in eukaryotes describe anthracycline intercalators like doxorubicin to act as human type IIA topoisomerase (Top2)

poison that block Top2 binding to DNA (at high concentrations), DNA religation (at low concentrations), induce DNA double and single strand breaks, and generate reactive oxygen species (compare additional weak induction of P_{ypuA}-*lacZ* by doxorubicin in chapter 2.1.1.) (Pommier et al., 2010). Interestingly, doxorubicin strongly induces the DNA stress bioreporter P_{yorB}-*lacZ,* which was confirmed to be LexA-dependent and therefore belongs to the SOS response. The SOS response is a highly sensitive control pathway that is initiated upon RecA-dependent sensing of elevated levels of single stranded DNA. The following activation of RecA results in the proteolytic autodigestion of the LexA repressor and the subsequent transcription of the SOS response regulon (Lovett et al., 1994; Au et al., 2005). The dependency of the stress response on the detection of single stranded DNA indicates that doxorubicin most likely also induces DNA strand breaks in *B. subtilis*. In addition, this implies that DNA-binding agents that only show P_{rpt}-*lacZ* induction, do not cause DNA strand breaks in *B. subtilis*. This hypothesis is supported by the DNA-binding agent echinomycin, which selectively induces P_{rpt}-*lacZ*, and is not known for any strand break capability (Huang et al., 1982). The combinational MOA profiling using P_{yorB}-*lacZ* and the newly established bioreporter P_{rpt}-*lacZ* supports an early discrimination of the diverse activities of DNA-binding agents, helping to dissect the primary *B. subtilis* stress response initiated upon antibiotic impairment.

3.1.2. Microcionamide A and C act on the bacterial cell envelope

The validation of the agar-based bioreporter approach with antibiotics of known MOA allowed the subsequent testing and MOA profiling of uncharacterized antimicrobial compounds. Our collaboration partners provided us with the pure agents microcionamide A and C, which were tested against the bioreporter panel. Both compounds showed selective and combined induction of the cell envelope stress bioreporters P_{ypuA}-*lacZ* and P_{lial}-*lacZ*. While P_{ypuA} is broadly induced upon stress inflicted on the cell envelope, the induction of P_{lial} hinted at a membrane associated target, most likely inhibiting steps of the bactoprenol-mediated precursor cycling. Furthermore, the induction signals excluded a mechanism comparable to the MOA of ionophores, as none of the previously tested ionophores yielded a P_{ypuA}-*lacZ* or P_{lial}-*lacZ* induction signal. This bioreporter-based MOA profiling facilitated the selection of adequate follow-up studies. The subsequent investigation of the *S. aureus* NCTC8325 membrane potential revealed the strong membrane depolarization even after treatment with low antibiotic concentrations of microcionamide A and C further showing that those compounds indeed act on the bacterial cell envelope, and thereby independently confirm the bioreporter MOA profiling. The results indicate a

mechanism comparable to nisin, which is known to bind to the carbohydrate pyrophosphate moiety of lipid-II and form a membrane pore (Schneider and Sahl, 2010). The lantibiotic would show similar bioreporter signals (Table S1, Publication 1) and would also destabilize the membrane potential (Ruhr and Sahl, 1985). The Gram-positive-only activity of microcionamide A and C suggests that the compounds are not able to pass through the outer membrane to reach their cytoplasmic membrane target, which can be explained by their molecular mass of approximately 875 Da and 889 Da, respectively, or by active efflux, counteracting their intracellular retainment. The observed cytotoxicity of microcionamide A and C, as well as their induction of apoptosis, could be due to an additional, unrelated eukaryotic target. Then again, *lial* induction was previously speculated to be responsive to interference with phospholipid components of the cytoplasmic membrane, like cardiolipin (compare chapter 3.1.1.). The impairment of membrane integrity by interaction with a phospholipid component that is equally present in eukaryotes (cardiolipin can be found in the inner membrane of mitochondria (Schlame, 2008)), could putatively also account for the detected cytotoxic effects. This hypothesis is further supported by the observed inhibition of autophagy by microcionamide C, as cardiolipin was recently proposed to play a role in autophagosome formation (Manganelli et al., 2021). Nevertheless, the exact underlying mechanisms of the cytotoxic activity of microcionamide A and C remain unclear and would need to be elucidated in further studies.

3.1.3. Applicability in direct screening of antibiotic producer strains

The agar-based bioreporter approach was further investigated for its applicability in direct screening of antibiotic producer strains. For validation, cultivated samples of six known antibiotic producer strains were directly tested in the agar-based bioreporter screening. After overnight incubation, MOA-informed ZOI could confidently be detected, matching the MOA of the antibiotic described to be produced by the respective producer strain. The setting allowed a direct MOA classification of produced antimicrobials with no need for initial time-consuming and laborious compound purification. This represents a big advantage in comparison to other MOA profiling tools, as they are often only suitable for the investigation of pure or at least partly purified antimicrobial agents (Urban et al., 2007; Nonejuie et al., 2016; O'Rourke et al., 2020). One limitation of the agar-based bioreporter assay is its deficiency to directly elucidate the exact molecular target, which makes substance purification for downstream MOA analysis unavoidable. Nevertheless, the rapid and reliant bioreporter information generally allows to prioritize activities of interest before purification, e.g., by solely investigating bioactivities that interfere with only one specific

metabolic pathway, or by the selective follow-up on non-inducing compounds, that most likely interfere with other, but also potentially new cellular target structures.

The agar-based bioreporter approach was further verified by the investigation of approximately 500 uncharacterized actinomycetes strains of the Tübingen strain collection. For validation purposes, different producer strains which either had or had not triggered a bioreporter signal were chosen for further investigation. Chemical analytics resulted in the dereplication of 28 antimicrobial substances. Of note, during the purification process, the bioreporters proved a useful tool to monitor the presence of the compound of interest, allowing to test supernatants, extracts, fractions, and purified compounds for the previously observed reporter signal. Furthermore, the bioreporter information added a MOA-informed dimension to the dereplication process, which accelerated compound deconvolution. For all 21 bioreporter-positive producer strains, the previously observed induction signal matched the antibiotic MOA described in literature. For example, Tü6430 strongly induced the bioreporter for translation arrest (P_{bmrC}-*lacZ*). Purification and dereplication uncovered the produced antibiotic pactamycin, which binds to the 30S subunit and affects translational initiation and elongation by preventing the release of the initiation factors and blocking tRNA-binding to the ribosome (Brodersen et al., 2000). Consequently, this interference hinders ribosomal progression, which was sensitively detected by the induction of P_{bmrC}-*lacZ.* Of note, the induction specificity of the respective bioreporter strains is discussed in chapter 3.1.1. in more detail. The remaining seven antimicrobial activities were initially chosen for further investigation, as they were not covered by the bioreporter panel. Although not showing an induction, they were not devoid of MOA information, containing the information of non-interference with the main metabolic pathways. And indeed, the dereplicated substances clustered with antibiotic classes that were previously shown not to be covered by the applied bioreporter panel, including three ionophores (monactin, omomycin, and boromycin), a siderophoric tRNA synthesis inhibitor (albomycin δ_1), and three substances with to date uncharacterized MOA (griseorhodin A, lobophorin A and E). The additional MOA information obtained from the direct agar-based bioreporter screening not only allowed monitoring of the purification process, but also enabled an early discrimination of diverse or multiple antibiotic production of a single producer strain, which is especially useful as producer strains are often genetically capable of producing different bioactive secondary metabolites (Seyedsayamdost, 2014; Yoon and Nodwell, 2014). For example, strain Tü2401 was shown to synthesize C-1027 or albomycin δ_1 when grown on agar or in liquid culture, respectively. In a solely activity-based screening the diverse antibiotic production would have been overlooked, as both samples displayed similar

bioactivity against *B. subtilis*. However, the additional bioreporter-based MOA information immediately uncovered the production of two differently acting antimicrobial agents. One strain many compounds (OSMAC) describes a strategy to exploit the full potential of an antibiotic producer strain by application of different cultivation conditions including changes in physical parameters (e.g., temperature, aeration, pH, or salinity), nutrient availability (e.g., carbon, nitrogen, or sulfur sources), fermentation (liquid or solid cultivation), or by application of epigenetic modifiers (e.g., DNA methyltransferase or histone deacetylase inhibitors) (Bode et al., 2002; Romano et al., 2018; Pan et al., 2019). Furthermore, cocultivation with other bacterial strains or fungi was also proven to modulate antimicrobial production (Oh et al., 2007; Pan et al., 2019). As OSMAC strategies are often laborious and quickly yield great amounts of conditioned samples, the application of the agar-based bioreporter approach represents an efficient screening tool to directly monitor differences in antimicrobial production. Of note, this is also the case for other strategies of activating silent gene clusters, like genome editing or heterologous expression (Nah et al., 2017; Mao et al., 2018). For initial validation of the direct agar-based bioreporter approach, we investigated the well explored order of actinomycetes producer strains, which are known to yield a high antibiotic rediscovery rate (Tulp and Bohlin, 2005; Genilloud, 2017). The high number of rediscovered antibiotics was useful for MOA comparison and validation of the direct agar-based bioreporter approach. Nevertheless, the bioreporter assay is not limited to this order of producer strains as cultivation of antibiotic producers happens independently, while the approach is suitable for concomitant screening of a variety of different samples.

3.2. In-depth characterization of the *B. subtilis* genes *rpt* and *helD*

3.2.1. P_{rpt} and P_{helD} share a similar antibiotic induction specificity

The induction specificity and strength of the newly established RNA stress bioreporter (P_{rpt}-*lacZ*) was additionally profiled in a quantitative system (P_{rpt}-*luxABCDE*). All luminescence signals (RLU) were normalized to an OD_{600} of 1, while the induction threshold was set to 200 %, always comparing with the background luminescence signal of untreated *B. subtilis* cells. Analysis confirmed the reliant and specific upregulation of P_{rpt}-*luxABCDE* only upon treatment with RNA synthesis inhibitors up to 240 min of incubation, after which the stated induction threshold was no longer suitable for discrimination. Interestingly, inhibitors of RNA synthesis initiation could already sensitively be detected for P_{rpt}-*luxABCDE* after 10 min of antibiotic treatment. Generally, the initiation process represents the crucial step in the regulation of RNA synthesis. Upon RNAP holoenzyme binding to the σ factor binding site in the promoter region, the formation

of a transcription-competent open promoter complex is critical for RNA synthesis initiation. Interestingly, promoter escape and therefore a stable transcription of full-length RNA in *E. coli* only takes place in 30-50 % of all initiation attempts. For the remaining cases, the initiation complex is prone to abortive cycling, leading to the repeated production and release of short mRNAs (Henderson et al., 2017). The length of those abortive mRNA oligomers can vary, while different studies propose their regulatory role in transcription initiation at other promoter sites (Goldman et al., 2011; Nickels, 2012; Druzhinin et al., 2015; Henderson et al., 2017). Transcription initiation is best investigated in *E. coli*, while it remains elusive if abortive cycling is as frequently utilized in *B. subtilis* (Whipple and Sonenshein, 1992). The rapid and strong upregulation of P_{rpt}-*luxABCDE* by RNA synthesis initiation inhibitors could indicate that interference with the highly dynamic initial step of transcription is generally less tolerated and therefore stress affecting transcription initiation might more sensitively be sensed. In chapter 3.2.3., the stalling of RNAP is discussed to most likely account for the *rpt* inducing stress signal. As *E. coli* data indicates that only about half of the RNAPs proceed to stable full-length transcription (Henderson et al., 2017), this means that only half of the promoter-bound RNAP complexes reach downstream mRNA regions. Hence, RNAP stalling stress (and therefore *rpt* induction) might more rapidly and strongly accumulate upon inhibition of the initiation process in comparison to downstream inhibitory effects on RNAP progression executed by RNA synthesis elongation inhibitors.

The quantitative luciferase-based setup also allowed sensitive comparison of the two RNA stress bioreporters. It could be shown, that P_{rpt}-*luxABCDE* and P_{helD}-*luxABCDE* are actually induced by the same panel of antibiotics, with P_{rpt} displaying a more powerful induction strength in both systems. For this reason, P_{helD}-*lacZ* induction by DNA-binding agents like echinomycin was not detectable in the generally less sensitive agar-based setup. Of note, P_{helD} was previously characterized in a firefly luciferase-based system, showing no induction of DNA-binding agents like actinomycin D after 90 min (Urban et al., 2007). This was also the case after 90 min using our bacterial luciferase-based bioreporter setup. However, we also monitored P_{helD}-*luxABCDE* expression at later time points. After 240 min of actinomycin D treatment, we could observe P_{helD}-*luxABCDE* luminescence signals exceeding the threshold of 200 %, while specificity for RNA synthesis inhibitors was still given at this time point. Furthermore, other DNA-binding agents that were not investigated by Urban and colleagues, but are described to interfere with RNA synthesis like the intercalator echinomycin (Foster et al., 1985), also showed induction of P_{rpt}-*luxABCDE* and P_{helD}-*luxABCDE* after 210 min (the more sensitive P_{rpt}-*luxABCDE* already exceeded the induction threshold of 200 % after 90 min). The observed, similar induction patterns of

P_{rpt}-*luxABCDE* and P_{helD}-*luxABCDE* upon treatment with different antibiotics supported a similar way of gene regulation. This result was especially interesting as previously published microarray data had only shown very few genes that displayed this selective and strong upregulation solely upon treatment with the RNA synthesis inhibitors rifampin and corallopyronin (Freiberg et al., 2006). Furthermore, none of the two *B. subtilis* genes had been elucidated for its gene regulation prior to the current project.

3.2.2. Function of Rpt and HelD in adaptation to RNA stress

The strong and selective upregulation of *rpt* and *helD* in response to RNA stress made us investigate their potential function in adaptation to those antibiotics, especially as the function of Rpt had not previously been characterized in *B. subtilis*. The knockout strains *B. subtilis* 168 Δ*rpt* and *B. subtilis* 168 Δ*helD* were tested for their antibiotic susceptibility against a panel of RNA synthesis inhibitors that had previously induced the bioreporter genes in our study. For comparison, the isogenic reference strain *B. subtilis* 168 Δ*amyE* was investigated for WT MIC levels. *B. subtilis* 168 Δ*rpt* displayed a selective drop in MIC only for rifamycin antibiotics. Due to sequence homologies, *B. subtilis* Rpt is annotated as putative phosphoenolpyruvate synthetase or rifampin phosphotransferase. While both enzymes possess an ATP binding domain, and a histidine domain important for phospho-transfer, parallels which explain the annotation of the two different genes, they possess different functions: the phosphoenolpyruvate synthetase is an enzyme involved in gluconeogenesis (McCormick and Jakeman, 2015) and the rifampin phosphotransferase is a resistance enzyme that selectively inactivates rifamycins by phosphorylation (Spanogiannopoulos et al., 2014). The decreased MIC of *B. subtilis* 168 Δ*rpt* only after treatment with rifamycins indicated that Rpt acts as rifampin phosphotransferase in *B. subtilis*. Heterologous overexpression of S707-*rpt* from a high-copy plasmid in *E. coli* XL1 blue, which is naturally devoid of a rifampin phosphotransferase gene, yielded high level resistance (128-fold MIC increase), as has been previously shown for rifampin phosphotransferases from other species (Spanogiannopoulos et al., 2014). Furthermore, complementation of the knockout *B. subtilis* 168 Δ*rpt* by IPTG-induced overexpression of S707-*rpt* in the *aprE* locus yielded WT MIC levels. Of note, S707 is described as 5'UTR preceding *rpt* (Nicolas et al., 2012). This construct was generated before the investigation of the gene regulation of *rpt* and *helD*. With the knowledge that we acquired during the regulatory studies (compare chapter 3.2.4.), it might be likely that overexpression of S707-*rpt* only returned to WT MIC levels in the *B. subtilis* 168 Δ*rpt* background, due to the presence of the regulatory 5'UTR region. While the 5'UTR promoter region possesses the

ability to repress SigA-dependent *rpt* expression under unstressed growth conditions, it likely also does so if preceded by an IPTG-inducible promoter instead of the native SigA σ factor binding site. A deletion of *helD* showed no changes in MIC in comparison to WT susceptibility for most tested RNA synthesis inhibitors, with the exception of the closely related α-pyrone antibiotics corallopyronin A and myxopyronin A, which showed strongly decreased MIC values for the Δ*helD* mutant. The underlying mechanism of this observation is elusive so far. However, function and RNAP binding of HelD are well investigated in *B. subtilis* (Wiedermannová et al., 2014; Newing et al., 2020; Pei et al., 2020). On the one hand, the binding site for myxopyronin (Ho et al., 2009) lies in close vicinity to the one described for HelD (Wiedermannová et al., 2014), which might sterically hinder antibiotic binding to RNAP in the presence of HelD and therefore decrease antibiotic potency. On the other hand, the function of HelD might counteract the MOA of corallopyronin A and myxopyronin A in the inhibition of RNA synthesis. While myxopyronin blocks clamp opening and DNA loading to the active site by a still unknown mechanism (Mukhopadhyay et al., 2008; Belogurov et al., 2009; Artsimovitch et al., 2012), HelD introduces large conformational changes that cause RpoC clamp opening, thereby releasing the DNA template from the active site of the stalled RNAP (Newing et al., 2020). Interestingly, we could detect the same selective drop in corallopyronin A and myxopyronin A MIC using *B. subtilis* 168 Δ*rpoE*. RpoE is an accessory RNAP subunit that was shown to enhance transcription and RNAP recycling and to act synergistically with HelD (Wiedermannová et al., 2014). However, further studies are needed to elucidate the molecular mechanism of corallopyronin A and myxopyronin A inhibition by HelD and RpoE.

Although *rpt* and *helD* could be induced by a broad range of structurally and mechanistically different transcription inhibitors, they only affected *B. subtilis* sensitivity for some selected compounds (e.g., inactivation of rifamycins by Rpt). Hence, *rpt* and *helD* are induced upon transcriptional stress that is common to all inducing RNA synthesis inhibiting substances, and not by direct compound sensing.

3.2.3. Induction of the RNA stress response genes *rpt* and *helD* is correlated with enhanced intracellular levels of stalled RNAP

Rpt and *helD* are induced by a diverse group of RNA synthesis inhibitors. In order to elucidate the stress signal that leads to induction, we tried to deduce a common mechanism of antibiotic interference from the described MOA. Interestingly, induction was observed for antimicrobial agents that directly bind to the RNAP complex in different ways (e.g., rifampin, fidaxomicin, streptolydigin) (Ho et al., 2009; Lin et al., 2018) but also by DNA-binding agents,

which inhibit transcription by sterically blocking RNAP progression (e.g., actinomycin D, echinomycin) (Gause et al., 1968; Hollstein, 1974). Therefore, elevated intracellular levels of stalled RNAP were suspected to initiate the stress response that led to upregulation of *rpt* and *helD*. This idea was further addressed by monitoring P_{rpt}-*luxABCDE* background expression (luminescence signal of untreated strains after 210 min of growth in BMM) in different *B. subtilis* 168 knockout mutants, affecting transcription efficacy. In comparison to the reference luminescence of *B. subtilis* 168 Δ*amyE*, *B. subtilis* 168 Δ*helD* and Δ*rpoE* showed significantly enhanced P_{rpt}-*luxABCDE* background expression. As previously mentioned, HelD and RpoE are both described to enhance transcriptional cycling and facilitate the recovery of stalled RNAP, which is further potentiated by them acting in synergism (Wiedermannová et al., 2014; Newing et al., 2020; Pei et al., 2020). Those findings support the hypothesis of *rpt* and *helD* expression being responsive to enhanced levels of stalled RNAP. For the mutants *B. subtilis* 168 Δ*uvrB* and Δ*mfd,* no enhanced P_{rpt}-*luxABCDE* background expression levels could be detected. The selection of those two genes was based on the expression profiles of P_{yorB}-*lacZ* and P_{rpt}-*lacZ* upon treatment with RNA and DNA synthesis inhibitors (compare chapter 3.1.1). It could be seen that *rpt* induction was responsive to DNA-binding agents that did not evoke chromosomal fragmentation (DNA strand breaks) but rather acted as DNA-bound roadblocks, most likely causing replication-transcription conflicts (Merrikh et al., 2012). As the nucleotide excision repair (NER) regulates the repair of DNA lesions (Kisker et al., 2013), we presumed that elimination of the major players of the prokaryotic NER pathway, UvrB and Mfd, might potentially affect *rpt* expression levels. UvrB is part of the UvrABC excinuclease complex, which is involved in the detection and repair of DNA lesions (Lenhart et al., 2012; Kisker et al., 2013). Of note, *uvrA*, *uvrB* and *uvrC* are all LexA-dependent and therefore part of the SOS response (Au et al., 2005). Mfd belongs to a subpathway of the NER, called transcription-coupled repair (TCR). The protein was shown to translocate along DNA and is able to dislodge stalled RNAP from DNA lesions, subsequently promoting DNA repair by the NER machinery (Ayora et al., 1996; Adebali et al., 2017). Furthermore, Mfd is discussed to produce genetic diversity by error-prone repair under starving conditions (Leyva-Sánchez et al., 2020). In general, the observed, unchanged background expression of P_{rpt}-*luxABCDE* in the Δ*uvrB* and Δ*mfd* mutants might be explained by the applied assay conditions. Under rather unstressed growth conditions (readout after 210 min of growth in BMM), the impact of the deletions might not be severe, especially as *B. subtilis* is not exposed to any DNA lesions inducing stressors (e.g., UV radiation, chemical treatment, or oxidative stress), where Mfd and UvrB are crucial to maintain genome fidelity.

3.2.4. Gene expression of *rpt* and *helD* may be regulated by a *cis*-encoded asRNA mechanism

To identify the promoter regions important for regulation of *rpt* and *helD*, we compared sequence identity, promoter composition, and putative TF binding sites (Sierro et al., 2008; Nicolas et al., 2012; Zhu and Stülke, 2017). Furthermore, expression was monitored upon promoter deletion or modification. The upstream promoter region could be deleted up to the proposed SigA binding site (Nicolas et al., 2012) with no changes in *rpt* and *helD* induction specificity after treatment with RNA synthesis inhibitors. Upon deletion of the -35 region of the SigA binding sites, both promoters lost their strong inducibility, which confirmed their SigA-dependent expression. Furthermore, this attested the existence of a 5'UTR preceding both genes, as the translational start site is located ~100 bp downstream of the SigA binding site. The general distribution in length of different putative 5' leader regions in *B. subtilis* indicated that most of them possess a length of up to 40 nucleotides (~52 %), with ~15 % being larger than 100 bp (Irnov et al., 2010). However, it remains elusive if those short 5'UTRs (< 40 bp) possess a regulatory function, as further RNA-seq data indicated that most mRNAs in *B. subtilis* have short unprocessed 5' ends (Nicolas et al., 2012). For their annotation of RNA features, Nicolas and colleagues excluded 5'UTRs smaller than 50 bp. The length distribution of the remaining 5'UTRs (> 50 bp) demonstrated that 5' leader regions of 50-150 bp are most abundant in *B. subtilis* (Nicolas et al., 2012). Of note, SigA was shown to be the most prevalent σ factor initiating transcription of the 5'UTR features in *B. subtilis* (> 65 %) (Mars et al., 2016).

For the *helD* promoter, two additional σ factor binding sites were postulated that are located upstream and downstream of the SigA binding site (Nicolas et al., 2012). Nonetheless, as the upstream promoter region of P_{helD} could be deleted up to the SigA binding site (P_{helD_120bp}-*lacZ*) causing no changes in induction specificity, while deletion of the -35 region of the SigA binding site (P_{helD_113bp}-*lacZ*) led to complete loss of its inducibility, it can be concluded that the alternatively described σ factor binding sites do not play a regulatory role under our applied growth conditions. Although *B. subtilis* possesses the ability to modulate gene expression by implementation of stress-responsive alternative σ factors (Helmann and Moran, 2001), this regulation mechanism was excluded to selectively upregulate *rpt* and *helD* upon RNA stress, as both genes showed a prominent dependence on the housekeeping σ factor SigA. However, SigA-dependent expression alone could not explain the specific induction of *rpt* and *helD* upon RNA stress, which strongly indicated the involvement of one or more additional regulatory element(s) located inside or downstream of the SigA binding sites. An alignment of the two shortened promoter regions of *rpt* and

helD that still retained specificity, revealed a 13 bp consensus motif at the downstream end of both promoter regions (Erb et al., 2012). Interestingly, a deletion of those 13 nucleotides in P_{rpt} or P_{helD} ($P_{rpt\_Del14bpDS}$-*lacZ* and $P_{helD\_Del15bpDS}$-*lacZ*, respectively) resulted in complete deregulation of gene expression, showing enhanced background expression and loss of RNA synthesis inhibitor-specific induction. To ensure that this deregulation is not due to a difference in length of the preceding 5'UTR, induction specificity was also investigated in a construct that was modified in 6 out of the 13 conserved nucleotides. Nonetheless, a modification of the consensus motif also displayed the same deregulated phenotype. A further construct only containing the SigA binding site of P_{rpt} fused to the *lacZ* reporter construct confirmed that the observed deregulated expression upon deletion or modification of the 13 bp consensus motif resembled a constitutive expression from a SigA-dependent promoter. However, the lacZ-dependent agar-based bioreporter approach does not allow for exact quantification of a bioreporter signal. Quantitative analysis of *lacZ* reporters is generally also possible in a liquid system, using fluorescent substrates like 4-Methylumbelliferyl-ß-D-glucuronide hydrate (MUG). Nevertheless, it only allows for a single readout upon cell disruption and substrate addition at a specific time point (Kuklin et al., 2003). Reporter systems using the bacterial luciferase are in general more sensitive and allow for quantitative *in vivo* real-time monitoring as the substrate is inherently produced in the same operon with the luciferase enzyme (La Rosa et al., 2012; Kuklin et al., 2003). Quantitative comparison of the unmodified and selective P_{rpt}-*luxABCDE* construct and $P_{rpt\_Del14bpDS}$-*luxABCDE*, which was devoid of 14 bp at the downstream end of the *rpt* promoter, including the conserved 13 nucleotides, demonstrated a 68-fold higher background luminescence signal after 210 min of growth for $P_{rpt\_Del14bpDS}$-*luxABCDE*. Interestingly, upon induction of P_{rpt}-*luxABCDE* with different RNA synthesis inhibitors, the measured values (RLU/OD_{600}) approximated to the background levels observed for $P_{rpt\_Del14bpDS}$-*luxABCDE.* $P_{rpt\_Del14bpDS}$-*luxABCDE* could not further be induced by RNA synthesis inhibitors, just showing unchanged background expression upon antibiotic treatment. Therefore, a deletion of the downstream 13 bp consensus motif seemed to eliminate the regulatory element that repressed SigA-dependent transcription under unstressed growth conditions, while in the unmodified *rpt* promoter construct this derepression could be selectively regulated by a yet unknown stress response mechanism only upon antibiotic treatment with RNA synthesis inhibitors. Of note, transcriptomic data indicates that mRNA levels of *rpt* and *helD* are comparable, but largely lowered in comparison to SigA-regulated housekeeping genes like *rpsJ, tufA,* or *rpoA* under all growth

conditions tested (Zhu and Stülke, 2017; Nicolas et al., 2012), supporting the idea of their repression under unstressed growth.

In order to identify a repressive element that confers induction specificity to *rpt* and *helD*, promoter regions were investigated for DNA-binding proteins that might selectively bind to P_{rpt} and modulate transcription. DBTBS database was consulted to investigate P_{rpt_123bp} and P_{helD_120bp} for known TF binding sites present in both promoter regions, but there was no match (Sierro et al., 2008). In previous studies, DACA experiments were conducted to unravel transcriptional regulators that specifically bind to the respective promoter regions and regulate expression of the gene(s) of interest (Park et al., 2009; Bekiesch et al., 2016). For example, Bekiesch and colleagues could identify 17 proteins specifically binding to the promoter region of the novobiocin gene cluster, while three of them could be proven to modulate expression (Bekiesch et al., 2016). While DACA followed by mass spectrometry sensitively detects DNA-binding proteins, further downstream approaches are required to elucidate the impact of the detected protein in regulating gene expression. To identify a TF that regulates *rpt* induction, three *rpt* promoter fragments were examined in the DACA: fragment 1 containing the entire P_{rpt} sequence that confirmed induction specificity (200 bp), fragment 2 that was shortened by the RBS and the 13 consensus nucleotides at the downstream end of P_{rpt} (170bp), and fragment 3 that was further shortened (126 bp). While experiments had shown that induction specificity was conferred by the 13 bp at the downstream end of the promoter, potential TFs were expected to bind selectively or most prominently to fragment 1, which still contained this promoter region. To exclude DNA-binding proteins that non-specifically interact with double stranded DNA, the unrelated *yorB* promoter fragment (fragment 4) was included in the DACA. Fragment 4 was further used as positive control, as *yorB* was previously suspected to be repressed by the DNA-binding protein LexA (Au et al., 2005). The DACA combined with NanoLC-MS/MS identified 54 proteins that were detected in higher abundance for the *yorB* promoter fragment, including the suspected LexA protein. For the *rpt* promoter fragments, 74 proteins were detected with elevated LFQ intensities. Some of those proteins were excluded for further analysis due to their well-described function, which could not selectively regulate *rpt* expression, leaving 45 promising candidates with 16 of them showing most prominent LFQ values for fragment 1. Of note, as an additional binding site of the putative regulatory TF in the upstream region of P_{rpt} could not be excluded, we also investigated DNA-binding candidates that showed general enhanced LFQ intensities for all *rpt* fragments (fragments 1-3) in comparison to fragment 4. To elucidate if one of the detected DNA-binding proteins is responsible for gene regulation, P_{rpt} or P_{yorB} bioreporter constructs were

expressed in the respective knockout mutant. And indeed, after transferring P_{yorB}-*lacZ* into a *B. subtilis* 168 Δ*lexA* mutant, an enhanced background expression and loss of induction specificity could be observed, proving its dependency on the LexA-repressor. Urban and colleagues postulated that the *yorB* bioreporter delivered the strongest signal-to-noise ratio among all promoters of the SOS regulon, indicating that it might be strongly repressed under unstressed growth conditions by additional regulators (Urban et al., 2007). The additional detection of TFs, like Xre or GamR (YbgA), binding more prominently to fragment 4 might likewise support this hypothesis. Of note, expression of P_{yorB}-*lacZ* in a *B. subtilis* 168 Δ*gamR* mutant did not yield a deregulated phenotype, showing that induction specificity is selectively conferred by LexA-regulation. However, GamR might possess a regulatory role under different growth or stress conditions, which would have to be addressed in further studies. None of the 45 candidates that were found in higher abundance for the P_{rpt} fragments could be confirmed for specific *rpt* regulation upon RNA stress. While the expression of P_{rpt}-*lacZ* in some knockout mutants led to a slightly enhanced background expression, none displayed complete loss of induction specificity as has been observed upon deletion or modification of the 13 bp consensus motif. Changes in background expression in those mutants might be caused by minor modulatory effects on *rpt* gene regulation or by generally enhanced cellular stress signals that are responsible for *rpt* induction, as has been seen for the expression of P_{rpt}-*luxABCDE* in *B. subtilis* 168 Δ*helD* or Δ*rpoE* (compare chapter 2.2.3.). As no TF responsible for regulation of *rpt* induction specificity could be identified, all 45 candidates were further checked for *B. subtilis* paralogous proteins (Kanehisa and Goto, 2000) that might compensate for the loss of the regulator in a single knockout mutant. None of the 16 candidates that showed selective binding to fragment 1 possessed a paralog with a sequence identity > 0.5 in *B. subtilis* 168. For the remaining proteins that displayed elevated LFQ intensities for P_{rpt}, e.g., the paralogous proteins AbrB and Abh as well as YxaF and LmrA were identified (Kanehisa and Goto, 2000). AbrB and Abh are TFs described to control gene expression in the transition to stationary phase. Both are discussed to play a role in antibiotic production and resistance development, while they show partly dissimilar regulation at shared promoter sites (Qian et al., 2002; Strauch et al., 2007). The transcriptional repressors YxaF and LmrA are both able to regulate the expression of *yxaF* and the operons *lmrAB* and *yxaGH*, with *lmrB*, *yxaG*, and *yxaH* encoding for a multidrug efflux transporter, quercetin 2,3-dioxygenase and a putative membrane protein, respectively (Yoshida et al., 2004; Hirooka et al., 2007). Inactivation of YxaF and LmrA and therefore derepression of controlled genes was observed in response to certain flavonoids (Hirooka et al., 2007). Generally, we would have anticipated at least slight effects upon

single deletion of one paralogous protein, as they often cannot fully compensate for each other (Strauch et al., 2007). In the DACA AbrB, Abh and YxaF displayed the same LFQ intensities for all P_{rpt} fragments (fragments 1-3), not showing any specificity for fragment 1. LmrA was only detected at low intensities and did not reproducibly show the same results in all 3 biological replicates. For P_{rpt} a putative AbrB binding site could be mapped to the -35 region of the SigA binding site (Sierro et al., 2008), which fits the DACA results, as the SigA binding site is present in all three P_{rpt} fragments. However, it rather excludes AbrB's participation in regulating induction specificity, as the region conferring specificity was mapped to the downstream end of the 5'UTR. Furthermore, microarray data of Freiberg and colleagues only displayed very few genes that showed selective upregulation only upon treatment with RNA synthesis interfering antibiotics (Freiberg et al., 2006), while in comparison AbrB regulates gene expression during transition to stationary phase and is known to control transcription of over 250 genes (Qian et al., 2002; Hoch, 2017), which reduces the probability of AbrB being prominently responsible for the selective induction of only *rpt* and *helD*. Nevertheless, further studies would need to examine *rpt* expression in different double mutants to finally exclude those paralogous candidates. In general, the data from the promoter deletion studies strongly indicated that the 13 bp consensus sequence found in P_{rpt} and P_{helD} confers induction specificity upon RNA stress by repression of a SigA-dependent transcription under unstressed growth condition. As in *B. subtilis* the majority of DNA-binding TFs act by repression of the respective gene(s) (Moreno-Campuzano et al., 2006), the DACA investigation and the identification of repressors selectively binding to fragment 1 seemed to represent a promising strategy. While the method to elucidate the regulatory TF by combining a DACA investigation with subsequent bioreporter verification in the respective deletion background was validated for *yorB,* it could not uncover a DNA-binding protein that specifically binds to the 13 bp consensus sequence and controls *rpt* upregulation upon RNA stress. The DACA results left us with different options: *rpt* expression is not regulated by a TF, the regulating DNA-binding protein is dependent on a co-factor or not stable under our DACA conditions, or alternatively, paralogous TFs can fully compensate for the loss in a single knockout mutant.

Further investigation of P_{rpt} revealed a potential regulatory involvement of a previously annotated sRNA, called ncr1015/S708, that is located on the opposite DNA strand of P_{rpt} and partly overlaps with the 5'UTR of *rpt* (Irnov et al., 2010; Nicolas et al., 2012). Although a deletion or modification of the 13 conserved nucleotides of P_{rpt}, does not modify the sRNA itself, it likely interferes with its expression, as the 13 nucleotides, overlap with the -35 region of the complementary SigA binding site of ncr1015/S708 (Nicolas et al., 2012). The

existence of an additional SigA binding site on the complementary strand further explained the elevated LFQ intensities for SigA, RpoA, RpoB, and RpoC observed for fragment 1 compared to fragment 2 and 3 in the DACA. Interestingly, Nicolas and colleagues also identified a SigA binding site on the opposite DNA strand of P_{helD} (Nicolas et al., 2012), which again overlaps in its -35 region with the conserved 13 bp motif of P_{helD}. While no sRNA has been annotated complementary to P_{helD}, transcriptomic data might indicate slightly elevated transcript levels under some growth conditions (Nicolas et al., 2012; Zhu and Stülke, 2017). To investigate if the complementary transcription of an sRNA could be responsible for the selective regulation of *rpt* expression, a construct was generated that was unmodified in the 13 conserved nucleotides, leaving the -35 region of the SigA binding site of ncr1015/S708 intact, but modified in the -10 region of the SigA binding site of ncr1015/S708, thereby again impairing complementary sRNA expression. And indeed, this modification also led to the observed deregulation of induction specificity, that was previously detected upon deletion or modification of the 13 bp consensus motif. The result strongly supports transcriptional regulation of *rpt* expression by the complementary sRNA expression, a mechanism called *cis*-encoded asRNA regulation. Of note, all alterations of the *rpt* promoter region always affected both, the 5'UTR of *rpt* as well as (the expression of) the complementary sRNA ncr1015/S708. Therefore, a deletion or modification of the 13 bp consensus sequence of P_{rpt} or the modulation of the -10 region of the SigA binding site of ncr1015/S708 might not only influence the transcription of the *cis*-encoded asRNA, but also the structure and stability of the *rpt* preceding 5'UTR. However, different arguments speak against a regulation that is solely conferred by the structure and stability of the 5'UTR. First of all, microarray data shows that *rpt* transcript levels increased 100-fold after 10 min of rifampin treatment (Freiberg et al., 2006). If *rpt* mRNA levels would be solely upregulated due to a more stable mRNA conferred by the 5'UTR, this would mean that *rpt* mRNA is constantly expressed by one of the strongest SigA-dependent promoters (belonging to the M17 cluster of SigA binding sites) (Nicolas et al., 2012), while under unstressed growth conditions, *rpt* mRNA is not accessible for translation and/or quickly degraded. Nevertheless, it is questionable for mRNA stability to yield differences in mRNA levels of this dimension after 10 min of rifampin treatment, with general *B. subtilis* mRNA half-lives varying between 2-7 min, while more extreme half-lives of more than 2 min and less than 15 min have been detected in rare cases (Hambraeus et al., 2003). Furthermore, all 5'UTRs of the promoter deletion or modification constructs were analyzed *in silico* for their minimum free energy and their potential to form secondary structures in comparison to S707 (native 5'UTR of *rpt*) (Zuker, 2003). While it is difficult to predict the impact of such structural modifications (Hambraeus et al., 2003; Xiao et al.,

2020), only minor changes in minimum free energy and secondary structure between the different constructs could be observed. Although 5'UTR-mediated regulation of mRNA stability could not fully be excluded, the results hinted at a different mechanism controlling *rpt* induction specificity. Notably, all bioreporter constructs possessed the same ribosomal bindings site (RBS) located in equal distance to the translational start site of the respective reporter gene. Reports that postulate the enhanced stability of mRNAs containing stronger RBSs due to the better ribosomal binding can therefore not explain the observed differences in *rpt* transcript levels (Xiao et al., 2020).

Cis-encoded asRNA regulation is predominantly executed by four mechanisms: attenuation of translation, attenuation of transcription (transcription termination), alteration of target RNA stability, and/or transcriptional interference (Georg and Hess, 2011; Mars et al., 2016). In asRNA translation attenuation, the asRNA interacts with the target mRNA and influences translation by blocking its ribosomal accessibility (Brantl, 2007). As changes in gene expression were already observed for *rpt* mRNA levels (Freiberg et al., 2006), the likelihood of the translation attenuation mechanism to regulate *rpt* expression can rather be excluded, although not fully suspending the option of its involvement in regulatory fine-tuning. Attenuation of transcription by an asRNA was previously described to lead to premature transcription termination (Chai and Winans, 2005). The direct binding of the asRNA to its complementary mRNA target promotes the formation of an intrinsic terminator structure in the nascent mRNA that inhibits further transcription (Brantl, 2007; Giangrossi et al., 2010). Alteration of target mRNA stability can e.g., be achieved by asRNA-mediated regulation of nuclease accessibility (Brantl, 2007; Stazic et al., 2011). Interestingly, upon depletion of the major and essential 5'-3' exoribonuclease RNase J1 (RnjA), Durand and colleagues could detect 10-fold and 2-fold enhanced abundance of *helD* and *rpt* mRNA, respectively (Durand et al., 2012). Hence, RnjA might participate in degradation of the mRNAs of *rpt* and *helD* or their potential regulatory asRNAs. However, upregulated mRNA levels of *rpt* and *helD* upon RnjA depletion could also be explained by RnjAs ability to resolve stalled RNAP complexes upon collision (Šiková et al., 2020), a mechanism that might also affect the potential *rpt* and *helD* inducing stress response (compare chapter 3.2.3.). Of note, a depletion of RNase Y and III, two further essential ribonucleases of *B. subtilis* weakly affect *helD* (approximately 2-fold increase in abundance) but not *rpt* mRNA levels, while ncr1015/S708 sRNA abundance stayed unchanged upon depletion of any of the three ribonucleases (Durand et al., 2012). Transcriptional interference describes the mutual impairment of gene expression by the sense mRNA and the *cis*-encoded asRNA, e.g., by RNAP collision or promoter occlusion due to steric hindrance of complementarily bound RNAP (Bordoy and Chatterjee,

2015; Brophy and Voigt, 2016). Until now, with the exception of translation attenuation, none of the above mentioned *cis*-encoded asRNA regulation mechanisms can be excluded with certainty, while it further remains elusive if the strong *rpt* upregulation upon RNA stress could potentially be conferred collectively by combined regulation of those mechanisms. A study of Giangrossi and colleagues investigated the gene regulation of *icsA*, a virulence gene of *Shigella flexneri* that facilitates the invasion of intestine epithelial cells crucial for host colonization. They could show that expression of *icsA* is regulated by transcriptional interference upon strong, complementary expression of the *cis*-encoded asRNA RnaG. In addition, RnaG can directly repress *icsA* transcription by hetero-duplex formation with the nascent mRNA of the invasion protein, thereby promoting premature transcription termination (transcription attenuation mechanism) (Giangrossi et al., 2010). The data on the regulation of *rpt* and *helD* expression in *B. subtilis*, that has been gathered in this thesis, would perfectly fit a similar kind of gene regulation mechanism.

In a recent experiment, we tried to complement ncr1015/S708 in *trans* (*aprE* locus) to compensate for the loss of ncr1015/S708 sRNA expression upon deletion or modification of the 13 conserved nucleotides, which we suspect to regulate *rpt* transcription. Nevertheless, complementation in *trans* did not recover induction specificity of $P_{rpt\_Del14bpDS}$-*lacZ* (data not shown). However, *cis*-encoded regulation is often very dependent on high asRNA concentrations that are located in close vicinity to their complementary expressed target mRNAs (Saberi et al., 2016). Therefore, a ncr1015/S708 complementation in *trans* might not yield asRNAs that are sufficiently stable or concentrated high enough to influence *rpt* regulation. Furthermore, an asRNA mechanism by transcriptional interference could impossibly be complemented by ncr1015/S708 expression in *trans.*

3.2.5. Conservation of *rpt* regulation in other Bacillales

B. subtilis Rpt homologs could be identified in several Actinomycetales, Bacillales, Clostridiales, and Myxococcales. In actinomycetes, *rpt* (called *rph*) gene expression is dependent on the RAE, that was also shown to be present in different promoter regions of other rifampin inactivating enzymes like monooxygenases or glycosyltransferases (Spanogiannopoulos et al., 2014). Looking at different promoter regions of the *rpt* homologs, we could also identify minor variations of the RAE motif in some Myxococcales, indicating that the RAE is more broadly distributed than previously suspected (Spanogiannopoulos et al., 2014). However, it remains elusive if the modified RAEs in Myxococcales actually regulate rifampin-associated expression of their *rpt* homologs or if they are just a remnant of horizontal gene transfer upon acquisition of the resistance gene. All other investigated

strains were devoid of the RAE, leaving the question of their way of *rpt* gene regulation unanswered. As previous results of this thesis indicated that in *B. subtilis*, *rpt* and *helD* gene expression was dependent on 13 conserved nucleotides (compare chapter 3.2.4.), the promoter regions of the different bacteria were investigated for this motif. Interestingly, we could detect the motif (or slight variations of it) for a subgroup of different Bacillales strains. In those strains, *rpt* was located at disperse chromosomal positions and flanked by a variety of different genes. However, an alignment of the respective preceding promoter regions of this subset of strains uncovered a conserved promoter sequence of approximately 200 bp, that contained all regulatory elements previously shown to be important for selective *rpt* expression: the SigA binding site and RBS of P_{rpt} as well as the SigA binding site on the complementary strand (compare chapter 3.2.4.). Interestingly, transcriptomic data of *B. licheniformis* also revealed the expression of a *rpt* 5'UTR and a complementarily transcribed sRNA (Wiegand et al., 2013). In *B. subtilis* 168, *rpt* was proposed to be acquired by horizontal gene transfer, as it is located in the *P6* prophage-like region (Kunst et al., 1997; Rocha et al., 1999). The broad distribution and integration of *rpt* at different genomic positions in different species supports this hypothesis, while the conservation of the promoter region in a subset of different Bacillales shows that they also maintained a similar way of *rpt* regulation. However, it remains elusive if the *rpt* homologs combined with the 200 bp promoter region were (solely) acquired by a transduction mechanism. Studies in *B. thuringiensis* BMB171 did not map the *rpt* homolog to a putative prophage region (Fu et al., 2019), indicating that it must be obtained by other horizontal gene transfer mechanisms like transformation or conjugation (Douglas and Langille, 2019). Within Bacillaceae, development of natural competence is described for *B. subtilis* and some closely related *B. licheniformis* and *B. amyloliquefaciens* strains (Dubnau, 1991; Koumoutsi et al., 2004; Jakobs et al., 2014). However, the ability to take up functional DNA from the environment is discussed to be widespread among Bacilli (Mirończuk et al., 2008; Kovács et al., 2009), making a transformation mechanism responsible for *rpt* gene transfer appear likely.

REFERENCES

Adebali, O., Chiou, Y.-Y., Hu, J., Sancar, A., and Selby, C. P. (2017). Genome-wide transcription-coupled repair in *Escherichia coli* is mediated by the Mfd translocase. Proceedings of the National Academy of Sciences 114, E2116.

Alm, R. A., and Lahiri, S. D. (2020). Narrow-spectrum antibacterial agents-benefits and challenges. Antibiotics (Basel, Switzerland) 9, 418.

Arnaouteli, S., Bamford, N. C., Stanley-Wall, N. R., and Kovács, Á. T. (2021). *Bacillus subtilis* biofilm formation and social interactions. Nature Reviews Microbiology.

Artsimovitch, I., Seddon, J., and Sears, P. (2012). Fidaxomicin is an inhibitor of the initiation of bacterial RNA synthesis. Clinical Infectious Diseases 55 Suppl 2, S127-S131.

Aslam, B., Wang, W., Arshad, M. I., Khurshid, M., Muzammil, S., Rasool, M. H., Nisar, M. A., Alvi, R. F., Aslam, M. A., Qamar, M. U., et al. (2018). Antibiotic resistance: a rundown of a global crisis. Infection and drug resistance 11, 1645-1658.

Au, N., Kuester-Schoeck, E., Mandava, V., Bothwell, L. E., Canny, S. P., Chachu, K., Colavito, S. A., Fuller, S. N., Groban, E. S., Hensley, L. A., et al. (2005). Genetic composition of the *Bacillus subtilis* SOS system. Journal of Bacteriology 187, 7655-7666.

Aviner, R. (2020). The science of puromycin: From studies of ribosome function to applications in biotechnology. Computational and Structural Biotechnology Journal 18, 1074-1083.

Ayala, F. R., Bartolini, M., and Grau, R. (2020). The stress-responsive alternative sigma factor SigB of *Bacillus subtilis* and its relatives: An old friend with new functions. Frontiers in Microbiology 11.

Ayora, S., Rojo, F., Ogasawara, N., Nakai, S., and Alonso, J. C. (1996). The Mfd protein of *Bacillus subtilis*168 is involved in both transcription-coupled DNA repair and DNA recombination. Journal of Molecular Biology 256, 301-318.

Bandow, J. E., Brötz, H., Leichert, L. I. O., Labischinski, H., and Hecker, M. (2003). Proteomic approach to understanding antibiotic action. Antimicrobial Agents and Chemotherapy 47, 948-955.

Basarab, G. S., Doig, P., Galullo, V., Kern, G., Kimzey, A., Kutschke, A., Newman, J. P., Morningstar, M., Mueller, J., Otterson, L., et al. (2015a). Discovery of novel DNA gyrase inhibiting spiropyrimidinetriones: Benzisoxazole fusion with N-linked oxazolidinone substituents leading to a clinical candidate (ETX0914). Journal of Medicinal Chemistry 58, 6264-6282.

Basarab, G. S., Kern, G. H., Mcnulty, J., Mueller, J. P., Lawrence, K., Vishwanathan, K., Alm, R. A., Barvian, K., Doig, P., Galullo, V., et al. (2015b). Responding to the challenge of untreatable gonorrhea: ETX0914, a first-in-class agent with a distinct mechanism-of-action against bacterial Type II topoisomerases. Scientific reports 5, 11827-11827.

Bassetti, M., Merelli, M., Temperoni, C., and Astilean, A. (2013). New antibiotics for bad bugs: where are we? Annals of clinical microbiology and antimicrobials 12, 22-22.

Bechhofer, D. H., and Dubnau, D. (1987). Induced mRNA stability in *Bacillus subtilis*. Proceedings of the National Academy of Sciences 84, 498.

Bekiesch, P., Franz-Wachtel, M., Kulik, A., Brocker, M., Forchhammer, K., Gust, B., and Apel, A. K. (2016). DNA affinity capturing identifies new regulators of the heterologously expressed novobiocin gene cluster in *Streptomyces coelicolor* M512. Applied Microbiology and Biotechnology 100, 4495-509.

Belogurov, G. A., Vassylyeva, M. N., Sevostyanova, A., Appleman, J. R., Xiang, A. X., Lira, R., Webber, S. E., Klyuyev, S., Nudler, E., Artsimovitch, I., et al. (2009).

Transcription inactivation through local refolding of the RNA polymerase structure. Nature 457, 332-335.
Bérdy, J. (2012). Thoughts and facts about antibiotics: Where we are now and where we are heading. The Journal of Antibiotics 65, 385-395.
Bervoets, I., and Charlier, D. (2019). Diversity, versatility and complexity of bacterial gene regulation mechanisms: opportunities and drawbacks for applications in synthetic biology. FEMS Microbiology Reviews 43, 304-339.
Bhaduri, S., Ranjan, N., and Arya, D. P. (2018). An overview of recent advances in duplex DNA recognition by small molecules. Beilstein Journal of Organic Chemistry 14, 1051-1086.
Bode, H. B., Bethe, B., Höfs, R., and Zeeck, A. (2002). Big effects from small changes: possible ways to explore nature's chemical diversity. ChemBioChem 3, 619-27.
Bordoy, A. E., and Chatterjee, A. (2015). *Cis*-antisense transcription gives rise to tunable genetic switch behavior: a mathematical modeling approach. PLOS ONE 10, e0133873.
Borg, A., Holm, M., Shiroyama, I., Hauryliuk, V., Pavlov, M., Sanyal, S., and Ehrenberg, M. (2015). Fusidic acid targets elongation factor G in several stages of translocation on the bacterial ribosome. The Journal of biological chemistry 290, 3440-3454.
Borovinskaya, M. A., Shoji, S., Fredrick, K., and Cate, J. H. D. (2008). Structural basis for hygromycin B inhibition of protein biosynthesis. RNA (New York) 14, 1590-1599.
Borovinskaya, M. A., Shoji, S., Holton, J. M., Fredrick, K., and Cate, J. H. D. (2007). A steric block in translation caused by the antibiotic spectinomycin. ACS Chemical Biology 2, 545-552.
Brandish, P. E., Kimura, K. I., Inukai, M., Southgate, R., Lonsdale, J. T., and Bugg, T. D. (1996). Modes of action of tunicamycin, liposidomycin B, and mureidomycin A: inhibition of phospho-N-acetylmuramyl-pentapeptide translocase from *Escherichia coli*. Antimicrobial Agents and Chemotherapy 40, 1640-1644.
Brantl, S. (2007). Regulatory mechanisms employed by *cis*-encoded antisense RNAs. Current Opinion in Microbiology 10, 102-109.
Brennan, R. G., and Matthews, B. W. (1989). The helix-turn-helix DNA binding motif. Journal of Biological Chemistry 264, 1903-6.
Brito, P. H., Chevreux, B., Serra, C. R., Schyns, G., Henriques, A. O., and Pereira-Leal, J. B. (2018). Genetic competence drives genome diversity in *Bacillus subtilis*. Genome Biology and Evolution 10, 108-124.
Britton, R. A., Eichenberger, P., Gonzalez-Pastor, J. E., Fawcett, P., Monson, R., Losick, R., and Grossman, A. D. (2002). Genome-wide analysis of the stationary-phase sigma factor (sigma-H) regulon of *Bacillus subtilis*. Journal of Bacteriology 184, 4881-4890.
Brodersen, D. E., Clemons, W. M., Carter, A. P., Morgan-Warren, R. J., Wimberly, B. T., and Ramakrishnan, V. (2000). The structural basis for the action of the antibiotics tetracycline, pactamycin, and hygromycin B on the 30S ribosomal subunit. Cell 103, 1143-1154.
Brophy, J. A., and Voigt, C. A. (2016). Antisense transcription as a tool to tune gene expression. Molecular Systems Biology 12, 854.
Brötz-Oesterhelt, H., Beyer, D., Kroll, H.-P., Endermann, R., Ladel, C., Schroeder, W., Hinzen, B., Raddatz, S., Paulsen, H., Henninger, K., et al. (2005). Dysregulation of bacterial proteolytic machinery by a new class of antibiotics. Nature Medicine 11, 1082-1087.
Brötz-Oesterhelt, H., and Sass, P. (2010). Postgenomic strategies in antibacterial drug discovery. Future Microbiology 5, 1553-1579.

Brötz, H., Josten, M., Wiedemann, I., Schneider, U., Götz, F., Bierbaum, G., and Sahl, H.-G. (1998). Role of lipid-bound peptidoglycan precursors in the formation of pores by nisin, epidermin and other lantibiotics. Molecular Microbiology 30, 317-327.
Bush, K., Courvalin, P., Dantas, G., Davies, J., Eisenstein, B., Huovinen, P., Jacoby, G. A., Kishony, R., Kreiswirth, B. N., Kutter, E., et al. (2011). Tackling antibiotic resistance. Nature Reviews Microbiology 9, 894-896.
Bush, K., and Pucci, M. J. (2011). New antimicrobial agents on the horizon. Biochemical Pharmacology 82, 1528-1539.
Campbell, E. A., Korzheva, N., Mustaev, A., Murakami, K., Nair, S., Goldfarb, A., and Darst, S. A. (2001). Structural mechanism for rifampicin inhibition of bacterial RNA polymerase. Cell 104, 901-912.
Campbell, E. A., Pavlova, O., Zenkin, N., Leon, F., Irschik, H., Jansen, R., Severinov, K., and Darst, S. A. (2005). Structural, functional, and genetic analysis of sorangicin inhibition of bacterial RNA polymerase. The EMBO Journal 24, 674-682.
Carrano, L., and Marinelli, F. (2015). The relevance of chemical dereplication in microbial natural product screening. Journal of Applied Bioanalysis 1, 55-67.
Centers for Disease Control and Prevention (2013). Antibiotic resistance threats in the United States (Georgia (U.S.): U.S. Department of Health and Human Services.)
Centers for Disease Control and Prevention. 2020. *About Antibiotic Resistance* [Online]. Available: https://www.cdc.gov/drugresistance/about.html [Accessed: 8 March 2021].
Chai, Y., and Winans, S. C. (2005). A small antisense RNA downregulates expression of an essential replicase protein of an *Agrobacterium tumefaciens* Ti plasmid. Molecular Microbiology 56, 1574-85.
Chan, A. N., Shiver, A. L., Wever, W. J., Razvi, S. Z. A., Traxler, M. F., and Li, B. (2017). Role for dithiolopyrrolones in disrupting bacterial metal homeostasis. Proceedings of the National Academy of Sciences 114, 2717.
Choi, U., and Lee, C.-R. (2019). Antimicrobial agents that inhibit the outer membrane assembly machines of Gram-negative bacteria. Journal of Microbiology and Biotechnology 29, 1-10.
Chopra, I., Hawkey, P. M., and Hinton, M. (1992). Tetracyclines, molecular and clinical aspects. Journal of Antimicrobial Chemotherapy 29, 245-277.
Clatworthy, A. E., Pierson, E., and Hung, D. T. (2007). Targeting virulence: a new paradigm for antimicrobial therapy. Nature Chemical Biology 3, 541-548.
Cohen, S. S., Flaks, J. G., Barner, H. D., Loeb, M. R., and Lichtenstein, J. (1958). The mode of action of 5-fluorouracil and its derivatives. Proceedings of the National Academy of Sciences 44, 1004-1012.
Cudic, P., Kranz, J. K., Behenna, D. C., Kruger, R. G., Tadesse, H., Wand, A. J., Veklich, Y. I., Weisel, J. W., and Mccafferty, D. G. (2002). Complexation of peptidoglycan intermediates by the lipoglycodepsipeptide antibiotic ramoplanin: Minimal structural requirements for intermolecular complexation and fibril formation. Proceedings of the National Academy of Sciences 99, 7384.
Culp, E. J., Yim, G., Waglechner, N., Wang, W., Pawlowski, A. C., and Wright, G. D. (2019). Hidden antibiotics in actinomycetes can be identified by inactivation of gene clusters for common antibiotics. Nature Biotechnology 37, 1149-1154.
Dambach, M., Irnov, I., and Winkler, W. C. (2013). Association of RNAs with *Bacillus subtilis* Hfq. PLOS ONE 8, e55156.
Dapa, T., Fleurier, S., Bredeche, M.-F., and Matic, I. (2017). The SOS and RpoS regulons contribute to bacterial cell robustness to genotoxic stress by synergistically regulating DNA polymerase Pol II. Genetics 206, 1349-1360.
Davies, J., and Davies, D. (2010). Origins and evolution of antibiotic resistance. Microbiology and Molecular Biology Reviews 74, 417-433.

Davis, B. D., Chen, L. L., and Tai, P. C. (1986). Misread protein creates membrane channels: an essential step in the bactericidal action of aminoglycosides. Proceedings of the National Academy of Sciences 83, 6164-6168.
De Hoon, M. J. L., Eichenberger, P., and Vitkup, D. (2010). Hierarchical evolution of the bacterial sporulation network. Current Biology 20, R735-R745.
Doherty, G. P., Meredith, D. H., and Lewis, P. J. (2006). Subcellular partitioning of transcription factors in *Bacillus subtilis*. Journal of Bacteriology 188, 4101-4110.
Douglas, G. M., and Langille, M. G. I. (2019). Current and promising approaches to identify horizontal gene transfer events in metagenomes. Genome Biology and Evolution 11, 2750-2766.
Druzhinin, S. Y., Tran, N. T., Skalenko, K. S., Goldman, S. R., Knoblauch, J. G., Dove, S. L., and Nickels, B. E. (2015). A conserved pattern of primer-dependent transcription initiation in *Escherichia coli* and *Vibrio cholerae* revealed by 5' RNA-seq. PLOS Genetics 11, e1005348.
Du Toit, A. (2014). Promoter melting by alternative sigma factors. Nature Reviews Microbiology 12, 235-235.
Dubnau, D. (1991). Genetic competence in *Bacillus subtilis*. Microbiological reviews 55, 395-424.
Durand, S., Gilet, L., Bessières, P., Nicolas, P., and Condon, C. (2012). Three essential ribonucleases-RNase Y, J1, and III-control the abundance of a majority of *Bacillus subtilis* mRNAs. PLOS Genetics 8, e1002520-e1002520.
Dwyer, D. J., Kohanski, M. A., Hayete, B., and Collins, J. J. (2007). Gyrase inhibitors induce an oxidative damage cellular death pathway in *Escherichia coli*. Molecular systems biology 3, 91-91.
Eagle, H. (1954). The multiple mechanisms of penicillin resistance. Journal of Bacteriology 68, 610-616.
Economou, N. J., Cocklin, S., and Loll, P. J. (2013). High-resolution crystal structure reveals molecular details of target recognition by bacitracin. Proceedings of the National Academy of Sciences 110, 14207.
Eiamphungporn, W., and Helmann, J. D. (2008). The *Bacillus subtilis* sigma(M) regulon and its contribution to cell envelope stress responses. Molecular microbiology 67, 830-848.
Elsholz, A. K. W., Birk, M. S., Charpentier, E., and Turgay, K. (2017). Functional diversity of AAA+ protease complexes in *Bacillus subtilis*. Frontiers in Molecular Biosciences 4.
Epand, R. M., Walker, C., Epand, R. F., and Magarvey, N. A. (2016). Molecular mechanisms of membrane targeting antibiotics. Biochimica Biophysica Acta - Biomembranes 1858, 980-987.
Erb, I., González-Vallinas, J. R., Bussotti, G., Blanco, E., Eyras, E., and Notredame, C. (2012). Use of ChIP-Seq data for the design of a multiple promoter-alignment method. Nucleic Acids Research 40, e52-e52.
Errington, J. (2003). Regulation of endospore formation in *Bacillus subtilis*. Nature Reviews Microbiology 1, 117-126.
Fabret, C., Feher, V. A., and Hoch, J. A. (1999). Two-component signal transduction in *Bacillus subtilis*: how one organism sees its world. Journal of Bacteriology 181, 1975-1983.
Field, D., Seisling, N., Cotter, P. D., Ross, R. P., and Hill, C. (2016). Synergistic nisin-polymyxin combinations for the control of pseudomonas biofilm formation. Frontiers in Microbiology 7, 1713-1713.
Fischer, H. P., Brunner, N. A., Wieland, B., Paquette, J., Macko, L., Ziegelbauer, K., and Freiberg, C. (2004). Identification of antibiotic stress-inducible promoters: a

systematic approach to novel pathway-specific reporter assays for antibacterial drug discovery. Genome Research 14, 90-98.
Floss, H. G., and Yu, T.-W. (2005). Rifamycin-Mode of action, resistance, and biosynthesis. Chemical Reviews 105, 621-632.
Fornelos, N., Browning, D. F., Pavlin, A., Podlesek, Z., Hodnik, V., Salas, M., and Butala, M. (2018). Lytic gene expression in the temperate bacteriophage GIL01 is activated by a phage-encoded LexA homologue. Nucleic Acids Research 46, 9432-9443.
Foster, B. J., Clagett-Carr, K., Shoemaker, D. D., Suffness, M., Plowman, J., Trissel, L. A., Grieshaber, C. K., and Leyland-Jones, B. (1985). Echinomycin: the first bifunctional intercalating agent in clinical trials. Investigational New Drugs 3, 403-10.
Fournier, B., Zhao, X., Lu, T., Drlica, K., and Hooper, D. C. (2000). Selective targeting of topoisomerase IV and DNA gyrase in *Staphylococcus aureus*: different patterns of quinolone-induced inhibition of DNA synthesis. Antimicrobial Agents and Chemotherapy 44, 2160-2165.
Freiberg, C., Brunner, N., Macko, L., and Fischer, H. P. (2006). Discovering antibiotics efficacy biomarkers: towards mechanism-specific high-content compound screening. Molecular and Cellular Proteomics.
Frieri, M., Kumar, K., and Boutin, A. (2017). Antibiotic resistance. Journal of Infection and Public Health 10, 369-378.
Fu, Y., Wu, Y., Yuan, Y., and Gao, M. (2019). Prevalence and diversity analysis of candidate prophages to provide an understanding on their roles in *Bacillus thuringiensis*. Viruses 11, 388.
Funabashi, H., Kawaguchi, A., Tomoda, H., Omura, S., Okuda, S., and Iwasaki, S. (1989). Binding site of cerulenin in fatty acid synthetase. Journal of Biochemistry 105, 751-5.
Gaballa, A., Guariglia-Oropeza, V., Dürr, F., Butcher, B. G., Chen, A. Y., Chandrangsu, P., and Helmann, J. D. (2017). Modulation of extracytoplasmic function (ECF) sigma factor promoter selectivity by spacer region sequence. Nucleic Acids Research 46, 134-145.
Gale, F. G., Cundliffe, E., Reynolds, P. E., Richmond, M. H., and Waring, M. J. (1981). The Molecular Basis of Antibiotic Action (London: John Wiley and Sons.
Gause, G. G., Jr., Loshkareva, N. P., and Zbarsky, I. B. (1968). Effect of olivomycin and echinomycin on initiation and growth of RNA chains catalyzed by RNA polymerase. Biochimica Biophysica Acta 166, 752-4.
Genilloud, O. (2017). Actinomycetes: still a source of novel antibiotics. Natural Product Reports 34, 1203-1232.
Georg, J., and Hess, W. R. (2011). *Cis*-antisense RNA, another level of gene regulation in bacteria. Microbiology and Molecular Biology Reviews 75, 286-300.
Giangrossi, M., Prosseda, G., Tran, C. N., Brandi, A., Colonna, B., and Falconi, M. (2010). A novel antisense RNA regulates at transcriptional level the virulence gene icsA of *Shigella flexneri*. Nucleic Acids Research 38, 3362-3375.
Giedroc, D. P. (2009). Hydrogen peroxide sensing in *Bacillus subtilis*: it is all about the (metallo)regulator. Molecular Microbiology 73, 1-4.
Godzieba, M., and Ciesielski, S. (2020). Natural DNA intercalators as promising therapeutics for cancer and infectious diseases. Current Cancer Drug Targets 20, 19-32.
Goldman, S. R., Sharp, J. S., Vvedenskaya, I. O., Livny, J., Dove, S. L., and Nickels, B. E. (2011). NanoRNAs prime transcription initiation *in vivo*. Molecular Cell 42, 817-825.
González-Pastor, J. E. (2011). Cannibalism: a social behavior in sporulating *Bacillus subtilis*. FEMS Microbiology Reviews 35, 415-24.
Grein, F., Müller, A., Scherer, K. M., Liu, X., Ludwig, K. C., Klöckner, A., Strach, M., Sahl, H.-G., Kubitscheck, U., and Schneider, T. (2020). Ca^{2+}-Daptomycin targets cell wall

biosynthesis by forming a tripartite complex with undecaprenyl-coupled intermediates and membrane lipids. Nature Communications 11, 1455.
Hambraeus, G., Von Wachenfeldt, C., and Hederstedt, L. (2003). Genome-wide survey of mRNA half-lives in *Bacillus subtilis* identifies extremely stable mRNAs. Molecular Genetics and Genomics 269, 706-714.
Hancock, R. E. (1997). The bacterial outer membrane as a drug barrier. Trends in Microbiology 5, 37-42.
Hart, E. M., Mitchell, A. M., Konovalova, A., Grabowicz, M., Sheng, J., Han, X., Rodriguez-Rivera, F. P., Schwaid, A. G., Malinverni, J. C., Balibar, C. J., et al. (2019). A small-molecule inhibitor of BamA impervious to efflux and the outer membrane permeability barrier. Proceedings of the National Academy of Sciences 116, 21748.
Härtl, B., Wehrl, W., Wiegert, T., Homuth, G., and Schumann, W. (2001). Development of a new integration site within the *Bacillus subtilis* chromosome and construction of compatible expression cassettes. Journal of Bacteriology 183, 2696-2699.
Harvey, A. M., Batt, R. D., and Prichard, G. G. (1976). Inhibition of RNA synthesis in *Chlorella pyrenoidos*a and *Bacillus megaterium* by the pine-blight toxin, Dothistromin. Microbiology 95, 268-276.
Heath, R. J., and Rock, C. O. (2004). Fatty acid biosynthesis as a target for novel antibacterials. Current Opinion in Investigational Drugs 5, 146-153.
Heath, R. J., Rubin, J. R., Holland, D. R., Zhang, E., Snow, M. E., and Rock, C. O. (1999). Mechanism of triclosan inhibition of bacterial fatty acid synthesis. Journal of Biological Chemistry 274, 11110-4.
Hecker, M., Pané-Farré, J., and Völker, U. (2007). SigB-dependent general stress response in *Bacillus subtilis* and related gram-positive bacteria. Annual Review of Microbiology 61, 215-36.
Hecker, M., Schumann, W., and Völker, U. (1996). Heat-shock and general stress response in *Bacillus subtilis*. Molecular Microbiology 19, 417-428.
Helmann, J. D. (2016). *Bacillus subtilis* extracytoplasmic function (ECF) sigma factors and defense of the cell envelope. Current Opinion in Microbiology 30, 122-132.
Helmann, J. D., and Moran, C. P. J. 2001. RNA Polymerase and Sigma Factors. *Bacillus subtilis* and Its Closest Relatives.
Henderson, K. L., Felth, L. C., Molzahn, C. M., Shkel, I., Wang, S., Chhabra, M., Ruff, E. F., Bieter, L., Kraft, J. E., and Record, M. T. (2017). Mechanism of transcription initiation and promoter escape by *E. coli* RNA polymerase. Proceedings of the National Academy of Sciences 114, E3032.
Higgins, D., and Dworkin, J. (2012). Recent progress in *Bacillus subtilis* sporulation. FEMS Microbiology Reviews 36, 131-148.
Hirooka, K., Kunikane, S., Matsuoka, H., Yoshida, K.-I., Kumamoto, K., Tojo, S., and Fujita, Y. (2007). Dual regulation of the *Bacillus subtilis* regulon comprising the *lmrAB* and *yxaGH* operons and *yxaF* gene by two transcriptional repressors, LmrA and YxaF, in response to flavonoids. Journal of bacteriology 189, 5170-5182.
Ho, M. X., Hudson, B. P., Das, K., Arnold, E., and Ebright, R. H. (2009). Structures of RNA polymerase-antibiotic complexes. Current Opinion in Structural Biology 19, 715-723.
Hoch, J. A. (2017). A life in *Bacillus subtilis* signal transduction. Annual Review of Microbiology 71, 1-19.
Hollstein, U. (1974). Actinomycin. Chemistry and mechanism of action. Chemical Reviews 74, 625-652.
Hong, Y., Zeng, J., Wang, X., Drlica, K., and Zhao, X. (2019). Post-stress bacterial cell death mediated by reactive oxygen species. Proceedings of the National Academy of Sciences 116, 10064.

Huang, C. H., Prestayko, A. W., and Crooke, S. T. (1982). Bifunctional intercalation of antitumor antibiotics BBM-928A and echinomycin with deoxyribonucleic acid. Effects of intercalation on deoxyribonucleic acid degradative activity of bleomycin and phleomycin. Biochemistry 21, 3704-10.
Huang, X., Lopez De Saro, F. J., and Helmann, J. D. (1997). Sigma factor mutations affecting the sequence-selective interaction of RNA polymerase with -10 region single-stranded DNA. Nucleic Acids Research 25, 2603-2609.
Hutchings, M. I., Truman, A. W., and Wilkinson, B. (2019). Antibiotics: past, present and future. Current Opinion in Microbiology 51, 72-80.
Hutter, B., Fischer, C., Jacobi, A., Schaab, C., and Loferer, H. (2004). Panel of *Bacillus subtilis* reporter strains indicative of various modes of action. Antimicrobial Agents and Chemotherapy 48, 2588-2594.
Irnov, I., Sharma, C. M., Vogel, J., and Winkler, W. C. (2010). Identification of regulatory RNAs in *Bacillus subtilis*. Nucleic Acids Research 38, 6637-6651.
Jakobs, M., Hoffmann, K., Grabke, A., Neuber, S., Liesegang, H., Volland, S., and Meinhardt, F. (2014). Unravelling the genetic basis for competence development of auxotrophic *Bacillus licheniformis* 9945A strains. Microbiology 160, 2136-2147.
Jervis, A. J., Thackray, P. D., Houston, C. W., Horsburgh, M. J., and Moir, A. (2007). SigM-responsive genes of *Bacillus subtilis* and their promoters. Journal of Bacteriology 189, 4534-4538.
Johnson, J. W., Fisher, J. F., and Mobashery, S. (2013). Bacterial cell-wall recycling. Annals of the New York Academy of Sciences 1277, 54-75.
Johnston, C. W., Skinnider, M. A., Dejong, C. A., Rees, P. N., Chen, G. M., Walker, C. G., French, S., Brown, E. D., Bérdy, J., Liu, D. Y., et al. (2016). Assembly and clustering of natural antibiotics guides target identification. Nature Chemical Biology 12, 233-239.
Jordan, S., Junker, A., Helmann, J. D., and Mascher, T. (2006). Regulation of LiaRS-dependent gene expression in *Bacillus subtilis*: identification of inhibitor proteins, regulator binding sites, and target genes of a conserved cell envelope stress-sensing two-component system. Journal of Bacteriology 188, 5153-5166.
Juhas, M., and Ajioka, J. W. (2016). Integrative bacterial artificial chromosomes for DNA integration into the *Bacillus subtilis* chromosome. Journal of Microbiological Methods 125, 1-7.
Kalamara, M., Spacapan, M., Mandic-Mulec, I., and Stanley-Wall, N. R. (2018). Social behaviours by *Bacillus subtilis*: quorum sensing, kin discrimination and beyond. Molecular Microbiology 110, 863-878.
Kanehisa, M., and Goto, S. (2000). KEGG: kyoto encyclopedia of genes and genomes. Nucleic Acids Research 28, 27-30.
Kevin Ii, D. A., Meujo, D. A., and Hamann, M. T. (2009). Polyether ionophores: broad-spectrum and promising biologically active molecules for the control of drug-resistant bacteria and parasites. Expert Opinion on Drug Discovery 4, 109-146.
Khan, T., Sankhe, K., Suvarna, V., Sherje, A., Patel, K., and Dravyakar, B. (2018). DNA gyrase inhibitors: progress and synthesis of potent compounds as antibacterial agents. Biomedicine and Pharmacotherapy 103, 923-938.
Khoshnood, S., Heidary, M., Asadi, A., Soleimani, S., Motahar, M., Savari, M., Saki, M., and Abdi, M. (2019). A review on mechanism of action, resistance, synergism, and clinical implications of mupirocin against *Staphylococcus aureus*. Biomedicine and Pharmacotherapy 109, 1809-1818.
Kindrachuk, K. N., Fernández, L., Bains, M., and Hancock, R. E. W. (2011). Involvement of an ATP-dependent protease, PA0779/AsrA, in inducing heat shock in response to tobramycin in *Pseudomonas aeruginosa*. Antimicrobial agents and chemotherapy 55, 1874-1882.

Kirstein, J., Hoffmann, A., Lilie, H., Schmidt, R., Rübsamen-Waigmann, H., Brötz-Oesterhelt, H., Mogk, A., and Turgay, K. (2009). The antibiotic ADEP reprogrammes ClpP, switching it from a regulated to an uncontrolled protease. EMBO Molecular Medicine 1, 37-49.
Kisker, C., Kuper, J., and Van Houten, B. (2013). Prokaryotic nucleotide excision repair. Cold Spring Harbor Perspectives in Biology 5, a012591-a012591.
Koumoutsi, A., Chen, X.-H., Henne, A., Liesegang, H., Hitzeroth, G., Franke, P., Vater, J., and Borriss, R. (2004). Structural and functional characterization of gene clusters directing nonribosomal synthesis of bioactive cyclic lipopeptides in *Bacillus amyloliquefaciens* strain FZB42. Journal of bacteriology 186, 1084-1096.
Kovács, A. T., Smits, W. K., Mirończuk, A. M., and Kuipers, O. P. (2009). Ubiquitous late competence genes in *Bacillus species* indicate the presence of functional DNA uptake machineries. Environ Microbiol 11, 1911-22.
Kraemer, S. A., Ramachandran, A., and Perron, G. G. (2019). Antibiotic pollution in the environment: from microbial ecology to public policy. Microorganisms 7, 180.
Krause, K. M., Serio, A. W., Kane, T. R., and Connolly, L. E. (2016). Aminoglycosides: an overview. Cold Spring Harbor Perspectives in Medicine 6, a027029.
Kuklin, N. A., Pancari, G. D., Tobery, T. W., Cope, L., Jackson, J., Gill, C., Overbye, K., Francis, K. P., Yu, J., Montgomery, D., et al. (2003). Real-time monitoring of bacterial infection *in vivo*: development of bioluminescent staphylococcal foreign-body and deep-thigh-wound mouse infection models. Antimicrobial agents and chemotherapy 47, 2740-2748.
Kumar, P., Kizhakkedathu, J. N., and Straus, S. K. (2018). Antimicrobial peptides: diversity, mechanism of action and strategies to improve the activity and biocompatibility *in vivo*. Biomolecules 8, 4.
Kunst, F., Ogasawara, N., Moszer, I., Albertini, A. M., Alloni, G., Azevedo, V., Bertero, M. G., Bessières, P., Bolotin, A., Borchert, S., et al. (1997). The complete genome sequence of the Gram-positive bacterium *Bacillus subtilis*. Nature 390, 249-256.
La Rosa, S. L., Diep, D. B., Nes, I. F., and Brede, D. A. (2012). Construction and application of a *luxABCDE* reporter system for real-time monitoring of *Enterococcus faecalis* gene expression and growth. Applied and Environmental Microbiology 78, 7003-7011.
Lambert, M. P., and Neuhaus, F. C. (1972). Mechanism of D-cycloserine action: alanine racemase from *Escherichia coli* W. Journal of Bacteriology 110, 978.
Landers, T. F., Cohen, B., Wittum, T. E., and Larson, E. L. (2012). A review of antibiotic use in food animals: perspective, policy, and potential. Public health reports (Washington, D.C. : 1974) 127, 4-22.
Laws, M., Shaaban, A., and Rahman, K. M. (2019). Antibiotic resistance breakers: current approaches and future directions. FEMS Microbiology Reviews 43, 490-516.
Lenhart, J. S., Schroeder, J. W., Walsh, B. W., and Simmons, L. A. (2012). DNA repair and genome maintenance in *Bacillus subtilis*. Microbiology and Molecular Biology Reviews 76, 530-564.
Leyva-Sánchez, H. C., Villegas-Negrete, N., Abundiz-Yañez, K., Yasbin, R. E., Robleto, E. A., and Pedraza-Reyes, M. (2020). Role of Mfd and GreA in *Bacillus subtilis* base excision repair-dependent stationary-phase mutagenesis. Journal of Bacteriology 202, e00807-19.
Li, Q., Cebrián, R., Montalbán-López, M., Ren, H., Wu, W., and Kuipers, O. P. (2021). Outer-membrane-acting peptides and lipid II-targeting antibiotics cooperatively kill Gram-negative pathogens. Communications Biology 4, 31.
Lin, W., Das, K., Degen, D., Mazumder, A., Duchi, D., Wang, D., Ebright, Y. W., Ebright, R. Y., Sineva, E., Gigliotti, M., et al. (2018). Structural basis of transcription inhibition by fidaxomicin (lipiarmycin A3). Molecular cell 70, 60-71.e15.

Ling, L. L., Schneider, T., Peoples, A. J., Spoering, A. L., Engels, I., Conlon, B. P., Mueller, A., Schäberle, T. F., Hughes, D. E., Epstein, S., et al. (2015). A new antibiotic kills pathogens without detectable resistance. Nature 517, 455-459.
Liu, P. T., Stenger, S., Li, H., Wenzel, L., Tan, B. H., Krutzik, S. R., Ochoa, M. T., Schauber, J., Wu, K., Meinken, C., et al. (2006). Toll-like receptor triggering of a vitamin D-mediated human antimicrobial response. Science 311, 1770-3.
Longley, D. B., Harkin, D. P., and Johnston, P. G. (2003). 5-Fluorouracil: mechanisms of action and clinical strategies. Nature Reviews Cancer 3, 330-338.
Lovett, C. M., Jr., O'gara, T. M., and Woodruff, J. N. (1994). Analysis of the SOS inducing signal in *Bacillus subtilis* using *Escherichia coli* LexA as a probe. Journal of bacteriology 176, 4914-4923.
Macpherson, D. W., Gushulak, B. D., Baine, W. B., Bala, S., Gubbins, P. O., Holtom, P., and Segarra-Newnham, M. (2009). Population mobility, globalization, and antimicrobial drug resistance. Emerging Infectious Diseases 15, 1727-1732.
Maffioli, S. I., Zhang, Y., Degen, D., Carzaniga, T., Del Gatto, G., Serina, S., Monciardini, P., Mazzetti, C., Guglierame, P., Candiani, G., et al. (2017). Antibacterial nucleoside-analog inhibitor of bacterial RNA polymerase. Cell 169, 1240-1248.e23.
Mak, P. A., Rao, S. P. S., Ping Tan, M., Lin, X., Chyba, J., Tay, J., Ng, S. H., Tan, B. H., Cherian, J., Duraiswamy, J., et al. (2012). A high-throughput screen to identify inhibitors of ATP homeostasis in non-replicating *Mycobacterium tuberculosis*. ACS Chemical Biology 7, 1190-1197.
Manganelli, V., Capozzi, A., Recalchi, S., Riitano, G., Mattei, V., Longo, A., Misasi, R., Garofalo, T., and Sorice, M. (2021). The role of cardiolipin as a scaffold mitochondrial phospholipid in autophagosome formation: *in vitro* evidence. Biomolecules 11, 222.
Manyi-Loh, C., Mamphweli, S., Meyer, E., and Okoh, A. (2018). Antibiotic use in agriculture and its consequential resistance in environmental sources: potential public health implications. Molecules (Basel, Switzerland) 23, 795.
Mao, D., Okada, B. K., Wu, Y., Xu, F., and Seyedsayamdost, M. R. (2018). Recent advances in activating silent biosynthetic gene clusters in bacteria. Current opinion in microbiology 45, 156-163.
Mars, R. a. T., Nicolas, P., Denham, E. L., and Van Dijl, J. M. (2016). Regulatory RNAs in *Bacillus subtilis*: a Gram-positive perspective on bacterial RNA-mediated regulation of gene expression. Microbiology and Molecular Biology Reviews 80, 1029-1057.
Martin, J. K., Sheehan, J. P., Bratton, B. P., Moore, G. M., Mateus, A., Li, S. H.-J., Kim, H., Rabinowitz, J. D., Typas, A., Savitski, M. M., et al. (2020). A dual-mechanism antibiotic kills Gram-negative bacteria and avoids drug resistance. Cell 181, 1518-1532.e14.
Martínez, F. O., Cardoso, M. H., Ribeiro, S. M., and Franco, O. L. (2019). Recent advances in anti-virulence therapeutic strategies with a focus on dismantling bacterial membrane microdomains, toxin neutralization, quorum-sensing interference and biofilm inhibition. Frontiers in Cellular and Infection Microbiology 9.
Mascher, T., Zimmer, S. L., Smith, T.-A., and Helmann, J. D. (2004). Antibiotic-inducible promoter regulated by the cell envelope stress-sensing two-component system LiaRS of *Bacillus subtilis*. Antimicrobial Agents and Chemotherapy 48, 2888-2896.
Mccormick, N. E., and Jakeman, D. L. (2015). On the mechanism of phosphoenolpyruvate synthetase (PEPs) and its inhibition by sodium fluoride: potential magnesium and aluminum fluoride complexes of phosphoryl transfer. Biochemistry and Cell Biology 93, 236-40.
Mcvey, A. C., Bartlett, S., Kajbaf, M., Pellacani, A., Gatta, V., Tammela, P., Spring, D. R., and Welch, M. (2020). 2-Aminopyridine analogs inhibit both enzymes of the

glyoxylate shunt in *Pseudomonas aeruginosa*. International Journal of Molecular Sciences 21, 2490.
Melander, R. J., and Melander, C. (2017). The challenge of overcoming antibiotic resistance: an adjuvant approach? ACS Infectious Diseases 3, 559-563.
Melander, R. J., Zurawski, D. V., and Melander, C. (2018). Narrow-spectrum antibacterial agents. MedChemComm 9, 12-21.
Merrikh, H., Zhang, Y., Grossman, A. D., and Wang, J. D. (2012). Replication-transcription conflicts in bacteria. Nature Reviews Microbiology 10, 449-458.
Miller, W. R., Bayer, A. S., and Arias, C. A. (2016). Mechanism of action and resistance to daptomycin in *Staphylococcus aureus* and Enterococci. Cold Spring Harbor Perspectives in Medicine 6, a026997.
Mirończuk, A. M., Kovács, Á. T., and Kuipers, O. P. (2008). Induction of natural competence in *Bacillus cereus* ATCC14579. Microbial biotechnology 1, 226-235.
Mondal, S., Yakhnin, A. V., Sebastian, A., Albert, I., and Babitzke, P. (2016). NusA-dependent transcription termination prevents misregulation of global gene expression. Nature Microbiology 1, 15007-15007.
Moreno-Campuzano, S., Janga, S. C., and Pérez-Rueda, E. (2006). Identification and analysis of DNA-binding transcription factors in *Bacillus subtilis* and other Firmicutes-a genomic approach. BMC genomics 7, 147-147.
Mukherjee, S., and Kearns, D. B. (2014). The structure and regulation of flagella in *Bacillus subtilis*. Annual review of genetics 48, 319-340.
Mukhopadhyay, J., Das, K., Ismail, S., Koppstein, D., Jang, M., Hudson, B., Sarafianos, S., Tuske, S., Patel, J., Jansen, R., et al. (2008). The RNA polymerase "switch region" is a target for inhibitors. Cell 135, 295-307.
Müller, A., Wenzel, M., Strahl, H., Grein, F., Saaki, T. N. V., Kohl, B., Siersma, T., Bandow, J. E., Sahl, H. G., Schneider, T., et al. (2016). Daptomycin inhibits cell envelope synthesis by interfering with fluid membrane microdomains. Proceedings of the National Academy of Sciences 113, E7077-e7086.
Murray, E. M., Allen, C. F., Handy, T. E., Huffine, C. A., Craig, W. R., Seaton, S. C., and Wolfe, A. L. (2019). Development of a robust and quantitative high-throughput screening method for antibiotic production in bacterial libraries. ACS Omega 4, 15414-15420.
Nah, H.-J., Pyeon, H.-R., Kang, S.-H., Choi, S.-S., and Kim, E.-S. (2017). Cloning and heterologous expression of a large-sized natural product biosynthetic gene cluster in *Streptomyces* species. Frontiers in Microbiology 8.
Nakano, M. M., and Zuber, P. (1998). Anaerobic growth of a "strict aerobe" (*Bacillus subtilis*). Annual Review of Microbiology 52, 165-190.
Netzker, T., Fischer, J., Weber, J., Mattern, D. J., König, C. C., Valiante, V., Schroeckh, V., and Brakhage, A. A. (2015). Microbial communication leading to the activation of silent fungal secondary metabolite gene clusters. Frontiers in Microbiology 6.
Neuhaus, F. C., and Lynch, J. L. (1964). The enzymatic synthesis of D-alanyl-D-alanine. III. On the inhibition of D-alanyl-D-alanine synthetase by the antibiotic D-cycloserine. Biochemistry 3, 471-480.
Newing, T. P., Oakley, A. J., Miller, M., Dawson, C. J., Brown, S. H. J., Bouwer, J. C., Tolun, G., and Lewis, P. J. (2020). Molecular basis for RNA polymerase-dependent transcription complex recycling by the helicase-like motor protein HelD. Nature Communications 11, 6420.
Newman, D. J., and Cragg, G. M. (2016). Natural products as sources of new drugs from 1981 to 2014. Journal of Natural Products 79, 629-661.
Nickels, B. E. (2012). A new way to start: nanoRNA-mediated priming of transcription initiation. Transcription 3, 300-304.

Nicolas, P., Mäder, U., Dervyn, E., Rochat, T., Leduc, A., Pigeonneau, N., Bidnenko, E., Marchadier, E., Hoebeke, M., Aymerich, S., et al. (2012). Condition-dependent transcriptome reveals high-level regulatory architecture in *Bacillus subtilis*. Science 335, 1103.

Nithya, K., Muthukumar, C., Biswas, B., Alharbi, N. S., Kadaikunnan, S., Khaled, J. M., and Dhanasekaran, D. (2018). Desert actinobacteria as a source of bioactive compounds production with a special emphases on pyridine-2,5-diacetamide a new pyridine alkaloid produced by *Streptomyces* sp. DA3-7. Microbiological Research 207, 116-133.

Nomura, S., Horiuchi, T., Omura, S., and Hata, T. (1972). The action mechanism of cerulenin: I. Effect of cerulenin on sterol and fatty acid biosyntheses in yeast. Journal of Biochemistry 71, 783-796.

Nonejuie, P., Trial, R. M., Newton, G. L., Lamsa, A., Ranmali Perera, V., Aguilar, J., Liu, W. T., Dorrestein, P. C., Pogliano, J., and Pogliano, K. (2016). Application of bacterial cytological profiling to crude natural product extracts reveals the antibacterial arsenal of *Bacillus subtilis*. Journal of Antibiotics (Tokyo) 69, 353-61.

O'rourke, A., Beyhan, S., Choi, Y., Morales, P., Chan, A. P., Espinoza, J. L., Dupont, C. L., Meyer, K. J., Spoering, A., Lewis, K., et al. (2020). Mechanism-of-action classification of antibiotics by global transcriptome profiling. Antimicrobial Agents and Chemotherapy 64.

O´Neill, J. (2014). Review on antimicrobial resistance: tackling a crisis for the health and wealth of nations (London: Review on Antimicrobial Resistance.)

Oe, C., Hayashi, H., Hirata, K., Kawaji, K., Hashima, F., Sasano, M., Furuichi, M., Usui, E., Katsumi, M., Suzuki, Y., et al. (2020). Pyrimidine analogues as a new class of Gram-positive antibiotics, mainly targeting thymineless-death related proteins. ACS Infectious Diseases 6, 1490-1500.

Oh, D.-C., Kauffman, C. A., Jensen, P. R., and Fenical, W. (2007). Induced production of emericellamides A and B from the marine-derived fungus *Emericella* sp. in competing co-culture. Journal of Natural Products 70, 515-520.

Oliva, G., Sahr, T., and Buchrieser, C. (2015). Small RNAs, 5′ UTR elements and RNA-binding proteins in intracellular bacteria: impact on metabolism and virulence. FEMS Microbiology Reviews 39, 331-349.

Opperman, T. J., Kwasny, S. M., Li, J. B., Lewis, M. A., Aiello, D., Williams, J. D., Peet, N. P., Moir, D. T., Bowlin, T. L., and Long, E. C. (2016). DNA targeting as a likely mechanism underlying the antibacterial activity of synthetic bis-indole antibiotics. Antimicrobial Agents and Chemotherapy 60, 7067.

Pan, R., Bai, X., Chen, J., Zhang, H., and Wang, H. (2019). Exploring structural diversity of microbe secondary metabolites using OSMAC strategy: a literature review. Frontiers in Microbiology 10.

Park, S.-S., Yang, Y.-H., Song, E., Kim, E.-J., Kim, W. S., Sohng, J. K., Lee, H. C., Liou, K. K., and Kim, B.-G. (2009). Mass spectrometric screening of transcriptional regulators involved in antibiotic biosynthesis in *Streptomyces coelicolor* A3(2). Journal of Industrial Microbiology and Biotechnology 36, 1073-1083.

Pei, H.-H., Hilal, T., Chen, Z. A., Huang, Y.-H., Gao, Y., Said, N., Loll, B., Rappsilber, J., Belogurov, G. A., Artsimovitch, I., et al. (2020). The δ subunit and NTPase HelD institute a two-pronged mechanism for RNA polymerase recycling. Nature Communications 11, 6418.

Pham, T. D. M., Ziora, Z. M., and Blaskovich, M. a. T. (2019). Quinolone antibiotics. MedChemComm 10, 1719-1739.

Phillips, R. M., Burger, A. M., Loadman, P. M., Jarrett, C. M., Swaine, D. J., and Fiebig, H.-H. (2000). Predicting tumor responses to mitomycin C on the basis of DT-

diaphorase activity or drug metabolism by tumor homogenates: Implications for enzyme-directed bioreductive drug development. Cancer Research 60, 6384.
Piggot, P. J. (1973). Mapping of asporogenous mutations of *Bacillus subtilis*: a minimum estimate of the number of sporulation operons. Journal of Bacteriology 114, 1241-1253.
Piggot, P. J. 2009. *Bacillus subtilis*. *In:* SCHAECHTER, M. (ed.) *Encyclopedia of Microbiology* 3rd ed. Oxford: Academic Press.
Pommier, Y., Leo, E., Zhang, H., and Marchand, C. (2010). DNA topoisomerases and their poisoning by anticancer and antibacterial drugs. Chemistry and Biology 17, 421-433.
Prezioso, S. M., Brown, N. E., and Goldberg, J. B. (2017). Elfamycins: inhibitors of elongation factor-Tu. Molecular microbiology 106, 22-34.
Qian, Q., Lee, C. Y., Helmann, J. D., and Strauch, M. A. (2002). AbrB is a regulator of the σW regulon in *Bacillus subtilis*. FEMS Microbiology Letters 211, 219-223.
Radeck, J., Fritz, G., and Mascher, T. (2017). The cell envelope stress response of *Bacillus subtilis*: from static signaling devices to dynamic regulatory network. Current Genetics 63, 79-90.
Rasko, D. A., and Sperandio, V. (2010). Anti-virulence strategies to combat bacteria-mediated disease. Nature Reviews Drug Discovery 9, 117-128.
Ravikumar, V., Nalpas, N. C., Anselm, V., Krug, K., Lenuzzi, M., Šestak, M. S., Domazet-Lošo, T., Mijakovic, I., and Macek, B. (2018). In-depth analysis of *Bacillus subtilis* proteome identifies new ORFs and traces the evolutionary history of modified proteins. Scientific Reports 8, 17246.
Reusser, F. (1969). Mode of action of berninamycin. An inhibitor of protein biosynthesis. Biochemistry 8, 3303-8.
Reynolds, P. E. (1989). Structure, biochemistry and mechanism of action of glycopeptide antibiotics. European Journal of Clinical Microbiology and Infectious Diseases 8, 943-50.
Rezzoagli, C., Archetti, M., Mignot, I., Baumgartner, M., and Kümmerli, R. (2020). Combining antibiotics with antivirulence compounds can have synergistic effects and reverse selection for antibiotic resistance in *Pseudomonas aeruginosa*. PLOS Biology 18, e3000805.
Rocha, E. P., Danchin, A., and Viari, A. (1999). Analysis of long repeats in bacterial genomes reveals alternative evolutionary mechanisms in *Bacillus subtilis* and other competent prokaryotes. Molecular Biology and Evolution 16, 1219-30.
Rolain, J. M., and Baquero, F. (2016). The refusal of the Society to accept antibiotic toxicity: missing opportunities for therapy of severe infections. Clinical Microbiology and Infection 22, 423-427.
Romano, S., Jackson, S. A., Patry, S., and Dobson, A. D. W. (2018). Extending the "one strain many compounds" (OSMAC) principle to marine microorganisms. Marine drugs 16, 244.
Ruhr, E., and Sahl, H. G. (1985). Mode of action of the peptide antibiotic nisin and influence on the membrane potential of whole cells and on cytoplasmic and artificial membrane vesicles. Antimicrobial Agents and Chemotherapy 27, 841-845.
Saberi, F., Kamali, M., Najafi, A., Yazdanparast, A., and Moghaddam, M. M. (2016). Natural antisense RNAs as mRNA regulatory elements in bacteria: a review on function and applications. Cellular and Molecular Biology Letters 21, 6.
Sass, P., and Brötz-Oesterhelt, H. (2013). Bacterial cell division as a target for new antibiotics. Current Opinion in Microbiology 16, 522-30.
Sass, P., Josten, M., Famulla, K., Schiffer, G., Sahl, H.-G., Hamoen, L., and Brötz-Oesterhelt, H. (2011). Antibiotic acyldepsipeptides activate ClpP peptidase to

degrade the cell division protein FtsZ. Proceedings of the National Academy of Sciences 108, 17474-17479.
Schäberle, T. F., Vollmer, W., Frasch, H.-J., Hüttel, S., Kulik, A., Röttgen, M., Von Thaler, A.-K., Wohlleben, W., and Stegmann, E. (2011). Self-resistance and cell wall composition in the glycopeptide producer *Amycolatopsis balhimycina*. Antimicrobial Agents and Chemotherapy 55, 4283-4289.
Schlame, M. (2008). Cardiolipin synthesis for the assembly of bacterial and mitochondrial membranes. Journal of lipid research 49, 1607-1620.
Schneider, T., and Sahl, H. G. (2010). An oldie but a goodie - cell wall biosynthesis as antibiotic target pathway. International Journal of Medical Microbiology 300, 161-9.
Schroeck, J. L., Ruh, C. A., Sellick, J. A., Jr., Ott, M. C., Mattappallil, A., and Mergenhagen, K. A. (2015). Factors associated with antibiotic misuse in outpatient treatment for upper respiratory tract infections. Antimicrobial Agents and Chemotherapy 59, 3848-3852.
Seyedsayamdost, M. R. (2014). High-throughput platform for the discovery of elicitors of silent bacterial gene clusters. Proceedings of the National Academy of Sciences 111, 7266-7271.
Shaw, K. J., Miller, N., Liu, X., Lerner, D., Wan, J., Bittner, A., and Morrow, B. J. (2003). Comparison of the changes in global gene expression of *Escherichia coli* induced by four bactericidal agents. Microbial Physiology 5, 105-122.
Shimotsu, H., and Henner, D. J. (1986). Construction of a single-copy integration vector and its use in analysis of regulation of the trp operon of *Bacillus subtilis*. Gene 43, 85-94.
Sierro, N., Makita, Y., De Hoon, M., and Nakai, K. (2008). DBTBS: a database of transcriptional regulation in *Bacillus subtilis* containing upstream intergenic conservation information. Nucleic Acids Research 36, D93-D96.
Šiková, M., Wiedermannová, J., Převorovský, M., Barvík, I., Sudzinová, P., Kofroňová, O., Benada, O., Šanderová, H., Condon, C., and Krásný, L. (2020). The torpedo effect in *Bacillus subtilis*: RNase J1 resolves stalled transcription complexes. The EMBO Journal 39, e102500-e102500.
Silber, N., Pan, S., Schäkermann, S., Mayer, C., Brötz-Oesterhelt, H., and Sass, P. (2020). Cell division protein FtsZ is unfolded for N-terminal degradation by antibiotic-activated ClpP. mBio 11, e01006-20.
Silver, L. L. (2011). Challenges of antibacterial discovery. Clinical Microbiology Reviews 24, 71.
Silver, L. L. (2017). Fosfomycin: mechanism and resistance. Cold Spring Harbor Perspectives in Medicine 7, a025262.
Singh, S. B., Young, K., and Miesel, L. (2011). Screening strategies for discovery of antibacterial natural products. Expert Review of Anti-Infective Therapy 9, 589-613.
Singh, V., Brecik, M., Mukherjee, R., Evans, J. C., Svetlíková, Z., Blaško, J., Surade, S., Blackburn, J., Warner, D. F., Mikušová, K., et al. (2015). The complex mechanism of antimycobacterial action of 5-fluorouracil. Chemistry and Biology 22, 63-75.
Souza, B. M., Castro, T. L. D. P., Carvalho, R. D. D. O., Seyffert, N., Silva, A., Miyoshi, A., and Azevedo, V. (2014). σ(ECF) factors of gram-positive bacteria: a focus on *Bacillus subtilis* and the CMNR group. Virulence 5, 587-600.
Spanogiannopoulos, P., Waglechner, N., Koteva, K., and Wright, G. (2014). A rifamycin inactivating phosphotransferase family shared by environmental and pathogenic bacteria. Proceedings of the National Academy of Sciences 111.
Stazic, D., Lindell, D., and Steglich, C. (2011). Antisense RNA protects mRNA from RNase E degradation by RNA-RNA duplex formation during phage infection. Nucleic Acids Research 39, 4890-4899.

Stogios, P. J., Cox, G., Spanogiannopoulos, P., Pillon, M. C., Waglechner, N., Skarina, T., Koteva, K., Guarné, A., Savchenko, A., and Wright, G. D. (2016). Rifampin phosphotransferase is an unusual antibiotic resistance kinase. Nature Communications 7, 11343-11343.
Strauch, M. A., Bobay, B. G., Cavanagh, J., Yao, F., Wilson, A., and Le Breton, Y. (2007). Abh and AbrB control of *Bacillus subtilis* antimicrobial gene expression. Journal of Bacteriology 189, 7720.
Straus, S. K., and Hancock, R. E. W. (2006). Mode of action of the new antibiotic for Gram-positive pathogens daptomycin: Comparison with cationic antimicrobial peptides and lipopeptides. Biochimica Biophysica Acta - Biomembranes 1758, 1215-1223.
Susanna, K. A., Den Hengst, C. D., Hamoen, L. W., and Kuipers, O. P. (2006). Expression of transcription activator ComK of *Bacillus subtilis* in the heterologous host *Lactococcus lactis* leads to a genome-wide repression pattern: a case study of horizontal gene transfer. Applied and Environmental Microbiology 72, 404-411.
Taylor, S. D., and Palmer, M. (2016). The action mechanism of daptomycin. Bioorganic and Medicinal Chemistry 24, 6253-6268.
Temiakov, D., Zenkin, N., Vassylyeva, M. N., Perederina, A., Tahirov, T. H., Kashkina, E., Savkina, M., Zorov, S., Nikiforov, V., Igarashi, N., et al. (2005). Structural basis of transcription inhibition by antibiotic streptolydigin. Molecular Cell 19, 655-666.
Tenson, T., Lovmar, M., and Ehrenberg, M. (2003). The mechanism of action of macrolides, lincosamides and streptogramin B reveals the nascent peptide exit path in the ribosome. Journal of Molecular Biology 330, 1005-1014.
Thompson, J., Pratt, C. A., and Dahlberg, A. E. (2004). Effects of a number of classes of 50S inhibitors on stop codon readthrough during protein synthesis. Antimicrobial Agents and Chemotherapy 48, 4889-4891.
Ting, D. S. J., Beuerman, R. W., Dua, H. S., Lakshminarayanan, R., and Mohammed, I. (2020). Strategies in translating the therapeutic Potentials of host defense peptides. Frontiers in Immunology 11.
Tommasi, R., Brown, D. G., Walkup, G. K., Manchester, J. I., and Miller, A. A. (2015). ESKAPEing the labyrinth of antibacterial discovery. Nature Reviews Drug Discovery 14, 529-542.
Torres, C., Galián, C., Freiberg, C., Fantino, J.-R., and Jault, J.-M. (2009). The YheI/YheH heterodimer from *Bacillus subtilis* is a multidrug ABC transporter. Biochimica Biophysica Acta - Biomembranes 1788, 615-622.
Trimble, M. J., Mlynárčik, P., Kolář, M., and Hancock, R. E. W. (2016). Polymyxin: alternative mechanisms of action and resistance. Cold Spring Harbor Perspectives in Medicine 6, a025288.
Tulp, M., and Bohlin, L. (2005). Rediscovery of known natural compounds: Nuisance or goldmine? Bioorganic and Medicinal Chemistry 13, 5274-5282.
Tupin, A., Gualtieri, M., Leonetti, J.-P., and Brodolin, K. (2010). The transcription inhibitor lipiarmycin blocks DNA fitting into the RNA polymerase catalytic site. The EMBO Journal 29, 2527-2537.
Ul Haq, I., Müller, P., and Brantl, S. (2020). Intermolecular communication in *Bacillus subtilis*: RNA-RNA, RNA-protein and small protein-protein interactions. Frontiers in Molecular Biosciences 7.
Urban, A., Eckermann, S., Fast, B., Metzger, S., Gehling, M., Ziegelbauer, K., Rübsamen-Waigmann, H., and Freiberg, C. (2007). Novel whole-cell antibiotic biosensors for compound discovery. Applied and Environmental Microbiology 73, 6436-6443.
Van Eijk, E., Wittekoek, B., Kuijper, E. J., and Smits, W. K. (2017). DNA replication proteins as potential targets for antimicrobials in drug-resistant bacterial pathogens. Journal of Antimicrobial Chemotherapy 72, 1275-1284.

Vannuffel, P., and Cocito, C. (1996). Mechanism of action of streptogramins and macrolides. Drugs 51, 20-30.
Vargas-Blanco, D. A., and Shell, S. S. (2020). Regulation of mRNA stability during bacterial stress responses. Frontiers in Microbiology 11.
Vázquez-Laslop, N., and Mankin, A. S. (2018). How macrolide antibiotics work. Trends in Biochemical Sciences 43, 668-684.
Ventura, S. P. M., E Silva, F. A., Quental, M. V., Mondal, D., Freire, M. G., and Coutinho, J. a. P. (2017). Ionic-liquid-mediated extraction and separation processes for bioactive compounds: past, present, and future trends. Chemical Reviews 117, 6984-7052.
Walsh, C. T., and Wencewicz, T. A. (2014). Prospects for new antibiotics: a molecule-centered perspective. The Journal of Antibiotics 67, 7-22.
Walter, J. D., Hunter, M., Cobb, M., Traeger, G., and Spiegel, P. C. (2011). Thiostrepton inhibits stable 70S ribosome binding and ribosome-dependent GTPase activation of elongation factor G and elongation factor 4. Nucleic Acids Research 40, 360-370.
Wang, B., Guo, F., Dong, S.-H., and Zhao, H. (2019). Activation of silent biosynthetic gene clusters using transcription factor decoys. Nature Chemical Biology 15, 111-114.
Wang Erickson, A. F., Deighan, P., Chen, S., Barrasso, K., Garcia, C. P., Martínez-Lumbreras, S., Alfano, C., Krysztofinska, E. M., Thapaliya, A., Camp, A. H., et al. (2017). A novel RNA polymerase-binding protein that interacts with a sigma-factor docking site. Molecular microbiology 105, 652-662.
Wehrli, W., and Staehelin, M. (1971). Actions of the rifamycins. Bacteriological reviews 35, 290-309.
Wei, T. T., Byrne, K. M., Warnick-Pickle, D., and Greenstein, M. (1982). Studies on the mechanism of actin of gilvocarcin V and chrysomycin A. Journal of Antibiotics (Tokyo) 35, 545-8.
Weiss, A., Moore, B. D., Tremblay, M. H. J., Chaput, D., Kremer, A., and Shaw, L. N. (2016). The ω subunit governs RNA polymerase stability and transcriptional specificity in *Staphylococcus aureus*. Journal of Bacteriology 199, e00459-16.
Weiss, A., and Shaw, L. N. (2015). Small things considered: the small accessory subunits of RNA polymerase in Gram-positive bacteria. FEMS Microbiology Reviews 39, 541-554.
Welsch, M. (1952). Some aspects of microbial resistance to streptomycin. Bulletin of the World Health Organization 6, 173-183.
Wenzel, M., Chiriac, A. I., Otto, A., Zweytick, D., May, C., Schumacher, C., Gust, R., Albada, H. B., Penkova, M., Krämer, U., et al. (2014). Small cationic antimicrobial peptides delocalize peripheral membrane proteins. Proceedings of the National Academy of Sciences 111, E1409.
Wetzel, C., Lonneman, M., and Wu, C. (2021). Polypharmacological drug actions of recently FDA approved antibiotics. European Journal of Medicinal Chemistry 209, 112931.
Wex, K. W., Saur, J. S., Handel, F., Ortlieb, N., Mokeev, V., Kulik, A., Niedermeyer, T. H. J., Mast, Y., Grond, S., Berscheid, A., et al. (2021). Bioreporters for direct mode of action-informed screening of antibiotic producer strains. Cell Chemical Biology, DOI: 10.1016/j.chembiol.2021.02.022
Whipple, F. W., and Sonenshein, A. L. (1992). Mechanism of initiation of transcription by *Bacillus subtilis* RNA polymerase at several promoters. Journal of Molecular Biology 223, 399-414.
Wiedermannová, J., Sudzinová, P., Kovaľ, T., Rabatinová, A., Šanderova, H., Ramaniuk, O., Rittich, Š., Dohnálek, J., Fu, Z., Halada, P., et al. (2014). Characterization of HelD, an interacting partner of RNA polymerase from *Bacillus subtilis*. Nucleic Acids Research 42, 5151-5163.

Wiegand, S., Dietrich, S., Hertel, R., Bongaerts, J., Evers, S., Volland, S., Daniel, R., and Liesegang, H. (2013). RNA-Seq of *Bacillus licheniformis*: active regulatory RNA features expressed within a productive fermentation. BMC Genomics 14, 667.
Wilson, D. N. (2009). The A–Z of bacterial translation inhibitors. Critical Reviews in Biochemistry and Molecular Biology 44, 393-433.
Wohlleben, W., Mast, Y., Stegmann, E., and Ziemert, N. (2016). Antibiotic drug discovery. Microbial Biotechnology 9, 541-548.
Wolf, D., and Mascher, T. (2016). The applied side of antimicrobial peptide-inducible promoters from Firmicutes bacteria: expression systems and whole-cell biosensors. Applied Microbiology and Biotechnology 100, 4817-4829.
World Health Organization (2015). Antibiotic resistance: multi-country public awareness survey (Geneva: World Health Organization.)
Wormser, G. P., Keusch, G. T., and Heel, R. C. (1982). Co-trimoxazole (Trimethoprim-sulfamethoxazole). Drugs 24, 459-518.
Wright, G. D. (2017). Opportunities for natural products in 21st century antibiotic discovery. Natural Product Reports 34, 694-701.
Xiao, J., Peng, B., Su, Z., Liu, A., Hu, Y., Nomura, C., Chen, S., and Wang, Q. (2020). Facilitating protein expression with portable 5'-UTR secondary structures in *Bacillus licheniformis*. ACS Synthetic Biology.
Yakhnin, A. V., and Babitzke, P. (2002). NusA-stimulated RNA polymerase pausing and termination participates in the *Bacillus subtilis* operon attenuation mechanism *in vitro*. Proceedings of the National Academy of Sciences 99, 11067.
Yang, Y., Ashworth, A. J., Willett, C., Cook, K., Upadhyay, A., Owens, P. R., Ricke, S. C., Debruyn, J. M., and Moore Jr., P. A. (2019). Review of antibiotic resistance, ecology, dissemination, and mitigation in U.S. broiler poultry systems. Frontiers in Microbiology 10.
Yoon, V., and Nodwell, J. R. (2014). Activating secondary metabolism with stress and chemicals. Journal of Industrial Microbiology and Biotechnology 41, 415-424.
Yoshida, K.-I., Ohki, Y.-H., Murata, M., Kinehara, M., Matsuoka, H., Satomura, T., Ohki, R., Kumano, M., Yamane, K., and Fujita, Y. (2004). *Bacillus subtilis* LmrA is a repressor of the *lmrAB* and *yxaGH* operons: identification of its binding site and functional analysis of *lmrB* and *yxaGH*. Journal of bacteriology 186, 5640-5648.
Yun, U.-J., Lee, J.-H., Shim, J., Yoon, K., Goh, S.-H., Yi, E. H., Ye, S.-K., Lee, J.-S., Lee, H., Park, J., et al. (2019). Anti-cancer effect of doxorubicin is mediated by downregulation of HMG-Co A reductase via inhibition of EGFR/Src pathway. Laboratory Investigation 99, 1157-1172.
Zellmeier, S., Hofmann, C., Thomas, S., Wiegert, T., and Schumann, W. (2005). Identification of σV-dependent genes of *Bacillus subtilis*. FEMS Microbiology Letters 253, 221-229.
Zeng, D., Debabov, D., Hartsell, T. L., Cano, R. J., Adams, S., Schuyler, J. A., Mcmillan, R., and Pace, J. L. (2016). Approved glycopeptide antibacterial drugs: mechanism of action and resistance. Cold Spring Harbor Perspectives in Medicine 6, a026989.
Zhang, N., Yang, D., Kendall, J. R. A., Borriss, R., Druzhinina, I. S., Kubicek, C. P., Shen, Q., and Zhang, R. (2016). Comparative genomic analysis of *Bacillus amyloliquefacien*s and *Bacillus subtilis* reveals evolutional traits for adaptation to plant-associated habitats. Frontiers in Microbiology 7.
Zhu, B., and Stülke, J. (2017). SubtiWiki in 2018: from genes and proteins to functional network annotation of the model organism *Bacillus subtilis*. Nucleic Acids Research 46, D743-D748.
Zipperer, A., Konnerth, M. C., Laux, C., Berscheid, A., Janek, D., Weidenmaier, C., Burian, M., Schilling, N. A., Slavetinsky, C., Marschal, M., et al. (2016). Human

commensals producing a novel antibiotic impair pathogen colonization. Nature 535, 511-516.
Zuker, M. (2003). Mfold web server for nucleic acid folding and hybridization prediction. Nucleic Acids Research 31, 3406-3415.

APPENDIX

Publication 1

Resource

Cell Chemical Biology

Bioreporters for direct mode of action-informed screening of antibiotic producer strains

Graphical abstract

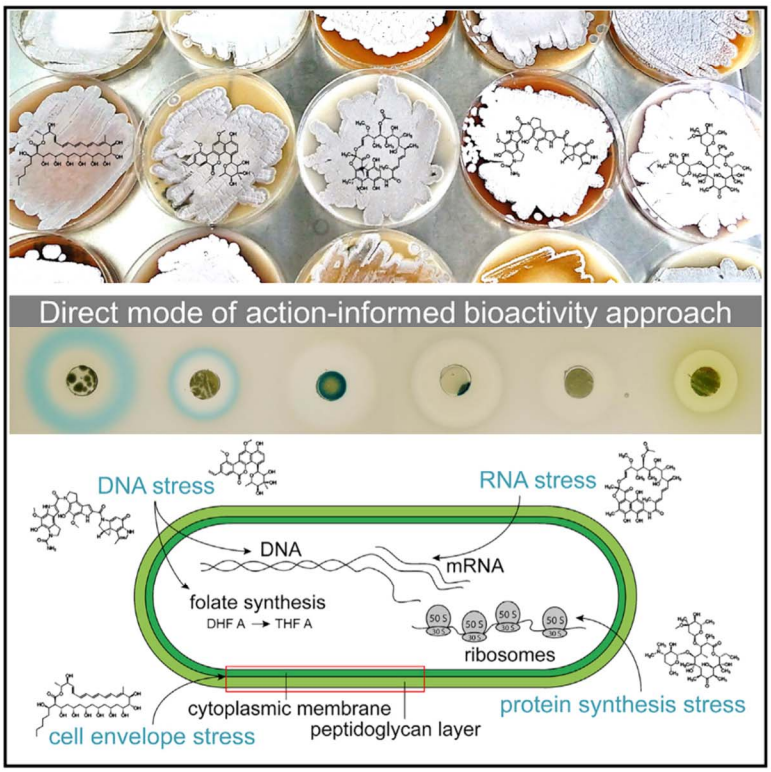

Authors

Katharina W. Wex, Julian S. Saur, Franziska Handel, ..., Stephanie Grond, Anne Berscheid, Heike Brötz-Oesterhelt

Correspondence

heike.broetz-oesterhelt@uni-tuebingen.de

In brief

Wex et al. established a robust, sensitive, and rapid bioreporter-based approach for broad mode of action profiling of antibiotic producer strains, detecting also polypharmacology and synergism. Bioreporter specificity was validated with 90 known reference compounds and proof-of-concept was provided by screening 500 actinomycete producers of the Tübingen strain collection.

Highlights

- Direct mode of action-informed bioreporter screening of antibiotic producer strains
- Rapid mode of action profiling of unknown antimicrobials after overnight incubation
- Detection of polypharmacology and synergism
- Facilitated deconvolution process by an additional mode of action dimension

Wex et al., 2021, Cell Chemical Biology *28*, 1–11
August 19, 2021
https://doi.org/10.1016/j.chembiol.2021.02.022

CellPress

Please cite this article in press as: Wex et al., Bioreporters for direct mode of action-informed screening of antibiotic producer strains, Cell Chemical Biology (2021), https://doi.org/10.1016/j.chembiol.2021.02.022

Cell Chemical Biology

CellPress

Resource

Bioreporters for direct mode of action-informed screening of antibiotic producer strains

Katharina W. Wex,[1,6] Julian S. Saur,[2] Franziska Handel,[3,6] Nico Ortlieb,[3,6] Vladislav Mokeev,[1,7] Andreas Kulik,[1,3,7] Timo H.J. Niedermeyer,[3,4,6] Yvonne Mast,[3,5,6] Stephanie Grond,[2,7] Anne Berscheid,[1,6,8] and Heike Brötz-Oesterhelt[1,6,7,8,9,*]

[1]Department of Microbial Bioactive Compounds, Interfaculty Institute of Microbiology and Infection Medicine, University of Tuebingen, Tuebingen, Baden-Württemberg 72076, Germany
[2]Biomolecular Chemistry, Institute of Organic Chemistry, University of Tuebingen, Tuebingen, Baden-Württemberg 72076, Germany
[3]Department of Microbiology and Biotechnology, Interfaculty Institute of Microbiology and Infection Medicine, University of Tuebingen, Tuebingen, Baden-Württemberg 72076, Germany
[4]Department of Pharmaceutical Biology/Pharmacognosy Institute of Pharmacy, Martin-Luther-University Halle-Wittenberg, Halle, Sachsen-Anhalt 06120, Germany
[5]Department Bioresources for Bioeconomy and Health Research, Leibniz Institute DSMZ-German Collection of Microorganisms and Cell Cultures, Braunschweig, Niedersachsen 38124, Germany
[6]German Center for Infection Research (DZIF), Partner Site Tuebingen, Tuebingen, Baden-Württemberg 72076, Germany
[7]Cluster of Excellence EXC 2124 – Controlling Microbes to Fight Infections, Tuebingen, Baden-Württemberg 72076, Germany
[8]Senior author
[9]Lead contact
*Correspondence: heike.broetz-oesterhelt@uni-tuebingen.de
https://doi.org/10.1016/j.chembiol.2021.02.022

SUMMARY

A big challenge in natural product research of today is rapid dereplication of already known substances, to free capacities for the exploration of new agents. Prompt information on bioactivities and mode of action (MOA) speeds up the lead discovery process and is required for rational compound optimization. Here, we present a bioreporter approach as a versatile strategy for combined bioactivity- and MOA-informed primary screening for antimicrobials. The approach is suitable for directly probing producer strains grown on agar, without need for initial compound enrichment or purification, and works along the entire purification pipeline with culture supernatants, extracts, fractions, and pure substances. The technology allows for MOA-informed purification to selectively prioritize activities of interest. In combination with high-resolution mass spectrometry, the biosensor panel is an efficient and sensitive tool for compound deconvolution. Concomitant information on the affected metabolic pathway enables the selection of appropriate follow-up assays to elucidate the molecular target.

INTRODUCTION

We are facing a post-antibiotic future, due to the rise of antibiotic resistance and the dried-out pipelines in antibiotic discovery and development (Aslam et al., 2018; Frieri et al., 2017; O'Neill, 2014). In recent years, the number of approved antibacterial drugs has been low, and the vast majority of these agents are derivatives of known antibiotic classes (Hutchings et al., 2019). The imprudent medical and economical handling of our available applicable antibiotics counteracts a sustainable use and further promotes rapid resistance development (Yang et al., 2019; WHO, 2015). The problem needs to be addressed from multiple sides to tackle this antibiotic crisis: we have to learn to handle our available precious drugs responsibly and stably finance antibiotic research and development. Furthermore, we urgently need to find new anti-infective agents, which are structurally different and either act on new targets or show novel binding modes on well-characterized targets, thereby avoiding cross-resistance (Bush et al., 2011). Resistance-breaking agents in combination with currently applied therapeutics are also of interest (Bush and Pucci, 2011; Laws et al., 2019; Melander and Melander, 2017). Although huge efforts have been made to overcome this problem by screening or rational design of optimized (semi-)synthetic molecules in target-based approaches, it became clear that the complexity of natural products is difficult to predict computationally or mimic by total synthesis (Brötz-Oesterhelt and Sass, 2010). A major issue in screening campaigns with synthetic libraries was the lack of bacterial cell entry or efflux problems of inhibitors identified against purified targets *in vitro* (Tommasi et al., 2015). The significant advantage of natural products is that they evolved for efficient target-binding and resistance-slowing polypharmacology. At the same time, their physicochemical properties facilitate entry and retainment within the bacterial cell. Therefore, natural products remain the most

Please cite this article in press as: Wex et al., Bioreporters for direct mode of action-informed screening of antibiotic producer strains, Cell Chemical Biology (2021), https://doi.org/10.1016/j.chembiol.2021.02.022

promising source in antibiotic discovery (Bérdy, 2012; Brötz-Oesterhelt and Sass, 2010).

After the golden age of antibiotic discovery (1940–1960), one of the main problems was the rediscovery of already known antibacterial agents, when following the classical phenotypic bioactivity-based screening approach mainly using actinomycetes producer strains isolated from soil (Genilloud, 2017; Tulp and Bohlin, 2005). To overcome this problem, current research is focusing on underexplored antibiotic producer species, e.g., those living in unique environmental niches, microbiomes, or those requiring specialized growth conditions (Niedermeyer, 2015; Zhang et al., 2017; Zipperer et al., 2016). Other approaches aim at harnessing the silent genomic capacity of known antibiotic producers (Wang et al., 2019). Producer strains often possess a large number of antibiotic gene clusters, and therefore have the genetic potential to produce a panel of different antimicrobial secondary metabolites when adapting to altered nutritional or environmental conditions, including microbe-microbe interactions (Culp et al., 2019; Handayani et al., 2018; Hug et al., 2018). Nevertheless, strains are usually discarded if they produce a known antibacterial agent, thereby potentially missing interesting compounds that are synthesized, e.g., in smaller amounts or under different growth conditions. The further development of effective screening tools, cultivation conditions, and extraction or dereplication methods form crucial steps in the discovery process of new bioactive molecules (Carrano and Marinelli, 2015; Wright, 2017). Cell-based screening methods that combine information on whole-cell bioactivity and mode of action (MOA) are promising tools to rapidly identify and characterize interesting bioactive molecules with the potential to cross the bacterial cell envelope and achieve sufficient target engagement in the whole-cell setting (Fischer et al., 2004; Wolf and Mascher, 2016; Nonejuie et al., 2016). Gathering MOA information at an early stage allows to prioritize activities targeting a specific metabolic pathway of interest. Identifying the targeted metabolic pathway also enables straightforward follow-up studies for tracking down the precise molecular target, which in turn is a prerequisite for rational lead optimization approaches.

The process of natural product discovery benefits from an MOA-informed screening and purification procedure in several ways. For known agents with known targets, the MOA information can confirm mass spectrometry-based compound identity by an independent method, facilitating compound dereplication. Besides, overlapping bioactivities in complex mixtures can be easily monitored and separated. Ideally, the setup of such a combined screening tool for antibacterial whole-cell activity and MOA should be easy to handle, suitable for high-throughput, quick to execute, and robust throughout the entire screening and purification process. Urban et al. (2007) reported on a panel of *Bacillus subtilis* whole-cell biosensors, derived from a large transcriptome study (Freiberg et al., 2006; Hutter et al., 2004), that are specifically induced upon antibiotic interference with the major biosynthetic bacterial pathways: DNA synthesis, RNA synthesis, protein synthesis, and cell envelope integrity. Their firefly luciferase-based reporter strain panel allowed for high-throughput screening of pure antimicrobial agents in solution. A substantial problem of most MOA analysis procedures is their dependency on preceding substance purification, which is time-consuming and requires separation processes with an inherent risk to miss out on interesting activities, especially in complex extract mixtures.

Here, we present an agar-based screening approach, which provides combined bioactivity and MOA information. Capitalizing on known and identifying a new biomarker, we developed a robust and versatile MOA profiling method that allows to directly screen antibiotic producer strains grown on agar without any purification, as well as culture supernatants, extracts, fractions, and pure substances. We verified the specificity and sensitivity of our bioreporters and assay conditions using an extensive library of reference antibiotics with known MOA and validated its suitability for direct screening with a set of characterized antibiotic producer strains. In a pilot screening campaign, we further tested 500 uncharacterized actinomycetes strains of the Tübingen strain collection. By following up on some activities from these strains, we could confirm that the metabolic stress sensed by the bioreporters matched the described MOA of the dereplicated substances in all cases.

RESULTS AND DISCUSSION

Selection of biomarker genes and optimization criteria for the setup of an agar-based bioreporter screening

As model organism we chose the best-investigated Gram-positive species *B. subtilis*, as there are extended datasets on the physiological stress response of this organism to antibiotic exposure, including transcriptome (Fischer et al., 2004; Freiberg et al., 2006), proteome (Bandow et al., 2003), or cytological profiling studies (Nonejuie et al., 2016). Furthermore, its high antibiotic susceptibility allows for a sensitive detection of most bioactive molecules, while the deduced MOA information can be often directly transferred to pathogenic species. To establish a bioreporter panel suitable for direct screening of producer strains, we selected biomarkers indicative of interference with the main bacterial metabolic pathways. We chose the promoters of the *B. subtilis* genes *yorB*, *bmrC* (*yhel*), *ypuA*, and *lial*, which had previously been shown to be specifically induced upon antibiotic stress (Urban et al., 2007; Freiberg et al., 2006; Mascher et al., 2004; Wenzel et al., 2014). The *yorB* gene encodes for a SPβ prophage protein of unknown function and is proposed to be part of the LexA regulon involved in the SOS response (Urban et al., 2007; Au et al., 2005). Its expression was described to be induced by compounds interfering with DNA synthesis and structure. Impairment of protein synthesis, or more specifically the occurrence of translation arrest, results in a specific induction of *bmrC*. In contrast, protein synthesis inhibitors which induce miscoding (e.g., most aminoglycosides) or result in truncated peptides (e.g., puromycin) do not increase *bmrC* expression (Urban et al., 2007). The BmrC protein is a subunit of a putative multidrug ABC transporter and it is still an enigma, why is it induced by a range of mechanistically similar yet structurally very diverse translation stalling agents. Besides, a deletion mutant of this transporter did not show increased sensitivity to compounds inducing its expression (Torres et al., 2009). Both the *ypuA* and *lial* promoters (P_{ypuA} and P_{lial}) serve as biomarkers for cell envelope stress. While P_{ypuA} reacts broadly to various kinds of stress affecting the cell wall or the cytoplasmic membrane, P_{lial} seems more selectively induced upon interference with the lipid-II cycle

Please cite this article in press as: Wex et al., Bioreporters for direct mode of action-informed screening of antibiotic producer strains, Cell Chemical Biology (2021), https://doi.org/10.1016/j.chembiol.2021.02.022

CellPress

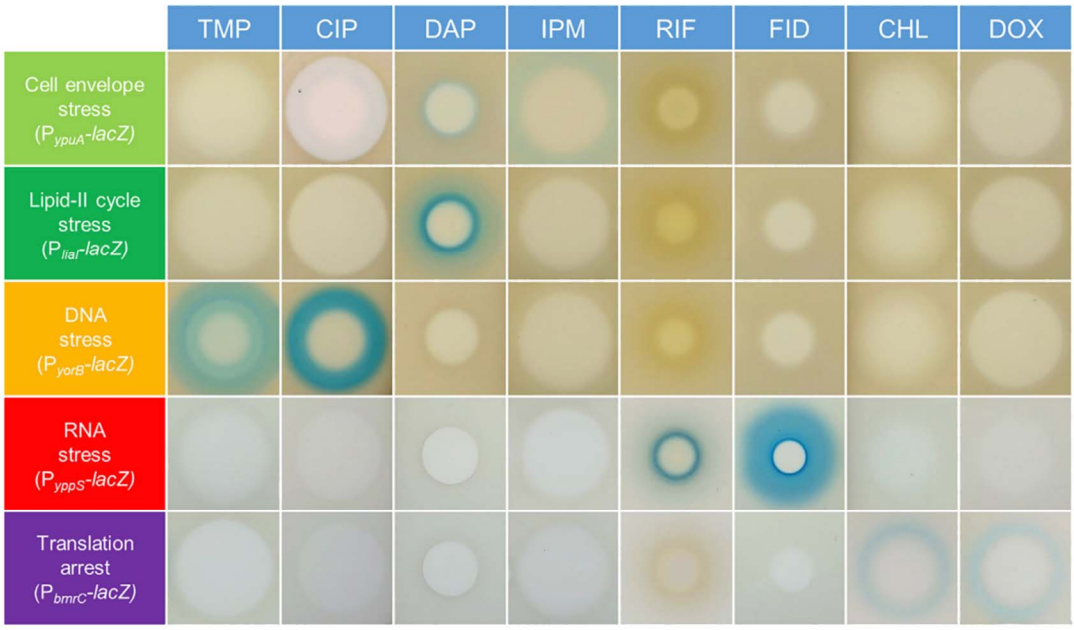

Figure 1. Induction pattern of exemplary reference antibiotics tested against the bioreporter strain panel

Pure compounds were spotted on agar, containing the respective *B. subtilis* reporter strain, in the following amounts: trimethoprim (TMP) 2 μg; ciprofloxacin (CIP) 5 μg; daptomycin (DAP) 2 μg; imipenem (IPM) 1 μg; rifampin (RIF) 1 μg; fidaxomicin (FID) 4 μg; chloramphenicol (CHL) 10 μg; and doxycycline (DOX) 10 μg. Promoter induction was detected as a blue halo following overnight incubation. The reporters for cell envelope stress (P_{ypuA}-*lacZ*, light green), lipid-II cycle stress (P_{liaI}-*lacZ*, green), and DNA stress (P_{yorB}-*lacZ*, yellow) were tested using lysogeny broth soft agar. RNA stress (P_{yppS}-*lacZ*, red) and translation arrest (P_{bmrC}-*lacZ*, violet) reporters were grown in Belitzky minimal soft agar.

as postulated by Mascher and colleagues (Urban et al., 2007; Jordan et al., 2006; Mascher et al., 2004), i.e., by compounds disturbing the cycling of the undecaprenyl phosphate carrier in the bacterial membrane. The gene of unknown function, *ypuA*, is regulated by SigM, an extracytoplasmic sigma factor involved in the cellular adaption to environmental stress (Jervis et al., 2007). The small membrane protein LiaI is encoded by the *liaIH-liaGFSR* operon, which is autoregulated via the two-component system LiaRS (Mascher et al., 2004). The promoter regions of the above-mentioned genes were individually fused to the β-galactosidase reporter gene *lacZ* and were chromosomally integrated into the *amyE* locus of *B. subtilis* 1S34, a sporulation-deficient derivative of *B. subtilis* 168 (Piggot, 1973). We also tried the *helD* (*yvgS*) promoter (P_{helD}) for our purpose, which was previously used to monitor stress within the RNA synthesis pathway (Urban et al., 2007), but P_{helD} only gave rise to a weak induction signal in the agar-based bioreporter setup, which did not meet the goal of robust detection. We re-analyzed previous microarray data (Freiberg et al., 2006) and identified an alternative, promising biomarker candidate, namely *yppS*, that had displayed strong upregulation upon treatment with the RNA polymerase inhibitors, rifampin and corallopyronin, in the transcriptome study. We constructed a reporter strain containing the chromosomal fusion of the *yppS* promoter (P_{yppS}) and the *lacZ* reporter gene, which reacted strongly to rifampin exposure and showed a more powerful induction signal than the P_{helD}-*lacZ* reporter strain (Figure S1). P_{yppS}-*lacZ* was selectively induced by direct inhibitors of the RNA polymerase and also allowed the detection of compounds interfering with RNA synthesis by intercalation into DNA, such as actinomycin D (compare Table S1). To yield sensitive detection in the agar-based assay setup, the handling of each bioreporter strain was optimized individually regarding growth phase, cell number, growth medium, supplements, substrate concentration, incubation time, and temperature, finally resulting in a robust protocol described in the STAR methods that can now be used for diverse applications without modification.

Induction specificity validated by pure antimicrobial substances with known MOA

Bacteria can show substantially different growth behavior and metabolism in liquid culture and agar. As previous studies employing some of our promoters were conducted in liquid media (Freiberg et al., 2006; Urban et al., 2007), we wanted to ensure that the bioreporters also generate reliable and selective signals in an agar-based setup. For a first round of validation, we tested 90 pure antibacterial agents with known MOA across the entire reporter panel. All of the five bioreporters showed selective induction by all tested antibiotics in accordance with their described MOA (Table S1). An exemplary panel of antibiotics is depicted in Figure 1. Reporter induction was detectable as a blue halo at the antibiotic diffusion borders, where the antibiotic concentration was not high enough to kill the *B. subtilis* reporter cells, but sufficient to cause a cellular stress response. Spotting of a concentration series of different antibiotics revealed a high sensitivity of the bioreporters, as already low antibiotic amounts gave rise to an induction signal (Figure S2). The most sensitive bioreporters even showed an induction at subinhibitory concentrations, i.e., a blue coloration of the agar was visible in the absence of a distinct zone of inhibition (ZOI).

Please cite this article in press as: Wex et al., Bioreporters for direct mode of action-informed screening of antibiotic producer strains, Cell Chemical Biology (2021), https://doi.org/10.1016/j.chembiol.2021.02.022

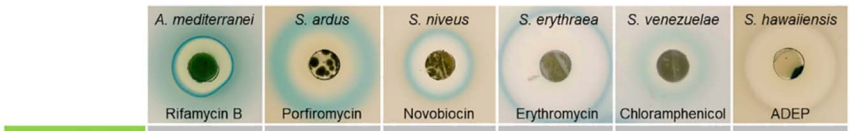

	A. mediterranei Rifamycin B	*S. ardus* Porfiromycin	*S. niveus* Novobiocin	*S. erythraea* Erythromycin	*S. venezuelae* Chloramphenicol	*S. hawaiiensis* ADEP
P_{ypuA}-*lacZ*	-	-	-	-	-	-
P_{lial}-*lacZ*	-	-	-	-	-	-
P_{yorB}-*lacZ*	-	+	+	-	-	-
P_{yppS}-*lacZ*	+	-	-	-	-	-
P_{bmrC}-*lacZ*	-	-	-	+	+	-

Figure 2. Induction of the bioreporter strain panel by agar-grown producer strains of antibiotics from different mechanistic classes

Amycolatopsis mediterranei NBRC 14843, *Streptomyces ardus* NBRC 13490, *Streptomyces niveus* NBRC 12917, *Saccharopolyspora erythraea* NBRC 13426, *Streptomyces venezuelae* NBRC 13096, and *Streptomyces hawaiiensis* NRRL 15010 were precultured on agar. Agar plugs of well-grown cultures were sampled and embedded in fresh agar containing the different bioreporter strains. The induction status of the tested reporter strain is indicated by + (inducing) and – (non-inducing), with the pictures showing the respective induction zone arising around the actinomycetes agar plug. The names of the antibiotics known to be produced by the respective antibiotic producer strain are indicated in the corresponding panel. Porfiromycin is a mitomycin C derivative.

Each bioreporter specifically signaled stress inflicted onto a particular metabolic pathway or cellular structure, without elucidating the exact molecular target of the respective antibiotics. The DNA stress reporter (P_{yorB}-*lacZ*), as an example, showed induction after treatment with trimethoprim (a folate synthesis inhibitor limiting the thymidine precursor supply) (Gleckman et al., 1981), ciprofloxacin (a DNA gyrase inhibitor) (Lebel, 1988), or mitomycin C (a DNA intercalating and alkylating agent) (Verweij and Pinedo, 1990). For the detection of cell envelope stress, our two different biomarkers (*ypuA* and *lial*) allowed to more specifically classify the MOA of compounds acting in this pathway. While P_{ypuA}-*lacZ* was induced by all tested cell envelope-targeting compounds, except for the membrane-active ionophores (Table S1), an additional induction of P_{lial}-*lacZ* conveyed the information that those substances rather target membrane-associated steps of the lipid-II cycle (e.g., nisin or teicoplanin). Interestingly, all quinolones, mitomycin C, and phleomycin, which interfere with DNA synthesis, showed an additional weak induction of the cell envelope stress promoter P_{ypuA} besides their prominent induction of the DNA damage-sensing promoter P_{yorB}. This observation had not been made by Urban and colleagues in their screening in liquid media, and could be due to our agar-based setup (Urban et al., 2007). The overnight incubation might reveal secondary antibiotic effects that had not manifested in the liquid assay, e.g., due to shorter incubation times. One potential explanation for the induction of P_{ypuA} by this group of agents could be oxidative stress and the corresponding impairment of membrane function (Goswami et al., 2006; Dwyer et al., 2007; Hong et al., 2019). None of the five reporter strains showed an induction upon treatment with ionophores (e.g., gramicidin A), fatty acid synthesis inhibitors (e.g., cerulenin), protein synthesis inhibitors that act by miscoding (e.g., gentamicin), by inhibition of aminoacyl-tRNA synthesis (e.g., mupirocin), or with agents causing protein stress (e.g., diamide), which is in accordance with the anticipated reporter coverage (Table S1). Of note, the aminocyclitol antibiotics spectinomycin and hygromycin B, often described as unusual aminoglycosides, rather cause blocking of translation than miscoding (Borovinskaya et al., 2007, 2008) and accordingly led to an induction of the translation arrest reporter (P_{bmrC}-*lacZ*).

Validation of the agar-based bioreporter assay as a MOA profiling tool for direct screening of antibiotic producer strains

Having positively evaluated the sensitivity and specificity of the agar-based bioreporter system with known reference compounds, we set out to directly test antibiotic producer strains, without previous extract generation or further purification of metabolites. We cultivated six actinomycetes strains, known to produce specific, well-characterized antibiotics, on solid media for several days, mostly until sporulation became visible. Agar plugs of the grown producer strains were directly tested against our bioreporter panel. All strains showed antibacterial activity combined with the expected promoter induction reflecting the MOA of the produced antibiotic (Figure 2). For example, *Streptomyces niveus* NBRC 12917 is a known producer of novobiocin, which inhibits DNA gyrase (Sugino et al., 1978). When we tested an agar plug of the grown *S. niveus* strain against the reporter panel, we detected a selective induction of P_{yorB}-*lacZ*, indicative of interference with DNA synthesis (Figure 2). In accordance, the pure compound novobiocin showed the same induction pattern on the reporter panel (Table S1). As expected, the acyldepsipeptide (ADEP)-producing strain *Streptomyces hawaiiensis* NRRL 15010 showed no induction, as the ClpP protease activator ADEP causes cellular protein stress (Brötz-Oesterhelt et al., 2005; Sass et al., 2011), which is not covered by our reporter panel.

Direct combined bioactivity and MOA screening of uncharacterized antibiotic producer strains

We proceeded to directly screen uncharacterized actinomycetes strains, without subjecting them to any kind of extraction, enrichment, or fractionation procedure. A schematic overview of the direct agar-based bioreporter screening process is depicted in Figure 3. In total, we included ~500 actinomycetes strains from the Tübingen strain collection in the bioreporter screening. Of note, 290 of these strains had previously shown bioactivity against *Staphylococcus aureus*. All actinomycetes were grown on at least two different solid media and were first tested for growth inhibition of the *B. subtilis* 1S34 wild type in the agar-based setup. In addition, a subset of approximately 280 producer strains was tested against *E. coli* ATCC25922 to check

Please cite this article in press as: Wex et al., Bioreporters for direct mode of action-informed screening of antibiotic producer strains, Cell Chemical Biology (2021), https://doi.org/10.1016/j.chembiol.2021.02.022

CellPress

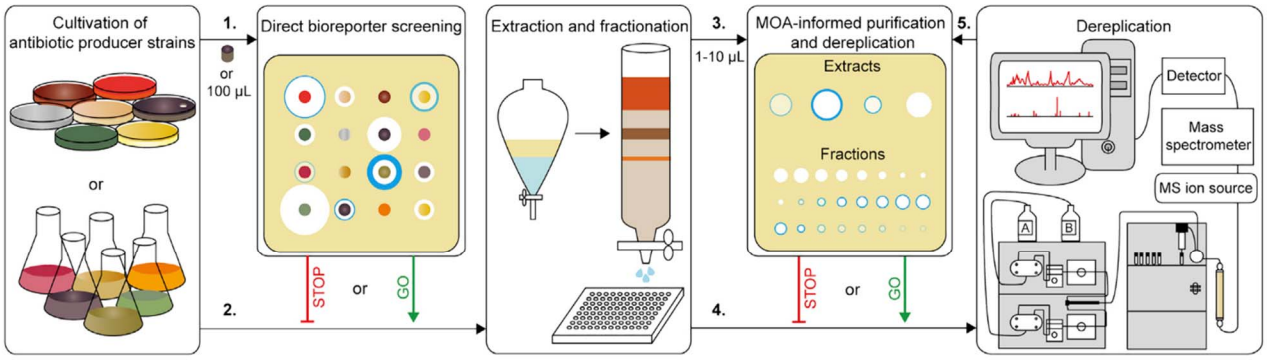

Figure 3. Schematic overview of the dereplication process using the agar-based bioreporter tool

(1) Well-grown samples of the antibiotic producer strains (agar plugs and/or supernatants) obtained under different growth conditions were directly tested against the reporter panel. (2) Samples with interesting bioactivities and reporter signals (blue halo) were selected for further investigation. Therefore, supernatants and/or agar plates were extracted and fractionated. (3) During this purification process, the previously shown activity and reporter signals were monitored in all samples. (4) This MOA-informed purification procedure allowed to selectively follow-up activities of interest, which could then be analyzed via high-resolution mass spectrometry. (5) Dereplicated, pure substances were again checked for the expected activity and reporter profile. The bioreporter setup allows for an evaluation at different steps (i.e., 2. and 4.) within the cultivation, purification, and dereplication processes, thereby enabling to specifically follow-up antibacterial activities of interest (indicated by "GO") or to deprioritize or set aside samples with less-interesting profiles (indicated by "STOP").

for anti-Gram-negative activity (Data S1). In this pilot study, none of the strains exhibited *E. coli*-only activity, which would have putatively hinted at a specific outer membrane target. All producer strains active against *E. coli* ATCC25922 also showed activity against *B. subtilis* 1S34, implicating conserved targets and demonstrating the capacity of the chosen bioreporter strain background for sensitive detection of a broad range of agents acting on a broad range of targets. Of course, antibacterial compounds selectively targeting the outer membrane without affecting the cytoplasmic membrane would be missed by our current bioreporter panel and would require the addition of an outer membrane stress bioreporter in a Gram-negative background. A total of 230 of the 500 tested producer strains showed no antibacterial activity against *B. subtilis* 1S34 and were excluded, while the remaining bioactive actinomycetes strains (~270) were tested against the full reporter panel. Figure S3 shows an exemplary screening plate containing the P_{yorB}-*lacZ* bioreporter. For some actinomycetes strains, we detected a blue coloration of the agar test plug. Generally, such agar plug coloration occurred with all five tested bioreporters and was considered unspecific, as it is most likely due to an inherent β-galactosidase production of the antibiotic producer strain. Promoter induction was only considered certain if a blue halo occurred at the borders of a defined ZOI. As 94 of the bioactive producer strains showed a reliable induction of at least one biomarker, we achieved a coverage of ~36%. An induction of more than one promoter (with the exception of the commonly observed P_{ypuA}-*lacZ* and P_{lial}-*lacZ* combination) may either hint at the production of a single substance with a dual MOA or causing secondary antibiotic effects, or the production of multiple bioactive agents. Subsequent to the initial screening, we started to follow-up on several of the producer strains that had led to an induction of the bioreporter strains. Extracts were generated from the same agar plate or liquid culture previously used for the bioreporter assay, fractionated, and again checked for the previously detected reporter signal before analyzing them via high-performance liquid chromatography-mass spectrometry (HPLC-MS) and/or HPLC-tandem MS. The bioreporter signals not only allowed to monitor the purification procedure, but facilitated compound deconvolution by adding an additional MOA-informed dimension to the dereplication process. If a certain mass found in an extract suggested a known compound and the bioreporter signal matched the expected MOA, two independent technologies immediately confirmed each other in the occurrence of a particular agent.

For assay validation, we also considered certain compounds present in growth media of the producer strains (e.g., isoflavones, such as genistein and daidzein) or common metabolites from actinomycetes (e.g., N-acetyltyramine or aromatic compounds, such as indol-3-acetic acid and indole-3-propionic acid), which are often co-extracted and detected by HPLC-MS. To exclude unspecific induction signals, resulting from solvents or commonly purified media components or metabolites, we tested a subset of these substances on the bioreporter panel (Table S2). While some of these agents showed very weak antibacterial activity resulting in a turbid ZOI, none of them led to an induction of one of our five bioreporter strains.

In total, 28 compounds were dereplicated from different strains of the Tübingen strain collection, all of them matching the MOA proposed by the respective promoter induction (Table 1). Additional information on the antibiotic structures, detection methods, mass spectra, and a strain-specific assignment of the dereplicated substances can be found in Table S3 and Data S2.

One example for a correct MOA prediction was the detection of berninamycin C in the P_{bmrC}-inducing strain Tü2108 (Table 1). Berninamycin, a cyclic thiopeptide antibiotic, is known to inhibit protein synthesis by binding to the 50S subunit of the ribosome, thereby hindering the incorporation of amino acids (Reusser, 1969). The resulting stress response due to ribosomal stalling elicited the reporter signal indicating translation arrest. Strain Tü104 showed induction of both cell envelope stress promoters, P_{ypuA} and P_{lial}. The combined induction suggested interference of a produced metabolite with biosynthesis, function, or integrity

Please cite this article in press as: Wex et al., Bioreporters for direct mode of action-informed screening of antibiotic producer strains, Cell Chemical Biology (2021), https://doi.org/10.1016/j.chembiol.2021.02.022

Table 1. Dereplicated antibiotics identified by direct bioreporter screening of antibiotic producers from the Tübingen strain collection

Reporter induction	Dereplicated antibiotics[a] (producer strain)
DNA stress (P_{yorB}-*lacZ*)	chartreusin (GöK9/13; GöK16/4); chrysomycin A (Tü2471); C-1027 (Tü2401); daunomycin (TüG111); rachelmycin (GöOber505)
RNA stress (P_{yppS}-*lacZ*)	actinomycin D, C_2 (GöWind756); chartreusin (GöK9/13; GöK16/4); cosmomycin B (Tü40/15; Tü2626); cosmomycin C (GöK8/12)
Translation arrest (P_{bmrC}-*lacZ*)	amicetin (KNN49.3e); berninamycin (Tü2108); chartreusin (GöK16/4); cycloheximide (A4/2); griseoviridin, viridogrisein (Tü3180); pactamycin (Tü6430); pristinamycin I, II (Tü2975)
Cell envelope and lipid-II cycle stress (P_{ypuA}-*lacZ* and P_{liaI}-*lacZ*)	aborycin (TüG349); FD-594 (Tü104); pentamycin (GöK12/7); telomycin (Tü2641)
No induction signal	albomycin δ_1 (Tü2401); boromycin (GöK12/9); griseorhodin A (TüG117); lobophorin A, E (GöSöt11); monactin (TüG102); omomycin (TüG343)

[a]The signals of the bioreporters concurred with the described MOA of the dereplicated antibiotics in all cases.

of the cell envelope, especially hinting at interference with the bacterial lipid-II cycle, also seen for antibiotics, such as teicoplanin (Table S1). HPLC-MS analysis revealed the production of antibiotic FD-594 (Data S2), belonging to the aromatic polyketides (Kudo et al., 2011). FD-594 is not well characterized but shares a related structural backbone with lysolipin I. It was proposed that lysolipin I would inhibit peptidoglycan synthesis by targeting bactoprenol-containing molecules (Drautz et al., 1975). The structural similarity and the shared reporter induction pattern (Table S1) hint at a similar MOA of antibiotic FD-594 and lysolipin I, a hypothesis that can now be tested by focused follow-up studies.

We were also interested to see what kinds of substances produced by the actinomycetes strains are not covered by our reporter panel. Therefore, we followed up some of the producer strains that showed antibacterial activity without inducing any of the five bioreporters. For these strains, seven different antimicrobial compounds could be identified. Among those were ionophores (monactin, boromycin, and omomycin), a siderophoric tRNA synthesis inhibitor (albomycin δ_1), and substances with unknown or poorly characterized MOA and target structures (lobophorins A and E, griseorhodin A) (Table 1). Mechanism-wise, these non-inducing compounds are in accordance with our expected coverage of the reporter panel that we had evaluated on the basis of 90 reference antibiotics with known MOA (Table S1). We further suspect some of the ZOI without reporter signal to be caused by aminoglycosides, which are known to be frequently produced by actinomycetes (Cox et al., 2017; Culp et al., 2019). Aminoglycosides would most likely be missed by our current screening strategy for two reasons, the *bmrC* bioreporter detects ribosome stalling but not miscoding and our applied purification procedure favors the extraction of hydrophobic substances. The expansion of the bioreporter panel is subject of current work. A bioreporter detecting interference with fatty acid synthesis as well as a bioreporter sensing protein stress, e.g., caused by the accumulation of mistranslated proteins (e.g., aminoglycosides), peptide fragments (e.g., ADEP), or prematurely terminated proteins (e.g., puromycin), are presently being developed. In addition, a Gram-negative bioreporter specifically responding to outer membrane stress is under investigation.

Exploiting the full potential of antibiotic producer strains

The advantages of our direct reporter screening approach are the large variety of compatible samples (agar plugs, supernatants, extracts, fractions, pure compounds) and the immediate detection of antibiotic activity combined with MOA information. This makes our technology a particularly useful tool to investigate changing antibiotic production patterns. When following up the hit strain Tü2401 that yielded an induction of the DNA stress reporter in the direct agar-based screening, we noted that we lost promoter induction, but not bioactivity, when the producer strain was grown in liquid media (Figure 4A). The ZOI were not distinguishable without the additional information of the divergent promoter signal. Substance extractions from agar and liquid media confirmed the cultivation-dependent production of two different natural products: albomycin δ_1 and C-1027 (lidamycin) (Figure 4B). When grown on agar, the strain produced C-1027 (Data S2), a very potent DNA intercalator that is able to introduce single- and double-strand breaks (Shao and Zhen, 2008), and our DNA stress reporter P_{yorB}-*lacZ* reacted accordingly (Figure 4A). In liquid culture, Tü2401 produced albomycin δ_1 (Data S2), a siderophore, which exerts intracellular activity against the seryl-tRNA synthetase (Zeng et al., 2012). Antibiotics interfering with tRNA synthesis are not covered by our reporter panel (compare mupirocin in Table S1), which concurred with the lack of promoter induction. This example highlights the potential of the direct MOA-informed bioreporter screening to quickly dissect divergent production of secondary metabolites that may occur under different growth conditions in a single producer strain.

The reporter strains were also useful to monitor the different steps of antibiotic purification. In cases where multiple antibacterial agents are produced, the additional information of the specific reporter signal helps to distinguish between these activities already at an early stage in the purification process. To demonstrate the potential to distinguish different substances hidden behind a single ZOI, we simulated the production of multiple bioactive metabolites by applying several combinations of two antibiotics, targeting different metabolic pathways, together in the same spot. Reporter induction sensitively detected the MOA of all agents in the different combinations (Figure S4). However, it should be kept in mind that the detection of reporter signals from both antibiotics is dependent on their concentration in the mixture and their diffusion coefficient in the agar. In particular, if one of the agents is quickly diffusing, very potent, or rapidly bactericidal, it might extinguish the signal of another

Please cite this article in press as: Wex et al., Bioreporters for direct mode of action-informed screening of antibiotic producer strains, Cell Chemical Biology (2021), https://doi.org/10.1016/j.chembiol.2021.02.022

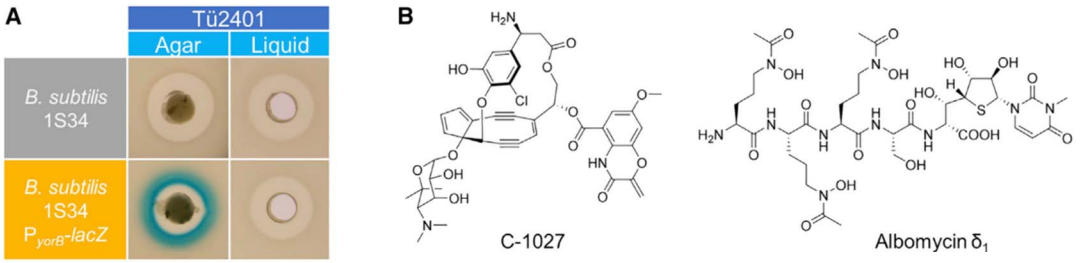

Figure 4. Rapid discrimination of distinct antibacterial metabolites synthesized by Tü2401 under different growth conditions

(A) Agar-based reporter screening of Tü2401 precultured either on OM agar or in OM liquid medium. An agar plug (left) or 100 μL of the liquid culture supernatant (right) were tested against *B. subtilis* 1S34 as well as our DNA stress reporter *B. subtilis* 1S34 P_{yorB}-*lacZ*. Both samples showed antibacterial activity against *B. subtilis* 1S34. Induction of the DNA stress reporter was only detected for the Tü2401 agar sample, allowing an immediate discrimination, and hinting at the production of two different substances.

(B) Structure of the isolated substances C-1027 (agar) and albomycin δ_1 (liquid).

less potent or less diffusible agent. Nonetheless, our reporter setup enables a bioactivity- and MOA-informed fractionation process, which will immediately solve the issues projected for simultaneous probing of two agents within the same ZOI. In an exemplary extract fractionation from Tü104, different active fractions separately eluted from the HPLC column could clearly be distinguished due to their divergent reporter signal (Figure S5). In combination with HPLC-MS data, the bioactivity- and MOA-based fractionation provides a valuable tool for selective compound identification and purification. The entire screening process is rapid and efficient and agar extraction has already worked well in many cases, omitting the prevalently used liquid cultivation for compound identification.

Promoter induction patterns provide information about dual and/or secondary MOA

For strain GöK16/4, we observed the induction of three different promoters, which corresponded to DNA, RNA, and protein synthesis stress, respectively (Table 1). This result initially suggested the production of several antibiotic agents with different MOA. However, dereplication revealed only a single bioactive substance: the antitumor glycoside antibiotic chartreusin (Data S2). For the pure compound chartreusin, we obtained the same promoter induction pattern (Figure 5A), thereby disproving the idea of several antibiotics produced by strain GöK16/4. At lower chartreusin concentrations, the signal on our translation arrest reporter was not detectable in the agar-based reporter setup (Figure 5A). Chartreusin-mediated P_{bmrC}-*lacZ* induction mainly appeared in the inner radius of the ZOI, indicating that higher concentrations might be required to induce the protein synthesis stress. In comparison, the DNA or RNA synthesis stress signals, induced by the intercalating MOA of chartreusin (Portugal, 2003), could be detected at all concentrations (Figure 5A). This observation might also explain why we could only detect P_{yorB}-*lacZ* and P_{yppS}-*lacZ* signals for the less bioactive strain GöK9/13, which was also shown to produce chartreusin but in lower amounts (Table 1). Our triple promoter induction pattern of chartreusin is supported by an observation of Li et al. (1978), who detected strong effects of chartreusin on RNA and DNA synthesis in an incorporation assay with radioactive precursors. Protein synthesis was also affected; however, to a lesser extent and requiring a higher concentration of chartreusin. The weak induction of the P_{bmrC} promoter upon chartreusin treatment in our study hinted at an additional bacterial target structure or a secondary metabolic effect, which led to translation arrest. The interference with protein synthesis had also been observed in a study using reticulocyte ribosomes. Here, it was shown that chartreusin is attached to ribosomes and inhibits the binding of aminoacyl tRNAs, thereby hindering polypeptide chain elongation (Gregg and Heintz, 1972). This finding was confirmed by demonstrating the binding of chartreusin to human tonsil ribosomes and its inhibition of peptide translocation from the A to the P site (Vazquez et al., 1974).

The detection of polypharmacology by our bioreporter system was also verified for the pure substances 5′-fluorouracil and SCH-79797. 5′-Fluorouracil induced both the DNA stress and translation arrest biomarkers (Table S1). The detection of both signals concurs with its known dual MOA. 5′-Fluorouracil inhibits thymidylate synthase, which restricts and unbalances pyrimidine *de novo* synthesis leading to DNA stress. In addition, metabolites of 5′-fluorouracil are incorporated into RNA and DNA (Cohen et al., 1958; Longley et al., 2003; Noordhuis et al., 2004). Incorporation into RNA was described to disturb mRNA processing in eukaryotes and protein synthesis in general (Horowitz and Chargaff, 1959; Noordhuis et al., 2004; Will and Dolnick, 1989), the latter matching the observed ribosome stalling reporter signal. SCH-79797 is a recently reported antibacterial agent with broad-spectrum activity, very low induction of resistance, and a new, dual MOA (Martin et al., 2020). Motivated by the emerging pharmacological profile of the compound, the authors put substantial efforts into elucidating the molecular mechanism of the new compound and applied a range of different assays, including rather demanding methodology, such as cytological profiling, thermal proteome profiling, and metabolomics, to narrow down on the target (Martin et al., 2020). As a result, they found that SCH-79797 inhibits dihydrofolate reductase and disturbs membrane integrity. Interested in finding out what our easy-to-handle bioreporter strains would reveal about the compound, we also tested SCH-79797 and could immediately detect an interference with both cell envelope reporters, as well as the DNA stress reporter (Figure 5B). The combined induction of P_{ypuA}-*lacZ* and P_{liaI}-*lacZ* hinted at a membrane target (lipid-II cycle), while a P_{yorB}-*lacZ* signal indicated the induction of the SOS response due to DNA stress, which is induced e.g., by gyrase

Please cite this article in press as: Wex et al., Bioreporters for direct mode of action-informed screening of antibiotic producer strains, Cell Chemical Biology (2021), https://doi.org/10.1016/j.chembiol.2021.02.022

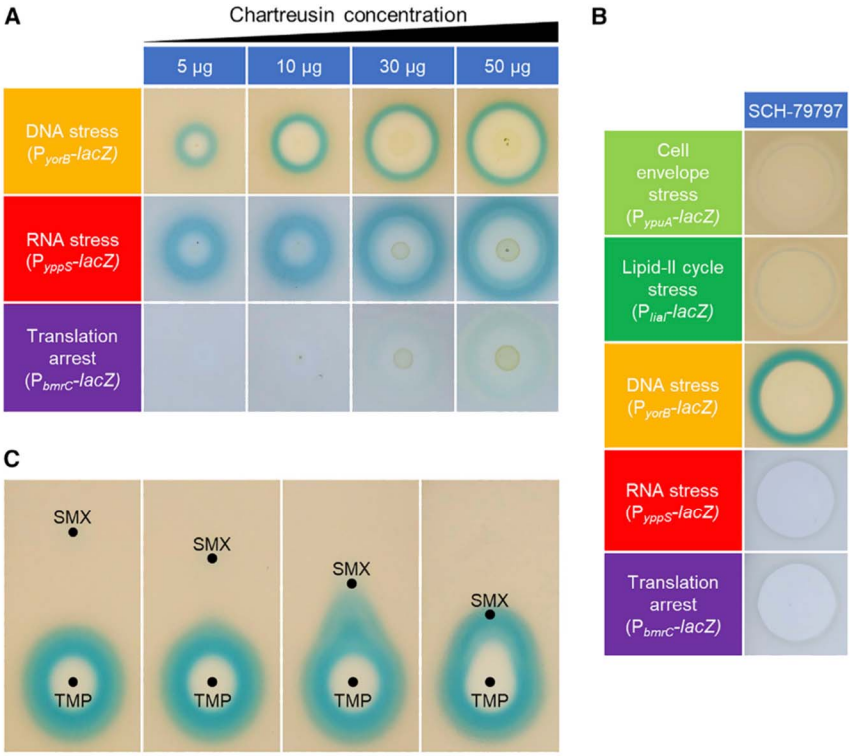

Figure 5. Reporter-dependent visualization of antibiotic polypharmacology and synergism

(A) Induction of the DNA, RNA, and protein synthesis stress reporters after treatment with a concentration range of chartreusin (5, 10, 30, or 50 µg). All tested concentrations induced the DNA and RNA stress reporters, while induction of P_{bmrC}-*lacZ* indicative of translation arrest was only detected at increased chartreusin concentrations.

(B) Diverse induction pattern after treatment with 40 µg SCH-79797. A strong induction for P_{yorB}-*lacZ* could be detected. SCH-79797 also showed weak signals for both cell envelope stress bioreporters P_{ypuA}-*lacZ* and P_{liaI}-*lacZ*.

(C) The synergistic effect of sulfamethoxazole (SMX) and trimethoprim (TMP) visualized by reporter induction. SMX at an amount of 10 µg showed no antibiotic activity. Trimethoprim at 1 µg showed a large ZOI and an induction of P_{yorB}-*lacZ*. After reducing the spotting distance, the synergistic effect of both substances was detectable by an additional induction zone between both antibiotic spots.

inhibitors, folate synthesis inhibitors, or some intercalators (Table S1). The latter example demonstrates that the reporter panel is well suited for rapid MOA profiling of new bioactive agents.

Detection of synergistic effects with the bioreporter tool

Having evaluated this reliable screening approach for sensitive MOA verification, we were interested to see if we could also detect synergistic antibiotic effects. The combination treatment and the synergism of trimethoprim and sulfamethoxazole, two folate synthesis inhibitors, is well established in antibiotic therapy (Minato et al., 2018). We spotted the two substances on agar, containing the DNA stress reporter, and gradually reduced the spotting distance. Sulfamethoxazole was used in a concentration showing no activity against *B. subtilis* 1S34 and neither did it elicit a reporter signal. As soon as the two compounds came into close vicinity, the induction signal of P_{yorB}-*lacZ* became visible where both antibiotic diffusions zones overlapped, clearly visualizing their synergistic effect on DNA synthesis (Figure 5C). This particular application could be of special interest not only for purified compounds, but also in co-cultivation studies with diverse producer species grown in close proximity.

Conclusions and perspectives

In summary, we developed and extensively evaluated a panel of bacterial bioreporters suitable for agar-based screening that respond specifically to distinct modes of antibiotic action, thereby signaling DNA stress, RNA stress, translation arrest, and interference with cell envelope integrity. Assay conditions were probed and optimized to enable reliable and sensitive signal detection after overnight incubation with the antibiotic. The assay proved to be fast, suitable for substantial throughput, and robustly worked with any material along the purification pipeline, from unprocessed producer strains, extracts, and partially purified fractions to pure compounds. To reliably validate the approach, in this study we focused on actinomycetes producer strains from the Tübingen strain collection grown under standard laboratory growth conditions. Knowing this to be a rather richly mined source and expecting to encounter many known compounds, we wanted to evaluate if the bioreporters manage to reliably signal the expected MOA of a broad range of diverse agents during the production and purification process, which indeed they did. In addition, they led us to a range of compounds that had not been isolated from the Tübingen strain collection before. However, importantly, our assay is not limited to this bacterial order of antibiotic producers, and there is also no preference for certain groups of bacteria.

The current proof-of-concept study aimed at demonstrating the broad applicability of the bioreporter-based technology. By using the different bioreporters in parallel, their MOA profiling capacity can be harnessed best. Screening campaigns benefit from the additional MOA information that adds a further dimension to the dereplication process. Known compounds with known MOA can be rapidly deconvoluted by correlating the HPLC-MS data with the bioreporter signal(s). Agar extraction of the single Petri dish of the cultivated producer strain, previously used for the bioreporter screening, is more than sufficient for dereplication of most bioactive agents. With an aim to expand the MOA coverage, to ideally assign a target area to most natural products tested, we are working toward the detection of further antibacterial mechanisms. Besides such global profiling, our bioreporter method offers potential as a direct selection tool in a screening process. For instance, if a certain target area is of particular interest, only a single bioreporter from the current set can be utilized.

Please cite this article in press as: Wex et al., Bioreporters for direct mode of action-informed screening of antibiotic producer strains, Cell Chemical Biology (2021), https://doi.org/10.1016/j.chembiol.2021.02.022

Notably, the potential of the technology extends beyond screening and can be applied to a variety of further research questions, such as unraveling challenging compound mixtures, detecting synergistic activities, or exploring multiple mechanisms inherent in a single compound. The bioreporter assay is also ideally suited as a rapid entry assay to guide the selection of appropriate follow-up experiments for elucidating the molecular target.

SIGNIFICANCE

With the dramatic increase in infections caused by antibiotic-resistant bacteria, there is an urgent need for new antibacterial agents to replenish dwindling antibiotic development pipelines. Although microbial secondary metabolites are acknowledged as the most promising source of antibiotics and efforts are directed toward finding new ones, rediscovery of known compounds binds valuable capacities. An efficient, sensitive, and rapid deconvolution strategy is mandatory to identify already known compounds quickly, reliably, and without the need for laborious compound purification. High-resolution mass spectrometry has made tremendous progress and serves as the mainstay of current dereplication procedures, while at the biological end of the natural product discovery process, classical agar-based screening for bacterial growth inhibition is still the most widely used procedure, not least due to its ease of handling. Our agar-based bioreporter toolbox links such classical activity-based screening with the simultaneous acquisition of reporter-based MOA information. When combined with high-resolution mass spectrometry, this MOA-informed bioactivity screening represents a powerful dereplication tool. Without much additional effort in time and resources, the information content generated in the screening process is greatly enhanced. A particular strength of the bioreporter assay is its ease of handling, speed, low cost, and the fact that it can be performed with basic microbiological equipment, which in principle allows its application in any natural product isolating laboratory worldwide. Another great strength is its versatility. Biosynthesis-related applications include, but are not limited to, the assessment of the biosynthetic potential of unprocessed producer strains, tracking of substances throughout the purification process, detection of bioactive compounds in mixtures, and evaluation of the synergistic potential. Mechanism-wise, MOA hypotheses emerge already during the initial screening process, and polypharmacology is detected. Any producer of secondary metabolites is suitable for testing, which makes the setup highly instrumental in the early steps of antibiotic discovery.

STAR★METHODS

Detailed methods are provided in the online version of this paper and include the following:

- KEY RESOURCES TABLE
- RESOURCE AVAILABILITY
  - Lead contact
  - Materials availability
  - Data and code availability
- EXPERIMENTAL MODEL AND SUBJECT DETAILS
  - Bacterial strains
- METHOD DETAILS
  - Recombinant plasmid construction
  - Agar-based bioactivity screening
  - Agar-based bioreporter screening
  - Dereplication procedures
- QUANTIFICATION AND STATISTICAL ANALYSIS

SUPPLEMENTAL INFORMATION

Supplemental information can be found online at https://doi.org/10.1016/j.chembiol.2021.02.022.

ACKNOWLEDGMENTS

This study was funded by the German Center for Infection Research (DZIF) projects TTU 09.811, TTU 09.812, TTU 09.818, and TTU 09.819. J.S.S. gratefully acknowledges funding by the "Promotionskolleg Initiative" (Ministry for Science, Research and Arts Baden-Württemberg). H.B.-O., S.G., A.K., and V.M. also acknowledge infrastructural support from the Cluster of Excellence EXC 2124 funded by the German Research Foundation (Deutsche Forschungsgemeinschaft, DFG). We thank Damaris Mayer and Elisa Liebhart for expert technical assistance. We are further grateful to Hans-Peter Fiedler and Wolfgang Wohlleben for providing lysolipin I, chartreusin, echinomycin, holomycin, rinamycin, thiolutin, streptolydigin, streptovaricin, and sorangicin A, Gabriele König for providing corallopyronin A, and Leendert Hamoen for the kind gift of plasmid pHJS105.

AUTHOR CONTRIBUTIONS

H.B.-O. and A.B. devised the study concept. K.W.W., A.B., H.B.-O., J.S.S., S.G., F.H., Y.M., N.O., and T.H.J.N. designed experiments. K.W.W. designed and generated the bioreporter panel, established the assay conditions, and conducted all reporter screening experiments. J.S.S., F.H., N.O., and V.M. cultivated the uncharacterized producer strains. J.S.S., F.H., N.O., V.M., and A.K. purified and dereplicated the antimicrobial compounds. A.B., H.B.-O., S.G., Y.M., and T.H.J.N. supervised experiments. All authors discussed and analyzed data. K.W.W., A.B., and H.B.-O. wrote the paper. H.B.-O., S.G., Y.M., and T.H.J.N. acquired funding.

DECLARATION OF INTERESTS

The authors declare no competing interests.

Received: October 27, 2020
Revised: January 27, 2021
Accepted: February 23, 2021
Published: March 23, 2021

REFERENCES

Aslam, B., Wang, W., Arshad, M.I., Khurshid, M., Muzammil, S., Rasool, M.H., Nisar, M.A., Alvi, R.F., Aslam, M.A., Qamar, M.U., et al. (2018). Antibiotic resistance: a rundown of a global crisis. Infect. Drug Resist. *11*, 1645–1658.

Au, N., Kuester-Schoeck, E., Mandava, V., Bothwell, L.E., Canny, S.P., Chachu, K., Colavito, S.A., Fuller, S.N., Groban, E.S., Hensley, L.A., et al. (2005). Genetic composition of the *Bacillus subtilis* SOS system. J. Bacteriol. *187*, 7655–7666.

Bandow, J.E., Brötz, H., Leichert, L.I.O., Labischinski, H., and Hecker, M. (2003). Proteomic approach to understanding antibiotic action. Antimicrob. Agents Chemother. *47*, 948–955.

Bérdy, J. (2012). Thoughts and facts about antibiotics: where we are now and where we are heading. J. Antibiot. *65*, 385–395.

Please cite this article in press as: Wex et al., Bioreporters for direct mode of action-informed screening of antibiotic producer strains, Cell Chemical Biology (2021), https://doi.org/10.1016/j.chembiol.2021.02.022

Borovinskaya, M.A., Shoji, S., Fredrick, K., and Cate, J.H.D. (2008). Structural basis for hygromycin B inhibition of protein biosynthesis. RNA *14*, 1590–1599.

Borovinskaya, M.A., Shoji, S., Holton, J.M., Fredrick, K., and Cate, J.H.D. (2007). A steric block in translation caused by the antibiotic spectinomycin. ACS Chem. Biol. *2*, 545–552.

Brötz-Oesterhelt, H., Beyer, D., Kroll, H.-P., Endermann, R., Ladel, C., Schroeder, W., Hinzen, B., Raddatz, S., Paulsen, H., Henninger, K., et al. (2005). Dysregulation of bacterial proteolytic machinery by a new class of antibiotics. Nat. Med. *11*, 1082–1087.

Brötz-Oesterhelt, H., and Sass, P. (2010). Postgenomic strategies in antibacterial drug discovery. Future Microbiol. *5*, 1553–1579.

Bush, K., Courvalin, P., Dantas, G., Davies, J., Eisenstein, B., Huovinen, P., Jacoby, G.A., Kishony, R., Kreiswirth, B.N., Kutter, E., et al. (2011). Tackling antibiotic resistance. Nat. Rev. Microbiol. *9*, 894–896.

Bush, K., and Pucci, M.J. (2011). New antimicrobial agents on the horizon. Biochem. Pharmacol. *82*, 1528–1539.

Carrano, L., and Marinelli, F. (2015). The relevance of chemical dereplication in microbial natural product screening. J. Appl. Bioanal. *1*, 55–67.

Cohen, S.S., Flaks, J.G., Barner, H.D., Loeb, M.R., and Lichtenstein, J. (1958). The mode of action of 5-fluorouracil and its derivatives. Proc. Natl. Acad. Sci. U S A *44*, 1004–1012.

Cox, G., Sieron, A., King, A.M., De Pascale, G., Pawlowski, A.C., Koteva, K., and Wright, G.D. (2017). A common platform for antibiotic dereplication and adjuvant discovery. Cell Chem. Biol. *24*, 98–109.

Culp, E.J., Yim, G., Waglechner, N., Wang, W., Pawlowski, A.C., and Wright, G.D. (2019). Hidden antibiotics in actinomycetes can be identified by inactivation of gene clusters for common antibiotics. Nat. Biotechnol. *37*, 1149–1154.

Drautz, H., Keller-Schierlein, W., and Zähner, H. (1975). Stoffwechselprodukte von Mikroorganismen. Arch. Microbiol. *106*, 175–190.

Dwyer, D.J., Kohanski, M.A., Hayete, B., and Collins, J.J. (2007). Gyrase inhibitors induce an oxidative damage cellular death pathway in *Escherichia coli*. Mol. Syst. Biol. *3*, 91.

Fischer, H.P., Brunner, N.A., Wieland, B., Paquette, J., Macko, L., Ziegelbauer, K., and Freiberg, C. (2004). Identification of antibiotic stress-inducible promoters: a systematic approach to novel pathway-specific reporter assays for antibacterial drug discovery. Genome Res. *14*, 90–98.

Freiberg, C., Brunner, N., Macko, L., and Fischer, H.P. (2006). Discovering antibiotics efficacy biomarkers: towards mechanism-specific high-content compound screening. Mol. Cell Proteomics *5*, 2326–2335.

Frieri, M., Kumar, K., and Boutin, A. (2017). Antibiotic resistance. J. Infect. Public Health *10*, 369–378.

Genilloud, O. (2017). Actinomycetes: still a source of novel antibiotics. Nat. Prod. Rep. *34*, 1203–1232.

Gleckman, R., Blagg, N., and Joubert, D.W. (1981). Trimethoprim: mechanisms of action, antimicrobial activity, bacterial resistance, pharmacokinetics, adverse reactions, and therapeutic indications. Pharmacotherapy *1*, 14–20.

Goswami, M., Mangoli, S.H., and Jawali, N. (2006). Involvement of reactive oxygen species in the action of ciprofloxacin against *Escherichia coli*. Antimicrob. Agents Chemother. *50*, 949–954.

Gregg, R.E., and Heintz, R.L. (1972). The inhibition of eukaryotic aminoacyl transferase I by chartreusin. Arch. Biochem. Biophys. *152*, 451–456.

Handayani, I., Ratnakomala, S., Lisdiyanti, P., Fahrurrozi, Kusharyoto, W., Alanjary, M., Ort-Winklbauer, R., Kulik, A., Wohlleben, W., and Mast, Y. (2018). Complete genome sequence of *Streptomyces* sp. strain SHP22-7, a new species isolated from mangrove of Enggano Island, Indonesia. Microbiol. Resour. Announc. *7*, e01317–e01318.

Hong, Y., Zeng, J., Wang, X., Drlica, K., and Zhao, X. (2019). Post-stress bacterial cell death mediated by reactive oxygen species. Proc. Natl. Acad. Sci. U S A *116*, 10064.

Horowitz, J., and Chargaff, E. (1959). Massive incorporation of 5-fluorouracil into a bacterial ribonucleic acid. Nature *184*, 1213–1215.

Hug, J.J., Bader, C.D., Remškar, M., Cirnski, K., and Müller, R. (2018). Concepts and methods to access novel antibiotics from actinomycetes. Antibiotics (Basel) *7*, 44.

Hutchings, M.I., Truman, A.W., and Wilkinson, B. (2019). Antibiotics: past, present and future. Curr. Opin. Microbiol. *51*, 72–80.

Hutter, B., Fischer, C., Jacobi, A., Schaab, C., and Loferer, H. (2004). Panel of *Bacillus subtilis* reporter strains indicative of various modes of action. Antimicrob. Agents Chemother. *48*, 2588–2594.

Jahn, N., Brantl, S., and Strahl, H. (2015). Against the mainstream: the membrane-associated type I toxin BsrG from *Bacillus subtilis* interferes with cell envelope biosynthesis without increasing membrane permeability. Mol. Microbiol. *98*, 651–666.

Jervis, A.J., Thackray, P.D., Houston, C.W., Horsburgh, M.J., and Moir, A. (2007). SigM-responsive genes of *Bacillus subtilis* and their promoters. J. Bacteriol. *189*, 4534–4538.

Jordan, S., Junker, A., Helmann, J.D., and Mascher, T. (2006). Regulation of LiaRS-dependent gene expression in *Bacillus subtilis*: identification of inhibitor proteins, regulator binding sites, and target genes of a conserved cell envelope stress-sensing two-component system. J. Bacteriol. *188*, 5153–5166.

Kieser, T., and Foundation, J.I. (2000). Practical *Streptomyces* Genetics (John Innes Foundation).

Krause, J., Handayani, I., Blin, K., Kulik, A., and Mast, Y. (2020). Disclosing the potential of the SARP-type regulator PapR2 for the activation of antibiotic gene clusters in streptomycetes. Front. Microbiol. *11*, 225.

Kudo, F., Yonezawa, T., Komatsubara, A., Mizoue, K., and Eguchi, T. (2011). Cloning of the biosynthetic gene cluster for naphthoxanthene antibiotic FD-594 from *Streptomyces* sp. TA-0256. J. Antibiot. *64*, 123–132.

Laws, M., Shaaban, A., and Rahman, K.M. (2019). Antibiotic resistance breakers: current approaches and future directions. FEMS Microbiol. Rev. *43*, 490–516.

Lebel, M. (1988). Ciprofloxacin: chemistry, mechanism of action, resistance, antimicrobial spectrum, pharmacokinetics, clinical trials, and adverse reactions. Pharmacotherapy *8*, 3–33.

Li, L.H., Clark, T.D., Murch, L.L., Wooden, J.M., Pschigoda, L.M., and Krueger, W.C. (1978). Biological and biochemical effects of chartreusin on mammalian cells. Cancer Res. *38*, 3012.

Longley, D.B., Harkin, D.P., and Johnston, P.G. (2003). 5-Fluorouracil: mechanisms of action and clinical strategies. Nat. Rev. Cancer *3*, 330–338.

Martin, J.K., Sheehan, J.P., Bratton, B.P., Moore, G.M., Mateus, A., Li, S.H.-J., Kim, H., Rabinowitz, J.D., Typas, A., Savitski, M.M., et al. (2020). A dual-mechanism antibiotic kills gram-negative bacteria and avoids drug resistance. Cell *181*, 1518–1532.e14.

Mascher, T., Zimmer, S.L., Smith, T.-A., and Helmann, J.D. (2004). Antibiotic-inducible promoter regulated by the cell envelope stress-sensing two-component system LiaRS of *Bacillus subtilis*. Antimicrob. Agents Chemother. *48*, 2888–2896.

Melander, R.J., and Melander, C. (2017). The challenge of overcoming antibiotic resistance: an adjuvant approach? ACS Infect. Dis. *3*, 559–563.

Minato, Y., Dawadi, S., Kordus, S.L., Sivanandam, A., Aldrich, C.C., and Baughn, A.D. (2018). Mutual potentiation drives synergy between trimethoprim and sulfamethoxazole. Nat. Commun. *9*, 1003.

Niedermeyer, T.H.J. (2015). Anti-infective natural products from cyanobacteria. Planta Med. *81*, 1309–1325.

Nonejuie, P., Trial, R.M., Newton, G.L., Lamsa, A., Ranmali Perera, V., Aguilar, J., Liu, W.T., Dorrestein, P.C., Pogliano, J., and Pogliano, K. (2016). Application of bacterial cytological profiling to crude natural product extracts reveals the antibacterial arsenal of *Bacillus subtilis*. J. Antibiot. (Tokyo) *69*, 353–361.

Noordhuis, P., Holwerda, U., Van Der Wilt, C.L., Van Groeningen, C.J., Smid, K., Meijer, S., Pinedo, H.M., and Peters, G.J. (2004). 5-Fluorouracil incorporation into RNA and DNA in relation to thymidylate synthase inhibition of human colorectal cancers. Ann. Oncol. *15*, 1025–1032.

OŃeill, J. (2014). Review on Antimicrobial Resistance: Tackling a Crisis for the Health and Wealth of Nations (Review on Antimicrobial Resistance).

Please cite this article in press as: Wex et al., Bioreporters for direct mode of action-informed screening of antibiotic producer strains, Cell Chemical Biology (2021), https://doi.org/10.1016/j.chembiol.2021.02.022

Ortlieb, N. (2019). Characterization of Natural Products from Actinobacteria of the Tübingen Strain Collection—Screening, Isolation & Structure Elucidation, Doctoral Dissertation (Eberhard-Karls-University Tübingen).

Piggot, P.J. (1973). Mapping of asporogenous mutations of *Bacillus subtilis*: a minimum estimate of the number of sporeulation operons. J. Bacteriol. *114*, 1241–1253.

Portugal, J. (2003). Chartreusin, elsamicin A and related anti-cancer antibiotics. Curr. Med. Chem. Anticancer Agents *3*, 411–420.

Reusser, F. (1969). Mode of action of berninamycin. An inhibitor of protein biosynthesis. Biochemistry *8*, 3303–3308.

Ruttkies, C., Schymanski, E.L., Wolf, S., Hollender, J., and Neumann, S. (2016). MetFrag relaunched: incorporating strategies beyond in silico fragmentation. J. Cheminformatics *8*, 3.

Sass, P., Josten, M., Famulla, K., Schiffer, G., Sahl, H.-G., Hamoen, L., and Brötz-Oesterhelt, H. (2011). Antibiotic acyldepsipeptides activate ClpP peptidase to degrade the cell division protein FtsZ. Proc. Natl. Acad. Sci. U S A *108*, 17474–17479.

Shao, R.G., and Zhen, Y.S. (2008). Enediyne anticancer antibiotic lidamycin: chemistry, biology and pharmacology. Anticancer Agents Med. Chem. *8*, 123–131.

Stülke, J., Hanschke, R., and Hecker, M. (1993). Temporal activation of β-glucanase synthesis in *Bacillus subtilis* is mediated by the GTP pool. Microbiology *139*, 2041–2045.

Sugino, A., Higgins, N.P., Brown, P.O., Peebles, C.L., and Cozzarelli, N.R. (1978). Energy coupling in DNA gyrase and the mechanism of action of novobiocin. Proc. Natl. Acad. Sci. U S A *75*, 4838–4842.

Taylor and Francis Group (2019). Dictionary of Natural Products (CRC Press).

Tommasi, R., Brown, D.G., Walkup, G.K., Manchester, J.I., and Miller, A.A. (2015). ESKAPEing the labyrinth of antibacterial discovery. Nat. Rev. Drug Discov. *14*, 529–542.

Torres, C., Galián, C., Freiberg, C., Fantino, J.-R., and Jault, J.-M. (2009). The YheI/YheH heterodimer from *Bacillus subtilis* is a multidrug ABC transporter. Biochim. Biophys. Acta *1788*, 615–622.

Tulp, M., and Bohlin, L. (2005). Rediscovery of known natural compounds: nuisance or goldmine? Bioorg. Med. Chem. *13*, 5274–5282.

Urban, A., Eckermann, S., Fast, B., Metzger, S., Gehling, M., Ziegelbauer, K., Rübsamen-Waigmann, H., and Freiberg, C. (2007). Novel whole-cell antibiotic biosensors for compound discovery. Appl. Environ. Microbiol. *73*, 6436–6443.

Vagner, V., Dervyn, E., and Ehrlich, S.D. (1998). A vector for systematic gene inactivation in *Bacillus subtilis*. Microbiology *144*, 3097–3104.

Vazquez, D., Barbacid, M., and Carrasco, L. (1974). Inhibitors of mammalian protein synthesis. Hamatol. Bluttransfus. *14*, 327–340.

Verweij, J., and Pinedo, H.M. (1990). Mitomycin C: mechanism of action, usefulness and limitations. Anticancer Drugs *1*, 5–13.

Wang, B., Guo, F., Dong, S.-H., and Zhao, H. (2019). Activation of silent biosynthetic gene clusters using transcription factor decoys. Nat. Chem. Biol. *15*, 111–114.

Wang, M., Carver, J.J., Phelan, V.V., Sanchez, L.M., Garg, N., Peng, Y., Nguyen, D.D., Watrous, J., Kapono, C.A., Luzzatto-Knaan, T., et al. (2016). Sharing and community curation of mass spectrometry data with global natural products social molecular networking. Nat. Biotechnol. *34*, 828–837.

Wenzel, M., Chiriac, A.I., Otto, A., Zweytick, D., May, C., Schumacher, C., Gust, R., Albada, H.B., Penkova, M., Krämer, U., et al. (2014). Small cationic antimicrobial peptides delocalize peripheral membrane proteins. Proc. Natl. Acad. Sci. U S A *111*, E1409.

WHO (2015). Antibiotic Resistance: Multi-Country Public Awareness Survey (World Health Organization).

Will, C.L., and Dolnick, B.J. (1989). 5-Fluorouracil inhibits dihydrofolate reductase precursor mRNA processing and/or nuclear mRNA stability in methotrexate-resistant KB cells. J. Biol. Chem. *264*, 21413–21421.

Wolf, D., and Mascher, T. (2016). The applied side of antimicrobial peptide-inducible promoters from *Firmicutes* bacteria: expression systems and whole-cell biosensors. Appl. Microbiol. Biotechnol. *100*, 4817–4829.

Wright, G.D. (2017). Opportunities for natural products in 21st century antibiotic discovery. Nat. Prod. Rep. *34*, 694–701.

Yang, Y., Ashworth, A.J., Willett, C., Cook, K., Upadhyay, A., Owens, P.R., Ricke, S.C., Debruyn, J.M., and Moore, P.A., Jr. (2019). Review of antibiotic resistance, ecology, dissemination, and mitigation in U.S. Broiler poultry systems. Front. Microbiol. *10*, 2639.

Zeng, Y., Kulkarni, A., Yang, Z., Patil, P.B., Zhou, W., Chi, X., Van Lanen, S., and Chen, S. (2012). Biosynthesis of albomycin δ(2) provides a template for assembling siderophore and aminoacyl-tRNA synthetase inhibitor conjugates. ACS Chem. Biol. *7*, 1565–1575.

Zhang, Y., Mu, J., Essmann, F., Feng, Y., Kramer, M., Bao, H.Y., and Grond, S. (2017). A new quinolinone and its natural/artificial derivatives from a shark gill-derived fungus *Penicillium polonicum* AP2T1. Nat. Prod. Res. *31*, 985–989.

Zipperer, A., Konnerth, M.C., Laux, C., Berscheid, A., Janek, D., Weidenmaier, C., Burian, M., Schilling, N.A., Slavetinsky, C., Marschal, M., et al. (2016). Human commensals producing a novel antibiotic impair pathogen colonization. Nature *535*, 511–516.

Please cite this article in press as: Wex et al., Bioreporters for direct mode of action-informed screening of antibiotic producer strains, Cell Chemical Biology (2021), https://doi.org/10.1016/j.chembiol.2021.02.022

STAR★METHODS

KEY RESOURCES TABLE

REAGENT or RESOURCE	SOURCE	IDENTIFIER
Bacterial and virus strains		
Bacillus subtilis 1S34	(Piggot, 1973)	N/A
B. subtilis 1S34 *amyE*::pHJS105-P_{yorB}-*lacZ*	This study	N/A
B. subtilis 1S34 *amyE*::pHJS105-P_{ypuA}-*lacZ*	This study	N/A
B. subtilis 1S34 *amyE*::pHJS105-P_{liaI}-*lacZ*	This study	N/A
B. subtilis 1S34 *amyE*::pHJS105-P_{bmrC}-*lacZ*	This study	N/A
B. subtilis 1S34 *amyE*::pHJS105-P_{yppS}-*lacZ*	This study	N/A
B. subtilis 1S34 *amyE*::pHJS105-P_{helD}-*lacZ*	This study	N/A
Escherichia coli XL1 Blue	Agilent	Cat# 200249
Amycolatopsis mediterranei NBRC 14843	National Institute of Technology and Evaluation (NITE) Biological Resource Centre (NBRC)	Cat# 14843
Streptomyces ardus NBRC 13490	NBRC	Cat# 13490
Streptomyces niveus NBRC 12917	NBRC	Cat# 12917
Saccharopolyspora erythraea NBRC 13426	NBRC	Cat# 13426
Streptomyces venezuelae NBRC 13096	NBRC	Cat# 13096
Streptomyces hawaiiensis NRRL 15010	Agricultural Research Service (ARS) Culture Collection	Cat# 15010
Biological samples		
~500 cultivated actinomycetes producer strains	Tübingen strain collection	N/A
Chemicals, peptides, and recombinant proteins		
5-bromo-4-chloro-3-indolyl-beta-D-galactopyranoside (X-Gal)	Thermo Scientific	Cat# R0402
Vancomycin antibiotic discs (30 μg)	Thermo Scientific	Cat# CT0058B
Teicoplanin antibiotic discs (30 μg)	Thermo Scientific	Cat# CT0647B
Ciprofloxacin antibiotic discs (5 μg)	Thermo Scientific	Cat# CT0425B
Rifampin antibiotic discs (30 μg)	Thermo Scientific	Cat# CT0104B
Chloramphenicol antibiotic discs (10 μg)	Thermo Scientific	Cat# CT0012B
Oligonucleotides		
Primers used in this study are listed in Table S4.	Integrated DNA Technologies (IDT)	N/A
Recombinant DNA		
pHJS105	Leendert Hamoen, University of Amsterdam	N/A
Software and algorithms		
Bruker Daltonics DataAnalysis 4.2	Bruker Daltonics	N/A

RESOURCE AVAILABILITY

Lead contact

Heike Brötz-Oesterhelt (heike.broetz-oesterhelt@uni-tuebingen.de), Department of Microbial Bioactive Compounds; Interfaculty Institute of Microbiology and Infection Medicine, University of Tübingen; Tübingen, Baden-Württemberg, 72076; Germany.

Materials availability

Requests for plasmids and reagents generated in this study may be sent to the lead contact.

Please cite this article in press as: Wex et al., Bioreporters for direct mode of action-informed screening of antibiotic producer strains, Cell Chemical Biology (2021), https://doi.org/10.1016/j.chembiol.2021.02.022

CellPress

Data and code availability

This study did not generate datasets to be deposited.

EXPERIMENTAL MODEL AND SUBJECT DETAILS

Bacterial strains

All reporter strains were developed on the basis of the sporulation deficient *B. subtilis* 1S34 strain (Piggot, 1973). The integrative plasmid pHJS105 was used for the transformation of the respective reporter construct. pHJS105 integrates into the *amyE* locus and contains the antibiotic resistance marker spectinomycin (SPT) (Jahn et al., 2015). All reporter strains were grown in lysogeny broth (LB) (1% tryptone, 1% NaCl, 0.5% yeast extract, pH7.2) containing the antibiotic selection marker SPT at a final concentration of 100 μg/mL. For sub-cloning, the *E. coli* strain XL1 Blue was used for the construction and propagation of all plasmids.

METHOD DETAILS

Recombinant plasmid construction

The plasmid pHJS105 contains a xylose-inducible promoter fused to an N-terminal *gfp* tag, which was replaced by the respective promoter reporter construct. To modify the vector, we used a standard restriction-ligation protocol. The restriction sites *Sph*I and *Kpn*I were used to exchange the xylose-inducible promoter for the promoter regions of the chosen biomarker genes (P_{ypuA}, P_{liaI}, P_{yorB}, P_{yppS}, P_{bmrC}, and P_{helD}), which were amplified via PCR (phusion high-fidelity polymerase (NEB)) from *B. subtilis* 1S34 genomic DNA, gel-purified and then ligated using T4 DNA ligase (NEB). In a second step, the *gfp* reporter was replaced for a *B. subtilis*-optimized *lacZ* gene amplified from pMutin4 (Vagner et al., 1998), using the restriction sites *Kpn*I and *Hin*dIII. Primers used in this work are listed in Table S4. After transformation of chemically competent *E. coli* XL1 Blue, transformants were selected on LB agar containing 100 μg/mL ampicillin overnight. Single colonies were inoculated in 5 mL LB (37°C, 190 rpm). Plasmids were isolated (GeneJET Plasmid Miniprep Kit (Thermo Scientific)) and verified by Sanger sequencing (LGC genomics GmbH). The plasmids were transferred into competent *B. subtilis* 1S34 cells and selected on LB agar, containing 100 μg/mL of SPT. Integration into the *amyE* locus was confirmed by streaking single colonies on starch containing agar (0.3% meat extract, 1% starch, 1.2% agar). Successful transformants were unable to metabolize the starch, which was detectable after iodine staining (3.3% iodine, 6.7% potassium iodide). For confirmation of sequence integrity, the integrated sequence was amplified via PCR (DreamTaq polymerase (Thermo Scientific)). Purified PCR products (Monarch PCR & DNA Cleanup Kit (NEB)) were then confirmed by Sanger sequencing.

Agar-based bioactivity screening

Before the bioreporter assay was conducted, antibiotic producer strains were pre-tested for antimicrobial activity against the *B. subtilis* 1S34 wildtype. A subset of producer strains was additionally tested for activity against *E. coli* ATCC25922. An overnight culture of the respective strain was diluted to an OD_{600} of 0.05 and re-grown to an OD_{600} of 1 (37°C, 190 rpm). *B. subtilis* 1S34 cells were concentrated 1:10 (4700 rpm, 4°C) and used to inoculate the LB soft agar with an adjusted cell number of 3×10^7 colony forming units per mL (CFU/mL). For *E. coli* ATCC25922, we adjusted the cell number to 1.5×10^6 CFU/mL to inoculate the LB soft agar. Agar plugs of the antibiotic producer strains were arranged in square Petri dishes, and the soft agar containing either *B. subtilis* 1S34 or *E. coli* ATCC25922 was poured around. Agar plates were left to solidify for 15 min and subsequently incubated overnight (37°C).

Agar-based bioreporter screening

For reporter testing, overnight cultures were inoculated from glycerol stocks in LB, containing 100 μg/mL of SPT. Overnight cultures of the bioreporter strains were diluted to an OD_{600} of 0.05 and incubated for ~3.5 h (37°C, 190 rpm) until they reached an OD_{600} of 1. Cells were concentrated 1:10 (4700 rpm, 4°C) and used to inoculate the soft agar. For testing the P_{ypuA}-*lacZ*, P_{liaI}-*lacZ*, P_{yorB}-*lacZ*, and P_{helD}-*lacZ* reporter strains LB soft agar was used (1% tryptone, 1% NaCl, 0.5% yeast extract, and 0.75% agar). The P_{yppS}-*lacZ* and P_{bmrC}-*lacZ* reporter strains were tested in Belitzky minimal soft agar (Stülke et al., 1993). Cell numbers were adjusted to 3×10^7 CFU/mL for the P_{liaI}-*lacZ*, P_{yorB}-*lacZ*, P_{yppS}-*lacZ*, P_{helD}-*lacZ*, and P_{bmrC}-*lacZ* reporter strains and 6×10^7 CFU/mL for the P_{ypuA}-*lacZ* reporter strain. The agar was supplemented with 5 mM $MgCl_2$ and 150 μg/mL X-Gal (Thermo Scientific). As positive controls antibiotic discs of 30 μg vancomycin (P_{ypuA}-*lacZ*), 30 μg teicoplanin (P_{liaI}-*lacZ*), 5 μg ciprofloxacin (P_{yorB}-*lacZ*), 30 μg rifampin (P_{yppS}-*lacZ*), and 10 μg chloramphenicol (P_{bmrC}-*lacZ*) were used for reliable induction (see key resources table). For the screening of pure substances, extracts, and supernatants, the agar containing the reporter strain was poured in square Petri dishes and let to solidify for approximately 15 min. Subsequently, the respective amount of 1–5 μL test substance was spotted on the agar, and the plates were incubated overnight at 30°C for LB and 37°C for Belitzky minimal soft agar, respectively. For testing larger volumes, e.g. low-concentrated supernatants or weakly active substances, the samples were filled into holes, which were punched into the dried agar plates with a cork borer. Direct screening of actinomycetes strains was performed by transferring pre-stamped agar plugs of the grown antibiotic producer strains to a square Petri dish, before embedding them in soft agar containing the respective reporter strains. Control experiments, with different solvents used in the extraction and purification process, as well as agar plugs, and extracts of cultivation media (without bacterial growth), were always performed in parallel to exclude unspecific inhibitory effects or induction signals.

Please cite this article in press as: Wex et al., Bioreporters for direct mode of action-informed screening of antibiotic producer strains, Cell Chemical Biology (2021), https://doi.org/10.1016/j.chembiol.2021.02.022

Dereplication procedures

a) Agar cultivation conditions and compound extraction procedure (strains GöK8/12, GöK9/13, GöK12/7, GöK12/9, GöK16/4, GöOber505, GöSöt11, GöWind756, Tü40/15, TüG102, TüG111, TüG117, TüG343, TüG349). Agar plates were inoculated with 100 μL of cryo stock. Cryo stocks were prepared from a three-day culture by 1:1 (v/v) dilution with glycerol/water (1:1, v/v) and stored at −80°C. Actinomycetes strains were cultivated for 7–10 days at 28°C on the respective agar plates (Table S5).

Grown agar plate(s) were cut in ~5 × 5 mm pieces and transferred to a 50 mL falcon tube. The content was poured over by a mixture of isopropyl acetate/chloroform/isopropyl alcohol (3:1:1 v/v/v, 40 mL) and extracted two times for 1.5 h on an overhead shaker. Residual solids were filtered off, and the combined organic extracts were dried *in vacuo* to complete dryness. The extracts were stored at −20°C.

Pre-fractionation of the extract by normal-phase solid-phase extraction (NP-SPE) (strains GöK8/12, GöK9/13, GöK12/7, GöK12/9, GöK16/4, GöOber505, GöSöt11, GöWind756, Tü40/15, Tü104, Tü2626, Tü2641, TüG102, TüG111, TüG117, TüG343, TüG349). Bioactive extracts were fractionated at room temperature (25°C) by normal-phase SPE (Macherey-Nagel Chromabond® SiOH, 200 mg, 3 mL). The SPE cartridge was conditioned with 4 mL dichloromethane (DCM), DCM/n-hexane (1:1, v/v, 4 mL), n-hexane (4 mL). The extract (20 mg/mL in methanol, 50 μL) was loaded onto the silica bed and dried extensively by pressurized air to remove residual methanol. A stepwise gradient was used to elute the NP-SPE cartridge into a 96-well microtiter plate (PP): n-hexane (100%, 2 mL), n-hexane/EtOAc/MeOH (8/1.8/0.2, v/v/v, 2 mL), n-hexane/EtOAc/MeOH (7.25/2.35/0.4, v/v/v, 2 mL), n-hexane/EtOAc/MeOH (6.5/2.9/0.6, v/v/v, 2 mL), n-hexane/EtOAc/MeOH (5.75/3.45/0.8, v/v/v, 2 mL), n-hexane/EtOAc/MeOH (5/4/1, v/v/v, 2 mL), n-hexane/EtOAc/MeOH (4.25/4.55/1.2, v/v/v, 2 mL), n-hexane/EtOAc/MeOH (3.5/5.1/1.4, v/v/v, 2 mL), MeOH (100%, 2 mL). The volume of the eluent was set to 200 μL/well. After complete evaporation of the solvents using pressurized air, the fractions were re-suspended in methanol (100 μL). Daughter plates for HPLC-UV-HR-MS analysis were prepared by transferring an aliquot (20 μL) from each well of the master plate. The master plate was used for antimicrobial biological testing after evaporation, whereas the daughter plate was stored at −20°C for HPLC-UV-HR-MS analysis of the bioactive wells.

HPLC-UV-HR-MS setup (strains GöK8/12, GöK9/13, GöK12/7, GöK12/9, GöK16/4, GöOber505, GöSöt11, GöWind756, Tü40/15, Tü104, Tü2626, Tü2641, TüG102, TüG111, TüG117, TüG343, TüG349). 3 μL of the extract (3 mg/mL in methanol) and the pooled bioactive wells of the micro-fractionation daughter plate (no defined concentration) were subjected to HPLC-UV-HR-MS analysis performed on a Bruker MaXis 4G ESI-QTOF mass spectrometer equipped with a Dionex Ultimate 3000 HPLC system (Thermo Scientific). HPLC instrumental setup: Column: Macherey-Nagel Nucleoshell EC RP-C18 (150/2 RP18, 2.7 μm), flow rate: 0.3 mL min^{-1}, eluting solvents: Methanol (system B, containing 0.06% formic acid) and H_2O (system A, containing 0.1% formic acid), gradient: 0 min (10% B), 20 min (100% B), 25 min (100% B), 26 min (10% B), 30 min (10% B). Mass spectrometer instrumental setup: Electrospray ionization mass spectra (positive and negative ions) were recorded in the range of 100–1250 Da. The elemental composition was derived from the averaged mass spectra with high mass accuracy below 3 ppm. Sodium formate was used as internal calibrant. Nebulizer pressure of the ESI source was set to 0.4 bar with a dry gas flow of 4.0 l min^{-1} and a dry gas temperature of 200°C. The endplate offset was 500 V and capillary voltage = 3,000 V. Bruker Daltonics DataAnalysis 4.2 was used as software for the analysis of the HPLC-UV-HR-MS data.

HPLC-UV-HR-MS dereplication strategy (strains GöK8/12, GöK9/13, GöK12/7, GöK12/9, GöK16/4, GöOber505, GöSöt11, GöWind756, Tü40/15, Tü104, Tü2626, Tü2641, TüG102, TüG111, TüG117, TüG343, TüG349). For the dereplication process, the UV-DAD spectra of the extracts were analyzed for relevant signals first. The UV_{max} of prominent UV-signals were extracted and a database search was performed (UV_{max} +/− 10 nm). The Dictionary of Natural Products served as underlying database (Taylor and Francis Group, 2019). Additionally, the search criteria were extended by the molecular masses as well as molecular formulas of relevant peaks. In this step, the high abundant masses in the peaks observed in the Base Peak Chromatogram (BPC, m/z +/− 1) as well as the adduct pattern was used to select masses for the database search. For the selected masses, the molecular formulas were estimated (+/− 3 ppm) and added to the search criteria. Finally, the MS/MS spectra of positive hits were matched with an *in-house* natural product database, Global Natural Products Social Molecular Networking (Wang et al., 2016) or spectra from the literature and medfrag (Ruttkies et al., 2016). The same procedure was carried out for the bioactive fractions of the micro-fractionation. A substance was classified as 'clearly identified', if especially the match with the in-house database confirmed even regioisomers or if all four criteria (UV_{max}, MS, molecular formula, MS/MS) were in agreement with the database entry.

b) Liquid cultivation conditions and compound extraction procedure (strains Tü104, Tü2626, Tü2641, Tü2108, Tü2975, Tü6430, Tü3180, A4/2, KNN49.3e). For antibiotic production, strains were cultivated in 50 mL preculture medium (R5 or NL410) for 3 days at 30°C in 500 mL Erlenmeyer flasks (with steel springs) on an orbital shaker (180 rpm) (Kieser and Foundation, 2000). 5 or 10 mL of preculture were inoculated in 50 or 100 mL of production medium (Table S5), respectively, and cultures were grown for 4–10 days at 30°C in 500 mL Erlenmeyer flasks (with steel springs) on an orbital shaker (180 rpm). 5 mL culture were extracted with 5 mL ethyl acetate or butanol for 30 min at room temperature. Ethyl acetate and butanol samples were dried *in vacuo,* and redissolved in 0.25 mL of methanol. The culture extracts were stored at 4°C or −20°C. Methanolic and butanolic extracts were used for bioassays and HPLC-MS analysis.

HPLC-MS analysis (strains Tü2108, Tü6430, Tü3180, Tü2975, A4/2, KNN49.3e-for strains Tü104, Tü2626, Tü2641 see section "a)"). HPLC analysis was performed as described previously with a HP1090M system with ChemStation 3D software rev. A.08.03 (Agilent Technologies, Waldbronn, Germany) on a Nucleosil C18 column (5 μm, 125 mm × 3 mm) fitted with a precolumn (20 × 3 mm) and with a flow rate of 850 mL min-1 (Krause et al., 2020). HPLC-MS was performed with an Agilent 1200 series chromatography system (binary pump, high performance autosampler, DAD-detector) coupled with an LC/MSD Ultra Trap System XCT 6330

Please cite this article in press as: Wex et al., Bioreporters for direct mode of action-informed screening of antibiotic producer strains, Cell Chemical Biology (2021), https://doi.org/10.1016/j.chembiol.2021.02.022

(Agilent Technologies, Waldbronn, Germany). The sample was injected on a Nucleosil 100 C18 column (3 μm, 100 × 2 mm) fitted with a precolumn (3 μm, 10 × 2 mm) at a flow rate of 400 μL/min and a linear gradient from 10% solvent A (0.1% formic acid in water) to 100% solvent B (0.06% formic acid in acetonitrile) over 15 min at 40°C.

c) Cultivation conditions and compound extraction procedure for Tü2401.

Liquid precultures of Tü2401 were inoculated either with spores from the respective agar plates, or with 50 μL of the respective suspension of cryo-preserved spores. Precultures were inoculated in NL410 medium and incubated for three days at 29°C (180 rpm). 500 mL of preculture were used to inoculate 9.5 L OM medium for fermentation. Liquid cultures were cultivated at 27°C in a 10 L bioreactor at a rotor speed of 200 rpm, and an airflow of 5 L/min. For the growth on solid medium, ISP2 agar plates were inoculated with 50 μL of the preculture and incubated at 29°C for four days until sporulation occurred. The respective media used for cultivation are noted in Table S5.

For the extraction from agar, Tü2401 was cultivated on ISP2 agar plates. Two plates (approx. 40 mL) were sliced, transferred into a 50 mL falcon tube, and subsequently centrifuged at 20,000 g for 30 min, resulting in 10 mL supernatant. After filtration through a folded filter, the pH was adjusted to pH 4.0 using 0.1 M HCl. After centrifugation, $(NH_4)_2SO_4$ was added to the supernatant up to the saturation point and incubated for 4 hr at 4°C. Afterward, the precipitate was separated and dissolved in 10 mL 0.1 M K_2HPO_4 at a pH of 8.0. Finally, this solution was extracted with 10 mL ethyl acetate. After drying under reduced pressure, the pellet was dissolved in 2.0 mL MeOH. Methanolic extracts were used for bioassays and HPLC-MS analysis.

For the extraction of liquid culture, the supernatant of Tü2401 was filtrated (0.2 μm) and extracted five times for 30 min with 2 L of ethyl acetate. The aqueous phase was collected, frozen at −80°C, and subsequently dried using a Lyovac GT2 (Heraeus Holding, Hanau; Germany). Further detailed information on the dereplication strategy has been described previously (Ortlieb, 2019).

QUANTIFICATION AND STATISTICAL ANALYSIS

Bruker Daltonics DataAnalysis 4.2 was used as software for the analysis of the HPLC-UV-HR-MS data.

Supplemental Information

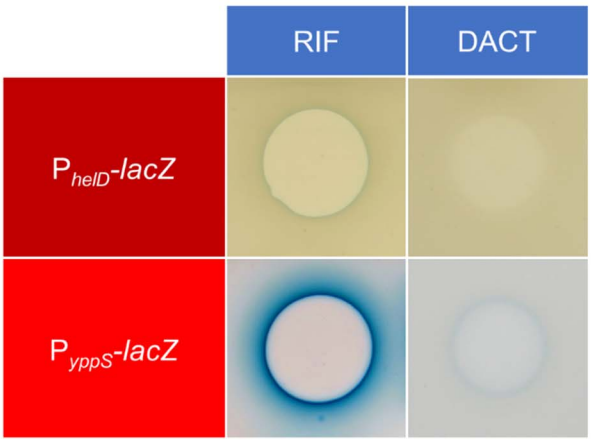

Figure S1, related to Figure 1. Comparison of the induction strength of two RNA stress bioreporter strains

Pure compounds were spotted on agar, containing the respective *B. subtilis* reporter strain, in the following amounts: rifampin (RIF) 20 µg, actinomycin D (DACT) 0.5 µg. The P_{yppS}-*lacZ* reporter strain was grown in Belitzky minimal soft agar, while P_{helD}-*lacZ* was grown in LB soft agar to match the luciferase-based conditions applied by Urban and colleagues (Urban et al., 2007). P_{yppS}-*lacZ* yielded a substantially stronger induction signal upon treatment with both antibiotics compared to P_{helD}-*lacZ*. Induction of P_{helD}-*lacZ* in Belitzky minimal soft agar showed a similar result.

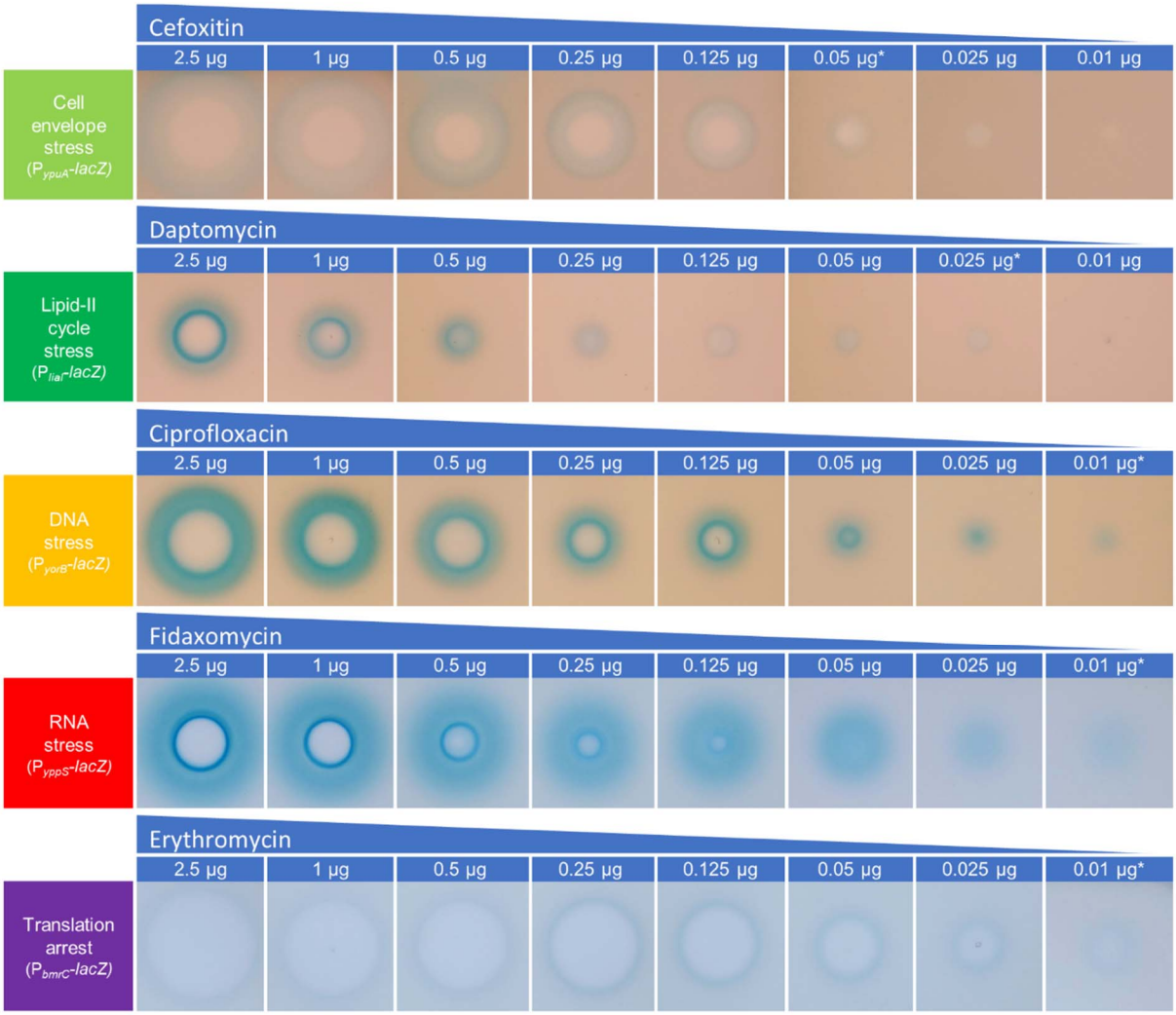

Figure S2, related to Figure 1. Determination of the detection limit of the bioreporter panel
Respective antibiotic amounts were directly spotted on the bioreporter containing soft agar. The diameter of a zone of inhibition (ZOI) is determined by the antibiotic potency and its diffusion potential in agar. Induction occurred at the borders of the ZOI, with some bioreporters (P_{yorB}-*lacZ*, P_{yppS}-*lacZ,* and P_{liaI}-*lacZ*) already effectively signaling at subinhibitory antibiotic concentrations. The lowest antibiotic concentration still yielding a detectable induction signal is indicated by „*“.

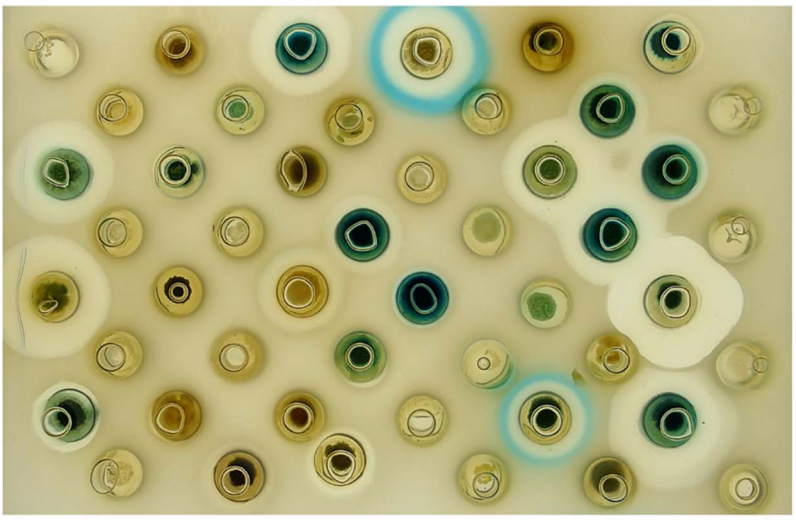

Figure S3, related to Figure 3. Direct agar-based bioreporter screening against actinomycetes strains of the Tübingen strain collection

Agar plugs of the precultured actinomycetes strains were tested against the DNA stress reporter (P_{yorB}-*lacZ*) for antibacterial activity with combined MOA analysis. One exemplary screening plate is shown depicting the activities of 48 actinomycetes strains on P_{yorB}-*lacZ*.

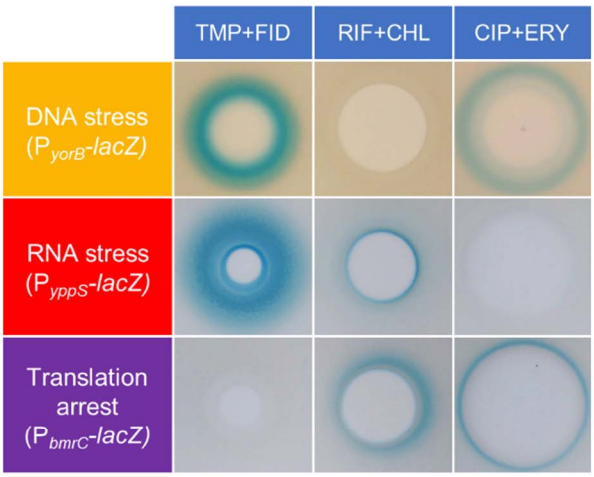

Figure S4, related to Figure 4. Sensitivity of the agar-based bioreporter approach for the detection of distinct substances present in same zone of inhibition

Antibiotics were spotted on the bioreporter strain containing agar in the following amounts and combinations: trimethoprim (TMP) 0.5 µg and fidaxomicin (FID) 2 µg (first column); rifampin (RIF) 5 µg and chloramphenicol (CHL) 5 µg (second column); ciprofloxacin (CIP) 2.5 µg and erythromycin (ERY) 5 µg (third column). Induction of the respective promoters for DNA stress (P_{yorB}-*lacZ)*, RNA stress (P_{yppS}-*lacZ),* and translation arrest (P_{bmrC}-*lacZ)* reflects the expected MOA of the antibiotics (Table S1).

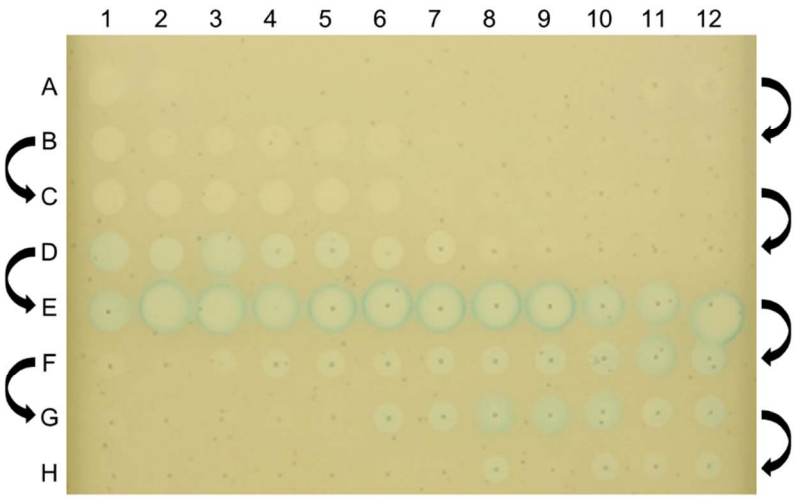

Figure S5, related to Figure 3. Bioactivity- and MOA-informed fractionation pattern

Fractionation of an extract of the antibiotic producer strain Tü104 into a microtiter plate. Collection order of the 96 HPLC fractions is indicated by the black arrows (A1-H1). 2 µL of each fraction were spotted in parallel on the P_{lial}-*lacZ* reporter strain containing agar, using a multichannel liquid handling device.

Table S1, related to Figure 1. Promoter induction pattern of pure antibacterial agents evaluated in the bioreporter system. The main bacterial metabolic pathways that antibiotics interfere with are highlighted in bold font. Promoter induction is indicated by "–" (no induction), "(+)" (weak induction) and "+" (good induction).

MOA[a]	Antibiotic [µg][b]	Promoter induction				
		P_{ypuA}	P_{lial}	P_{yorB}	P_{yppS}	P_{bmrC}
Cell envelope inhibition						
PG[c] synthesis enzymes inhibitors	Ampicillin [20]	+	-	-	-	-
	Cefadroxil [0.5]	+	-	-	-	-
	Cefalexin [0.5]	+	-	-	-	-
	Cefotaxime [5]	+	-	-	-	-
	Cefoxitin [5]	+	-	-	-	-
	Cefuroxime [10]	+	-	-	-	-
	D-Cycloserine [20]	+	-	-	-	-
	Flavomycin [20]	+	-	-	-	-
	Fosfomycin [20]	+	-	-	-	-
	Imipenem [1]	+	-	-	-	-
	Meropenem [0.5]	+	-	-	-	-
	Methicillin [1]	+	-	-	-	-
	Oxacillin [1]	+	-	-	-	-
	Penicillin G [20]	+	-	-	-	-
Lipid-II cycle inhibitors	Bacitracin [10]	+	+	-	-	-
	Daptomycin [2]	+	+	-	-	-
	Lysolipin I	(+)	+	-	-	-
	Mersacidin [30]	+	+	-	-	-
	Nisin [30]	+	+	-	-	-
	Ramoplanin [20]	+	+	-	-	-
	Teicoplanin [10]	+	+	-	-	-
	Vancomycin [15]	+	+	-	-	-
Cell membrane disturbers	Colistin [20]	+	-	-	-	-
	Polymyxin B [20]	+	-	-	-	-
Ionophores	CCCP[d] [5]	-	-	-	-	-
	Gramicidin A [20]	-	-	-	-	-
	Nigericin [20]	-	-	-	-	-
	Monensin [30]	-	-	-	-	-
	Valinomycin [30]	-	-	-	-	-
DNA synthesis inhibitors						
DNA gyrase binders	Ciprofloxacin [1]	(+)	-	+	-	-
	Levofloxacin [1]	(+)	-	+	-	-
	Moxifloxacin [0.5]	(+)	-	+	-	-
	Nalidixic acid [25]	(+)	-	+	-	-
	Norfloxacin [2]	(+)	-	+	-	-
	Novobiocin [2]	-	-	+	-	-
Intercalators	Cisplatin [25]	-	-	+	-	-
	Mitomycin C [2]	(+)	-	+	-	-
	Mitoxantrone [20]	-	-	+	-	-
	Phleomycin [10]	(+)	-	+	-	-
Nucleotide synthesis inhibitors	Azaserine [3]	-	-	+	(+)	-
	Sulfamethoxazole [20]	-	-	+	-	-
	Trimethoprim [0.5]	-	-	+	-	-
RNA synthesis inhibitors						
RNA polymerase binders	Corallopyronin A [30]	-	-	-	+	-
	Fidaxomicin [4]	-	-	-	+	-
	Rifabutin [20]	-	-	-	+	-
	Rifampin [30]	-	-	-	+	-
	Rifamycin SV [20]	-	-	-	+	-
	Sorangicin A [20]	-	-	-	+	-
	Streptolydigin [20]	-	-	-	+	-
	Streptovaricin [20]	-	-	-	+	-
Intercalators	Actinomycin D [0.5]	-	-	-	+	-
	Actinomycin X2 [0.5]	-	-	-	+	-
	Echinomycin [20]	-	-	-	+	-

MOA[a]	Antibiotic [µg][b]	Promoter induction				
		P_{ypuA}	P_{lial}	P_{yorB}	P_{yppS}	P_{bmrC}
Protein synthesis inhibitors						
Translation stallers	Anhydrotetracycline [6]	-	-	-	-	+
	Azithromycin [10]	-	-	-	-	+
	Clindamycin [20]	-	-	-	-	+
	Chloramphenicol [5]	-	-	-	-	+
	Doxycycline [2]	-	-	-	-	+
	Erythromycin [2]	-	-	-	-	+
	Ferrimycin A [20]	-	-	-	-	+
	Fusidic acid [0.5]	-	-	-	-	+
	Hygromycin B [50]	-	-	-	-	+
	Kirromycin [20]	-	-	-	-	+
	Linezolid [20]	-	-	-	-	+
	Lincomycin [20]	-	-	-	-	+
	Pactamycin [0.5]	-	-	-	-	+
	Spectinomycin[e] [150]	-	-	-	-	+
	Telithromycin [20]	-	-	-	-	+
	Tetracycline [20]	-	-	-	-	+
	Tiamulin [40]	-	-	-	-	+
	Tigecycline [20]	-	-	-	-	+
Miscoding inducers	Amikacin [20]	-	-	-	-	-
	Apramycin [1]	-	-	-	-	-
	Gentamicin [1]	-	-	-	-	-
	Kanamycin [1]	-	-	-	-	-
	Neomycin [1]	-	-	-	-	-
	Streptomycin [20]	-	-	-	-	-
	Tobramycin [20]	-	-	-	-	-
Abortive translation	Puromycin [30]	-	-	-	-	-
Protein stress	Diamide [30]	-	-	-	-	-
	N-ethylmaleimide [5]	-	-	-	-	-
tRNA synthetase inhibitors	Mupirocin [0.1]	-	-	-	-	-
Fatty acid synthesis inhibitors						
	Cerulenin [10]	-	-	-	-	-
	Triclosan [5]	-	-	-	-	-
Diverse MOA						
	ADEP7[f] [20]	-	-	-	-	-
	Holomycin [10]	-	-	-	-	-
	5´-Fluorouracil [10]	-	-	+	-	+
	Nitrofurantoin [20]	-	-	+	-	-
	Thiolutin [20]	-	-	-	-	-
	SCH-79797 [40]	+	+	+	-	-

[a] Based on current knowledge of the mechanism of action (MOA).
[b] Antibiotic amount spotted on agar.
[c] Peptidoglycan
[d] Carbonyl cyanide m-chlorophenyl hydrazine
[e] All biosensors contain a spectinomycin-resistance cassette (requires higher concentrations for activity/induction).
[f] Acyldepsipeptide 7

Table S2, related to STAR methods (Agar-based bioreporter screening). Solvents and commonly purified media components / bacterial metabolites tested against the bioreporter panel. Promoter induction is indicated by "–" (no induction) and "+" (induction).

Test substance	Amount or volume tested[a]	*B. subtilis* 1S34 activity [diameter of zone of inhibition]	Promoter induction				
			P_{ypuA}	P_{liaI}	P_{yorB}	P_{yppS}	P_{bmrC}
DMSO[b]	10 µl	turbid zone [7 mm]	-	-	-	-	-
Methanol[b]	5 µl	no	-	-	-	-	-
Ethanol[b]	5 µl	no	-	-	-	-	-
Buthanol[b]	5 µl	yes [6 mm]	-	-	-	-	-
Ethylacetate[b]	10 µl	no	-	-	-	-	-
Glycerin[b]	10 µl	no	-	-	-	-	-
Genistein	100 µg	turbid zone [8 mm][c]	-	-	-	-	-
Daidzein	100 µg	no[c]	-	-	-	-	-
N-acetyltyramine	20 µg	turbid zone [5 mm]	-	-	-	-	-
Indol-3-acetic acid	100 µg	turbid zone [8 mm]	-	-	-	-	-
Indole-3-propionic acid	100 µg	turbid zone [12 mm]	-	-	-	-	-
2,4-Dihydroxy-6-methylbenzoic acid	100 µg	turbid zone [9 mm]	-	-	-	-	-
4-Hydroxybenzamide	100 µg	turbid zone [7 mm]	-	-	-	-	-
4-Oxonon-2-enolic acid	50 µg	turbid zone [10 mm]	-	-	-	-	-
Prodigiosin	5 µg	yes [8 mm]	-	-	-	-	-

[a] amount or volume of test substance was directly spotted on the bioreporter-containing agar
[b] concentration of 100 %
[c] substance precipitates on agar

Table S3, related to Table 1. Additional information on the dereplicated antibiotics identified by screening of producer strains and their respective biosensor signal.

Producer strain	Reporter induction	Dereplicated antibiotics	CAS[a] Registry Number and InChI[b] Code
GöK9/13 (K9/13)	P_{yorB}-*lacZ*, P_{yppS}-*lacZ*	Chartreusin[c, d, e]	CAS Registry Number: 6377-18-0 InChI=1S/C32H32O14/c1-10-8-9-15-18-16(10)29(38)45-26-17-13(23(35)20(19(18)26)30(39)43-15)6-5-7-14(17)44-32-28(24(36)21(33)11(2)42-32)46-31-25(37)27(40-4)22(34)12(3)41-31/h5-9,11-12,21-22,24-25,27-28,31-37H,1-4H3
GöK16/4 (K16/4)	P_{yorB}-*lacZ*, P_{yppS}-*lacZ*, P_{bmrC}-*lacZ*	Chartreusin[c, d, e]	
Tü2471	P_{yorB}-*lacZ*	Chrysomycin A[c, d, e]	CAS Registry Number: 82196-88-1 InChI=1S/C28H28O9/c1-6-13-9-16-20(18(10-13)34-4)15-11-19(35-5)22-17(29)8-7-14(21(22)23(15)37-27(16)32)24-26(31)28(3,33)25(30)12(2)36-24/h6-12,24-26,29-31,33H,1H2,2-5H3
Tü2401 agar cultivation	P_{yorB}-*lacZ*	C-1027 (Lidamycin)[c, d]	CAS Registry Number: 120177-69-7 InChI=1S/C43H42ClN3O13/c1-21-39(52)46-34-26(17-25(54-6)18-30(34)56-21)40(53)57-31-20-55-33(49)19-28(45)23-15-27(44)37(29(48)16-23)58-32-11-7-9-22(31)12-13-24-10-8-14-43(24,32)60-41-36(51)35(50)38(47(4)5)42(2,3)59-41/h8-10,14-18,28,31-32,35-36,38,41,48,50-51H,1,19-20,45H2,2-6H3,(H,46,52)/b22-9+/t28-,31-,32+,35-,36+,38-,41-,43+/m0/s1
TüG111 (MB11)	P_{yorB}-*lacZ*	Daunomycin (Daunorubicin)[c, d, e]	CAS Registry Number: 20830-81-3 InChI=1S/C27H29NO10/c1-10-22(30)14(28)7-17(37-10)38-16-9-27(35,11(2)29)8-13-19(16)26(34)21-20(24(13)32)23(31)12-5-4-6-15(36-3)18(12)25(21)33/h4-6,10,14,16-17,22,30,32,34-35H,7-9,28H2,1-3H3
GöOber505 (Ober505)	P_{yorB}-*lacZ*	Rachelmycin (CC-1065)[c, d, e]	CAS Registry Number: 69866-21-3 InChI=1S/C37H33N7O8/c1-14-12-39-27-22(45)10-23-37(24(14)27)11-15(37)13-44(23)35(49)21-9-18-16-4-6-42(28(16)30(46)32(51-2)25(18)41-21)34(48)20-8-19-17-5-7-43(36(38)50)29(17)31(47)33(52-3)26(19)40-20/h8-10,12,14-15,40-41,46-47H,4-7,11,13H2,1-3H3,(H2,38,50)
GöWind756 (Wind756)	P_{yppS}-*lacZ*	Actinomycin D (C_1,IV) (Dactinomycin)[c, d, e]	CAS Registry Number: 50-76-0 InChI=1S/C62H86N12O16/c1-27(2)42-59(84)73-23-17-19-36(73)57(82)69(13)25-38(75)71(15)48(29(5)6)61(86)88-33(11)44(55(80)65-42)67-53(78)35-22-21-31(9)51-46(35)64-47-40(41(63)50(77)32(10)52(47)90-51)54(79)68-45-34(12)89-62(87)49(30(7)8)72(16)39(76)26-70(14)58(83)37-20-18-24-74(37)60(85)43(28(3)4)66-56(45)81/h21-22,27-30,33-34,36-37,42-45,48-49H,17-20,23-26,63H2,1-16H3,(H,65,80)(H,66,81)(H,67,78)(H,68,79)
		Actinomycin C_2 (VI)[c, d, e]	CAS Registry Number: 2612-14-8 InChI=1S/C63H88N12O16/c1-17-31(8)44-61(86)75-25-19-21-38(75)59(84)71(14)27-40(77)73(16)50(30(6)7)63(88)90-35(12)46(57(82)67-44)69-55(80)41-42(64)51(78)33(10)53-48(41)65-47-36(23-22-32(9)52(47)91-53)54(79)68-45-34(11)89-62(87)49(29(4)5)72(15)39(76)26-70(13)58(83)37-20-18-24-74(37)60(85)43(28(2)3)66-56(45)81/h22-23,28-31,34-35,37-38,43-46,49-50H,17-21,24-27,64H2,1-16H3,(H,66,81)(H,67,82)(H,68,79)(H,69,80)/t31-,34+,35+,37-,38-,43+,44+,45-,46-,49-,50-/m0/s1
Tü40/15	P_{yppS}-*lacZ*	Cosmomycin B[c, d, e]	CAS Registry Number: 77517-27-2 InChI=1S/C40H53NO14/c1-7-40(49)14-13-21-30(36(48)32-31(34(21)46)35(47)29-20(33(32)45)9-8-10-24(29)43)39(40)55-27-15-22(41(5)6)37(18(3)51-27)54-28-16-25(44)38(19(4)52-28)53-26-12-11-23(42)17(2)50-26/h8-10,17-19,22-23,25-28,37-39,42-44,46,48-49H,7,11-16H2,1-6H3
		Echinosporin[c, d, e]	CAS Registry Number: 79127-35-8 InChI=1S/C10H9NO5/c11-7(12)6-3-5-4-1-2-10(5,14)9(13)16-8(4)15-6/h1-5,8,14H,(H2,11,12)
Tü2626	P_{yppS}-*lacZ*	Cosmomycin B [c, d]	CAS Registry Number: 77517-27-2 InChI=1S/C40H53NO14/c1-7-40(49)14-13-21-30(36(48)32-31(34(21)46)35(47)29-20(33(32)45)9-8-10-24(29)43)39(40)55-27-15-22(41(5)6)37(18(3)51-27)54-28-16-25(44)38(19(4)52-28)53-26-12-11-23(42)17(2)50-26/h8-10,17-19,22-23,25-28,37-39,42-44,46,48-49H,7,11-16H2,1-6H3
		Cytorhodin X [c, d]	CAS Registry Number: 133914-58-6 InChI=1S/C48H68N2O15/c1-10-48(65-37-18-28(49(6)7)42(53)24(4)60-37)20-27-39(46(57)40-41(44(27)55)45(56)38-26(43(40)54)12-11-13-31(38)52)33(21-48)63-36-19-29(50(8)9)47(25(5)61-36)64-35-17-15-32(23(3)59-35)62-34-16-14-30(51)22(2)58-34/h11-13,22-25,28-30,32-37,42,47,51-53,55,57H,10,14-21H2,1-9H3
GöK8/12 (K8/12)	P_{yppS}-*lacZ*	Cosmomycin C[c, d, e]	CAS Registry Number: 55945-22-7 InChI=1S/C60H88N2O21/c1-12-60(71)25-40(79-44-22-33(61(8)9)57(30(6)75-44)82-46-24-38(66)58(31(7)77-46)81-42-20-17-36(64)27(3)73-42)48-51(55(70)49-50(54(48)68)69)53(68)47-32(52(49)67)14-13-15-37(47)65)59(60)83-45-23-34(62(10)11)56(29(5)76-45)80-43-21-18-39(28(4)74-43)78-41-19-16-35(63)26(2)72-41/h13-15,26-31,33-36,38-46,56-59,63-66,69-71H,12,16-25H2,1-11H3

Producer strain	Reporter induction	Dereplicated antibiotics	CAS[a] Registry Number and InChI[b] Code
KNN49.3e	P*bmrC*-*lacZ*	Amicetin[c, d]	CAS Registry Number: 17650-86-1 InChI=1S/C29H42N6O9/c1-15-19(44-26-24(38)23(37)22(34(4)5)16(2)43-26)10-11-21(42-15)35-13-12-20(33-28(35)41)32-25(39)17-6-8-18(9-7-17)31-27(40)29(3,30)14-36/h6-9,12-13,15-16,19,21-24,26,36-38H,10-11,14,30H2,1-5H3,(H,31,40)(H,32,33,39,41)/t15-,16-,19+,21-,22-,23+,24-,26-,29+/m1/s1
Tü2108	P*bmrC*-*lacZ*	Berninamycin C[c, d]	InChI=1S/C48H48N14O14S/c1-12-26-46-61-32(24(9)76-46)42(71)52-19(4)37(66)62-34(48(10,11)73)43(72)54-21(6)45-60-31(23(8)75-45)41(70)51-18(3)36(65)53-20(5)44-57-28(15-74-44)33-25(13-14-27(55-33)38(67)50-17(2)35(49)64)47-58-29(16-77-47)39(68)59-30(22(7)63)40(69)56-26/h12-16,22,30,34,63,73H,2-6H2,1,7-11H3,(H2,49,64)(H,50,67)(H,51,70)(H,52,71)(H,53,65)(H,54,72)(H,56,69)(H,59,68)(H,62,66)/b26-12-/t22-,30+,34-/m1/s1
A4/2	P*bmrC*-*lacZ*	Cycloheximide (Actidione)[c, d]	CAS Registry Number: 66-81-9 InChI=1S/C15H23NO4/c1-8-3-9(2)15(20)11(4-8)12(17)5-10-6-13(18)16-14(19)7-10/h8-12,17H,3-7H2,1-2H3,(H,16,18,19)/t8-,9-,11-,12+/m0/s1
Tü3180	P*bmrC*-*lacZ*	Griseoviridin[c, d]	CAS Registry Number: 53216-90-3 InChI=1S/C22H27N3O7S/c1-13-6-7-18-21(29)23-8-4-2-3-5-14(26)9-15(27)10-19-24-16(11-31-19)20(28)25-17(12-33-18)22(30)32-13/h2-5,7,11,13-15,17,26-27H,6,8-10,12H2,1H3,(H,23,29)(H,25,28)/b4-2+,5-3+,18-7-/t13-,14-,15-,17-/m1/s1
		Viridogrisein[c, d]	CAS Registry Number: 102646-56-0 InChI=1S/C44H62N8O11/c1-23(2)19-30-42(60)52-21-29(53)20-31(52)43(61)49(8)22-33(55)50(9)36(25(5)24(3)4)40(58)46-26(6)41(59)51(10)37(28-15-12-11-13-16-28)44(62)63-27(7)34(38(56)47-30)48-39(57)35-32(54)17-14-18-45-35/h11-18,23-27,29-31,34,36-37,53-54H,19-22H2,1-10H3,(H,46,58)(H,47,56)(H,48,57)
Tü6430	P*bmrC*-*lacZ*	Pactamycin[c, d]	CAS Registry Number: 23668-11-3 InChI=1S/C28H38N4O8/c1-15-9-7-12-20(35)21(15)24(36)40-14-27(39)23(30-19-11-8-10-18(13-19)16(2)33)22(29)28(17(3)34,26(27,4)38)31-25(37)32(5)6/h7-13,17,22-23,30,34-35,38-39H,14,29H2,1-6H3,(H,31,37)/t17-,22-,23-,26-,27+,28-/m0/s1
Tü2975	P*bmrC*-*lacZ*	Pristinamycin IA (Streptogramin B, Virginiamycin B)[c, d]	CAS Registry Number: 3131-03-1 InChI=1S/C45H54N8O10/c1-6-31-42(59)52-22-11-14-32(52)43(60)51(5)34(24-27-16-18-29(19-17-27)50(3)4)44(61)53-23-20-30(54)25-33(53)39(56)49-37(28-12-8-7-9-13-28)45(62)63-26(2)36(40(57)47-31)48-41(58)38-35(55)15-10-21-46-38/h7-10,12-13,15-19,21,26,31-34,36-37,55H,6,11,14,20,22-25H2,1-5H3,(H,47,57)(H,48,58)(H,49,56)
		Pristinamycin IIA (Streptogramin A, Virginiamycin M1)[c, d]	CAS Registry Number: 21411-53-0 InChI=1S/C28H35N3O7/c1-17(2)26-19(4)9-10-24(34)29-11-5-7-18(3)13-20(32)14-21(33)15-25-30-22(16-37-25)27(35)31-12-6-8-23(31)28(36)38-26/h5,7-10,13,16-17,19-20,26,32H,6,11-12,14-15H2,1-4H3,(H,29,34)
TüG349 (LHO49)	P*ypuA*-*lacZ*, P*lial*-*lacZ*	Aborycin[c, d, e]	CAS Registry Number: 152835-17-1 InChI=1S/C97H131N23O26S4/c1-11-50(8)80-93(141)104-40-75(126)108-68(42-121)90(138)113-63(31-53-20-14-12-15-21-53)87(135)105-51(9)81(129)101-38-76(127)110-69-44-149-150-45-70(91(139)112-61(30-47(2)3)84(132)102-41-77(128)118-80)109-73(124)36-67-97(145)146-96(144)66(34-56-37-100-60-25-19-18-24-58(56)60)115-88(136)64(32-54-22-16-13-17-23-54)114-92(140)71(46-148-147-43-59(98)83(131)111-65(35-72(99)123)89(137)116-67)117-94(142)78(48(4)5)120-95(143)79(49(6)7)119-82(130)52(10)106-86(134)62(107-74(125)39-103-85(69)133)33-55-26-28-57(122)29-27-55/h12-29,37,47-52,59,61-71,78-80,100,121-122H,11,30-36,38-46,98H2,1-10H3,(H2,99,123)(H,101,129)(H,102,132)(H,103,133)(H,104,141)(H,105,135)(H,106,134)(H,107,125)(H,108,126)(H,109,124)(H,110,127)(H,111,131)(H,112,139)(H,113,138)(H,114,140)(H,115,136)(H,116,137)(H,117,142)(H,118,128)(H,119,130)(H,120,143)/t50?,51-,52-,59-,61-,62-,63-,64-,65-,66-,67-,68-,69-,70-,71-,78-,79-,80-/m0/s1
GöK12/7 (K12/7)	P*ypuA*-*lacZ*, P*lial*-*lacZ*	Pentamycin (Lagosin, Fungichromin)[c, d, e]	CAS Registry Number: 6834-98-6 InChI=1S/C35H58O12/c1-4-5-11-16-29(41)32-30(42)20-26(38)18-24(36)17-25(37)19-27(39)21-31(43)34(45)33(44)22(2)14-12-9-7-6-8-10-13-15-28(40)23(3)47-35(32)46/h6-10,12-15,23-34,36-45H,4-5,11,16-21H2,1-3H3/b7-6-,10-8+,12-9+,15-13+,22-14+
Tü2641	P*ypuA*-*lacZ*, P*lial*-*lacZ*	Telomycin (Antibiotic 128)[c, d]	CAS Registry Number: 19246-24-3 InChI=1S/C59H77N13O19/c1-25(2)49(79)46-57(87)72-18-16-40(76)48(72)59(90)91-29(6)45(69-52(82)38(24-73)65-41(77)20-34(60)58(88)89)55(85)68-44(28(5)74)54(84)64-27(4)50(80)63-23-42(78)71-17-15-39(75)47(71)56(86)66-37(19-30-21-61-35-13-9-7-11-31(30)35)51(81)67-43(53(83)70-46)26(3)33-22-62-36-14-10-8-12-32(33)36/h7-14,19,21-22,25-29,34,38-40,43-49,61-62,73-76,79H,15-18,20,23-24,60H2,1-6H3,(H,63,80)(H,64,84)(H,65,77)(H,66,86)(H,67,81)(H,68,85)(H,69,82)(H,70,83)(H,88,89)/b37-19-

Producer strain	Reporter induction	Dereplicated antibiotics	CAS[a] Registry Number and InChI[b] Code
Tü2401 liquid cultivation	-	Albomycin δ_1[c, d]	CAS Registry Number: 1414-39-7 InChI=1S/C36H58N10O18S.Fe/c1-17(48)44(62)12-5-8-20(37)30(55)38-21(9-6-13-45(63)18(2)49)31(56)39-22(10-7-14-46(64)19(3)50)32(57)40-23(16-47)33(58)41-25(35(59)60)26(52)29-27(53)28(54)34(65-29)43-15-11-24(51)42(4)36(43)61;/h11,15,20-23,25-29,34,47,52-54,62-64H,5-10,12-14,16,37H2,1-4H3,(H,38,55)(H,39,56)(H,40,57)(H,41,58)(H,59,60);/t20-,21-,22-,23-,25+,26-,27+,28+,29+,34+;/m0./s1
Tü104	P_{ypuA}-*lacZ*, P_{lial}-*lacZ*	FD-594[c, d, e]	CAS Registry Number: 175644-46-9 InChI=1S/C47H56O20/c1-7-8-20-11-19-12-21-31(39(53)30(19)47(57)63-20)33-34(42(56)37(21)51)45(59-6)46-35(41(33)55)40(54)32-24(65-46)9-10-25(38(32)52)64-27-13-22(48)43(17(3)61-27)66-28-14-23(49)44(18(4)62-28)67-29-15-26(58-5)36(50)16(2)60-29/h9-10,12,16-18,20,22-23,26-29,36-37,42-44,48-53,55-56H,7-8,11,13-15H2,1-6H3
		Naphthomycin B[c, d, f]	CAS Registry Number: 86825-88-9 InChI=1S/C39H44ClNO9/c1-20-11-9-7-8-10-12-30(45)41-34-33(40)39(50)31-27(38(34)49)18-25(6)37(48)32(31)36(47)24(5)17-23(4)35(46)22(3)14-16-26(42)15-13-21(2)29(44)19-28(20)43/h7-14,16-18,20,22-23,26,28,35,42-43,46,48H,15,19H2,1-6H3,(H,41,45)/b8-7+,11-9?,12-10+,16-14+,21-13+,24-17+
		Naphthomycin J[c, d, f]	CAS Registry Number: 214482-56-1 InChI=1S/C44H52N2O12S/c1-22-12-10-8-9-11-13-34(51)46-37-41(55)30-19-27(6)40(54)36(35(30)42(56)43(37)59-21-31(44(57)58)45-28(7)47)39(53)26(5)18-25(4)38(52)24(3)15-17-29(48)16-14-23(2)33(50)20-32(22)49/h8-15,17-19,22,24-25,29,31-32,38,48-49,52,54H,16,20-21H2,1-7H3,(H,45,47)(H,46,51)(H,57,58)/b9-8+,12-10+,13-11+,17-15+,23-14+,26-18+
GöK12/9 (K12/9)	-	Boromycin[c, d, e]	CAS Registry Number: 34524-20-4 InChI=1S/C45H73BNO15/c1-24(2)36(47)39(50)54-27(5)30-16-12-11-13-17-32(48)42(7,8)34-21-19-26(4)45(57-34)38-41(52)56-31-23-29(53-28(31)6)15-14-18-33(49)43(9,10)35-22-20-25(3)44(58-35)37(40(51)55-30)59-46(60-38,61-44)62-45/h11-12,24-38,48-49H,13-23,47H2,1-10H3/q-1/p+1/b12-11+
TüG117 (MB17)	-	Griseorhodin A[c, d, e]	CAS Registry Number: 11048-91-2 InChI=1S/C25H16O12/c1-6-3-7-4-8-19(17(29)11(7)24(32)34-6)36-25(23-20(8)35-23)22(31)14-16(28)12-9(26)5-10(33-2)15(27)13(12)18(30)21(14)37-25/h3-5,20,22-23,28-31H,1-2H3
GöSöt11 (Söt11)	-	Lobophorin A[c, d, e]	CAS Registry Number: 247171-46-6 InChI=1/C61H92N2O19/c1-27-14-17-42(78-47-25-59(10,62)54(35(9)77-47)63-58(71)73-13)28(2)19-37-20-36(26-64)31(5)24-61(37)56(69)48(57(70)82-61)55(68)60(11)39(27)16-15-38-49(60)29(3)18-30(4)51(38)80-46-23-43(50(67)32(6)74-46)79-44-22-41(66)53(34(8)76-44)81-45-21-40(65)52(72-12)33(7)75-45/h14-16,19-20,29-35,37-47,49-54,64-67,69H,17-18,21-26,62H2,1-13H3,(H,63,71)/b27-14+,28-19+
		Lobophorin E[c, d, e]	CAS Registry Number: 1352053-60-1 InChI=1/C61H90N2O20/c1-27-15-18-42(79-47-26-59(11,63(71)72)54(36(10)78-47)62-58(70)74-14)29(3)21-37-20-28(2)32(6)25-61(37)56(68)48(57(69)83-61)55(67)60(12)39(27)17-16-38-49(60)30(4)19-31(5)51(38)81-46-24-43(50(66)33(7)75-46)80-44-23-41(65)53(35(9)77-44)82-45-22-40(64)52(73-13)34(8)76-45/h15-17,20-21,30-47,49-54,64-66,68H,18-19,22-26H2,1-14H3,(H,62,70)/b27-15+,29-21+
TüG102 (MB2)	-	Monactin[c, d, e]	CAS Registry Number: 6833-84-7 InChI=1S/C40H64O12/c1-21-17-29-9-13-34(49-29)26(6)38(42)46-23(3)19-31-11-15-36(51-31)28(8)40(44)48-24(4)20-32-12-16-35(52-32)27(7)39(43)47-22(2)18-30-10-14-33(50-30)25(5)37(41)45-21/h21-36H,9-20H2,1-8H3
TüG343 (LHO43)	-	Omomycin[c, d, f]	CAS Registry Number: 117615-33-5 InChI=1S/C29H39NO4/c1-4-20(28-18(2)13-16-25(34-28)19(3)29(32)33)8-5-10-22-15-14-21-9-6-11-23(21)26(22)27(31)24-12-7-17-30-24/h5,7-8,10,12,14-15,17-19,21-23,25-26,28,30H,4,6,9,11,13,16H2,1-3H3,(H,32,33)/b10-5-,20-8-

[a] Chemical Abstracts Service
[b] International Chemical Identifier
[c] Confirmed by ultraviolet-visible (UV-Vis) spectrophotometry.
[d] Confirmed by high-performance liquid chromatography-mass spectrometry (HPLC-MS).
[e] Confirmed by tandem mass spectrometry (MS-MS).
[f] no MS-MS data confirmation due to missing reference spectrum.

Table S4, related to STAR methods (Key Resource Table). Oligonucleotides used in this study.

Name	Use	Sequence (5'-3')	Source
yorB-for	Cloning of pHJS105-P*yorB*-*gfp*	TATAGCATGCCGGGATATATTGGGATAAAGAT	IDT[a]
yorB-rev	Cloning of pHJS105- P*yorB*-*gfp*	TATAGGTACCTTTTTCCTCCTTACTGCAGGTC	IDT
bmrC-for	Cloning of pHJS105- P*bmrC*-*gfp*	TATAGCATGCTTCTTACTATTTTCACTTCCGTCA	IDT
bmrC-rev	Cloning of pHJS105- P*bmrC*-*gfp*	TATAGGTACCTTTTTCCTCCTTACTGCAGGTC	IDT
ypuA-for	Cloning of pHJS105- P*ypuA*-*gfp*	TATAGCATGCCCGCCTCATGTGTATGCGGG	IDT
ypuA-rev	Cloning of pHJS105- P*ypuA*-*gfp*	TATAGGTACCTTTTTCCTCCTTACTGCAGCAATT	IDT
lial-for	Cloning of pHJS105- P*lial*-*gfp*	TATAGCATGCCGGGTATCGGAATCTTGCTGT	IDT
lial-rev	Cloning of pHJS105- P*lial*-*gfp*	TATAGGTACCTTTTTCCTCCTTACTGCAGTCC	IDT
yppS-for	Cloning of pHJS105- P*yppS*-*gfp*	TATAGCATGCCAGATCATCCTTAATCAGGGGT	IDT
yppS-rev	Cloning of pHJS105- P*yppS*-*gfp*	TATAGGTACCTTTTTCCTCCTTACTGCAGAAAAAT ATTGACAAGAGCTTCC	IDT
lacZ_for	Cloning of the *lacZ* reporter constructs (exchanging *gfp*)	AAAGGTACCGTGGAAGTTACTGACGTAAGAT	IDT
lacZ_rev	Cloning of the *lacZ* reporter constructs (exchanging *gfp*)	AAAAAGCTTGCCTGCCCGGTTATTATTATT	IDT
pHJS105-ctrl	Control primer for sequencing of the promoter fragments	ATAGAAAGAAATTGTTCCTTCGA	IDT

[a]Integrated DNA Technology

Table S5, related to STAR methods (Dereplication procedures). Composition of the production media used for of the respective antibiotic producers. All quantities refer to 1 L of medium. For agar plates a concentration of 20 g/L agar was used.

Medium	Composition	Amount	Cultivation medium of antibiotic producer strain
Cycloheximide cultivation medium (CCM) (Kominek, 1975)	Glucose Soy meal Yeast extract $(NH_4)_2SO_4$ NaCl KH_2PO_4	60 g 15 g 2.5 g 8 g 4 g 0.2 g	A4/2
ISP2 (YMG) (Shomura et al., 1979)	Yeast extract Malt extract Glucose	4 g 10 g 4 g pH 7.3	Tü2401 (agar cultivation), Tü2471, Tü3180
ISP3 (OM) (Shomura et al., 1979)	Oatmeal Holo Trace metal mix	20 g 5 mL pH 7.3	Tü2401 (liquid cultivation)
Trace metal mix	$CaCl_2 \times 2H_2O$ Iron(III)-citrate $MnSO_4 \times 1H_2O$ $ZnCl_2$ $CuSO_4 \times 5H_2O$ $Na_2B_4O_7 \times 10H_2O$ $CoCl_2 \times 6H_2O$ $Na_2MoO_4 \times 2H_2O$	3 g 1 g 200 mg 100 mg 25 mg 20 mg 4 mg 10 mg	
M2+	Malt extract Yeast extract Glucose $CaCO_3$	10 g 4 g 4 g 0.5 g pH 7.2	GöK8/12, GöK9/13, GöK12/7, GöK12/9, GöOber505, GöSöt11, GöWind756, TüG102, TüG111, TüG117, TüG349
NL19	Mannitol Soy meal	20 g 20 g	Tü104
NL200	Mannitol Cornsteep powder	20 g 20 g pH 7,5	Tü2641
NL333	Glucose Starch, soluble Malt extract Yeast extract Bacto™ Peptone Ammonium nitrate $CaCO_3$	5 g 10 g 10 g 3 g 3 g 3 g 2 g pH 7.2	Tü2975, Tü2626
NL400	Glucose Starch Bacto™ Peptone Yeast extract Meat extract $CaCO_3$	10 g 2 g 3 g 5 g 3 g 3 g pH 7.0	KNN49.3e
NL410	Glucose Glycerol Oatmeal Holo Soy meal Yeast extract Casamino acids $CaCO_3$	10 g 10 g 5 g 10 g 5 g 5 g 1 g pH 7.0	precultures
NL800	Glucose Glycerol Starch, soluble Oatmeal Holo Yeast extract NaCl $CaCO_3$	5 g 10 g 10 g 58 g 2 g 1 g 1 g pH 7.2	Tü6430

Medium	Composition	Amount	Cultivation medium of antibiotic producer strain
R5	Saccharose	103 g	precultures, Tü2108
	Glucose	10 g	
	K_2SO_4,	0.25 g	
	$MgCl_2$	10.12 g	
	Casamino acids	0.1 g	
	Yeast extract	5 g	
	TES[a]	5.73 g	
	Trace element solution	2 ml	
		pH 7.2	
	After autoclavation:		
	1 M $CaCl_2$,	20 mL	
	0.54% KH_2PO_4	10 mL	
	20 % L-Proline	15 mL	
Starch -glycerol -glucose (SGG)	Soluble starch	10 g	GöK8/12, GöK12/7, GöK12/9, GöK16/4, GöSöt11, GöWind756, Tü40/15, TüG343
	Glucose	10 g	
	Glycerol	10 g	
	Cornsteep powder	2.5 g	
	Casein peptone	5 g	
	Yeast extract	2 g	
	NaCl	1 g	
	$CaCO_3$	3 g	
		pH 7.3	

[a] N-Tris(hydroxymethyl)methyl-2-aminoethanesulfonic acid

Data S1, related to STAR methods (Agar-based bioactivity screening). Activity of different antibiotic producer strains tested against *B. subtilis* 1S34 and *E. coli* ATCC25922 in the agar-based setup. Antimicrobial activity is indicated by "–" (no zone of inhibition), "(+)" (radius of zone of inhibition < 1mm), "+" (radius of zone of inhibition 1-3 mm), "++" (radius of zone of inhibition 3-7 mm) and "+++" (radius of zone of inhibition >7 mm). For all radius values the radius of the agar plug of the producer strain was subtracted.

Antibiotic producer strain[a]	Antimicrobial activity		Dereplicated antibiotic	*B. subtilis* 1S34 bioreporter induction
	B. subtilis 1S34	*E. coli* ATCC25922		
Nº1	-	-		no
Nº2	-	-		no
Nº3	-	-		no
Nº4	-	-		no
Nº5	+	-		no
Nº6	-	-		no
Nº7	-	-		no
GöK12/7	++	-	Pentamycin[b]	P_{ypuA}, P_{lial}
Nº8	-	-		no
GöK12/9	+	-	Boromycin[b]	no
Nº9	+	-		no
Nº10	-	-		no
Nº11	-	-		no
Nº12	-	-		no
Nº13	-	-		no
Nº14	-	-		no
Nº15	-	-		no
Nº16	-	-		no
Nº17	+	-		no
Nº18	+	-		no
Nº19	-	-		no
Nº20	(+)	-		no
Nº21	-	-		no
Nº22	+	-		no
Nº23	-	-		no
GöK16/4	++	-	Chartreusin[b]	P_{yorB}, P_{yppS}, P_{bmrC}
Nº24	-	-		no
Nº25	-	-		no
Nº26	++	-		P_{ypuA}
Nº27	-	-		-
GöK8/12	++	-	Cosmomycin C[b]	P_{yppS}
Nº28	+	-		P_{ypuA}
Nº29	-	-		no
Nº30	-	-		no
Nº31	-	-		no
Nº32	-	-		no
Nº33	-	-		no
GöK9/13	++	-	Chartreusin[b]	P_{yorB}, P_{yppS}
Nº34	-	-		no
Nº35	-	-		no
Nº36	++	-		no
Tü40/15	+	-	Cosmomycin B[b]	P_{yppS}
Nº37	-	-		no
Nº38	-	-		no
Nº39	-	-		no
Nº40	-	-		no
Nº41	-	-		no

Antibiotic producer strain[a]	Antimicrobial activity		Dereplicated antibiotic	*B. subtilis* 1S34 bioreporter induction
	B. subtilis 1S34	*E. coli* ATCC25922		
Nº42	-	-		no
Nº43	-	-		no
Nº44	(+)	-		no
Nº45	+	-		no
Nº46	-	-		no
Nº47	-	-		no
Nº48	-	-		no
Nº49	-	-		no
Nº50	-	-		no
Nº51	-	-		no
Nº52	-	-		no
Nº53	-	-		no
Nº54	-	-		no
Nº55	-	-		no
Nº56	-	-		no
Nº57	-	-		no
Nº58	-	-		no
Nº59	-	-		no
GöSöt11	++	-	Lobophorin A and E[b]	no
Nº60	-	-		no
Nº61	-	-		no
Nº62	(+)	-		no
GöWind756	++	-	Actinomycin D, C_2[b]	P_{yppS}
Nº63	(+)	-		(P_{bmrC})
Nº64	-	-		no
Nº65	-	-		no
Nº66	-	-		no
Nº67	-	-		N/A
GöOber505	+	-	Rachelmycin[b]	P_{yorB}
Nº68	-	-		N/A
Nº69	-	-		N/A
Nº70	-	-		N/A
Nº71	-	-		N/A
Nº72	+	-		no
Nº73	+	-		no
Nº74	-	-		N/A
Nº75	-	-		N/A
Nº76	+	-		no
Nº77	-	-		N/A
Nº78	-	-		N/A
Nº79	-	-		N/A
Nº80	-	-		N/A
Nº81	-	-		N/A
Nº82	-	-		N/A
Nº83	-	-		N/A
TüG102	+	-	Monactin[b]	no
TüG117	+	-	Griseorhodin A[b]	no
Nº84	-	-		N/A
Nº85	+	-		no
Nº86	+	-		no
Nº87	-	-		N/A
TüG111	++	(+)	Daunomycin[b]	P_{yorB}
Nº88	-	-		N/A
Nº89	+	-		no
Nº90	+	-		no
Nº91	+	+	Under investigation	P_{yppS}
Nº92	-	-		N/A
Nº93	+	-		no

Antibiotic producer strain[a]	Antimicrobial activity		Dereplicated antibiotic	*B. subtilis* 1S34 bioreporter induction
	B. subtilis 1S34	*E. coli* ATCC25922		
Nº94	-	-		N/A
Nº95	(+)	-		no
Nº96	+	-		no
Nº97	-	-		N/A
Nº98	-	-		N/A
Nº99	-	-		N/A
Nº100	-	-		N/A
Nº101	-	-		N/A
Nº102	-	-		N/A
Nº103	-	-		N/A
Nº104	-	-		N/A
Nº105	-	-		N/A
Nº106	-	-		N/A
Nº107	-	-		N/A
Nº108	-	-		N/A
Nº109	-	-		N/A
Nº110	++	+		no
Nº111	+++	+++		no
Nº112	-	-		N/A
Nº113	-	-		N/A
Nº114	++	-		P_{yorB}
Nº115	+	-		no
Nº116	+	++		no
Nº117	-	-		N/A
Nº118	-	-		N/A
Nº119	-	-		N/A
Nº120	-	-		N/A
Nº121	-	-		N/A
Nº122	-	-		N/A
Nº123	-	-		N/A
Nº124	-	-		N/A
Nº125	+	++		no
Nº126	-	-		N/A
Nº127	+	+		no
Nº128	+	-		no
Nº129	-	-		N/A
Nº130	-	-		N/A
Nº131	+	++		no
Nº132	-	-		N/A
Nº133	-	-		N/A
Nº134	-	-		N/A
Nº135	-	-		N/A
Nº136	-	-		N/A
Nº137	-	-		N/A
TüG343	++	-	Omomycin[b]	no
Nº138	-	-		N/A
TüG349	++	-	Aborycin[b]	P_{ypuA}, P_{lial}
Nº139	-	-		N/A
Nº140	+	-		no
Nº141	+	-		no
Nº142	++	++		no
Nº143	+	-		no
Nº144	+	++	Oxytetracyclin[c]	P_{bmrC}
Nº145	+	-		no
Nº146	+	-		no
Nº147	++	-		no
Nº148	++	-		no
Nº149	+	-		no

Data S2, related to Table 1. HPLC-MS spectra of the dereplicated antibiotics identified in the bioreporter screening of antibiotic producers of the Tübingen strain collection.

Characteristic mass fragments of each dereplicated antibiotic are outlined in red.

Dereplicated substance (producer strain)	
Mass spectrum	**Structure**
Characteristic mass fragment(s)	**Supporting information**
Chartreusin (GöK9/13)	
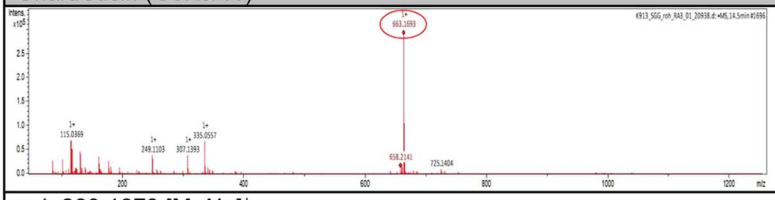	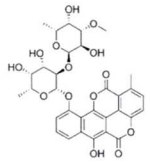
m/z 663.1679 $[M+Na]^+$	(Xu et al., 2005; Maskey et al., 2002)
Chartreusin (GöK16/4)	
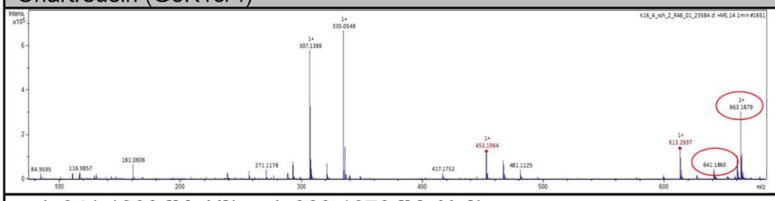	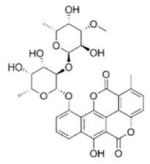
m/z 641.1860 $[M+H]^+$, *m/z* 663.1679 $[M+Na]^+$	(Maskey et al., 2002; Xu et al., 2005)
Chrysomycin A (Tü2471)	
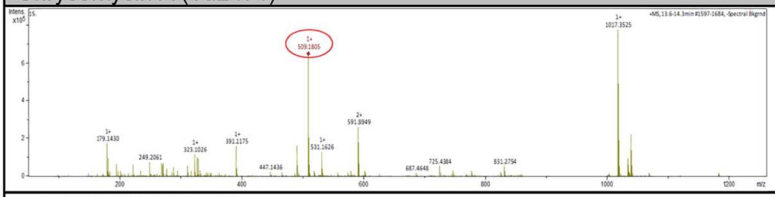	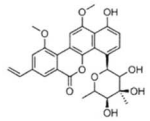
m/z 509.1805 $[M+H]^+$	(Muralikrishnan et al., 2017)
C-1027 and Albomycin δ_1 (Tü2401)	
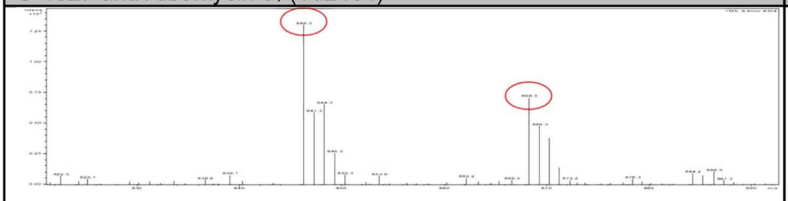 See (Ortlieb, 2019) for MS spectrum of Albomycin δ_1	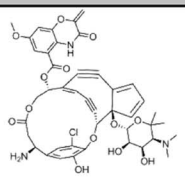 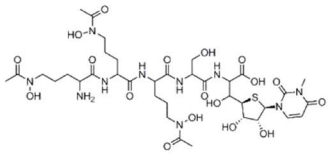
C-1027 *m/z* 846,3 $[M+H]^+$, *m/z* 868,3 $[M+Na]^+$	(Shao and Zhen, 2008; Zeng et al., 2012)
Daunomycin (TüG111)	
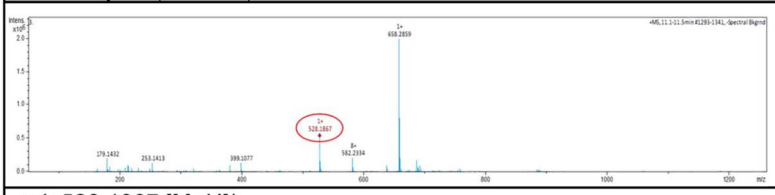	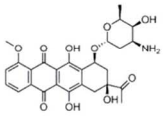
m/z 528.1867 $[M+H]^+$	(Pethő et al., 2019; Sottani et al., 2004)

Rachelmycin (GöOber505)	
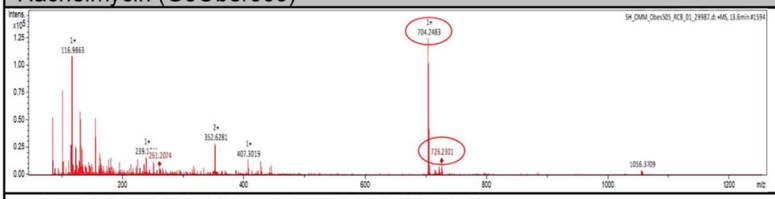	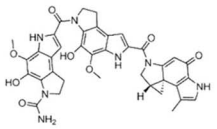
m/z 704.2483 $[M+H]^+$, *m/z* 726.2301 $[M+Na]^+$	
Actinomycin D and Actinomycin C_2 (GöWind756)	
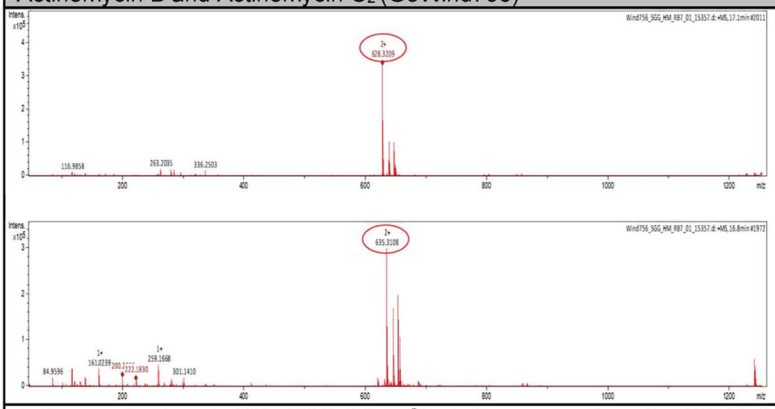	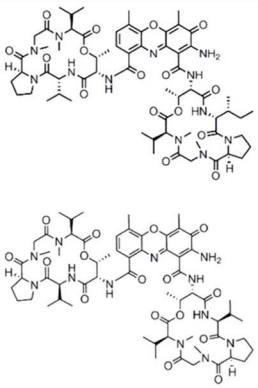
Actinomycin D *m/z* 628.3209 $[M+H]^{2+}$; Actinomycin C_2 *m/z* 635.3108 $[M+H]^{2+}$	(Vater et al., 2014)
Cosmomycin B and Echinosporin (Tü40/15)	
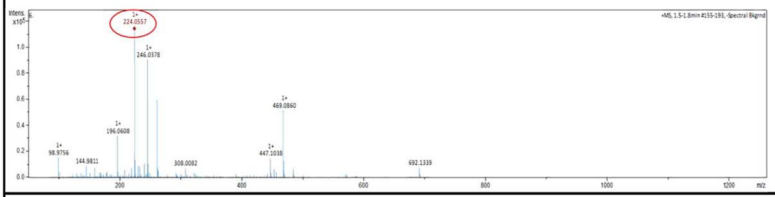	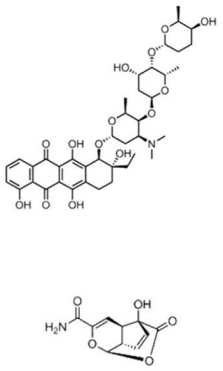
Cosmomycin B *m/z* 772.3549 $[M+H]^+$; Echinosporin *m/z* 224.0557 $[M+H]^+$	
Cosmomycin B and Cytorhodin X (Tü2626)	
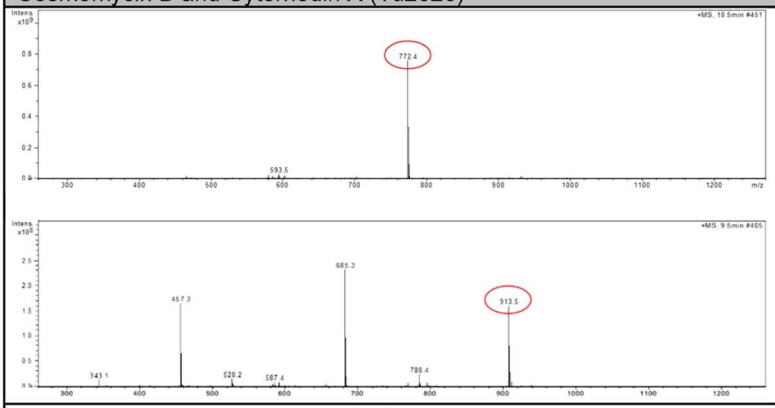	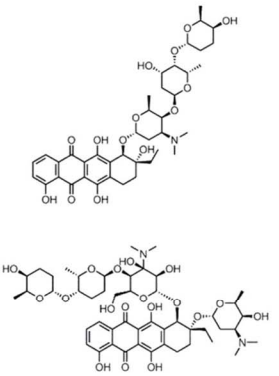
Cosmomycin B *m/z* 772.4 $[M+H]^+$; Cytorhodin X *m/z* 913.5 $[M+H]^+$	(Ando et al., 1985; Hedtmann et al., 1992)

Cosmomycin C (GöK8/12)	
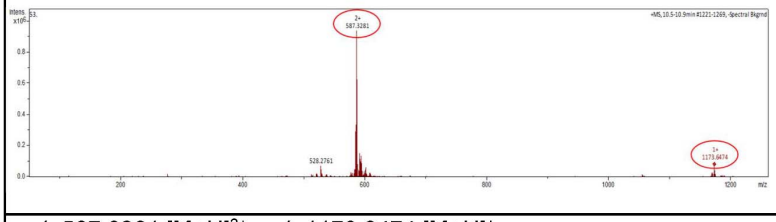	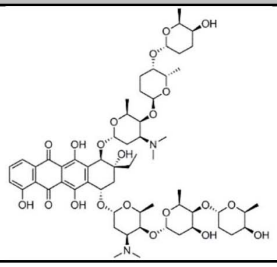
m/z 587.3281 $[M+H]^{2+}$, *m/z* 1173.6474 $[M+H]^{+}$	
Amicetin (KNN49.3e)	
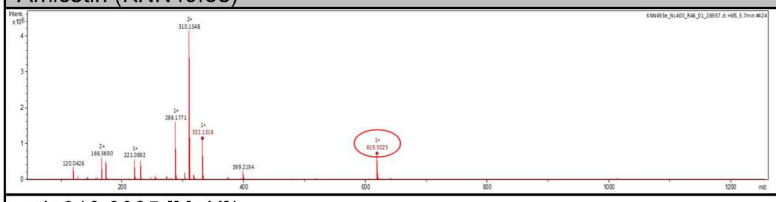	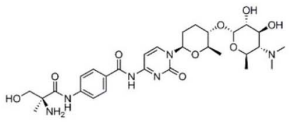
m/z 619.3025 $[M+H]^{+}$	(Zhang et al., 2012)
Berninamycin C (Tü2180)	
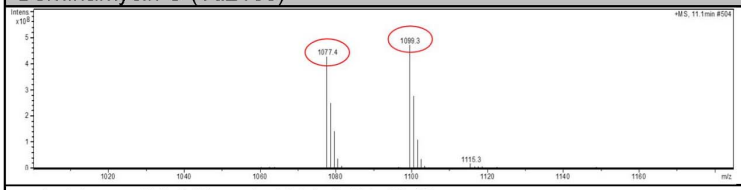	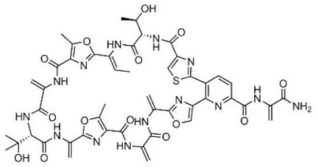
m/z 1077.4 $[M+H]^{+}$, *m/z* 1099.3 $[M+Na]^{+}$	(Lau and Rinehart, 1994)
Cycloheximide (A4/2)	
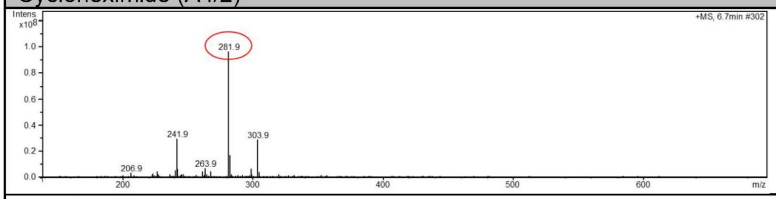	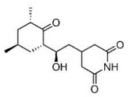
m/z 281.9 $[M+H]^{+}$	(Haesler et al., 2008)
Griseoviridin and Viridogrisein (Tü3180)	
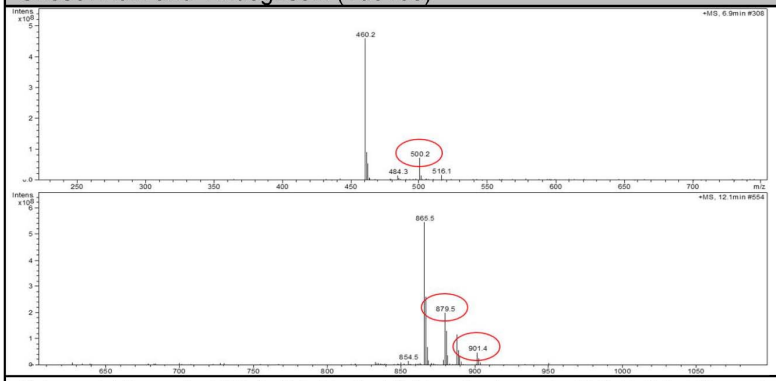	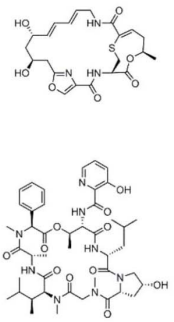
Griseoviridin *m/z* 500.2 $[M+Na]^{+}$; Viridogrisein *m/z* 879.5 $[M+H]^{+}$, *m/z* 901.4 $[M+Na]^{+}$	(Xie et al., 2012)
Pactamycin (Tü6430)	
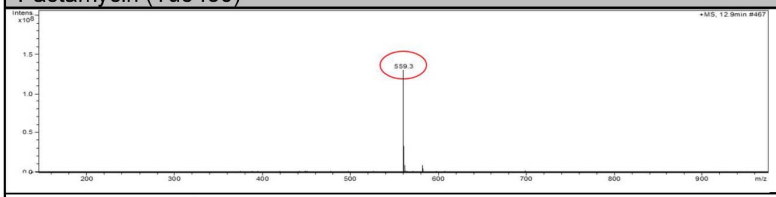	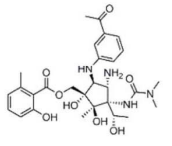
m/z 559.3 $[M+H]^{+}$	(Adams and Rinehart, 1994)

Pristinamycin IA and Pristinamycin IIA (Tü2975)	
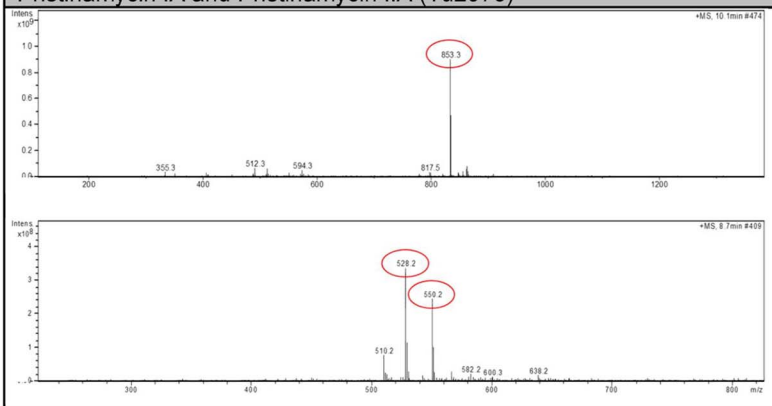	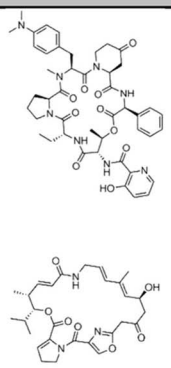
Pristinamycin IA *m/z* 853.3 $[M+Na]^+$; Pristinamycin IIA *m/z* 528.2 $[M+H]^+$, *m/z* 550.2 $[M+Na]^+$	(Cocito, 1979)
Aborycin (TüG349)	
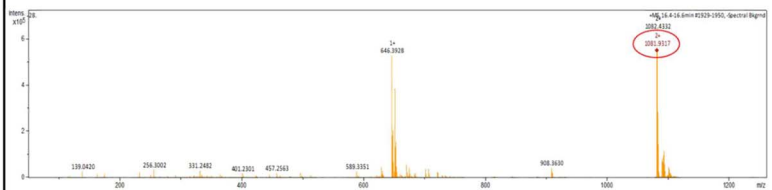	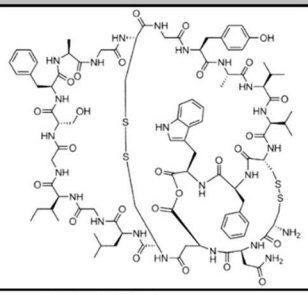
m/z 1081.9317 $[M+H]^{2+}$	(Shao et al., 2019)
FD-594, Naphthomycin B and Naphthomycin J (Tü104)	
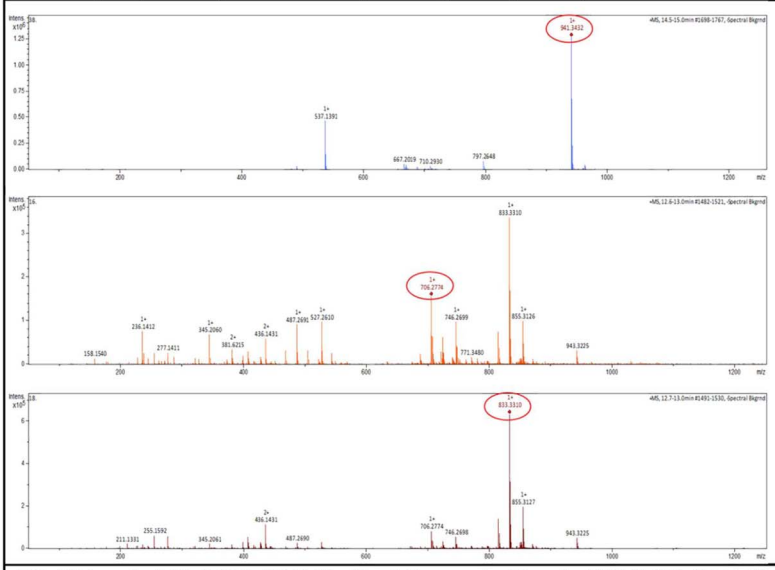	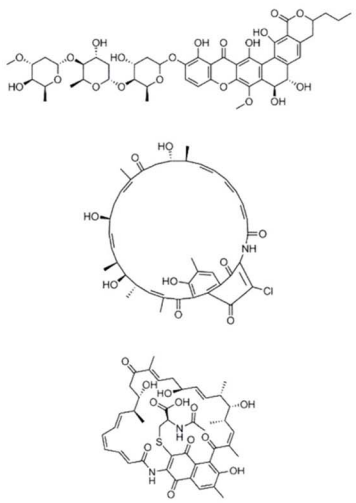
FD-594 *m/z* 941.3432 $[M+H]^+$; Naphthomycin B *m/z* 706.2774 $[M+H]^+$; Naphthomycin J *m/z* 833.3310 $[M+H]^+$	(Kondo et al., 1998; Kudo et al., 2011)
Pentamycin (GöK12/7)	
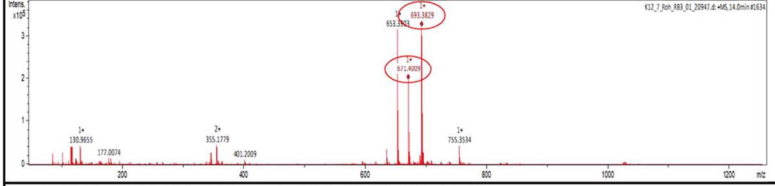	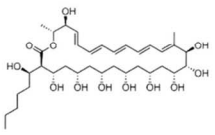
m/z 671.4009 $[M+H]^+$, *m/z* 693.3829 $[M+Na]^+$	(Zhou et al., 2019; Awla et al., 2016)

Telomycin (Tü2641)	
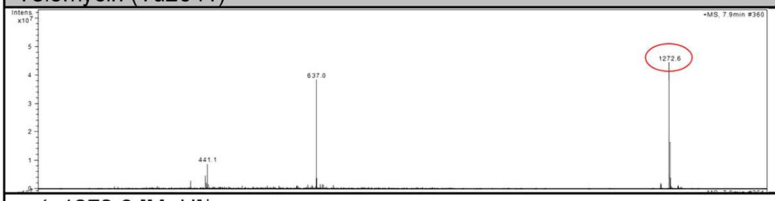	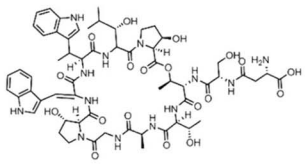
m/z 1272.6 $[M+H]^+$	(Fu et al., 2015)
Boromycin (GöK12/9)	
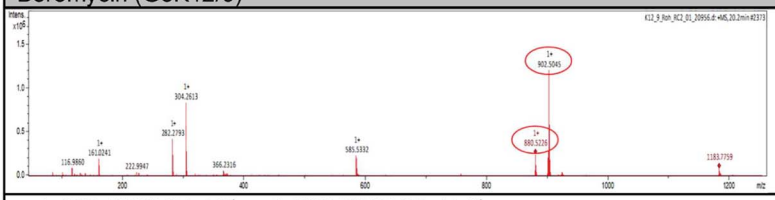	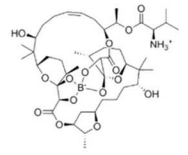
m/z 880.5226 $[M+H]^+$, *m/z* 902.5045 $[M+Na]^+$	(Kohno et al., 1996)
Griseorhodin A (TüG117)	
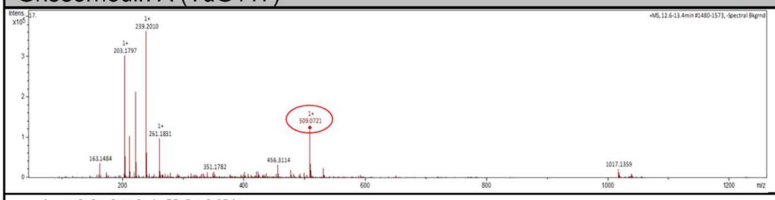	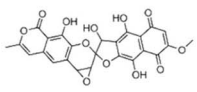
m/z 509.0721 $[M+H]^+$	
Lobophorin A and Lobophorin E (GöSöt11)	
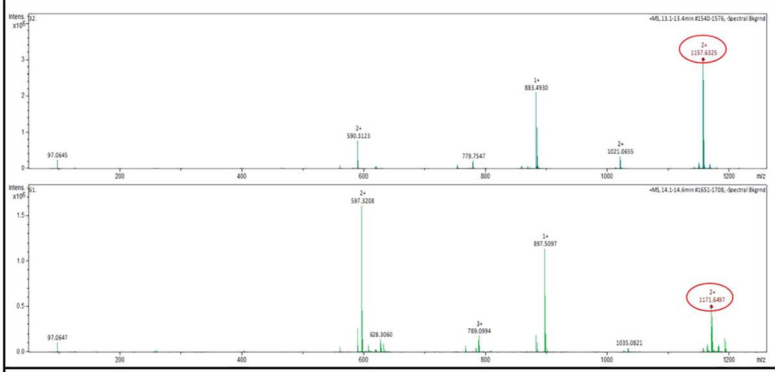	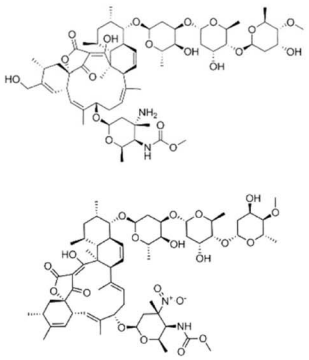
Lobophorin A *m/z* 1157.6325 $[M+H]^+$; Lobophorin E *m/z* 1171.6497 $[M+H]^+$	(Jiang et al., 1999)
Monactin (TüG102)	
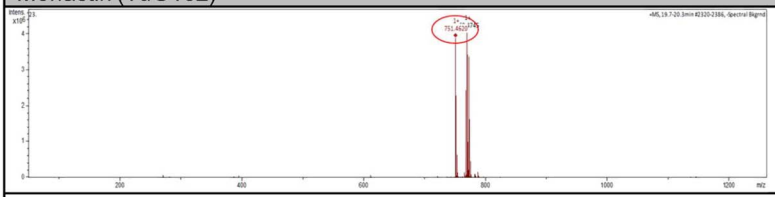	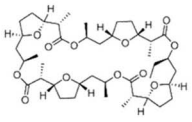
m/z 751.4620 $[M+H]^+$	(Crevelin et al., 2014)
Omomycin (TüG343)	
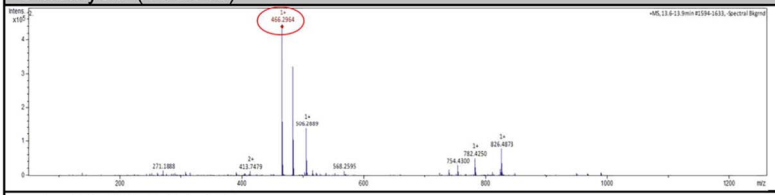	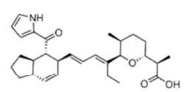
m/z 466.2970 $[M+H]^+$	

SUPPLEMENTAL REFERENCES Data S2

Adams, E. S., and Rinehart, K. L. (1994). Directed biosynthesis of 5''-fluoropactamycin in *Streptomyces pactum*. J Antibiot (Tokyo) 47, 1456-65.

Ando, T., Hirayama, K., Takahashi, R., Horino, I., Etoh, Y., Morioka, H., Shibai, H., and Murai, A. (1985). The structures of anthracycline antibiotics, cosmomycins A and B. Agricultural and Biological Chemistry 49, 1207-1209.

Awla, H., Kadir, J., Othman, R., Rashid, T., and Wong, M.-Y. (2016). Bioactive compounds produced by *Streptomyces* sp. isolate UPMRS4 and antifungal activity against *Pyricularia oryzae*. American Journal of Plant Sciences 07, 1077-1085.

Cocito, C. (1979). Antibiotics of the virginiamycin family, inhibitors which contain synergistic components. Microbiological Reviews 43, 145-192.

Crevelin, E. J., Crotti, A. E. M., Zucchi, T. D., Melo, I. S., and Moraes, L. a. B. (2014). Dereplication of *Streptomyces* sp. AMC 23 polyether ionophore antibiotics by accurate-mass electrospray tandem mass spectrometry. Journal of Mass Spectrometry 49, 1117-1126.

Fu, C., Keller, L., Bauer, A., Brönstrup, M., Froidbise, A., Hammann, P., Herrmann, J., Mondesert, G., Kurz, M., Schiell, M., et al. (2015). Biosynthetic studies of telomycin reveal new lipopeptides with enhanced activity. Journal of the American Chemical Society 137, 7692-7705.

Haesler, F., Hagn, A., Frommberger, M., Hertkorn, N., Schmitt-Kopplin, P., Munch, J. C., and Schloter, M. (2008). *In vitro* antagonism of an actinobacterial *Kitasatospora* isolate against the plant pathogen *Phytophthora citricola* as elucidated with ultrahigh resolution mass spectrometry. Journal of Microbiological Methods 75, 188-195.

Hedtmann, U., Fehlhaber, H. W., Sukatsch, D. A., Weber, M., Hoffmann, D., and Kraemer, H. P. (1992). The new cytotoxic antibiotic cytorhodin X, an unusual anthracyclinone-9 alpha-glycoside. Journal of Antibiotics (Tokyo) 45, 1373-5.

Jiang, Z.-D., Jensen, P. R., and Fenical, W. (1999). Lobophorins A and B, new antiinflammatory macrolides produced by a tropical marine bacterium. Bioorganic and Medicinal Chemistry Letters 9, 2003-2006.

Kohno, J., Kawahata, T., Otake, T., Morimoto, M., Mori, H., Ueba, N., Nishio, M., Kinumaki, A., Komatsubara, S., and Kawashima, K. (1996). Boromycin, an anti-HIV antibiotic. Bioscience, Biotechnology, and Biochemistry 60, 1036-1037.

Kondo, K., Eguchi, T., Kakinuma, K., Mizoue, K., and Qiao, Y. F. (1998). Structure and biosynthesis of FD-594; a new antitumor antibiotic. Journal of Antibiotics (Tokyo) 51, 288-95.

Kudo, F., Yonezawa, T., Komatsubara, A., Mizoue, K., and Eguchi, T. (2011). Cloning of the biosynthetic gene cluster for naphthoxanthene antibiotic FD-594 from *Streptomyces* sp. TA-0256. The Journal of Antibiotics 64, 123-132.

Lau, R. C., and Rinehart, K. L. (1994). Berninamycins B, C, and D, minor metabolites from *Streptomyces bernensis*. Journal of Antibiotics (Tokyo) 47, 1466-72.

Maskey, R. P., Pusecker, K., Speitling, M., Monecke, P., Helmke, E., and Laatsch, H. (2002). 2''-Chartreusin-monoacetate, a New Natural Product with Unusual Anisotropy Effects from the Marine Isolate *Streptomyces* sp. B5525, and its 4''-Isomer. Zeitschrift für Naturforschung B 57, 823-829.

Muralikrishnan, B., Dan, V. M., Vinodh, J. S., Jamsheena, V., Ramachandran, R., Thomas, S., Dastager, S. G., Kumar, K. S., Lankalapalli, R. S., and Kumar, R. A. (2017). Anti-microbial activity of chrysomycin A produced by *Streptomyces* sp. against *Mycobacterium tuberculosis*. RSC Advances 7, 36335-36339.

Ortlieb, N. (2019). Characterization of natural products from actinobacteria of the Tübingen strain collection – Screening, isolation and structure elucidation. Doctoral dissertation. Eberhard-Karls-University Tübingen.

Pethő, L., Mező, G., and Schlosser, G. (2019). Overcharging effect in electrospray ionization mass spectra of daunomycin-tuftsin bioconjugates. Molecules (Basel, Switzerland) 24, 2981.

Shao, M., Ma, J., Li, Q., and Ju, J. (2019). Identification of the anti-infective aborycin biosynthetic gene cluster from deep-sea-derived *Streptomyces* sp. SCSIO ZS0098 enables production in a heterologous host. Marine Drugs 17, 127.

Shao, R. G., and Zhen, Y. S. (2008). Enediyne anticancer antibiotic lidamycin: chemistry, biology and pharmacology. Anti-Cancer Agents in Medicinal Chemistry 8, 123-31.

Sottani, C., Tranfo, G., Bettinelli, M., Faranda, P., Spagnoli, M., and Minoia, C. (2004). Trace determination of anthracyclines in urine: a new high-performance liquid

chromatography/tandem mass spectrometry method for assessing exposure of hospital personnel. Rapid Communications in Mass Spectrometry 18, 2426-2436.
Vater, J., Crnovčić, I., Semsary, S., and Keller, U. (2014). MALDI-TOF mass spectrometry, an efficient technique for *in situ* detection and characterization of actinomycins. Journal of Mass Spectrometry 49, 210-222.
Xie, Y., Wang, B., Liu, J., Zhou, J., Ma, J., Huang, H., and Ju, J. (2012). Identification of the biosynthetic gene cluster and regulatory cascade for the synergistic antibacterial antibiotics griseoviridin and viridogrisein in *Streptomyces griseoviridis*. ChemBioChem 13, 2745-2757.
Xu, Z., Jakobi, K., Welzel, K., and Hertweck, C. (2005). Biosynthesis of the antitumor agent chartreusin involves the oxidative rearrangement of an anthracyclic polyketide. Chemistry and Biology 12, 579-588.
Zeng, Y., Kulkarni, A., Yang, Z., Patil, P. B., Zhou, W., Chi, X., Van Lanen, S., and Chen, S. (2012). Biosynthesis of albomycin δ(2) provides a template for assembling siderophore and aminoacyl-tRNA synthetase inhibitor conjugates. ACS Chemical Biology 7, 1565-75.
Zhang, G., Zhang, H., Li, S., Xiao, J., Zhang, G., Zhu, Y., Niu, S., Ju, J., and Zhang, C. (2012). Characterization of the amicetin biosynthesis gene cluster from *Streptomyces vinaceusdrappus* NRRL 2363 implicates two alternative strategies for amide bond formation. Applied and Environmental Microbiology 78, 2393-2401.
Zhou, S., Song, L., Masschelein, J., Sumang, F. a. M., Papa, I. A., Zulaybar, T. O., Custodio, A. B., Zabala, D., Alcantara, E. P., De Los Santos, E. L. C., et al. (2019). Pentamycin biosynthesis in philippine *Streptomyces* sp. S816: cytochrome P450-catalyzed installation of the C-14 hydroxyl group. ACS Chemical Biology 14, 1305-1309.

JOURNAL OF NATURAL PRODUCTS

Article

Cite This: J. Nat. Prod. 2017, 80, 2941-2952

pubs.acs.org/jnp

Cyclic Cystine-Bridged Peptides from the Marine Sponge *Clathria basilana* Induce Apoptosis in Tumor Cells and Depolarize the Bacterial Cytoplasmic Membrane

Amin Mokhlesi,[†,‡] Fabian Stuhldreier,[§] Katharina W. Wex,[⊥] Anne Berscheid,[⊥] Rudolf Hartmann,[∥] Nidja Rehberg,[†] Parichat Sureechatchaiyan,[▽] Chaidir Chaidir,[○] Matthias U. Kassack,[▽] Rainer Kalscheuer,[†] Heike Brötz-Oesterhelt,[⊥] Sebastian Wesselborg,[§] Björn Stork,[§] Georgios Daletos,*[,†] and Peter Proksch*[,†]

[†]Institute of Pharmaceutical Biology and Biotechnology, Heinrich Heine University, Universitätsstraße 1, D-40225 Düsseldorf, Germany

[‡]Department of Marine Biology, Faculty of Marine Sciences, Tarbiat Modares University, Noor, Iran

[§]Institute of Molecular Medicine I, Medical Faculty, Heinrich Heine University, Universitätsstraße 1, D-40225 Düsseldorf, Germany

[⊥]Department of Microbial Bioactive Compounds, Interfaculty Institute of Microbiology and Infection Medicine, University of Tübingen, Auf der Morgenstelle 28/E8, 72076 Tübingen, Germany

[∥]Institute of Complex Systems: Strukturbiochemie, Forschungszentrum Jülich, Wilhelm-Johnenstrasse, 52428 Jülich, Germany

[▽]Institute of Pharmaceutical and Medicinal Chemistry, Heinrich Heine University, Universitätsstraße 1, D-40225 Düsseldorf, Germany

[○]Center for Pharmaceutical and Medical Technology, Agency for the Assessment and Application Technology, 10340 Jakarta, Indonesia

Supporting Information

ABSTRACT: Investigation of the sponge *Clathria basilana* collected in Indonesia afforded five new peptides, including microcionamides C (**1**) and D (**2**), gombamides B (**4**), C (**5**), and D (**6**), and an unusual amide, (*E*)-2-amino-3-methyl-*N*-styrylbutanamide (**7**), along with 11 known compounds, among them microcionamide A (**3**). The structures of the new compounds were elucidated by one- and two-dimensional NMR spectroscopy as well as by high-resolution mass spectrometry. The absolute configurations of the constituent amino acid residues in **1**−**7** were determined by Marfey's analysis. Microcionamides A, C, and D (**1**−**3**) showed *in vitro* cytotoxicity against lymphoma (Ramos) and leukemia cell lines (HL-60, Nomo-1, Jurkat J16), as well as against a human ovarian carcinoma cell line (A2780) with IC_{50} values ranging from 0.45 to 28 μM. Mechanistic studies showed that compounds **1**−**3** rapidly induce apoptotic cell death in Jurkat J16 and Ramos cells and that **1** and **2** potently block autophagy upon starvation conditions, thereby impairing pro-survival signaling of cancer cells. In addition, microcionamides C and A (**1** and **3**) inhibited bacterial growth of *Staphylococcus aureus* and *Enterococcus faecium* with minimal inhibitory concentrations between 6.2 and 12 μM. Mechanistic studies indicate dissipation of the bacterial membrane potential.

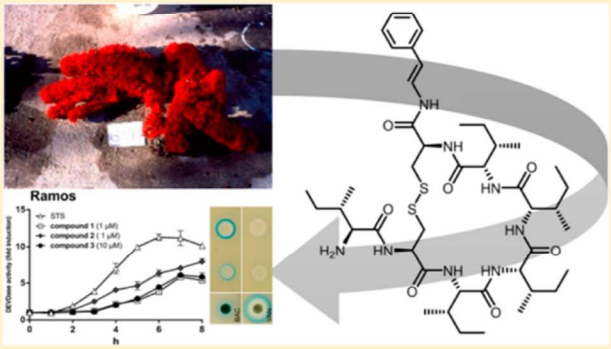

Marine sponges represent a prolific source of structurally unique peptides possessing diverse bioactivities, primarily as antibiotic, anticancer, and neuroprotective agents, thus suggesting their potential value for the development of leads in drug discovery.[1] Prominent examples of bioactive sponge-derived peptides include koshikamide A_1 and calyxamide A reported from *Theonella* sp. and *Discodermia calyx*, respectively, both showing strong cytotoxicity toward P388 murine leukemia cells,[2,3] as well as the diaminoacrilic acid-containing cyclic peptides callyaerins A and B possessing inhibitory activity against *Mycobacterium tuberculosis*.[4]

The genus *Clathria* (order Poecilosclerida, family Microcionidae)[5] includes more than 800 species that are widely distributed in the shallow waters of tropical and temperate regions. Chemical investigation of sponges belonging to this genus has provided a diverse array of secondary metabolites, such as alkaloids,[6,7] carotenoids,[8] steroids,[9,10] and peptides.[11,12] The latter class of compounds includes microcionamides A and B as well as gombamide A from *Clathria abietina* and *Clathria*

Received: June 4, 2017
Published: November 2, 2017

DOI: 10.1021/acs.jnatprod.7b00477
J. Nat. Prod. 2017, 80, 2941−2952

Table 1. ^{1}H (600 MHz), ^{13}C (150 MHz), HMBC, and ROESY NMR Data (DMSO-d_6, δ in ppm) of Microcionamide C (1)

Uunit	position	δ_C,[a] type	δ_H (J in Hz)	HMBC	ROESY[b]
E-PEA	NH		10.02, d (10.0)		Cys_1-α, *E*-PEA-β
	α	122.8, CH	7.35, dd (10.0, 14.8)	Cys_1-CO, *E*-PEA-β, *E*-PEA-1	
	β	112.5, CH	6.26, d (14.8)	*E*-PEA-α, *E*-PEA-1, *E*-PEA-2/6	Ile_2-γ'
	aromatic	1:136.0, C			
		2:124.9, CH	7.32, br dd (7.4, 1.4)	*E*-PEA-β, *E*-PEA-1, *E*-PEA-6, *E*-PEA-4	
		3:128.5, CH	7.28, br dd (7.4, 7.1)	*E*-PEA-1, *E*-PEA-5, *E*-PEA-4	
		4:126.1, CH	7.16, tt (7.1, 1.4)	*E*-PEA-2/6, *E*-PEA-3/5	
		5:128.5, CH	7.28, br dd (7.4, 7.1)	*E*-PEA-1, *E*-PEA-3, *E*-PEA-4	
		6:124.9, CH	7.32, br dd (7.4, 1.4)	*E*-PEA-β, *E*-PEA-1, *E*-PEA-2, *E*-PEA-4	
Cys_1	NH		8.15, d (7.8)	Ile_2-CO	Ile_2-α
	CO	167.2, C			
	α	52.6, CH	4.34[c]	Cys_1-CO, Cys_1-β, Ile_2-CO	*E*-PEA-α, *E*-PEA-NH
	β	40.7, CH_2	3.19, br t (13.2); 3.30, dd (13.2, 4.7)	Cys_1-CO, Cys_1-α	
Ile_2	NH		7.99, br s		
	CO	170.4, C			
	α	57.7, CH	3.96, t (7.6)	Ile_2-CO, Ile_3-CO, Ile_2-β, Ile_2-γ, Ile_2-γ'	Cys_1-NH
	β	34.6, CH	1.88, m	Ile_2-α	
	γ	24.5, CH_2	1.51, m; 1.06, m	Ile_2-α	Ile_3-α
	γ'	15.4, CH_3	0.86, d (6.9)	Ile_2-α	
	δ	11.0, CH_3	0.81[c]		
Ile_3	NH		7.75, br s		
	CO	171.2, C			
	α	57.6, CH	4.04, br s	Ile_3-γ, Ile_3-γ'	Ile_2-γ
	β	36.2, CH	1.82, m	Ile_3-γ, Ile_3-γ', Ile_3-δ, Ile_3-CO	
	γ	24.5, CH_2	1.20, m; 1.54, m	Ile_3-α	
	γ'	15.1, CH_3	0.93, d (6.8)	Ile_3-α	
	δ	11.2, CH_3	0.87[c]		
Ile_4	NH		7.34[c]		
	CO	n.d.[d]			
	α	56.7, CH	4.33[c]	Ile_4-γ, Ile_4-γ'	Ile_5-β
	β	35.9, CH	2.00, br s		
	γ	23.5, CH_2	1.16, m; 1.35, m	Ile_4-α, Ile_4-γ', Ile_4-δ	
	γ'	15.6, CH_3	0.89[c]	Ile_4-α, Ile_4-γ	
	δ	11.1, CH_3	0.82[c]	Ile_4-β	
Ile_5	NH		8.53, d (9.8)	Cys_6-CO	Cys_6-α
	CO	170.4, C			
	α	57.8, CH	4.19, dd (9.8, 6.9)	Ile_5-CO, Cys_6-CO, Ile_5-β, Ile_5-γ, Ile_5-γ'	
	β	36.2, CH	1.84, m	Ile_5-α, Ile_5-γ'	Ile_4-α
	γ	23.9, CH_2	1.40, m; 1.10, m	Ile_5-α	
	γ'	15.2, CH_3	0.84[c]	Ile_5-α, Ile_5-β	
	δ	10.7, CH_3	0.80[c]		
Cys_6	NH		8.83, d (8.1)	Cys_6-β	Ile_7-α, Ile_7-β, Ile_7-γ
	CO	168.9, C			
	α	52.3, CH	4.62, br ddd (10.3, 8.1, 4.6)	Cys_6-CO, Ile_7-CO, Cys_6-β	Ile_5-NH
	β	40.1, CH_2	3.11, br dd (12.8, 10.3); 3.39, dd (12.8, 4.6)	Cys_6-CO, Cys_6-α	
Ile_7	NH_2		8.10, br d (5.4)	Ile_7-CO, Ile_7-α, Ile_7-β	Ile_7-α, Ile_7-β, Ile_7-γ'
	CO	167.8, C			
	α	56.0, CH	3.66, br t (5.4)	Ile_7-CO, Ile_7-γ, Ile_7-γ'	Cys_6-NH
	β	36.2, CH	1.79, m	Ile_7-CO, Ile_7-δ	Cys_6-NH
	γ	23.4, CH_2	1.10, m; 1.47, m	Ile_7-α	Cys_6-NH
	γ'	14.1, CH_3	0.89[c]	Ile_7-α	
	δ	10.8, CH_3	0.83[c]		

[a]Data extracted from HSQC and HMBC spectra. [b]Sequential NOEs. [c]Signal overlap prevents determination of couplings. [d]n.d.: not detected.

gombawuiensis, respectively, all featuring a disulfide linkage that is rarely found in sponge-derived metabolites.[11,12]

During our ongoing research for bioactive metabolites from marine sponges, we investigated a specimen of the marine sponge *Clathria basilana*, which was collected at Ambon Island, Indonesia. Notably, the MeOH extract completely inhibited the growth of the murine lymphoma L5178Y cell line at a concentration of 10 μg/mL. Bioactivity-guided isolation afforded five new peptides (**1**, **2**, **4**–**6**) and one new amide derivative (**7**), in addition to one known peptide (**3**) and 10 known, structurally unrelated aromatic compounds. In this study, the structure elucidation of the new compounds as well as results of cytotoxicity

DOI: 10.1021/acs.jnatprod.7b00477
J. Nat. Prod. 2017, 80, 2941−2952

and antibacterial assays, followed by mechanistic studies, are reported.

RESULTS AND DISCUSSION

The MeOH extract of *C. basilana* was subjected to liquid−liquid fractionation to yield *n*-hexane, EtOAc, and *n*-BuOH fractions. Subsequent column chromatography of the EtOAc or *n*-BuOH fraction followed by semipreparative reversed-phase HPLC afforded five new peptides (**1**, **2**, **4**−**6**) and a new amide derivative (**7**).

Compound **1** was obtained as a white, amorphous solid. Its molecular formula was determined to be $C_{44}H_{72}N_8O_7S_2$ on the basis of the prominent ion peak at m/z 889.5033 $[M + H]^+$ in the HRESIMS spectrum, accounting for 13 degrees of unsaturation. In the ^{1}H NMR spectrum, measured in DMSO-d_6, the peptidic nature of **1** was evident from the presence of NH signals in the amide region (δ_H 7.34−10.02) and characteristic signals of α-amino protons (δ_H 3.66−4.62), as well as from a cluster of primary and secondary methyl groups in the aliphatic region (δ_H 0.81−2.00). Detailed analysis of the 2D NMR (HSQC, TOCSY, ROESY, and HMBC) spectra of **1** allowed the assignment of seven spin systems, including those of five isoleucine (Ile) and two cysteine (Cys) residues (Table 1). The remaining signals included those of a monosubstituted phenyl ring [δ_H 7.32 (2H, dd, J = 7.4, 1.4 Hz), 7.28 (2H, dd, J = 7.4, 7.1 Hz), and 7.16 (1H, tt, J = 7.1, 1.4 Hz)] and two olefinic protons at δ_H 6.26 (PEA-Hβ) and 7.35 (PEA-Hα), suggesting the presence of a 2-phenylethen-1-amine (PEA) unit, as supported by the HMBC correlations from PEA-Hα to PEA-C1 (δ_C 136.0) and from PEA-Hβ to PEA-C2/6 (δ_C 124.9), as well as by the TOCSY correlations of both PEA-Hα and PEA-Hβ with PEA-NH. The configuration of the double bond of PEA was deduced as *E* on the basis of the large coupling constant (^3J = 14.8 Hz) measured for the respective protons.

The connectivity of the amino acid residues and of *E*-PEA was established by key HMBC and ROESY correlations (Figure 1).

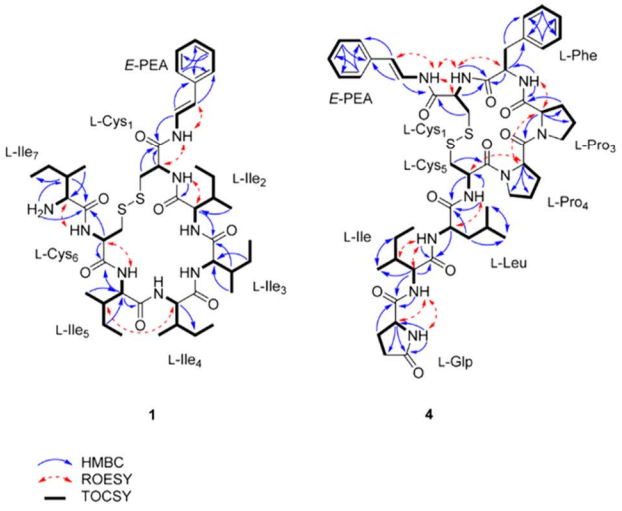

Figure 1. Key HMBC, ROESY, and TOCSY correlations of **1** and **4**.

Accordingly, the HMBC correlations from *E*-PEA-Hα to Cys_1-CO (δ_C 167.2), from Cys_1-NH to Ile_2-CO (δ_C 170.4), and from Ile_2-Hα to Ile_3-CO (δ_C 171.2), along with the ROESY correlations between Cys_1-Hα and *E*-PEA-NH and between Ile_2-Hα and Cys_1-NH, suggested the peptide substructure *E*-PEA-Cys_1-Ile_2-Ile_3. Moreover, the sequence Ile_4-Ile_5-Cys_6 was supported by the HMBC correlations from Ile_5-NH and Ile_5-Hα to Cys_6-CO, as well as by the ROESY correlations between Ile_4-Hα and Ile_5-Hβ and between Ile_5-NH and Cys_6-Hα (Figure 1). The latter cysteine moiety (Cys_6) was linked to Ile_7 based on the HMBC cross-peak from Cys_6-Hα to Ile_7-CO (δ_C 167.8) and the ROESY correlation between Cys_6-NH and Ile_7-Hα, thus leading to the overall peptide structure *E*-PEA-Cys_1-Ile_2-Ile_3-Ile_4-Ile_5-Cys_6-Ile_7. Additionally, the cyclic nature of **1** was evident from the disulfide linkage of the two cysteine residues that formed a cystine moiety, thus accounting for the last degree of unsaturation based on the molecular formula ($C_{44}H_{72}N_8O_7S_2$). The assignment was further supported by HRESIMS/MS, which showed the fragmentation ions at m/z 770.4297 for $[M - E\text{-PEA}]^+$ and at m/z 657.3454 for $[M - (E\text{-PEA+Ile}_7)]^+$, originating from subsequent cleavage of the *E*-PEA and Ile_7 units, both located at the linear parts of the peptide (Figure S1-7). Hence, compound **1** was identified as a new natural product, and the name microcionamide C was proposed given the structural relationship between this compound and the known compounds microcionamides A (**3**) and B.[11]

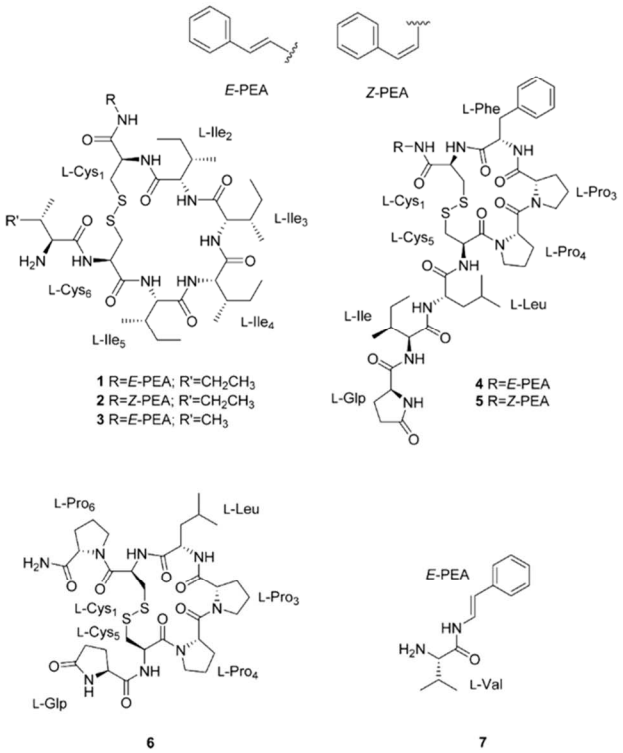

Compound **2** was isolated as a white, amorphous solid. The molecular formula of **2** was established as $C_{44}H_{72}N_8O_7S_2$ by HRESIMS, identical to that found for **1**. Moreover, the ^{1}H NMR data of **2** were almost superimposable to those of **1**, the only notable difference being the resonances and coupling constants of the olefinic protons at δ_H 5.74 (1H, d, J = 10.0 Hz) and 6.72 (1H, t, J = 10.0 Hz), suggesting a (*Z*)-2-phenylethen-1-amine (*Z*-PEA) unit in **2** instead of a *E*-PEA unit, as in the case of **1** (Table S2-1). Likewise, HRESIMS/MS of **2** showed fragmentation ions originating from cleavage of the *Z*-PEA and Ile_7 units (Figure S2-9). Hence, the structure of **2** was assigned as the *Z* isomer of **1** and was named microcionamide D.

Compound **4** was obtained as a white, amorphous solid. The molecular formula of **4** was deduced to be $C_{50}H_{67}N_9O_9S_2$ based on the prominent ion peak at m/z 1002.4572 $[M + H]^+$ in

DOI: 10.1021/acs.jnatprod.7b00477
J. Nat. Prod. 2017, 80, 2941−2952

Table 2. ^{1}H (600 MHz), ^{13}C (150 MHz), HMBC, and ROESY NMR Data (DMSO-d_6, δ in ppm) of Gombamide B (4)

unit	position	δ_C, type	δ_H (J in Hz)	HMBC	ROESY[a]
E-PEA	NH		10.32, d (10.0)		Cys_1-NH, Cys_1-α
	α	123.0, CH	7.36, dd (14.7, 10.0)	Cys_1-CO, *E*-PEA-1	
	β	113.2, CH	6.33, d (14.7)	*E*-PEA-NH, *E*-PEA-α, *E*-PEA-2/6, *E*-PEA-1	*E*-PEA-NH
	aromatic	1: 136.2, C			
		2: 125.3, CH	7.37, br d (7.7)	*E*-PEA-β, *E*-PEA-1, *E*-PEA-6, *E*-PEA-4	
		3: 128.6, CH	7.30, br t (7.7)	*E*-PEA-1, *E*-PEA-5	
		4: 126.4, CH	7.17, br t (7.7)	*E*-PEA-2/6	
		5: 128.6, CH	7.30, br t (7.7)	*E*-PEA-1, *E*-PEA-3	
		6: 125.3, CH	7.37, br d (7.7)	*E*-PEA-β, *E*-PEA-1, *E*-PEA-2	
Cys_1	NH		7.72, d (8.6)	Phe-CO, Cys_1-α, Cys_1-β	*E*-PEA-NH, Phe-α
	CO	167.8, C			
	α	51.6, CH	4.64, ddd (12.0, 8.6, 3.5)	Cys_1-CO, Cys_1-β, Phe-CO	*E*-PEA-NH
	β	42.1, CH_2	2.93, dd (14.4, 12.0); 3.15, dd (14.4, 3.5)	Cys_1-CO, Cys_1-α	
Phe	NH		8.97, d (8.8)	Phe-α, Phe-β, Pro_3-CO	Pro_3-α
	CO	170.8, C			
	α	53.5, CH	4.81, m	Phe-CO, Phe-β, Phe-1, Pro_3-CO	Cys_1-NH
	β	34.0, CH_2	2.99, m; 3.02, m	Phe-CO, Phe-α, Phe-1, Phe-2/6	
	aromatic	1: 138.3, C			
		2: 129.3, CH	7.43, br d (7.5)	Phe-β, Phe-6, Phe-4	
		3: 128.1, CH	7.29, br t (7.5)	Phe-1, Phe-5	
		4: 126.2, CH	7.20, br t (7.5)	Phe-2/6	
		5: 128.1, CH	7.29, br t (7.5)	Phe-1, Phe-3	
		6: 129.3, CH	7.43, br d (7.5)	Phe-β, Phe-2, Phe-4	
Pro_3	CO	171.4, C			
	α	60.3, CH	4.36, d (7.8)	Pro_3-CO, Pro_4-CO, Pro_3-β, Pro_3-γ, Pro_3-δ	Pro_4-α, Pro_4-β, Phe-NH
	β	31.2, CH_2	1.73, m; 1.88, m	Pro_3-CO, Pro_3-α, Pro_3-γ	
	γ	20.1, CH_2	1.42, m; 0.55, m	Pro_3-α	
	δ	45.9, CH_2	3.29, m; 3.26, m	Pro_3-α, Pro_3-β	
Pro_4	CO	169.3, C			
	α	59.2, CH	4.84, dd (9.5, 2.0)	Pro_4-β, Pro_4-γ, Pro_4-δ	Pro_3-α, Cys_5-α
	β	30.2, CH_2	1.87, m; 2.22, m	Pro_4-CO, Pro_4-α, Pro_4-δ	Pro_3-α
	γ	21.9, CH_2	1.76, m	Pro_4-α	
	δ	46.3, CH_2	3.34, m; 3.48, m	Pro_4-β, Pro_4-γ	
Cys_5	NH		8.01, d (10.0)	Leu-CO, Cys_5-α, Cys_5-β	Leu-α
	CO	167.9, C			
	α	48.4, CH	4.56, td (10.0, 5.2)	Leu-CO, Cys_5-CO, Cys_5-β	Pro_4-α
	β	38.0, CH_2	2.61, br dd (12.0, 10.0); 3.22, br dd (12.0, 5.2)	Cys_5-α, Cys_5-CO	
Leu	NH		8.05, d (9.2)	Leu-α, Leu-β, Ile-CO	Ile-α, Ile-β
	CO	170.5, C			
	α	50.5, CH	4.49, ddd (9.2, 8.0, 7.7)	Leu-CO, Leu-β, Leu-γ, Ile-CO	Cys_5-NH
	β	41.2, CH_2	1.58, m	Leu-CO, Leu-α, Leu-γ, Leu-δ, Leu-δ'	
	γ	24.0, CH	1.63, m	Leu-δ, Leu-δ'	
	δ	21.3, CH_3	0.86, d (6.3)	Leu-β, Leu-γ, Leu-δ'	
	δ'	23.3, CH_3	0.89, d (6.4)	Leu-β, Leu-γ, Leu-δ	
Ile	NH		8.07, d (8.8)	Glp-CO, Ile-α, Ile-β	Glp-α, Glp-NH
	CO	170.7, C			
	α	57.0, CH	4.16, t (8.8)	Ile-CO, Ile-β, Ile-γ, Ile-γ', Glp-CO	Leu-NH
	β	35.5, CH	1.73, m	Ile-CO, Ile-α, Ile-γ	
	γ	24.2, CH_2	1.02, m; 1.42, m	Ile-α, Ile-β, Ile-δ, Ile-γ'	
	γ'	15.4, CH_3	0.75, d (6.7)	Ile-α, Ile-β, Ile-γ	
	δ	10.4, CH_3	0.72, t (7.4)	Ile-β, Ile-γ	
Glp	NH		7.80, s	Glp-CO′, Glp-α, Glp-β, Glp-γ	Ile-NH
	CO	172.4, C			
	CO′	177.4, C			
	α	55.1, CH	4.10, dd (8.7, 4.0)	Glp-CO, Glp-CO′, Glp-β, Glp-γ	Ile-NH
	β	25.3, CH_2	1.78, m; 2.21, m	Glp-CO, Glp-CO′	
	γ	29.0, CH_2	2.09, m; 2.07, m	Glp-CO′, Glp-α, Glp-β	

[a]Sequential NOEs.

DOI: 10.1021/acs.jnatprod.7b00477
J. Nat. Prod. 2017, 80, 2941−2952

the HRESIMS spectrum, accounting for 22 degrees of unsaturation. The planar peptidic structure of **4** was distinguished by the abundance of the amide (NH) (δ_H 7.72−10.32) and α-amino (δ_H 4.10−4.84) protons, as well as by the cluster of primary and secondary methyl groups in the aliphatic region of the ^{1}H NMR spectrum (Table 2). Analysis of the COSY and TOCSY NMR spectra revealed the spin systems of seven amino acid residues, including Pro (2 equiv), Cys (2 equiv), Phe, Leu, and Ile, together with the *E*-PEA unit and the unusual amino acid residue pyroglutamic acid (Glp). The presence of the latter was confirmed by key HMBC correlations from Glp-Hα to Glp-CO′ (δ_C 177.4) and Glp-Cγ (δ_C 29.0), from Glp-NH to Glp-CO′ and Glp-Cα (δ_C 55.1), and from Glp-Hβ to Glp-CO (δ_C 172.4). In analogy to **1** and **2**, the linkages and assignments of the amino acid residues in **4** were established by HMBC and ROESY NMR data (Table 2). Accordingly, the connection between *E*-PEA and Cys_1 was deduced by the HMBC correlation from *E*-PEA-Hα to Cys_1-CO (δ_C 167.8) as well as the ROESY cross-peak between *E*-PEA-NH and Cys_1-Hα. Moreover, the HMBC correlations from Cys_1-Hα and Cys_1-NH to Phe-CO (δ_C 170.8), from Phe-Hα and Phe-NH to Pro_3-CO (δ_C 171.4), and from Pro_3-Hα to Pro_4-CO (δ_C 169.3) disclosed the peptide fragment *E*-PEA-Cys_1-Phe-Pro_3-Pro_4 (Figure 1). This was further corroborated by the ROESY cross-peaks between Cys_1-NH/Phe-Hα, Phe-NH/Pro_3-Hα, and Pro_3-Hα/Pro_4-Hα. Likewise, the HMBC correlations from Cys_5-Hα to Leu-CO (δ_C 170.5), from Leu-Hα to Ile-CO (δ_C 170.7), as well as from Ile-Hα to Glp-CO (δ_C 172.4), in addition to the ROESY correlations between Pro_4-Hα/Cys_5-Hα, Cys_5-NH/Leu-Hα, Leu-NH/Ile-Hα, and Ile-NH/Glp-Hα extended this fragment, leading to the overall peptide sequence *E*-PEA-Cys_1-Phe-Pro_3-Pro_4-Cys_5-Leu-Ile-Glp. Finally, a disulfide bond between the two Cys residues was evident, consistent with the 22 elements of unsaturation required by the molecular formula. The structure of **4** was further corroborated by the fragment ions at *m*/*z* 665.2566 [M − Leu-Ile-Glp]$^+$ and 883.3826 [M − *E*-PEA]$^+$ in the HRESIMS/MS spectrum, originating from cleavage of the linear peptide sequence Leu-Ile-Glp and the PEA unit, respectively (Figure S4-9). Hence, compound **4** was identified as a new natural product and was named gombamide B, based on the structural relationship with the known compound gombamide A.[12]

Compound **5** was isolated as a white, amorphous solid. The molecular formula of **5** was deduced to be $C_{50}H_{67}N_9O_9S_2$ by HRESIMS analysis, as in the case of **4**. In analogy to **1** and **2**, the ^{1}H NMR spectrum of **5** was similar to that of **4**, the only difference being the *Z*-configuration of the ethylene protons in the PEA moiety instead of the *E*-configuration, as deduced by their vicinal coupling constant ($^3J_{H\alpha,H\beta}$ = 9.7 Hz; Table S5-1). In a similar manner to **4**, HRESIMS/MS of **5** showed MS fragment ions of [M − *Z*-PEA]$^+$ and [M − Leu-Ile-Glp]$^+$ (Figure S5-7). Thus, compound **5** was characterized as a new natural product and was named gombamide C.

Compound **6** was isolated as a white, amorphous solid. The molecular formula of **6** was determined as $C_{32}H_{48}N_8O_8S_2$ by HRESIMS, consistent with 13 degrees of unsaturation. Detailed interpretation of the COSY and HMBC NMR spectra of **6** established the presence of six amino acid residues, including Pro (3 equiv), Cys (2 equiv), and Leu, along with a Glp unit. As described for peptides **1**, **2**, **4**, and **5**, key HMBC correlations from Pro_6-Hα to Cys_1-CO (δ_C 168.1), from Cys_1-NH to Leu-CO (δ_C 170.9), from Leu-NH to Pro_3-CO (δ_C 171.0), from Pro_3-Hα to Pro_4-CO (δ_C 169.6), and from Cys_5-NH to Glp-CO (δ_C 171.5) established the overall amino acid sequence of **6** as Pro_6-Cys_1-Leu-Pro_3-Pro_4-Cys_5-Glp. This assignment was also evident by the ROESY cross-peaks between Cys_1-NH/Leu-NH, Leu-NH/Pro_3-Hα, and Cys_5-NH/Glp-Hα. The remaining two NH protons at δ_H 6.90 (1H, s) and 7.27 (1H, s) were attributed to a terminal carboxamide group, as supported by their HMBC correlations to Pro_6-CO and Pro_6-Cα (Figure 2, Table 3). Finally,

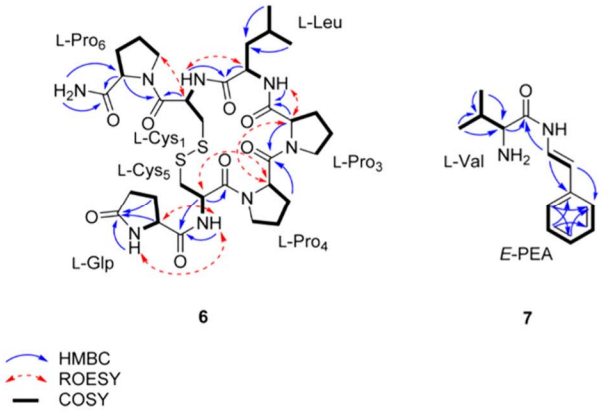

Figure 2. Key HMBC, ROESY, and COSY correlations of **6** and **7**.

cyclization via a disulfide bond between the two Cys residues was suggested to satisfy the remaining element of unsaturation in the structure of **6**. This assignment was further corroborated by the fragment ions at *m*/*z* 623.2317 [M − Pro_6-NH_2]$^+$ and 595.2367 [M − (Pro_6-NH_2 + CO)]$^+$, which were observed in the HRESIMS/MS spectrum of **6** (Figure S6-8). Accordingly, compound **6** was identified as a new natural product and was given the name gombamide D.

Compound **7** was isolated as a white, amorphous solid. The molecular formula of **7** was determined as $C_{13}H_{18}N_2O$ based on HRESIMS analysis, consistent with six degrees of unsaturation. Detailed analysis of the 2D NMR (COSY and HMBC) spectra of **7** allowed the assignment of an unusual amide consisting of Val and *E*-PEA residues, connected through an amide linkage, as supported by the HMBC correlation from *E*-PEA-Hα to Val-CO (δ_C 167.2) (Figure 2, Table 4). Thus, compound **7** was assigned as (*E*)-2-amino-3-methyl-*N*-styrylbutanamide, which is a new natural product.

The remaining compounds were identified on the basis of NMR, HRESIMS, and specific rotation data analysis, as well as by comparison with published data as microcionamide A (**3**),[11] six indole derivatives, namely, 1*H*-indole-3-carbaldehyde, 1*H*-indole-3-carboxylic acid, 6-bromo-1*H*-indole-3-carbaldehyde, 6-bromo-1*H*-indole-3-carboxylic acid, methyl 6-bromo-1*H*-indole-3-carboxylate, and ethyl 6-bromo-1*H*-indole-3-carboxylate,[13,14] along with 7-bromo-4(1*H*)-quinolinone,[15] the δ-lactam derivative (3-(2-(4-hydroxyphenyl)-2-oxoethyl)-5,6-dihydropyridin-2(1*H*)-one),[16] 2-deoxythymidine,[17] and 4-hydroxybenzoic acid (Figure S9-1).

The absolute configuration of each amino acid residue was determined by Marfey's method following acid hydrolysis (6 N HCl) of the isolated peptides **1**−**7** (0.5 mg each).[18] Comparison of the resulting derivatives with those of standard amino acids by HPLC led to the assignment of the L-configuration for all amino acid residues (Table S8-1). Moreover, in an attempt to improve the HPLC resolution between L/D-Ile and L/D-*allo*-Ile residues, a C_4 HPLC RP-column was successfully employed, instead of the commonly used C_{18} column, in analogy to the C_3 Marfey's method,[19] revealing the presence of only L-Ile residues

DOI: 10.1021/acs.jnatprod.7b00477
J. Nat. Prod. 2017, 80, 2941−2952

Table 3. ^{1}H (600 MHz), ^{13}C (150 MHz), HMBC, and ROESY NMR Data (DMSO-d_6, δ in ppm) of Gombamide D (**6**)

unit	position	δ_C, type	δ_H (J in Hz)	HMBC	ROESY[a]
Pro_6	$CONH_2$		6.90, s; 7.27, s	Pro_6-CO, Pro_6-α	Pro_6-α, Cys_1-β
	CO	173.4, C			
	α	59.9, CH	4.16, dd (8.8, 3.5)	Pro_6-CO, Cys_1-CO, Pro_6-β, Pro_6-γ, Pro_6-δ	
	β	29.3, CH_2	1.80, m; 2.02, m	Pro_6-CO, Pro_6-α, Pro_6-γ, Pro_6-δ	
	γ	24.3, CH_2	1.87, m	Pro_6-α, Pro_6-β, Pro_6-δ	
	δ	46.6, CH_2	3.52[b]; 3.63, ddd (9.7, 7.4, 4.5)	Pro_6-α, Pro_6-β	Cys_1-α
Cys_1	NH		7.87, d (8.3)	Leu-CO, Cys_1-β, Cys_1-α	Leu-α, Leu-NH
	CO	168.1, C			
	α	49.2, CH	4.75, ddd (11.6, 8.3, 3.2)	Cys_1-CO, Cys_1-β	Pro_6-δ
	β	41.3, CH_2	2.78, dd (14.6, 11.6); 3.12, dd (14.6, 3.2)	Cys_1-CO, Cys_1-α	
Leu	NH		9.17, d (9.0)	Leu-α, Pro_3-CO	Cys_1-NH, Pro_3-α, Pro_3-δ
	CO	170.9, C			
	α	50.1, CH	4.53[b]	Leu-CO, Leu-β, Leu-γ	Cys_1-NH
	β	37.7, CH_2	1.37, m; 1.71, m	Leu-CO, Leu-α, Leu-γ, Leu-δ, Leu-δ'	
	γ	24.2, CH	1.42, m	Leu-α, Leu-δ, Leu-δ'	
	δ	21.4, CH_3	0.79, d (6.4)	Leu-β, Leu-γ, Leu-δ'	
	δ'	23.1, CH_3	0.88, d (6.4)	Leu-β, Leu-γ, Leu-δ	
Pro_3	CO	171.0, C			
	α	60.6, CH	4.52[b]	Pro_3-CO, Pro_4-CO, Pro_3-β, Pro_3-γ, Pro_3-δ	Leu-NH, Pro_4-α
	β	31.2, CH_2	2.08, m; 2.21, m	Pro_3-CO, Pro_3-α, Pro_3-γ, Pro_3-δ	
	γ	21.2, CH_2	1.56, m; 1.91, m	Pro_3-α	
	δ	45.9, CH_2	3.27, br t (10.4); 3.43[b]	Pro_3-β, Pro_3-γ	Leu-NH
Pro_4	CO	169.6, C			
	α	59.4, CH	4.91, dd (8.7, 2.5)	Pro_4-β, Pro_4-γ, Pro_4-δ	Pro_3-α, Cys_5-α
	β	30.4, CH_2	2.30, m; 1.94, m	Pro_4-CO, Pro_4-α, Pro_4-δ	
	γ	21.8, CH_2	1.73, m; 1.79, m		
	δ	46.5, CH_2	3.50[b]; 3.35, dt (11.7, 7.7)	Pro_4-β	
Cys_5	NH		8.54, d (9.7)	Glp-CO, Cys_5-α	Glp-α, Glp-NH
	CO	168.2, C			
	α	48.4, CH	4.58, ddd (11.1, 9.7, 5.2)	Cys_5-CO, Glp-CO, Cys_5-β	Pro_4-α
	β	37.5, CH_2	2.62, dd (12.4, 11.1); 3.23, dd (12.4, 5.2)	Cys_5-α, Cys_5-CO	
Glp	NH		7.67, s	Glp-CO′, Glp-α, Glp-β, Glp-γ	Cys_5-NH
	CO	171.5, C			
	CO′	177.6, C			
	α	54.9, CH	4.02, br dd (9.0, 2.6)	Glp-CO′, Glp-β	Cys_5-NH
	β	25.1, CH_2	2.07, m; 2.15, td (9.2, 3.4)	Glp-CO, Glp-CO′, Glp-γ	
	γ	28.9, CH_2	2.00, m; 2.24, m	Glp-CO′, Glp-α	

[a]Sequential NOEs. [b]Signal overlap prevents determination of couplings.

as constituents of the respective peptides (**1**–**5**) (Table S8-2). Moreover, the ROESY correlations between Pro_3-Hα/Pro_4-Hα and Pro_4-Hα/Cys_5-Hα (Figure 1) in **4** and **5** suggested a *cis* configuration for the amide peptide bonds, which was further corroborated by the large Pro-Cβ and Pro-Cγ shift difference values ($\Delta\delta_{C\beta\text{-}C\gamma} \approx 8$–$11$ ppm). Similarly, in the case of **6** a *cis* peptide bond was deduced between Pro_3-Pro_4 and Pro_4-Cys_5, whereas the ROESY correlation between Cys_1-Hα and Pro_6-Hδ in addition to the carbon resonances of Cβ and Cγ in Pro_6 (29.3 and 24.3 ppm, respectively) suggested a *trans* peptide bond between Pro_6-Cys_1.[4,20]

Microcionamides C (**1**) and D (**2**) are stereoisomers differing in the *E*/*Z* double-bond configuration of the PEA moiety, as previously observed for the known analogues microcionamides A (**3**) and B.[11] The only difference between the structures of **1** and **2** compared to **3** and microcionamide B is the replacement of the terminal Val residue in the latter compounds by Ile. In analogy to **1** and **2**, compounds **4** and **5** were found to be *E*/*Z* stereoisomers. It should be noted, however, that the *Z*-PEA derivatives **2** and **5** were detected as the minor components in the crude extract, and thus these compounds may be artifacts arising from the respective *E*-PEA analogues **1** and **4** during extraction and/or isolation (e.g., upon exposure to natural light), as previously suggested for **3** and microcionamide B.[11] Compounds **4** and **5** are structurally related to the known peptide gombamide A from the sponge *Clathria gombawuiensis*, the latter compound bearing pyroglutamic acid (Glp) and *para*-hydroxystyrylamide units instead of the linear peptide chain Leu-Ile-Glp and PEA, respectively.[12] Interestingly, Glp is rarely reported from marine invertebrates. In addition to the aforementioned gombamide A, other examples of peptides bearing this unit include didemnins from the tunicate *Tridemnum solidum*,[21] as well as asteropsin A and two pyroglutamyl dipeptides from *Asteropus* sp. sponges.[22,23] The intramolecular cyclization of N-terminal glutamine residues into Glp is of special interest, as it protects peptides from degradation by the action of exopeptidase enzymes or even enables them to adopt the right conformation for binding to their receptors.[24] Gombamide D (**6**) possesses a similar cyclic part to **4** and **5**, the only difference being that the Phe residue is substituted by Leu, as in the case of the cyclic thiopeptides eudistomides A and B, reported from a Fijian ascidian of the genus *Eudistoma*.[25] The promiscuous occurrence of these

DOI: 10.1021/acs.jnatprod.7b00477
J. Nat. Prod. 2017, 80, 2941–2952

Table 4. ^{1}H (600 MHz), ^{13}C (150 MHz), and HMBC NMR Data (MeOH-d_4, δ in ppm) of (*E*)-2-Amino-3-methyl-*N*-styrylbutanamide (7)

unit	position	δ_C, type	δ_H (*J* in Hz)	HMBC
E-PEA	α	122.8, CH	7.46, d (14.7)	Val-CO, *E*-PEA-1
	β	116.4, CH	6.32, d (14.7)	*E*-PEA-2/6
	aromatic	1: 137.2, C		
		2: 126.6, CH	7.35, dt (8.3, 1.5)	*E*-PEA-β, *E*-PEA-6, *E*-PEA-4
		3: 129.8, CH	7.29, br dd (8.3, 7.3)	*E*-PEA-1, *E*-PEA-5
		4: 128.1, CH	7.19, tt (7.3, 1.5)	*E*-PEA-2/6
		5: 129.8, CH	7.29, br dd (8.3, 7.3)	*E*-PEA-1, *E*-PEA-3
		6: 126.6, CH	7.35, dt (8.3, 1.5)	*E*-PEA-β, *E*-PEA-2, *E*-PEA-4
Val	CO	167.2, C		
	α	59.9, CH	3.69, d (5.8)	Val-CO, Val-γ, Val-γ'
	β	31.6, CH	2.24, m	Val-γ, Val-γ'
	γ	17.8, CH_3	1.07, d (6.9)	Val-β, Val-α
	γ'	18.9, CH_3	1.10, d (6.9)	Val-β, Val-α

peptide analogues in different phyla of marine invertebrates argues for symbiont microorganisms as true producers.

Cytotoxicity of the isolated metabolites (**1**–**7** and known compounds) was investigated using different tumor cell lines. Microcionamides A, C, and D (**1**–**3**) showed *in vitro* cytotoxicity against lymphoma (Ramos) and leukemia cell lines (HL-60, Nomo-1, Jurkat J16), as well as against a human ovarian carcinoma cell line (A2780) with IC_{50} values ranging from 0.45 to 28 μM (Figures S10-1 and 3, Table 5). The remaining

Table 5. Cytotoxicity of Compounds 1–3 after Incubation for 24 h Reported as IC_{50} (μM)

compd	A 2780	Ramos	Jurkat J16	Nomo-1	HL-60
1	0.45	1.4	0.81	1.4	1.9
2	0.53	1.9	1.3	2.4	2.5
3	2.6	5.9	4.6	10	28

isolated compounds proved to be inactive in concentrations up to 10 μM.

Due to their strong cytotoxic activity, we next addressed the question of whether **1**–**3** cause apoptotic cell death. Activation of caspase-3 was measured employing two different methods: first by immunoblotting for the cleavage of the caspase-3 substrate poly(ADP-ribose) polymerase-1 (PARP-1) and second by measuring the fluorescence of the profluorescent caspase-3 substrate Ac-DEVD-AMC. Activated caspase-3 cleaves the latter substrate between aspartate (D) and 7-amino-4-methylcoumarin (AMC), hence releasing the fluorogenic AMC, which can be subsequently detected with a spectrofluorometer. Because cysteine-dependent aspartate-directed proteases (caspases) in general and caspase-3 as an effector caspase in particular are central players of apoptotic processes, activation of caspase-3 indicates induction of apoptosis. As shown in Figure 3A, compounds **1**–**3** induced the activation of caspases in Jurkat and Ramos cells with rapid kinetics within 4 h and reached a maximum after 6 to 7 h, indicating a fast induction of apoptotic processes. However, compound **3** induced caspase activation only at 10 μM, whereas in contrast to **1** and **2** it displayed no effect at 1 μM (data not shown), which is in accordance with the higher IC_{50}. To confirm activation of caspase-3 via a further end point, we detected cleavage of the caspase-3 substrate PARP after treatment with **1**, **2**, and **3** (same concentrations as in Figure 3A). In line with the results of the caspase-3 activity assay, all compounds induced cleavage of PARP within 4 to 8 h, indicating again activation of caspase-3 and thus execution of apoptosis. To prove caspase dependency of the observed PARP cleavage, we additionally performed co-incubation with the pan-caspase inhibitor QVD (Figure 3B). QVD completely blocked cleavage of PARP after treatment with **1**, **2**, and **3**, demonstrating a causative role of caspases and thereby occurrence of apoptosis.

Autophagy is a major intracellular degradation route responsible for the lysosome-mediated breakdown of soluble cytosolic components and therefore plays a crucial role in maintaining cellular homeostasis.[26] Cancer cells in particular suffer from metabolic stress and nutrient deprivation due to fast proliferation. Thus, autophagy can support cancer cells to overcome microenvironmental stress by allowing them to recycle dysfunctional or unessential components. Autophagy thereby acts as a mechanism of cell survival. Accordingly, inhibition of autophagy is a promising therapeutic target for anticancer chemotherapy.[27,28] In order to investigate potential inhibitory or stimulating effects of **1**–**3** with regard to autophagy, we used murine embryonic fibroblast (MEF) cells stably expressing mCitrine-hLC3B and measured lysosomal degradation of mCitrine-hLC3B under starvation conditions and after treatment with compounds **1**–**3** or alternatively with the known autophagy inhibitor bafilomycin A1 via flow cytometry.[29] LC3 is an essential component of autophagosomes (double-membraned key structures of autophagy), which deliver engulfed cytoplasmic components to lysosomes and get degraded by the lysosomal system during autophagy. Thus, breakdown of LC3 is a suitable indicator of autophagic processes. Incubation with 10 μM compound **1** or **2** distinctly blocked starvation-induced degradation of LC3, indicating inhibition of autophagy by these compounds (Figure 4). Compound **3** on the other hand was inactive in this experiment, indicating the relevance of the terminal Ile for the autophagy-inhibitory effect. In order to determine whether the observed inhibition of autophagy by compounds **1** and **2** is caspase-dependent, we additionally performed experiments with cotreatment of QVD. Because QVD counteracted compound **1**-related inhibition of autophagy, this inhibitory effect was at least partially due to apoptotic processes. In contrast, the inhibitory effect mediated by compound **2** was completely unaffected by cotreatment with QVD, indicating independence of apoptosis.

Finding new antibacterial agents unaffected by available resistance determinants is of paramount importance in light of increasing bacterial resistance development. Thus, we were also interested in the antibacterial potential of the compounds (Table S10-2). Compounds **1** and **3** showed antibacterial activity against the Gram-positive bacterial species *Enterococcus faecium* and *Staphylococcus aureus* in the low μM range. For both compounds, the minimal inhibitory concentrations (defined as the lowest concentrations completely preventing visible bacterial growth) were 6.2 μM for *S. aureus* and 12 μM for *E. faecium*, respectively (Table S10-2). *Mycobacterium tuberculosis* as well as the Gram-negative species *Klebsiella pneumoniae*, *Enterobacter aerogenes*, *Escherichia coli*, *Pseudomonas aeruginosa*, and *Acinetobacter baumannii* were not inhibited up to 100 μM. Compounds **2** and **5** were not investigated due to compound limitation. The remaining compounds showed no antibacterial activity.

In order to investigate the mechanism of bacterial growth inhibition, we employed as a first step a panel of bacterial reporter strains that we constructed in the background of the Gram-positive

DOI: 10.1021/acs.jnatprod.7b00477
J. Nat. Prod. 2017, 80, 2941–2952

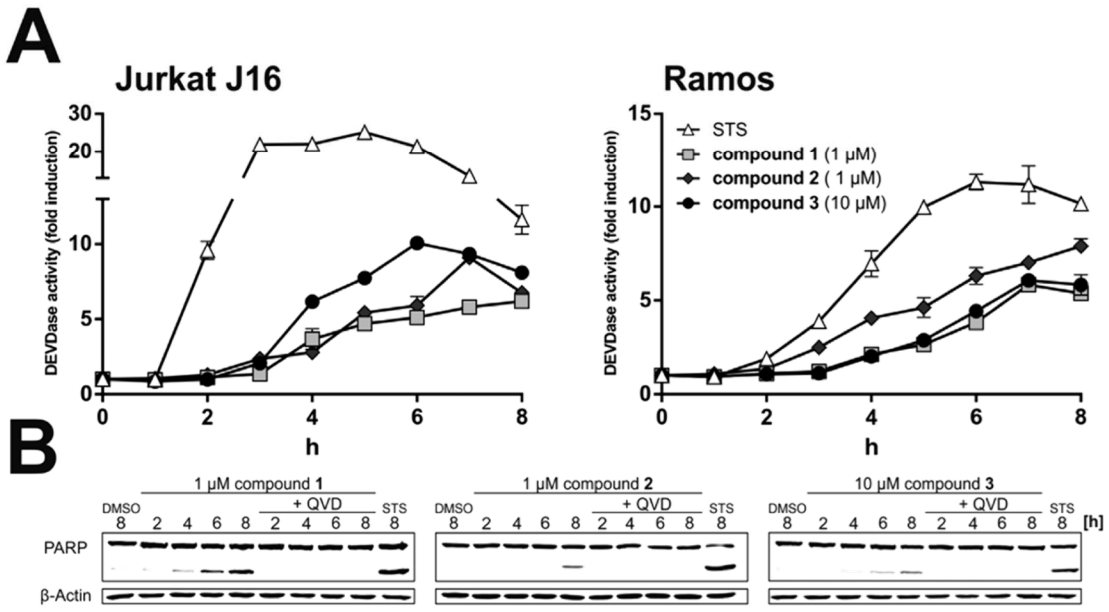

Figure 3. Compounds **1**–**3** rapidly induce apoptosis in human lymphoma and leukemia cell lines. (A) The kinetics of caspase-3 activation in Jurkat J16 (acute T cell leukemia; left panel) and Ramos (Burkitt's lymphoma; right panel) cells after treatment with indicated concentrations of compounds **1**–**3** were compared to those of staurosporine (STS, 2.5 μM), a well-established inducer of apoptosis. Caspase-3 activity was measured by the rate of cleavage of the profluorescent caspase-3 substrate Ac-DEVD-AMC. Relative caspase-3 activity in DMSO (0.1% v/v)-treated control cells was set to 1. Data shown are the mean ± SD from a representative experiment performed in triplicate. (B) Ramos cells were treated with compounds **1** (1 μM), **2** (1 μM), or **3** (10 μM) in the absence or presence of the caspase inhibitor Q-VD-OPh (QVD, 10 μM) for the indicated duration between 2 and 8 h. After the incubation period cleavage of PARP was determined by Western blot analysis. The expression of β-actin was determined as a protein loading control. Shown is the result of a representative blot. STS (2.5 μM) served as the positive control for caspase-dependent cleavage of PARP.

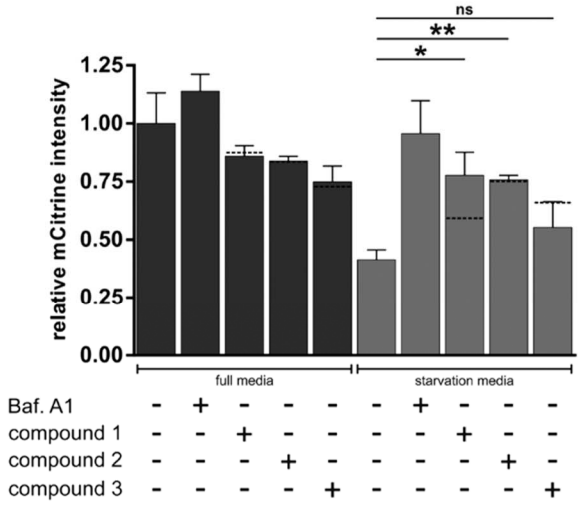

Figure 4. Compounds **1** and **2** impair amino acid starvation-induced autophagy. MEFs stably expressing mCitrine-hLC3B were cultivated in full medium or starvation medium (EBSS) with 10 μM compounds **1**, **2**, or **3** for 4 h. Ten nM bafilomycin A_1 (Baf. A1) served as the positive control for inhibition of autophagy. Total cellular mCitrine-hLC3B signals were analyzed by flow cytometry. The median of fluorescence intensity was plotted in a bar diagram. Values are normalized to DMSO (0.1% v/v)-treated cells cultivated in full medium (1.0) and represent mean ± SD of 3 independent analyses. * = $p \leq 0.05$, ** = $p \leq 0.01$ (Student's t test, two-sample assuming unequal variances). Dashed lines represent median mCitrine fluorescence intensity of cells cotreated with caspase inhibitor Q-VD-OPh (10 μM) performed in triplicate.

model organism *Bacillus subtilis*. These strains express the reporter gene β-galactosidase from five selected promoters that were previously found and validated to react specifically to disturbances of certain metabolic pathways or cell structures.[30] Previous whole genome mRNA profiling of *B. subtilis* after treatment with a broad range of antibiotic classes had identified these promoters as particularly responsive to DNA, RNA, protein, or cell envelope damage. Compounds **1** and **3** showed a specific induction of the cell envelope stress sensing promoters *liaI* and *ypuA* (Figure 5). While *ypuA* is known to respond broadly to disturbances at the bacterial cell envelope, *liaI* showed in previous studies a particularly strong reaction to compounds that interfere with cycling of undecaprenyl precursors in cell wall synthesis.[31]

With the aim to further explore the effects of the microcionamides on the bacterial cell envelope, we determined effects of compounds **1** and **3** on the membrane potential of *S. aureus*. The membrane potential is an electrical gradient across the bacterial cytoplasmic membrane, with a surplus of positive charge outside, that bacteria establish in the course of respiration. The membrane potential is essential for ATP generation by the F_OF_1-ATPase and for active transport processes across the cytoplasmic membrane. For measurement of the membrane potential the fluorescent dye $DiOC_2(3)$ was used, which enters bacterial cells to some extent and emits green fluorescence. The higher the membrane potential, the more dye molecules accumulate in the cells and aggregation triggers a red-shift of fluorescence emission. Addition of compounds **1** and **3** efficiently dissipated the membrane potential of *S. aureus*, as indicated by the strong loss of red fluorescence (Figure 6). The effect occurred already at submicromolar concentrations of **1** and **3**, the latter compound being slightly more potent. Consequently, microcionamides A (**3**) and C (**1**) seem to kill bacteria by energy depletion.

Notably, while some energy depleting agents induce the *liaI* promoter, e.g. the lantibiotic nisin, which uses the undecaprenyl

DOI: 10.1021/acs.jnatprod.7b00477
J. Nat. Prod. 2017, 80, 2941–2952

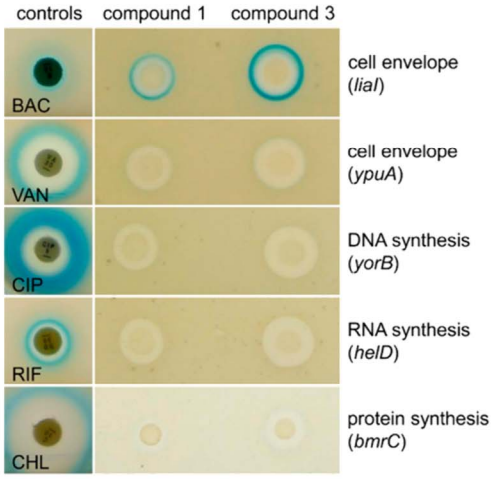

Figure 5. Reporter gene assay with compounds **1** and **3** for orienting mode of action studies. Compounds **1** and **3** strongly induced the *liaI* promoter, and a weak induction was detected for the *ypuA* promoter, indicating that these compounds cause cell envelope stress. The other three promoters indicating DNA damage (*yorB*), RNA damage (*helD*), or translation arrest (*bmrC*) were not induced. The five different promoters showed a strong induction when treated with the respective positive controls: bacitracin (BAC), vancomycin (VAN), ciprofloxacin (CIP), rifampicin (RIF), and chloramphenicol (CHL).

precursor lipid II as a docking molecule to form pores within the bacterial cytoplasmic membrane,[32] many energy-depleting agents, such as ionophores, do not effectively induce *liaI*. Whether or not the strong *liaI* signal triggered by the microcionamides indicates that bacterial cells sense an interference with their undecaprenyl precursor cycle will require further studies.

In summary, microcionamides A, B, and C (**1**–**3**) exhibited cytotoxicity on different human cancer cell lines via both induction of apoptosis and inhibition of starvation-induced autophagy. Furthermore, microcionamides A (**3**) and C (**1**) showed a significant inhibitory effect on Gram-positive bacteria, which is probably correlated with their abilities to depolarize bacterial cytoplasmic membranes. It is noteworthy that microcionamide C (**1**) showed increased cytotoxic activity over microcionamide A (**3**) by a factor of 5 or more on different eukaryotic cell lines, while **3** was more potent against Gram-positive bacteria compared to **1**. Even though the difference in the MIC between **1** and **3** against *S. aureus* was smaller than a whole titration step in the MIC assay, a larger zone of inhibition of **3** was detected on agar (Figure 5), and lower concentrations of **3** were able to cause a disruption of the membrane potential in comparison to **1** (Figure 6). Conversely, gombamides B (**4**) and D (**6**) proved to be inactive against both human and bacterial cells.

■ EXPERIMENTAL SECTION

General Experimental Procedures. Optical rotations were measured with a JASCO P-2000 polarimeter. UV data were recorded on a PerkinElmer Lambda 25 UV/vis spectrometer. ^{1}H, ^{13}C, and 2D NMR spectra (HH-ROESY, HH-TOCSY, HC-HSQC, and HC-HMBC) were recorded with standard pulse sequences on a Bruker AVIII HD 600 spectrometer equipped with a QXI/QCI cryoprobe. The sweep width for the homonuclear experiments (HH-ROESY, HH-TOCSY) was 7000 Hz in F2 and F1. Two thousand data points were collected in F2, and 512 data points in F1 with quadrature detection in both dimensions. The mixing time for the HH-ROESY experiment was 450 ms with a spin lock field of 5000 Hz and 80ms for the HH-TOCSY with a spin lock field of 9500 Hz. The HC-HSQC

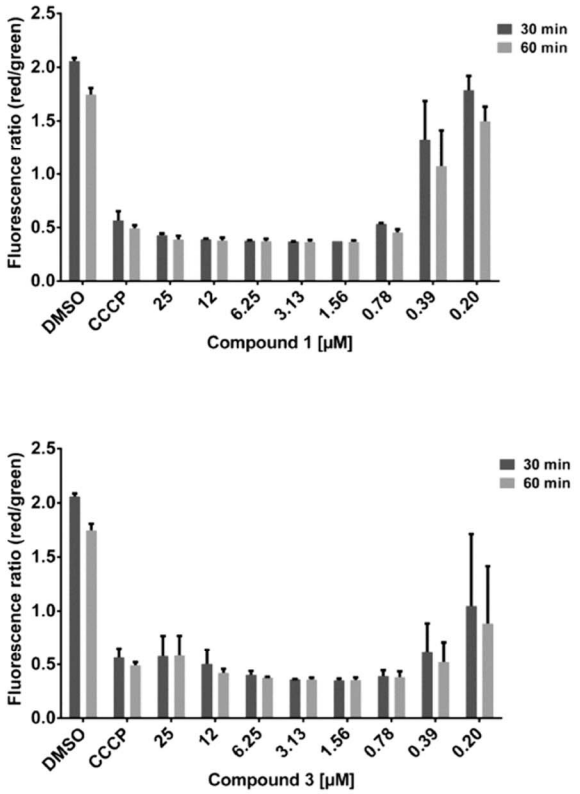

Figure 6. Effect of microcionamides A (**3**) and C (**1**) on the membrane potential of *Staphylococcus aureus* NCTC 8325. A prominent loss of red fluorescence indicative of strong membrane potential dissipation occurs already at 0.8 μM of **1** or 0.2 μM of **3**. The protonophore carbonyl cyanide *m*-chlorophenyl hydrazone (CCCP) at 5 μM served as a positive control, and DMSO was the negative control. Samples were analyzed after 30 and 60 min of exposure to compounds. The experiment was performed two times on two different days with independent bacterial cultures. Results for both biological replicates are shown in the graphs. Error bars indicate the standard error of the mean.

experiment was measured with a sweep width of 7000 Hz in F2 and 26400 Hz in F1. Two thousand data points were collected in F2, and 512 data points in F1 with quadrature detection in both dimensions. The sweep width for the HC-HMBC experiments was set to 7000 Hz in F2 and 27900 Hz in F1. Two thousand data points in F2 and 512 data points in F1 were collected with quadrature detection in F2. The chemical shifts were referenced to the residual solvent peaks at δ_H 3.31(MeOH-d_4) and 2.50 (DMSO-d_6) for ^{1}H and at δ_C 49.0 (MeOH-d_4) and 39.5 (DMSO-d_6) for ^{13}C NMR. Low-resolution ESI mass spectra were recorded on a Thermoquest Finnigan LCQ Deca connected to an Agilent 1100 series LC. High-resolution mass measurements were obtained on an LTQ Orbitrap Velos Pro (Thermo Scientific). Solvents were distilled prior to use, and spectral grade solvents were used for spectroscopic measurements. HPLC analysis was performed using a Dionex UltiMate3400 SD coupled to a photodiode array detector (DAD3000RS) with detection wavelengths at 235, 254, 280, and 340 nm. The separation column (125 × 4 mm, L × i.d) was prefilled with Eurospher 100-10, C18 (Knauer, Germany). HPLC analysis of L/D-Ile and L/D-*allo*-Ile following Marfey's derivatization was carried out on the EC 250/4.6 Nucleosil 120-5, C_4 (Macherey-Nagel) separation column. Column chromatography was performed using Sephadex LH-20 or reversed-phase silica (RP C_{18}) as stationary phase. Semipreparative purification was accomplished on a Merck Hitachi system (pump L7100 and UV detector L7400; Eurospher 100 C_{18}, 300 × 8 mm, L × i.d; Knauer) with a flow rate of 5.0 mL/min. Thin-layer chromatography (TLC) was performed using

DOI: 10.1021/acs.jnatprod.7b00477
J. Nat. Prod. 2017, 80, 2941−2952

precoated silica gel 60 F_{254} plates (Merck) followed by detection under UV at 254 nm or after spraying the plates with anisaldehyde reagent.

Sponge Material. The sponge was collected by scuba at Ambon, Indonesia. The sponge was identified as *Clathria basilana* by Dr. Nicole de Voogd (Naturalis Biodiversity Center, Leiden, The Netherlands), and a voucher specimen was deposited at the Naturalis Biodiversity Center, Leiden, The Netherlands (reference number RMNH POR 8636). The sponge was preserved in a mixture of EtOH and H_2O (70:30) and stored in a −20 °C freezer prior to extraction.

Extraction and Isolation. The thawed sponge material (820 g wet) was cut into small pieces and exhaustively extracted with MeOH (3 × 2L) at room temperature (rt). The extracts were combined and concentrated under vacuum to yield 6.5 g of crude extract. Subsequent liquid−liquid partitioning afforded *n*-hexane, EtOAc, *n*-BuOH, and aqueous fractions at amounts of 420 mg, 700 mg, 540 mg, and 4.9 g, respectively. The EtOAc fraction was further purified by column chromatography on Sephadex LH-20 (MeOH as mobile phase), followed by reversed-phase vacuum liquid chromatography (RP-VLC) and semipreparative HPLC in a gradient system of H_2O/MeOH, respectively, to yield **1** (7.7 mg), **2** (2 mg), **3** (1 mg), **4** (4.5 mg), **5** (1 mg), 7 (0.8 mg), 1*H*-indole-3-carbaldehyde (0.6 mg), 1*H*-indole-3-carboxylic acid (0.5 mg), 6-bromo-1*H*-indole-3-carbaldehyde (1.2 mg), 6-bromo-1*H*-indole-3-carboxylic acid (1 mg), methyl 6-bromo-1*H*-indole-3-carboxylate (1 mg), ethyl 6-bromo-1*H*-indole-3-carboxylate (1.7 mg), 7-bromo-4(1*H*)-quinolinone (1 mg), (3-(2-(4-hydroxyphenyl)-2-oxoethyl)-5,6-dihydropyridin-2(1*H*)-one) (2.2 mg), 2-deoxythymidine (2.5 mg), and 4-hydroxybenzoic acid (4 mg). The *n*-BuOH fraction was subjected to column chromatography on Sephadex LH-20 (MeOH as mobile phase), followed by RP-VLC and semipreparative HPLC to yield **6** (5.6 mg).

*Microcionamide C (**1**):* white, amorphous solid; $[\alpha]^{20}_D$ −56 (*c* 0.1, MeOH); UV (λ_{max}, MeOH) (log ε) 201 (3.72), 287 (3.09); ^{1}H (600 MHz) and ^{13}C (150 MHz) NMR data (DMSO-d_6), Table 1; HRESIMS *m*/*z* 889.5033 $[M + H]^+$ (calcd for $C_{44}H_{73}N_8O_7S_2$, 889.5038); HRESIMS/MS *m*/*z* 770.4297 $[M - E\text{-PEA}]^+$ (calcd for $C_{36}H_{64}N_7O_7S_2$, 770.4303); 657.3454 $[M - (E\text{-PEA} + Ile_7)]^+$ (calcd for $C_{30}H_{52}N_6O_6S_2$, 657.3463).

*Microcionamide D (**2**):* white, amorphous solid; $[\alpha]^{20}_D$ −40 (*c* 0.1, MeOH); UV (λ_{max}, MeOH) (log ε) 210 (3.8), 271 (4.01); ^{1}H (600 MHz) and ^{13}C (150 MHz) NMR data (DMSO-d_6), Table S2-1; HRESIMS *m*/*z* 889.5034 $[M + H]^+$ (calcd for $C_{44}H_{73}N_8O_7S_2$, 889.5038); HRESIMS/MS *m*/*z* 770.4294 $[M - Z\text{-PEA}]^+$ (calcd for $C_{36}H_{64}N_7O_7S_2$, 770.4294); 657.3451 $[M - (Z\text{-PEA} + Ile_7)]^+$ (calcd for $C_{30}H_{52}N_6O_6S_2$, 657.3451); 776.4184 $[M - Ile_7]^+$ (calcd for $C_{38}H_{60}N_7O_6S_2$, 776.4184).

*Gombamide B (**4**):* white, amorphous solid; $[\alpha]^{20}_D$ +28 (*c* 0.1, MeOH); UV (λ_{max}, MeOH) (log ε) 212 (4.1), 290 (4.56); ^{1}H (600 MHz) and ^{13}C (150 MHz) NMR data (DMSO-d_6), Table 2; HRESIMS *m*/*z* 1002.4572 $[M + H]^+$ (calcd for $C_{50}H_{68}N_9O_9S_2$, 1002.4576); HRESIMS/MS *m*/*z* 883.3826 $[M - E\text{-PEA}]^+$ (calcd for $C_{42}H_{59}N_8O_9S_2$, 883.3826); 665.2566 $[M -$ Leu-Ile-Glp$]^+$ (calcd for $C_{33}H_{41}N_6O_5S_2$, 665.2566); 546.1833 $[M - (E\text{-PEA} +$ Leu-Ile-Glp$)]^+$ (calcd for $C_{25}H_{32}N_5O_5S_2$, 546.1833).

*Gombamide C (**5**):* white, amorphous solid; $[\alpha]^{20}_D$ +16 (*c* 0.1, MeOH); UV (λ_{max}, MeOH) (log ε) 214 (4.01), 288 (4.4); ^{1}H (600 MHz) and ^{13}C (150 MHz) NMR data (DMSO-d_6), Table S5-1; HRESIMS *m*/*z* 1002.4576 $[M + H]^+$ (calcd for $C_{50}H_{68}N_9O_9S_2$, 1002.4576); HRESIMS/MS *m*/*z* 883.3826 $[M - Z\text{-PEA}]^+$ (calcd for $C_{42}H_{59}N_8O_9S_2$, 883.3841); 665.2566 $[M -$ Leu-Ile-Glp$]^+$ (calcd for $C_{33}H_{41}N_6O_5S_2$, 665.2566); 546.1833 $[M - (Z\text{-PEA} +$ Leu-Ile-Glp$)]^+$ (calcd for $C_{25}H_{32}N_5O_5S_2$, 546.1839).

*Gombamide D (**6**):* white, amorphous solid; $[\alpha]^{20}_D$ −6 (*c* 0.1, MeOH); UV (λ_{max}, MeOH) (log ε) 210 (3.8), 271 (4.01); ^{1}H (600 MHz) and ^{13}C (150 MHz) NMR data (DMSO-d_6), Table 3; HRESIMS *m*/*z* 737.3107 $[M + H]^+$ (calcd for $C_{32}H_{49}N_8O_8S_2$, 737.3109); HRESIMS/MS *m*/*z* 623.2317 $[M - Pro_6\text{-}NH_2]^+$ (calcd for $C_{27}H_{39}N_6O_7S_2$, 623.2317); 595.2367 $[M - (Pro_6\text{-}NH_2 + CO)]^+$ (calcd for $C_{26}H_{39}N_6O_6S_2$, 595.2367).

*(E)-2-Amino-3-methyl-N-styrylbutanamide (**7**):* white, amorphous solid; $[\alpha]^{20}_D$ −38 (*c* 0.1, MeOH); UV (λ_{max}, MeOH) (log ε) 220 (3.07), 285 (3.22); ^{1}H (600 MHz) and ^{13}C (150 MHz) NMR data (MeOH-d_4), Table 4; HRESIMS *m*/*z* 219.1490 $[M + H]^+$ (calcd for $C_{13}H_{19}N_2O$, 219.1492).

Marfey's Analysis. For acid hydrolysis of the isolated peptides (**1**−**7**), 0.5 mg of each was treated separately with 2 mL of 6 N HCl and heated at 110 °C for 24 h. The resulting solutions were concentrated, with consecutive addition of H_2O (5 mL each) to ensure complete elimination of HCl. Accordingly, the mixture of 50 μL of each acid hydrolysate, 100 μL of FDNPL (1% *N*-(5-fluoro-2,4-dinitrophenyl)-L-leucinamide in acetone), and 20 μL of 1 M $NaHCO_3$ was heated at 40 °C for 1 h with frequent mixing. After cooling, 10 μL of 2 N HCl was added into the reaction solution. Subsequently, the derivatized product was concentrated to dryness and prepared for HPLC analysis by dissolving in 1000 μL of MeOH. The same procedure was followed for L- and D-amino acid standards. HPLC (C_{18}) analysis of the derivatized amino acids was performed by comparing their retention times with those of standards [gradient (MeOH, 0.1% HCOOH in H_2O): 0 min (10% MeOH); 5 min (10% MeOH); 35 min (100% MeOH); 45 min (100% MeOH); 25 °C, 1 mL/min] (Table S8-1). For improved resolution, HPLC analysis of the derivatized L/D-Ile and L/D-*allo*-Ile residues was performed on a C_4 analytical column [gradient (MeOH, 0.1% HCOOH in H_2O): 0% to 60% (MeOH) for 160 min; 25 °C, 1 mL/min] (Table S8-2).[18,33]

Eukaryotic Cell Lines and Reagents. Acute T cell leukemia cells (Jurkat J16, no. ACC- 282), Burkitt's lymphoma B lymphocytes (Ramos, no. ACC-603), acute promyelocytic leukemia cells (HL-60, no. ACC-3), and acute myeloid leukemia cells (Nomo-1, no. ACC-542) were obtained from the German Collection of Microorganisms and Cell Cultures (DSMZ). Wild-type murine embryonic fibroblasts (kindly provided by Xiaodong Wang)[34] expressing mCitrine-hLC3B were generated by retroviral gene transfer using pMSCVpuro/mCitrine-hLC3B. To generate pMSCVpuro/mCitrine-hLC3B, full-length human *MAP1LC3B* cDNA was cloned into pMSCVpuro/mCitrine vector (kindly provided by Michael Engelke, University of Göttingen). All cell lines were grown at 37 °C under humidified air supplemented with 5% CO_2 in RPMI 1640 (HL-60, Jurkat J16, Nomo-1, Ramos) or DMEM (mCitrine-hLC3B-MEF) containing 10% fetal calf serum, 1% HEPES, 120 IU/mL penicillin, and 120 μg/mL streptomycin. The broad-range caspase inhibitor *N*-(2-quinolyl)-L-valyl-L-aspartyl-(2,6-difluorophenoxy) methyl ketone [(QVD) #SML0063], the autophagy inhibitor bafilomycin A1 [(Baf. A1) #B1793], and the kinase inhibitor staurosporine [(STS) #S5921], used as positive control for induction of apoptosis, were obtained from Sigma-Aldrich. The profluorescent caspase-3 substrate Ac-DEVD-AMC was purchased from Biomol (#ABD-13402). Human ovarian carcinoma (A2780) cells were obtained from ECACC (Salisbury, Wiltshire, UK) and cultivated in RPMI-1640 medium supplemented with 10% fetal bovine serum, 120 μg/mL streptomycin, and 120 U/mL penicillin. Cells were grown at 37 °C in a humidified atmosphere containing 5% CO_2.

Determination of Eukaryotic Cell Viability. HL-60, Jurkat J16, Nomo-1, and Ramos cells were seeded at a density of 5×10^5 cells/mL and incubated with different concentrations of compounds **1**, **2**, and **3** for 24 h. Cells treated with DMSO (0.1% v/v) for 24 h were used as the negative control. After the incubation period MTT (3-(4,5-dimethyl-2-thiazolyl)-2,5-diphenyl-2*H*-tetrazolium bromide; Calbiochem #475989) was added to the cells to a final concentration of 1 mg/mL, and the cells were incubated further for 60 min and then centrifuged at 600 rcf for 5 min. The medium was aspirated, and 100 μL of DMSO was added to each well to extract the formazan product from the cells. After 25 min of incubation on a shaker at rt, the absorbances at 650 nm (reference wavelength) and 570 nm (test wavelength) were measured using a multiplate reader (Synergy Mx, BioTek). Viability and IC_{50} values (IC_{50} = half-maximal inhibitory concentration) were calculated using Prism 6 (GraphPad Software). Relative viability in DMSO (0.1% v/v)-treated control cells was set to 100%. A2780 cells were plated into 96-well microtiter plates (approximately 9000 cells/well) (Sarstedt) and preincubated with growth medium overnight. Then, cells were incubated with increasing concentrations of test compounds for 72 h. After 72 h, 25 μL of a solution of MTT was added to each well. After approximately 10 min, formazan crystals were formed, and

DOI: 10.1021/acs.jnatprod.7b00477
J. Nat. Prod. 2017, 80, 2941−2952

medium was removed. Formazan crystals were then dissolved in 75 μL of DMSO. Absorptions were measured at 544 nm (test wavelength) and 690 nm (reference wavelength) using the BMG FLUOstar (BMG Labtechnologies, Offenburg, Germany). Absorption of the reference wavelength was subtracted from the absorption of the test wavelength.

Determination of Antibacterial Activity. MIC values for bacterial strains were determined in cation-adjusted Mueller-Hinton broth by the broth microdilution method according to the recommendations of the Clinical and Laboratory Standards Institute (CLSI).[35] For preparation of the inoculum the direct colony suspension method was used. Briefly, serial 2-fold dilutions of test compounds were prepared in microtiter plates and seeded with a final bacterial inoculum of 5×10^5 colony forming units per mL (CFU/mL). After 16 to 20 h at 37 °C and ambient air, the minimal inhibitory concentration was read as the lowest compound concentration preventing visible bacterial growth. The strain panel included antibiotic-susceptible CLSI quality control strains obtained from the American Type Culture Collection as indicated by the ATCC strain label. *E. faecium* BM 4147-1 is a clinical isolate cured of its vancomycin resistance plasmid,[36] and *A. baumannii* 09987 is a clinical isolate from the University of Bonn, Germany.

Cells of *M. tuberculosis* H37Rv were grown aerobically in Middlebrook 7H9 medium supplemented with 10% (v/v) ADS enrichment (5%, w/v, bovine serum albumin fraction V; 2%, w/v, glucose; 0.85%, w/v, sodium chloride), 0.5% (v/v) glycerol, and 0.05% (v/v) tyloxapol at 37 °C. For the determination of MIC against *M. tuberculosis*, bacteria were precultured until log-phase (OD_{600nm} = 0.5−1) and then seeded at 1×10^5 cells per well in a total volume of 100 μL in 96-well round-bottom microtiter plates containing 2-fold serially diluted compounds at a concentration range of 100−0.78 μM. Microplates were incubated at 37 °C for 5 days. Afterward, 10 μL/well of a 100 μg/mL resazurin solution was added and incubated at ambient temperature for a further 16 h. Then cells were fixed for 30 min after formalin addition (5%, v/v, final concentration). For viability determination, fluorescence was quantified using a microplate reader (excitation 540 nm, emission 590 nm). Percentage of growth was calculated relative to rifampicin-treated (0% growth) and DMSO-treated (100% growth) controls.

Western Blot Analysis. Ramos cells were treated for the indicated durations with 1 μM of **1**, 1 μM of **2**, or 10 μM of **3**, respectively. Co-incubation with the caspase inhibitor QVD at a concentration of 10 μM was used as proof of caspase dependency of the observed effects. Subsequently, cells were pelletized at 600 rcf at 4 °C for 5 min, washed with phosphate-buffered saline (PBS), and frozen in liquid nitrogen. The cells were lysed in ice-cold lysis buffer [20 mM Tris-HCl, pH 7.5, 150 mM NaCl, 0.5 mM EDTA, 1% Triton X-100, 10 mM NaF, 2.5 mM $Na_4P_2O_7$, 10 μM Na_2MoO_4, 1 mM Na_3VO_4, protease inhibitor cocktail (Sigma #P2714)]. The lysates were cleared from cell debris by centrifugation at 11 000 rcf at 4 °C for 15 min, and the total protein concentration was measured by Bradford assay and adjusted to equal concentrations. After loading with Laemmli buffer and heating to 95 °C for 5 min, 25 μg of the protein extract was separated by SDS-PAGE [10% tris-glycine polyacrylamide gel (v/v)] and transferred to a PVDF membrane by Western blotting according to the standard protocol. Analysis of proteins of interest was performed using primary mouse antibodies to poly(ADP-ribose) polymerase-1 (Enzo Life Sciences #BML-SA250) or β-actin (Sigma-Aldrich #A5316) and IRDye800-conjugated secondary antibodies (LI-COR Biosciences #926-32210/11). Signals were detected with an infrared imaging system.

Caspase-3 Activity Assay. Caspase activity was analyzed as previously described.[37] Briefly, Jurkat J16 cells and Ramos cells were seeded at a density of 1×10^6 cells/mL in 96-well microtiter plates and incubated with different concentrations of **1**, **2**, and **3** for the indicated times. Cells treated with DMSO (0.1% v/v) were used as negative control. After the incubation period, cells were harvested by centrifugation at 600 rcf at 4 °C and lysed by incubation with ice-cold lysis buffer (20 mM HEPES, 84 mM KCl, 10 mM $MgCl_2$, 200 μM EDTA, 200 μM EGTA, 0.5% NP-40, 1 μg/mL leupeptin, 1 μg/mL pepstatin, 5 μg/mL aprotinin)) for 10 min. After addition of 150 μL of reaction buffer (50 mM HEPES, 100 mM NaCl, 10% sucrose, 0.1% CHAPS, 2 mM $CaCl_2$, 13.35 mM DTT, 70 μM DEVD-AMC) per well, fluorescence (Ex 360 nm, Em 450 nm) was measured at 37 °C over a time course of 150 min using a multiplate reader (Synergy Mx, BioTek). Caspase activity was determined as the slope of the resulting linear regressions. Data points shown are the mean of triplicates; error bars = SD. Values are normalized to DMSO (0.1% v/v)-treated cells (fold change = 1.00).

FACS-Based Analysis of Autophagy. The FACS-based analysis of autophagy was adapted from a protocol previously described by Shvets et al.[38] MEF cells stably expressing mCitrine-hLC3B were cultured in the indicated medium for 4 h with bafilomycin A1 (10 nM) and compound **1**, **2**, or **3** (10 μM), harvested with 0.05% trypsin-EDTA, and washed once with PBS. Subsequently, the intensity of mCitrine fluorescence was analyzed by flow cytometry using FACSDiva software. Reduction of mCitrine-hLC3B compared to medium control indicates autophagy induction. Baf. A1 served as positive control for inhibition of autophagy. Co-treatment with QVD was performed to exclude caspase-dependent processes.

Bacterial Reporter Gene Assay. For mode of action studies, five bacterial reporter strains were constructed in the genetic background of *B. subtilis* 1S34, each carrying one of the following promoters fused to the β-galactosidase reporter gene and inserted into the chromosomal *amyE* locus. Induction of the *yorB* promoter indicates DNA damage, the *helD* promoter (synonym *yvgS*) senses RNA damage, and the *bmrC* promoter senses translation arrest. Induction of the *ypuA* or *liaI* (synonym *yvqI*) promoters indicates cell envelope stress. Promoter regions were chosen according to a previous publication by Urban et al.[30] For the agar-based reporter gene assay 20 mL of lysogeny broth (LB) containing spectinomycin (50 μg/mL) were inoculated with 500 μL of an overnight culture of *B. subtilis* 1S34 and grown to the stationary phase. Cells were adjusted to a total cell number of 3×10^7 CFU/mL in 50 mL of LB soft agar (0.7% agar) containing 150 μg/mL of 5-bromo-4-chloro-3-indolyl-β-D-galactopyranoside (X-Gal) and poured into a square Petri dish. After solidification, test compounds (20 nmol) were spotted onto the agar plates. Paper discs (Oxoid) containing the following reference antibiotics were used as positive controls: bacitracin (10 μg), chloramphenicol (10 μg), ciprofloxacin (5 μg), rifampicin (30 μg), and vancomycin (30 μg). Plates were analyzed for promoter induction after incubation at 30 °C for 14 to 18 h. In the case of the *bmrC* promoter, soft agar was prepared from Belitzky minimal medium, and the plates were incubated at 37 °C.[39]

Measurement of Bacterial Membrane Potential. Determination of membrane potential changes upon antibiotic treatment was performed using the membrane potential-sensitive fluorescent dye 3,3′-diethyloxacarbocyanine iodide ($DiOC_2(3)$, Molecular Probes). *S. aureus* NCTC 8325 was grown to the exponential phase in LB medium, harvested, and resuspended to an optical density at 600 nm (OD_{600}) of 0.5 in PBS. Cells were incubated with 30 μM $DiOC_2(3)$ for 15 min and subsequently treated with compounds **1** and **3** at different concentrations for 30 min. The protonophore carbonyl cyanide *m*-chlorophenyl hydrazone (Sigma-Aldrich) at a concentration of 5 μM was used as a positive control and DMSO as a negative control. Fluorescence was measured 30 and 60 min after addition of the respective compound at an excitation wavelength of 485 nm and two emission wavelengths, 530 nm (green) as well as 630 nm (red), using a microplate reader (TECAN Infinite M200). Increased membrane potential promotes intracellular dye accumulation, self-association of which causes a red-shift of the fluorescence emission signal.

■ ASSOCIATED CONTENT

Supporting Information

The Supporting Information is available free of charge on the ACS Publications website at DOI: 10.1021/acs.jnatprod.7b00477.

^{1}H NMR spectra of **1**−**7**; ^{13}C NMR spectra of **4**, **6**, and **7**; 2D NMR and HRESIMS spectra of the new compounds **1**, **2**, and **4**−**7**; HRESIMS/MS spectra of **1**, **2**, and **4**−**6**; tables of ^{1}H, ^{13}C, and 2D NMR data for **2** and **5**; HPLC analysis of the acid hydrolysates of **1**−**7** using Marfey's method; structures of known compounds; cytotoxicity effects of **1**−**3** on human lymphoma and leukemia cell lines, measured by MTT assay; table of antibacterial

DOI: 10.1021/acs.jnatprod.7b00477
J. Nat. Prod. 2017, 80, 2941−2952

activity of **1**–**7** and known compounds reported as MIC (PDF)

AUTHOR INFORMATION

Corresponding Authors

*Tel: ++492118114163. E-mail: georgios.daletos@uni-duesseldorf.de.

*E-mail: proksch@uni-duesseldorf.de.

ORCID

Georgios Daletos: 0000-0002-1636-6424

Notes

The authors declare no competing financial interest.

ACKNOWLEDGMENTS

Support of this project to P.P., H.B.-O., M.U.K., R.K., and A.B. by the BMBF (project BALIPEND) and to K.W.W. by the German Center for Infection Research is gratefully acknowledged. We thank Dr. N. de Voogd (Leiden, Naturalis Biodiversity Center, Leiden, The Netherlands) for identification of the sponge. We appreciate the help of Prof. W. E. G. Müller (Johannes Gutenberg University, Mainz, Germany) for cytotoxicity assays with the L5178Y mouse lymphoma cell line. A.M. gratefully acknowledges the Ministry of Science, Research and Technology (MSRT) of Iran for awarding him a scholarship. The authors acknowledge access to the Jülich-Düsseldorf Biomolecular NMR Center. We furthermore wish to acknowledge Ms. Okoniewski and Mr. Straetener for expert technical assistance. The authors wish to thank Dr. E. Ferdinandus (University Pattimura, Ambon, Indonesia) and Prof. Dr. S. Wiryowidagdo (University Hassanudin, Makassar, Indonesia) for their support and help during sponge collection.

REFERENCES

(1) Toshiyuki, W.; Karen, C. T.; Hiroki, T.; Ikuro, A. Cytotoxic Cyclic Peptides from the Marine Sponges. In *Handbook of Anticancer Drugs from Marine Origin*; Springer International Publishing: Switzerland, 2015; pp 113–144.

(2) Fusetani, N.; Warabi, K.; Nogata, Y.; Nakao, Y.; Matsunaga, S.; Van Soest, R. R. M. *Tetrahedron Lett.* **1999**, *40*, 4687–4690.

(3) Kimura, M.; Wakimoto, T.; Egami, Y.; Tan, K. C.; Ise, Y.; Abe, I. *J. Nat. Prod.* **2012**, *75*, 290–294.

(4) Daletos, G.; Kalscheuer, R.; Koliwer, B. H.; Hartmann, R.; de Voogd, N. J.; Wray, V.; Lin, W.; Proksch, P. *J. Nat. Prod.* **2015**, *78*, 1910–1925.

(5) Van Soest, R. W. M.; Boury-Esnault, N.; Hooper, J. N. A.; Rützler, K.; de Voogd, N. J.; Alvarez de Glasby, B.; Hajdu, E.; Pisera, A. B.; Manconi, R.; Schoenberg, C.; Klautau, M.; Picton, B.; Kelly, M.; Vacelet, J.; Dohrmann, M.; Díaz, M.-C.; Cárdenas, P.; Carballo, J. L.; Rios Lopez, P. (2017). World Porifera database. Accessed at http://www.marinespecies.org/porifera on 2017–06–01.

(6) El-Naggar, M.; Conte, M.; Capon, R. J. *Org. Biomol. Chem.* **2010**, *8*, 407–412.

(7) Sperry, S.; Crews, P. *Tetrahedron Lett.* **1996**, *37*, 2389–2390.

(8) Tanaka, Y.; Katayama, T. *Nippon Suisan Gakkaishi* **1976**, *42*, 801–805.

(9) Aiello, A.; Ciminiello, P.; Fattorusso, E.; Magno, S. *Steroids* **1988**, *52*, 533–542.

(10) Keyzers, R. A.; Northcote, P. T.; Webb, V. *J. Nat. Prod.* **2002**, *65*, 598–600.

(11) Davis, R. A.; Mangalindan, G. C.; Bojo, Z. P.; Antemano, R. R.; Rodriguez, N. O.; Concepcion, G. P.; Samson, S. C.; de Guzman, D.; Cruz, L. J.; Tasdemir, D.; Harper, M. K.; Feng, X.; Carter, G. T.; Ireland, C. M. *J. Org. Chem.* **2004**, *69*, 4170–4176.

(12) Woo, J. K.; Jeon, J. e.; Kim, C. K.; Sim, C. J.; Oh, D. C.; Oh, K. B.; Shin, J. *J. Nat. Prod.* **2013**, *76*, 1380–1383.

(13) Cardellina, J. H.; Nigh, D.; VanWagenen, B. C. *J. Nat. Prod.* **1986**, *49*, 1065–1067.

(14) Rasmussen, T.; Jensen, J.; Anthoni, U.; Christophersen, C.; Nielsen, P. H. *J. Nat. Prod.* **1993**, *56*, 1553–1558.

(15) AlTarabeen, M.; Hassan Aly, A.; Perez Hemphill, C.; Catalina, F.; Rasheed, M.; Wray, V.; Proksch, P. *Z. Naturforsch., C: J. Biosci.* **2015**, *70*, 75–78.

(16) Gopichand, Y.; Schmitz, F. J. *J. Org. Chem.* **1979**, *44*, 4995–4997.

(17) Lidgren, G.; Bohlin, L.; Christophersen, C. *J. Nat. Prod.* **1988**, *51*, 1277–1280.

(18) Marfey, P. *Carlsberg Res. Commun.* **1984**, *49*, 591–596.

(19) Vijayasarathy, S.; Prasad, P.; Fremlin, L. J.; Ratnayake, R.; Salim, A. A.; Khalil, Z.; Capon, R. J. *J. Nat. Prod.* **2016**, *79*, 421–427.

(20) Siemion, I. Z.; Wieland, T.; Pook, K. H. *Angew. Chem., Int. Ed. Engl.* **1975**, *14*, 702–703.

(21) Rinehart, K. L.; Kishore, V.; Bible, K. C.; Sakai, R.; Sullins, D. W.; Li, K.-M. *J. Nat. Prod.* **1988**, *51*, 1–21.

(22) Li, H.; Bowling, J. J.; Fronczek, F. R.; Hong, J.; Jabba, S. V.; Murray, T. F.; Ha, N. C.; Hamann, M. T.; Jung, J. H. *Biochim. Biophys. Acta, Gen. Subj.* **2013**, *1830*, 2591–2599.

(23) Li, H.; Dang, H. T.; Li, J.; Sim, C. J.; Hong, J.; Kim, D. K.; Jung, J. H. *Biochem. Syst. Ecol.* **2010**, *38*, 1049–1051.

(24) Calvaresi, M.; Garavelli, M.; Bottoni, A. *Proteins: Struct., Funct., Genet.* **2008**, *73*, 527–538.

(25) Whitson, E. L.; Ratnayake, A. S.; Bugni, T. S.; Harper, M. K.; Ireland, C. M. *J. Org. Chem.* **2009**, *74*, 1156–1162.

(26) Mizushima, N. *Genes Dev.* **2007**, *21*, 2861–2873.

(27) Guo, J. Y.; Chen, H. Y.; Mathew, R.; Fan, J.; Strohecker, A. M.; Karsli-Uzunbas, G.; Kamphorst, J. J.; Chen, G.; Lemons, J. M. S.; Karantza, V.; Coller, H. A.; DiPaola, R. S.; Gelinas, C.; Rabinowitz, J. D.; White, E. *Genes Dev.* **2011**, *25*, 460–470.

(28) Degenhardt, K.; Mathew, R.; Beaudoin, B.; Bray, K.; Anderson, D.; Chen, G.; Mukherjee, C.; Shi, Y.; Gélinas, C.; Fan, Y.; Nelson, D. A.; Jin, S.; White, E. *Cancer Cell* **2006**, *10*, 51–64.

(29) Klionsky, D. J.; Abdelmohsen, K.; Abe, A.; Abedin, M. J.; Abeliovich, H.; Acevedo Arozena, A.; Adachi, H.; Adams, C. M.; Adams, P. D.; Adeli, K. *Autophagy* **2016**, *12*, 1–222.

(30) Urban, A.; Eckermann, S.; Fast, B.; Metzger, S.; Gehling, M.; Ziegelbauer, K.; Rübsamen-Waigmann, H.; Freiberg, C. *Appl. Environ. Microbiol.* **2007**, *73*, 6436–6443.

(31) Mascher, T.; Zimmer, S. L.; Smith, T. A.; Helmann, J. D. *Antimicrob. Agents Chemother.* **2004**, *48*, 2888–2896.

(32) Brötz, H.; Josten, M.; Wiedemann, I.; Schneider, U.; Götz, F.; Bierbaum, G.; Sahl, H. G. *Mol. Microbiol.* **1998**, *30*, 317–327.

(33) Ibrahim, S. R. M.; Min, C. C.; Teuscher, F.; Ebel, R.; Kakoschke, C.; Lin, W.; Wray, V.; Edrada-Ebel, R.; Proksch, P. *Bioorg. Med. Chem.* **2010**, *18*, 4947–4956.

(34) Shang, L.; Chen, S.; Du, F.; Li, S.; Zhao, L.; Wang, X. *Proc. Natl. Acad. Sci. U. S. A.* **2011**, *108*, 4788–4793.

(35) Patel, J. B.; Cockerill, F. R.; Bradford, P. A.; Eliopoulos, G. M.; Hindler, J. A.; Jenkins, S. G.; Lewis, J. S.; Limbago, B.; Miller, L. A.; Nicolau, D. P.; Powell, M.; Swenson, J. M.; Turnidge, J. D.; Weinstein, M. P.; Zimmer, B. L. *Methods for dilution antimicrobial susceptibility tests for bacteria that grow aerobically. Approved Standard*, 10th ed.; Clinical and Laboratory Standards Institute: USA, 2015; Vol. *35*.

(36) Woodford, N.; Adebiyi, A. M. A.; Palepou, M. F. I.; Cookson, B. D. *Antimicrob. Agents Chemother.* **1998**, *42*, 502–508.

(37) Czugala, M.; Mykhaylyk, O.; Böhler, P.; Onderka, J.; Stork, B.; Wesselborg, S.; Kruse, F. E.; Plank, C.; Singer, B. B.; Fuchsluger, T. A. *Nanomedicine* **2016**, *11*, 1787–1800.

(38) Shvets, E.; Fass, E.; Elazar, Z. *Autophagy* **2008**, *4*, 621–628.

(39) Stülke, J.; Hanschke, R.; Hecker, M. *J. Gen. Microbiol.* **1993**, *139*, 2041–2045.

DOI: 10.1021/acs.jnatprod.7b00477
J. Nat. Prod. 2017, 80, 2941–2952

Supplemental Information

S1. Microcionamide C (1)

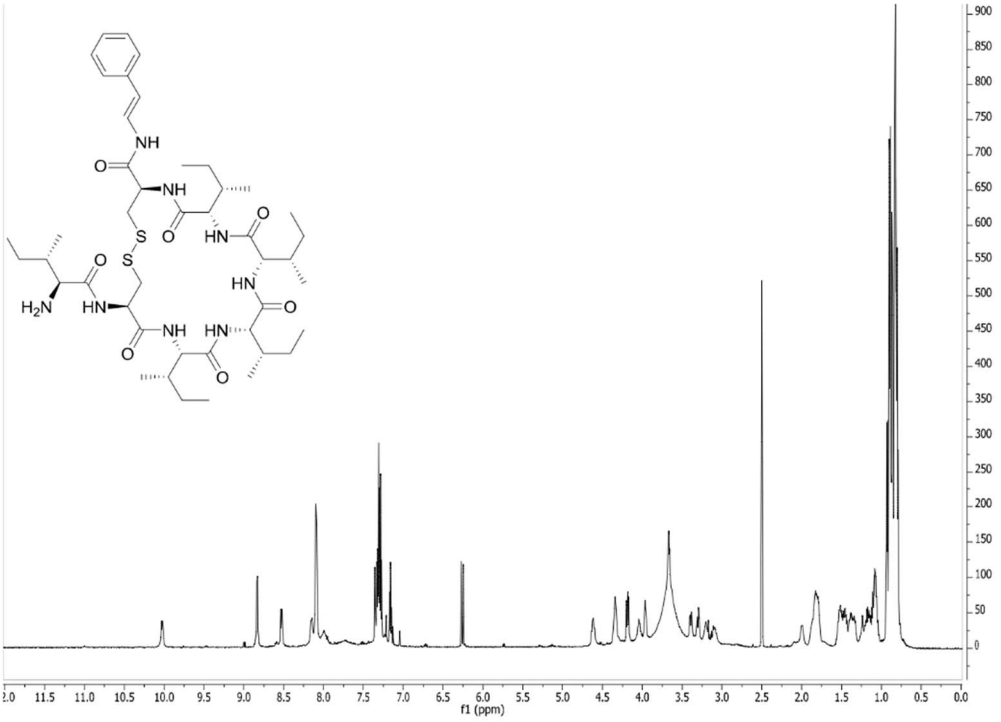

S1-1. ^{1}H NMR (DMSO-d_6, 600 MHz) spectrum of **1**

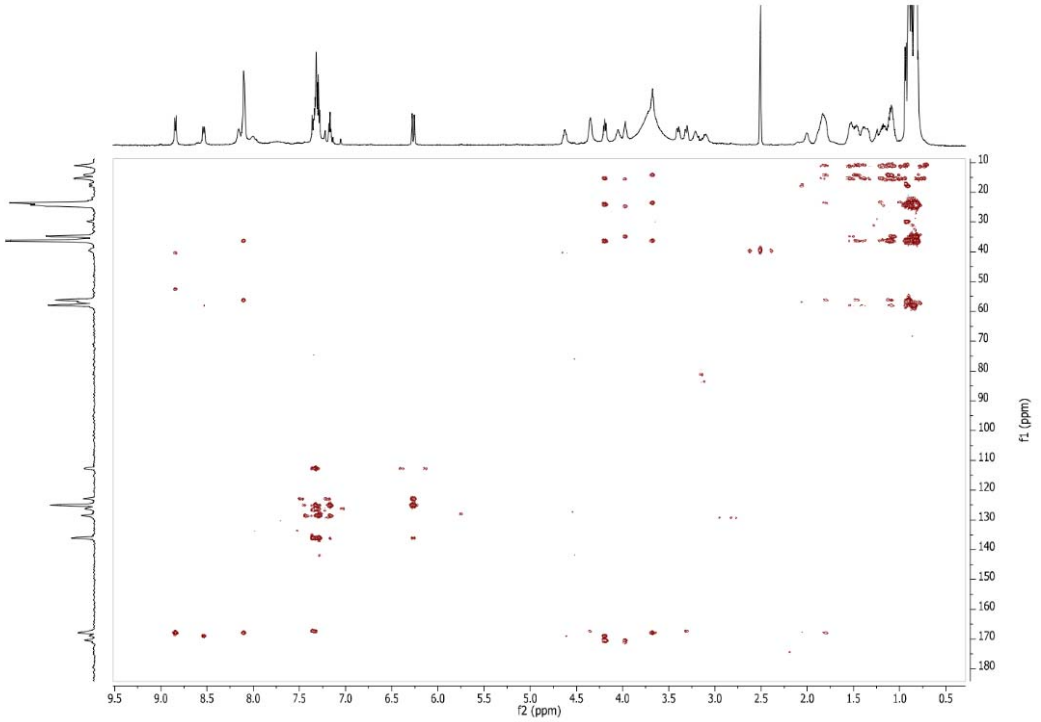

S1-2. HMBC NMR (DMSO-d_6, 600 MHz) spectrum of **1**

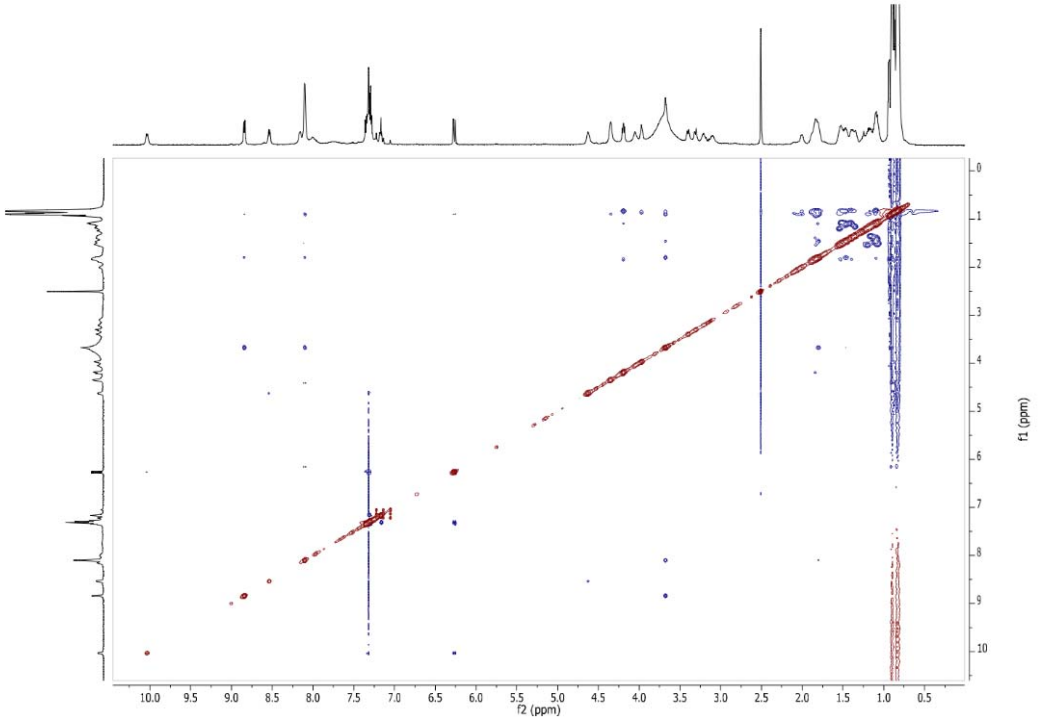

S1-3. ROESY NMR (DMSO-d_6, 600 MHz) spectrum of **1**

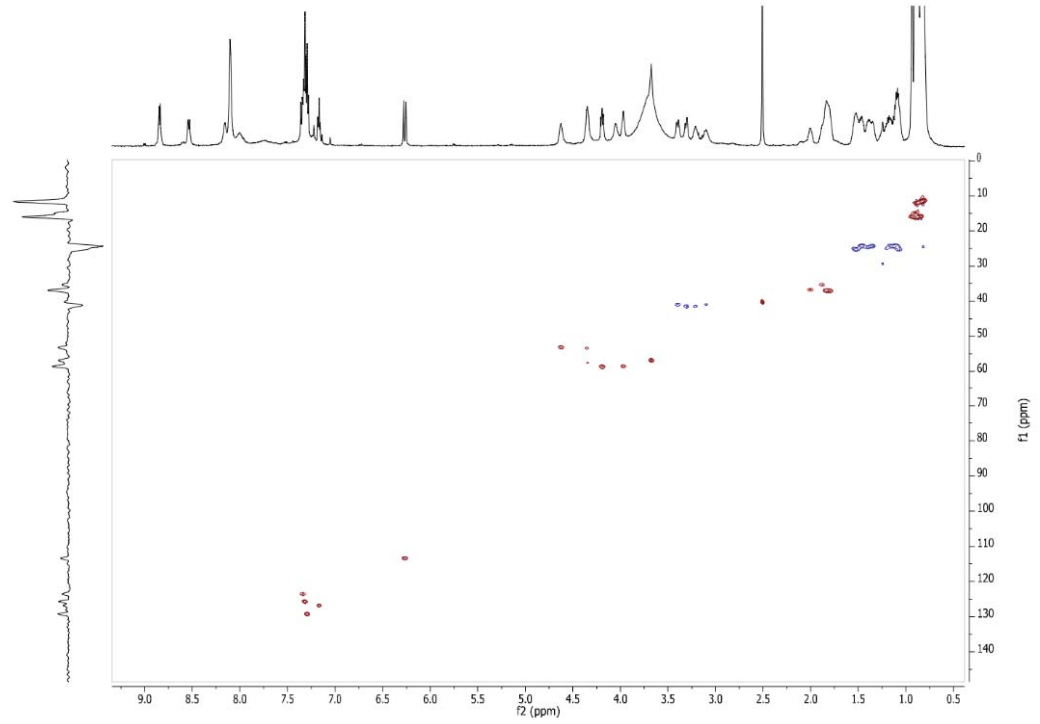

S1-4. HSQC NMR (DMSO-d_6, 600 MHz) spectrum of **1**

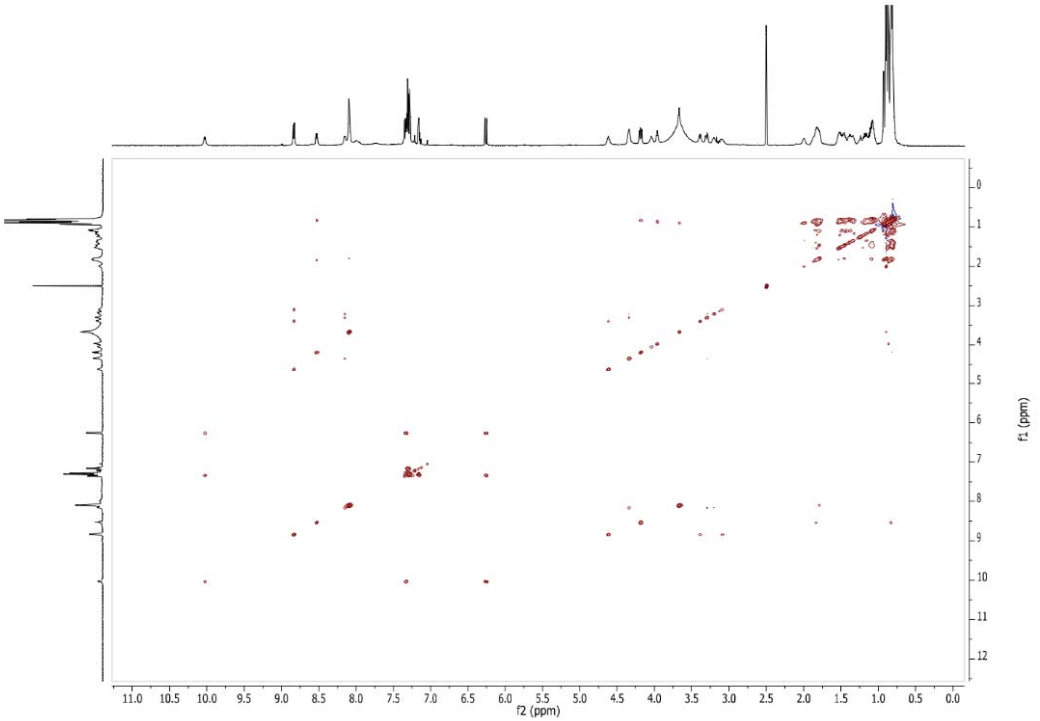

S1-5. TOCSY NMR (DMSO-d_6, 600 MHz) spectrum of **1**

Mass Spectrum SmartFormula Report

Analysis Info

Analysis Name	D:\Data\spektren2016\Proksch16HR000001.d	Acquisition Date	1/5/2016 2:58:54 PM
Method	tune_low_new.m	Operator	Peter Tommes
Sample Name	Amin Mokhlesi CE1SiA1P2 (CH3OH)	Instrument	maXis 288882.20213
Comment	2 ug/ml		

Acquisition Parameter

Source Type	ESI	Ion Polarity	Positive	Set Nebulizer	0.3 Bar
Focus	Not active	Set Capillary	4000 V	Set Dry Heater	180 °C
Scan Begin	50 m/z	Set End Plate Offset	-500 V	Set Dry Gas	4.0 l/min
Scan End	1500 m/z	Set Collision Cell RF	600.0 Vpp	Set Divert Valve	Source

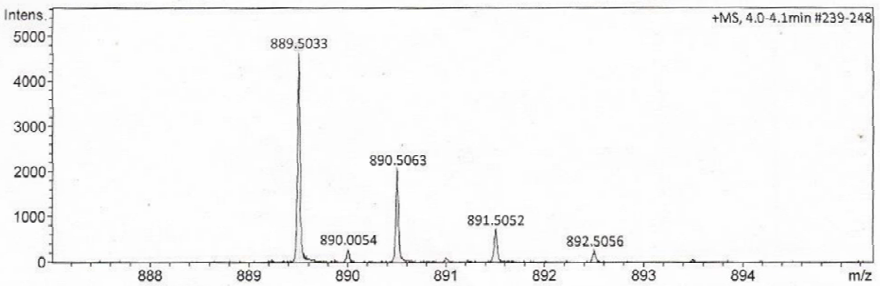

Meas. m/z	#	Ion Formula	m/z	err [ppm]	mSigma	# mSigma	Score	rdb	e⁻ Conf	N-Rule
889.5033	1	C43H77N4O11S2	889.5025	-1.0	49.2	1	100.00	7.5	even	ok
	2	C41H65N18OS2	889.5025	-1.0	53.6	2	86.79	18.5	even	ok
	3	C44H73N8O7S2	889.5038	0.5	57.3	3	95.07	12.5	even	ok
	4	C45H69N12O3S2	889.5052	2.0	66.4	4	31.39	17.5	even	ok
	5	C56H69N6S2	889.5020	-1.6	115.5	5	4.74	25.5	even	ok
	6	C60H73O2S2	889.5047	1.5	129.2	6	2.33	24.5	even	ok

S1-6. HRESIMS spectrum of **1**

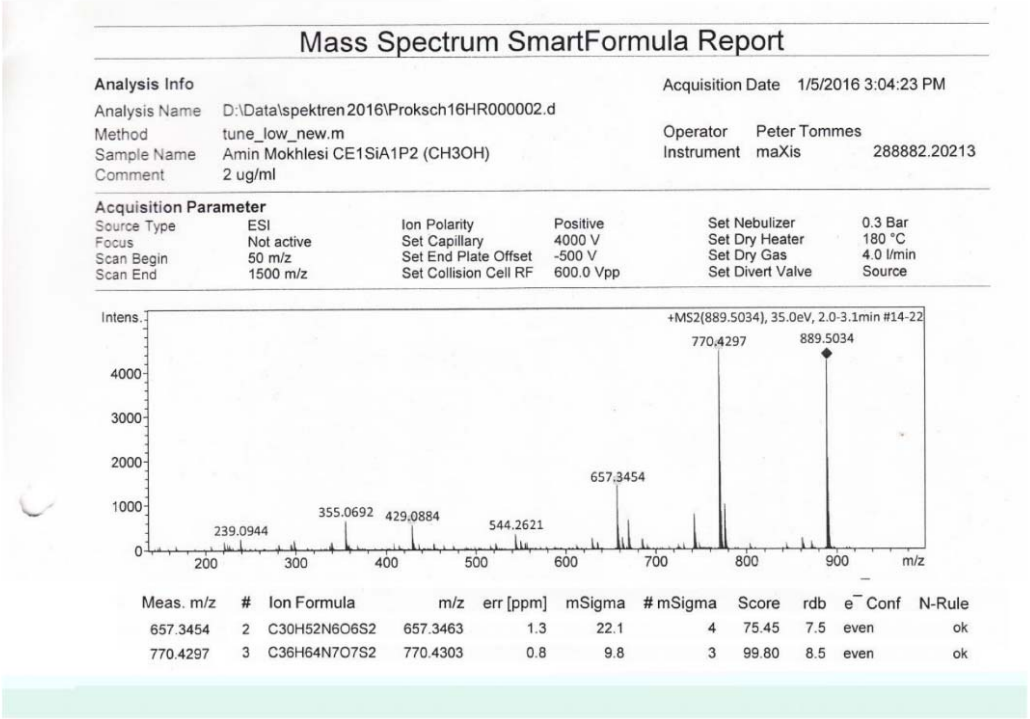

S1-7. HRESIMS/MS spectrum of **1**

S2. Microcionamide D (2)

S2-1. Table of ^{1}H (600 MHz), ^{13}C (150 MHz), HMBC, and ROESY NMR Data (DMSO-d_6, δ in ppm) of Microcionamide D (**2**)

Unit	Position	δ_c,[a] type	δ_H (J in Hz)	HMBC	ROESY[b]
Z-PEA	NH		9.46, d (10.5)	Cys_1-CO	Cys_1-α, Cys_1-NH
	α	121.1, CH	6.72, d (10.0)	Cys_1-CO, *Z*-PEA-β, *Z*-PEA-1	
	β	110.8, CH	5.74, d (10.0)	*Z*-PEA-α, *Z*-PEA-1, *Z*-PEA-2/6	
	aromatic	1: 134.7, C			
		2: 127.9, CH	7.35[c]	*Z*-PEA-β, *Z*-PEA-1, *Z*-PEA-6, *Z*-PEA-4	
		3: 128.3, CH	7.35[c]	*Z*-PEA-1, *Z*-PEA-5, *Z*-PEA-4	
		4: 126.4, CH	7.24, m	*Z*-PEA-2/6	
		5: 128.3, CH	7.35[c]	*Z*-PEA-1, *Z*-PEA-3, *Z*-PEA-4	
		6: 127.9, CH	7.35[c]	*Z*-PEA-β, *Z*-PEA-1, *Z*-PEA-2, *Z*-PEA-4	
Cys_1	NH		8.24, br s		*Z*-PEA-NH, Ile_2-α
	CO	168.0, C			
	α	51.7, CH	4.62[c]	Cys_1-CO, Ile_2-CO, Cys_1-β	*Z*-PEA-NH
	β	40.9, CH_2	3.07, br t (11.0); 3.28[c]	Cys_1-α, Cys_1-CO	
Ile_2	NH		7.77, br s		
	CO	170.9, C			
	α	57.2, CH	4.01, br t (8.5)	Ile_2-CO, Ile_3-CO, Ile_2-β, Ile_2-γ, Ile_2-γ'	Cys_1-NH
	β	34.3, CH	1.77, m	Ile_2-α	
	γ	24.3, CH_2	1.07, m; 1.48, m	Ile_2-α	
	γ'	15.1, CH_3	0.78[c]	Ile_2-α	
	δ	11.0, CH_3	0.81[c,d]		
Ile_3	NH		n.d.[e]		
	CO	170.5			
	α	n.d.[e]	4.08[c]		
	β	36.4, CH	1.79, m		
	γ	24.4, CH_2	1.07, m; 1.51, m		
	γ'	15.2, CH_3	0.89[c]		
	δ	11.0, CH_3	0.83[c,d]		

Ile_4	NH		7.39[c]		
	CO	n.d.[e]			
	α	57.0, CH	4.31, br s		Ile_5-β
	β	35.9, CH	2.08, br s		
	γ	23.5, CH_2	1.16, m; 1.33, m		
	γ'	15.6, CH_3	0.87[c]		
	δ	11.1, CH_3	0.86[c,d]		
Ile_5	NH		8.59, d (9.3)	Cys_6-CO	Cys_6-α
	CO	170.4, C			
	α	58.0, CH	4.17, dd (9.7, 7.5)	Ile_5-CO, Cys_6-CO, Ile_5-β, Ile_5-γ, Ile_5-γ'	Cys_6-α
	β	36.4, CH	1.80, m	Ile_5-α	Ile_4-α, Cys_6-NH, Cys_6-α
	γ	24.3, CH_2	1.08, m; 1.41, m	Ile_5-α	
	γ'	15.2, CH_3	0.84[c]	Ile_5-α	
	δ	10.9, CH_3	0.80[c,d]		
Cys_6	NH		8.82, br d (7.0)	Ile_7-CO	Ile_7-α, Ile_7-β, Ile_7-γ, Ile_5-β
	CO	168.6, C			
	α	52.5, CH	4.61[c]	Ile_7-CO	Ile_5-NH, Ile_7-α, Ile_5-α
	β	40.2, CH_2	3.19, m; 3.35, m		
Ile_7	NH_2		8.06, br s		
	CO	167.8, C			
	α	56.1, CH	3.66, br t (5.0)	Ile_7-CO, Ile_7-β, Ile_7-γ, Ile_7-γ'	Cys_6-α, Cys_6-NH
	β	36.2, CH	1.79, m	Ile_7-α	Cys_6-NH
	γ	23.4, CH_2	1.10, m; 1.46, m	Ile_7-α	Cys_6-NH
	γ'	14.2, CH_3	0.89[c]	Ile_7-α	
	δ	10.8, CH_3	0.83[c,d]		

[a]Data extracted from HSQC and HMBC spectra. [b]Sequential NOEs. [c]Signal overlap prevents determination of couplings. [d]Assignments within the same column may be interchanged. [e]n.d. : not detected

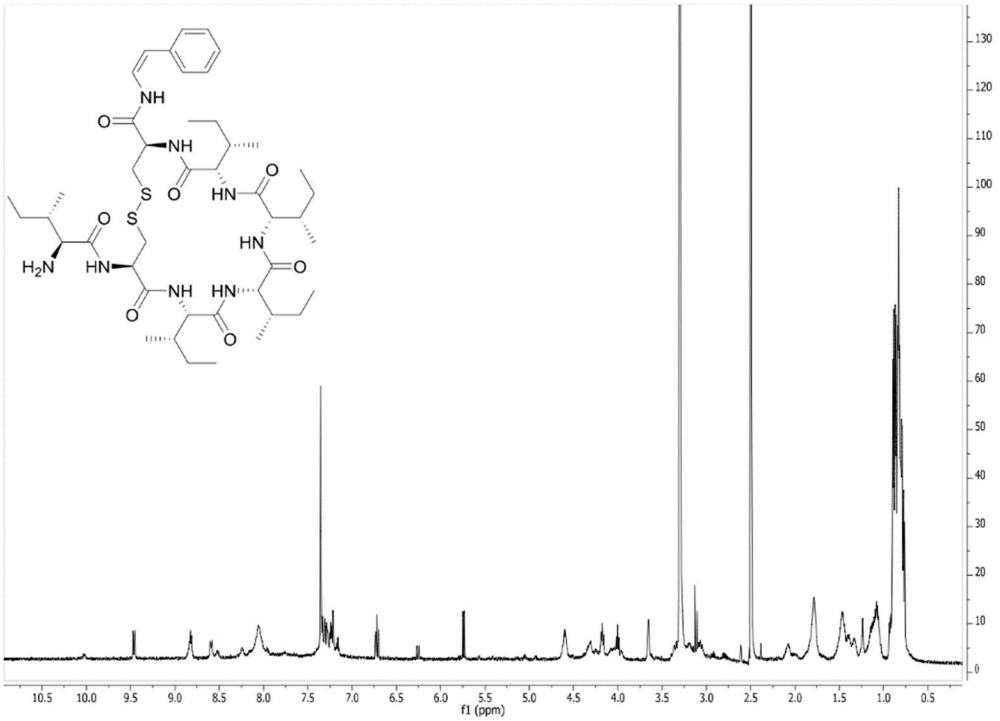

S2-2. ^{1}H NMR (DMSO-d_6, 600 MHz) spectrum of **2**

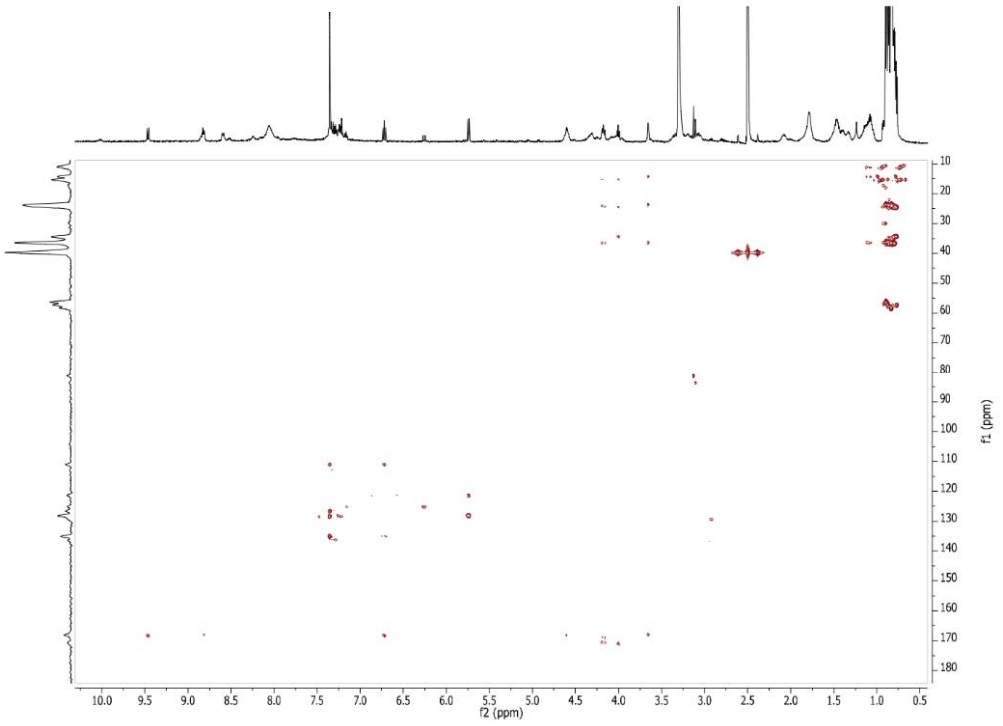

S2-3. HMBC NMR (DMSO-d_6, 600 MHz) spectrum of **2**

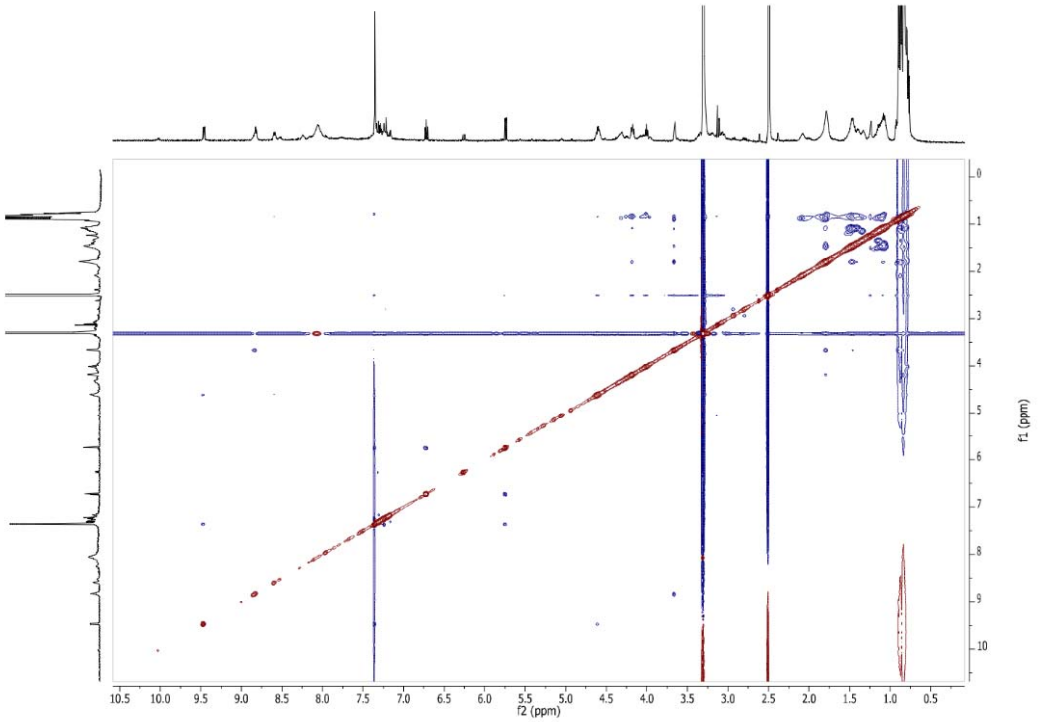

S2-4. ROESY NMR (DMSO-d_6, 600 MHz) spectrum of **2**

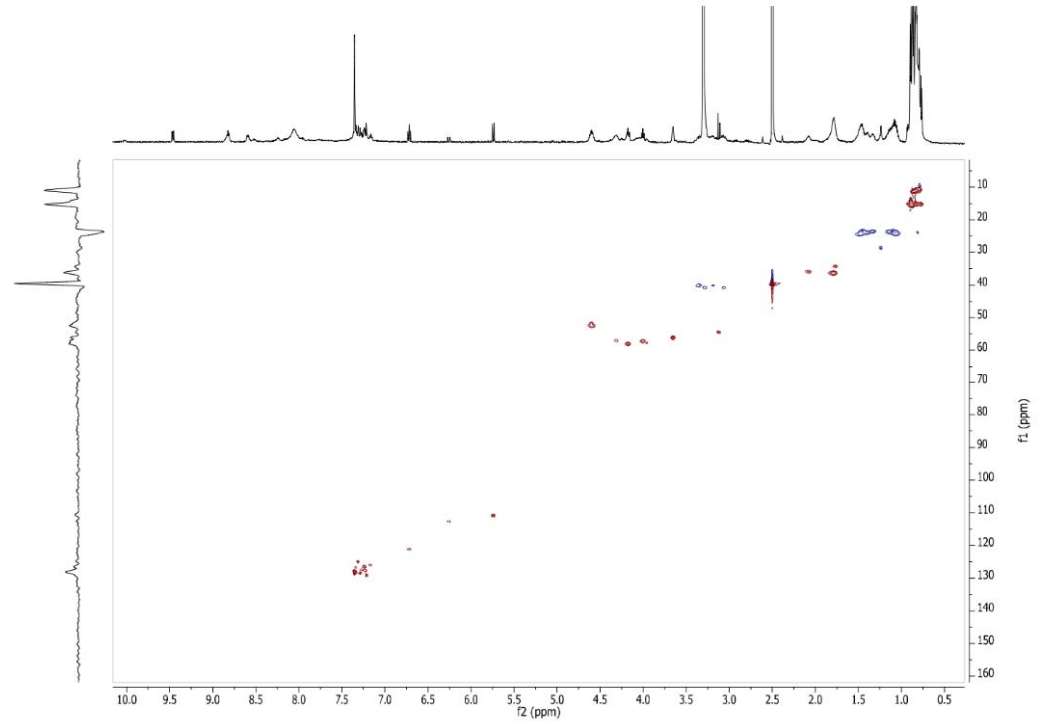

S2-5. HSQC NMR (DMSO-d_6, 600 MHz) spectrum of **2**

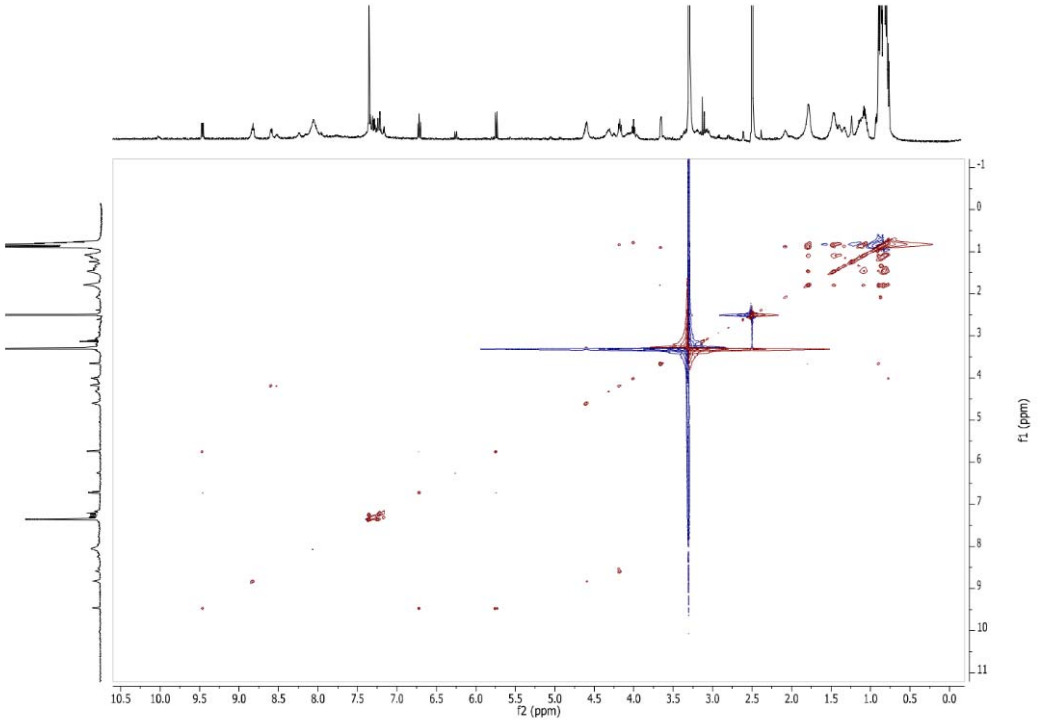

S2-6. TOCSY NMR (DMSO-d_6, 600 MHz) spectrum of **2**

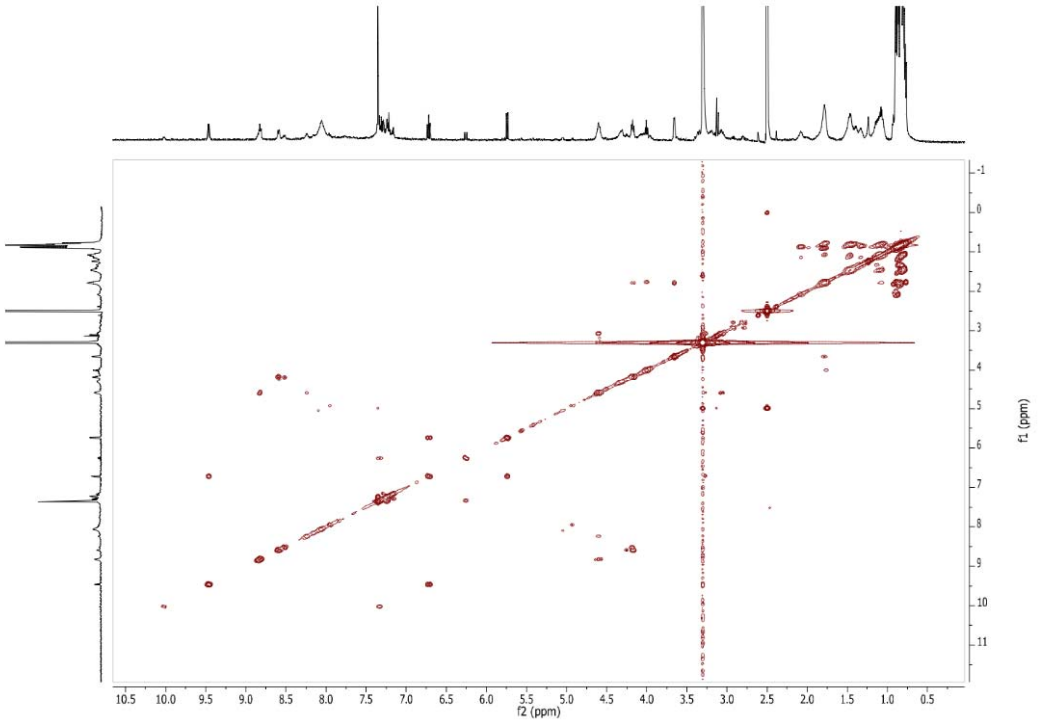

S2-7. COSY NMR (DMSO-d_6, 600 MHz) spectrum of **2**

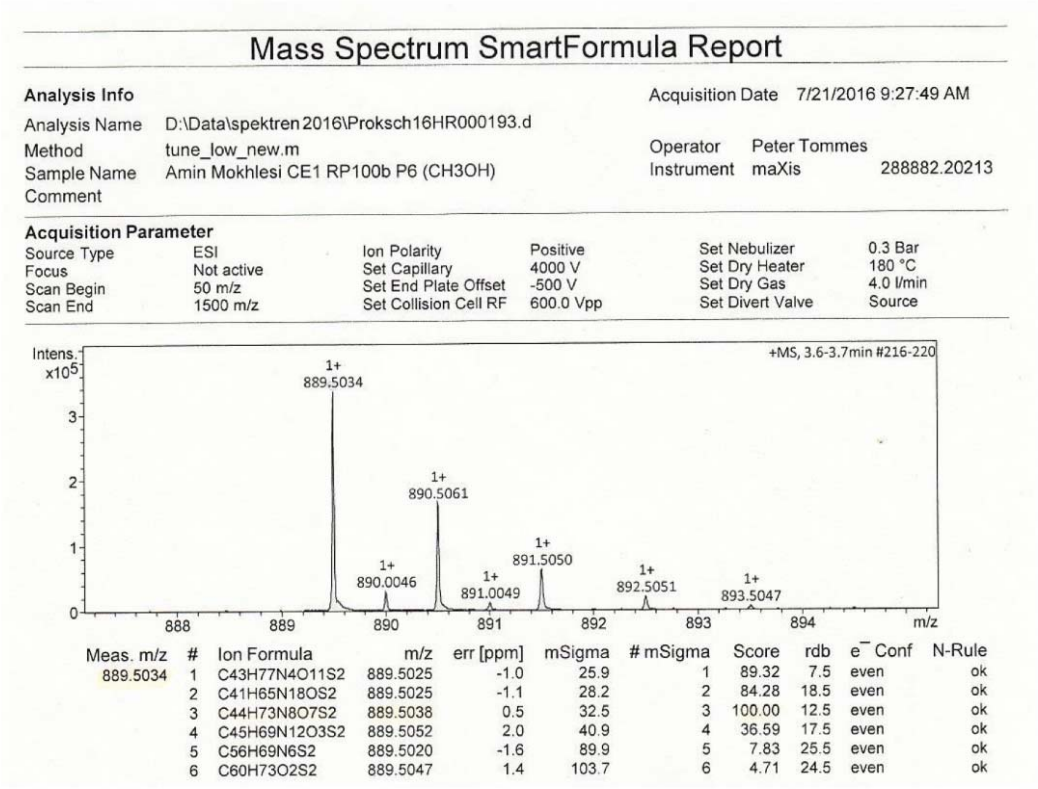

Mass Spectrum SmartFormula Report

Analysis Info

Analysis Name D:\Data\spektren 2016\Proksch16HR000193.d
Method tune_low_new.m
Sample Name Amin Mokhlesi CE1 RP100b P6 (CH3OH)
Comment

Acquisition Date 7/21/2016 9:27:49 AM
Operator Peter Tommes
Instrument maXis 288882.20213

Acquisition Parameter

Source Type	ESI	Ion Polarity	Positive	Set Nebulizer	0.3 Bar
Focus	Not active	Set Capillary	4000 V	Set Dry Heater	180 °C
Scan Begin	50 m/z	Set End Plate Offset	-500 V	Set Dry Gas	4.0 l/min
Scan End	1500 m/z	Set Collision Cell RF	600.0 Vpp	Set Divert Valve	Source

Meas. m/z	#	Ion Formula	m/z	err [ppm]	mSigma	# mSigma	Score	rdb	e¯ Conf	N-Rule
889.5034	1	C43H77N4O11S2	889.5025	-1.0	25.9	1	89.32	7.5	even	ok
	2	C41H65N18OS2	889.5025	-1.1	28.2	2	84.28	18.5	even	ok
	3	C44H73N8O7S2	889.5038	0.5	32.5	3	100.00	12.5	even	ok
	4	C45H69N12O3S2	889.5052	2.0	40.9	4	36.59	17.5	even	ok
	5	C56H69N6S2	889.5020	-1.6	89.9	5	7.83	25.5	even	ok
	6	C60H73O2S2	889.5047	1.4	103.7	6	4.71	24.5	even	ok

S2-8. HRESIMS spectrum of **2**

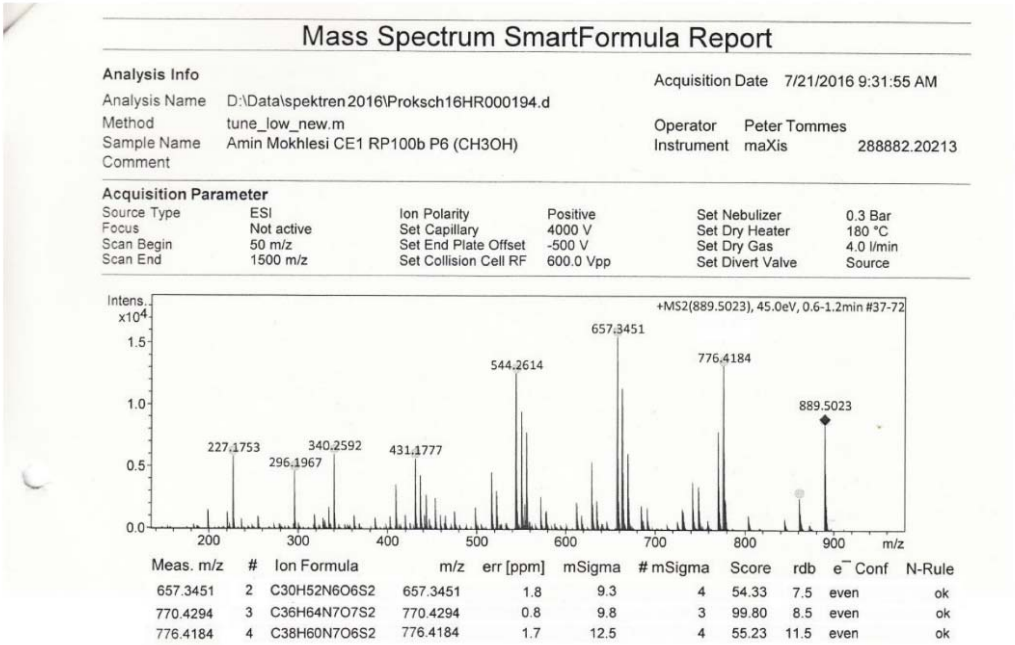

Mass Spectrum SmartFormula Report

Analysis Info

Analysis Name D:\Data\spektren 2016\Proksch16HR000194.d
Method tune_low_new.m
Sample Name Amin Mokhlesi CE1 RP100b P6 (CH3OH)
Comment

Acquisition Date 7/21/2016 9:31:55 AM
Operator Peter Tommes
Instrument maXis 288882.20213

Acquisition Parameter

Source Type	ESI	Ion Polarity	Positive	Set Nebulizer	0.3 Bar
Focus	Not active	Set Capillary	4000 V	Set Dry Heater	180 °C
Scan Begin	50 m/z	Set End Plate Offset	-500 V	Set Dry Gas	4.0 l/min
Scan End	1500 m/z	Set Collision Cell RF	600.0 Vpp	Set Divert Valve	Source

Meas. m/z	#	Ion Formula	m/z	err [ppm]	mSigma	# mSigma	Score	rdb	e¯ Conf	N-Rule
657.3451	2	C30H52N6O6S2	657.3451	1.8	9.3	4	54.33	7.5	even	ok
770.4294	3	C36H64N7O7S2	770.4294	0.8	9.8	3	99.80	8.5	even	ok
776.4184	4	C38H60N7O6S2	776.4184	1.7	12.5	4	55.23	11.5	even	ok

S2-9. HRESIMS/MS spectrum of **2**

S3. Microcionamide A (3)

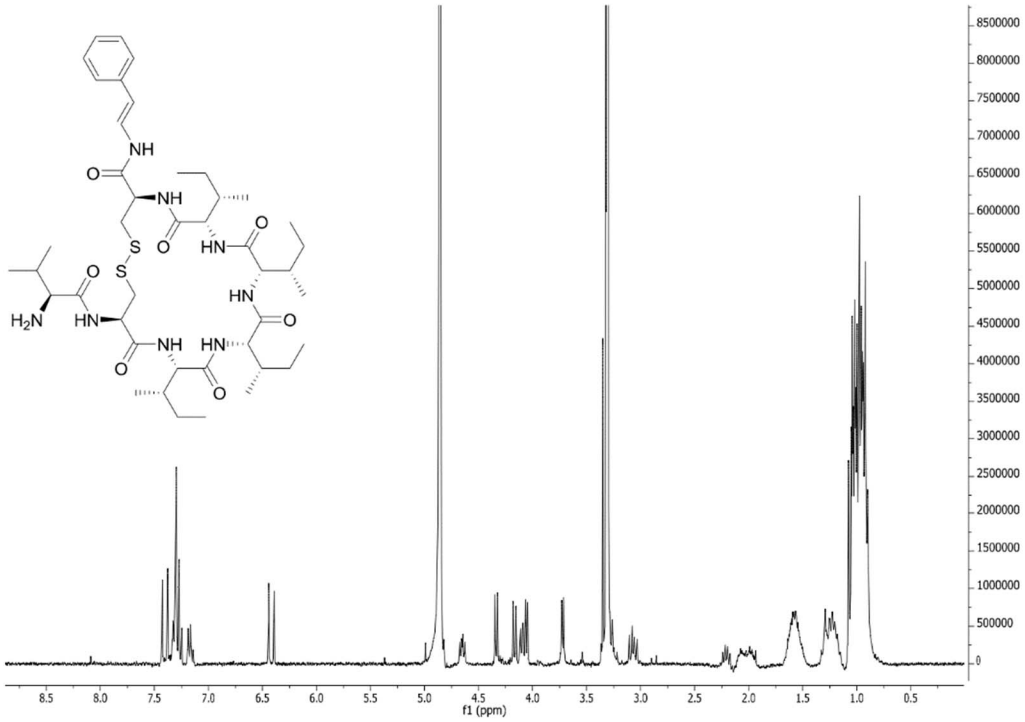

S3-1. ^{1}H NMR (MeOH-d_4, 600 MHz) spectrum of **3**

S4. Gombamide B (4)

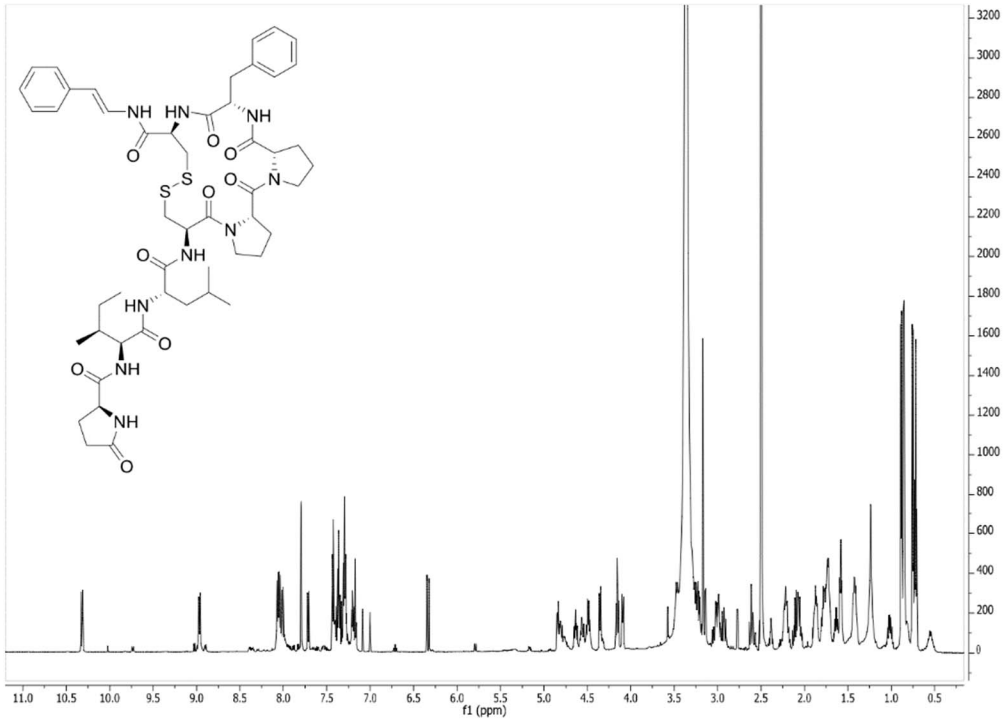

S4-1. ^{1}H NMR (DMSO-d_6, 600 MHz) spectrum of **4**

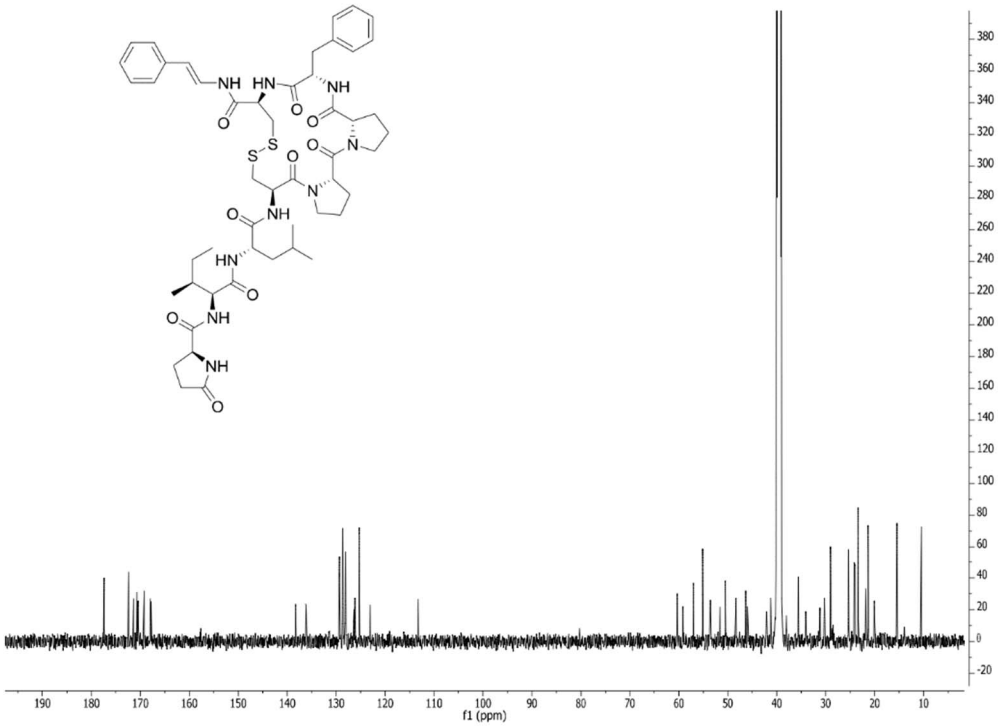

S4-2. ^{13}C NMR (DMSO-d_6, 600 MHz) spectrum of **4**

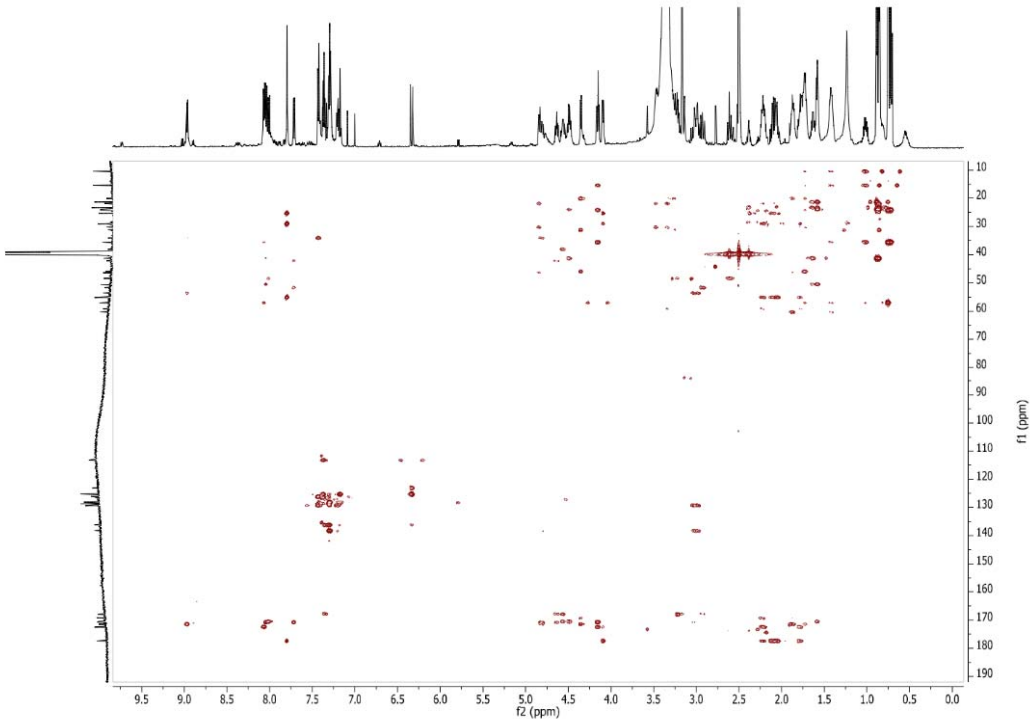

S4-3. HMBC NMR (DMSO-d_6, 600 MHz) spectrum of **4**

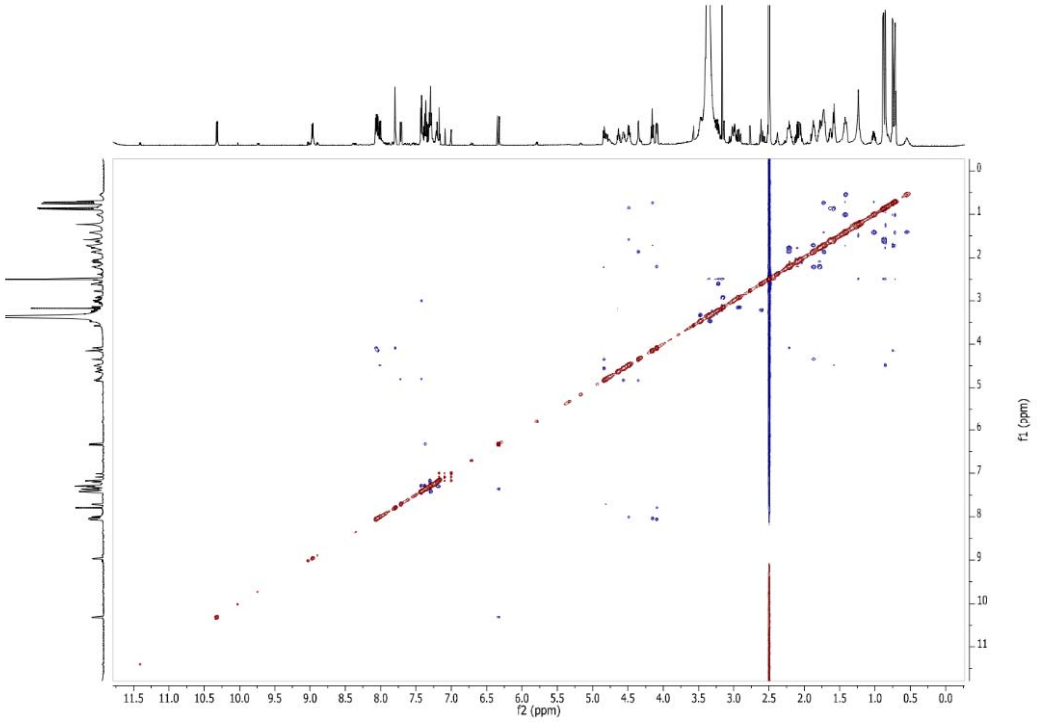

S4-4. ROESY NMR (DMSO-d_6, 600 MHz) spectrum of **4**

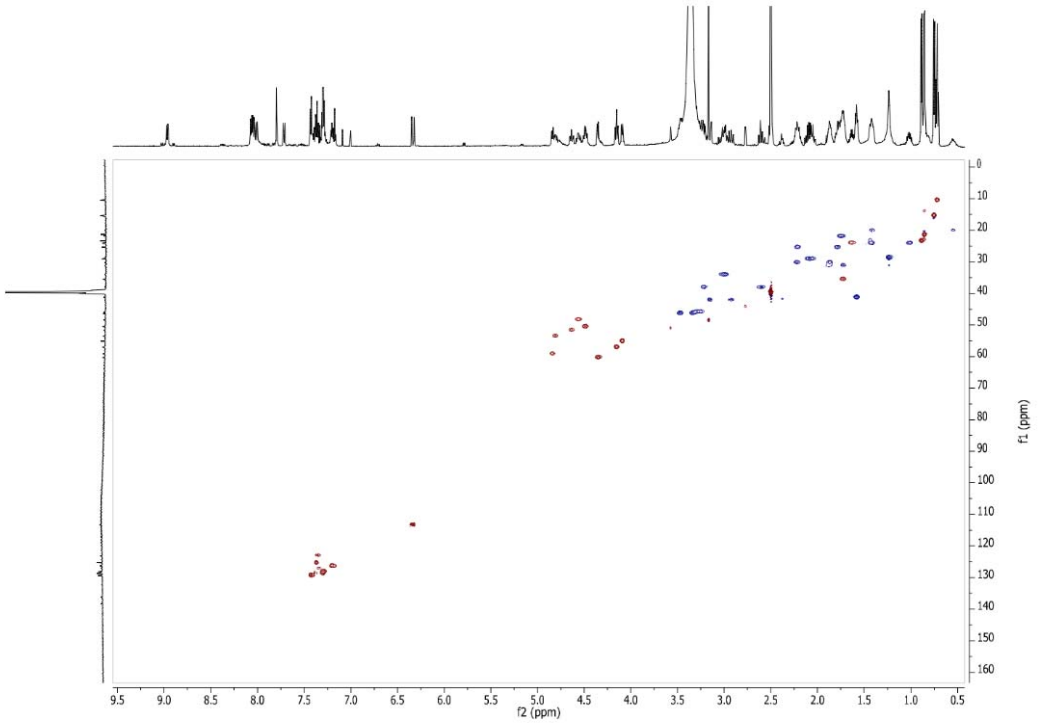

S4-5. HSQC NMR (DMSO-d_6, 600 MHz) spectrum of **4**

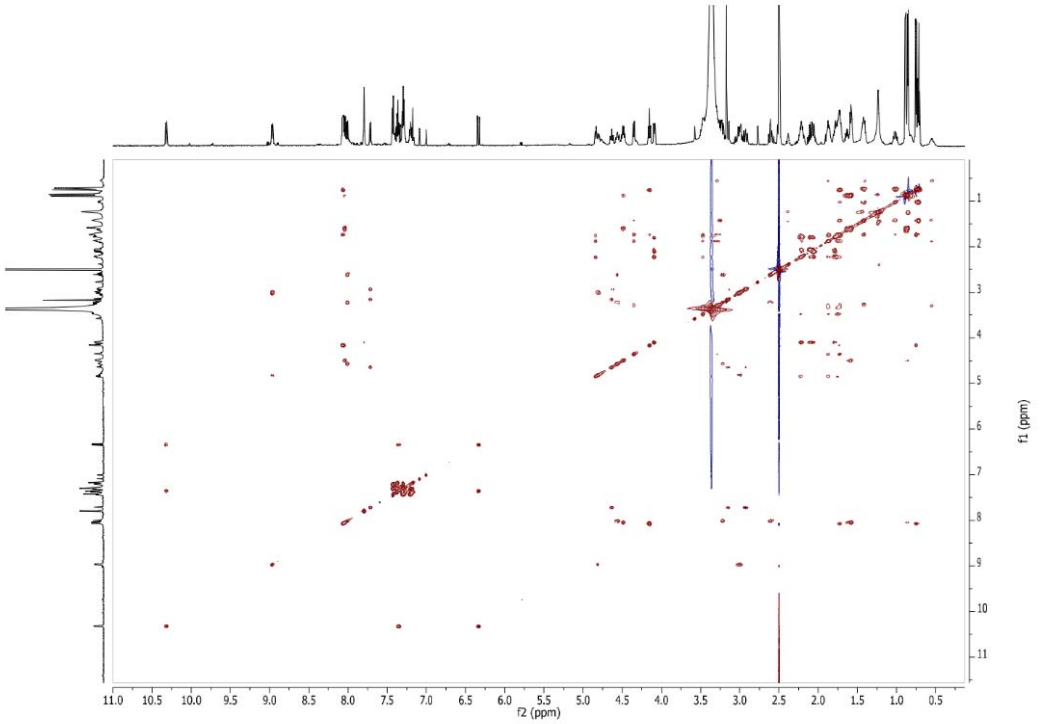

S4-6. TOCSY NMR (DMSO-d_6, 600 MHz) spectrum of **4**

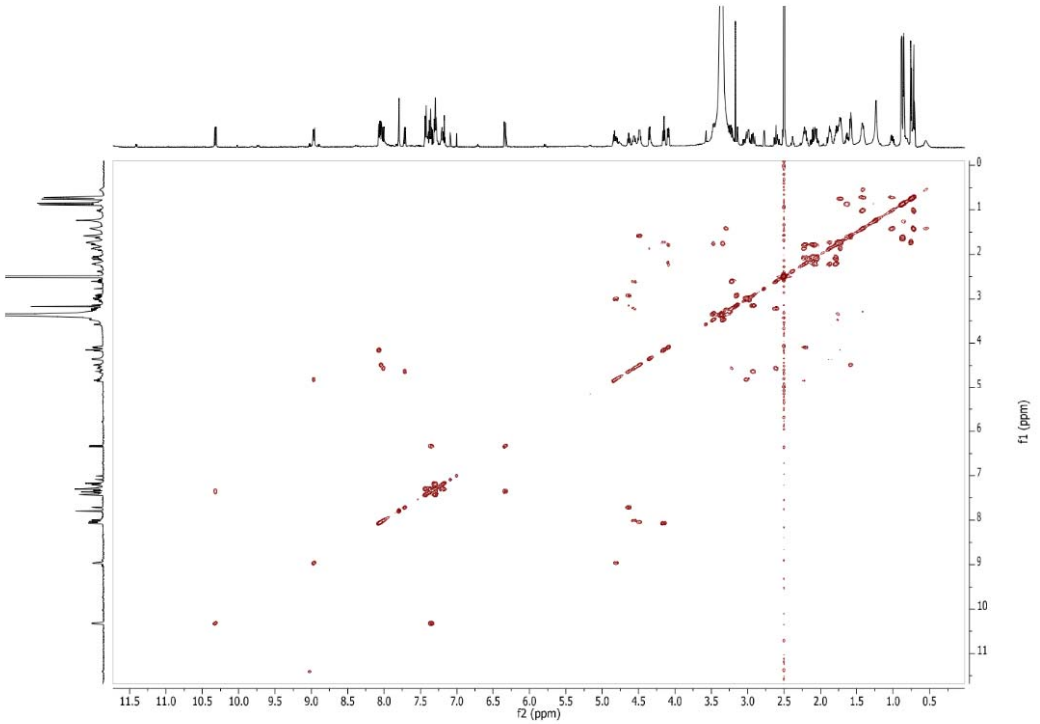

S4-7. COSY NMR (DMSO-d_6, 600 MHz) spectrum of **4**

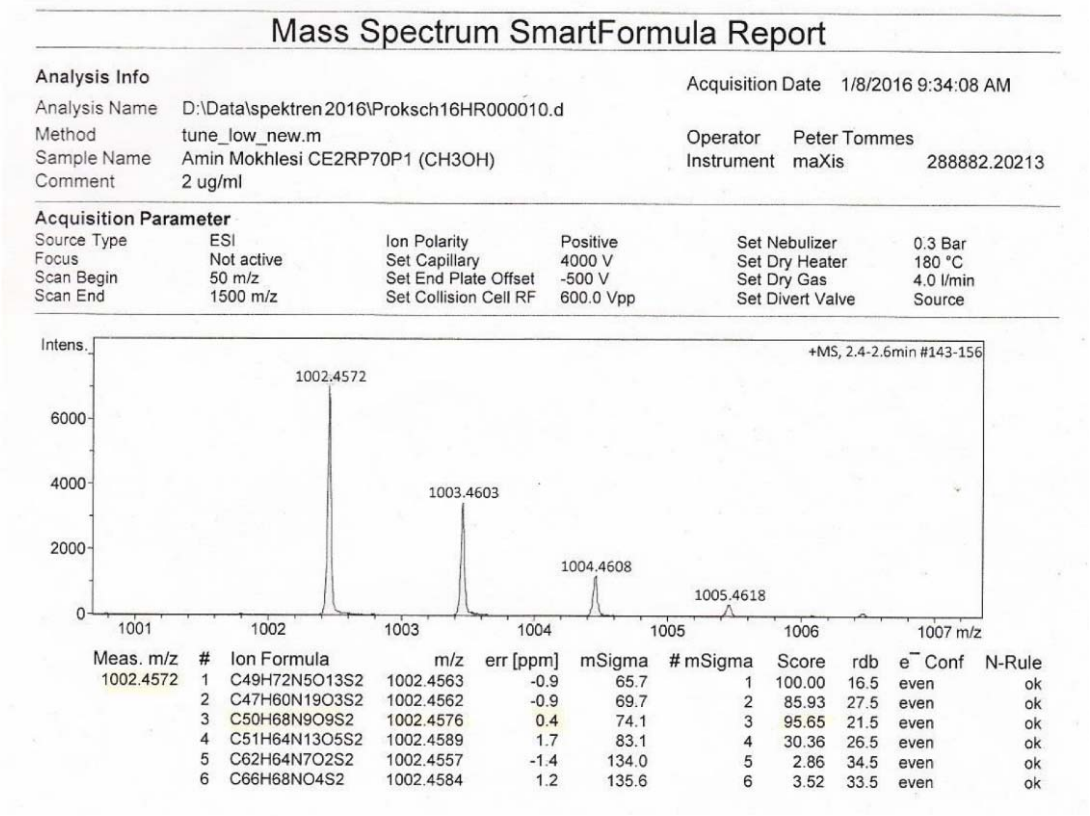

Mass Spectrum SmartFormula Report

Analysis Info

Analysis Name	D:\Data\spektren 2016\Proksch16HR000010.d	Acquisition Date	1/8/2016 9:34:08 AM
Method	tune_low_new.m	Operator	Peter Tommes
Sample Name	Amin Mokhlesi CE2RP70P1 (CH3OH)	Instrument	maXis 288882.20213
Comment	2 ug/ml		

Acquisition Parameter

Source Type	ESI	Ion Polarity	Positive	Set Nebulizer	0.3 Bar
Focus	Not active	Set Capillary	4000 V	Set Dry Heater	180 °C
Scan Begin	50 m/z	Set End Plate Offset	-500 V	Set Dry Gas	4.0 l/min
Scan End	1500 m/z	Set Collision Cell RF	600.0 Vpp	Set Divert Valve	Source

Meas. m/z	#	Ion Formula	m/z	err [ppm]	mSigma	# mSigma	Score	rdb	e⁻ Conf	N-Rule
1002.4572	1	C49H72N5O13S2	1002.4563	-0.9	65.7	1	100.00	16.5	even	ok
	2	C47H60N19O3S2	1002.4562	-0.9	69.7	2	85.93	27.5	even	ok
	3	C50H68N9O9S2	1002.4576	0.4	74.1	3	95.65	21.5	even	ok
	4	C51H64N13O5S2	1002.4589	1.7	83.1	4	30.36	26.5	even	ok
	5	C62H64N7O2S2	1002.4557	-1.4	134.0	5	2.86	34.5	even	ok
	6	C66H68NO4S2	1002.4584	1.2	135.6	6	3.52	33.5	even	ok

S4-8. HRESIMS spectrum of **4**

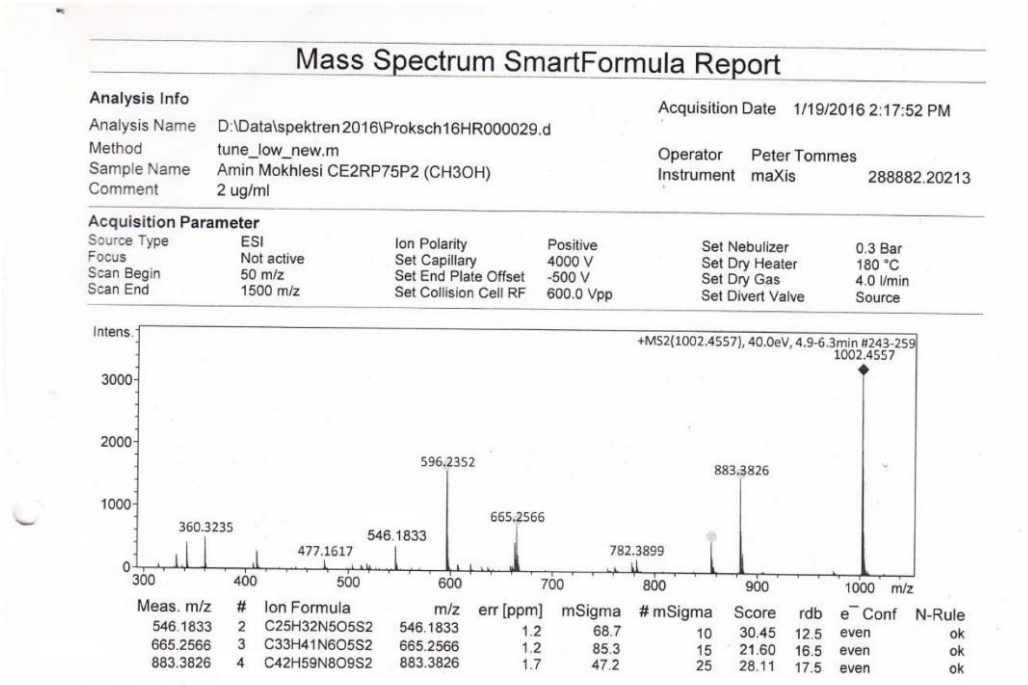

Mass Spectrum SmartFormula Report

Analysis Info

Analysis Name	D:\Data\spektren 2016\Proksch16HR000029.d	Acquisition Date	1/19/2016 2:17:52 PM
Method	tune_low_new.m	Operator	Peter Tommes
Sample Name	Amin Mokhlesi CE2RP75P2 (CH3OH)	Instrument	maXis 288882.20213
Comment	2 ug/ml		

Acquisition Parameter

Source Type	ESI	Ion Polarity	Positive	Set Nebulizer	0.3 Bar
Focus	Not active	Set Capillary	4000 V	Set Dry Heater	180 °C
Scan Begin	50 m/z	Set End Plate Offset	-500 V	Set Dry Gas	4.0 l/min
Scan End	1500 m/z	Set Collision Cell RF	600.0 Vpp	Set Divert Valve	Source

Meas. m/z	#	Ion Formula	m/z	err [ppm]	mSigma	# mSigma	Score	rdb	e⁻ Conf	N-Rule
546.1833	2	C25H32N5O5S2	546.1833	1.2	68.7	10	30.45	12.5	even	ok
665.2566	3	C33H41N6O5S2	665.2566	1.2	85.3	15	21.60	16.5	even	ok
883.3826	4	C42H59N8O9S2	883.3826	1.7	47.2	25	28.11	17.5	even	ok

S4-9. HRESIMS/MS spectrum of **4**

S5. Gombamide C (5)

S5-1. Table of ^{1}H (600 MHz), ^{13}C (150 MHz), and HMBC NMR Data (DMSO-d_6, δ in ppm) of Gombamide C (**5**)

Unit	Position	δ_c,[a] type	δ_H (J in Hz)	HMBC
Cys_1	NH		7.89, br d (8.6)	Phe-CO
	CO	168.4, C		
	α	51.5, CH	4.76[b]	
	β	41.7, CH_2	2.91, dd (14.4, 12.4); 3.14, dd (14.4, 3.4)	
Z-PEA	NH		9.72, br d (10.1)	Cys_1-CO
	α	121.3, CH	6.71, dd (10.1, 9.7)	Cys_1-CO, *Z*-PEA-β
	β	111.6, CH	5.79, d (9.7)	*Z*-PEA-α, *Z*-PEA-2/6, *Z*-PEA-1
	aromatic	1: 135.2, C		
		2: 128.1, CH	7.38[b]	
		3: 128.4, CH	7.38[b]	
		4: 126.6, CH	7.38[b]	
		5: 128.4, CH	7.38[b]	
		6: 128.1, CH	7.38[b]	
Phe	NH		9.00, br d (8.8)	
	CO	170.5, C		
	α	53.4, CH	4.75[b]	Phe-CO, Phe-β, Pro_3-CO
	β	34.1, CH_2	2.98, m	Phe-α, Phe-1, Phe-2/6
	aromatic	1: 138.0, C		
		2: 129.1, CH	7.40, br d (7.5)	Phe-β, Phe-6, Phe-4
		3: 128.0, CH	7.28, br t (7.5)	Phe-1, Phe-5
		4: 126.1, CH	7.19, br t (7.5)	Phe-2/6
		5: 128.0, CH	7.28, br t (7.5)	Phe-1, Phe-3
		6: 129.1, CH	7.40, br d (7.5)	Phe-β, Phe-6, Phe-4
Pro_3	CO	171.2, C		
	α	60.7, CH	4.34, d (8.0)	Pro_3-CO, Pro_4-CO, Pro_3-β, Pro_3-γ, Pro_3-δ
	β	31.1, CH_2	1.72, m; 1.87, m	
	γ	20.0, CH_2	1.42, m; 0.58, m	
	δ	45.9, CH_2	3.28, m	

Pro_4	CO	169.2, C		
	α	59.0, CH	4.80, dd (8.8, 3.0)	Pro_4-γ
	β	30.1, CH_2	1.86, m; 2.22, m	
	γ	21.6, CH_2	1.74, m	
	δ	46.7, CH_2	3.34, m; 3.47, m	
Cys_5	NH		8.00, br d (10.0)	Leu-CO
	CO	167.9, C		
	α	48.1, CH	4.55, td (10.0, 5.1)	Leu-CO, Cys_5-CO, Cys_5-β
	β	37.9, CH_2	2.58, dd (13.0, 10.0); 3.20, dd (13.0, 5.1)	Cys_5-α, Cys_5-CO
Leu	NH		8.04, br d (9.9)	
	CO	170.3, C		
	α	50.3, CH	4.47, ddd (9.9, 8.6, 6.1)	Leu-CO, Leu-β, Ile-CO
	β	41.0, CH_2	1.58, m	Leu-α, Leu-δ, Leu-δ', Leu-CO
	γ	23.8, CH	1.62, m	
	δ	21.2, CH_3	0.85, d (6.5)	Leu-β, Leu-δ'
	δ'	23.2, CH_3	0.88, d (6.6)	Leu-β, Leu-δ
Ile	NH		8.06, br d (8.7)	
	CO	170.5, C		
	α	56.8, CH	4.15, t (8.5)	Glp-CO, Ile-CO, Ile-β, Ile-γ, Ile-γ'
	β	35.4, CH	1.72, m	Ile-α, Ile-δ
	γ	24.0, CH_2	1.01, m; 1.42, m	Ile-α, Ile-δ
	γ'	15.2, CH_3	0.75, d (6.8)	Ile-α
	δ	10.2, CH_3	0.71, t (7.4)	Ile-β, Ile-γ
Glp	NH		7.80, s	Glp-CO', Glp-α, Glp-β, Glp-γ
	CO	172.2, C		
	CO'	177.4, C		
	α	55.0, CH	4.09, dd (8.7, 3.6)	Glp-CO', Glp-β, Glp-γ
	β	25.2, CH_2	1.79, m; 2.22, m	Glp-CO, Glp-α
	γ	28.8, CH_2	2.05, m; 2.09, m	Glp-α

[a]Data extracted from HSQC and HMBC spectra. [b]Signal overlap prevents determination of couplings.

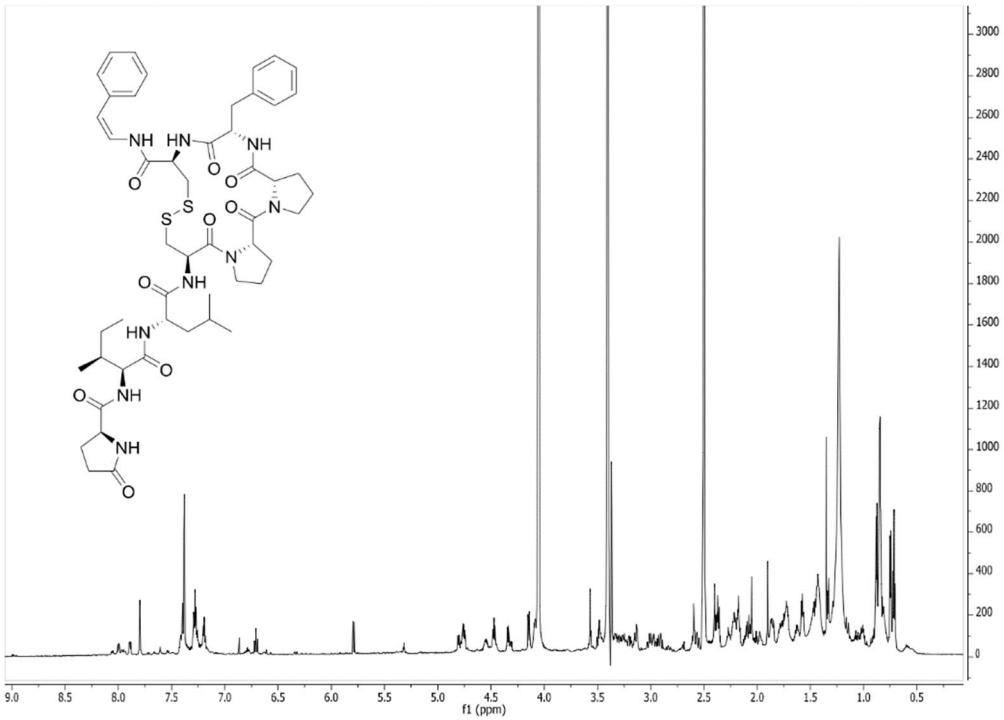

S5-2. ^{1}H NMR (DMSO-d_6, 600 MHz) spectrum of **5**

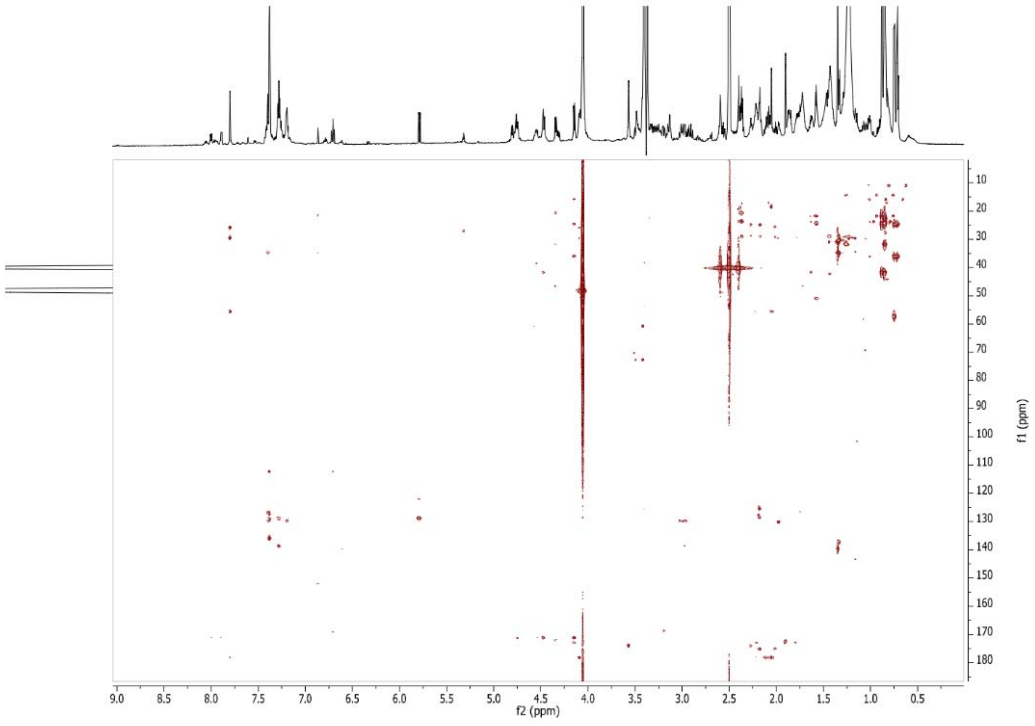

S5-3. HMBC NMR (DMSO-d_6, 600 MHz) spectrum of **5**

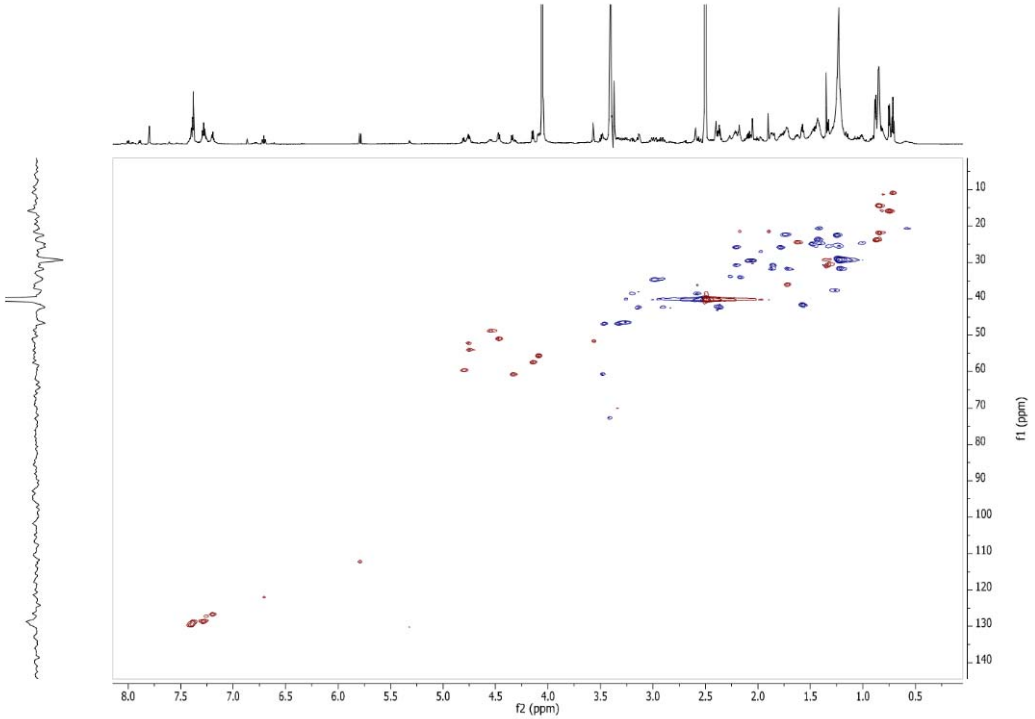

S5-4. HSQC NMR (DMSO-d_6, 600 MHz) spectrum of **5**

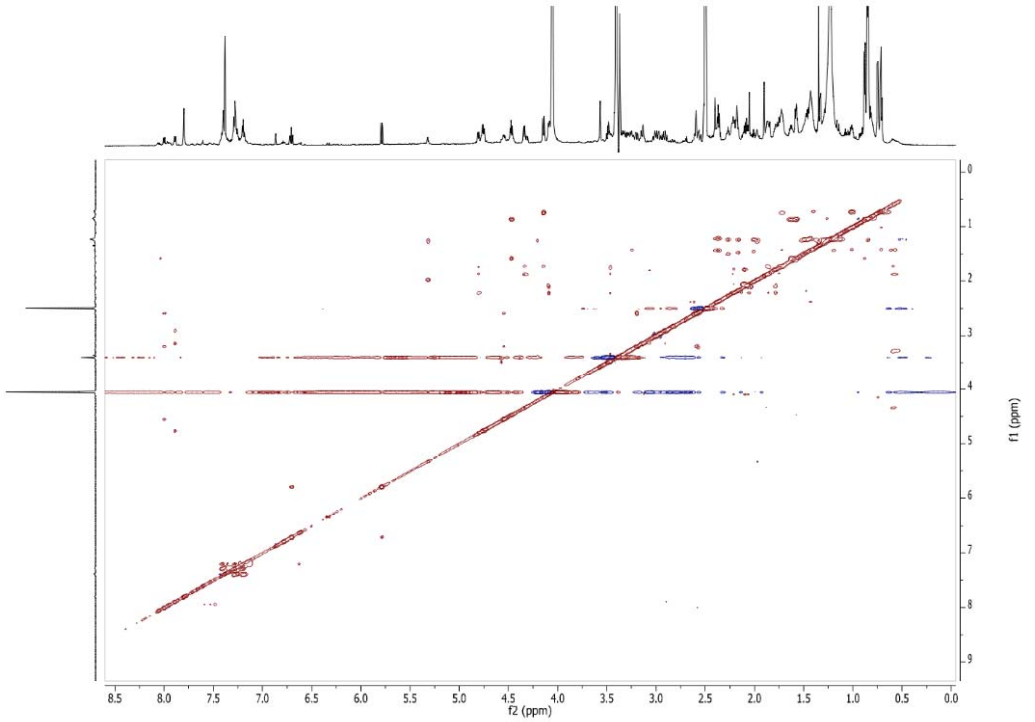

S5-5. TOCSY NMR (DMSO-d_6, 600 MHz) spectrum of **5**

Mass Spectrum SmartFormula Report

Analysis Info

Analysis Name	D:\Data\Spektren 2015\Proksch15HR000119.d	Acquisition Date	3/27/2015 1:47:25 PM
Method	tune_midneu.m	Operator	Peter Tommes
Sample Name	Amin CE2RP70P3 in CH3OH (ACN/H2O)	Instrument	maXis 288882.20213
Comment			

Acquisition Parameter

Source Type	ESI	Ion Polarity	Positive	Set Nebulizer	0.3 Bar
Focus	Active	Set Capillary	4000 V	Set Dry Heater	180 °C
Scan Begin	300 m/z	Set End Plate Offset	-500 V	Set Dry Gas	4.0 l/min
Scan End	2800 m/z	Set Collision Cell RF	2500.0 Vpp	Set Divert Valve	Source

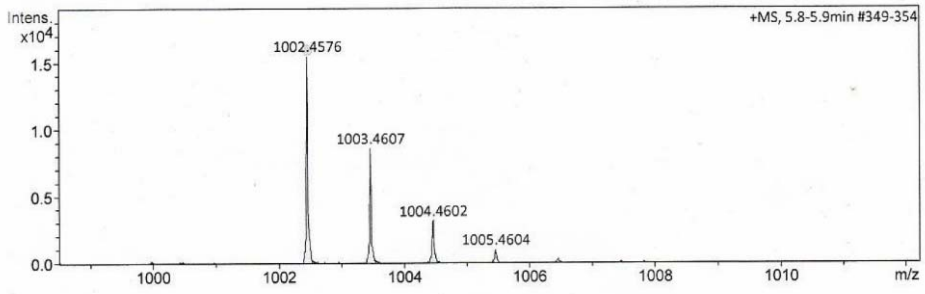

Meas. m/z	#	Ion Formula	m/z	err [ppm]	mSigma	# mSigma	Score	rdb	e¯ Conf	N-Rule
1002.4576	1	C43H60N19O8S	1002.4587	1.2	5.6	1	65.86	23.5	even	ok
	2	C42H64N15O12S	1002.4574	-0.1	12.1	2	100.00	18.5	even	ok
	3	C45H72N5O18S	1002.4588	1.2	14.0	3	56.06	12.5	even	ok
	4	C49H64N9O14	1002.4567	-0.8	14.2	4	68.98	22.5	even	ok
	5	C53H68N3O16	1002.4594	1.8	20.9	5	31.37	21.5	even	ok
	6	C50H60N13O10	1002.4581	0.5	22.4	6	68.71	27.5	even	ok
	7	C44H76NO22S	1002.4574	-0.1	22.9	7	80.22	7.5	even	ok
	8	C47H52N23O4	1002.4567	-0.8	27.3	8	41.36	33.5	even	ok
	9	C51H56N17O6	1002.4594	1.8	35.3	9	17.97	32.5	even	ok
	10	C48H48N27	1002.4581	0.5	37.2	10	38.54	38.5	even	ok
	11	C49H72N5O13S2	1002.4563	-1.3	39.3	11	29.25	16.5	even	ok
	12	C47H60N19O3S2	1002.4562	-1.3	40.4	12	28.20	27.5	even	ok
	13	C50H68N9O9S2	1002.4576	0.0	45.5	13	46.91	21.5	even	ok
	14	C54H60N13O5S	1002.4556	-2.0	50.3	14	13.12	31.5	even	ok

S5-6. HRESIMS spectrum of **5**

Mass Spectrum SmartFormula Report

Analysis Info

Analysis Name	D:\Data\spektren 2016\Proksch16HR000030.d	Acquisition Date	1/19/2016 3:13:09 PM
Method	tune_low_new.m	Operator	Peter Tommes
Sample Name	Amin Mokhlesi CE2RP75P3 (CH3OH)	Instrument	maXis 288882.20213
Comment	2 ug/ml		

Acquisition Parameter

Source Type	ESI	Ion Polarity	Positive	Set Nebulizer	0.3 Bar
Focus	Not active	Set Capillary	4000 V	Set Dry Heater	180 °C
Scan Begin	50 m/z	Set End Plate Offset	-500 V	Set Dry Gas	4.0 l/min
Scan End	1500 m/z	Set Collision Cell RF	600.0 Vpp	Set Divert Valve	Source

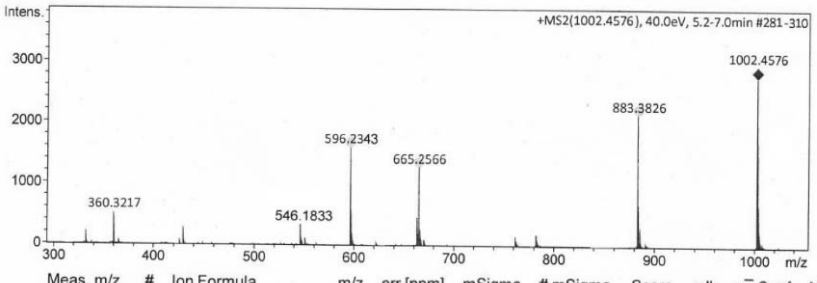

Meas. m/z	#	Ion Formula	m/z	err [ppm]	mSigma	# mSigma	Score	rdb	e¯ Conf	N-Rule
546.1833	2	C25H32N5O5S2	546.1839	0.2	15.6	8.5	100.00	2.5	even	ok
665.2566	3	C33H41N6O5S2	665.2566	1.4	32.1	10	98.38	13.5	even	ok
883.3826	4	C42H59N8O9S2	883.3841	1.3	18.5	19	66.25	8.5	even	ok

S5-7. HRESIMS/MS spectrum of **5**

S6. Gombamide D (6)

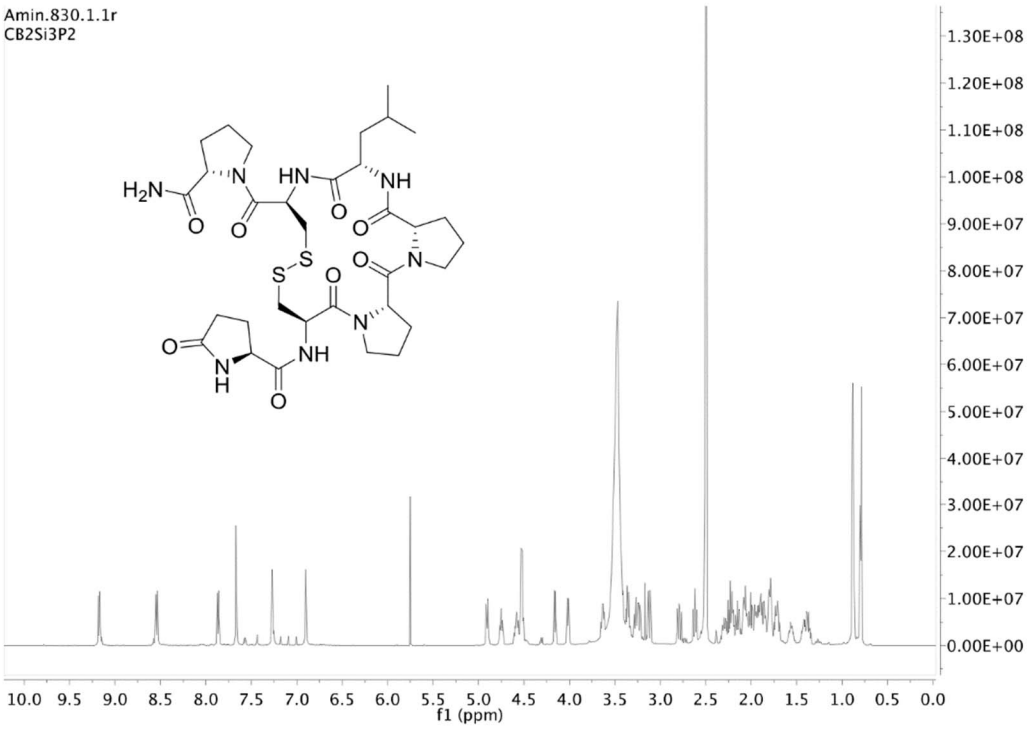

S6-1. ^{1}H NMR (DMSO-d_6, 600 MHz) spectrum of **6**

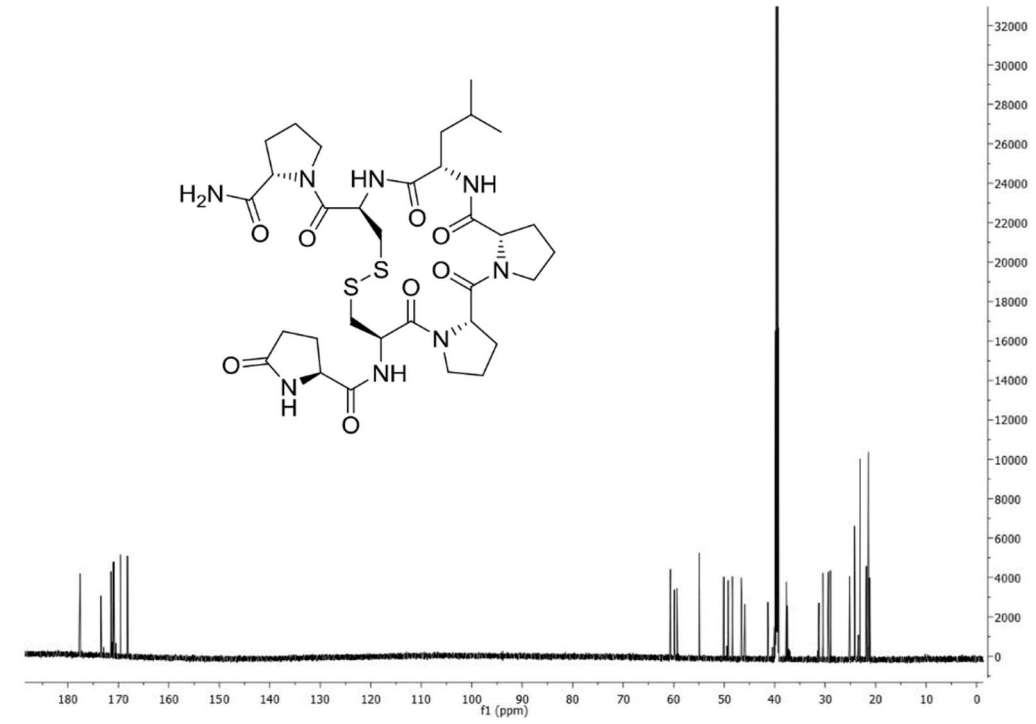

S6-2. ^{13}C NMR (DMSO-d_6, 150 MHz) spectrum of **6**

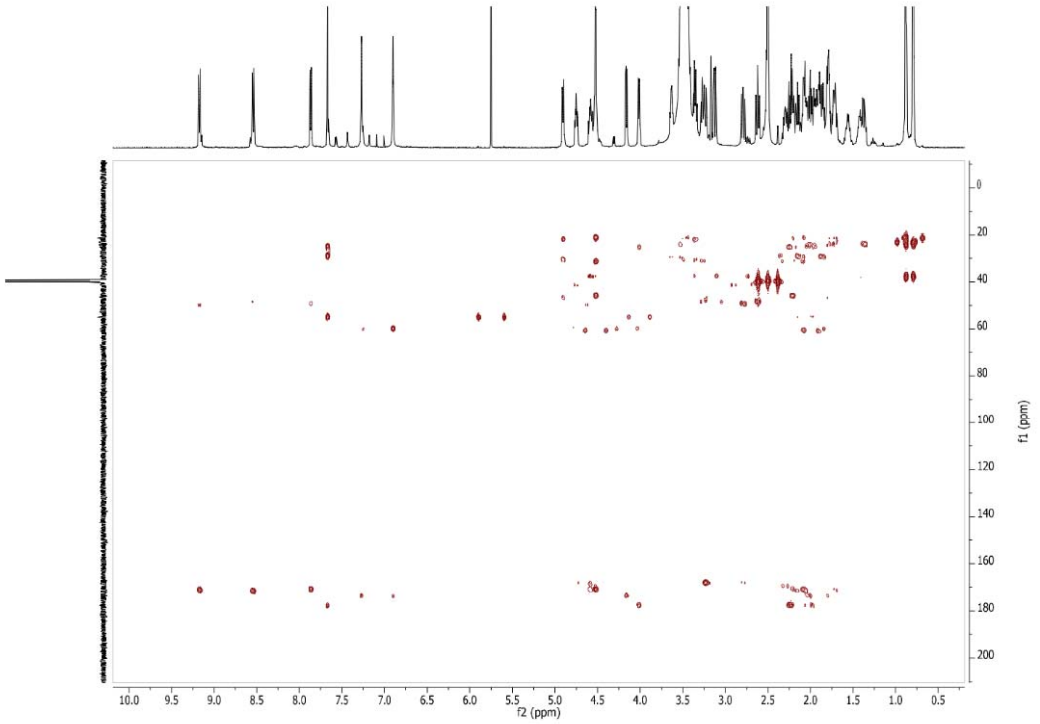

S6-3. HMBC NMR (DMSO-d_6, 600 MHz) spectrum of **6**

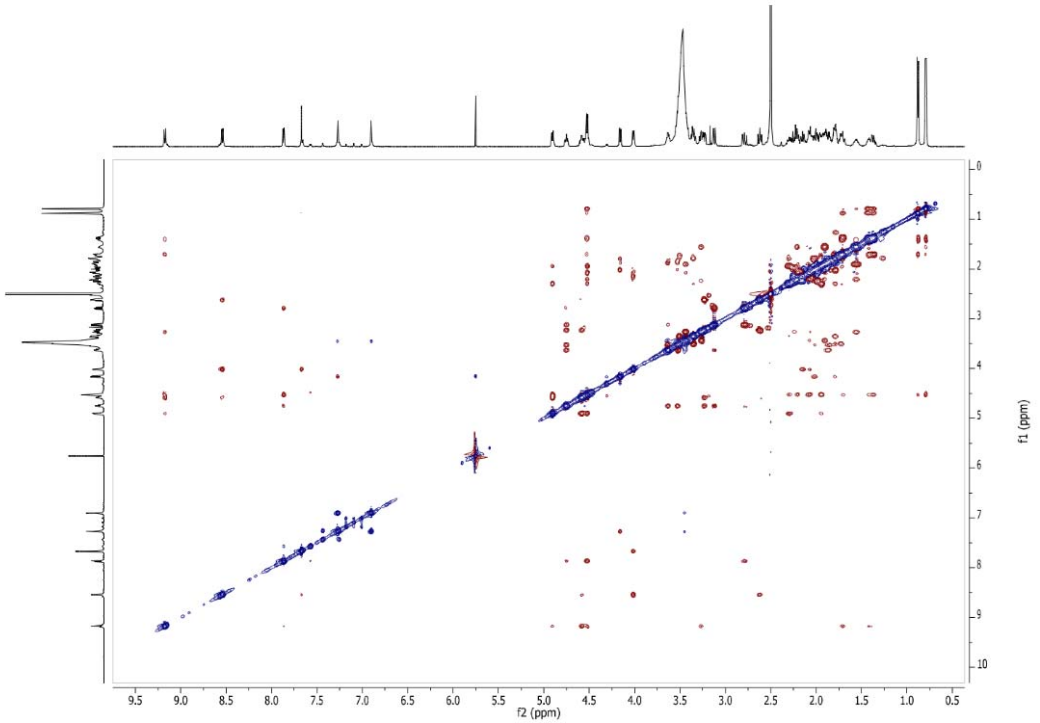

S6-4. ROESY NMR (DMSO-d_6, 600 MHz) spectrum of **6**

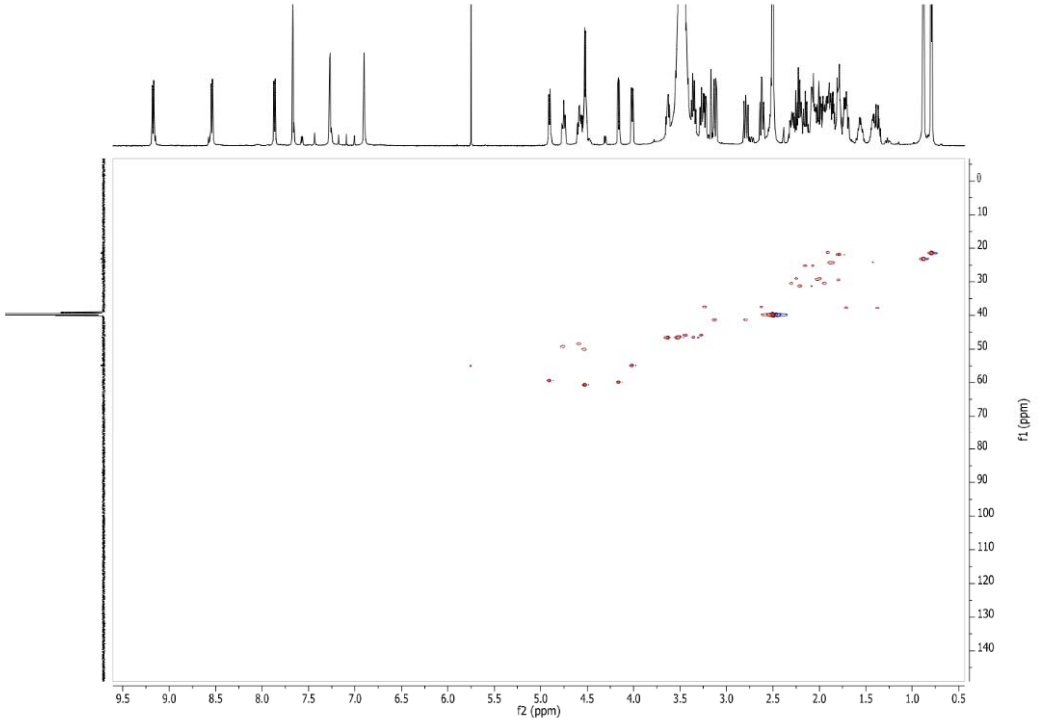

S6-5. HSQC NMR (DMSO-d_6, 600 MHz) spectrum of **6**

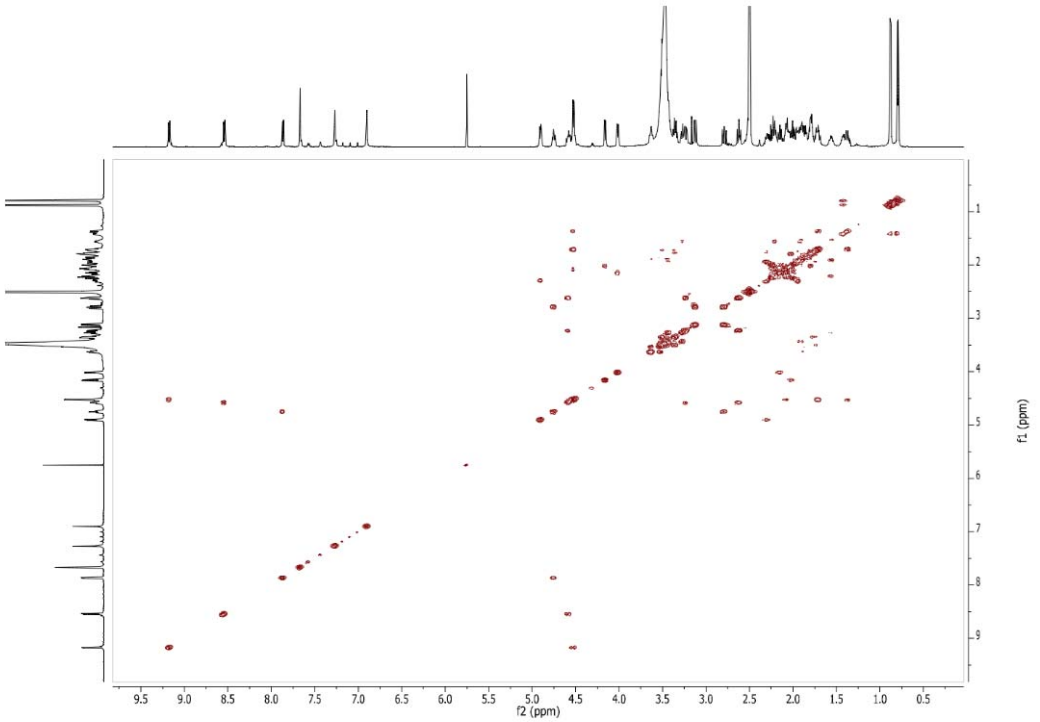

S6-6. COSY NMR (DMSO-d_6, 600 MHz) spectrum of **6**

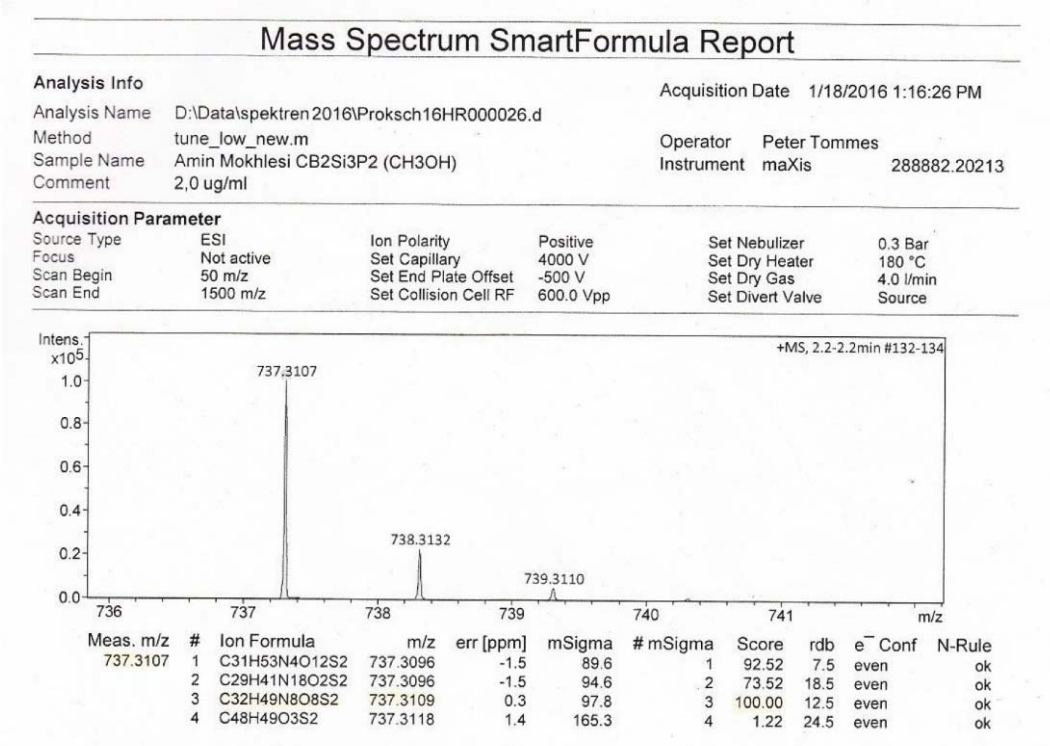

Mass Spectrum SmartFormula Report

Analysis Info

Analysis Name	D:\Data\spektren 2016\Proksch16HR000026.d	Acquisition Date	1/18/2016 1:16:26 PM
Method	tune_low_new.m	Operator	Peter Tommes
Sample Name	Amin Mokhlesi CB2Si3P2 (CH3OH)	Instrument	maXis 288882.20213
Comment	2,0 ug/ml		

Acquisition Parameter

Source Type	ESI	Ion Polarity	Positive	Set Nebulizer	0.3 Bar
Focus	Not active	Set Capillary	4000 V	Set Dry Heater	180 °C
Scan Begin	50 m/z	Set End Plate Offset	-500 V	Set Dry Gas	4.0 l/min
Scan End	1500 m/z	Set Collision Cell RF	600.0 Vpp	Set Divert Valve	Source

Meas. m/z	#	Ion Formula	m/z	err [ppm]	mSigma	# mSigma	Score	rdb	e⁻ Conf	N-Rule
737.3107	1	C31H53N4O12S2	737.3096	-1.5	89.6	1	92.52	7.5	even	ok
	2	C29H41N18O2S2	737.3096	-1.5	94.6	2	73.52	18.5	even	ok
	3	C32H49N8O8S2	737.3109	0.3	97.8	3	100.00	12.5	even	ok
	4	C48H49O3S2	737.3118	1.4	165.3	4	1.22	24.5	even	ok

S6-7. HRESIMS spectrum of **6**

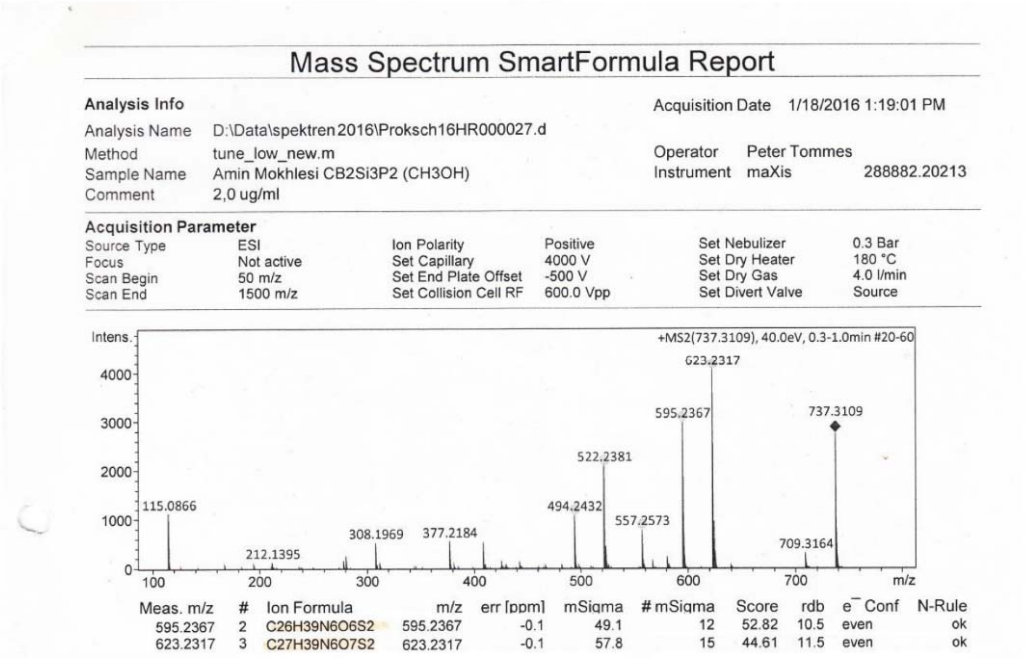

Mass Spectrum SmartFormula Report

Analysis Info

Analysis Name	D:\Data\spektren 2016\Proksch16HR000027.d	Acquisition Date	1/18/2016 1:19:01 PM
Method	tune_low_new.m	Operator	Peter Tommes
Sample Name	Amin Mokhlesi CB2Si3P2 (CH3OH)	Instrument	maXis 288882.20213
Comment	2,0 ug/ml		

Acquisition Parameter

Source Type	ESI	Ion Polarity	Positive	Set Nebulizer	0.3 Bar
Focus	Not active	Set Capillary	4000 V	Set Dry Heater	180 °C
Scan Begin	50 m/z	Set End Plate Offset	-500 V	Set Dry Gas	4.0 l/min
Scan End	1500 m/z	Set Collision Cell RF	600.0 Vpp	Set Divert Valve	Source

Meas. m/z	#	Ion Formula	m/z	err [ppm]	mSigma	# mSigma	Score	rdb	e⁻ Conf	N-Rule
595.2367	2	C26H39N6O6S2	595.2367	-0.1	49.1	12	52.82	10.5	even	ok
623.2317	3	C27H39N6O7S2	623.2317	-0.1	57.8	15	44.61	11.5	even	ok

S6-8. HRESIMS/MS spectrum of **6**

S7. (*E*)-2-amino-3-methyl-N-styrylbutanamide (7)

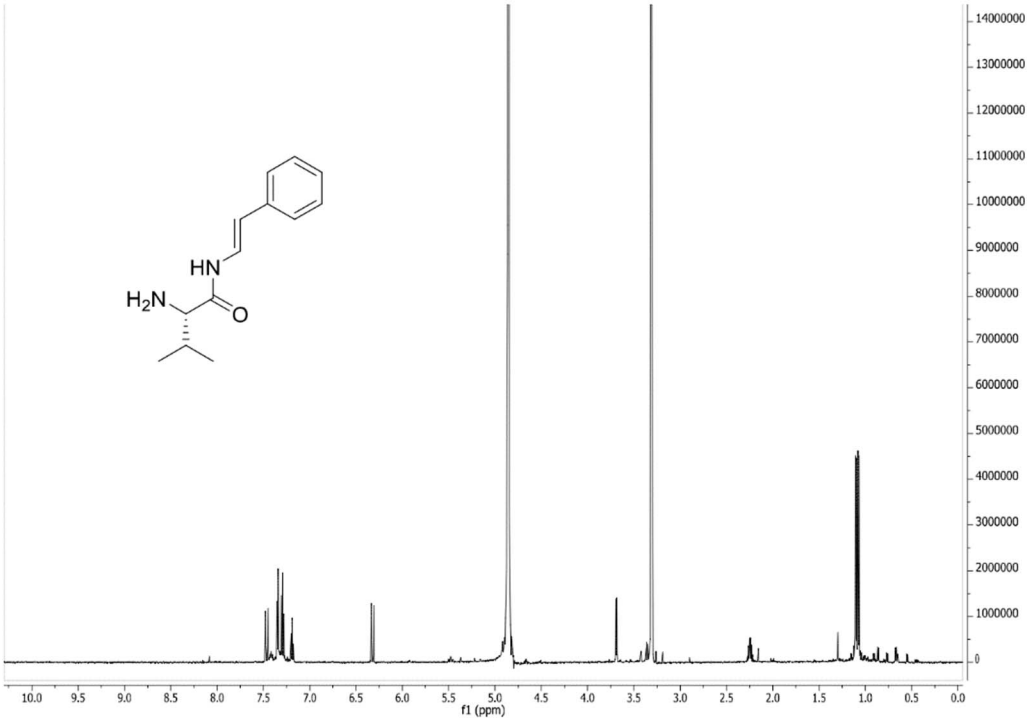

S7-1. ^{1}H NMR (MeOH-*d4*, 600 MHz) spectrum of **7**

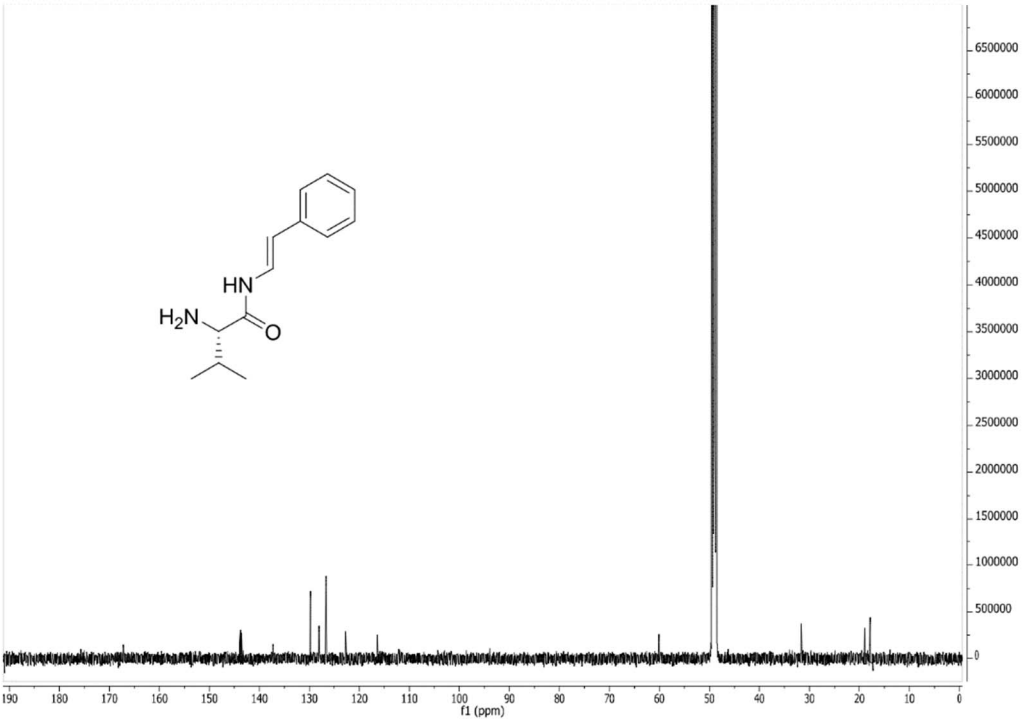

S7-2. ^{13}C NMR (MeOH-*d4*, 600 MHz) spectrum of **7**

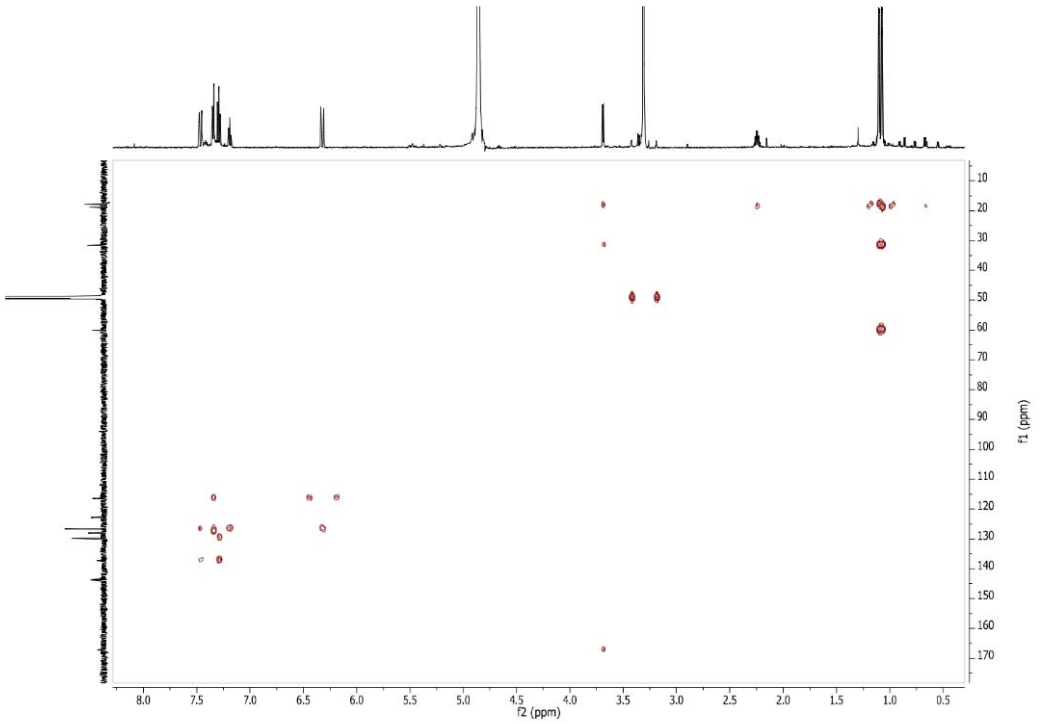

S7-3. HMBC NMR (MeOH-*d4*, 600 MHz) spectrum of **7**

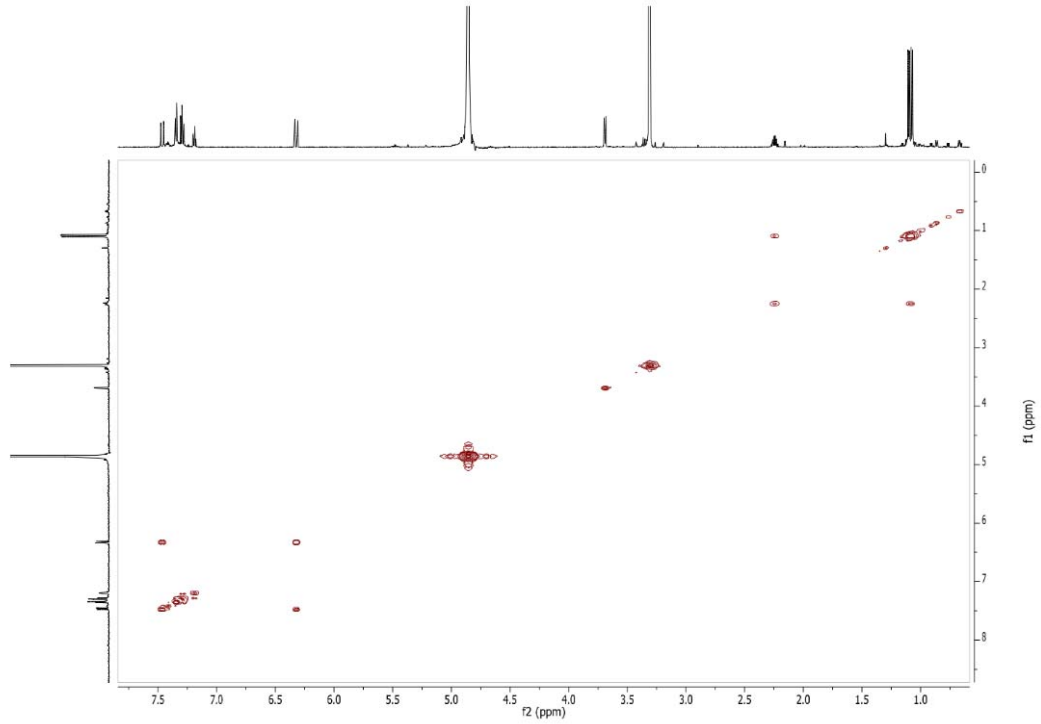

S7-4. COSY NMR (MeOH-*d4*, 600 MHz) spectrum of **7**

Mass Spectrum SmartFormula Report

Analysis Info

Analysis Name	D:\Data\spektren 2016\Proksch16HR000195.d	Acquisition Date	7/21/2016 10:03:47 AM
Method	tune_low_new.m	Operator	Peter Tommes
Sample Name	Amin Mokhlesi CE3 Si4 P3 (CH3OH)	Instrument	maXis 288882.2021
Comment			

Acquisition Parameter

Source Type	ESI	Ion Polarity	Positive	Set Nebulizer	0.3 Bar
Focus	Not active	Set Capillary	4000 V	Set Dry Heater	180 °C
Scan Begin	50 m/z	Set End Plate Offset	-500 V	Set Dry Gas	4.0 l/min
Scan End	1500 m/z	Set Collision Cell RF	600.0 Vpp	Set Divert Valve	Source

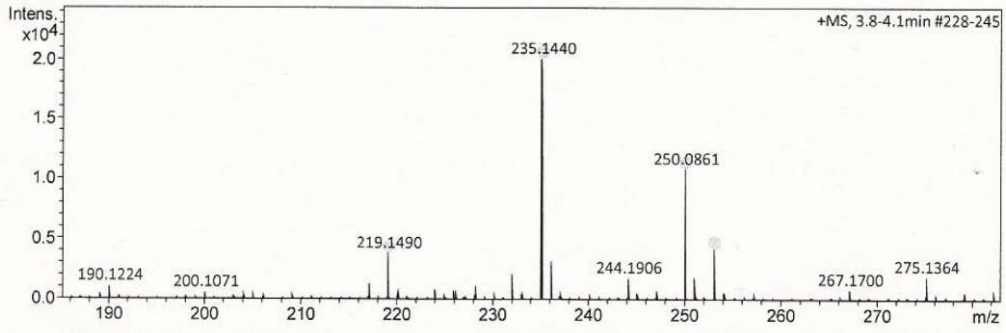

Meas. m/z	#	Ion Formula	m/z	err [ppm]	mSigma	# mSigma	Score	rdb	e⁻ Conf	N-Rule
219.1490	1	C13H19N2O	219.1492	0.9	10.8	1	100.00	5.5	even	ok
235.1440	1	C13H19N2O2	235.1441	0.5	2.6	1	100.00	5.5	even	ok
250.0861	1	C16H12NO2	250.0863	0.5	3.7	1	100.00	11.5	even	ok
253.1545	1	C13H21N2O3	253.1547	0.7	13.1	1	100.00	4.5	even	ok

S7-5. HRESIMS spectrum of **7**

S8. Marfey's analysis

S8-1. Table of HPLC (C_{18}) retention times of acid hydrolysates of **1**–**7** using Marfey's method

Amino acid	Standard	**1**	**2**	**3**	**4**	**5**	**6**	**7**
L-Cys	20.0	19.9	19.8	20.4	19.9	20.0	20.0	
D-Cys	21.2							
L-Ile	21.4	21.4	21.3	21.9	20.8	21.0		
D-Ile	24.2							
L-Leu	21.7				21.3	21.5	21.5	
D-Leu	24.3							
L-Val	14.5							
D-Val	19.4			19.9				19.4
L-Pro	8.8				8.5	8.5	8.8	
D-Pro	11.4							
L-Glu	12.4	12.3			12.4	12.3		
D-Glu	14.2							
L-Phe	20.9				20.8	21.0		
D-Phe	23.3							

S8-2. Table of HPLC (C_4) retention times for L-Ile and L-*allo*-Ile of **1**–**5** using Marfey's method

Amino acid	Standard	**1**	**2**	**3**	**4**	**5**
L-Ile	40.6	40.4	40.6	40.2	40.5	40.5
L-*allo*-Ile	39.5					

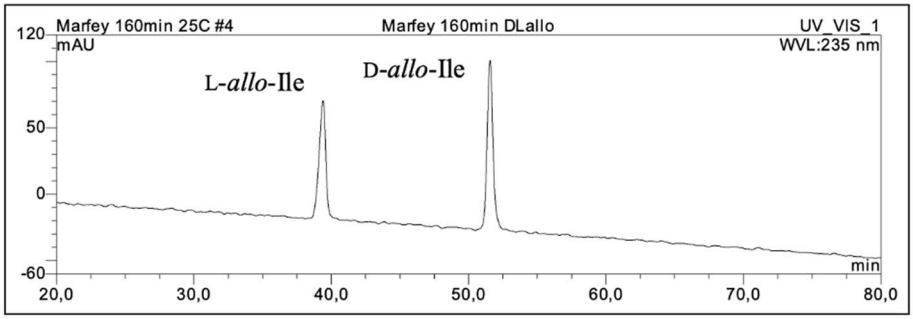

S8-2-1. HPLC chromatogram of derivatized L- and D-*allo*-Ile standards

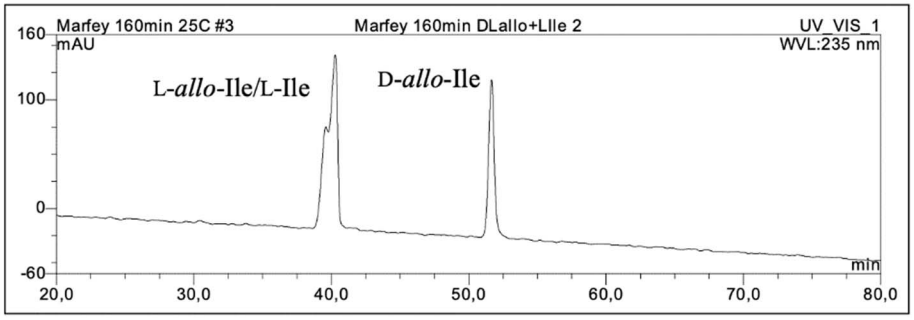

S8-2-2. HPLC chromatogram of derivatized D-*allo*-Ile, L-*allo*-Ile, and L-Ile standards

S9. Structures of known compounds

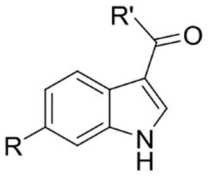

8 R=H; R'=H
9 R=H; R'=OH
10 R=Br; R'=H
11 R=Br; R'=OH
12 R=Br; R'=OCH_3
13 R=Br; R'=OCH_2CH_3

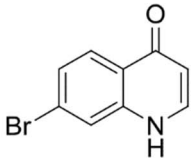

14

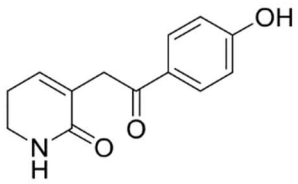

15

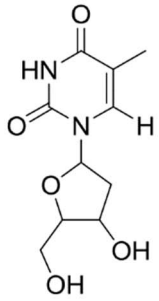

16

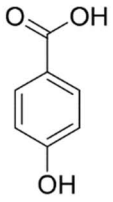

17

S9-1. Structures of known compounds, including 1*H*-indole-3-carbaldehyde (8), 1*H*-indole-3-carboxylic acid (9), 6-bromo-1*H*-indole-3-carbaldehyde (10), 6-bromo-1*H*-indole-3-carboxylic acid (11), methyl 6-bromo-1*H*-indole-3-carboxylate (12), ethyl 6-bromo-1*H*-indole-3-carboxylate (13), 7-bromo-4(1*H*)-quinolinone (14), (3-(2-(4-hydroxyphenyl)-2-oxoethyl)-5,6-dihydropyridin-2(1*H*)-one) (15), 2-deoxythymidine (16), and 4-hydroxybenzoic acid (17).

S10. Bioactivity results

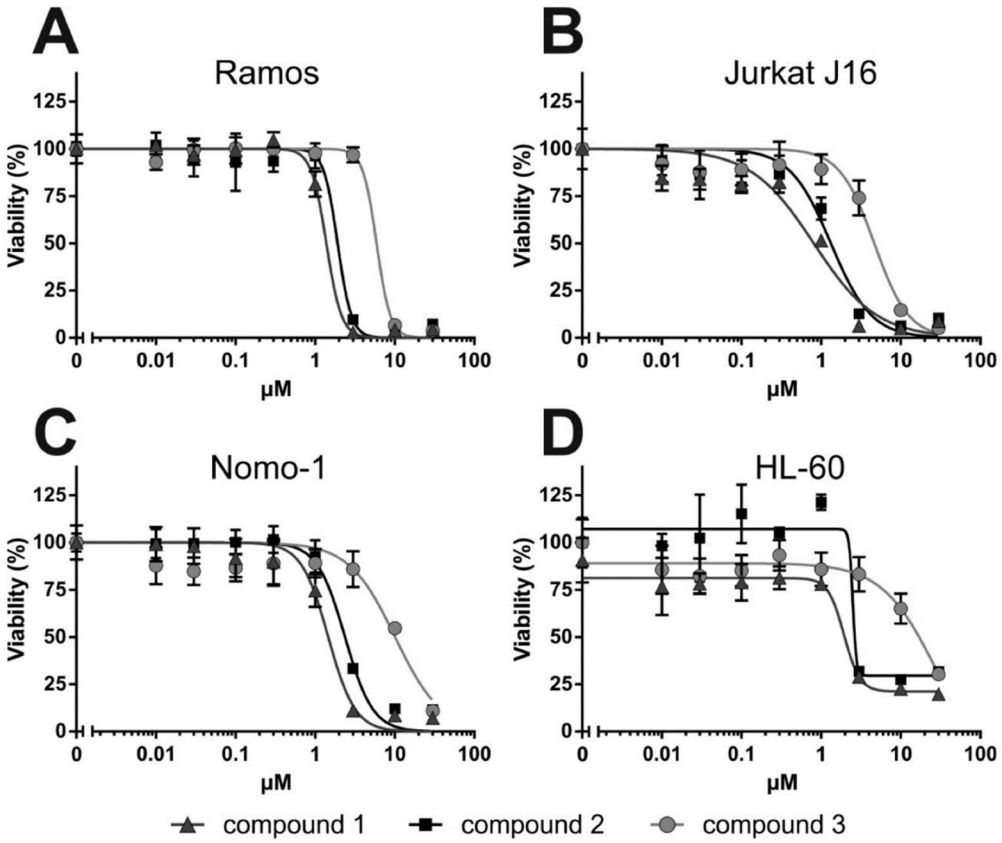

S10-1. Cytotoxicity effects of **1**–**3** on human lymphoma and leukemia cell lines, measured by MTT assay. (A) Ramos (Burkitt's lymphoma), (B) Jurkat J16 (acute T cell leukemia), (C) Nomo-1 (acute myeloid leukemia) and (D) HL-60 (acute promyelocytic leukemia) cells were seeded at a density of 5×10^5 cells/mL and incubated with increasing concentrations of **1**, **2** and **3**, respectively. Cells treated with DMSO (0.1% v/v) for 24 h were used as the negative control. After an incubation period of 24 h cell viability was monitored using the MTT assay as described in methods. Relative viability in DMSO-treated control cells was set to 100%. Data points shown are the mean of triplicates, error bars = SD. Viability and IC_{50} values (IC_{50} = half maximal inhibitory concentration) were calculated using Prism 6 (GraphPad Software).

S10-2. Table of antibacterial activity of new **1**–**7** and known (8 – 17) compounds reported as minimal inhibitory concentration (MIC)[a]

Compound	*Staphylococcus aureus* ATCC 29213	*Enterococcus faecium* BM 4147-1	*Escherichia coli* ATCC 25922	*Klebsiella pneumoniae* ATCC 12657	*Enterobacter aerogenes* ATCC 13048	*Pseudomonas aeruginosa* ATCC 27853	*Acinetobacter baumannii* 09987	*Mycobacterium tuberculosis* H37Rv
1	6.3	12.5	> 100	> 100	> 100	> 100	> 100	100
2	n.i.[b]	n.i.	n.i.	n.i.	n.i.	n.i.	n.i.	n.i.
3	6.3[c]	12.5	> 100	> 100	> 100	> 100	> 100	100
4	> 50	> 50	> 100	> 100	> 100	> 100	> 100	> 100
5	n.i.	n.i.	n.i.	n.i.	n.i.	n.i.	n.i.	n.i.
6–17	> 50	> 50	> 100	> 100	> 100	> 100	> 100	n.i.
ciprofloxacin	0.12	2	0.01	≤ 0.25	≤ 0.01	0.25	0.03	n.i.
doxycycline	0.5	4	2	2	4	n.i.	n.i.	n.i.
vancomycin	1	4	> 64	> 64	> 64	> 64	> 64	n.i.

[a]MIC values are reported for test compounds in μM and for reference antibiotics in μg/ml and indicate the lowest concentration fully inhibiting visible bacterial growth. [b]n.i. : not investigated. [c]Growth reduction was already observed at 3.1 μM

Manuscript 1

Expression of the *Bacillus subtilis* genes *rpt* (formerly *pps*/*yppS*) and *helD* is specifically induced by RNA polymerase stalling and regulated by a *cis*-encoded antisense RNA

Katharina W. Wex[1,3#], Mirita Franz-Wachtel[2], Andreas Kulik[1], Boris Macek[2,4], Heike Brötz-Oesterhelt[1,3,4], Anne Berscheid[1,3#]

[1] Department of Microbial Bioactive Compounds; Interfaculty Institute of Microbiology and Infection Medicine, University of Tuebingen; Tuebingen, Baden-Wuerttemberg, 72076; Germany

[2] Proteome Center Tuebingen, Interfaculty Institute for Cell Biology, University of Tuebingen; Tuebingen, Baden-Wuerttemberg, 72076; Germany

[3] German Center for Infection Research (DZIF), Partner Site Tuebingen; Tuebingen, Baden-Wuerttemberg, 72076; Germany

[4] Cluster of Excellence Controlling Microbes to Fight Infection

[#]Correspondence to Katharina W. Wex, katharina.wex@student.uni-tuebingen.de or Anne Berscheid, anne.berscheid@uni-tuebingen.de

INTRODUCTION

Transcription constitutes one of the most important cellular processes in bacteria, archaea, and eukaryotes. Interference cannot be tolerated as all cellular processes depend on a highly regulated, efficient, and yet quickly adaptable gene expression. Nevertheless, its tight entanglement with replication requires an additional level of coordination, which is prone to errors (Merrikh et al., 2012; Hamperl and Cimprich, 2016). Furthermore, the lack of resources (e.g., nutrient supply) (Sharma and Chatterji, 2010; Lyer et al., 2018), the divergent gene regulation in different growth phases (Resnekov et al., 1990), the adaptation to different environmental conditions (Helmann et al., 2001; Brillard et al., 2010), or the encounter with RNA synthesis tackling antibiotics (Freiberg et al., 2006) complicate the maintenance of a functional transcription process. Therefore, bacteria have evolved an optimized genome organization (Srivatsan et al., 2010) and a fine-meshed net of regulatory

mechanisms consisting of, i.e., an adaptive transcriptional stress response (e.g., by alternative sigma factors) (Ayala et al., 2020), different DNA repair mechanisms (Lenhart et al., 2012; Kisker et al., 2013), antibiotic detoxification or adaptation processes (Koteva et al., 2018; Xu et al., 2018) or transcription pausing strategies (Esyunina et al., 2016; Lerner et al., 2016).

The *Bacillus subtilis* genes *ppS*/*yppS* and *helD* as well as *yorB* were selectively upregulated in response to antibiotic interference with RNA or DNA synthesis (Freiberg et al., 2006). In previous studies, they have been employed as bioreporters for antibiotic screening and mode of action (MOA) profiling (Urban et al., 2007; Wex et al., 2021). Nevertheless, until now the regulation of their gene expression and their affiliation to a specific stress response has not been characterized.

Also, the function of PpS/YppS is not elucidated in *B. subtilis.* Due to sequence homologies, it is annotated as putative phosphoenolpyruvate synthetase or as rifampin phospho-transferase. Both enzymes contain an energy-conferring ATP domain as well as a histidine domain important for phospho-transfer, which explains the divergent annotation (Spanogiannopoulos et al., 2014; McCormick and Jakeman, 2015). Phosphoenolpyruvate synthetase is a metabolic enzyme that takes part in gluconeogenesis (McCormick and Jakeman, 2015). Rifampin phosphotransferase represents a resistance factor found in different actinobacteria and firmicutes (Spanogiannopoulos et al., 2014; Stogios et al., 2016). It was shown to specifically phosphorylate and inactivate rifamycins, by attenuating their affinity for the RNA polymerase (RNAP) RpoB subunit (Spanogiannopoulos et al., 2014). *Pps*/*yppS* from *B. subtilis* is located in a prophage-like region and therefore has presumably been acquired by horizontal gene transfer (Kunst et al., 1997; Rocha et al., 1999).

B. subtilis HelD (formerly YvgS) was first described in 2011, when it was consistently copurified with the RNAP complex throughout all growth phases (Delumeau et al., 2011). It was annotated as putative helicase, due to its sequence homology to other DNA and RNA helicases of the superfamily I, like the distantly related UvrD from *Escherichia coli*, but showed no helicase activity *in vitro* (Fairman-Williams et al., 2010; Wiedermannová et al., 2014). Wiedermannová and colleagues demonstrated that the helicase-like enzyme enhances transcriptional cycling and elongation in an ATP-dependent manner, thereby helping *B. subtilis* to rapidly adapt to a changing environment (Wiedermannová et al., 2014). The stimulating effect on transcription as well as the release of stalled RNAP from DNA can be further enhanced by the addition of the RpoE protein, a small accessory RNAP subunit acting synergistically (Wiedermannová et al., 2014; Weiss and Shaw, 2015). HelD was

shown to be associated with the core RNAP subunits RpoB and RpoC, but also possesses the ability to directly bind to DNA (Wiedermannová et al., 2014; Kovaľ et al., 2019; Pei et al., 2020). The protein can be sub-structured into three domains: the N-terminal domain, that shows no sequence homology to other helicases, and the ATPase- and C-terminal domains, which are related to UvrD but possess different topology (Wiedermannová et al., 2014; Kovaľ et al., 2019). After ATP-binding, HelD undergoes a strong conformational change (Kovaľ et al., 2019). A deletion of the unique N-terminal domain hampered its transcription-related functions, but had no effect on ATPase activity or DNA and RNAP binding properties (Kovaľ et al., 2019). Therefore, this domain was proposed to be essential for the transcription modulating function. In recent studies, the exact molecular mechanism conferring the ability of HelD to successfully remove stalled RNAP complexes could be elucidated (Kouba et al., 2020; Newing et al., 2020; Pei et al., 2020). The 2-armed structure of the enzyme allows for deep penetration into the primary and secondary channels of the RNAP, thereby removing nucleic acids from the active site and recycling the stalled polymerase (Newing et al., 2020; Pei et al., 2020). Furthermore, HelD was proposed to keep the RNAP in an inactive (dimeric) state, that allows to restart transcription under more favorable environmental conditions (Kouba et al., 2020; Pei et al., 2020). Also, HelD was reported to possess the tendency to oligomerize and form amyloid or amyloid-like fibrils *in vitro*, although it predominantly occurred as a monomeric protein in solution (Kaur et al., 2018). Deletion of *helD* coincides with a prolonged lag phase (similar to deletion of *rpoE*) (Wiedermannová et al., 2014), while overexpression induces premature initiation of sporulation (Meeske et al., 2016).

YorB encodes for a SPß-prophage gene of unknown function, which was proposed to be LexA-dependent, as it showed strong upregulation during the SOS response and a putative LexA binding site was predicted (Au et al., 2005; Urban et al., 2007).

Here, we confirm the function of *B. subtilis* PpS/YppS as a rifampin phosphotransferase enzyme, which confers increased resistance to rifamycin antibiotics and propose the name Rpt. Concerning gene regulation, we finely discriminate the response of the *B. subtilis* bioreporters P_{yorB}-*lacZ*, P_{rpt}-*lacZ* and P_{helD}-*lacZ* to an extended panel of RNA and DNA synthesis inhibitors with distinct modes of action. Our results shed light on the stress signal that leads to selective high-level expression of *rpt* and *helD* upon RNA synthesis interference in *B. subtilis*. The selective regulation of both genes seems to depend on a *cis*-encoded antisense transcription mechanism, that represses constitutive *rpt* and *helD* expression from a sigma factor A (SigA)-dependent promoter under unstressed growth conditions.

RESULTS and DISCUSSION

B. subilis PpS/YppS is a rifampin phosphotransferase resistance enzyme.

In a previous study we established a new RNA stress bioreporter P_{yppS} (Wex et al., 2021), which was selected based on its strong and selective upregulation upon antibiotic interference with RNA synthesis in a former transcriptome study (Freiberg et al., 2006). The function of *B. subtilis* PpS/YppS has not been elucidated. In some databases it is named *ppS* corresponding to its former annotation as putative phosphoenolpyruvate synthetase (Kanehisa and Goto, 2000; Zhu and Stülke, 2017), while it can also be found under the name *yppS* (Sayers et al., 2022), relating to its to date unknown function. Due to sequence homologies, *ppS*/*yppS* was recently further annotated as putative rifampin phosphotransferase, a resistance enzyme that selectively phosphorylates and thereby inactivates rifamycin antibiotics (Spanogiannopoulos et al., 2014; Stogios et al., 2016).

In order to elucidate if PpS/YppS possesses the proposed rifamycins inactivating function, we investigated the rifampin susceptibility of different *B. subtilis* 168 deletion and complementation mutants (Table S1). For the determination of the wildtype (WT) MIC, the isogenic strain *B. subtilis* 168 Δ*amyE* from the *B. subtilis* knockout library was used as a reference strain (Koo et al., 2017). We chose the Δ*amyE* strain as an unrelated control, as it had undergone the same knockout procedure as our deletion mutant of interest, and the *amyE* locus, encoding an α-amylase, is not considered important under common laboratory conditions (Juhas and Ajioka, 2016), while it is often used as a standard locus for gene insertions (Shimotsu and Henner, 1986; Härtl et al., 2001). Interestingly, the deletion of Δ*pps/yppS* lead to a 32-fold higher rifampin susceptibility in *B. subtilis* 168 in comparison to the reference strain Δ*amyE*. Complementation of *B. subtilis* 168 Δ*ppS*/*yppS* with an isopropyl-β-D-thiogalactopyranoside (IPTG)-inducible S707-*ppS*/*yppS* construct in the *aprE* locus, restored WT rifampin MIC upon induction (Table S1). Of note, S707 represents the 5’ untranslated region (UTR) preceding the *ppS*/*yppS* gene, which contains crucial regulatory elements as described below. An heterologous overexpression of *B. subtilis* S707-*ppS*/*yppS* in *E. coli* XL-1 blue (*E. coli* XL1 blue pBS2E-P_{Spac}-S707-*ppS*/*yppS*) led to high-level resistance (128-fold MIC increase) (Table S1), as previously described for the *Bacillus cereus* rifampin phosphotransferase (Spanogiannopoulos et al., 2014) (74 % identity to *B. subtilis* PpS/YppS).

To verify the function of *B. subtilis* PpS/YppS as rifampin phosphorylating enzyme, the supernatants of rifampin-treated and IPTG-induced cultures of *E. coli* XL1 blue pBS2E-P_{Spac} and *E. coli* XL1 blue pBS2E-P_{Spac}-S707-*ppS*/*yppS* were investigated via high-performance liquid chromatography-mass spectrometry (HPLC-MS). The mass of unmodified rifampin

(*m/z* 821.3) was present in both samples, while the mass of phosphorylated rifampin (*m/z* 901.3) could only be detected in the IPTG-induced culture of *E. coli* XL1 blue pBS2E-P_{Spac}-S707-*ppS*/*yppS* (Figure S1), proving that *B. subtilis ppS*/*yppS* encodes a rifampin phosphotransferase resistance enzyme. Based to the elucidated function, we propose the name *rpt* for *B. subtilis ppS*/*yppS* and Rpt for the corresponding protein. Of note, the name *rph* - in the style of the first discovered rifampin phosphotransferase found in actinomycetes called *rph* (Spanogiannopoulos et al., 2014) - was already taken in the *B. subtilis* gene annotation and thus no longer available.

Induction spectra of the *rpt*, *helD* and *yorB* genes upon treatment with antibiotics interfering with RNA and/or DNA synthesis.

In a previous study, we had generated and validated the *B. subtilis* bioreporters P_{yorB}-*lacZ*, P_{rpt}-*lacZ* and P_{helD}-*lacZ,* that show induction upon interference of antimicrobial agents with DNA synthesis and structure (P_{yorB}-*lacZ*) or RNA synthesis (P_{rpt}-*lacZ* and P_{helD}-*lacZ*), thereby yielding important information on the MOA of unknown antimicrobial agents (Wex et al., 2021). The specific induction of the promoter P_{helD} after RNA stress was first described by Urban and colleagues in a luciferase-based screening setup (Urban et al., 2007). For our agar-based screening approach employing the ß-galactosidase *lacZ* as the reporter gene, we had replaced the P_{helD} promoter with the P_{rpt} promoter, as it showed the same induction specificity but stronger induction signals and was additionally able to detect intercalating agents that inhibit RNA synthesis (e.g., actinomycin D) (Wex et al., 2021). As RNA and DNA synthesis are both DNA-dependent processes, they need to be tightly coordinated to exclude replication-transcription conflicts that might have dramatic consequences for cellular survival. To further discriminate the stress responses signaled by the bioreporters P_{rpt}-*lacZ,* P_{helD}-*lacZ,* and P_{yorB}-*lacZ* and initiated by antibiotics affecting RNA and/or DNA synthesis, we tested additional compounds acting in those pathways. Figure 1 shows an exemplary panel of RNA and DNA synthesis inhibitors, which are all covered by the induction of at least one bioreporter. All bioreporters were investigated using previously described, standardized growth and media conditions (P_{yorB} and P_{helD} were grown in LB soft agar and P_{rpt} in Belitzky minimal soft agar) (Wex et al., 2021). To exclude that the different growth media might have had an effect on the induction specificity, we additionally confirmed the results with P_{yorB}-*lacZ* and P_{helD}-*lacZ* grown in Belitzky minimal soft agar (Figure S2). An extended set of investigated antibiotic agents can be found in Table S2.

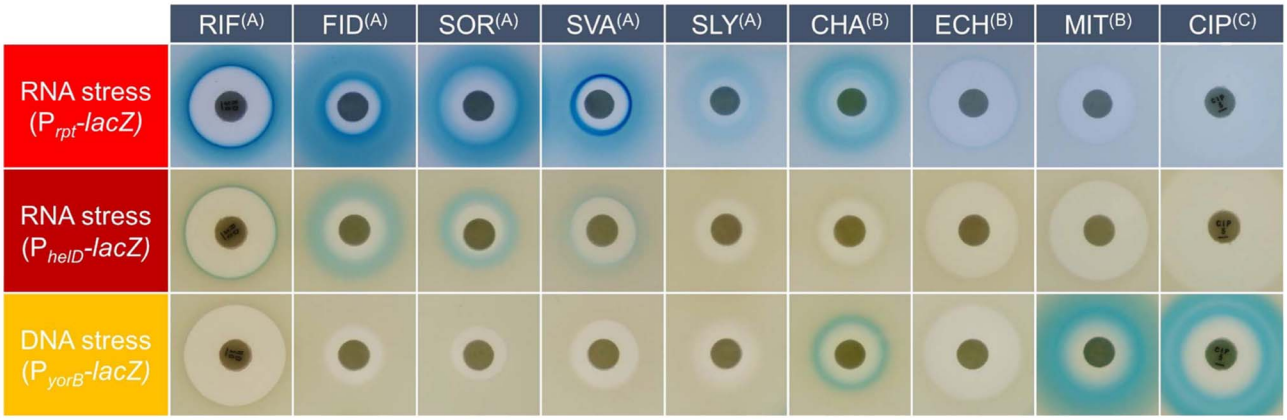

Figure 1. Induction pattern of exemplary reference antibiotics tested against our RNA and DNA stress bioreporters. Compounds were spotted on a filter disc and subsequently placed on the agar, containing the respective *B. subtilis* reporter strain. Filter discs contained the following antibiotic amounts: rifampin (RIF) 30 µg, fidaxomicin (FID) 8 µg, sorangicin A (SOR) 5 µg, streptovaricin (SVA) 10 µg, streptolydigin (SLY) 40 µg, chartreusin (CHA) 30 µg, echinomycin (ECH) 20 µg, mitomycin C (MIT) 1 µg, and ciprofloxacin (CIP) 5 µg. Categorization into DNA synthesis inhibitors (A), RNAP inhibitors (B), and DNA-binding agents (C) is indicated by the respective superscript. Promoter induction was detected as a blue halo following overnight incubation. As previously described, the DNA stress reporter P$_{yorB}$-*lacZ* and the RNA stress reporter P$_{helD}$-*lacZ* were tested using lysogeny broth (LB) soft agar, while the RNA stress reporter P$_{rpt}$-*lacZ* was grown in Belitzky minimal soft agar (Wex et al., 2021).

The compounds were clustered in DNA synthesis inhibitors that cover gyrase binders and nucleotide biosynthesis inhibitors, RNA synthesis inhibitors that directly bind to the RNAP, and DNA-binding agents that most likely have an effect on both, replication and transcription, but often show preferences for one of those pathways. RNAP binders were selectively detected by the two RNA stress bioreporters, except for streptolydigin, tirandamycin, and pseudouridimicin, which were only detected with P$_{rpt}$-*lacZ* in the agar-based assay. Streptolydigin rather acts on transcription elongation (Temiakov et al., 2005), and also showed a weaker induction signal on P$_{rpt}$-*lacZ* in comparison to the other RNAP binders, which interfere with transcription initiation (compare Figure 1). Gyrase binders and nucleotide synthesis inhibitors selectively induced the DNA stress reporter P$_{yorB}$, with the exception of azaserine, which also showed an additional weak signal on P$_{rpt}$-*lacZ*. Azaserine is a glutamine analog that is proposed to inhibit *de novo* purine synthesis, thereby most likely affecting both RNA and DNA synthesis (Williams and Tritz, 1977; Ahluwalia et al., 1990). In comparison, folate synthesis inhibitors like trimethoprim limit the thymidine precursor supply, which primarily effects DNA synthesis (Gleckman et al., 1981). DNA-binding agents show a diverse promoter induction. Some of them, like mitomycin C or doxorubicin, only induce the SOS response-dependent bioreporter P$_{yorB}$-*lacZ* (LexA-dependent regulation is confirmed in this study, compare Figure S6). Others induce both, P$_{yorB}$-*lacZ* and P$_{rpt}$-*lacZ*, like chartreusin or gilvocarcin V, and some antibiotics like actinomycin D, echinomycin or netropsin lead to a selective upregulation of only the P$_{rpt}$-*lacZ* bioreporter (Table S2). Due to the described MOA of those DNA-binding agents, we propose that compounds that

provoke the formation of DNA single or double strand breaks mainly induce a cellular SOS response and therefore lead to a strong induction of *yorB* in *B. subtilis* (Reiter et al., 1972; Vidal et al., 2006; Cardenas et al., 2014). This primary stress response might then hinder the activation of other stress pathway(s), i.e., transcriptional stress responsible for the induction of P_{rpt}-*lacZ.* Vice versa, DNA-binding agents that are not known for any strand break capability (e.g., echinomycin) (Huang et al., 1982) showed no induction of P_{yorB}-*lacZ*, in accordance with the lack of an SOS response. Therefore, the employed bioreporters allow a classification of DNA-binding agents according to their primary pathway of interference and the concomitant stress response. A preference of DNA-binding agents for either transcription or replication was also detected in incorporation assays with radioactive RNA- or DNA-specific nucleosides. Harvey and colleagues showed that low concentrations of actinomycin D selectively inhibited RNA synthesis, while they had no effect on DNA synthesis (Harvey et al., 1976), a result in accordance with the P_{rpt}-*lacZ* induction preference observed in our study. Higher concentrations of actinomycin D were shown to also interfere with DNA synthesis in eukaryotes (Reich and Goldberg, 1964). Vice versa, mitomycin C demonstrated a stronger effect on DNA synthesis than on RNA synthesis in precursor incorporation assays (Harvey et al., 1976), which matched our P_{yorB}-*lacZ* bioreporter signal. For P_{helD}-*lacZ*, we could not detect an induction by any of the DNA-binding agents in the agar-based setup. As the induction intensities for DNA-binding agents tested on P_{rpt}-*lacZ* appeared to be generally weaker in comparison to the signal caused by transcription initiation inhibitors, we suspected that an induction of P_{helD}-*lacZ* might be missed due to its overall weaker signaling strength. As the agar-based setup does not allow a reliable and precise quantification of the induction intensities, we decided to compare the induction intensities of both bioreporters, P_{rpt}-*lacZ* and P_{helD}-*lacZ*, in a luminescence-based setup in liquid culture, which bears the advantage of a more sensitive detection that can also be quantified in compound dilution series. In the following sections we will now focus on the RNA stress response sensed by P_{rpt} and P_{helD}, using the luciferase operon *luxABCDE* from *Photorhabdus luminescens* as readout.

Quantitative and comparative analysis of the induction specificity of P_{rpt} and P_{helD}.

The fusion of the described promoter regions P_{rpt} and P_{helD} to the *P. luminescens luxABCDE* operon allowed monitoring and quantification of the promoter induction signals over time, without the need for external substrate addition. The induction threshold of both *B. subtilis* bioreporters after antibiotic treatment was set to 2-fold the signal of the untreated control (200 %). All luminescence signals were normalized to OD_{600} = 1 to guarantee that growth

inhibitory effects would not obscure the induction signal, as better growing cell cultures potentially possess a higher background induction signal due to their higher cell number. For better comparison, both bioreporters were grown in Belitzky minimal medium (BMM) and treated with serial dilutions of 24 antibiotics with diverse MOA. As P_{rpt} had not been characterized in a quantitative bioreporter-based system before, we first monitored the induction specificity over time. Notably, already after 10 min of treatment with an antibiotic that interfered with RNA synthesis initiation (e.g., rifampin or fidaxomicin), a more than 2-fold increase in the P_{rpt}-*luxABCDE* signal was detectable (Table S3). The best signal-to-noise ratio was observed after 210 min, i.e., strong, reproducible signals triggered by RNA synthesis inhibitors, with a broad range of negative controls below threshold. The results confirmed that P_{rpt}-*luxABCDE* is indeed suitable for selective detection of RNA synthesis inhibitors (Figure 2). Furthermore, as previously observed in the agar-based setup, Figure 2 shows a comparable induction specificity for both RNA synthesis bioreporters after 210 min, with P_{rpt} exhibiting a generally higher maximal induction strength compared to P_{helD} (approximately 2-times higher). Analyzing the induction signals over time (compare Table S3 for different time points) both bioreporters displayed reliable induction specificity up to 240 min, after which the postulated threshold of 200 % was no longer suitable for discrimination.

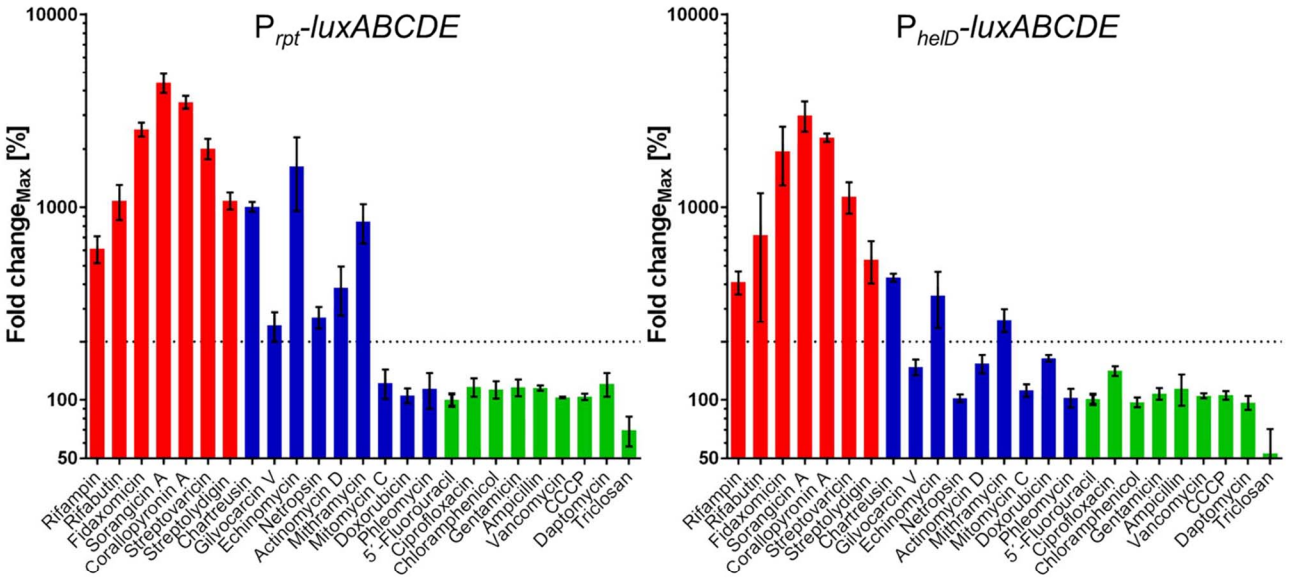

Figure 2. Induction of the bioreporters P_{rpt}-*luxABCDE* and P_{helD}-*luxABCDE* after 210 min of antibiotic treatment. Direct RNAP-binding antibiotics and DNA-binding agents are marked in red and blue, respectively. Other antibiotics (meant as negative controls), with a primary MOA unrelated to RNA synthesis, are marked in green. Depicted is the maximal fold change, i.e., the maximal induction signal after antibiotic treatment in comparison to the untreated control. The dotted line highlights the induction threshold of 200 %. All values were normalized to the untreated control (100%). Error bars indicate the standard deviation of the maximal fold change measured in three biological replicates.

As for the *lacZ* bioreporters in the agar-based setup, P_{rpt}-*luxABCDE* and P_{helD}-*luxABCDE* exhibited the strongest induction for antibiotics that hamper transcription initiation (e.g., rifamycins, fidaxomicin, or corallopyronin A), especially when only shorter incubation times (10 or 90 min) were considered. Inhibition of the transcription elongation step of RNA synthesis (e.g., streptolydigin) or interference via direct DNA-binding (e.g., netropsin, actinomycin D, or echinomycin) showed substantially weaker signals after short incubation times, but increased over time (Table S3). Due to the generally weaker induction strength of P_{helD}-*luxABCDE* not all DNA-binding agents detected by P_{rpt}-*luxABCDE* exceeded the induction threshold of 200 % for P_{helD}-*luxABCDE* after 210 min. Nevertheless, those antibiotics displayed a tendency by showing increased expression compared to the untreated control after 240 min, a time point where the induction specificity of P_{helD}-*luxABCDE* was still given (compare Table S3). Generally, the induction specificity as well as the induction pattern hinted at a similarly regulated expression of both bioreporters, which raised a number of different questions that we set out to investigate further. Do they help *B. subtilis* to adapt to or gain resistance against antibiotics that induce their expression? What kind of molecular stress signal is sensed by the bacterial cell (resulting in the induction of *rpt* and *helD*), that is triggered by all those structurally and mechanistically different RNA synthesis inhibiting antibiotics? And last but not least, how are the *rpt* and *helD* genes regulated, and are they regulated the same way?

helD and _rpt_ are commonly induced upon RNAP stalling.

As bioreporter assays showed an induction by all kinds of mechanistically different RNAP inhibitors, we were interested to see if the increased expression of Rpt and HelD helps the bacterial cell to counteract the antibiotic attack. Table 1 shows the minimal inhibitory concentration (MIC) values of *B. subtilis* 168 strains lacking *rpt*, *helD*, or *rpoE* for different RNA synthesis inhibitors. For the determination of the wildtype (WT) MIC, we again used the isogenic reference strain *B. subtilis* 168 Δ*amyE*. The deletion of *rpt* resulted in a higher susceptibility to all tested rifamycin derivatives, while it showed no effect for other RNA synthesis inhibiting antibiotics. Notably, the MIC against the rifamycin-related antibiotic streptovaricin (mixture of streptovaricins mainly containing the derivatives A, B, and C) was not affected by the *rpt* deletion. This result demonstrates a high selectivity of Rpt for rifamycins, as streptovaricin also possesses the hydroxyl group attached to the C21 of the ansa-chain, which constitutes the target site for the rifampin inactivating phosphorylation by the Rpt homolog Rph from actinomycetes (Spanogiannopoulos et al., 2014; Stogios et al., 2016).

Table 1. Antibiotic susceptibility of the *B. subtilis* 168 knockout mutants Δ*rpt*, Δ*helD*, and Δ*rpoE* upon treatment with different RNA synthesis inhibitors. *B. subtilis* 168 Δ*amyE* served as substitute for WT antibiotic susceptibility. MIC values that strongly deviated from WT MIC are marked in bold font. MIC determination was conducted in BMM. The streptovaricin natural product complex contains a mixture of different streptovaricins, mainly composed of the derivatives A, B, and C.

Antibiotic	MIC [µg/mL]			
	B. subtilis 168 Δ*amyE*	*B. subtilis* 168 Δ*rpt*	*B. subtilis* 168 Δ*helD*	*B. subtilis* 168 Δ*rpoE*
Actinomycin D	1-2	1-2	1-2	1
Chartreusin	16	16	16	16
Corallopyronin A	16	16	**1**	**1**
Fidaxomicin	4-8	4-8	4-8	4-8
Myxopyronin A	> 64	> 64	**2**	**2-4**
Rifamycin SV	0.125	**0.0039-0.0078**	0.0625-0.125	0.0625-0.125
Rifampin	0.5	**0.0625-0.125**	0.25-0.5	0.25-0.5
Rifabutin	1	**0.25**	0.5-1	0.5-1
Sorangicin A	4	4	4	4
Streptolydigin	64-128	64-128	64-128	64-128
Streptovaricin	4	4	2-4	2-4

For *B. subtilis* 168 Δ*helD*, the detected MIC values were close to WT level, with the exception of the closely related antibiotics corallopyronin A and myxopyronin A, which showed a markedly more sensitive phenotype (Table 1). As HelD is described to directly bind to the RNAP and to DNA, thereby accelerating transcriptional cycling and RNAP recycling (Wiedermannová et al., 2014; Newing et al., 2020; Pei et al., 2020), we excluded that HelD could be a specific corallopyronin/myxopyronin inactivating enzyme (like Rpt for rifamycins). Binding of HelD to the interface of the RpoB and RpoC RNAP subunits was previously investigated in *B. subtilis*. Wiedermannová and colleagues could show the weak binding of HelD to the fragment $RpoB_{(400-760)}$ and strongly to $RpoC_{(600-915)}$ (Wiedermannová et al., 2014). Myxopyronin is also described to bind to those two subunits of the *Thermus thermophilus* RNAP, with the RpoC binding sites V805, D806 and Q809 (converted to the conserved *B. subtilis* RNAP positions) overlapping with the proposed binding region of HelD (Ho et al., 2009). The ability of both, myxopyronin A and HelD, to bind to the RNAP subunits RpoB and RpoC in close vicinity might lead to competition at the respective binding regions. Thereby, the presence of HelD may inhibit binding of the two similarly acting antibiotics myxopyronin A and corallopyronin A to their target site. However, also an opposing function of HelD could explain the increased corallopyronin A and myxopyronin A susceptibility of the Δ*helD* mutant. While myxopyronin binds to the switch-2 region of RpoC, thereby blocking clamp opening and DNA loading to the active site by a yet unsolved mechanism (Mukhopadhyay et al., 2008; Belogurov et al., 2009; Artsimovitch et al., 2012),

HelD drives large conformational changes that lead to RpoC clamp opening and dissociation of the DNA template from the active site of the stalled RNAP (Newing et al., 2020). Arguably, we see the same selective drop in the corallopyronin A and myxopyronin A MIC for *B. subtilis* 168 Δ*rpoE,* with RpoE constituting an accessory RNAP subunit, that is described to act synergistically with HelD in the recycling of stalled RNAP (Wiedermannová et al., 2014). However, the exact molecular mechanism underlying this observation of *B. subtilis* 168 Δ*helD and* Δ*rpoE* being more sensitive to corallopyronin A and myxopyronin A would need to be confirmed in further studies. Of note, while *Staphylococcus aureus* does not contain a HelD homolog*, S. aureus* USA300 JE2 Δ*rpoE* did not show increased sensitivity in comparison to *S. aureus* USA300 JE2 for corallopyronin A (MIC for both strains at 4 µg/mL). However, the RpoE enzymes of *B. subtilis* and *S. aureus* only share 34 % identity, while other essential RNAP subunits, like RpoA are highly conserved (77 % identity) (Kanehisa and Goto, 2000).

Although Rpt is specific for inactivation of rifamycins and HelD selectively confers resistance against corallopyronin A and myxopyronin A, it was intriguing that both enzymes are induced by a broad variety of RNA synthesis inhibiting substances. We could therefore deduce that *rpt* and *helD* were not upregulated by directly sensing the specific compounds that they selectively inactivate, but rather by a physiological state, which is commonly induced by all kinds of structurally different RNA synthesis inhibitors.

Capitalizing on the mostly well-described MOA of all the inducing compounds we tried to deduce the common feature in their various mechanisms of RNA synthesis inhibition, that might serve as a trigger for the ubiquitous stress response. Some of the antibiotics directly bind to the RNAP, thereby inhibiting transcription initiation or elongation in diverse ways. Others disturb the transcription process by binding to DNA, thereby sterically hindering the progression of the RNAP holoenzyme without any direct binding to the transcription complex. Rifamycins strongly bind to the RNAP subunit RpoB, near the exit tunnel, thereby directly blocking the path of the elongating mRNA (Campbell et al., 2001; Floss and Yu, 2005; Ho et al., 2009). They can only effectively inhibit transcription, if the nascent mRNA chain does not exceed a length of 3-7 nucleotides, as otherwise rifamycin binding is blocked (Campbell et al., 2001). Sorangicin A was shown to share the same binding site and mechanism of action, but possesses a higher conformational flexibility, thereby better adapting to conformational changes (e.g., some RNAP mutations or RNAPs of different species) (Campbell et al., 2005; Ho et al., 2009). Fidaxomicin and myxopyronin both interfere with transcription initiation only if they are added before the formation of the open promoter complex and trap the RNAP holoenzyme in a partially melted, inactive promoter

complex intermediate (Tupin et al., 2010; Artsimovitch et al., 2012). Although they both bind to the RNAP switch region, their binding sites do not overlap but are located in close vicinity (Lin et al., 2018). However, fidaxomicin was shown to inhibit preceding steps in open complex formation in comparison to myxopyronin and completely abolishes the transcription bubble formation (Tupin et al., 2010). The antibiotic streptolydigin is described to bind to RpoB and RpoC, close to the RNAP active center, thereby inhibiting RNA synthesis initiation, elongation and pyrophosphorolysis (Tuske et al., 2005; Ho et al., 2009). Streptolydigin hampers the nucleotide addition cycle and other catalytic reactions of the RNAP, proposedly by stabilizing a substrate-bound transcription intermediate in the catalytically inactive pre-insertion site (Temiakov et al., 2005). The inducing DNA-binding agents have no direct RNAP binding site. They inhibit RNA synthesis by sterically blocking the progression of the RNAP (Gause et al., 1968; Hollstein, 1974). To our knowledge, all those inducing antibiotics directly or indirectly stop the progression of RNAP at a specific point during RNA synthesis. Interestingly, transcription initiation inhibitors showed the fastest and strongest induction for P_{rpt}-*luxABCDE*. By inhibiting the first and crucial step of RNA synthesis, this MOA subgroup exceeded the induction threshold already after 10 min (Table S3). Searching for a common physiological state, the accumulated information on the various MOA of the different antibiotics led us to the hypothesis that our P_{rpt}- and P_{helD}-based bioreporters reveal a stress response, which is specifically induced by an increased intracellular level of stalled RNAP. To further follow this lead, we investigated the background expression of P_{rpt}-*luxABCDE* in different strains of the *B. subtilis* knockout library (Koo et al., 2017), which might affect RNAP fidelity. The background expression refers to the luminescence signal in relation to the OD_{600} of the respective reporter strain during growth in BMM without addition of an external stressor (i.e., an antibiotic). As a reference strain we again used the *B. subtilis* 168 Δ*amyE* background. Of note, we only investigated knockout mutants that did not display growth defects, to exclude growth phase dependent differences in background expression. HelD and RpoE were previously described to enhance transcriptional cycling and to resolve stalled RNAP complexes (Wiedermannová et al., 2014; Pei et al., 2020). Mfd and UvrB are major players in the prokaryotic nucleotide excision repair (NER). The transcription-repair coupling factor Mfd was shown to dislodge stalled RNAP from DNA lesions and to initiate subsequent DNA repair mechanisms (Ayora et al., 1996; Adebali et al., 2017). UvrB is part of the UvrABC excinuclease complex that is able to detect and repair DNA lesions (Lenhart et al., 2012). The *B. subtilis* 168 Δ*perR* background was chosen as a negative control as it is not expected to directly influence P_{rpt}-*luxABCDE* expression. PerR represents a transcriptional repressor

that senses the intracellular Fe/Mn ratio and is responsive to peroxide stress (Giedroc, 2009; Helmann, 2014). We could detect a significantly enhanced background expression of P_{rpt}-*luxABCDE* in the knockout mutants *B. subtilis* 168 Δ*helD* and Δ*rpoE* in comparison to the reference strain *(B. subtilis* 168 Δ*amyE*) (Figure 3).

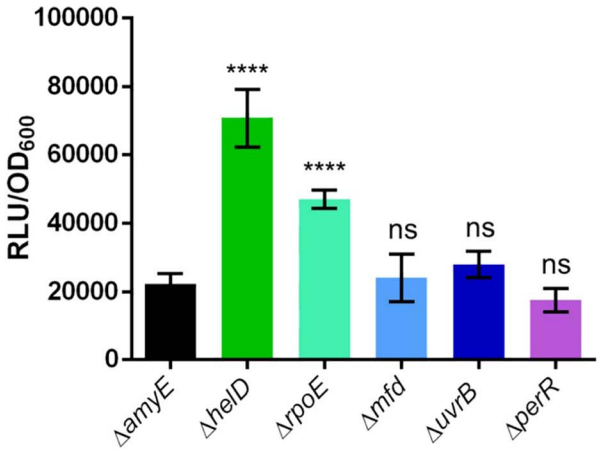

Figure 3. P_{rpt}-*luxABCDE* background expression in different *B. subtilis* deletion mutants (Δ*amyE*, Δ*helD*, Δ*rpoE*, Δ*mfd*, Δ*uvrB*, and Δ*perR*). Background expression in relation to the OD_{600} in BMM was determined after 210 min of untreated growth**.** Error bars show the standard deviation of the background luminescence signal measured in three biological replicates. Statistical significance was determined using the unpaired Students t-test with Holm-Bonferroni correction, always comparing the respective mutant with the reference strain *B. subtilis* Δ*amyE* (ns, $P > 0.01$; *, $P \leq 0.01$; **, $P \leq 0.001$; ***, $P \leq 0.0001$, ****, $P \leq 0.00001$).

As both enzymes were described to be involved in RNAP recycling, it is plausible that their deletion results in elevated levels of stalled RNAP. The raised P_{rpt}-*luxABCDE* background in their absence supports our hypothesis, that an elevated level of stalled RNAP forms the signal triggering upregulation of *rpt.* Background expression of P_{rpt}-*luxABCDE* in *B. subtilis* 168 Δ*mfd*, Δ*uvrB*, and Δ*perR* was not modulated and stayed close to Δ*amyE* level (Figure 3). Although we may have expected effects upon deletion of *mfd* or *uvrB*, it might likely be that their deletion is dispensable under the applied unstressed growth conditions (210 min in BMM), thereby not severely affecting the level of transcriptional stress.

Expression profiles, promoter composition and induction patterns suggest a similar regulation of *rpt* and *helD*.

The microarray data (Freiberg et al., 2006) and the corresponding induction specificity seen in our quantitative bioreporter setup suggested a similar regulation of *rpt* and *helD* (Figure 2), which both support the transcription process in very different ways. The comparison of different published data sets found yielded additional evidence that *rpt* and *helD* might be regulated in a similar way (Figure S3A). Although *rpt* and *helD* are located at distant positions in the *B. subtilis* 168 genome (accession number NC_000964.3, from 2053929 to 2051329 and from 3436651 to 3434327 respectively), they showed a nearly

identical expression pattern under different growth conditions (Figure S3A). For *rpt* expression the most positively correlated segments have been assigned to its own 5'UTR, called S707, and *helD* (Rasmussen et al., 2009; Zhu and Stülke, 2017). Figure S3B shows a schematic overview of the proposed promoter region. Both genes possess a SigA binding site (Nicolas et al., 2012). As the sequences of SigA factor binding sites in *B. subtilis* vary largely, Nicolas and colleagues further classified six consensus motif clusters, one of them M17, to which the promoter regions of *rpt* and *helD* were both categorized (Nicolas et al., 2012). Notably, they also described two further potential sigma factor binding sites for *helD* (Nicolas et al., 2012). Although not explicitly described for *helD*, both genes are preceded by a 5'UTR. For *rpt* the 5'UTR S707 was annotated with a length of 110 bp (Nicolas et al., 2012). For *helD* the length of the 5'UTR could be deduced from the SigA binding site and the translational start site, corresponding to approximately 102 bp (Nicolas et al., 2012).

Promoter deletion studies uncover 13 conserved nucleotides conferring specificity to P_{rpt} and P_{helD} expression upon RNA stress.

The initial promoter fragments for the bioreporter constructs P_{rpt}-*lacZ* and P_{helD}-*lacZ* were spaciously chosen in order not to miss upstream regulatory elements (Urban et al., 2007; Wex et al., 2021). Therefore, deletion studies were started with the removal of the upstream promoter regions up to the described SigA (M17) binding sites to investigate, if the bioreporters still retain induction and specificity. The promoter fragments P_{rpt_123bp} (Figure 4A) and P_{helD_120bp} (Figure 4B) still showed the specific induction upon treatment with RNA synthesis inhibitors. Progressing with the upstream promoter deletion, the next constructs were devoid of the -35 region of the SigA binding site (P_{rpt_108bp}-*lacZ* and P_{helD_113bp}-*lacZ*). After this deletion both bioreporters P_{rpt_108bp}-*lacZ* and P_{helD_113bp}-*lacZ* showed nearly no induction signal for all tested antibiotics (Figure 4A and Figure 4B, respectively). The remaining minimal activity seen for P_{rpt_108bp}-*lacZ* was still specific for RNA synthesis inhibitors, and can be explained by either upstream regulatory effects (e.g., additional promoters, readthroughs, or polar effects) or the residual binding capacity of the -10 region, and indicates that the specificity-conferring region must still be located in the remaining promoter fragment. For P_{helD} this shows that expression is mainly conferred by the SigA binding site, although of course not fully excluding an additional, divergent expression under different growth conditions from the described alternative promoter sites (Nicolas et al., 2012). We concluded that induction of *rpt* and *helD* is (mainly) initiated from the identified SigA (M17)-dependent promoters. Nevertheless, the highly expressed housekeeping sigma factor SigA could not solely be responsible for the specific induction

after RNA stress. We consulted the DBTBS database and investigated the minimal promoter sequence, that still showed specificity (P_{rpt_123bp}, P_{helD_120bp}) to find known transcription factor binding sites, but there was no match (Sierro et al., 2008). A direct alignment of the two promoter sequences revealed a 13 bp nucleotide sequence which was highly conserved at the downstream end of the 5'UTR of both promoters (Figure S4) (Erb et al., 2012). Figure 4A shows that deletion of 14 bp at the downstream end ($P_{rpt\_Del14bpDS}$-*lacZ*), including those 13 conserved nucleotides, resulted in a strong background signal under unstressed growth conditions, as well as the loss of induction specificity upon antibiotic treatment. Intriguingly, the same result could be detected after the deletion of the last 15 bp of the *helD* promoter region ($P_{helD\_Del15bpDS}$-*lacZ)*, which also included the 13 conserved nucleotides (Figure 4B). This result clearly indicated that the presence of those 13 nucleotides conferred induction specificity and regulated the selective expression of *rpt* and *helD*.

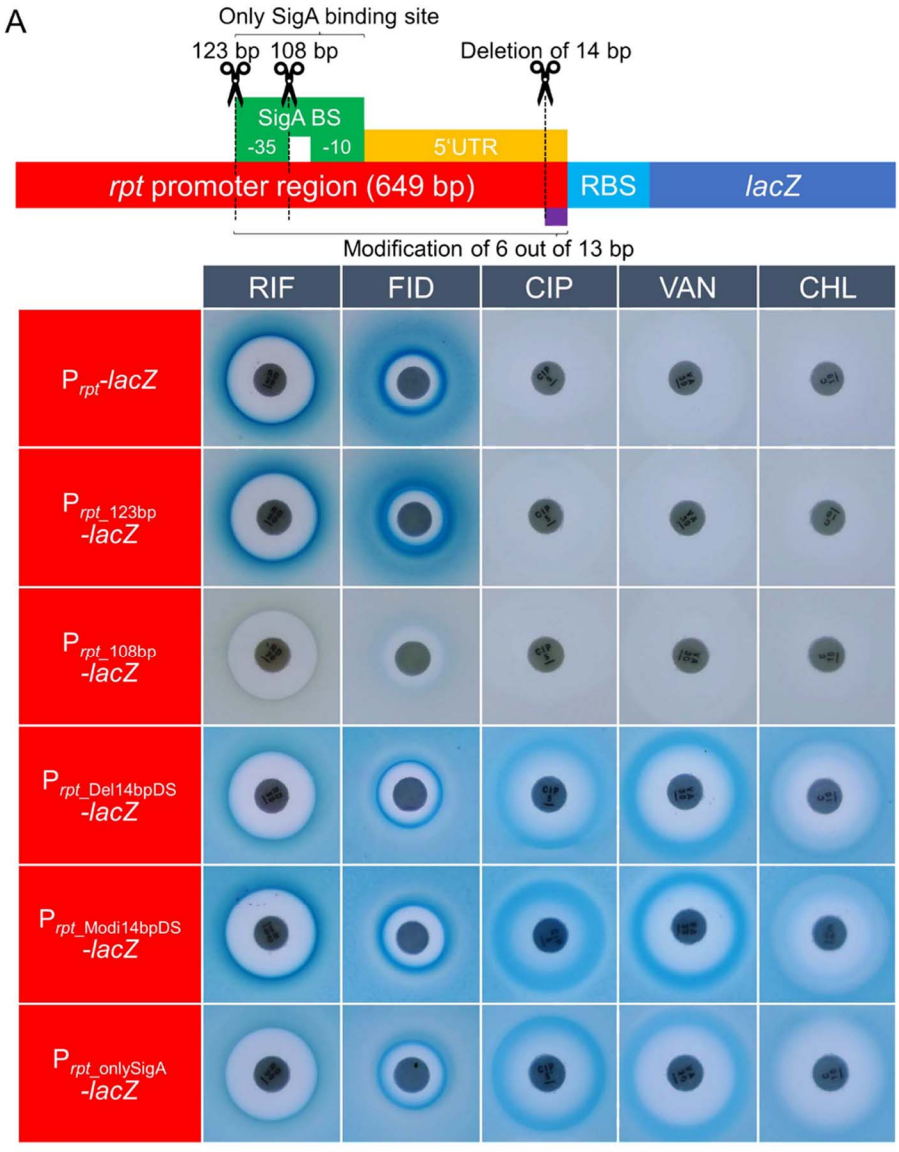

Figure 4. continued on the next page

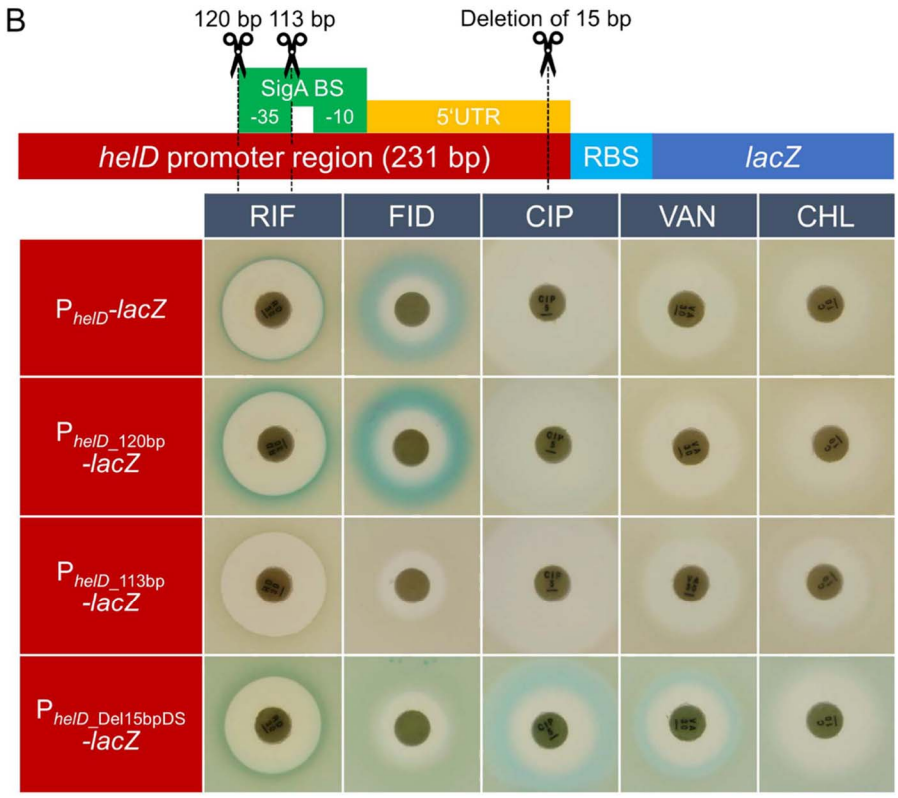

Figure 4. Promoter deletion and modification studies of the *rpt* and *helD* promoter regions. Schematic overviews at the top indicate the applied promoter modifications. (A) Different *rpt* promoter deletion and modification constructs tested in the agar-based bioreporter setup. P_{rpt}-*lacZ* and P_{rpt_123bp}-*lacZ* displayed the previously described induction specificity for RNA stress inducing compounds. P_{rpt_108bp}-*lacZ*, devoid of the -35 region of the SigA binding site, only showed marginal induction signals upon treatment with RIF and FID. The constructs $P_{rpt\_Del14bpDS}$-*lacZ, *$P_{rpt\_Modi14bpDS}$-*lacZ, and* $P_{rpt\_onlySigA}$-*lacZ* depicted a strong background upregulation and loss of induction specificity after antibiotic treatment. All *rpt* constructs were tested in Belitzky minimal soft agar. (B) Agar-based induction profiles of some corresponding promoter deletion constructs of *helD*. P_{helD_113bp}-*lacZ*, missing the -35 region of the SigA binding site, showed no induction signal for any of the tested antibiotics. For $P_{helD\_Del15bpDS}$-*lacZ* we could also detect an enhanced background expression in combination with loss of antibiotic induction specificity. All *helD* deletion mutants were tested in LB soft agar. Filter discs contained the following antibiotic amounts: rifampin (RIF) 30 µg, fidaxomicin (FID) 8 µg, ciprofloxacin (CIP) 5 µg, vancomycin (VAN) 30 µg, and chloramphenicol (CHL) 10 µg.

As 5'UTRs are described to confer stability to mRNA products and their stability is associated with the length and structure of the 5'UTR (Xiao et al., 2020), we also checked the induction specificity of a construct that retains the length of the initial 5'UTR of *rpt*, but was randomly modified in 6 of the 13 conserved nucleotides, changing the sequence from "TTGTCAATATTTT" to "TCATCTATGATCT" ($P_{rpt\_Modi14bpDS}$-*lacZ*). For this construct we could detect the same enhanced background signal combined with the unspecific induction pattern, excluding the idea that change in length of the 5'UTR would cause the observed deregulation (Figure 4A). Nevertheless, we still cannot fully exclude that a modified secondary structure of the 5'UTR may contribute to the loss of induction specificity. After deletion or modification of the conserved nucleotides, the predicted secondary structures of the 5'UTR region of the *rpt* mRNA only showed minor changes in the minimum free energy and modified secondary structure, suggesting similar accessibility of the

ribosomal binding site (RBS). An overview of the predicted secondary structures of P_{rpt} and all 5'UTR mutants can be found in Figure S5. Notably, all reporter constructs contained the same strong RBS with an equal distance to the reporter gene start codon. Reports that describe the enhanced stability of mRNAs containing stronger RBSs due to the better ribosomal binding (Xiao et al., 2020) can therefore not be the reason for the observed differences in transcript levels in our studies. The microarray data from Freiberg and colleagues showed upregulated levels of *rpt* mRNA after e.g., rifampin treatment (Freiberg et al., 2006), indicating that upregulation already manifests on the transcriptional level. Putatively, this RNA stress-specific upregulation phenomenon could be achieved by a more stable mRNA product being less prone to degradation, but as *rpt* mRNA levels increased by 100-fold after 10 min of incubation with rifampin (Freiberg et al., 2006), and structural changes were not that prominent (Figure S5), we rather presumed a transcription regulation mechanism to be responsible for the induced expression.

The high background induction and loss of induction specificity after deletion of the 13 nucleotides in both bioreporters hinted at a repressive element conferring induction specificity from a SigA (M17) regulated promoter. Vice versa that meant, that after deletion of this regulatory unit, we should mainly detect background expression from a SigA (M17)-dependent promoter. To verify this, we constructed a bioreporter only containing the SigA binding site of P_{rpt} fused to the *lacZ* reporter construct ($P_{rpt\_onlySigA}$-*lacZ)*. The expression of $P_{rpt\_onlySigA}$-*lacZ* resembled the results seen for $P_{rpt\_Del14bpDS}$-*lacZ* and $P_{rpt\_Modi14bpDS}$-*lacZ*, thereby supporting the idea of a mechanism of repression enabling induction specificity (Figure 4A). To further confirm that the results observed for $P_{rpt\_Del14bpDS}$-*lacZ* and $P_{rpt\_Modi14bpDS}$-*lacZ* complied with a loss of induction specificity, we also conducted the experiment in a quantitative setup. For this purpose, we constructed $P_{rpt\_Del14bpDS}$-*luxABCDE*, in which the last 14 bp of the downstream end of the 5'UTR were likewise deleted. Matching the agar-based results, we could also detect a highly enhanced background expression for the $P_{rpt\_Del14bpDS}$-*luxABCDE* construct in the quantitative setup (Figure 5A), which corresponded to an approximately 68-fold higher signal after 210 min compared to P_{rpt}-*luxABCDE*. Furthermore, the signal emitted by $P_{rpt\_Del14bpDS}$-*luxABCDE* could not be raised above that already high value by any of the applied antibiotics (Figure 5B; for induction specificity of the unmodified construct P_{rpt}-*luxABCDE* compare Figure 2). The induction level of P_{rpt}-*luxABCDE* upon treatment with RNA synthesis inhibitors, reached RLU values comparable to the deregulated construct $P_{rpt\_Del14bpDS}$-*luxABCDE* (Figure 5C).

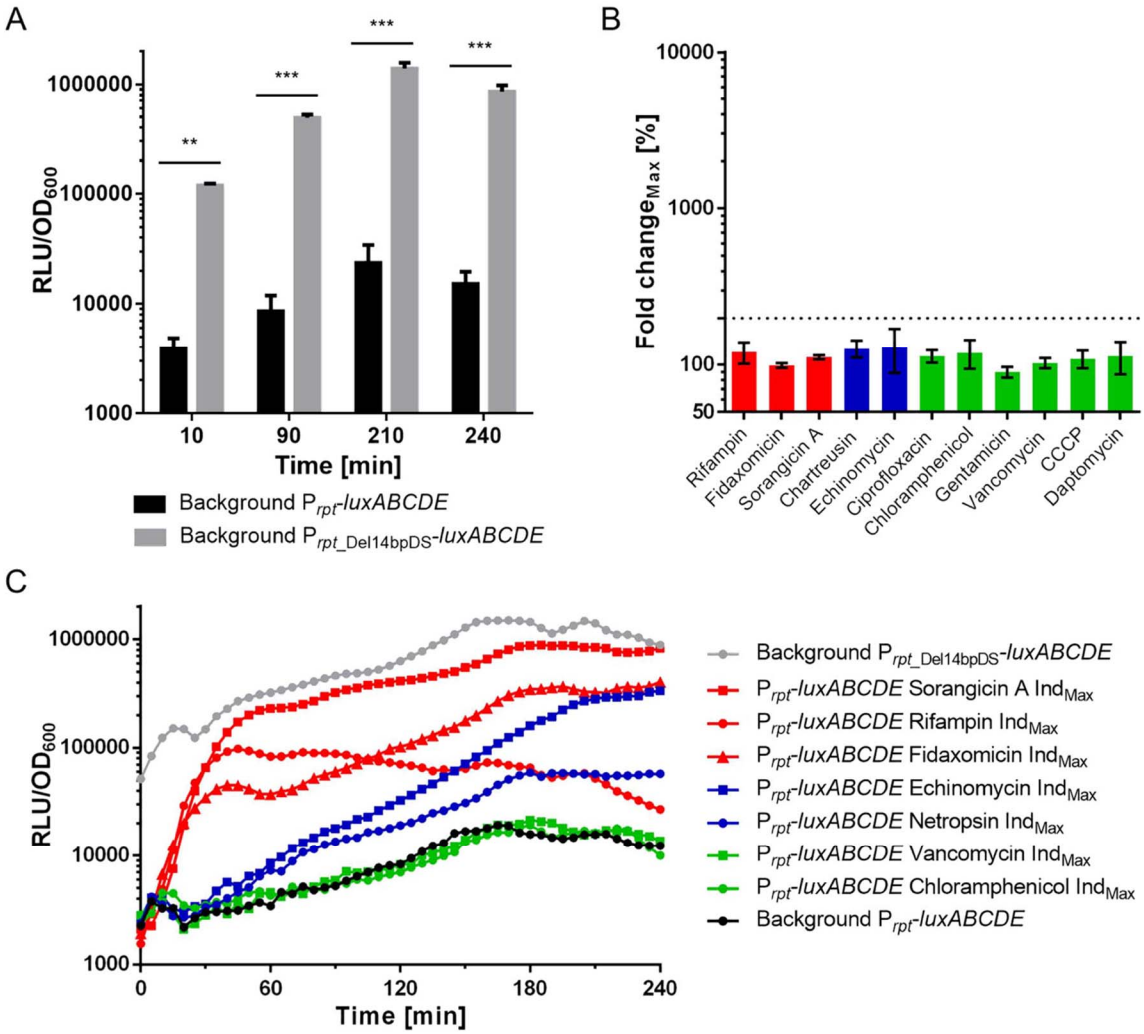

Figure 5. Expression level and induction specificity of $P_{rpt\_Del14bpDS}$-*luxABCDE*. (A) Background expression in relation to OD_{600} of the untreated bioreporter strains P_{rpt}-*luxABCDE* and $P_{rpt\_Del14bpDS}$-*luxABCDE* grown in BMM after stated incubation periods. Error bars indicate the standard deviation of the background luminescence signal measured in at least three biological replicates. Statistical significance was determined using unpaired Students t-test with Welch´s correction (ns, $P > 0.01$; *, $P \leq 0.01$; **, $P \leq 0.001$; ***, $P \leq 0.0001$). (B) Maximal fold change of $P_{rpt\_Del14bpDS}$-*luxABCDE* after antibiotic treatment. Direct RNAP-binding antibiotics and DNA-binding agents are marked in red and blue, respectively. Other antibiotics (meant as negative controls), with a primary MOA unrelated to RNA synthesis are marked in green. Depicted is the maximal fold change after 210 min of antibiotic treatment. Error bars show the standard deviation of the maximal fold change measured in three independent biological replicates. The dotted line indicates the induction threshold of 200 % that had been set on the basis of P_{rpt}-*luxABCDE*. In comparison to the unmodified P_{rpt}-*luxABCDE* construct (Figure 2), $P_{rpt\_Del14bpDS}$-*luxABCDE* could not be selectively induced by RNA synthesis inhibiting compounds. (C) Time course of luciferase expression in relation OD_{600} of the bioreporter strains (exemplary experiment from >3 independent repetitions). Background expression levels of P_{rpt}-*luxABCDE* (low background, black) and $P_{rpt\_Del14bpDS}$-*luxABCDE* (high background, grey) are correlated to the induction curves of P_{rpt}-*luxABCDE* treated with reference antibiotics (direct RNAP inhibitors (red), DNA-binding agents (blue), antibiotics that do not interfere with RNA synthesis (green)). Depicted are the antibiotic concentrations resulting in the maximal induction signal for the respective antibiotics: sorangicin A 4 µg/mL, rifampin 0.002 µg/mL, fidaxomicin 1 µg/mL, echinomycin 0.0156 µg/mL, netropsin 2 µg/mL, vancomycin 0.125 µg/mL, and chloramphenicol 0.125 µg/mL. All strains were grown in BMM.

Those results indicated that deletion of the 13 consensus nucleotides at the downstream promoter region of *rpt* yielded a constantly derepressed, constitutive SigA-regulated expression. In the presence of the 13 consensus nucleotides induction is repressed under unstressed growth conditions, while it can be specifically derepressed by RNA synthesis

inhibitors. A study of Bandow and colleagues discussed the observation that upon rifampin-dependent growth arrest the cells after some time became tolerant to the antibiotic and resumed growth (Bandow et al., 2002). The high-level expression of *rpt* upon RNA stress could constitute to such a quick adaptation mechanism in *B. subtilis*. Rifampin treatment initiates *rpt* expression which leads to enhanced levels of inactivated rifamycins that would again allow growth at later time points.

Induction specificity could not be correlated with a specific transcription factor binding to the 13 bp consensus sequence.

First, we investigated if the potential repressor sequence constitutes a target site for a specific transcription factor. For this purpose, a DNA affinity capturing assay (DACA) was conducted, which was combined with semi-quantitative MS to identify DNA-binding proteins. We used four different DNA fragments (Table S4) and compared the results to identify proteins, which potentially only bind to the fragment containing the 13 bp consensus sequence. Fragment 1 contained 200 bp of the P_{rpt} promoter region including the SigA (M17) binding site, the 5'UTR including the 13 bp consensus sequence, as well as the RBS employed in the bioreporter construct. Fragment 2 was shortened by 30 bp at the downstream end, thereby deleting the RBS and the 13 bp consensus sequence. Fragment 3 was further shortened downstream to a length of 126 bp. As a control to exclude unspecific DNA-binding proteins, we also included an *rpt*-unrelated promoter fragment of 200 bp of P_{yorB} (fragment 4), which has been previously suspected to be LexA-regulated (Au et al., 2005; Urban et al., 2007). For the four promoter fragments, 1228 different proteins were detected in semi-quantitative MS in at least one of three biological replicates. Approximately 1/3 of those proteins were detected in very low abundance and were excluded as they did not reproducibly show in all biological replicates. Most of the identified proteins were retained by all fragments, as they are known DNA-binding proteins, like the DNA topoisomerase subunits ParC or ParE, or constitute ubiquitous transcription proteins like the RNAP subunits RpoA, RpoB or RpoC. In some cases, fragments 2 and 3 showed generally weaker label-free quantification (LFQ) intensities in comparison to fragments 1 and 4, which might be caused by their overall smaller fragment size. We also detected non-DNA-binding proteins, that were rather copurified with other proteins or remnants of highly concentrated intracellular proteins, like the elongation factor G. We concentrated on proteins, that displayed elevated LFQ intensities for fragments 1-3 (fragments of P_{rpt}) in comparison to fragment 4 (fragment of P_{yorB}) and especially on such retained strongest by fragment 1. Nevertheless, we also followed up on proteins that could likewise be identified

for fragment 2 and/or fragment 3, as we could not fully exclude that the potential transcription factor might have an additional binding site that is still present in fragments 2 and 3, thereby allowing a weaker binding to DNA, without possessing full functionality. For the identification of the regulatory protein responsible for induction specificity, we integrated the bioreporter construct P_{rpt}-*lacZ* into the genome of the respective deletion strain of the identified DNA-binding protein. In the decisive knockout strain, we expected a deregulation of the bioreporter as had been noted for the deletion/modification of the 13 nucleotides on the downstream end of the 5'UTR of *rpt*. The control fragment 4 showed enhanced binding of 54 different proteins in comparison to fragments 1-3, but most importantly of the expected regulatory protein LexA. As proof of principle, we transformed the P_{yorB}-*lacZ* construct into the *B. subtilis* 168 Δ*lexA* deletion mutant. Figure S6 shows the highly increased background signal of *B. subtilis* 168 Δ*lexA amyE*::P_{yorB}-*lacZ* as well as the loss of induction specificity upon antibiotic treatment, comparable to the deregulation seen for $P_{rpt\_Del14bpDS}$-*lacZ* and $P_{rpt\_Modi14bpDS}$-*lacZ.* Therefore, the results confirmed the previously suspected SOS-dependent LexA regulation of *yorB* induction (Au et al., 2005; Urban et al., 2007) and further validated our strategy to identify regulatory proteins by monitoring expression of the bioreporter in a deletion mutant background. Of note, we could also detect further transcription factors (e.g., Xre or GamR (YbgA)) more prominently binding to P_{yorB} than to the P_{rpt} related fragments 1-3 (compare Table S6). However, the expression of P_{yorB}-*lacZ* in *B. subtilis* 168 Δ*gamR* had no influence on the bioreporters' background expression and induction specificity (Figure S6), showing that induction upon DNA stress is selectively conferred by LexA repression. Nevertheless, those additionally binding transcription factors might contribute to the regulation of *yorB* under different growth conditions and generally participate in the strong repression of *yorB* under unstressed growth conditions, as previously suspected by Urban and colleagues (Urban et al., 2007). For *rpt* regulation, identified 73 proteins that showed higher LFQ values for fragments 1-3 in comparison to fragment 4 (Table S5). Some could be excluded to specifically regulate *rpt* expression due to their described function (e.g., Noc or PriA), yielding a list of 45 final candidates, with 16 of them most prominently showing for fragment 1 (Table S7). We transformed the bioreporter construct P_{rpt}-*lacZ* in each of those deletion mutants and monitored the general background expression as well as the preservation of the induction specificity upon antibiotic treatment. The loss of none of those 45 proteins led to an unspecific deregulation of P_{rpt}-*lacZ* (Table S7) as has been seen for $P_{rpt\_Del14bpDS}$-*lacZ* and $P_{rpt\_Modi14bpDS}$-*lacZ* (Figure 4A). Some deletion mutants displayed a modulated background expression (e.g., Δ*ycnK* or Δ*iolR*), but maintained induction specificity for RNA synthesis inhibitors.

We also checked for paralogous proteins (Table S7), that might take over the function of the knocked-out gene and e.g., found the paralogous proteins AbrB and Abh as well as YxaF and LmrA, which had all been identified in the DACA. Generally, if they were responsible for the selective induction of *rpt* (and putatively *helD*) we would have expected even slight effects upon deletion of one of the paralogs as they often cannot fully compensate for each other (Strauch et al., 2007). Nevertheless, unequivocal exclusion of those transcriptional regulators would require the construction and validation of double mutants in further studies.

Even though we could sensitively detect and verify the repressor LexA binding to the *yorB* promoter region, thereby validating the method itself, we were unable to identify a transcription factor responsible for conferring induction specificity to P_{rpt}. The results left us with different options concerning the regulation of *rpt*: the transcription factor of interest might not be stable or dependent on a co-factor for DNA-binding, which is not present or unstable under our DACA experimental procedure, the trypsin-digest of the protein is not suitable for detection via MS analysis, the cell can fully compensate for the deletion of the respective transcription factor, or induction specificity of P_{rpt} is simply not conferred by transcription factor binding. However, although not solely responsible for the regulation of *rpt* under RNA stress inducing conditions, the detected transcription factors that bind to the *rpt* promoter region (Table S5 and Table S7) may still play a role in the regulation of *rpt* under other growth or stress conditions, as some of them displayed a modulation of the background expression.

Cis-encoded asRNA regulation may be responsible for induction specificity of P_{rpt} and P_{helD}.

As we could not find a regulator in the DACA conferring induction specificity, we hypothesized that the selective induction observed upon RNA stress might not be dependent on transcription factor binding. Furthermore, we were surprised to see that fragment 1 displayed approximately 10-fold higher LFQ values for SigA in comparison to fragment 3, although both fragments contained the SigA (M17) binding site of P_{rpt}. Interestingly, the opposite strand of the *rpt* promoter, covering the 5'UTR of *rpt* only partially, encodes a previously annotated small RNA (sRNA) called ncr1015 (120 bp) or S708 (628 bp), depending on the study (Irnov et al., 2010; Nicolas et al., 2012). Figure 6A shows, that although deletion of the 13 conserved nucleotides that led to the loss of induction specificity ($P_{rpt\_Del14bpDS}$-*lacZ* construct) did not directly modify the complementary sRNA itself, it most likely interfered with its expression, as it overlapped with and thereby deleted the -35 region

of the SigA (M14) binding site of ncr1015/S708 (Nicolas et al., 2012). This additional binding site on the complementary strand might also explain the elevated levels of sigma factor (SigA) and different RNAP subunits (RpoA, RpoB, and RpoC) binding to fragment 1 in the DACA. Looking at the supplemental data provided by Nicolas and colleagues, we could also identify a SigA (M19) binding site on the opposite strand of the *helD* promoter (Figure 6A). Furthermore, transcript levels show a slight upregulatory shift in proximity of this chromosomal location for several growth conditions (Nicolas et al., 2012; Zhu and Stülke, 2017). Again the -35 region of the SigA (M19) binding site of the proposed complementary sRNA of *helD* overlapped with the conserved 13 nucleotides identified P_{helD} (Figure 6A). A deletion or modification of the 13 nucleotides would therefore simultaneously change the -35 region of the complementary SigA binding site in both promoters, potentially hindering SigA from binding and thereby suppressing expression of the sRNA.

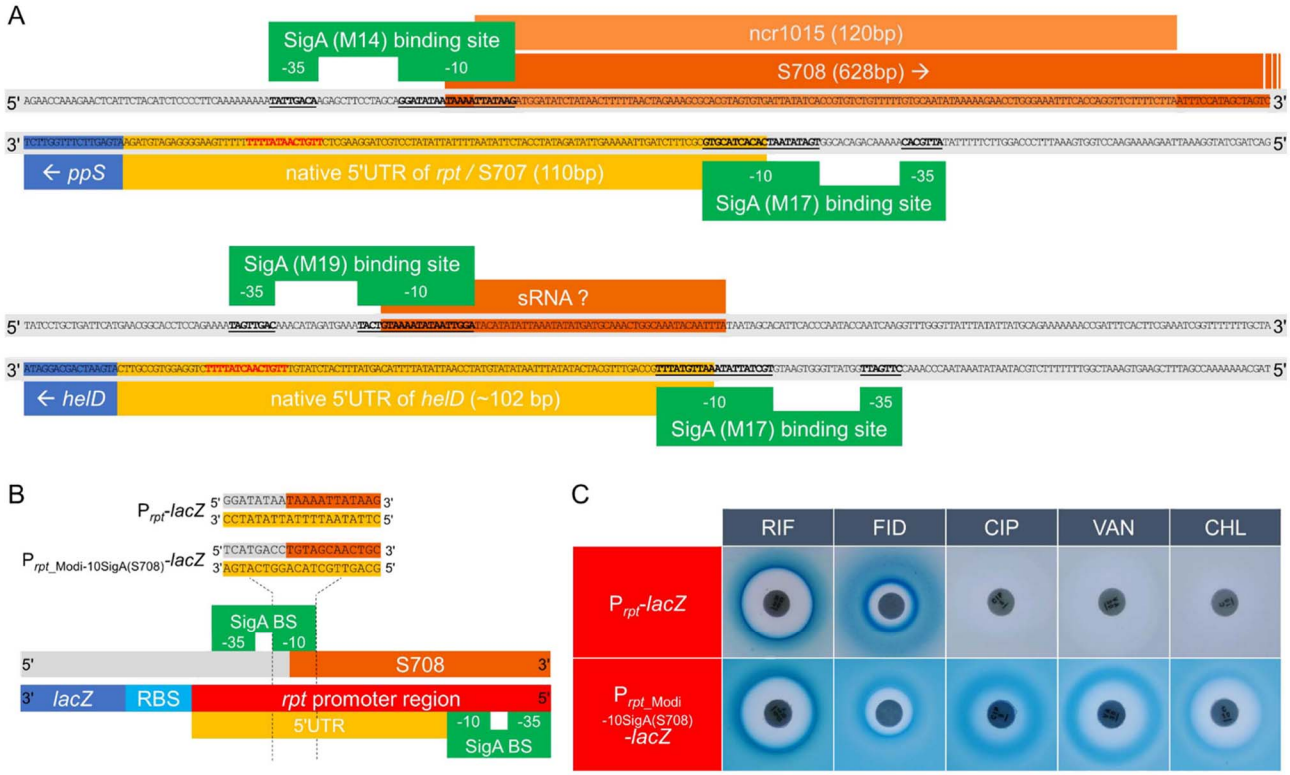

Figure 6. Overview of the regulatory important promoter regions of *rpt* and *helD*. (A) Schematic view of the native promoter regions of *rpt* and *helD*, including the 5'UTR (yellow) and the complementary sRNA. S708 and the proposed complementary sRNA of *helD* have been chosen on the basis of previously conducted transcriptomic data (both marked in orange) (Nicolas et al., 2012; Zhu and Stülke, 2017). Ncr1015, which is alternatively described to S708, is highlighted in light orange (Irnov et al., 2010). The sequence of the SigA binding sites is indicated by the underlined bases in bold. The conserved 13 nucleotides in the *helD* and *rpt* promoter are highlighted in red. (B) Schematic view of the modification of the -10 region of the SigA binding site of ncr1015/S708, which likewise changed the nucleotide sequence of the *rpt* 5'UTR. (C) Induction of $P_{rpt\_Modi\text{-}10regionSigA(S708)}$-*lacZ* in comparison to the unmodified bioreporter P_{rpt}-*lacZ*. The modified construct showed enhanced background signal and loss of antibiotic induction specificity. Filter discs with the respective antibiotic amount were directly placed on the bioreporter containing Belitzky minimal soft agar. Antibiotics were used in the following amounts: rifampin (RIF) 30 µg, fidaxomicin (FID) 8 µg, ciprofloxacin (CIP) 5 µg, vancomycin (VAN) 30 µg, and chloramphenicol (CHL) 10 µg.

We hypothesized that by abolishing the expression of the complementary sRNA, the expression of *rpt* (or *helD*) is no longer repressed, which would lead to the observed enhanced background expression and deregulation of induction specificity. This kind of sRNA regulation constitutes a *cis*-encoded antisense RNA (asRNA) regulation. Generally, *cis*-encoded RNA regulation is suspected to be quite commonly employed by Firmicutes (Irnov et al., 2010). To confirm the idea of a *cis*-encoded asRNA regulation, we kept the -35 region of the SigA (M14) binding site of ncr1015/S708 intact, but modified its -10 region ($P_{rpt\_Modi\text{-}10SigA(S708)}$-*lacZ*) (Figure 6B). Indeed, a modification of the -10 region of the complementary sRNA also led to loss of induction specificity (Figure 6C), supporting the idea that specific derepression of the SigA-dependent *rpt* expression upon RNA stress is regulated by the complementary *cis*-encoded asRNA. However, those nucleotide substitutions of course also inevitably modified the complementary 5'UTR of *rpt.* Figure S5C displays the 5'UTR of *rpt* upon modification of the -10 region of the SigA binding site of ncr1015/S708. Although the impact of such variation in the 5'UTR are difficult to predict, the even lowered minimum free energy and the similarly structured RBS of the modified 5'UTR in comparison to the unmodified 5'UTR of P_{rpt}-*lacZ* (Figure S5B), rather contradict the idea of a regulation via 5'UTR stability and structure.

Regulation via a *cis*-encoded asRNA is predominantly implemented by four main mechanisms: attenuation of translation, alteration of target RNA stability, transcriptional interference, and attenuation of transcription (transcription termination) (Georg and Hess, 2011; Mars et al., 2016). Translation attenuation regulates gene expression by controlling mRNA secondary structure and thereby the ribosomal accessibility of the RBS for subsequent translation. As transcriptome studies already revealed a 100-fold difference in *rpt* and *helD* mRNA levels between rifampin-treated and untreated *B. subtilis* cells (Freiberg et al., 2006), we rather exclude that a translation attenuation mechanism is responsible for main regulation of *rpt* and *helD*, but of course cannot rule out an additional fine-tuning.
The impact of the remaining mechanisms on P_{rpt} and P_{helD} regulation remains elusive, while none of them can be excluded with certainty. Alteration of target mRNA stability can e.g., be modulated by RNA-binding proteins or achieved by asRNA-mediated regulation of nuclease-dependent degradation (Brantl, 2007; Stazic et al., 2011). Hfq is a well described RNA-binding chaperone that was shown to strongly effect sRNA stability and structure in many Gram-negative bacteria (Fantappiè et al., 2009; dos Santos et al., 2019). Nevertheless, it does not seem to participate in *rpt* regulation, as the expression of P_{rpt}-*lacZ* in the knockout strain *B. subtilis* 168 Δ*ymaH,* which is devoid of the *B. subtilis* Hfq

homolog, did not show any difference in background signal or induction specificity. Of note, recent studies indicate that Hfq in *B. subtilis* does not play a central role in post-transcriptional regulation as has been observed for proteobacterial species (Rochat et al., 2015). Concerning nuclease accessibility, a study from Durand and colleagues demonstrated that upon depletion of the major and essential 5'-3' exoribonuclease RNase J1 (RnjA), mRNAs of *helD* and *rpt* were found 10-fold and 2-fold more abundant in the *B. subtilis* cell, respectively (Durand et al., 2012). Hence, RnjA could indeed play a role in degradation of the *rpt* and *helD* mRNAs or their proposed regulatory asRNAs. In contrast, the elevated mRNA levels upon RnjA depletion might also be caused by RnjAs ability to resolve stalled RNAP complexes upon collision (Šiková et al., 2020), a mechanism that might generally trigger the stress response leading to *rpt* and *helD* expression (compare section "*helD* and *rpt* are commonly induced upon RNAP stalling").

The expression of *rpt* and *helD* could also be regulated by transcriptional interference. This process describes the mutual impairment of transcription by complementary expression of sense mRNA and *cis*-encoded asRNA, e.g., by promoter occlusion, sitting duck interference or RNAP collision mechanisms (Bordoy and Chatterjee, 2015; Brophy and Voigt, 2016). Furthermore, an asRNA transcription attenuation mechanism that influences transcription termination of the corresponding sense mRNA (Giangrossi et al., 2010) could contribute to the observed selective *rpt* and *helD* expression. Of note, both regulatory processes, transcriptional interference and transcription attenuation, might also potentially act cooperatively as has been seen for the virulence gene *icsA* of *Shigella flexneri* (Giangrossi et al., 2010). However, in order to fully resolve the molecular mechanism of the proposed antisense regulation of *rpt* and *helD* further studies are needed.

Conservation of the *rpt* promoter regions in different bacteria.

Having gained information about regulatory important promoter regions in *B. subtilis* we had a look at the promoter compositions of other *rpt* containing strains. Figure 7 shows a phylogenetic tree of the *rpt* gene, which could be confidently detected in Actinomycetales, Myxococcales, Clostridiales and Bacillales (protein identity > 0.5 (Kanehisa and Goto, 2000); conservation of the described rifamycin-binding sites (Stogios et al., 2016)). Looking at the regulatory aspect, we quickly identified the previously described palindromic rifamycin-associated element (RAE) in the promoter regions of some of the Actinomycetales (Spanogiannopoulos et al., 2014), which is indicated in Figure 7 by a blue star. Variations of this RAE motif with 1-2 nucleotide substitutions were displayed by a blue bordered star. Interestingly, minor variations of the RAE motif were also found in the promoter region of

some Myxococcales, hinting at a broader distribution of this regulatory element (Figure 7). For the regulation in Bacillales we started screening different *rpt* promoter regions for the conserved 13 bp regulatory sequence, which was indeed traceable in different species as indicated by the red star (Figure 7). The cross-species conservation of the regulatory sequence is depicted in a consensus motif in Figure S7.

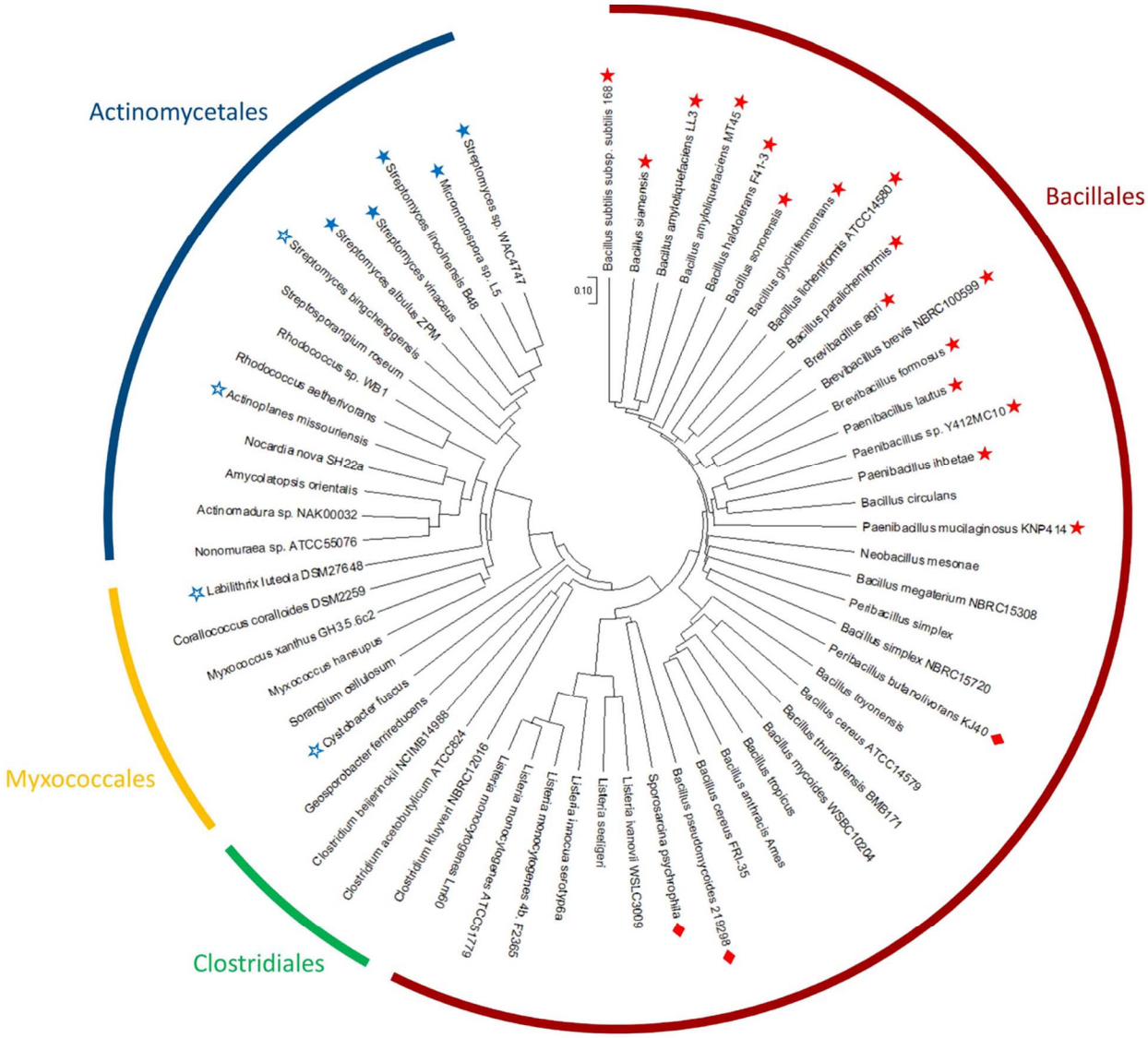

Figure 7. Phylogenic tree of different rifampin phosphotransferase encoding genes from various bacteria. A blue star indicates strains that contain the palindromic RAE motif in their promoter sequence, which has previously been described (Spanogiannopoulos et al., 2014). Strains that contain small modifications of the RAE motif are displayed by a blue bordered star. Bacterial strains that are highlighted by a red star all contain the conserved 13 nucleotides in their promoter region (the consensus motif is enclosed in Figure S7), that were shown to regulate induction specificity of *rpt* and *helD*. A red diamond marks strains that possess a potential variation of this consensus motif. Phylogenetic analysis was conducted with MEGA X using the Maximum Likelihood approach and Jones-Taylor-Thornton matrix-based model (Jones et al., 1992; Kumar et al., 2018), while all positions of the alignment of different rifampin phosphotransferases containing gaps and missing data were eliminated. Accession numbers of all strains used for the construction of the phylogenetic tree are listed in Table S8.

As this region contained the -35 region of the SigA binding site of ncr1015/S708 on the complementary strand in *B. subtilis*, the cross-species conservation might underline the important regulatory function of this region. Looking at the genomic locus of *rpt* in these 13 bp consensus motif containing Bacillales, one could quickly notice its divergent localization in the chromosome with a broad variety of different upstream and downstream located genes in different species. However, an alignment of the promoter regions revealed a conserved promoter region of ~200 bp (Figure S8). The alignment showed a high conservation especially in regions that were previously described to potentially possess regulatory functions: the SigA binding site and the RBS of P_{rpt}, the SigA binding site of the asRNA ncr1015/S708 (containing the conserved 13 bp motif of P_{rpt}), and a potential intrinsic terminator structure of the ncr1015/S708 *cis*-encoded asRNA (Figure S8) (Irnov et al., 2010). The high conservation in different Bacillales hints at the regulatory importance of those regions and a potentially common mechanism of regulation. Furthermore, the broad distribution in different genomic loci speaks for an acquisition by horizontal gene transfer, as has been proposed by its *B. subtilis* location in the *P6* prophage-like region (Kunst et al., 1997; Rocha et al., 1999). Noteworthy, in the alignment of the remaining Bacillales that did not contain the 13 bp consensus sequence (e.g., *Bacillus cereus*, *Bacillus megaterium*, or *Bacillus mycoides*) we could identify highly conserved regions that might play a role in their *rpt* regulation, e.g., a perfectly conserved “TTAATTATA” motif, that was exclusively present in all analyzed Bacillales (including *Listeria*) devoid of the previously described consensus motif.

MATERIAL AND METHODS

Strains, plasmids, and culture conditions.

All strains used in this study are listed in Table S9. All bioreporter strains (including all promoter deletion mutants) were generated on the basis of the sporulation deficient *B. subtilis* 1S34 strain (Piggot, 1973). For the bioreporter expression in different knockout mutants we utilized strains of the *B. subtilis* 168 deletion library (Koo et al., 2017). The integrative plasmid pHJS105 was used for the transformation of the respective *lacZ* reporter constructs. pHJS105 integrates into the *amyE* locus and contains the antibiotic resistance marker spectinomycin (SPT) (Jahn et al., 2015). For the *luxABCDE* reporter constructs the vector pBS3Clux was used, which integrates into the *sacA* locus and confers resistance to chloramphenicol (CHL) (Radeck et al., 2013).All bioreporter strains were grown in lysogeny broth (LB) (1 % tryptone, 1 % NaCl and 0.5 % yeast extract) containing the respective antibiotic selection marker in the following final concentration: SPT [100 µg/mL], CHL [5 µg/mL]. For sub-cloning, the *E. coli* strains XL1 blue and XL10 gold were utilized for the construction and propagation of all plasmids with the exception for the *B. subtilis rpt* overexpression strains which were all sub-cloned using *E. coli* Turbo cells.

Recombinant plasmid construction.

The luciferase constructs pBS3Clux-P_{rpt}-*luxABCDE* and pBS3Clux-P_{helD}-*luxABCDE* were generated on the basis of plasmid pBS3Clux (Radeck et al., 2013). The restriction sites *Eco*RI and *Sal*I of the plasmid pBS3Clux were utilized to integrate the respective promoter regions (P_{rpt} or P_{helD}), which were amplified via PCR (Phusion® high-fidelity DNA polymerase (NEB)) from *B. subtilis* 1S34 genomic DNA, gel-purified and then integrated via Gibson assembly (NEBuilder® HiFi DNA assembly master mix (NEB)). For the construct $P_{rpt\_Del14bpDS}$-*luxABCDE* we amplified the plasmid pBS3Clux-P_{rpt}-*luxABCDE* using 5'-phosphorylated primers that bound upstream and downstream of the 14 bp consensus region (Phusion® high-fidelity DNA polymerase (NEB)). The gel-purified fragment was then ligated back-to-back using the T4 DNA ligase (Thermo Scientific). Primers used in this work are listed in Table S10. After transformation of chemically competent *E. coli* XL10 gold cells, transformants were selected on LB agar containing 100 µg/mL ampicillin overnight. Single colonies were inoculated in 5 mL LB (37 °C, 190 rpm). Subsequently, plasmids were isolated (GeneJET Plasmid Miniprep Kit (Thermo Scientific)), and sequence integrity was controlled by Sanger sequencing (LGC genomics GmbH). The plasmids were transferred into naturally competent *B. subtilis* 1S34 cells and selected on LB agar, containing 5 µg/mL of CHL. Integration into the *sacA* locus was confirmed via PCR. Furthermore, the integrated

sequence was amplified via PCR (DreamTaq polymerase (Thermo scientific)), purified (Monarch PCR & DNA Cleanup Kit (NEB)) and subsequently confirmed by Sanger sequencing. The luciferase construct pHT304-P_{rpt}-*luc* was constructed on the bases of pHT304-P_{helD}-luc. After digestion of pHT304-P_{helD}-*luc* with *Kpn*I and *Pst*I, the vector was gel-purified. The insert was amplified via PCR (Phusion® high-fidelity DNA polymerase (NEB)) from *B. subtilis* genomic DNA, purified and ligated into the vector via Gibson assembly (NEBuilder® HiFi DNA assembly master mix (NEB)). Primers are listed in Table S10. After transformation of chemically competent *E. coli* XL1 blue cells, transformants were selected on LB agar containing 100 µg/mL ampicillin overnight. Single colonies were inoculated in 5 mL LB and incubated overnight (37 °C, 190 rpm), plasmids were isolated (GeneJET Plasmid Miniprep Kit (Thermo Scientific)) and controlled via Sanger sequencing (LGC genomics GmbH). After verification, the non-integrative plasmid was transformed into naturally competent *B. subtilis* 1S34 cells.

The plasmid of the *rpt* overexpression strain *E. coli* XL1 blue pBS2E-P_{Spac}-S707-*rpt* was constructed on the basis of pBS2E. For this, the pBS2E backbone was amplified via PCR (Phusion® high-fidelity DNA polymerase (NEB)) and purified via an agarose gel. The S707-*rpt* insert was amplified via PCR (Phusion® high-fidelity DNA polymerase (NEB)) from *B. subtilis* 1S34 genomic DNA, gel-purified and integrated using Gibson assembly (NEBuilder® HiFi DNA assembly master mix (NEB)). Primers are listed in Table S10. After transformation of chemically competent *E. coli* XL1 blue cells, transformants were selected on LB agar containing 100 µg/mL ampicillin overnight. Single colonies were inoculated in 5 mL LB and incubated overnight (37 °C, 190 rpm). Plasmids were isolated (GeneJET Plasmid Miniprep Kit (Thermo Scientific)), and Sanger sequencing (LGC genomics GmbH) was used to verify the sequence integrity.

For the construction of the *B. subtilis rpt* overexpression strain the plasmid pAPNC-mCherry was used. After digestion with *Sal*I and *Eco*RI the backbone of the plasmid was gel-purified. The insert S707-*rpt* was amplified from *B. subtilis* 1S34 genomic DNA, purified and then assembled using the Gibson cloning method (NEBuilder® HiFi DNA assembly master mix (NEB)). The respective primers can be found in Table S10. After transformation of chemically competent *E. coli* Turbo cells, transformants were selected on LB agar containing 100 µg/mL ampicillin overnight. Single colonies were inoculated in 5 mL LB containing the resistance marker and incubated overnight (37 °C, 190 rpm). Plasmids were isolated (GeneJET Plasmid Miniprep Kit (Thermo Scientific)), verified by Sanger sequencing (LGC genomics GmbH), transferred into competent *B. subtilis* 168 Δ*rpt* cells and selected on LB agar, containing 5 µg/mL of CHL. Integration into the *aprE* locus

was confirmed by PCR. The sequence integrity was confirmed via PCR (DreamTaq polymerase (Thermo scientific)) and subsequent Sanger sequencing of the amplificated fragments.

All P_{rpt} and P_{helD} promoter deletion constructs (except for pHJS105-$P_{rpt\_Modi14bpDS}$-*lacZ*, pHJS105-$P_{rpt\_onlySigA}$-*lacZ and* pHJS105-$P_{rpt\_Modi\text{-}10SigA(S708)}$-*lacZ*) were constructed similarly. The restriction sites *Sph*I and *Kpn*I of the plasmid pHJS105-P_{rpt}-*lacZ* (Wex et al., 2021) were used to exchange the P_{rpt} promoter for the respective promoter regions (P_{rpt_123bp}, P_{rpt_108bp}, $P_{rpt\_Del14bpDS}$, P_{helD_120bp}, P_{helD_113bp} and $P_{helD\_Del15bpDS}$), which were amplified via PCR (DreamTaq DNA polymerase (Thermo Scientific)) from *B. subtilis* 1S34 genomic DNA, gel-purified and then integrated via Gibson assembly (NEBuilder® HiFi DNA assembly master mix (NEB)). For the constructs pHJS105-$P_{rpt\_Modi14bpDS}$-*lacZ* and pHJS105-$P_{rpt\_Modi\text{-}10SigA(S708)}$-*lacZ* we amplified the entire plasmid pHJS105-P_{rpt_123bp}-*lacZ* using 5'-phosphorylated primers that contained the respective modification (Phusion® high-fidelity DNA polymerase (NEB)). The gel-purified fragment was then ligated back-to-back using the T4 DNA ligase (Thermo Scientific). For pHJS105-$P_{rpt\_onlySigA}$-*lacZ* we amplified two fragments of pHJS105- P_{rpt_123bp} -*lacZ,* thereby only maintaining the SigA binding site of the promoter. The fragments were gel-purified and then merged via Gibson assembly (NEBuilder® HiFi DNA assembly master mix (NEB)). All Primers are listed in Table S10. After transformation of chemically competent *E. coli* XL1 blue- or E. coli XL10 gold cells, transformants were selected on LB agar containing 100 µg/mL ampicillin overnight. Single colonies were inoculated in 5 mL LB (37 °C, 190 rpm). After overnight incubation plasmids were isolated (GeneJET Plasmid Miniprep Kit (Thermo Scientific)), and verified by Sanger sequencing (LGC genomics GmbH). The plasmids were transferred into competent *B. subtilis* 1S34 cells and selected on LB agar, containing 100 µg/mL of SPT. Integration into the *amyE* locus was investigated by streaking single colonies on starch containing agar (0.3 % meat extract, 1 % starch, 1.2 % agar). Successful transformants were unable to metabolize the starch, which was detectable after iodine staining (3.3 % iodine, 6.7 % potassium iodide). Furthermore, the integrated sequence was controlled by PCR (DreamTaq polymerase (Thermo scientific)) and purified PCR products (Monarch PCR & DNA Cleanup Kit (NEB)) were again confirmed via Sanger sequencing.

Agar-based bioreporter assay.

The method of the agar-based bioreporter assay has previously been described in detail (Wex et al., 2021). In this study, the bioreporters P_{helD}-*lacZ* and P_{yorB}-*lacZ* have additionally been tested in Belitzky minimal soft agar (Stülke et al., 1993) for better comparability (Figure S2).

For all *B. subtilis* 168 knockout strains that were tested for selective pHJS105- P_{rpt}-*lacZ* or pHJS105- P_{yorB}-*lacZ* induction in the agar-based bioreporter assay we applied the conditions previously described for the *B. subtilis* 1S34 bioreporter constructs (Wex et al., 2021).

In the promoter studies, all deleted or modified P_{rpt} constructs have been tested in Belitzky minimal soft agar under the same conditions described for P_{rpt}-*lacZ.* Promoter deletion constructs of *helD* were all tested in LB soft agar, thereby applying the same conditions as previously published for P_{helD} (Urban et al., 2007; Wex et al., 2021).

Luciferase-based liquid bioreporter assay.

The liquid bioreporter assay for all *P. luminescens* luciferase (*luxABCDE*)-based constructs in this study was conducted in BMM. Overnight cultures were diluted to an OD_{600} of 0.05 and re-grown to an OD_{600} of 0.9. Cells were diluted to an OD_{600} of 0.02. In parallel an antibiotic dilution series was conducted in each lane of a white 96-well microtiter plate (MTP) with transparent, flat bottom (A1-A11, B1-B11,…H1-H11) using 60 µL BMM. Antibiotics were used in the following concentration ranges: rifampin 0.0005-0.5 µg/mL, rifabutin 0.0009-1 µg/mL, fidaxomicin 0.0156-16 µg/mL, sorangicin A 0.0313-32 µg/mL, corallopyronin A 0.0313-32 µg/mL, streptovaricin 0.0019-2 µg/mL, streptolydigin 0.125-128 µg/mL, chartreusin 0.0313-32 µg/mL, echinomycin 0.0002-0.25 µg/mL, netropsin 0.0156-16 µg/mL, actinomycin D 0.0078-8 µg/mL, mithramycin 0.0039-4 µg/mL, mitomycin C 0.0078-8 µg/mL, doxorubicin 0.0078-8 µg/mL, phleomycin 0.0156-16 µg/mL, 5'-fluorouracil 0.0156-16 µg/mL, ciprofloxacin 0.0078-8 µg/mL, chloramphenicol 0.0313-32 µg/mL, gentamicin 0.0039-4 µg/mL, ampicillin 0.0156-16 µg/mL, vancomycin 0.0078-8 µg/mL, CCCP 0.0078-8 µg/mL, daptomycin 0.0313-32 µg/mL, triclosan 0.0019-2 µg/mL. The last column of the MTP contained only 60 µL of BMM with no antibiotic added, to serve as growth control (background luciferase production). The MTP plate was pre-warmed at 37 ºC before addition of the bioreporter strain. 60 µL of the *B. subtilis* bioreporter cell suspension (OD_{600} of 0.02) were added to each well of the MTP. The MTP was immediately incubated at 37 ºC in the Spark® multimode microplate reader (Tecan). Luminescence as well as OD_{600} measurements were performed automatically every 5 min for 16-20 h. The firefly luciferase (*luc*)-based construct pHT304-P_{rpt}-*luc* was tested as

described for before for other *luc*-based bioreporter constructs (Urban et al., 2007). It was grown in BMM, and induction was investigated after 90 and 210 min of incubation with the antibiotic.

Minimal inhibitory concentration (MIC) determination of single deletion mutants.

MIC was determined following the Clinical and Laboratory Standards Institute (CLSI) guidelines with several exceptions (Patel et al., 2015). The *B. subtilis* 168 knockout strains Δ*amyE*, Δ*rpt*, Δ*helD* and Δ*rpoE* were grown overnight on LB-agar plates. Of each strain 3-5 colonies were thoroughly resuspended in 0.9 % NaCl and the suspensions were adjusted to an OD_{600} of 0.1. All strains were further diluted in BMM to achieve an inoculum of 1 x 10^6 colony forming units per mL (CFU/mL). In parallel an antibiotic dilution series was conducted in lanes B-G (e.g., B2-B10, C2-C10 etc.) of a transparent, flat bottom 96-well MTP using 50 µL BMM. Column 11 comprised 100 µL of the sterile control (BMM but no antibiotic and no cells) (B11, C11, D11) as well as 50 µL of the growth control (BMM but no antibiotic) (E11, F11, G11). 50 µL of the previously diluted *B. subtilis* cells (1 x 10^6 CFU/mL) were added to each well of the prepared MTP, except for the sterile controls. The MTP was incubated under shaking conditions at 37 ºC in the microplate reader Tecan infinite M200. MIC was determined after 20 h of incubation. For each experiment CFU determinations were performed to control the initial inoculum.

MIC determination of S707-*rpt* overexpression strains.

For the MIC determination of the overexpression mutants (*E. coli* XL1 blue pBS2E-P_{Spac}-S707-*rpt* and *B. subtilis* 168 Δ*rpt aprE*::P_{Spac}-S707-*rpt* overnight cultures of the respective strains were used. *E. coli* XL1 blue pBS2E-P_{Spac} was used as unrelated control, which contained the same high-copy plasmid as the overexpression strain, but no integrated *rpt* gene. For the *B. subtilis* overexpression strain, we used two different control strains: *B. subtilis* 168 Δ*amyE*, which still possessed the native *rpt* gene and *B. subtilis* 168 Δ*rpt aprE*::P_{Spac}, which was devoid of the native *rpt* gene and only contained the integrative plasmid (without *rpt* gene sequence). The overnight cultures were diluted to an OD_{600} of 0.05 in LB containing the selection marker and parallelly in LB containing the selection marker and 1 mM IPTG and grown to an OD_{600} of 1. Cells were diluted to 1 x 10^6 CFU/mL in LB. In parallel a rifampin dilution series was conducted in lanes B-G (e.g., B2-B10, C2-C10 etc.) of a transparent, round bottom 96-well MTP using 50 µL LB (containing the selection marker) in lanes B, D, F and 50 µL LB (containing the selection marker and 2 mM IPTG) in lanes C, E, G. Column 11 of the MTP comprised 100 µL of the sterile control

(LB but no antibiotic and no cells) (B11, C11) as well as 50 µL of the growth control with (D11, E11) and without IPTG (LB but no antibiotic ± IPTG) (F11, G11). 50 µL of the previously diluted (1 x 10^6 CFU/mL) bacterial cells were added to each well of the prepared MTP, except for the sterile control. The MTP was incubated at 37 ºC and MIC results were determined after 20 h of incubation. For each experiment CFU determinations were performed to control the initial inoculum.

Detection of rifampin modifications via HPLC-MS analysis.

E. coli XL1 blue pBS2E-P_{Spac} and *E. coli* XL1 blue pBS2E-P_{Spac}-S707-*rpt* were inoculated in 20 mL LB containing rifampin [100 µg/mL] and IPTG [1 mM] and grown for 24 h (190 rpm, 37 ºC). Supernatants of the induced cultures were subsequently investigated via HPLC-MS analysis. HPLC-MS was performed using an Agilent 1200 series chromatography system (binary pump, high performance autosampler, column thermostat, diode array detector (DAD)) coupled with an LC/MSD Ultra Trap System XCT 6330.The sample (2.5 µL) was injected on a Nucleosil 100 C18 column (3 µm, 100 x 2 mm) fitted with a precolumn (3 µm, 10 x 2 mm) (Dr. Maisch GmbH, Ammerbuch) at a flow rate of 400 mL/min and a linear gradient from 10 % solvent A (0.1 % formic acid in water) to 100 % solvent B (0.06 % formic acid in acetonitrile) over 15 min at 40°C.

DNA affinity capturing assay (DACA).

For the DACA assay we amplified and parallelly biotinylated 4 different DNA fragments from *B. subtilis* 1S34 genomic DNA via PCR (Phusion® high-fidelity DNA polymerase (NEB)). All primers are listed in Table S10. Fragments were purified using the Monarch® PCR and DNA Cleanup Kit (NEB). 75 µg of each biotinylated promoter fragment was bound to 5 mg of the Dynabeads® M-280 Streptavidin (Invitrogen), following the manufacturers' instructions. The biotinylated beads were stored in TGED buffer (20 mM Tris-HCL, 1 mM EDTA, 100 mM NaCl, 0.1 % Triton-X-100, 10 % glycerol, pH 7.5) at 4 ºC. For the generation of the *B. subtilis* whole cell protein extract, 5 L of LB were inoculated with an overnight culture of *B. subtilis* 1S34 to an OD_{600} of 0.05 and grown to an OD_{600} of 1.8 (37 ºC, 170 rpm). Cells were harvested (20 min, 4000 g, 4 ºC) and resuspended in 25 mL of TGED cell lysis buffer (TGED buffer was mixed with 1 mM DTT and the proteinase inhibitor mix (cOmplete™, EDTA-free Protease Inhibitor Cocktail Tablets (Roche)), just before use). The cell suspension was homogenized using 3 cycles (6400 rpm for 20 s) of Precellys®, while the suspension was incubated for 3 min on ice between the cycles. Cell debris were sedimented via centrifugation (10 min, 50000 g, 4 ºC). The supernatant was collected and cooled on ice

before it was subsequently used in the protein binding studies of the 4 promoter fragments. For protein pulldown 4 mL of freshly prepared whole cell protein extract was mixed with 100 µg/mL salmon sperm DNA in a 50 mL falcon tube and incubated for 15 min on ice. The 5 mg of promoter fragment-coupled beads of one fragment were added to the protein whole cell extract and incubated for 45 min on ice, weakly inverting. Beads were purified in a stepwise procedure, at a time transferring 1.6 mL of the suspension to a 2 mL Eppendorf tube and separating the magnetic beads by binding them with a magnet to one side of the Eppendorf tube (binding took approximately 4 min) and removing the supernatant. Beads were washed in 3 steps: with 500 µL of TGED buffer, 400 µL TGED containing salmon sperm [100 µg/mL], and again using 500 µL of TGED buffer. Elution of the specifically bound proteins was carried out by washing two times with 350 µL TGED elution buffer (20 mM Tris-HCL, 1 mM EDTA, 2 M NaCl, 0.1 % Triton-X-100, 10 % glycerol, pH 7.5). The supernatant was collected and pooled. Proteins were precipitated with trichloroacetic acid (175 µL per 700 µL of supernatant) by incubating them for 30 min on ice. Precipitated proteins were pelleted via centrifugation (10 min, 16800 g, 4 ºC), the supernatant was removed, and pellets were two times washed with pure acetone. Pellets were subsequently air dried and stored at -70 ºC. After the elution step, the Dynabeads were recovered by washing them 2 times with TGED elution buffer, and 2 times with TGED buffer before storing them at 4 ºC in TGED buffer.

NanoLC-MS/MS analysis and data processing

Analysis of protein eluates was performed as previously described (Bekiesch et al., 2016), with slight modifications: Extracted and desalted peptides were run on an Easy-nLC 1200 system coupled to a Q Exactive HF mass spectrometer (both Thermo Fisher Scientific) as described elsewhere (Kliza et al., 2017) using a 57 minute segmented gradient of 10-33-50-90 % of HPLC solvent B (80 % acetonitrile in 0.1 % formic acid) in HPLC solvent A (0.1 % formic acid) at a flow rate of 200 nl/min. The 7 most intense precursor ions were sequentially fragmented in each scan cycle using higher energy collisional dissociation (HCD) fragmentation. In all measurements, sequenced precursor masses were excluded from further selection for 30 s. The target values for MS/MS fragmentation were 10^5 charges and $3x10^6$ charges for the MS scan. Each sample was run in technical duplicates.

Acquired MS spectra were processed with MaxQuant software package version 1.6.7.0 (Cox and Mann, 2008) with integrated Andromeda search engine (Cox et al., 2011). Database search was performed against a *B. subtilis* database obtained from Uniprot, containing 4,271 protein entries and 286 commonly observed contaminants. Endoprotease

trypsin was defined as protease with a maximum of two missed cleavages. Oxidation of methionine and N-terminal acetylation were specified as variable modifications, and carbamidomethylation on cysteine was set as fixed modification. Initial maximum allowed mass tolerance was set to 4.5 parts per million (ppm) for precursor ions and 20 ppm for fragment ions. Peptide, protein and modification site identifications were reported at a false discovery rate (FDR) of 0.01, estimated by the target-decoy approach (Elias and Gygi, 2007). The iBAQ (Intensity Based Absolute Quantification) and LFQ (Label-Free Quantification) algorithms were enabled, as was the “match between runs” option (Luber et al., 2010; Schwanhäusser et al., 2011).

REFERENCES

Adebali, O., Chiou, Y.-Y., Hu, J., Sancar, A., and Selby, C. P. (2017). Genome-wide transcription-coupled repair in *Escherichia coli* is mediated by the Mfd translocase. Proceedings of the National Academy of Sciences 114, E2116.

Ahluwalia, G. S., Grem, J. L., Hao, Z., and Cooney, D. A. (1990). Metabolism and action of amino acid analog anti-cancer agents. Pharmacology and Therapeutics 46, 243-271.

Artsimovitch, I., Seddon, J., and Sears, P. (2012). Fidaxomicin is an inhibitor of the initiation of bacterial RNA synthesis. Clinical Infectious Diseases 55 Suppl 2, S127-S131.

Au, N., Kuester-Schoeck, E., Mandava, V., Bothwell, L. E., Canny, S. P., Chachu, K., Colavito, S. A., Fuller, S. N., Groban, E. S., Hensley, L. A., et al. (2005). Genetic composition of the *Bacillus subtilis* SOS system. Journal of Bacteriology 187, 7655-7666.

Ayala, F. R., Bartolini, M., and Grau, R. (2020). The stress-responsive alternative sigma factor SigB of *Bacillus subtilis* and its relatives: An old friend with new functions. Frontiers in Microbiology 11.

Ayora, S., Rojo, F., Ogasawara, N., Nakai, S., and Alonso, J. C. (1996). The Mfd protein of *Bacillus subtilis*168 is involved in both transcription-coupled DNA repair and DNA recombination. Journal of Molecular Biology 256, 301-318.

Bandow, J. E., Brötz, H., and Hecker, M. (2002). Bacillus subtilis tolerance of moderate concentrations of rifampin involves the sigma(B)-dependent general and multiple stress response. Journal of Bacteriology 184, 459-467.

Bekiesch, P., Franz-Wachtel, M., Kulik, A., Brocker, M., Forchhammer, K., Gust, B., and Apel, A. K. (2016). DNA affinity capturing identifies new regulators of the heterologously expressed novobiocin gene cluster in *Streptomyces coelicolor* M512. Applied Microbiology and Biotechnology 100, 4495-509.

Belogurov, G. A., Vassylyeva, M. N., Sevostyanova, A., Appleman, J. R., Xiang, A. X., Lira, R., Webber, S. E., Klyuyev, S., Nudler, E., Artsimovitch, I., et al. (2009). Transcription inactivation through local refolding of the RNA polymerase structure. Nature 457, 332-335.

Bordoy, A. E., and Chatterjee, A. (2015). *Cis*-antisense transcription gives rise to tunable genetic switch behavior: a mathematical modeling approach. PLOS ONE 10, e0133873.

Brantl, S. (2007). Regulatory mechanisms employed by *cis*-encoded antisense RNAs. Current Opinion in Microbiology 10, 102-109.

Brillard, J., Jéhanno, I., Dargaignaratz, C., Barbosa, I., Ginies, C., Carlin, F., Fedhila, S., Nguyen-The, C., Broussolle, V., and Sanchis, V. (2010). Identification of *Bacillus cereus* genes specifically expressed during growth at low temperatures. Applied and Environmental Microbiology 76, 2562.

Brophy, J. A., and Voigt, C. A. (2016). Antisense transcription as a tool to tune gene expression. Molecular Systems Biology 12, 854.

Campbell, E. A., Korzheva, N., Mustaev, A., Murakami, K., Nair, S., Goldfarb, A., and Darst, S. A. (2001). Structural mechanism for rifampicin inhibition of bacterial RNA polymerase. Cell 104, 901-912.

Campbell, E. A., Pavlova, O., Zenkin, N., Leon, F., Irschik, H., Jansen, R., Severinov, K., and Darst, S. A. (2005). Structural, functional, and genetic analysis of sorangicin inhibition of bacterial RNA polymerase. The EMBO Journal 24, 674-682.

Cardenas, P. P., Gándara, C., and Alonso, J. C. (2014). DNA double strand break end-processing and RecA induce RecN expression levels in *Bacillus subtilis*. DNA Repair 14, 1-8.

Cox, J., and Mann, M. (2008). MaxQuant enables high peptide identification rates, individualized p.p.b.-range mass accuracies and proteome-wide protein quantification. Nature Biotechnology 26, 1367-1372.

Cox, J., Neuhauser, N., Michalski, A., Scheltema, R. A., Olsen, J. V., and Mann, M. (2011). Andromeda: A Peptide Search Engine Integrated into the MaxQuant Environment. Journal of Proteome Research 10, 1794-1805.

Delumeau, O., Lecointe, F., Muntel, J., Guillot, A., Guédon, E., Monnet, V., Hecker, M., Becher, D., Polard, P., and Noirot, P. (2011). The dynamic protein partnership of RNA polymerase in *Bacillus subtilis*. PROTEOMICS 11, 2992-3001.

Dos Santos, R. F., Arraiano, C. M., and Andrade, J. M. (2019). New molecular interactions broaden the functions of the RNA chaperone Hfq. Current Genetics 65, 1313-1319.

Durand, S., Gilet, L., Bessières, P., Nicolas, P., and Condon, C. (2012). Three essential ribonucleases-RNase Y, J1, and III-control the abundance of a majority of *Bacillus subtilis* mRNAs. PLOS Genetics 8, e1002520-e1002520.
Elias, J. E., and Gygi, S. P. (2007). Target-decoy search strategy for increased confidence in large-scale protein identifications by mass spectrometry. Nature Methods 4, 207-214.
Erb, I., González-Vallinas, J. R., Bussotti, G., Blanco, E., Eyras, E., and Notredame, C. (2012). Use of ChIP-Seq data for the design of a multiple promoter-alignment method. Nucleic Acids Research 40, e52-e52.
Esyunina, D., Agapov, A., and Kulbachinskiy, A. (2016). Regulation of transcriptional pausing through the secondary channel of RNA polymerase. Proceedings of the National Academy of Sciences 113, 201603531.
Fairman-Williams, M. E., Guenther, U.-P., and Jankowsky, E. (2010). SF1 and SF2 helicases: family matters. Current Opinion in Structural Biology 20, 313-324.
Fantappiè, L., Metruccio, M. M. E., Seib, K. L., Oriente, F., Cartocci, E., Ferlicca, F., Giuliani, M. M., Scarlato, V., and Delany, I. (2009). The RNA chaperone Hfq Is Involved in stress response and virulence in *Neisseria meningitidis* and is a pleiotropic regulator of protein expression. Infection and Immunity 77, 1842.
Floss, H. G., and Yu, T.-W. (2005). Rifamycin-Mode of action, resistance, and biosynthesis. Chemical Reviews 105, 621-632.
Freiberg, C., Brunner, N., Macko, L., and Fischer, H. P. (2006). Discovering antibiotics efficacy biomarkers: towards mechanism-specific high-content compound screening. Molecular and Cellular Proteomics.
Gause, G. G., Jr., Loshkareva, N. P., and Zbarsky, I. B. (1968). Effect of olivomycin and echinomycin on initiation and growth of RNA chains catalyzed by RNA polymerase. Biochimica Biophysica Acta 166, 752-4.
Georg, J., and Hess, W. R. (2011). *Cis*-antisense RNA, another level of gene regulation in bacteria. Microbiology and Molecular Biology Reviews 75, 286-300.
Giangrossi, M., Prosseda, G., Tran, C. N., Brandi, A., Colonna, B., and Falconi, M. (2010). A novel antisense RNA regulates at transcriptional level the virulence gene icsA of *Shigella flexneri*. Nucleic Acids Research 38, 3362-3375.
Giedroc, D. P. (2009). Hydrogen peroxide sensing in *Bacillus subtilis*: it is all about the (metallo)regulator. Molecular Microbiology 73, 1-4.
Gleckman, R., Blagg, N., and Joubert, D. W. (1981). Trimethoprim: mechanisms of action, antimicrobial activity, bacterial resistance, pharmacokinetics, adverse reactions, and therapeutic indications. Pharmacotherapy 1, 14-20.
Hamperl, S., and Cimprich, K. A. (2016). Conflict resolution in the genome: How transcription and replication make it work. Cell 167, 1455-1467.
Härtl, B., Wehrl, W., Wiegert, T., Homuth, G., and Schumann, W. (2001). Development of a new integration site within the *Bacillus subtilis* chromosome and construction of compatible expression cassettes. Journal of Bacteriology 183, 2696-2699.
Harvey, A. M., Batt, R. D., and Prichard, G. G. (1976). Inhibition of RNA synthesis in *Chlorella pyrenoidos*a and *Bacillus megaterium* by the pine-blight toxin, Dothistromin. Microbiology 95, 268-276.
Helmann, J. D. (2014). Specificity of metal sensing: iron and manganese homeostasis in *Bacillus subtilis*. The Journal of biological chemistry 289, 28112-28120.
Helmann, J. D., Wu, M. F. W., Kobel, P. A., Gamo, F.-J., Wilson, M., Morshedi, M. M., Navre, M., and Paddon, C. (2001). Global Transcriptional Response *Bacillus subtilis* to Heat Shock. Journal of Bacteriology 183, 7318.
Ho, M. X., Hudson, B. P., Das, K., Arnold, E., and Ebright, R. H. (2009). Structures of RNA polymerase-antibiotic complexes. Current Opinion in Structural Biology 19, 715-723.
Hollstein, U. (1974). Actinomycin. Chemistry and mechanism of action. Chemical Reviews 74, 625-652.
Huang, C. H., Prestayko, A. W., and Crooke, S. T. (1982). Bifunctional intercalation of antitumor antibiotics BBM-928A and echinomycin with deoxyribonucleic acid. Effects of intercalation on deoxyribonucleic acid degradative activity of bleomycin and phleomycin. Biochemistry 21, 3704-10.

Irnov, I., Sharma, C. M., Vogel, J., and Winkler, W. C. (2010). Identification of regulatory RNAs in *Bacillus subtilis*. Nucleic Acids Research 38, 6637-6651.
Jahn, N., Brantl, S., and Strahl, H. (2015). Against the mainstream: the membrane-associated type I toxin BsrG from *Bacillus subtilis* interferes with cell envelope biosynthesis without increasing membrane permeability. Molecular Microbiology 98, 651-666.
Jones, D. T., Taylor, W. R., and Thornton, J. M. (1992). The rapid generation of mutation data matrices from protein sequences. Computer Applications in the Biosciences 8, 275-82.
Juhas, M., and Ajioka, J. W. (2016). Integrative bacterial artificial chromosomes for DNA integration into the *Bacillus subtilis* chromosome. Journal of Microbiological Methods 125, 1-7.
Kanehisa, M., and Goto, S. (2000). KEGG: kyoto encyclopedia of genes and genomes. Nucleic Acids Research 28, 27-30.
Kaur, G., Kapoor, S., and Thakur, K. G. (2018). *Bacillus subtilis* HelD, an RNA polymerase interacting helicase, forms amyloid-like fibrils. Frontiers in Microbiology 9.
Kisker, C., Kuper, J., and Van Houten, B. (2013). Prokaryotic nucleotide excision repair. Cold Spring Harbor Perspectives in Biology 5, a012591-a012591.
Kliza, K., Taumer, C., Pinzuti, I., Franz-Wachtel, M., Kunzelmann, S., Stieglitz, B., Macek, B., and Husnjak, K. (2017). Internally tagged ubiquitin: a tool to identify linear polyubiquitin-modified proteins by mass spectrometry. Nature Methods 14, 504-512.
Koo, B.-M., Kritikos, G., Farelli, J. D., Todor, H., Tong, K., Kimsey, H., Wapinski, I., Galardini, M., Cabal, A., Peters, J. M., et al. (2017). Construction and analysis of two genome-scale deletion libraries for *Bacillus subtilis*. Cell systems 4, 291-305.e7.
Koteva, K., Cox, G., Kelso, J. K., Surette, M. D., Zubyk, H. L., Ejim, L., Stogios, P., Savchenko, A., Sørensen, D., and Wright, G. D. (2018). Rox, a Rifamycin Resistance Enzyme with an Unprecedented Mechanism of Action. Cell Chemical Biology 25, 403-412.e5.
Kouba, T., Koval', T., Sudzinová, P., Pospíšil, J., Brezovská, B., Hnilicová, J., Šanderová, H., Janoušková, M., Šiková, M., Halada, P., et al. (2020). Mycobacterial HelD is a nucleic acids-clearing factor for RNA polymerase. Nature Communications 11, 6419.
Kovaľ, T., Sudzinová, P., Perháčová, T., Trundová, M., Skálová, T., Fejfarová, K., Šanderová, H., Krásný, L., Dušková, J., and Dohnálek, J. (2019). Domain structure of HelD, an interaction partner of *Bacillus subtilis* RNA polymerase. FEBS Letters 593, 996-1005.
Kumar, S., Stecher, G., Li, M., Knyaz, C., and Tamura, K. (2018). MEGA X: Molecular Evolutionary Genetics Analysis across Computing Platforms. Molecular Biology and Evolution 35, 1547-1549.
Kunst, F., Ogasawara, N., Moszer, I., Albertini, A. M., Alloni, G., Azevedo, V., Bertero, M. G., Bessières, P., Bolotin, A., Borchert, S., et al. (1997). The complete genome sequence of the Gram-positive bacterium *Bacillus subtilis*. Nature 390, 249-256.
Lenhart, J. S., Schroeder, J. W., Walsh, B. W., and Simmons, L. A. (2012). DNA repair and genome maintenance in *Bacillus subtilis*. Microbiology and Molecular Biology Reviews 76, 530-564.
Lerner, E., Chung, S., Allen, B. L., Wang, S., Lee, J., Lu, S. W., Grimaud, L. W., Ingargiola, A., Michalet, X., Alhadid, Y., et al. (2016). Backtracked and paused transcription initiation intermediate of *Escherichia coli* RNA polymerase. Proceedings of the National Academy of Sciences 113, E6562.
Lin, W., Das, K., Degen, D., Mazumder, A., Duchi, D., Wang, D., Ebright, Y. W., Ebright, R. Y., Sineva, E., Gigliotti, M., et al. (2018). Structural basis of transcription inhibition by fidaxomicin (lipiarmycin A3). Molecular cell 70, 60-71.e15.
Luber, C. A., Cox, J., Lauterbach, H., Fancke, B., Selbach, M., Tschopp, J., Akira, S., Wiegand, M., Hochrein, H., O'keeffe, M., et al. (2010). Quantitative proteomics reveals subset-specific viral recognition in dendritic cells. Immunity 32, 279-89.
Lyer, S., Le, D., Park, B. R., and Kim, M. (2018). Distinct mechanisms coordinate transcription and translation under carbon and nitrogen starvation in *Escherichia coli*. Nature Microbiology 3, 741-748.
Mars, R. a. T., Nicolas, P., Denham, E. L., and Van Dijl, J. M. (2016). Regulatory RNAs in *Bacillus subtilis*: a Gram-positive perspective on bacterial RNA-mediated regulation of gene expression. Microbiology and Molecular Biology Reviews 80, 1029-1057.
Mccormick, N. E., and Jakeman, D. L. (2015). On the mechanism of phosphoenolpyruvate synthetase (PEPs) and its inhibition by sodium fluoride: potential magnesium and aluminum fluoride complexes of phosphoryl transfer. Biochemistry and Cell Biology 93, 236-40.

Meeske, A. J., Rodrigues, C. D. A., Brady, J., Lim, H. C., Bernhardt, T. G., and Rudner, D. Z. (2016). High-throughput genetic screens identify a large and diverse collection of new sporulation genes in *Bacillus subtilis*. PLOS Biology 14, e1002341-e1002341.

Merrikh, H., Zhang, Y., Grossman, A. D., and Wang, J. D. (2012). Replication-transcription conflicts in bacteria. Nature Reviews Microbiology 10, 449-458.

Mukhopadhyay, J., Das, K., Ismail, S., Koppstein, D., Jang, M., Hudson, B., Sarafianos, S., Tuske, S., Patel, J., Jansen, R., et al. (2008). The RNA polymerase "switch region" is a target for inhibitors. Cell 135, 295-307.

Newing, T. P., Oakley, A. J., Miller, M., Dawson, C. J., Brown, S. H. J., Bouwer, J. C., Tolun, G., and Lewis, P. J. (2020). Molecular basis for RNA polymerase-dependent transcription complex recycling by the helicase-like motor protein HelD. Nature Communications 11, 6420.

Nicolas, P., Mäder, U., Dervyn, E., Rochat, T., Leduc, A., Pigeonneau, N., Bidnenko, E., Marchadier, E., Hoebeke, M., Aymerich, S., et al. (2012). Condition-dependent transcriptome reveals high-level regulatory architecture in *Bacillus subtilis*. Science 335, 1103.

Patel, J. B., Cockerill, F. R., Bradford, P. A., Eliopoulos, G. M., Hindler, J. A., Jenkins, S. G., Lewis, J. S., Limbago, B., Miller, L. A., Nicolau, D. P., et al. (2015). Methods for dilution antimicrobial susceptibility tests for bacteria that grow aerobically (USA: Approved Standard - Tenth Edition, vol 35. Clinical and Laboratory Standards Institute.

Pei, H.-H., Hilal, T., Chen, Z. A., Huang, Y.-H., Gao, Y., Said, N., Loll, B., Rappsilber, J., Belogurov, G. A., Artsimovitch, I., et al. (2020). The δ subunit and NTPase HelD institute a two-pronged mechanism for RNA polymerase recycling. Nature Communications 11, 6418.

Piggot, P. J. (1973). Mapping of asporogenous mutations of *Bacillus subtilis*: a minimum estimate of the number of sporulation operons. Journal of Bacteriology 114, 1241-1253.

Radeck, J., Kraft, K., Bartels, J., Cikovic, T., Dürr, F., Emenegger, J., Kelterborn, S., Sauer, C., Fritz, G., Gebhard, S., et al. (2013). The Bacillus BioBrick Box: generation and evaluation of essential genetic building blocks for standardized work with *Bacillus subtilis*. Journal of Biological Engineering 7, 29-29.

Rasmussen, S., Nielsen, H. B., and Jarmer, H. (2009). The transcriptionally active regions in the genome of *Bacillus subtilis*. Molecular Microbiology 73, 1043-57.

Reich, E., and Goldberg, I. H. 1964. Actinomycin and Nucleic Acid Function. *In:* DAVIDSON, J. N. & COHN, W. E. (eds.) *Progress in Nucleic Acid Research and Molecular Biology.* Academic Press.

Reiter, H., Milewskiy, M., and Kelley, P. (1972). Mode of action of phleomycin on *Bacillus subtilis*. Journal of Bacteriology 111, 586-592.

Resnekov, O., Rutberg, L., and Von Gabain, A. (1990). Changes in the stability of specific mRNA species in response to growth stage in *Bacillus subtilis*. Proceedings of the National Academy of Sciences 87, 8355-8359.

Rocha, E. P., Danchin, A., and Viari, A. (1999). Analysis of long repeats in bacterial genomes reveals alternative evolutionary mechanisms in *Bacillus subtilis* and other competent prokaryotes. Molecular Biology and Evolution 16, 1219-30.

Rochat, T., Delumeau, O., Figueroa-Bossi, N., Noirot, P., Bossi, L., Dervyn, E., and Bouloc, P. (2015). Tracking the Elusive Function of *Bacillus subtilis* Hfq. PLOS ONE 10, e0124977-e0124977.

Sayers, E. W., Bolton, E. E., Brister, J. R., Canese, K., Chan, J., Comeau, D. C., Connor, R., Funk, K., Kelly, C., Kim, S., et al. (2022). Database resources of the national center for biotechnology information. Nucleic Acids Research 50, D20-d26.

Schwanhäusser, B., Busse, D., Li, N., Dittmar, G., Schuchhardt, J., Wolf, J., Chen, W., and Selbach, M. (2011). Global quantification of mammalian gene expression control. Nature 473, 337-342.

Sharma, U. K., and Chatterji, D. (2010). Transcriptional switching in *Escherichia coli* during stress and starvation by modulation of σ70 activity. FEMS Microbiology Reviews 34, 646-657.

Shimotsu, H., and Henner, D. J. (1986). Construction of a single-copy integration vector and its use in analysis of regulation of the trp operon of *Bacillus subtilis*. Gene 43, 85-94.

Sierro, N., Makita, Y., De Hoon, M., and Nakai, K. (2008). DBTBS: a database of transcriptional regulation in *Bacillus subtilis* containing upstream intergenic conservation information. Nucleic Acids Research 36, D93-D96.

Šiková, M., Wiedermannová, J., Převorovský, M., Barvík, I., Sudzinová, P., Kofroňová, O., Benada, O., Šanderová, H., Condon, C., and Krásný, L. (2020). The torpedo effect in *Bacillus subtilis*: RNase J1 resolves stalled transcription complexes. The EMBO Journal 39, e102500-e102500.

Spanogiannopoulos, P., Waglechner, N., Koteva, K., and Wright, G. (2014). A rifamycin inactivating phosphotransferase family shared by environmental and pathogenic bacteria. Proceedings of the National Academy of Sciences 111.

Srivatsan, A., Tehranchi, A., Macalpine, D. M., and Wang, J. D. (2010). Co-orientation of replication and transcription preserves genome integrity. PLOS Genetics 6, e1000810-e1000810.

Stazic, D., Lindell, D., and Steglich, C. (2011). Antisense RNA protects mRNA from RNase E degradation by RNA-RNA duplex formation during phage infection. Nucleic Acids Research 39, 4890-4899.

Stogios, P. J., Cox, G., Spanogiannopoulos, P., Pillon, M. C., Waglechner, N., Skarina, T., Koteva, K., Guarné, A., Savchenko, A., and Wright, G. D. (2016). Rifampin phosphotransferase is an unusual antibiotic resistance kinase. Nature Communications 7, 11343-11343.

Strauch, M. A., Bobay, B. G., Cavanagh, J., Yao, F., Wilson, A., and Le Breton, Y. (2007). Abh and AbrB control of *Bacillus subtilis* antimicrobial gene expression. Journal of Bacteriology 189, 7720.

Stülke, J., Hanschke, R., and Hecker, M. (1993). Temporal activation of β-glucanase synthesis in *Bacillus subtilis* is mediated by the GTP pool. Microbiology 139, 2041-2045.

Temiakov, D., Zenkin, N., Vassylyeva, M. N., Perederina, A., Tahirov, T. H., Kashkina, E., Savkina, M., Zorov, S., Nikiforov, V., Igarashi, N., et al. (2005). Structural basis of transcription inhibition by antibiotic streptolydigin. Molecular Cell 19, 655-666.

Tupin, A., Gualtieri, M., Leonetti, J.-P., and Brodolin, K. (2010). The transcription inhibitor lipiarmycin blocks DNA fitting into the RNA polymerase catalytic site. The EMBO Journal 29, 2527-2537.

Tuske, S., Sarafianos, S. G., Wang, X., Hudson, B., Sineva, E., Mukhopadhyay, J., Birktoft, J. J., Leroy, O., Ismail, S., Clark, A. D., et al. (2005). Inhibition of Bacterial RNA Polymerase by Streptolydigin: Stabilization of a Straight-Bridge-Helix Active-Center Conformation. Cell 122, 541-552.

Urban, A., Eckermann, S., Fast, B., Metzger, S., Gehling, M., Ziegelbauer, K., Rübsamen-Waigmann, H., and Freiberg, C. (2007). Novel whole-cell antibiotic biosensors for compound discovery. Applied and Environmental Microbiology 73, 6436-6443.

Vidal, L. S., Santos, L. B., Lage, C., and Leitão, A. C. (2006). Enhanced Sensitivity of Escherichia coli uvrB Mutants to Mitomycin C Points to a UV-C Distinct Repair for DNA Adducts. Chemical Research in Toxicology 19, 1351-1356.

Weiss, A., and Shaw, L. N. (2015). Small things considered: the small accessory subunits of RNA polymerase in Gram-positive bacteria. FEMS Microbiology Reviews 39, 541-554.

Wex, K. W., Saur, J. S., Handel, F., Ortlieb, N., Mokeev, V., Kulik, A., Niedermeyer, T. H. J., Mast, Y., Grond, S., Berscheid, A., et al. (2021). Bioreporters for direct mode of action-informed screening of antibiotic producer strains. Cell Chemical Biology, DOI: 10.1016/j.chembiol.2021.02.022

Wiedermannová, J., Sudzinová, P., Kovaľ, T., Rabatinová, A., Šanderova, H., Ramaniuk, O., Rittich, Š., Dohnálek, J., Fu, Z., Halada, P., et al. (2014). Characterization of HelD, an interacting partner of RNA polymerase from *Bacillus subtilis*. Nucleic Acids Research 42, 5151-5163.

Williams, M. V., and Tritz, G. J. (1977). Studies on the modes of action of azaserine inhibition of *Escherichia coli.* Potentiation of phenylalanine reversal. Journal of Antimicrobial Chemotherapy 3, 65-77.

Xiao, J., Peng, B., Su, Z., Liu, A., Hu, Y., Nomura, C., Chen, S., and Wang, Q. (2020). Facilitating protein expression with portable 5'-UTR secondary structures in *Bacillus licheniformis*. ACS Synthetic Biology.

Xu, Z., Zhou, A., Wu, J., Zhou, A., Li, J., Zhang, S., Wu, W., Karakousis, P. C., and Yao, Y.-F. (2018). Transcriptional approach for decoding the mechanism of rpoC compensatory mutations for the fitness cost in rifampicin-resistant *Mycobacterium tuberculosis*. Frontiers in Microbiology 9, 2895-2895.

Zhu, B., and Stülke, J. (2017). SubtiWiki in 2018: from genes and proteins to functional network annotation of the model organism *Bacillus subtilis*. Nucleic Acids Research 46, D743-D748.

Supplemental Information

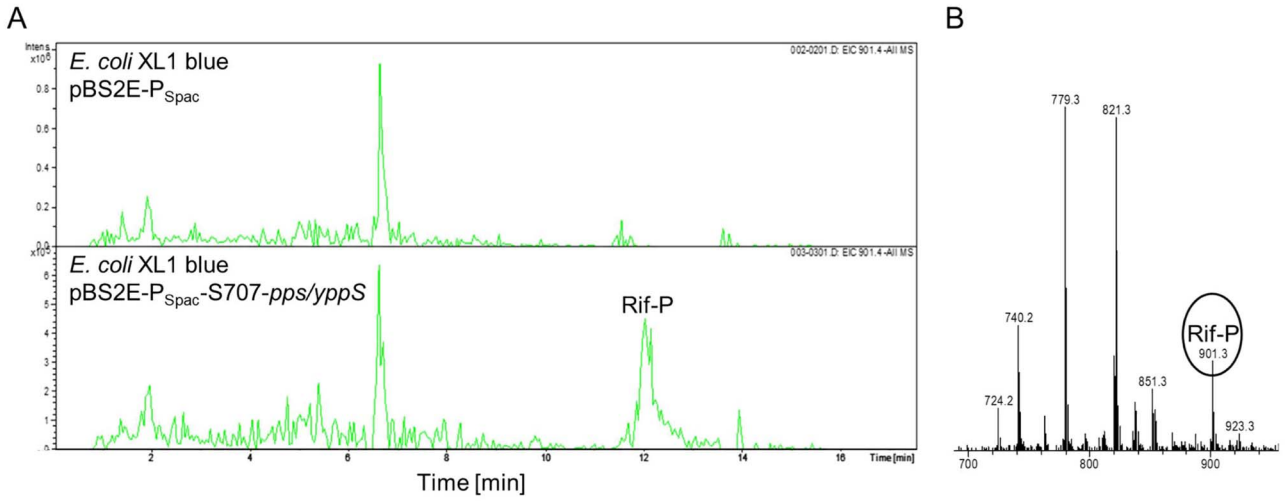

Figure S1. *B. subtilis* Pps/YppS is able to phosphorylate rifampin. *E. coli* XL1 blue pBS2E-P_{Spac} and *E. coli* XL1 blue pBS2E-P_{Spac}-S707-*pps/yppS* were grown in the presence of RIF(100 µg/mL) and the inducer IPTG (1 mM) for 24 h. S707 constitutes the 5'UTR preceding the *B. subtilis pps/yppS* gene (Nicolas et al., 2012). (A) HPLC-MS analysis of the conditioned media of *E. coli* XL1 blue pBS2E-P_{Spac} (upper graph) and *E. coli* XL1 blue pBS2E-P_{Spac}-S707- *pps/yppS* (lower graph). Phosphorylated rifampin was only detectable upon induction of *B. subtilis pps/yppS*. (B) Mass spectrum $[M-H]^-$ of the conditioned medium of *E. coli* XL1 blue pBS2E-P_{Spac}-S707- *pps/yppS* at a retention time of 12 min showing the detection of the mass of phosphorylated rifampin (*m/z* 901.3).

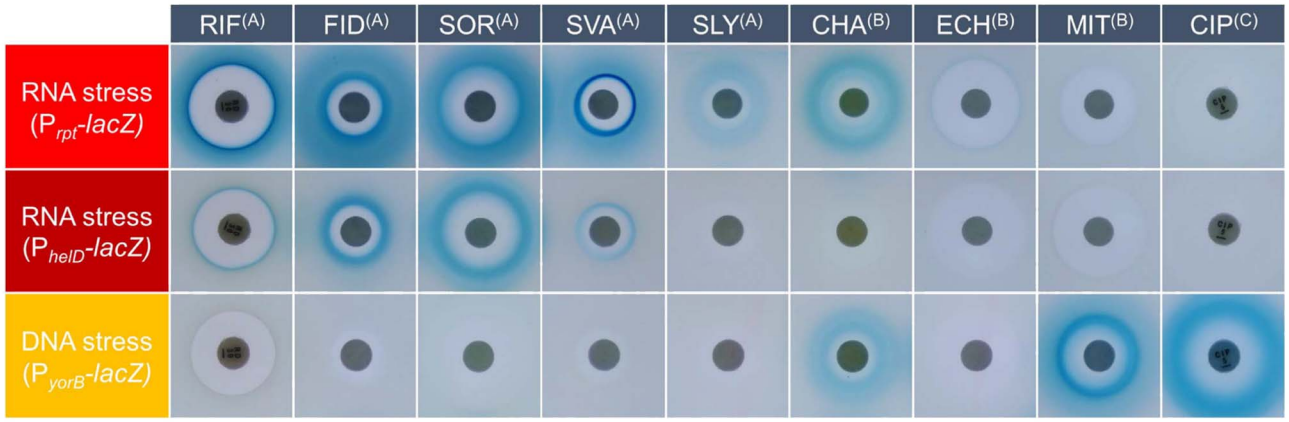

Figure S2. Induction pattern of exemplary reference antibiotics tested against our RNA and DNA stress bioreporters in Belitzky minimal soft agar. Compounds were spotted on a filter disc and subsequently placed on the agar, containing the respective *B. subtilis* reporter strain. Filter discs contained the following antibiotic amounts: rifampin (RIF) 30 µg, fidaxomicin (FID) 8 µg, sorangicin A (SOR) 5 µg, streptovaricin (SVA) 10 µg, streptolydigin (SLY) 40 µg, chartreusin (CHA) 30 µg, echinomycin (ECH) 20 µg, mitomycin C (MIT) 1 µg, and ciprofloxacin (CIP) 5 µg. Categorization into DNA synthesis inhibitors (A), RNAP inhibitors (B), and DNA-binding agents (C) is indicated by the respective superscript. Promoter induction was detected as a blue halo following overnight incubation.

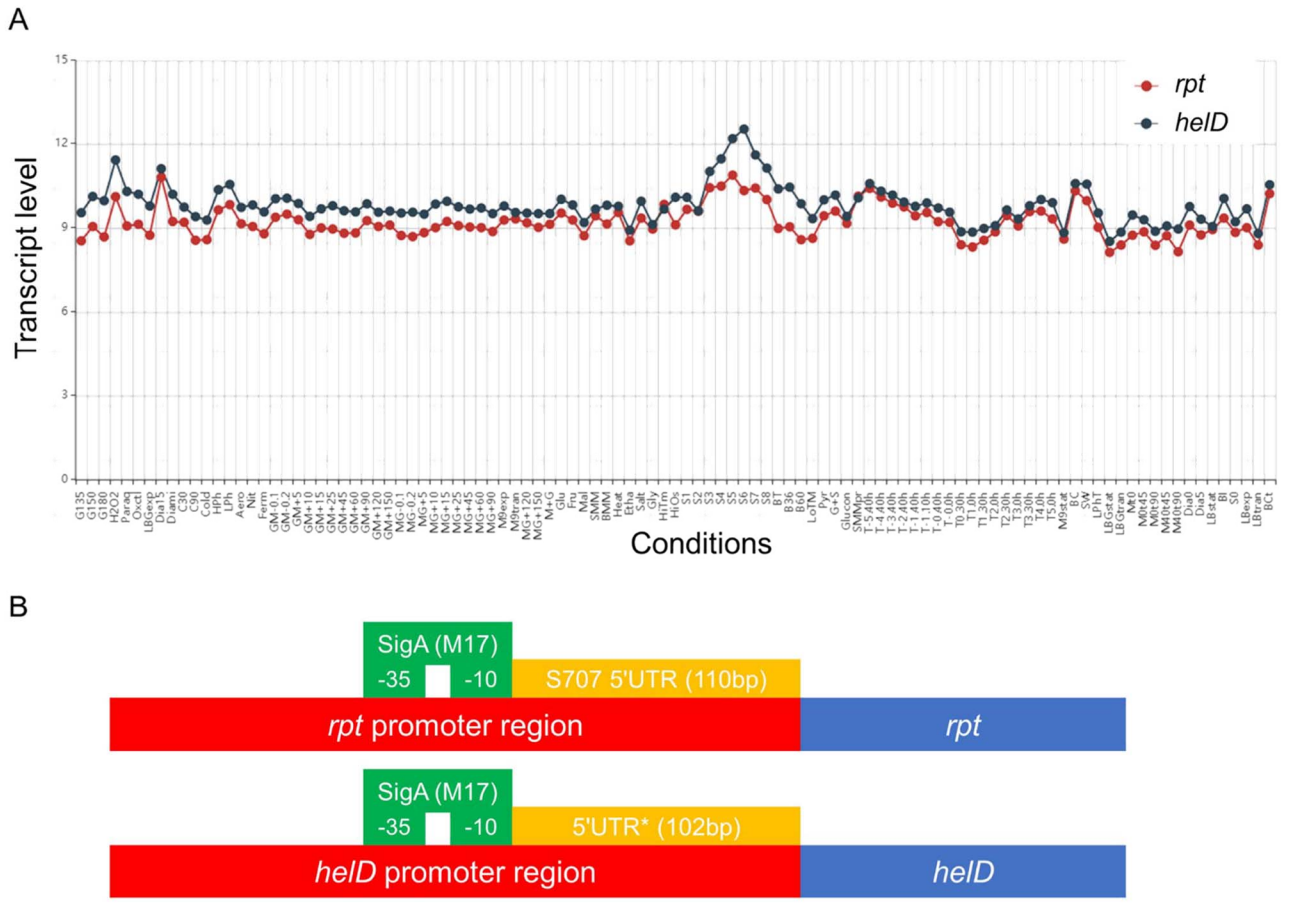

Figure S3. Comparison of *rpt* and *helD* transcriptional regulation. (A) Transcript levels of *rpt* and *helD* under different growth conditions. The data was obtained from the Expression browser available on SubtiWiki (Zhu and Stülke, 2017). (B) Schematic overview of the native promoter regions of *rpt* and *helD*. The SigA binding sites were both annotated by Nicolas and colleagues (Nicolas et al., 2012). A further subclassification of SigA binding sites based on their available consensus motifs yielded the subclass M17 for both, the *rpt* and *helD* promoter (Nicolas et al., 2012). S707 5'UTR was described with a length of 110 bp (Zhu and Stülke, 2017; Nicolas et al., 2012). For the *helD* promoter region, * indicates that this 5'UTR has not previously been annotated as such but can be deduced due to the described SigA binding site and the translational start site (Nicolas et al., 2012).

Figure S4. Sequence alignment of the promoter sequences P_{rpt} (123 bp fragment) and P_{helD} (120 bp fragment). For the alignment, the Pro-coffee alignment tool for homologous promoter regions was used (Erb et al., 2012). The conserved 13 nucleotides on the downstream end of the promoter regions are outlined in red.

A

Construct	Sequence	Induction specificity
5'UTR of *rpt* (natural composition in the *B. subtilis* chromosome)	CACACTACGTGCGCTTTCTAGTTAAAAAGTTATAGATATCCATCTTATAATTTTATTATATCCTGCTAGGAAGCTCTTGTCAATATTTTTTTTTGAAGGGGAGATGTAGAATG	Yes, based on microarray data (Freiberg et al., 2006)
5'UTR of P_{rpt}-*lacZ*	CACACTACGTGCGCTTTCTAGTTAAAAAGTTATAGATATCCATCTTATAATTTTATTATATCCTGCTAGGAAGCTCTTGTCAATATTTTTCTGCAGTAAGGAGGAAAAAGGTACCGTG	Yes (Wex et al., 2021)
5'UTR of P_{rpt}-*lacZ* after deletion of 14 bp at the downstream end ($P_{rpt\_Del14bpDS}$-*lacZ*)	CACACTACGTGCGCTTTCTAGTTAAAAAGTTATAGATATCCATCTTATAATTTTATTATATCCTGCTAGGAAGCTCCTGCAGTAAGGAGGAAAAAGGTACCGTG	No (this study)
5'UTR of P_{rpt}-*lacZ* after modification of 6 out of 13 bp ($P_{rpt\_Modi14bpDS}$-*lacZ*)	CACACTACGTGCGCTTTCTAGTTAAAAAGTTATAGATATCCATCTTATAATTTTATTATATCCTGCTAGGAAGCTCTCATCTATGATCTTCTGCAGTAAGGAGGAAAAAGGTACCGTG	No (this study)
5'UTR of P_{rpt}-*lacZ* after modification of the SigA -10 region of S708 ($P_{rpt\_Modi-10SigA(S708)}$-*lacZ*)	CACACTACGTGCGCTTTCTAGTTAAAAAGTTATAGATATCCATCGTCAACGATGTCCAGTACTTGCTAGGAAGCTCTTGTCAATATTTTTCTGCAGTAAGGAGGAAAAAGGTACCGTG	No (this study)

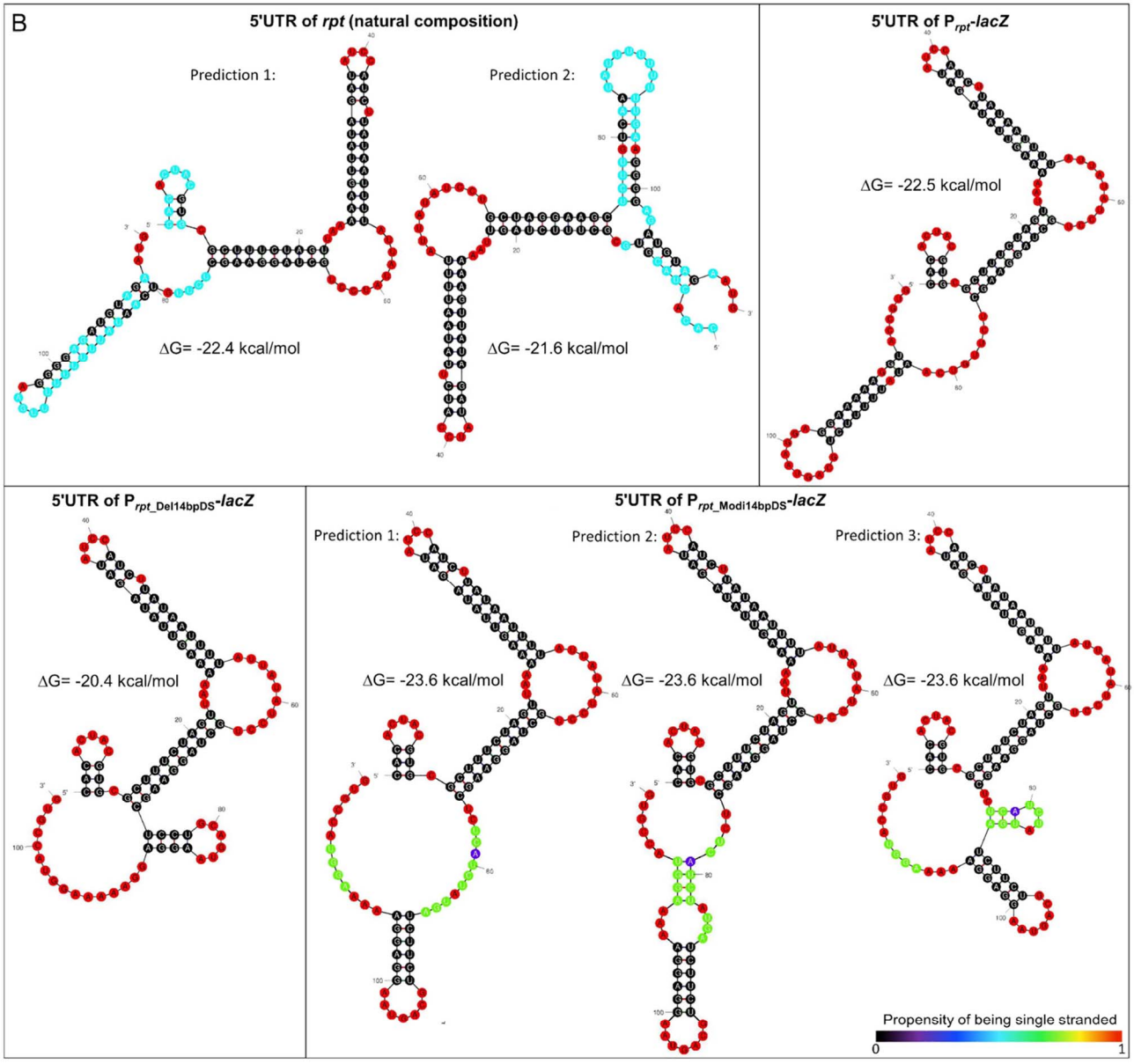

Figure S5. Continued on following page.

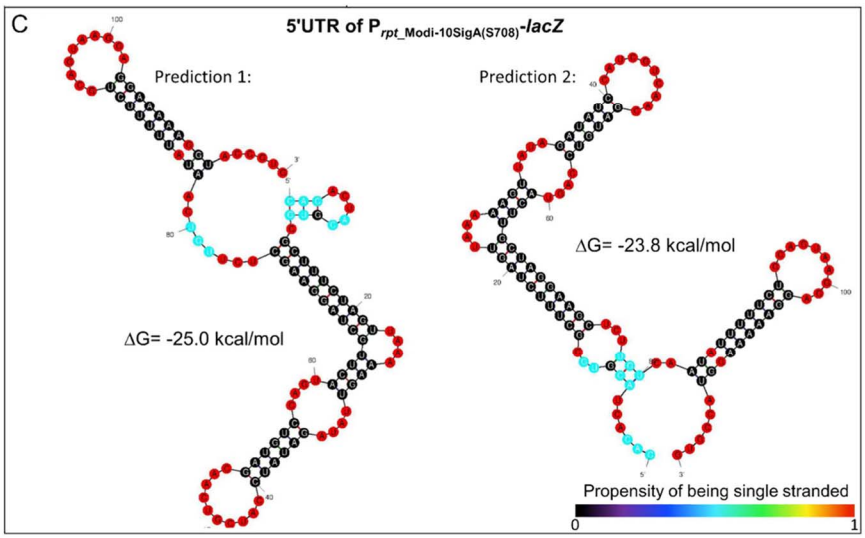

Figure S5. Predicted mRNA structures of the *rpt* promoter region with minimum free energy (ΔG). (A) Overview of the investigated 5'UTRs, their sequence and the induction specificity of the respective bioreporter construct. (B) Predicted 5'UTR structures of the *rpt* promoter deletion or modification studies. (C) Predicted 5'UTR structures after modification of the -10 region of the SigA binding site of the complementary sRNA ncr1015/S708**.** All 5'UTR structures have been analyzed using the RNA mfold version 2.3 (Zuker, 2003). The propensity of each base to be single stranded is color encoded.

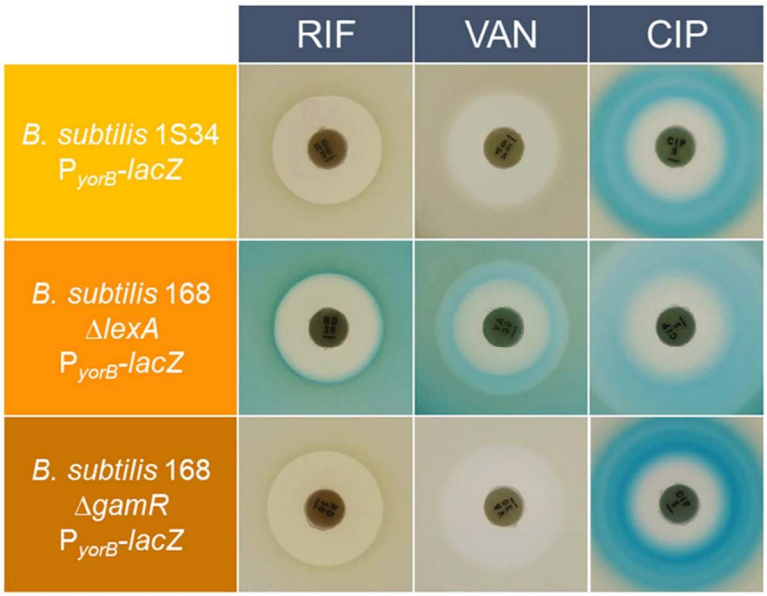

Figure S6. Antibiotic induction of the P_{yorB}-*lacZ* bioreporter in the different background strains *B. subtilis* 1S34, *B. subtilis* 168 Δ*lexA*, and *B. subtilis* 168 Δ*gamR*. Antibiotic discs contained the following antibiotic amounts, rifampin (RIF) 30 µg, vancomycin (VAN) 30 µg, and ciprofloxacin (CIP) 5 µg, and were directly placed on the bioreporter strain containing agar. Expression of P_{yorB}-*lacZ* in the deletion mutant *B. subtilis* 168 Δ*lexA*, which is devoid of the transcriptional repressor of the SOS response LexA, showed enhanced background expression and loss of induction specificity. Expression of P_{yorB}-*lacZ* in the *B. subtilis* 168 Δ*gamR* strain background had no influence on the bioreporter induction specificity.

Figure S7. Cross-species consensus motif of the conserved 13 nucleotides initially identified in the promoter regions of *B. subtilis rpt* and *helD*. Of note, the *helD* motif contains an additional cytosine compared to the *rpt* motif (compare Figure S4). The *rpt* promoter regions of the following strains were utilized for motif creation using Weblogo (Crooks et al., 2004): *Bacillus subtilis* subsp. *subtilis* 168 (NC_000964.3), *Bacillus licheniformis* ATCC14580 (NC_006270.3), *Bacillus amyloliquefaciens* MT45 (NC_014551.1), *Paenibacillus* sp. Y412MC10 (NC_013406.1), *Brevibacillus brevis* NBRC100599 (NC_012491.1), *Bacillus halotolerans* F41-3 (NZ_CP029364.1), *Bacillus sonorensis* (NZ_CP021920.1), *Paenibacillus mucilaginosus* KNP414 (NC_015690.1), *Brevibacillus brevis* NBRC100599 (NC_012491.1), *Brevibacillus formosus* (NZ_CP018145.1), *Paenibacillus ihbetae* (NZ_CP016809.1), *Brevibacillus agri* (NZ_CP026363.1), *Bacillus siamensis* (NZ_CP025001.1), *Bacillus glycinifermentans* (NZ_LT603683.1), *Bacillus amyloliquefaciens* LL3 (NC_017190.1), *Bacillus paralicheniformis* (NC_021362.1), *Paenibacillus lautus* (NZ_CP032412.1)

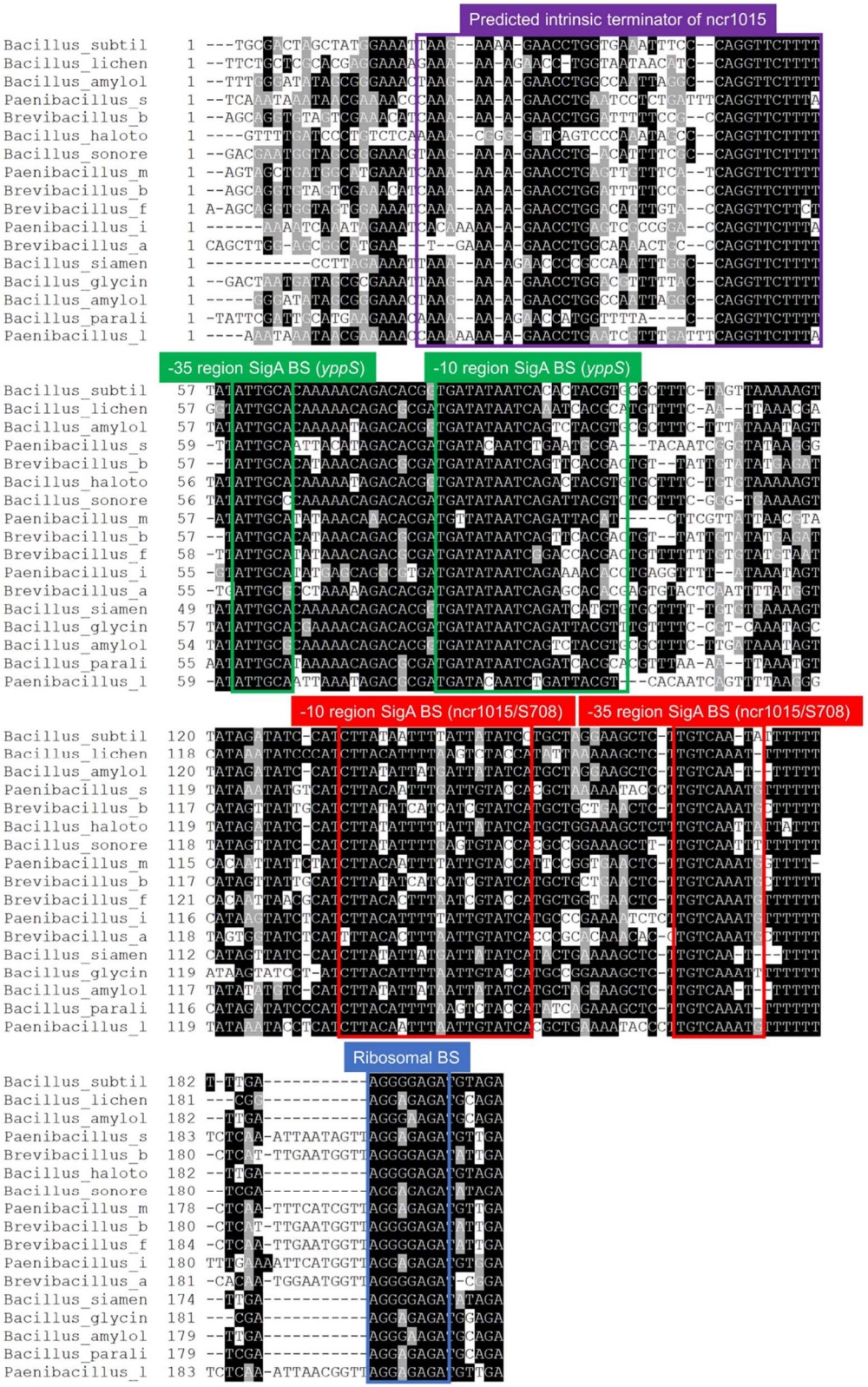

Figure S8. Promoter alignment of different Bacillales rpt homologs containing the conserved 13 nucleotides found in P_{rpt} and P_{helD}. Colored boxes highlight important regulatory regions of the rpt promoter region in different bacterial strains. The names of all analyzed strains are listed from first to last: Bacillus subtilis subsp. subtilis 168 (NC_000964.3), Bacillus licheniformis ATCC14580 (NC_006270.3), Bacillus amyloliquefaciens MT45 (NC_014551.1), Paenibacillus sp. Y412MC10 (NC_013406.1), Brevibacillus brevis NBRC100599 (NC_012491.1), Bacillus halotolerans F41-3 (NZ_CP029364.1), Bacillus sonorensis (NZ_CP021920.1), Paenibacillus mucilaginosus KNP414 (NC_015690.1), Brevibacillus brevis NBRC100599 (NC_012491.1), Brevibacillus formosus (NZ_CP018145.1), Paenibacillus ihbetae (NZ_CP016809.1), Brevibacillus agri (NZ_CP026363.1), Bacillus siamensis (NZ_CP025001.1), Bacillus glycinifermentans (NZ_LT603683.1), Bacillus amyloliquefaciens LL3 (NC_017190.1), Bacillus paralicheniformis (NC_021362.1), Paenibacillus lautus (NZ_CP032412.1)

Table S1. Rifampin susceptibility before and after complementation of the *ppS*/*yppS* (thereafter named *rpt*) gene. MIC determination was conducted in lysogeny broth.

Strain	IPTG [1mM]	Rifampin MIC [µg/mL]
B. subtilis 168 Δ*amyE*	-	0.25
	+	0.25
B. subtilis 168 Δ*pps*/*yppS*	-	0.0078
	+	0.0078
B. subtilis 168 Δ*pps*/*yppS aprE*::P_{Spac}	-	0.0078
	+	0.0078
B. subtilis 168 Δ*pps*/*yppS aprE*::P_{Spac}-S707- *pps*/*yppS*	-	0.0078
	+	0.25
E. coli XL1 blue pBS2E-P_{Spac}	-	4
	+	4
E. coli XL1 blue pBS2E-P_{Spac}-S707- *pps*/*yppS*	-	128
	+	512

Table S2. Promoter induction of antibacterial agents acting on RNA and DNA synthesis in the agar-based bioreporter assay. The three bioreporters have previously been shown to be selective only for RNA stress (P_{rpt}-*lacZ,* P_{helD}-*lacZ)* and DNA stress (P_{yorB}-*lacZ*) (Wex et al., 2021).

MOA[a]	Antimicrobial agent [µg][b]	Promoter induction		
		P_{yorB}	P_{rpt}	P_{helD}
DNA gyrase binders	Ciprofloxacin [1]	+	-	-
	Levofloxacin [1]	+	-	-
	Moxifloxacin [0.5]	+	-	-
	Nalidixic acid [25]	+	-	-
	Norfloxacin [2]	+	-	-
	Novobiocin [2]	+	-	-
Nucleotide synthesis inhibitors	Azaserine [3]	+	(+)	-
	5′-Fluorouracil [10]	+	-	-
	Sulfamethoxazole [20]	+	-	-
	SCH-79797 [40]	+	-	-
	Trimethoprim [0.5]	+	-	-
RNA polymerase binders	Corallopyronin A [30]	-	+	+
	Fidaxomicin [4]	-	+	+
	Myxopyronin A [30]	-	+	+
	Pseudouridimicin[c] [80]	-	+	-
	Rifabutin [20]	-	+	+
	Rifampin [30]	-	+	+
	Rifamycin SV [20]	-	+	+
	Sorangicin A [20]	-	+	+
	Streptolydigin [20]	-	+	-
	Streptovaricin[d] [20]	-	+	+
	Tirandamycin A [20]	-	+	-
DNA-binding agents	Actinomycin D [0.5]	-	+	-
	Actinomycin X2 [0.5]	-	+	-
	Cosmomycin B [10]	-	+	-
	Cosmomycin C [10]	-	+	-
	Cisplatin [25]	+	-	-
	Cinerubin A [20]	-	+	-
	Chartreusin [30]	+	+	-
	DAPI[e] [50]	-	+	-
	Daunomycin [5]	+	-	-
	Doxorubicin [1]	+	-	-
	Echinomycin [20]	-	+	-
	Gilvocarcin V [30]	+	+	-
	Mitomycin C [2]	+	-	-
	Mitoxantrone [20]	+	-	-
	Netropsin [15]	-	+	-
	Phleomycin [10]	+	-	-
	Rachelmycin [20]	+	-	-

[a] Based on current knowledge of the mechanism of action (MOA)
[b] Antibiotic amount spotted on agar
[c] Pseudouridimycin shows very weak antimicrobial activity against the bioreporter strains
[d] Mixture of different streptovaricins, mainly containing the derivatives A, B, and C
[e] 4′,6-diamidino-2-phenylindole

Table S3. Maximal antibiotic induction of P_{rpt}-*luxABCDE* and P_{helD}-*luxABCDE* after different incubation times (10, 90, 210 and 240 min). Presented is the maximal fold change of the antibiotic induction in comparison to the untreated control, including the standard deviation of at least 3 replicates. Measured values exceeding the induction threshold of 200 % are indicated in bold font.

Antibiotic	Induction$_{Max}$ P_{rpt}-*luxABCDE* [%]				Induction$_{Max}$ P_{helD}-*luxABCDE* [%]			
	10 min[a]	90 min	210 min	240 min	10 min[a]	90 min	210 min	240 min
Rifampin	**340 ± 16**	**1452 ± 272**	**611 ± 78**	**763 ± 242**	**206 ± 61**	**663 ± 165**	**411 ± 45**	**533 ± 89**
Rifabutin	**396 ± 37**	**2091 ± 251**	**1082 ± 181**	**1329 ± 277**	180 ± 58	**882 ± 113**	**718 ± 379**	**827 ± 61**
Fidaxomicin	**204 ± 19**	**1048 ± 275**	**2526 ± 171**	**3871 ± 275**	**206 ± 97**	**779 ± 51**	**1949 ± 533**	**3046 ± 454**
Sorangicin A	**369 ± 101**	**4511 ± 712**	**4397 ± 407**	**6851 ± 294**	**230 ± 110**	**1696 ± 87**	**2982 ± 432**	**3439 ± 470**
Corallopyronin A	**251 ± 81**	**1960 ± 204**	**3489 ± 215**	**4734 ± 476**	**220 ± 94**	**1175 ± 109**	**2290 ± 92**	**3401 ± 347**
Streptovaricin[b]	**493 ± 54**	**1944 ± 228**	**2010 ± 209**	**3073 ± 470**	**370 ± 95**	**831 ± 99**	**1136 ± 171**	**1919 ± 91**
Streptolydigin	104 ± 16	**425 ± 70**	**1083 ± 89**	**1768 ± 186**	121 ± 12	**218 ± 27**	**537 ± 108**	**877 ± 95**
Chartreusin	118 ± 9	**801 ± 107**	**1006 ± 48**	**1535 ± 87**	117 ± 5	**348 ± 30**	**434 ± 17**	**482 ± 67**
Echinomycin	151 ± 12	**605 ± 137**	**1629 ± 549**	**2788 ± 993**	110 ± 10	144 ± 14	**351 ± 93**	**591 ± 223**
Netropsin	114 ± 10	**285 ± 18**	**270 ± 30**	**304 ± 122**	114 ± 15	98 ± 8	102 ± 4	117 ± 7
Actinomycin D	107 ± 14	170 ± 37	**385 ± 89**	**698 ± 122**	120 ± 16	117 ± 2	154 ± 14	**281 ± 14**
Mithramycin	131 ± 21	**302 ± 68**	**845 ± 158**	**1384 ± 545**	109 ± 5	133 ± 13	**261 ± 30**	**554 ± 162**
Mitomycin C	136 ± 8	142 ± 27	122 ± 17	163 ± 22	112 ± 4	98 ± 4	112 ± 7	162 ± 58
Doxorubicin	121 ± 12	159 ± 27	106 ± 8	143 ± 33	129 ± 5	171 ± 21	164 ± 5	**214 ± 83**
Phleomycin	116 ± 7	122 ± 10	114 ± 20	161 ± 17	127 ± 6	102 ± 7	103 ± 9	142 ± 17
5'-Fluorouracil	123 ± 18	102 ± 8	100 ± 6	124 ± 17	126 ± 16	106 ± 10	101 ± 5	113 ± 2
Ciprofloxacin	123 ± 19	154 ± 20	117 ± 10	151 ± 37	121 ± 17	138 ± 20	141 ± 7	172 ± 7
Chloramphenicol	133 ± 10	105 ± 11	113 ± 9	132 ± 18	119 ± 7	103 ± 5	97 ± 5	121 ± 5
Gentamicin	128 ± 6	111 ± 14	116 ± 9	150 ± 6	135 ± 8	108 ± 3	108 ± 6	119 ± 8
Ampicillin	115 ± 5	118 ± 16	115 ± 3	137 ± 10	114 ± 8	113 ± 17	114 ± 17	143 ± 19
Vancomycin	129 ± 15	106 ± 6	103 ± 1	102 ± 2	132 ± 2	104 ± 9	105 ± 2	123 ± 25
CCCP	109 ± 8	101 ± 2	104 ± 3	113 ± 5	107 ± 25	97 ± 7	106 ± 4	115 ± 7
Daptomycin	116 ± 12	105 ± 12	121 ± 14	142 ± 11	89 ± 13	91 ± 6	97 ± 7	131 ± 15
Triclosan	110 ± 14	69 ± 9	70 ± 10	65 ± 10	95 ± 2	74 ± 7	53 ± 15	68 ± 19

[a] Values have not been adjusted to OD600 = 1 at this early timepoint, as growth differences were not yet detectable in BMM

[b] Mixture of different streptovaricins, mainly containing the derivatives A, B, and C

Table S4. Fragments used in the DNA affinity capturing assay (DACA). The SigA binding sites (-35 and -10 binding regions) of P_{rpt} (fragment 1-3) and P_{yorB} (fragment 4) are underlined. The 13 bp consensus sequence of P_{rpt} is highlighted in green. The potential LexA binding site of P_{yorB} is marked in red.

Fragment	Length	Sequence
1	200 bp	5´BIOTIN- tttttaatgcgactagctatggaaattaagaaaagaacctggtgaaatttcccaggttctttttatattgcacaaaaac agacacggtgatataatcacactacgtgcgctttctagttaaaaagttatagatatccatcttataattttattatatcct gctaggaagctcttgtcaatattttctgcagtaaggagg
2	170 bp	5´BIOTIN- tttttaatgcgactagctatggaaattaagaaaagaacctggtgaaatttcccaggttctttttatattgcacaaaaac agacacggtgatataatcacactacgtgcgctttctagttaaaaagttatagatatccatcttataattttattatatcct gctaggaagc
3	126 bp	5´BIOTIN- tttttaatgcgactagctatggaaattaagaaaagaacctggtgaaatttcccaggttctttttatattgcacaaaaac agacacggtgatataatcacactacgtgcgctttctagttaaaaagt
4	200 bp	5´BIOTIN- ggtgcaagagtgctttcgcatccatttgcaacgtttaatgcttccagtacaactttaatacataatacatacgacagc ggcacacctagattagccttagatgatacagtaatcgattataaataaaaaattcttaacgagaacacttgttccctttt atgggttttggtatataatttagtagtaccaaaaatttcaaaa

Table S5. All DACA candidates that showed increased LFQ intensities for the *rpt* promoter fragments (fragments 1-3; F1, F2, F3) in comparison to the *yorB* promoter fragment (fragment 4; F4). Interesting candidates that were further analyzed for their capability to modulate *rpt* expression are outlined in green.

Protein	Detected peptide fragments												Label-free quantification (LFQ) intensities											
	biological replicate 1				biological replicate 2				biological replicate 3				biological replicate 1				biological replicate 2				biological replicate 3			
	F1	F2	F3	F4	F1	F2	F3	F4	F1	F2	F3	F4	F1	F2	F3	F4	F1	F2	F3	F4	F1	F2	F3	F4
Noc	35	37	37	21	36	37	38	22	35	35	38	17	3.99E+11	1.29E+11	1.69E+11	5.26E+09	1.13E+11	2.00E+11	4.65E+11	3.53E+09	4.18E+11	3.92E+11	4.03E+11	3.98E+09
PriA	73	57	62	44	71	57	66	38	73	56	62	44	1.86E+11	1.29E+10	2.14E+10	5.59E+09	3.71E+10	1.30E+10	3.84E+10	1.86E+09	1.08E+11	1.59E+10	2.80E+10	5.69E+09
RpoB	88	76	69	79	91	77	65	74	94	74	66	77	1.39E+11	1.13E+10	7.60E+09	1.49E+10	4.31E+10	1.14E+10	7.17E+09	6.97E+09	1.28E+11	1.52E+10	8.21E+09	1.90E+10
RpoC	116	84	67	83	118	84	66	79	116	82	69	86	1.35E+11	1.24E+10	7.62E+09	1.40E+10	4.49E+10	1.06E+10	6.26E+09	6.91E+09	1.30E+11	1.38E+10	7.59E+09	2.05E+10
AdeR	30	29	30	22	30	31	32	23	29	28	29	23	7.54E+10	2.18E+10	2.45E+10	5.45E+09	3.15E+10	4.70E+10	8.64E+10	7.13E+09	8.87E+10	8.62E+10	7.07E+10	1.68E+10
RpoA	28	23	20	21	28	23	19	19	27	22	20	21	6.14E+10	5.68E+09	4.12E+09	7.74E+09	1.83E+10	6.71E+09	3.86E+09	4.39E+09	5.64E+10	1.03E+10	4.39E+09	9.79E+09
GlvR	19	20	22	7	20	20	22	8	19	18	19	6	5.66E+10	1.80E+10	2.34E+10	2.34E+08	2.02E+10	4.04E+10	7.97E+10	2.09E+08	2.11E+10	2.69E+10	2.14E+10	1.31E+08
AbrB	14	13	13	4	10	11	12	4	13	13	14	4	2.66E+10	6.03E+09	6.92E+09	2.80E+08	2.67E+09	4.17E+09	1.09E+10	2.82E+08	2.05E+10	2.08E+10	1.82E+10	3.85E+08
YonI	20	20	23	16	20	20	23	17	18	18	21	18	2.36E+10	1.20E+10	2.56E+10	5.37E+09	3.82E+09	1.04E+10	4.15E+10	1.65E+09	6.46E+09	1.08E+10	2.23E+10	3.71E+09
Hpr	11	10	8	3	12	10	8	4	9	8	7	3	1.89E+10	4.53E+09	7.65E+08	4.01E+07	1.14E+10	1.54E+10	5.28E+09	1.03E+08	3.37E+09	2.35E+09	4.26E+08	2.18E+07
SigB	19	15	1	5	19	15	1	5	19	15	1	5	9.88E+09	4.75E+08	0	8.37E+07	1.28E+09	5.68E+08	0	6.45E+07	6.02E+09	1.23E+09	0	1.33E+08
SigA	22	19	14	19	24	20	12	17	24	19	12	18	9.53E+09	8.96E+08	6.91E+08	1.48E+09	2.75E+09	1.03E+09	7.05E+08	9.35E+08	8.61E+09	2.37E+09	7.34E+08	1.84E+09
YxaF	11	10	11	1	10	10	11	1	11	11	11	1	8.33E+09	2.35E+09	2.40E+09	0	9.31E+08	1.73E+09	2.13E+09	0	3.38E+09	2.42E+09	2.21E+09	0
YdcH	14	12	12	0	12	12	12	0	12	12	11	0	7.18E+09	2.10E+09	2.75E+09	0	1.05E+09	2.05E+09	3.65E+09	0	3.69E+09	3.84E+09	2.71E+09	0
TreR	16	18	17	8	14	17	17	6	16	17	16	8	6.99E+09	2.08E+09	2.31E+09	4.56E+08	1.07E+09	2.35E+09	4.07E+09	1.60E+08	4.67E+09	3.79E+09	3.97E+09	4.63E+08
DisA	19	18	21	10	12	11	13	7	9	7	6	3	6.68E+09	4.24E+09	1.07E+10	4.30E+08	1.61E+08	7.17E+07	2.01E+08	3.55E+07	5.15E+07	4.15E+07	4.10E+07	1.01E+07
Rex	13	14	14	7	12	13	16	6	12	12	14	7	6.53E+09	2.72E+09	2.90E+09	3.16E+08	1.63E+09	3.23E+09	6.10E+09	1.95E+08	4.89E+09	7.03E+09	5.23E+09	5.46E+08
YprB	21	20	17	14	22	20	18	14	21	19	15	14	6.00E+09	1.85E+09	9.92E+08	8.57E+08	1.51E+09	2.74E+09	2.12E+09	3.89E+08	3.66E+09	3.32E+09	1.35E+09	6.98E+08
YprA	39	33	25	22	37	35	26	22	36	32	27	23	5.27E+09	1.34E+09	8.85E+08	6.77E+08	2.02E+09	2.23E+09	1.67E+09	4.45E+08	4.50E+09	2.12E+09	1.24E+09	8.35E+08
RocR	21	8	8	8	20	7	8	8	21	8	6	8	3.80E+09	2.38E+08	2.00E+08	2.90E+08	1.67E+09	4.25E+08	5.85E+08	2.02E+08	2.73E+09	3.83E+08	2.47E+08	3.60E+08
PolX	31	23	27	21	24	22	20	17	22	14	17	18	3.26E+09	1.07E+09	1.37E+09	8.90E+08	4.48E+08	5.22E+08	7.33E+08	4.11E+08	4.10E+08	3.08E+08	3.21E+08	6.48E+08
Abh	10	10	9	3	10	10	7	3	9	8	8	2	2.68E+09	5.66E+08	7.96E+08	3.30E+07	2.19E+08	2.88E+08	6.36E+08	4.92E+07	1.26E+09	9.35E+08	1.15E+09	0
SigD	15	0	0	1	16	0	0	2	16	0	0	3	2.52E+09	0	0	0	1.34E+09	0	0	2.08E+07	4.61E+09	0	0	4.83E+07
UvrB	33	35	12	11	30	35	14	10	30	34	15	11	2.45E+09	1.37E+09	2.99E+08	2.81E+08	5.72E+08	1.69E+09	4.61E+08	2.19E+08	1.58E+09	2.50E+09	7.48E+08	5.16E+08
IolR	14	13	13	10	15	14	13	12	14	12	14	12	2.25E+09	4.83E+08	5.30E+08	6.56E+08	1.04E+09	1.70E+09	2.30E+09	5.95E+08	2.20E+09	1.54E+09	1.25E+09	1.03E+09
DnaD[a]	9	0	1	0	9	0	1	0	9	0	1	0	2.13E+09	0	0	0	1.83E+08	0	0	0	5.66E+08	0	0	0
YorC	7	3	0	0	8	4	1	0	12	4	0	0	1.71E+09	1.15E+07	0	0	1.29E+09	1.81E+07	0	0	1.62E+10	1.98E+08	0	0

Protein	Detected peptide fragments												Label-free quantification (LFQ) intensities											
	biological replicate 1				biological replicate 2				biological replicate 3				biological replicate 1				biological replicate 2				biological replicate 3			
	F1	F2	F3	F4	F1	F2	F3	F4	F1	F2	F3	F4	F1	F2	F3	F4	F1	F2	F3	F4	F1	F2	F3	F4
YkrK	10	12	8	11	11	12	8	11	11	12	7	11	1.34E+09	5.49E+08	3.40E+08	8.04E+08	4.90E+08	6.35E+08	5.45E+08	3.59E+08	1.60E+09	1.02E+09	5.19E+08	1.09E+09
YdiP	15	10	7	10	12	10	7	10	15	10	7	10	1.24E+09	3.40E+08	2.35E+08	4.92E+08	3.78E+08	4.58E+08	3.60E+08	2.04E+08	1.58E+09	9.17E+08	4.46E+08	7.36E+08
YopP	13	10	10	3	12	10	10	3	13	10	10	5	1.01E+09	2.70E+08	2.59E+08	1.58E+08	1.81E+08	3.91E+08	5.77E+08	5.78E+07	1.36E+09	1.03E+09	8.21E+08	2.87E+08
YokA	17	15	17	9	16	16	19	6	20	16	19	9	8.57E+08	2.41E+08	2.69E+08	1.89E+08	3.87E+08	5.83E+08	1.07E+09	1.23E+08	9.15E+08	7.53E+08	7.82E+08	3.62E+08
YdeL	13	11	13	8	12	13	13	5	13	13	13	7	7.58E+08	2.98E+08	3.02E+08	3.70E+08	2.44E+08	3.87E+08	7.76E+08	1.13E+08	8.70E+08	8.04E+08	8.02E+08	2.99E+08
RnhB	7	3	3	3	5	3	3	2	7	2	3	2	7.00E+08	1.19E+08	9.34E+07	1.23E+08	4.19E+07	4.03E+07	1.08E+08	3.17E+07	2.10E+08	1.16E+08	6.92E+07	6.39E+07
BirA[a]	12	4	4	2	9	3	3	2	6	3	3	1	6.25E+08	8.33E+07	9.43E+07	0	3.87E+07	6.78E+07	2.71E+07	0	6.29E+07	0	2.27E+07	0
YfiR	9	6	0	0	5	5	0	1	7	5	0	0	6.21E+08	2.09E+08	0	0	2.85E+08	2.93E+08	0	0	5.08E+08	3.00E+08	0	0
YkzG	2	1	0	1	2	2	0	1	2	2	0	2	3.75E+08	0	0	0	1.02E+08	3.65E+07	0	0	5.21E+08	1.30E+08	0	8.77E+07
YybR*	9	7	7	4	8	7	5	4	6	5	5	5	3.31E+08	1.56E+08	1.32E+08	9.72E+07	5.97E+07	1.84E+08	2.71E+08	3.99E+07	1.87E+08	2.45E+08	1.70E+08	8.61E+07
LrgA	2	2	1	1	2	2	1	1	2	1	1	1	3.24E+08	3.40E+08	0	0	3.94E+08	3.06E+08	0	0	4.30E+08	0	0	0
RsmI	8	4	6	5	8	4	5	3	8	5	5	5	3.22E+08	1.20E+08	1.30E+08	9.24E+07	8.87E+07	1.34E+08	2.48E+08	6.34E+07	1.76E+08	1.27E+08	1.25E+08	7.78E+07
YwaE	4	4	5	3	4	4	5	3	3	1	2	2	3.19E+08	9.35E+07	8.85E+07	3.58E+07	7.21E+07	1.71E+08	1.84E+08	1.84E+07	2.65E+07	0	2.03E+07	9.57E+06
GmuR	6	3	2	2	4	3	2	2	6	3	1	1	2.76E+08	6.20E+07	7.54E+07	5.40E+07	4.27E+07	4.86E+07	6.42E+07	2.03E+07	1.50E+08	6.95E+07	0	0
CysL	7	0	0	10	5	0	0	7	7	0	0	10	2.47E+08	0	0	1.80E+08	6.12E+07	0	0	8.25E+07	1.11E+08	0	0	1.56E+08
YcnK	5	4	5	0	3	3	4	0	3	1	4	0	2.46E+08	8.66E+07	1.03E+08	0	3.07E+07	4.97E+07	1.37E+08	0	1.12E+08	0	6.23E+07	0
YybA	5	2	3	3	4	2	3	0	4	2	3	2	2.36E+08	0	9.12E+07	1.08E+08	6.98E+07	0	1.69E+08	0	1.37E+08	0	1.05E+08	1.13E+08
CoaBC	7	4	3	5	8	4	3	7	6	3	3	5	2.21E+08	7.07E+07	7.10E+07	5.45E+07	1.15E+08	6.48E+07	7.78E+07	8.45E+07	1.49E+08	5.70E+07	6.14E+07	4.68E+07
ManR	7	3	5	3	7	3	5	2	6	3	5	2	2.11E+08	0	9.63E+07	7.53E+07	2.40E+07	0	1.27E+08	0	1.45E+08	7.04E+07	1.49E+08	0
RpoZ	4	1	0	1	3	1	0	1	4	0	0	1	2.11E+08	0	0	0	3.84E+07	0	0	0	2.25E+08	0	0	0
XerC	7	3	6	2	6	5	6	1	7	5	6	2	1.80E+08	2.41E+07	4.60E+07	4.42E+07	5.96E+07	5.56E+07	1.13E+08	0	1.98E+08	6.96E+07	9.72E+07	6.75E+07
YydK	3	3	1	1	2	3	1	1	2	3	1	1	1.59E+08	2.89E+07	0	0	2.00E+07	1.88E+07	0	0	2.83E+07	1.99E+07	0	0
YurK	5	2	0	5	3	2	0	3	3	0	0	3	1.39E+08	2.99E+07	0	7.62E+07	1.97E+07	0	0	1.68E+07	2.54E+07	0	0	2.95E+07
AlsR	7	1	0	7	7	3	0	8	7	3	0	7	1.31E+08	0	0	1.24E+08	8.53E+07	8.40E+07	0	8.96E+07	1.29E+08	6.00E+07	0	2.13E+08
CcpN	4	4	0	1	3	3	0	1	3	1	1	1	1.23E+08	4.52E+07	0	0	4.18E+07	2.95E+07	0	0	5.04E+07	0	0	0
LicR	7	0	2	0	7	2	2	0	7	3	2	1	1.04E+08	0	0	0	6.40E+07	0	0	0	1.20E+08	0	0	0
LmrA	3	1	2	0	1	1	1	0	2	1	1	0	9.84E+07	0	2.46E+07	0	0	0	0	0	3.12E+07	0	0	0

Protein	Detected peptide fragments												Label-free quantification (LFQ) intensities											
	biological replicate 1				biological replicate 2				biological replicate 3				biological replicate 1				biological replicate 2				biological replicate 3			
	F1	F2	F3	F4	F1	F2	F3	F4	F1	F2	F3	F4	F1	F2	F3	F4	F1	F2	F3	F4	F1	F2	F3	F4
YulB	3	4	6	0	0	0	1	0	0	0	0	0	9.79E+07	4.42E+07	1.05E+08	0	0	0	0	0	0	0	0	0
SigI	3	1	1	1	2	1	0	0	3	0	0	1	9.35E+07	0	0	0	1.65E+07	0	0	0	2.96E+07	0	0	0
YcsD	3	1	2	0	2	1	2	0	2	1	1	1	7.49E+07	0	0	0	1.88E+07	0	0	0	2.48E+07	0	0	0
YkvZ	5	4	4	1	5	4	4	2	4	4	3	2	7.45E+07	1.67E+07	2.05E+07	0	2.27E+07	4.80E+07	7.60E+07	3.25E+07	7.81E+07	3.39E+07	4.80E+07	2.81E+07
YusI	3	2	1	1	2	2	1	1	2	2	1	1	7.41E+07	3.48E+07	0	0	0	2.57E+07	0	0	5.66E+07	5.26E+07	0	0
PerR	2	2	3	1	2	2	2	1	2	2	2	1	6.40E+07	4.39E+07	4.56E+07	0	3.47E+07	3.71E+07	4.20E+07	0	3.80E+07	3.83E+07	3.65E+07	0
MtlR	4	0	0	0	3	0	0	1	4	0	0	1	5.97E+07	0	0	0	1.66E+07	0	0	0	4.19E+07	0	0	0
YsfB	3	0	0	1	1	0	0	0	2	1	0	1	5.44E+07	0	0	0	0	0	0	0	0	0	0	0
YtlI	3	1	1	0	2	2	1	0	3	1	0	0	4.74E+07	0	0	0	3.82E+07	3.43E+07	0	0	3.05E+07	0	0	0
Alr1	2	4	4	2	2	3	4	2	2	3	2	1	4.72E+07	3.44E+07	3.60E+07	0	2.83E+07	3.48E+07	5.12E+07	4.79E+07	4.53E+07	6.90E+07	5.16E+07	0
PyrK	2	4	2	2	2	4	2	2	0	0	1	0	4.15E+07	5.09E+07	5.33E+07	0	7.15E+07	6.12E+07	4.84E+07	0	0	0	0	0
YjoB	3	5	6	3	5	5	4	5	1	1	3	3	3.94E+07	5.73E+07	4.99E+07	0	5.20E+07	3.40E+07	4.16E+07	0	0	0	5.65E+07	0
NtdR	2	2	3	1	2	2	3	1	0	0	0	0	3.55E+07	1.78E+07	2.02E+07	0	2.56E+07	2.87E+07	6.14E+07	0	0	0	0	0
YvmB	2	1	1	1	1	0	0	1	2	0	0	1	3.30E+07	0	0	0	0	0	0	0	2.84E+07	0	0	0
SpxA	2	0	0	0	0	0	0	0	4	0	0	0	2.47E+07	0	0	0	0	0	0	0	7.25E+07	0	0	0
NagA	2	3	3	3	2	3	3	2	2	2	3	3	2.25E+07	4.17E+07	4.77E+07	0	4.54E+07	3.30E+07	3.11E+07	0	2.45E+07	3.67E+07	3.93E+07	0
YtrF	2	2	1	2	2	2	1	2	2	2	1	2	1.45E+07	1.17E+07	1.42E+07	0	1.14E+07	8.94E+06	1.17E+07	0	1.83E+07	8.59E+06	0	0
RimM	2	2	2	4	2	2	2	4	2	1	2	3	1.03E+07	2.58E+07	2.24E+07	0	1.53E+07	1.41E+07	1.21E+07	0	1.11E+07	0	1.38E+07	0
YocD	2	0	0	1	2	0	0	1	1	0	0	1	5.19E+06	0	0	0	9.07E+06	0	0	0	0	0	0	0

[a] Essential gene
[b] Deletion mutant of this gene did not grow under any of the applied conditions.

Table S6. All DACA candidates that showed increased LFQ intensities for the *yorB* promoter fragment (fragment 4; F4) in comparison to the *rpt* promoter fragments (fragments 1-3; F1, F2, F3). The proposed regulatory candidate LexA, that was further shown to regulate *yorB* expression, is outlined in red. The interesting candidate GamR (YbgA), which was analyzed for its capability to modulate *yorB* expression, is outlined in green.

Protein	Detected peptide fragments												Label-free quantification (LFQ) intensities											
	biological replicate 1				biological replicate 2				biological replicate 3				biological replicate 1				biological replicate 2				biological replicate 3			
	F1	F2	F3	F4	F1	F2	F1	F2	F3	F4	F1	F2	F1	F2	F3	F4	F1	F2	F3	F4	F1	F2	F3	F4	F1	F2
RecG	27	30	23	46	23	30	21	44	26	29	21	45	3.05E+09	2.32E+09	9.92E+08	1.77E+10	7.70E+08	3.33E+09	1.81E+09	6.21E+09	1.88E+09	2.86E+09	1.21E+09	1.83E+10
YhaZ	9	6	7	18	8	6	10	16	8	7	8	19	8.10E+08	2.42E+08	2.01E+08	1.61E+09	1.91E+08	3.38E+08	4.58E+08	4.83E+08	4.87E+08	4.09E+08	2.90E+08	1.23E+09
WhiA	10	10	11	23	10	10	12	19	10	8	10	22	6.79E+08	3.71E+08	4.79E+08	4.72E+09	2.85E+08	6.32E+08	1.05E+09	2.10E+09	6.73E+08	6.30E+08	5.72E+08	5.86E+09
YeeA	18	7	2	49	15	8	1	41	18	1	2	48	6.42E+08	5.74E+07	1.99E+07	4.85E+09	1.15E+08	5.07E+07	0	1.12E+09	3.56E+08	0	1.50E+07	5.20E+09
SpoVG	7	8	7	10	7	8	8	11	7	9	7	11	4.71E+08	7.40E+08	3.28E+08	5.41E+09	4.41E+08	2.63E+09	1.40E+09	4.08E+09	7.33E+08	3.51E+09	5.44E+08	1.16E+10
CysL	7	0	0	10	5	0	0	7	7	0	0	10	2.47E+08	0	0	1.80E+08	6.12E+07	0	0	8.25E+07	1.11E+08	0	0	1.56E+08
LexA	4	4	7	20	4	4	8	16	4	2	1	16	1.69E+08	5.32E+07	2.15E+08	8.42E+10	3.01E+08	3.07E+08	1.11E+09	2.40E+10	3.31E+08	1.52E+08	1.82E+07	4.78E+10
Ung	3	7	5	12	3	6	4	11	3	6	2	12	1.64E+08	2.17E+08	1.23E+08	9.04E+08	3.26E+07	2.15E+08	8.37E+07	4.91E+08	1.05E+08	2.16E+08	7.18E+07	2.38E+09
YbgA	6	6	8	24	6	7	11	22	6	6	7	23	1.36E+08	4.88E+07	1.67E+08	7.97E+10	1.47E+08	2.35E+08	7.72E+08	2.36E+10	2.19E+08	1.40E+08	3.74E+07	6.84E+10
KdgR	7	1	2	13	6	1	3	10	5	1	2	12	1.33E+08	0	1.59E+07	1.17E+09	3.29E+07	0	8.46E+07	2.58E+08	8.62E+07	0	2.06E+07	6.22E+08
DinG	15	11	3	19	13	12	2	16	12	12	2	19	2.94E+08	1.10E+08	4.28E+07	5.70E+08	1.18E+08	3.35E+08	4.26E+07	1.41E+08	1.60E+08	1.49E+08	3.21E+07	5.42E+08
RecQ	8	22	8	30	7	23	8	28	8	18	5	32	2.39E+08	3.17E+08	9.28E+07	2.39E+09	6.92E+07	7.23E+08	1.97E+08	5.26E+08	1.96E+08	8.40E+08	1.07E+08	2.81E+09
AlkA	2	3	1	6	2	3	1	5	2	3	1	5	9.31E+07	5.00E+07	0	1.59E+08	3.11E+07	8.47E+07	0	5.32E+07	1.00E+08	1.40E+08	0	2.76E+08
YwqB	5	0	1	6	5	1	2	3	5	1	3	6	9.21E+07	0	0	3.80E+07	3.02E+07	0	5.43E+07	3.76E+07	9.11E+07	0	6.32E+07	6.20E+07
YuxN	5	3	1	10	6	3	3	9	9	4	3	13	7.90E+07	2.80E+07	0	2.61E+08	4.69E+07	6.55E+07	9.79E+07	1.69E+08	5.02E+08	1.95E+08	1.09E+08	1.82E+09
DacA	3	8	7	11	8	5	4	12	6	5	6	12	6.94E+07	1.53E+08	1.65E+08	1.35E+08	1.65E+08	8.03E+07	5.59E+07	1.73E+08	5.91E+07	7.52E+07	1.02E+08	1.49E+08
YdcG	2	4	0	7	1	5	0	6	2	5	0	7	6.63E+07	6.40E+07	0	1.32E+08	0	9.88E+07	0	5.31E+07	4.43E+07	1.27E+08	0	1.11E+08
YdiS	2	5	5	17	3	5	5	17	3	2	4	16	3.64E+07	6.25E+07	7.66E+07	1.81E+09	7.09E+07	8.43E+07	8.61E+07	1.24E+09	4.94E+07	5.08E+07	3.89E+07	8.65E+08
YdiR	1	2	0	10	1	2	0	11	0	1	0	10	0	3.25E+07	0	8.11E+08	0	4.19E+07	0	6.12E+08	0	0	0	3.85E+08
YdfD	4	2	2	17	2	2	3	15	1	2	3	15	0	0	4.12E+07	7.74E+08	0	0	9.84E+07	1.28E+08	0	0	8.80E+07	9.13E+08
RecS	0	2	2	16	0	2	3	14	0	2	3	16	0	5.68E+06	1.04E+07	5.25E+08	0	7.68E+06	3.03E+07	4.08E+07	0	1.74E+07	1.51E+07	5.53E+08
YpbB	0	0	3	10	0	0	4	9	0	0	3	10	0	0	4.10E+07	4.13E+08	0	0	9.38E+07	1.27E+08	0	0	4.33E+07	2.67E+08
YdjA	0	0	0	14	0	0	0	15	0	0	0	11	0	0	0	4.09E+08	0	0	0	3.72E+08	0	0	0	2.85E+08
Xre	0	0	0	5	0	0	0	5	0	0	0	4	0	0	0	2.28E+08	0	0	0	1.05E+08	0	0	0	8.47E+07
YazA	0	0	0	4	0	0	0	3	0	0	0	4	0	0	0	1.36E+08	0	0	0	2.77E+07	0	0	0	4.45E+07
YfjM	0	0	0	5	0	0	0	4	0	0	0	5	0	0	0	1.16E+08	0	0	0	4.80E+07	0	0	0	1.27E+08
PksA	1	1	1	5	1	1	1	4	1	1	1	6	0	0	0	1.09E+08	0	0	0	4.06E+07	0	0	0	1.24E+08
YjcM	0	1	1	1	0	1	1	1	0	1	1	1	0	0	0	0	0	0	0	0	0	0	0	9.16E+06

Protein	Detected peptide fragments												Label-free quantification (LFQ) intensities											
	biological replicate 1				biological replicate 2				biological replicate 3				biological replicate 1				biological replicate 2				biological replicate 3			
	F1	F2	F3	F4	F1	F2	F1	F2	F3	F4	F1	F2	F1	F2	F3	F4	F1	F2	F1	F2	F3	F4	F1	F2
YpsC	1	3	2	6	1	3	1	6	2	2	3	6	0	4.20E+07	0	3.63E+07	0	2.31E+07	0	3.80E+07	3.69E+07	3.34E+07	0	2.86E+07
YobJ	2	0	0	2	2	0	0	2	0	0	1	2	0	0	0	0	0	0	0	1.93E+07	0	0	0	0
MoaE	0	2	1	1	0	1	0	2	0	2	1	2	0	0	0	0	0	0	0	1.22E+07	0	0	0	1.27E+07
BmrA	0	1	2	2	0	1	2	2	0	0	1	2	0	0	0	0	0	0	0	2.05E+07	0	0	0	1.65E+07
HepS	0	1	1	2	0	1	1	3	0	0	1	2	0	0	0	1.38E+07	0	0	0	2.45E+07	0	0	0	1.66E+07
YdeS	0	0	1	2	0	0	0	2	0	0	0	1	0	0	0	1.80E+07	0	0	0	0	0	0	0	0
SunT	1	3	1	2	4	1	1	5	1	1	1	3	0	0	0	1.74E+07	0	0	0	1.93E+07	0	0	0	1.69E+07
MgsA	0	1	0	2	0	1	0	2	0	1	0	2	0	0	0	2.03E+07	0	0	0	2.06E+07	0	0	0	2.32E+07
LytE	1	1	1	2	1	1	1	2	0	0	0	2	0	0	0	1.83E+07	0	0	0	2.49E+07	0	0	0	1.45E+07
FapR	0	1	1	2	0	1	1	1	0	1	1	2	0	0	0	2.57E+07	0	0	0	0	0	0	0	1.76E+07
YpiA	2	1	2	2	2	1	2	3	2	1	2	2	0	0	0	3.31E+07	0	0	0	3.45E+07	0	0	0	2.98E+07
YdiF	1	2	0	3	2	2	0	3	0	1	0	3	0	0	0	3.33E+07	0	0	0	3.87E+07	0	0	0	3.11E+07
CoaX	0	1	2	3	0	1	2	3	0	1	2	3	0	0	0	3.48E+07	0	0	0	3.55E+07	0	0	0	3.36E+07
YpbR	0	0	1	2	1	0	1	2	0	0	1	2	0	0	0	5.57E+07	0	0	0	4.38E+07	0	0	0	0
YoeC	1	1	0	5	1	0	0	4	1	1	0	5	0	0	0	5.46E+07	0	0	0	3.32E+07	0	0	0	1.26E+08
LicT	0	0	1	2	1	0	0	3	0	0	1	2	0	0	0	1.19E+08	0	0	0	4.62E+07	0	0	0	1.02E+08
PksN	2	2	1	2	2	3	1	2	2	2	1	2	0	0	0	3.42E+08	0	0	0	3.29E+08	0	0	0	4.15E+08
Bmr3	0	0	0	1	0	0	0	1	0	0	0	1	0	0	0	1.03E+09	0	0	0	1.71E+08	0	0	0	5.66E+08
SigL	0	0	0	5	0	0	0	6	0	0	0	7	0	0	0	9.12E+07	0	0	0	5.74E+07	0	0	0	1.68E+08
YtoP	1	1	2	7	4	2	3	6	3	2	3	6	0	0	0	8.22E+07	1.51E+08	0	0	1.39E+08	7.07E+07	0	0	8.57E+07
Xpf	0	0	0	3	0	0	0	3	0	0	0	5	0	0	0	6.22E+07	0	0	0	2.55E+07	0	0	0	1.59E+08
GbsR	0	0	0	3	0	0	0	0	0	0	0	3	0	0	0	5.81E+07	0	0	0	0	0	0	0	6.55E+07
CisA	0	0	0	3	0	0	0	2	0	0	0	3	0	0	0	3.70E+07	0	0	0	3.25E+07	0	0	0	5.63E+07
UvsE	0	0	0	2	0	0	0	1	0	0	0	2	0	0	0	1.37E+07	0	0	0	0	0	0	0	3.92E+07
YndB	0	0	0	1	0	0	0	2	0	0	0	2	0	0	0	0	0	0	0	0	0	0	0	1.03E+09
YueD	0	0	0	2	0	0	0	3	0	0	0	3	0	0	0	0	0	0	0	1.54E+07	0	0	0	2.30E+07

Table S7. List of the most promising DACA candidates for the regulation of P_{rpt}, most prominently showing for DNA promoter fragments 1-3. For detected peptide fragments and LFQ intensities refer to Table S5.

Identified protein	Strain used for verification	Higher background expression	Loss of induction specificity	Paralogous proteins[a]
AdeR	*B. subtilis* 168 Δ*adeR* *amyE*::P_{rpt}-*lacZ*	Weakly	No	No
GlvR	*B. subtilis* 168 Δ*glvR* *amyE*::P_{rpt}-*lacZ*	No	No	No
AbrB	*B. subtilis* 168 Δ*abrB* pHT304-P_{rpt}-*luc*	No	No	Abh, SpoVT
Hpr (ScoC)[b]	*B. subtilis* 168 Δ*hpr* *amyE*::P_{rpt}-*lacZ*	No	No	No
SigB[b]	*B. subtilis* 168 Δ*sigB* *amyE*::P_{rpt}-*lacZ*	No	No	No
QdoR (YxaF)	*B. subtilis* 168 Δ*qdoR* *amyE*::P_{rpt}-*lacZ*	No	No	LmrA
PamR (ydcH)	*B. subtilis* 168 Δ*pamR* *amyE*::P_{rpt}-*lacZ*	No	No	No
TreR	*B. subtilis* 168 Δ*treR* *amyE*::P_{rpt}-*lacZ*	Weakly	No	No
Rex	*B. subtilis* 168 Δ*rex* *amyE*::P_{rpt}-*lacZ*	No	No	No
YprA	*B. subtilis* 168 Δ*yprA* *amyE*::P_{rpt}-*lacZ*	Weakly	No	No
YprB	*B. subtilis* 168 Δ*yprB* *amyE*::P_{rpt}-*lacZ*	Weakly	No	No
RocR[b]	*B. subtilis* 168 Δ*rocR* *amyE*::P_{rpt}-*lacZ*	No	No	No
Abh	*B. subtilis* 168 Δ*abh* *amyE*::P_{rpt}-*lacZ*	No	No	AbrB
SigD[b]	*B. subtilis* 168 Δ*sigD* *amyE*::P_{rpt}-*lacZ*	No	No	No
UvrB	*B. subtilis* 168 Δ*uvrB* *amyE*::P_{rpt}-*lacZ*	Yes	No	No
IolR	*B. subtilis* 168 Δ*iolR* *amyE*::P_{rpt}-*lacZ*	Yes	No	No
YorC[b]	*B. subtilis* 168 Δ*yorC* *amyE*::P_{rpt}-*lacZ*	No	No	No
YkrK	*B. subtilis* 168 Δ*ykrK* *amyE*::P_{rpt}-*lacZ*	No	No	No
YdeL	*B. subtilis* 168 Δ*ydeL* *amyE*::P_{rpt}-*lacZ*	No	No	YhdI
YfiR[b]	*B. subtilis* 168 Δ*yfiR* *amyE*::P_{rpt}-*lacZ*	No	No	No
RpoY (YkzG)[b]	*B. subtilis* 168 Δ*rpoY* *amyE*::P_{rpt}-*lacZ*	No	No	No
YwaE	*B. subtilis* 168 Δ*ywaE* *amyE*::P_{rpt}-*lacZ*	Weakly	No	No
GmuR	*B. subtilis* 168 Δ*gmuR* *amyE*::P_{rpt}-*lacZ*	No	No	No
CysL	*B. subtilis* 168 Δ*cysL* *amyE*::P_{rpt}-*lacZ*	No	No	No
YcnK	*B. subtilis* 168 Δ*ycnK* *amyE*::P_{rpt}-*lacZ*	Yes	No	No
YybA	*B. subtilis* 168 Δ*yybA* *amyE*::P_{rpt}-*lacZ*	Weakly	No	No
ManR	*B. subtilis* 168 Δ*manR* *amyE*::P_{rpt}-*lacZ*	No	No	No
RpoZ[b]	*B. subtilis* 168 Δ*rpoZ* *amyE*::P_{rpt}-*lacZ*	No	No	No

Identified protein	Strain used for verification	Higher background expression	Loss of induction specificity	Paralogous proteins[a]
YydK	*B. subtilis* 168 Δ*yydK amyE*::P*rpt*-*lacZ*	No	No	No
FrlR (YurK)	*B. subtilis* 168 Δ*frlR amyE*::P*rpt*-*lacZ*	Weakly	no	No
AlsR	*B. subtilis* 168 Δ*alsR amyE*::P*rpt*-*lacZ*	Weakly	no	No
CcpN	*B. subtilis* 168 Δ*ccpN amyE*::P*rpt*-*lacZ*	No	No	No
LicR[b]	*B. subtilis* 168 Δ*licR amyE*::P*rpt*-*lacZ*	Weakly	No	No
LmrA	*B. subtilis* 168 Δ*lmrA amyE*::P*rpt*-*lacZ*	No	No	YxaF
RhaR (YulB)	*B. subtilis* 168 Δ*rhaR amyE*::P*rpt*-*lacZ*	No	No	No
SigI[b]	*B. subtilis* 168 Δ*sigI amyE*::P*rpt*-*lacZ*	No	No	No
YcsD[b]	*B. subtilis* 168 Δ*ycsD amyE*::P*rpt*-*lacZ*	No	No	No
YkvZ	*B. subtilis* 168 Δ*ykvZ amyE*::P*rpt*-*lacZ*	No	No	No
YusI	*B. subtilis* 168 Δ*yusI amyE*::P*rpt*-*lacZ*	No	No	No
PerR	*B. subtilis* 168 Δ*perR* pHT304-P*rpt*-*luc*	No	No	No
MtlR[b]	*B. subtilis* 168 Δ*mtlR amyE*::P*rpt*-*lacZ*	No	No	No
YsfB[b]	*B. subtilis* 168 Δ*ysfB amyE*::P*rpt*-*lacZ*	Weakly	no	No
AscR (YtlI)[b]	*B. subtilis* 168 Δ*ascR amyE*::P*rpt*-*lacZ*	No	No	No
PchR (YvmB)[b]	*B. subtilis* 168 Δ*pchR amyE*::P*rpt*-*lacZ*	No	No	No
SpxA[b]	*B. subtilis* 168 Δ*spxA amyE*::P*rpt*-*lacZ*	No	No	No

[a] identified paralogs using the Kyoto encyclopedia of genes and genomes (KEGG) (Kanehisa and Goto, 2000) with a sequence identity > 0.5

[b] most prominent binding to fragment 1

Table S8. Strains utilized for the phylogenetic analysis of different rifampin-phosphotransferases (compare Figure 7).

Strain	Accession number
Actinomadura sp. NAK00032	NZ_CP054932.1
Actinoplanes missouriensis	NC_017093.1
Amycolatopsis orientalis	NZ_CP016174.1
Bacillus amyloliquefaciens LL3	NC_017190.1
Bacillus amyloliquefaciens MT45	NC_014551.1
Bacillus anthracis Ames	NC_003997.3
Bacillus cereus ATCC14579	NC_004722.1
Bacillus cereus FRI-35	NC_018491.1
Bacillus circulans	NZ_CP026031.1
Bacillus glycinifermentans	NZ_LT603683.1
Bacillus halotolerans F41-3	NZ_CP029364.1
Bacillus licheniformis ATCC14580	NC_006270.3
Bacillus megaterium NBRC 15308	NZ_CP009920.1
Bacillus mycoides WSBC10204	NZ_CP009746.1
Bacillus paralicheniformis	NC_021362.1
Bacillus pseudomycoides 219298	NZ_CP007626.1
Bacillus siamensis	NZ_CP025001.1
Bacillus simplex NBRC15720	NZ_CP017704.1
Bacillus sonorensis	NZ_CP021920.1
Bacillus subtilis subsp. *subtilis* 168	NC_000964.3
Bacillus thuringiensis BMB171	NC_014171.1
Bacillus toyonensis	NC_022781.1
Bacillus tropicus	NZ_CP041071.1
Brevibacillus agri	NZ_CP026363.1
Brevibacillus brevis NBRC100599	NC_012491.1
Brevibacillus formosus	NZ_CP018145.1
Clostridium acetobutylicum ATCC824	NC_003030.1
Clostridium beijerinckii NCIMB14988	NZ_CP010086.2
Clostridium kluyveri NBRC12016	NC_011837.1
Corallococcus coralloides DSM 2259	NC_017030.1
Cystobacter fuscus	NZ_CP022098.1
Geosporobacter ferrireducens	NZ_CP017269.1
Paenibacillus ihbetae	NZ_CP016809.1
Paenibacillus lautus	NZ_CP032412.1

Strain	Accession number
Paenibacillus mucilaginosus KNP414	NC_015690.1
Paenibacillus sp. Y412MC10	NC_013406.1
Peribacillus butanolivorans KJ40	NZ_CP030926.1
Peribacillus simplex	NZ_CP011008.1
Labilithrix luteola DSM 27648	NZ_CP012333.1
Listeria innocula serotyp6a	NC_003212.1
Listeria ivanovii WSLC3009	NZ_CP007172.1
Listeria monocytogenes ATCC51779	NC_018584.1
Listeria monocytogenes 4b. F2365	NC_002973.6
Listeria monocytogenes Lm60	NZ_CP009258.1
Listeria seeligeri	NC_013891.1
Micromonospora sp. L5	NC_014815.1
Myxococcus hansupus	NZ_CP012109.1
Myxococcus xanthus GH3.5.6c2	NZ_CP017169.1
Neobacillus mesonae	NZ_CP022572.1
Nocardia nova SH22a	NZ_CP006850.1
Nonomuraea sp. ATCC55076	NZ_CP017717.1
Sorangium cellulosum	NC_010162.1
Sporosarcina psychrophila	NZ_CP014616.1
Streptomyces albulus ZPM	NZ_CP006871.1
Streptomyces bingchenggensis	NC_016582.1
Streptomyces lincolnensis B48	NZ_CP046024.1
Streptomyces vinaceus	NZ_CP023692.1
Streptomyces sp. WAC4747, rifampin phosphotransferase gene	KJ151292
Streptosporangium roseum	NC_013595.1
Rhodococcus aetherivorans	NZ_CP011341.1
Rhodococcus sp. WB1	NZ_CP015529.1

Table S9. Strains used in this study. *B. subtilis* 168 knockout mutants (chosen on the basis of the DACA) containing the *amyE*::P$_{rpt}$-*lacZ* (Spt^r) or pHT304-P$_{rpt}$-*luc* (Erm^r) bioreporters are listed in Table S7.

Strain	Relevant genotype	Source/ reference
Escherichia coli XL1 blue	*recA1 endA1 gyrA96 thi-1 hsdR17 supE44 relA1 lac* [F´ *proAB lacI*^{q}ZΔ*M15* Tn*10* (Tet^r)]	Agilent (Cat#200249)
E. coli XL10 gold	Tet^{r}Δ(*mcrA*)183Δ(*mcrCB-hsdSMR-mrr*)173 *endA1 supE44 thi-1 recA1 gyrA96 relA1 lac* Hte [F´ *proAB lacI*^{q}ZΔ*M15* Tn*10*(Tet^r) Amy Cam^r]	Agilent (Cat#200314)
E. coli NEB Turbo	*F´ proA+B+ lacIq*Δ *lacZ M15/ fhuA2* Δ*(lac-proAB) glnV gal R(zgb-210::*Tn*10)Tet*^{S} *endA1 thi-1* Δ*(hsdS-mcrB)5*	NEB[a]
E. coli TOP 10 pHJS105	F$^-$ *mcrA* Δ(*mrr-hsdRMS-mcrBC*) ϕ80*lacZ*ΔM15 Δ*lacX74 nupG recA1 araD139* Δ(*ara-leu*)*7697 galE*15 *galK16 rpsL*(*StrR*) *endA1* λ-; pHJS105	Leendert Hamoen, University of Amsterdam
E. coli DH5α pBS3Clux	F$^-$ *endA1 glnV44 thi-1 recA1 relA1 gyrA96 deoR nupG* Φ80d*lacZ*Δ*M15* Δ(*lacZYA-argF*)U169, *hsdR17*(r_K^- m_K^+), λ–; pBS3Clux	Addgene (Cat#55172)
E. coli DH5α pBS2E	F$^-$ *endA1 glnV44 thi-1 recA1 relA1 gyrA96 deoR nupG* Φ80d*lacZ*Δ*M15* Δ(*lacZYA-argF*)U169, *hsdR17*(r_K^- m_K^+), λ–; pBS2E	Addgene (Cat#55169)
E. coli TOP 10 pAPNC-mCherry	F$^-$ *mcrA* Δ(*mrr-hsdRMS-mcrBC*) ϕ80*lacZ*ΔM15 Δ*lacX74 nupG recA1 araD139* Δ(*ara-leu*)*7697 galE*15 *galK16 rpsL*(*StrR*) *endA1* λ-; pAPNC-mCherry	Leendert Hamoen, University of Amsterdam
E. coli XL1 blue pBS2E-P$_{Spac}$	F$^-$ *endA1 glnV44 thi-1 recA1 relA1 gyrA96 deoR nupG* Φ80d*lacZ*Δ*M15* Δ(*lacZYA-argF*)U169, *hsdR17*(r_K^- m_K^+), λ–; pBS2E-P$_{Spac}$	This study
E. coli XL1 blue pBS2E-P$_{Spac}$-S707-*rpt*	F$^-$ *endA1 glnV44 thi-1 recA1 relA1 gyrA96 deoR nupG* Φ80d*lacZ*Δ*M15* Δ(*lacZYA-argF*)U169, *hsdR17*(r_K^- m_K^+), λ–; pBS2E-P$_{Spac}$-S707-*rpt*	This study
Bacillus subtilis 1S34	*trpC2 spoIIE61*	(Piggot, 1973)
B. subtilis 1S34 *amyE*::pHJS105-P$_{yorB}$-*lacZ*	*trpC2 spoIIE61, amyE*::P$_{yorB}$-*lacZ* Spt^r	(Wex et al., 2021)
B. subtilis 1S34 *amyE*::pHJS105-P$_{rpt}$-*lacZ*	*trpC2 spoIIE61, amyE*::P$_{rpt}$-*lacZ* Spt^r	(Wex et al., 2021)
B. subtilis 1S34 *amyE*::pHJS105-P$_{helD}$-*lacZ*	*trpC2 spoIIE61, amyE*::P$_{helD}$-*lacZ* Spt^r	(Wex et al., 2021)
B. subtilis 1S34 *amyE*::pHJS105-P$_{rpt_123bp}$-*lacZ*	*trpC2 spoIIE61, amyE*::P$_{rpt_123bp}$-*lacZ* Spt^r	This study
B. subtilis 1S34 *amyE*::pHJS105-P$_{rpt_108bp}$-*lacZ*	*trpC2 spoIIE61, amyE*::P$_{rpt_108bp}$-*lacZ* Spt^r	This study
B. subtilis 1S34 *amyE*::pHJS105-P$_{rpt_Del14bpDS}$-*lacZ*	*trpC2 spoIIE61, amyE*::P$_{rpt_Del14bpDS}$-*lacZ* Spt^r	This study
B. subtilis 1S34 *amyE*::pHJS105-P$_{rpt_Modi14bpDS}$-*lacZ*	*trpC2 spoIIE61, amyE*::P$_{rpt_Modi14bpDS}$-*lacZ* Spt^r	This study
B. subtilis 1S34 *amyE*::pHJS105-P$_{rpt_onlySigA}$-*lacZ*	*trpC2 spoIIE61, amyE*::-P$_{rpt_onlySigA}$-*lacZ* Spt^r	This study
B. subtilis 1S34 *amyE*::pHJS105-P$_{rpt_Modi-10SigA(S708)}$-*lacZ*	*trpC2 spoIIE61, amyE*::P$_{rpt_Modi-10SigA(S708)}$-*lacZ* Spt^r	This study
B. subtilis 1S34 *amyE*::pHJS105-P$_{helD_120bp}$-*lacZ*	*trpC2 spoIIE61, amyE*::P$_{helD_120bp}$-*lacZ* Spt^r	This study
B. subtilis 1S34 *amyE*::pHJS105-P$_{helD_113bp}$-*lacZ*	*trpC2 spoIIE61, amyE*::P$_{helD_113bp}$-*lacZ* Spt^r	This study
B. subtilis 1S34 *amyE*::pHJS105-P$_{helD_Del15bpDS}$-*lacZ*	*trpC2 spoIIE61, amyE*::P$_{helD_Del15bpDS}$-*lacZ* Spt^r	This study
B. subtilis 1S34 *sacA*::pBS3Clux-P$_{rpt}$-*luxABCDE*	*trpC2 spoIIE61, sacA*::P$_{rpt}$-*luxABCDE* Chl^r	This study
B. subtilis 1S34 *sacA*::pBS3Clux-P$_{helD}$-*luxABCDE*	*trpC2 spoIIE61, sacA*::P$_{helD}$-*luxABCDE* Chl^r	This study
B. subtilis 1S34 *sacA*::pBS3Clux-P$_{rpt_Del14bpDS}$*luxABCDE*	*trpC2 spoIIE61, sacA*::P$_{rpt_Del14bpDS}$-*luxABCDE* Chl^r	This study

Strain	Relevant genotype	Source/ reference
B. subtilis 168 single knockout mutants	*trpC2* Δ"gene"::Kan^r	Addgene (Cat#1000000115), (Koo et al., 2017)
B. subtilis 168 Δ*amyE* *sacA*::pBS3Clux-P$_{rpt}$-*luxABCDE*	*trpC2* Δ*amyE*::Kan^r, *sacA*::P$_{rpt}$-*luxABCDE* Chl^r	This study
B. subtilis 168 Δ*rpoE* *sacA*::pBS3Clux-P$_{rpt}$-*luxABCDE*	*trpC2* Δ*rpoE*::Kan^r, *sacA*::P$_{rpt}$-*luxABCDE* Chl^r	This study
B. subtilis 168 Δ*helD* *sacA*::pBS3Clux-P$_{rpt}$-*luxABCDE*	*trpC2* Δ*helD*::Kan^r, *sacA*::P$_{rpt}$-*luxABCDE* Chl^r	This study
B. subtilis 168 Δ*mfd* *sacA*::pBS3Clux-P$_{rpt}$-*luxABCDE*	*trpC2* Δ*mfd*::Kan^r, *sacA*::P$_{rpt}$-*luxABCDE* Chl^r	This study
B. subtilis 168 Δ*uvrB* *sacA*::pBS3Clux-P$_{rpt}$-*luxABCDE*	*trpC2* Δ*uvrB*::Kan^r, *sacA*::P$_{rpt}$-*luxABCDE* Chl^r	This study
B. subtilis 168 Δ*perR* *sacA*::pBS3Clux-P$_{rpt}$-*luxABCDE*	*trpC2* Δ*perR*::Kan^r, *sacA*::P$_{rpt}$-*luxABCDE* Chl	This study
B. subtilis 168 Δ*rpt* *aprE*::P$_{Spac}$	*trpC2* Δ*rpt*::Kan^r, *aprE*::P$_{Spac}$	This study
B. subtilis 168 Δ*rpt* *aprE*::P$_{Spac}$-S707-*rpt*	*trpC2* Δ*rpt*::Kan^r, *aprE*::P$_{Spac}$-S707-*rpt*	This study
B. subtilis 168 Δ*lexA* *amyE*::pHJS105-P$_{yorB}$-*lacZ*	*trpC2* Δ*lexA*::Kan^r, *amyE*::pHJS105-P$_{yorB}$-*lacZ* Spt^r	This study
B. subtilis 168 Δ*gamR* (*ybgA*) *amyE*::pHJS105-P$_{yorB}$-*lacZ*	*trpC2* Δ*gamR*::Kan^r, *amyE*::pHJS105-P$_{yorB}$-*lacZ* Spt^r	This study
B. subtilis 168 Δ*ymaH* *amyE*::pHJS105-P$_{rpt}$-*lacZ*	*trpC2* Δ*ymaH*::Kan^r, *amyE*::pHJS105-P$_{rpt}$-*lacZ* Spt^r	This study

[a] New England BioLabs

Table S10. Oligonucleotides used in this study.

Name	Use	Sequence (5'-3')
pBS2E-S707-*rpt*-insert-for	Cloning of pBS2E-P_{Spac}-S707-*rpt* forward primer insert	CACATACTAGAGAAAGAGGAGAAATACTAGA TGAGTTCTTTGGTTCTCGGTTTACATGAA
pBS2E-S707-*rpt*-insert-rev	Cloning of pBS2E-P_{Spac}-S707-*rpt* reverse primer insert	TAGCGATCTACACTAGCACTATCAGCGTTAT TAGAAGATTTCAATGTAGCCTTCTGTACC
pBS2E-S707-*rpt*-vector-for	Cloning of pBS2E-P_{Spac}-S707-*rpt* forward primer vector	CTAGTATTTCTCCTCTTTCTCTAGTATGTG
pBS2E-S707-*rpt*-vector-rev	Cloning of pBS2E-P_{Spac}-S707-*rpt* reverse primer vector	TAACGCTGATAGTGCTAGTGTAGATCGCTA
P_{rpt_123bp}-for	Cloning of pHJS105-P_{rpt_123bp}-*lacZ* forward primer	TATTAGTGACATTTGCATGCTATATTGCACAA AAACAGACAC
P_{rpt_108bp}-for	Cloning of pHJS105-P_{rpt_108bp}-*lacZ* forward primer	TATTAGTGACATTTGCATGCCAGACACGGTG ATATAATCAC
P_{rpt}-rev	Cloning of pHJS105-P_{rpt_123bp}-*lacZ* and pHJS105-P_{rpt_108bp}-*lacZ* reverse primer	ACGTCAGTAACTTCCACGGTACCTTTTTCCT CCTTACTGCAGAAAAATATTGACAAGAGC
$P_{rpt\_Del14bpDS}$-for	Cloning of pHJS105-$P_{rpt\_Del14bpDS}$-*lacZ* forward primer	TATTAGTGACATTTGCATGCTATATTGCACAA AAACAGACAC
$P_{rpt\_Del14bpDS}$-rev	Cloning of pHJS105-$P_{rpt\_Del14bpDS}$-*lacZ* reverse primer	ACGTCAGTAACTTCCACGGTACCTTTTTCCT CCTTACTGCAGGAGCTTCCTAGCAGGATA
$P_{rpt\_Modi14bpDS}$-for	Cloning of pHJS105-$P_{rpt\_Modi14bpDS}$-*lacZ* forward primer	5´-Phos-TGATCTTCTGCAGTAAGGAGGAAAA
$P_{rpt\_Modi14bpDS}$-rev	Cloning of pHJS105-$P_{rpt\_Modi14bpDS}$-*lacZ* reverse primer	5´-Phos-TAGATGAGAGCTTCCTAGCAGGATA
$P_{rpt_onlySigA}$_frag1-for	Cloning of pHJS105-$P_{rpt\_onlySigA}$-*lacZ* forward primer fragment 1	GGCTGTATATCCTGCATCATG
$P_{rpt_onlySigA}$_frag1-rev	Cloning of pHJS105-$P_{rpt\_onlySigA}$-*lacZ* reverse primer fragment 1	CACGTAGTGTGATTATATCACC
$P_{rpt_onlySigA}$_frag2-for	Cloning of pHJS105-$P_{rpt\_onlySigA}$-*lacZ* forward primer fragment 2	ACAGACACGGTGATATAATCACACTACGTGC TGCAGTAAGGAGGAAAAAGG
$P_{rpt_onlySigA}$_frag2-rev	Cloning of pHJS105-$P_{rpt\_onlySigA}$-*lacZ* reverse primer fragment 2	AAGGATATTCATGATGCAGGATATACAGCCA TTCAGACATCTCCGATTAACC
$P_{rpt\_Modi-10SigA(S708)}$-for	Cloning of pHJS105-$P_{rpt\_Modi-10SigA(S708)}$-*lacZ* forward primer	5´-Phos-GTCCAGTACTTGCTAGGAAGCTCTTGTCAAT AT
$P_{rpt\_Modi-10SigA(S708)}$-rev	Cloning of pHJS105-$P_{rpt\_Modi-10SigA(S708)}$-*lacZ* reverse primer	5´-Phos-ATCGTTGACGATGGATATCTATAACTTTTTAA CTAG
P_{helD_120bp}-for	Cloning of pHJS105-P_{helD_120bp}-*lacZ* forward primer	TATTAGTGACATTTGCATGCCTTGATTGGTAT TGGGTGAAT
P_{helD_113bp}-for	Cloning of pHJS105-P_{helD_111bp}-*lacZ* forward primer	TATTAGTGACATTTGCATGCGGTATTGGGTG AATGTGCTA
P_{helD}-rev	Cloning of pHJS105-P_{helD_120bp}-*lacZ* and pHJS105-P_{helD_111bp}-*lacZ* reverse primer	CTTACGTCAGTAACTTCCACGGTACCTTTTTC CTCCTTACTGCAGGAAAATAGTTGACAAACA TAGAT
$P_{helD\_Del15bpDS}$ -for	Cloning of pHJS105-$P_{helD\_Del15bpDS}$-*lacZ* forward primer	TATTAGTGACATTTGCATGCATGTTTAATTGG AAGCTGCCA
$P_{helD\_Del15bpDS}$-rev	Cloning of pHJS105-$P_{helD\_Del15bpDS}$-*lacZ* reverse primer	CTTACGTCAGTAACTTCCACGGTACCTTTTTC CTCCTTACTGCAGGTCGACACATAGATGAAA TACTGTAAAATA
P_{rpt}-*luxABCDE*-for	Cloning of pBS3Clux-P_{rpt}-*luxABCDE* forward primer	GATAAGCTGTCAAACATGAGAATTCCAGATC ATCCTTAATCAGGG
P_{rpt}-*luxABCDE*-rev	Cloning of pBS3Clux-P_{rpt}-*luxABCDE* reverse primer	CCAAATTTCATAGAGAGTCCTCCTGTCGACA AAAATATTGACAAGAGCTTCC
P_{helD}-*luxABCDE*-for	Cloning of pBS3Clux-P_{helD}-*luxABCDE* forward primer	GATAAGCTGTCAAACATGAGAATTCATGTTTA ATTGGAAGCTGCC
P_{helD}-*luxABCDE*-rev	Cloning of pBS3Clux-P_{helD}-*luxABCDE* reverse primer	TAGAGAGTCCTCCTGTCGACGAAAATAGTTG ACAAACATAG

Name	Use	Sequence (5'-3')
P_{rpt}-*luc*-for	Cloning of pHT304-P_{rpt}-luc forward primer	GGCCAGTGAATTCGAGCTCGGTACCCAGATCATCCTTAATCAGGG
P_{rpt}-*luc*-rev	Cloning of pHT304-P_{rpt}-*luc* reverse primer	TTCCATTTTTTCCTCCTTACTGCAGAAAAATATTGACAAGAGCTTCC
$P_{rpt\_Del14bpDS}$-*luxABCDE*-for	Cloning of pBS3Clux-$P_{rpt\_Del14bpDS}$-*luxABCDE* forward primer	5´-Phos-GTCGACAGGAGGACTCTCTATGAAATTTGG
$P_{rpt\_Del14bpDS}$-*luxABCDE*-rev	Cloning of pBS3Clux-$P_{rpt\_Del14bpDS}$-*luxABCDE* reverse primer	5´-Phos-GAGCTTCCTAGCAGGATATAATAAAATTAT
P_{Spac}-S707-*rpt*-for	Cloning of pAPNC-P_{Spac}-S707-*rpt* forward primer	AGGCATGCCTGCAGGTCGACCACACTACGTGCGCTTTCTA
P_{Spac}-S707-*rpt*-rev	Cloning of pAPNC-P_{Spac}-S707-*rpt* reverse primer	TGGGCTAACGCCCGAATTCTTAGAAGATTTCAATGTAGCCTT
pHJS105-ctrl_for	Control primer for sequencing of the promoter region	ATAGAAAGAAATTGTTCCTTCGA
pBS3Clux-ctrl_for	Control primer for sequencing of the promoter region	AAGGATTTGAGCGTAGCGAA
pBS3Clux-integration_for	Control primer for integration selectively binding genomically in the *sacA* region	CTGATTGGCATGGCGATTGC
pBS3Clux-integration_rev	Control primer for integration selectively binding in pBS3Clux	ACAGCTCCAGATCCTCTACG
pAPNC_ctrl1_for	Control primer for sequencing of the promoter region and the *rpt* gene start	CTACAAGGTGTGGCATAATG
pAPNC_ctrl2_for	Control primer for sequencing of the *rpt* sequence integrity	GCGACAGGAAGCTTTGAAG
pAPNC-integration_for	Control primer for integration selectively binding genomically in the *aprE* region	CCGGGACTCAGGAGCATTTAAC
pAPNC-integration_rev	Control primer for integration selectively binding in pAPNC	CGCTATCTTTACAGGTACATC
DACA_fragment1-3_for	Amplification of the biotinylated DACA fragments 1-3 forward primer	5´-Biotin-TTTTTAATGCGACTAGCTATGGAA
DACA_fragment1_rev	Amplification of the biotinylated DACA fragment 1 reverse primer	CCTCCTTACTGCAGAAAAATAT
DACA_fragment1_rev	Amplification of the biotinylated DACA fragment 2 reverse primer	GCTTCCTAGCAGGATATAATAA
DACA_fragment1_rev	Amplification of the biotinylated DACA fragment 3 reverse primer	ACTTTTTAACTAGAAAGCGCAC
DACA_fragment4_for	Amplification of the biotinylated DACA fragment 4 forward primer	5´-Biotin- GGTGCAAGAGTGCTTTCGC
DACA_fragment4_rev	Amplification of the biotinylated DACA fragment 4 reverse primer	TTTTGAAATTTTTGGTACTACTAAA

Supplemental References

Crooks, G. E., Hon, G., Chandonia, J. M., and Brenner, S. E. (2004). WebLogo: a sequence logo generator. Genome Research 14, 1188-90.

Erb, I., González-Vallinas, J. R., Bussotti, G., Blanco, E., Eyras, E., and Notredame, C. (2012). Use of ChIP-Seq data for the design of a multiple promoter-alignment method. Nucleic Acids Research 40, e52-e52.

Freiberg, C., Brunner, N., Macko, L., and Fischer, H. P. (2006). Discovering antibiotics efficacy biomarkers: towards mechanism-specific high-content compound screening. Molecular and Cellular Proteomics.

Kanehisa, M., and Goto, S. (2000). KEGG: kyoto encyclopedia of genes and genomes. Nucleic Acids Research 28, 27-30.

Koo, B.-M., Kritikos, G., Farelli, J. D., Todor, H., Tong, K., Kimsey, H., Wapinski, I., Galardini, M., Cabal, A., Peters, J. M., et al. (2017). Construction and analysis of two genome-scale deletion libraries for *Bacillus subtilis*. Cell systems 4, 291-305.e7.

Nicolas, P., Mäder, U., Dervyn, E., Rochat, T., Leduc, A., Pigeonneau, N., Bidnenko, E., Marchadier, E., Hoebeke, M., Aymerich, S., et al. (2012). Condition-dependent transcriptome reveals high-level regulatory architecture in *Bacillus subtilis*. Science 335, 1103.

Piggot, P. J. (1973). Mapping of asporogenous mutations of *Bacillus subtilis*: a minimum estimate of the number of sporulation operons. Journal of Bacteriology 114, 1241-1253.

Wex, K. W., Saur, J. S., Handel, F., Ortlieb, N., Mokeev, V., Kulik, A., Niedermeyer, T. H. J., Mast, Y., Grond, S., Berscheid, A., et al. (2021). Bioreporters for direct mode of action-informed screening of antibiotic producer strains. Cell Chemical Biology, DOI: 10.1016/j.chembiol.2021.02.022

Zhu, B., and Stülke, J. (2017). SubtiWiki in 2018: from genes and proteins to functional network annotation of the model organism *Bacillus subtilis*. Nucleic Acids Research 46, D743-D748.

Zuker, M. (2003). Mfold web server for nucleic acid folding and hybridization prediction. Nucleic Acids Research 31, 3406-3415.